

**Final Report:
Los Alamos Opacity
Verification and Validation
Workshop**

May 3-5, 2005

Los Alamos National Laboratory

Edited by David P. Kilcrease

Los Alamos Opacity Verification and Validation Workshop 2005

The purpose of this workshop is to bring together theorists and experimentalists in the area of plasma opacity and its applications to try to determine to what extent we can verify and validate our opacity calculations. Simply put, by validation we mean, “Are we solving the right equations?” and by verification “Are we solving them correctly?”.

More specifically, to verify an opacity calculation, we want to make sure that the equations that represent the particular opacity theory we have chosen have been implemented on the computer in such a way as to produce the exact solution of those equations to the desired numerical accuracy. Impediments to this goal can include interpolation errors, insufficiently converged atomic Hartree-Fock wave functions and similar numerical problems.

To validate calculated opacity values we want to determine if our theoretical model is sufficient to give results that agree, again with a desired accuracy, with the actual real-world value for the opacity. This is hampered by the fact that most of the density and temperature points for which we calculate opacities are not easily accessible in the laboratory.

Additionally, the term opacity here can refer not only to frequency averaged quantities such as the Rosseland and Planck means, but also to frequency dependent spectra. This would appear to be a daunting task but we are not without hope or means!

To address the verification problem we can take similar calculations performed by different groups and compare them at opacity code comparison workshops. These comparisons have many times pointed out errors in calculations that were not apparent at first. At the upcoming WorkOp at Lawrence Livermore National Lab we will continue these comparisons.

Validating the results of these calculations is the primary subject of the current Workshop here at Los Alamos. We will hear from those who perform laboratory opacity measurements; those who use opacity data to accurately explain stellar structures and behavior; those who use opacity data to model thermonuclear devices; and those who calculate the opacities. From these talks we hope to begin to construct a road map to quantify computed opacity uncertainties.

David P. Kilcrease
Atomic and Optical Theory
Los Alamos National Laboratory
Los Alamos, New Mexico

Los Alamos
Opacity Validation and Verification
Workshop
May 3-5, 2005
Los Alamos National Laboratory

Tuesday, May 3:

(8:00-8:30) Continental Breakfast

(8:30-8:45) Welcome by James Peery and Mark Chadwick
Introduction and Purpose of the Workshop (D. Kilcrease)

(8:45-9:30) Plasma Opacities and High Precision Atomic Physics (A. Pradhan)

(9:30-10:15) Opacity Development at Los Alamos (N. Magee)

(10:15-10:30) BREAK

(10:30-11:15) Neglected Opacity Issues (W. Huebner)

(11:15-12:00) Opacities in Astrophysics (A. Cox)

(12:00-2:00) LUNCH Catered
Briefing for Classified Session

(2:00-3:00) Exploring Warm Dense Matter with QMD (S. Mazevet)

(3:00-3:15) BREAK

(3:15-3:45) Improvements to the Finite Temperature AA Model (J. Colgan)

(3:45-4:15) ATOMIC Opacity Calculations using CHEMEOS (P. Hakel)

(4:15-4:45) Visualization Tools for Opacity Analysis (L. Welser)

Tuesday Evening Catered Banquet 6:30 pm Central Avenue Grill

Wednesday Morning, May 4:

(8:00-8:45) Continental Breakfast

(8:45-9:30) AWE Current and Future Opacity Experiments (D. Hoarty)

(9:30-10:15) Opacity Experiments at Omega and Trident (T. Tierney)

(10:15-10:30) BREAK

(10:30-11:15) Overview of LLNL Opacity Efforts (B. Heeter)

(11:15-12:00) Application of Stark Broadened Line Shapes in the Analysis
of Line Absorption Spectra (R. Mancini)

(12:00-1:30) LUNCH Catered

Wednesday Afternoon:

- | | | |
|-------------------|--|----------------|
| (1:30-1:45) | Introduction | (D. Kilcrease) |
| (1:45-2:15) | Review of Recent LLNL Opacity/EOS Workshop (U) | (S. Libby) |
| (2:15-3:00) | Opacity Theory at AWE (U) | (J. Harris) |
| (3:00-3:15) BREAK | | |
| (3:15-4:00) | Overview of LLNL Opacity Modeling (U) | (B. Wilson) |
| (4:00-4:30) | QMD Simulation of Heavy Elements (U) | (L. Collins) |

Thursday, May 5:

- | | | |
|---------------------|--|----------------|
| (8:00-8:30) | Continental Breakfast | |
| (8:30-9:30) | Opacity Experiments at LLNL (U) | (B. Heeter) |
| (9:30-10:15) | Opacity Experiments at Z (U) | (J. Bailey) |
| (10:15-10:30) BREAK | | |
| (10:30-11:15) | Historical Overview of Opacity Experiments at AWE (U) | (C. Smith) |
| (11:15-12:00) | Concept Development for Foam Blast Wave Opacity Experiments on Z (U) | (B. Peterson) |
| (12:00-1:30) | LUNCH | Not Catered |
| (1:30-2:15) | Design of a Continuum Lowering Experiment (U) | (J. Benage) |
| (2:15-3:00) | LLNL – LANL Opacity Comparisons (U) | (B. Wilson) |
| (3:00-3:15) BREAK | | |
| (3:15-4:00) | Discussion and Summary | (D. Kilcrease) |

Sessions marked in **green** (Tuesday and Wednesday morning) are open and unclassified. Sessions marked in **red** (Wednesday afternoon and Thursday) are closed and classified. There will be a complimentary continental breakfast and refreshments each day.

The Tuesday through Wednesday morning session will be located in room 203A of The Los Alamos Research Park, 4200 W Jemez Road directly across from the main LANL Administration Building. The classified Wednesday afternoon and Thursday session will be located in the Al McKnight Conference Room (aka “The Forum”) in Building 1498.

For more information contact David Kilcrease at dpk@lanl.gov and check our web page at www.t4.lanl.gov.

OPACITY WORKSHOP

May 3-5, 2005

LASTNAME	FIRSTNAME	ORGANIZATION	TELEPHONE	EMAIL
Abdallah	Joseph	Los Alamos National Laboratory	505-662-5855	abd@lanl.gov
Bailey	James	SNL	505-845-7203	jebaile@sandia.gov
Batha	Steven	Los Alamos National Laboratory	505-665-5898	sbatha@lanl.gov
Chisolm	Eric	Los Alamos National Laboratory	505-665-5020	echisolm@lanl.gov
Chrien	Robert	Los Alamos National Laboratory	505-667-1674	bchrien@lanl.gov
Cohen	James	Los Alamos National Laboratory	505-667-5982	cohen@lanl.gov
Colgan	James	Los Alamos National Laboratory	505-665-0291	jcolgan@lanl.gov
Cox	Arthur	Los Alamos National Laboratory	505-667-7380	anc@lanl.gov
Csanak	George	Los Alamos National Laboratory	505-667-4836	gc@t4..lanl.gov
Delamater	Normon	Los Alamos National Laboratory	505-667-7946	ndd@lanl.gov
Fincke	James	Los Alamos National Laboratory	505-667-5730	jfincke@lanl.gov
Fitzpatrick	Joseph	Los Alamos National Laboratory	505-665-6616	josephf@lanl.gov
Fontes	Christopher	Los Alamos National Laboratory	505-665-7676	cjf@lanl.gov
Gales	Steven	AWE	44-118-982-6859	Steven.gales@awe.com
Goldman	Sanford	Los Alamos National Laboratory	505-665-7873	srgo@lanl.gov
Grondalski	John	Los Alamos National Laboratory	505-664-0771	jcat@lanl.gov
Gunderson	Mark	Los Alamos National Laboratory	505-665-4495	magx@lanl.gov
Hakel	Peter	Los Alamos National Laboratory	505-667-9555	hakel@lanl.gov
Hammerberg	James	Los Alamos National Laboratory	505-667-0687	jeh@lanl.gov
Harris	James	AWE	44-118-982-6916	James.w.Harris@awe.co.uk
Haynes	Donald	Los Alamos National Laboratory	505-665-7783	dhaynes@lanl.gov
Heeter	Robert	LLNL	925-423-3761	heeter1@llnl.gov
Hoarty	David	AWE	44-118-982-7536	david.hoarty@awe.co.uk
Hoffman	Nelson	Los Alamos National Laboratory	505-667-8417	nmh@lanl.gov
Holmes	Richard	Los Alamos National Laboratory	505-667-3598	holmes@lanl.gov
Huebner	Walter	Southwest Research Institute	210-522-2730	Whuebner@swri.edu
Hueckstaedt	Robert	Los Alamos National Laboratory	505-665-0083	rmhx@lanl.gov
Iglesias	Carlos	LLNL	925-422-7252	iglesias1@llnl.gov
James	Steven	AWE	44-118-982-6859	steven.james@awe.co.uk
Keady	John	Los Alamos National Laboratory	505-667-8764	jjk@lanl.gov
Keiter	Paul	Los Alamos National Laboratory	505-665-8566	pkeiter@lanl.gov
Kilcrease	David	Los Alamos National Laboratory	505-665-7726	dpk@lanl.gov
Kowalski	Piotr	Los Alamos National Laboratory	505-667-3747	kowalski@lanl.gov
Kyrala	George	Los Alamos National Laboratory	505-667-7649	kyrala@lanl.gov
LaGattuta	Ken	Los Alamos National Laboratory	505-667-2933	jkl@lanl.gov
Libby	Steve	LLNL	925-422-9785	libby1@llnl.gov
Little	Robert	Los Alamos National Laboratory	505-665-3487	rcl@lanl.gov

OPACITY WORKSHOP

May 3-5, 2005

Magee	Norman	Los Alamos National Laboratory	505-667-5077	nhma@lanl.gov
Mancini	Roberto	University of Nevada/SNL	775-784-6595	rcman@physics.un.edu
Mazevet	Stephane	Los Alamos National Laboratory	505-667-0956	smazevet@lanl.gov
Mihalas	Dimitri	Los Alamos National Laboratory	505-665-4529	dmihalas@lanl.gov
Onifer	Andrew	Los Alamos National Laboratory	505-665-8330	aonifer@lanl.gov
Paisley	Dennis	Los Alamos National Laboratory	505-667-7837	paisley@lanl.gov
Peterson	Robert	Los Alamos National Laboratory	505-667-5392	rrpeter@lanl.gov
Pollak	Gregory	Los Alamos National Laboratory	505-665-2048	gdp@lanl.gov
Porter	James	Los Alamos National Laboratory	505-665-0736	porter@lanl.gov
Powers	William	Los Alamos National Laboratory	505-665-3614	wjp@lanl.gov
Pradhan	Anil	Ohio State University	614-292-5850	pradhan1@osu.edu
Saumon	Didier	Los Alamos National Laboratory	505-665-3469	dsaumon@lanl.gov
Sherrill	Manolo	Los Alamos National Laboratory	505-665-8559	manolo@lanl.gov
Shurter	Roger	Los Alamos National Laboratory	505-667-4408	shurter@lanl.gov
Smith	Colin	AWE	44-118-982-7979	colin.l.smith@awe.co.uk
Taccetti	Jose	Los Alamos National Laboratory	505-667-3555	taccetti@lanl.gov
Tierney	Thomas	Los Alamos National Laboratory	505-667-6944	tierney@lanl.gov
Timmes	Francis	Los Alamos National Laboratory	505-665-1468	timmes@lanl.gov
Upcraft	Lee	AWE	44-118-982-7891	lee.upcraft@awe.co.uk
Watt	Robert	Los Alamos National Laboratory	505-665-2310	watt_r@lanl.gov
Welser	Leslie	Los Alamos National Laboratory	505-665-9953	lwelser@lanl.gov
Wilson	Brian	LLNL	925-423-4636	wilson9@llnl.gov
Workman	Jonathan	Los Alamos National Laboratory	505-665-1784	workman@lanl.gov
Zhang	Honglin	Los Alamos National Laboratory	505-665-3676	zhang@lanl.gov

Plasma Opacities And High Precision Atomic Physics

LANL – EOS/Opacity V & V Workshop

Anil Pradhan
The Ohio State University

The Opacity Project Team: M. J. Seaton (UCL), et.al.
: D. Mihalas (LANL), et.al.

The OSU Team
(www.astronomy.ohio-state.edu/~pradhan)

Sultana Nahar – Senior Research Scientist
Graduate Students

- Guo-Xin Chen – (Ex) PDF (Harvard - ITAMP)
- Franck Delahaye (**Opacities**)
- Justin Oelgoetz (**Also LANL**)
- Maximiliano Montenegro
- Brian Larkins
- Rajni Tyagi

Honorary Permanent Members

- Hong Lin Zhang – (**LANL**)
- Werner Eissner – (**Stuttgart**)

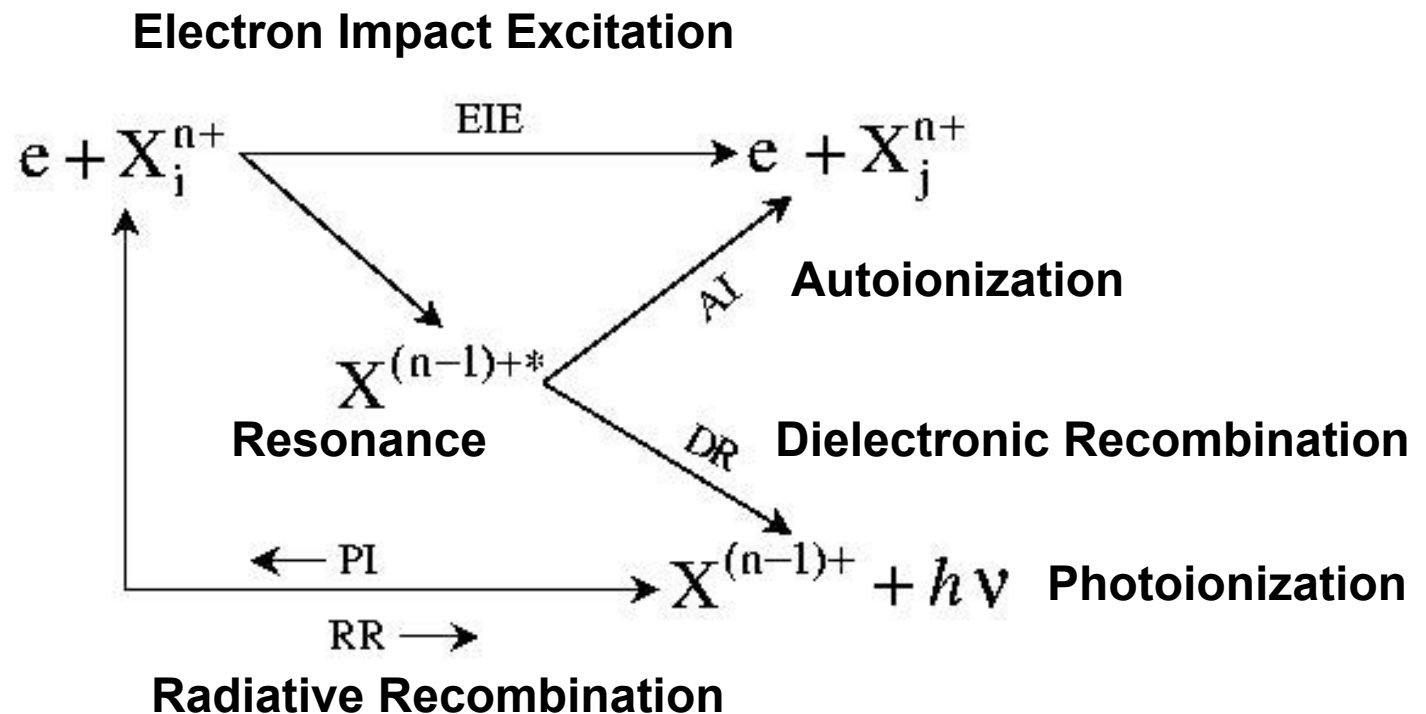
Outline: Validity and Verification of EOS/Opacities

- “Academic” Perspective:
 - Accuracy AND Completeness
- **Astrophysical opacities (OP and OPAL)**
 - Current Problems: Radiative Accelerations
New Solar abundances
- **High Precision Atomic Physics**
 - Theory and Experiment
- Monochromatic X-ray opacities
- Nanoscience and Nanotechnology
 - Biomedicine and Materials Research
- Plasma Fusion: ICF and Magnetic

V &V – Academic Issues: Are we there yet?

- State-of-the-art atomic theory
- Continuous code development
- Study individual atomic processes in detail and compare with latest experiments (radiative transitions, photoionization, recombination, electron impact excitation)
- Large-scale calculations for laboratory and astrophysical opacities and spectral models
 - **The Opacity Project**
 - **The Iron Project (Fe-peak elements)**

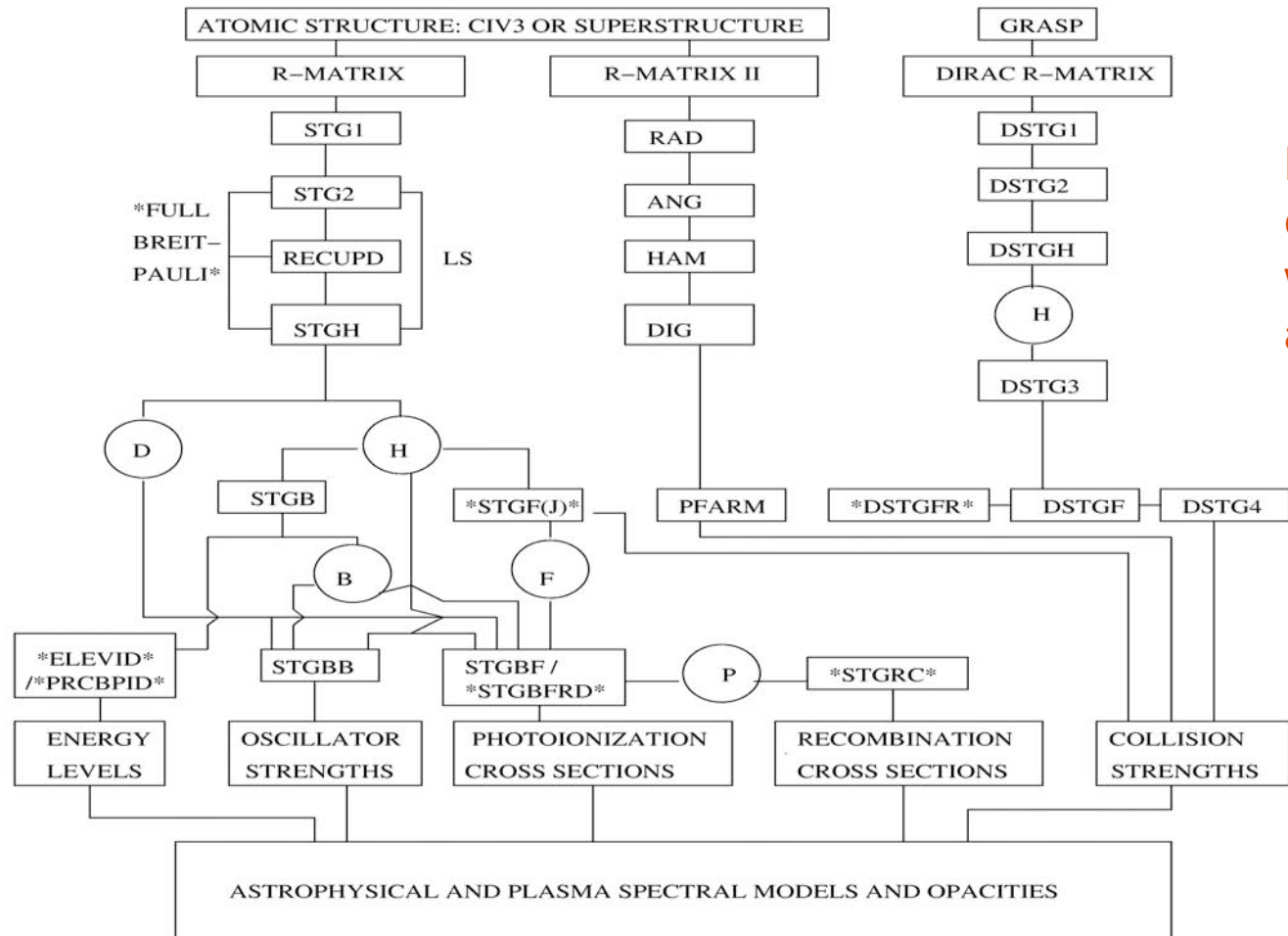
Primary Atomic Processes in Plasmas



The Coupled-Channel R-matrix method provides a self-consistent and unified treatment of all processes with one single wavefunction expansion

Relativistic and Non-Relativistic R-matrix Codes For Atomic Processes (Ohio Supercomputer Center)

THE R-MATRIX CODES AT OSU



Large-scale
calculations
with high precision
and self-consistency

The Opacity Project: Two independent sets of opacity codes for V&V
(i) M.J. Seaton, & Co., (ii) Yu, Mihalas, & Pradhan
Only (i) employed for final OP tabulations

The Opacity Project: 1983-2005

- Inception: 1983 → Group of > 30 researchers, 5 countries
UK, US, France, Germany, Venezuela
- Cr, Mn, Ni – Extrapolation + Kurucz
- First complete results 1994 → OP1
(Seaton, Yu, Mihalas, Pradhan, MNRAS, 266, 805, 1994)
- OP1 results for stellar **envelope** opacities;
did **not** include
 - inner-shell processes
 - stellar interior EOS for $\rho > 0.01 \text{ g/cc}$
- New OP work includes both
- On-line calculations for arbitrary composition
 - <http://www.osc.edu/hpc/opacities>
- CD-ROM from Anil Pradhan or Claude Zeippen

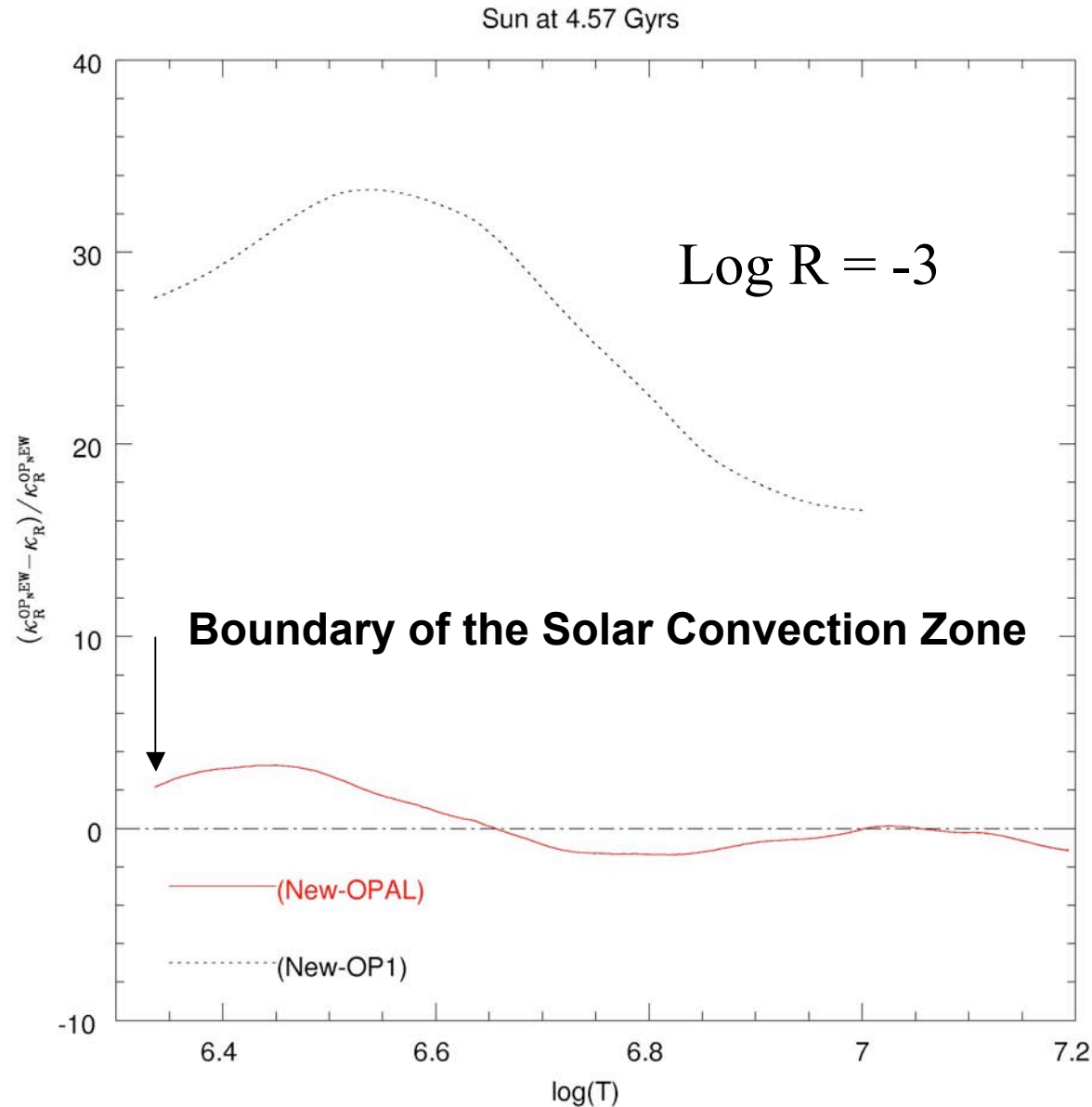
Astrophysical Opacities: The Opacity Project (OP) and LLNL (OPAL)

- The OP work used a combination of R-matrix and atomic structure calculations for bound-bound and bound-free
- Mihalas-Hummer-Dappen (MHD) EOS
- New OP work uses “extended” MHD-EOS
 - High-density uncertainties
 - Perturbed atom approximation
- Atomic data for inner-shell processes
 - K-, L-, shell opacity

Astrophysical Opacities – Validation and Verification

- New OP and OPAL agree in the **MEAN** opacities at the 5-10% level
- But radiative accelerations disagree by factors of 2-5 !!
 - Monochromatic opacity **resolution**
 - Atomic physics **accuracy**
- V&V using Solar models similar in EOS, composition, central temperature, density, base of convection zone → very small differences

OP vs. OPAL → % Differences in Rosseland Mean Opacities



OP1
Envelope
EOS only,
and Without
Inner-shell
Processes

New
Extended
EOS, and
including
Inner-shell
Processes
(Badnell et.al.
2005)

Delahaye & Pinsonneault (2005, ApJ in press)

The Opacity Project (OP) and the OPAL Rosselland Mean Opacities

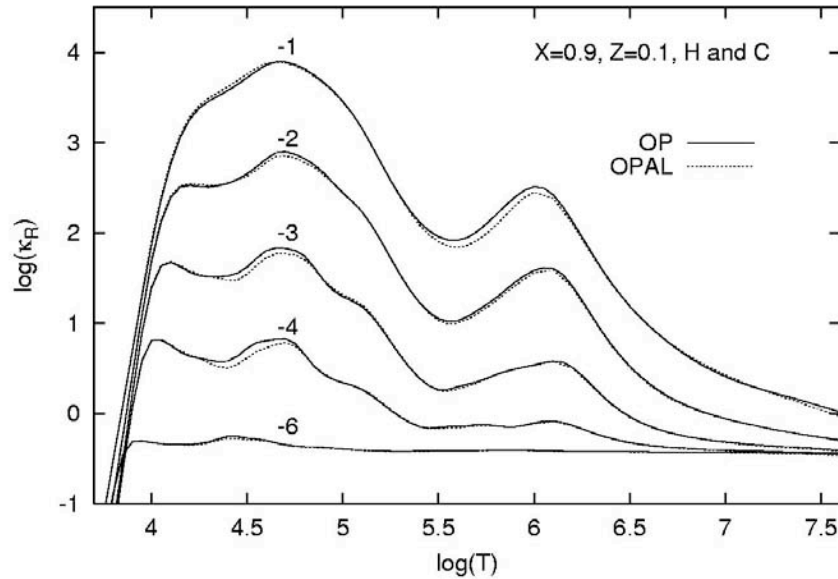


Figure 5. Comparisons of $\log(\kappa_R)$ from OP and OPAL for a H/C mixture with mass fractions $X = 0.9$ for H and $Z = 0.1$ for C. Curves are labelled by values of $\log(R)$.

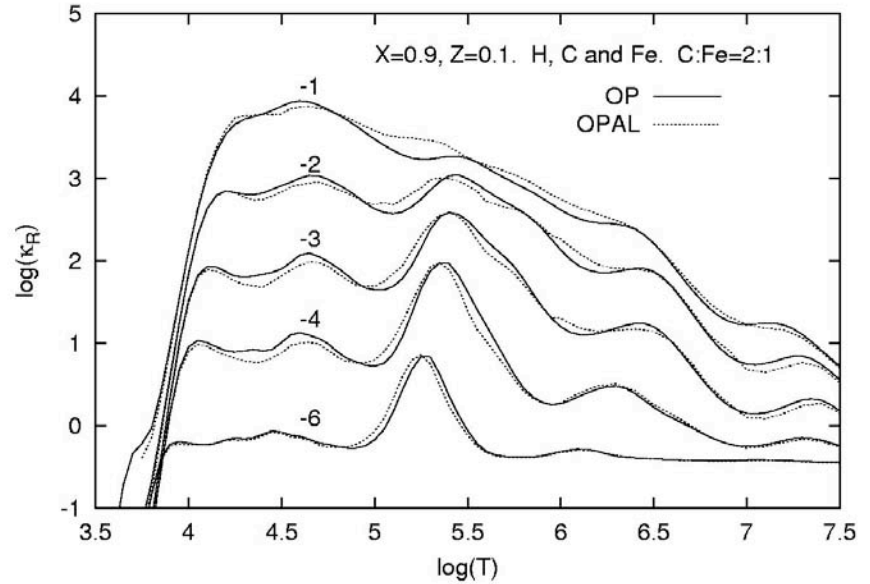


Figure 10. Comparisons of $\log(\kappa_R)$ from OP and OPAL for an iron-rich mixture: $X = 0.9$, $Z = 0.1$ and $C:Fe=2:1$ by number fraction. Curves are labelled by values of $\log(R)$.

(Log κ_R vs. Log T) at Log R = $\rho / (T/10^6)^3$

RADIATIVE ACCELERATION

Given BB radiative flux $F(r)$ at depth r in a star with T_{eff} and radius R_* , the radiative acceleration of element k is

$$g_{rad}(r) = \left(\frac{1}{c}\right)\left(\frac{M}{M_k}\right)\kappa_R\gamma_k F(r), \quad (1)$$

where κ_R is the Rosseland mean opacity at temperature T and density ρ at r , and γ_k is a dimensionless quantity representing the ratio of the momentum-transfer (mta) cross section to the total opacity cross section per atom

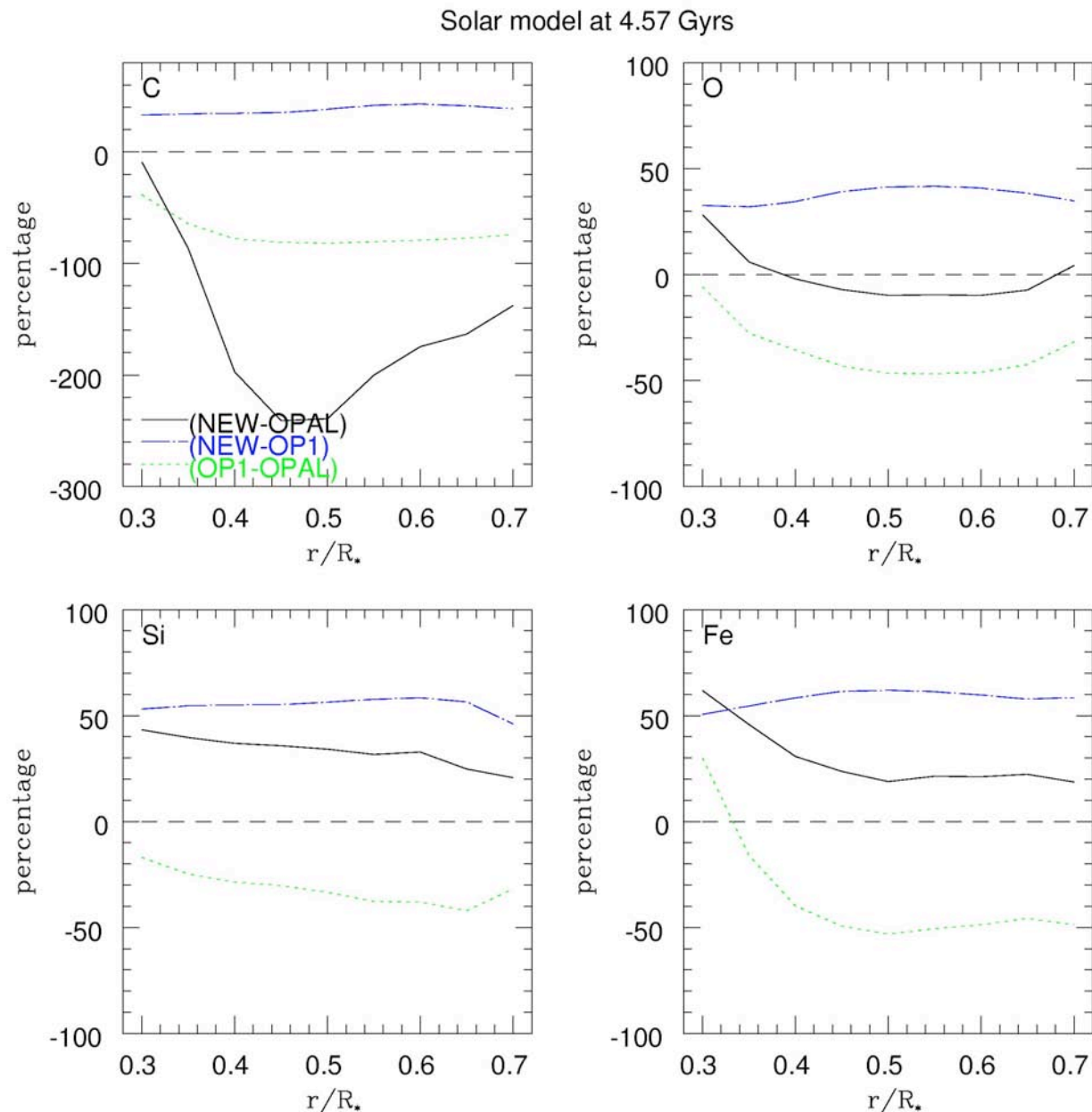
$$\gamma_k = \int \frac{\sigma_v^{mta}(k)}{\sigma_v^{tot}} f_v d\nu, \quad (2)$$

where

$$f_v = \frac{(dB_\nu/dT)}{(dB/dT)}. \quad (3)$$

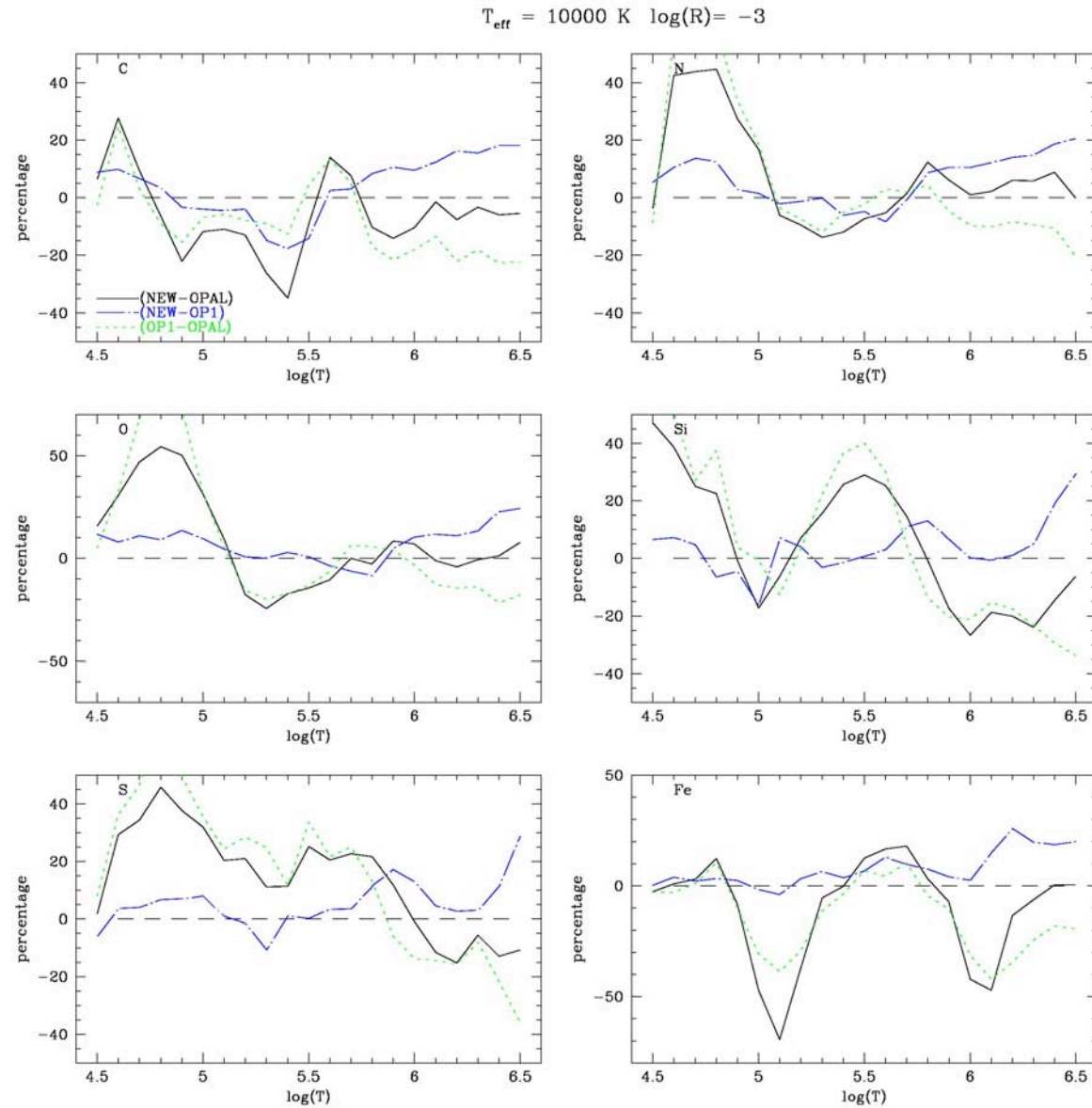
γ_k is a measure of the specific opacity of element k relative to the total opacity, therefore much more sensitive to resolution and accuracy of atomic data than the Rosseland mean.

OP vs. OPAL \rightarrow % Differences in g_{rad} for the Sun



Delahaye & Pinsonneault (2005, ApJ in press)

OP vs. OPAL \rightarrow % Differences in Radiative Accelerations



Delahaye & Pinsonneault (2005, ApJ in press)

New Solar Abundances (And Problems!)

- Latest determination of solar abundances (Asplund et.al. 2005) – measurements and 3D hydro NLTE models – yield
 - **30- 40% lower abundances of C,N,O,Ne,Ar**
- However, this disagrees with Helioseismology data (sound speed, BCZ, etc.), and
 - **would require the OP and OPAL opacities to be lower by about 10%; EOS has little effect (Bahcall et.al. 2004)**

Causes: Resolution

- Radiative acceleration g_{rad} or γ are more sensitive to resolution than the Rosseland mean opacities (RMO)
- Both OP and OPAL RMOs converge to 2% with 10^4 points, γ could differ by several factors depending on element and physical conditions
- OP data uses an adjustable mesh with better resolution

Causes: Accuracy of Atomic Physics

- Only a relatively small subset of OP atomic data is from the R-matrix calculations
- Both OP and OPAL data may not differ much in absolute accuracy
- New Calculations – Iron Project and Beyond
- Compare Close-Coupling R-matrix and other methods
- Verify results for fundamental atomic parameters for primary processes
- High precision atomic physics

Coupled Channel R-Matrix Theory vs. Distorted Wave

Coupled Channel Theory

The wavefunction expansion, $\Psi(E)$, for a total spin and angular symmetry $SL\pi$ or $J\pi$, of the $(N+1)$ electron system is represented in terms of the target ion states as:

$$\Psi(E) = A \sum_i \chi_i \theta_i + \sum_j c_j \Phi_j, \quad (1)$$

where χ_i is the target ion wave function in a specific state $S_i L_i \pi_i$ or level $J_i \pi_i$, and θ_i is the wave function for the $(N+1)$ th electron in a channel labeled as $S_i L_i (J_i) \pi_i \ k_i^2 \ell_i (SL\pi) [J\pi]$; k_i^2 is the incident kinetic energy. In the second sum the Φ_j 's are correlation wavefunctions of the $(N+1)$ electron system.

- Ab initio treatment of **important** atomic processes with the same expansion: Eq.(1)
- Electron impact excitation, radiative transitions, and a **self-consistent and unified treatment of photoionization and (e + ion) recombination, including radiative and dielectronic (RR+DR) (Nahar, Zhang, Pradhan)**

All **significant** effects may be included

- Infinite series of resonances are considered

Distorted Wave Theory

Central Field Approximation

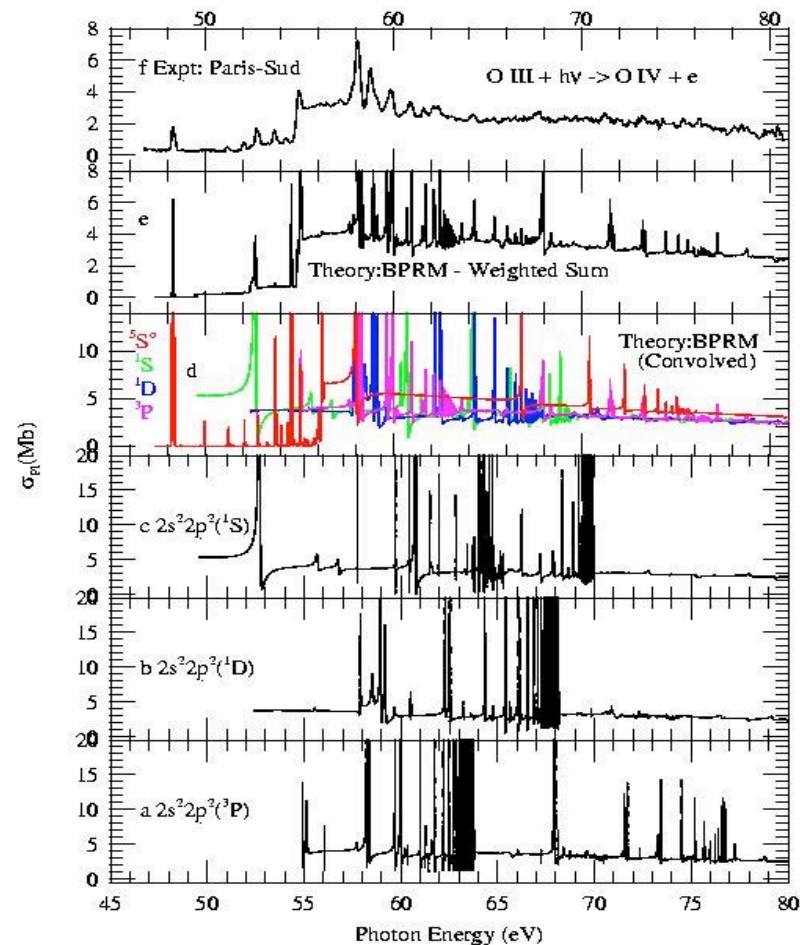
- Includes only initial and final channels in Eq. (1); no summation
- Neglects channel coupling
- Resonance states (intermediate channels) NOT included in wavefunction expansion
- Resonances may be considered indirectly in the Isolated Resonance Approximation
- Finite number of resonances with n-extrapolation

Accuracy AND Completeness: New Opacities Calculations

- Aim for high precision **first**, then completeness
- Benchmark state-of-the-art theoretical calculations with experiments for
 - Photoionization** - Accelerator based Advanced Light Sources (Reno/Berkeley, Aarhus, Paris)
 - Recombination** - Heavy ion storage rings (Heidelberg, Stockholm)
 - Electron-Ion Scattering** - Electron Beam Ion Traps (Livermore, NIST)

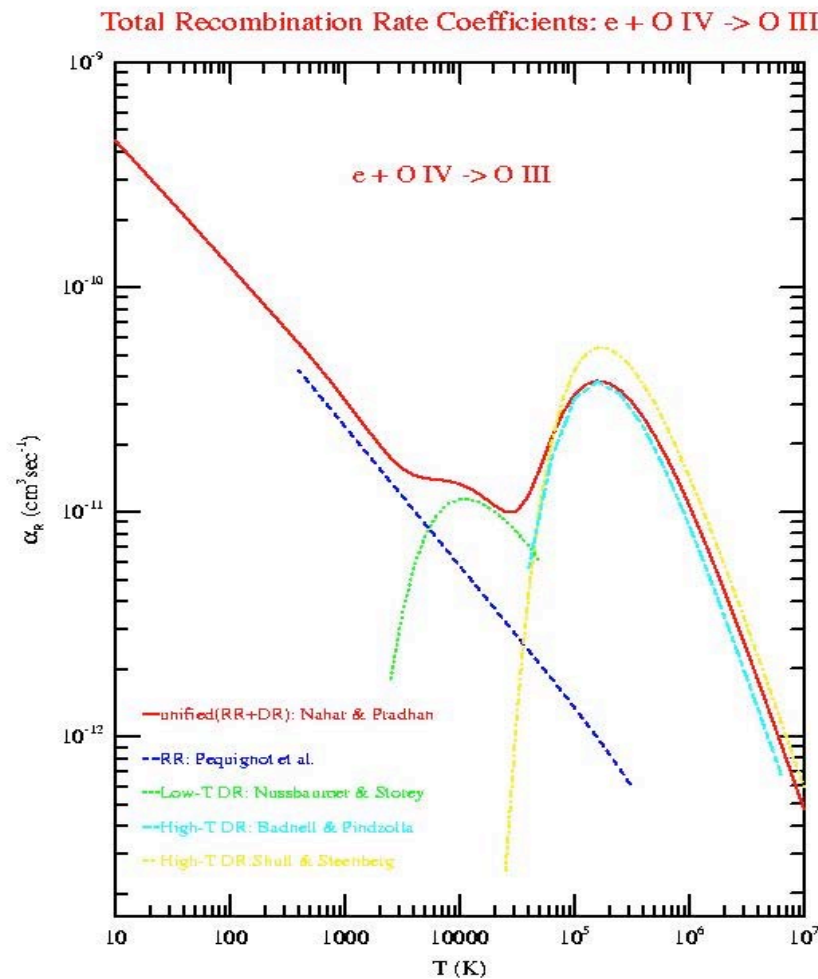
Photoionization of O III

Comparison of R-Matrix Theory (Nahar 2003) and Experiment (Bijeau et al 2003)



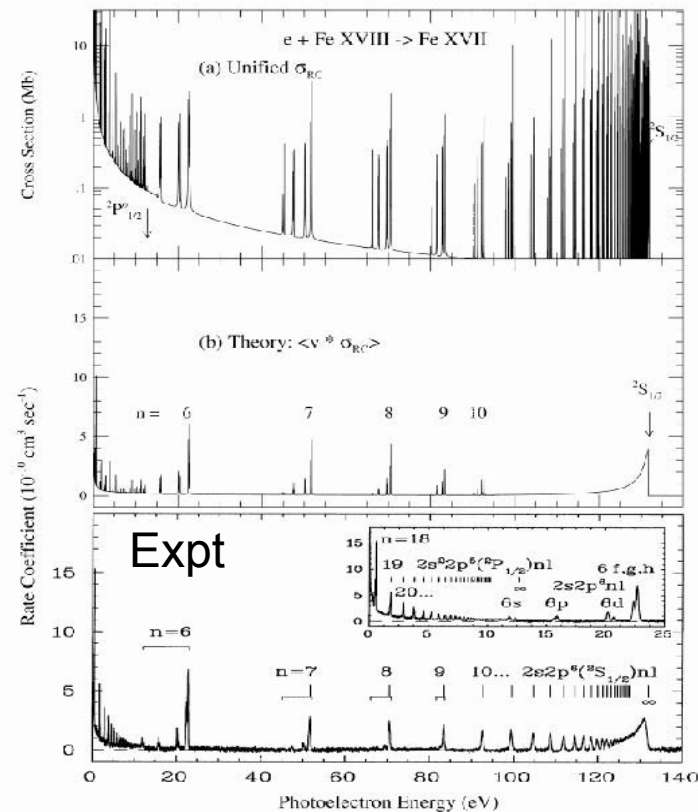
Experiment includes
the ground state and
metastable states
of O III in the beam

Unified (e+ion) Recombination Rate Coefficient (RR+DR)

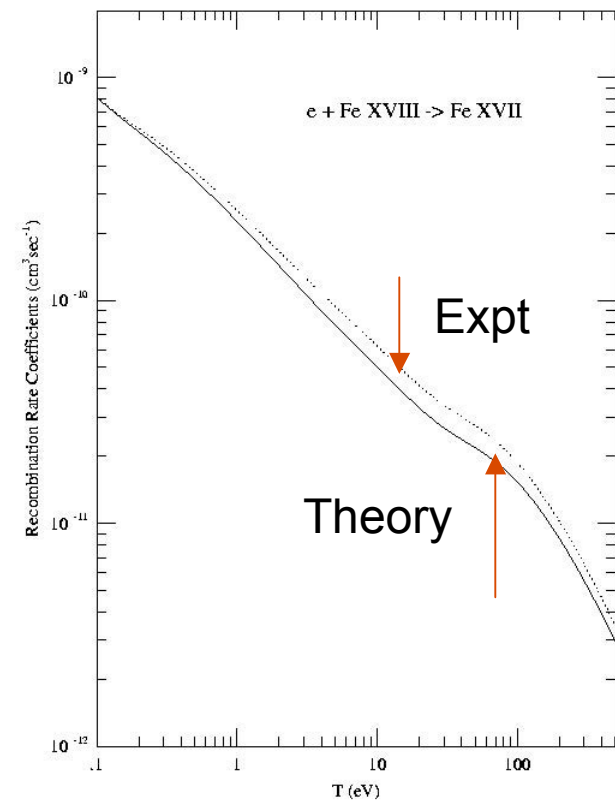


Unified (e+ion) recombination: R-Matrix Theory and Experiments

Gaussian Averaged X-sections



Maxwellian Averaged Rate



Rates agree to < 20%

Theory: Pradhan, Nahar, and Zhang (ApJL, 549, L265, 2001)

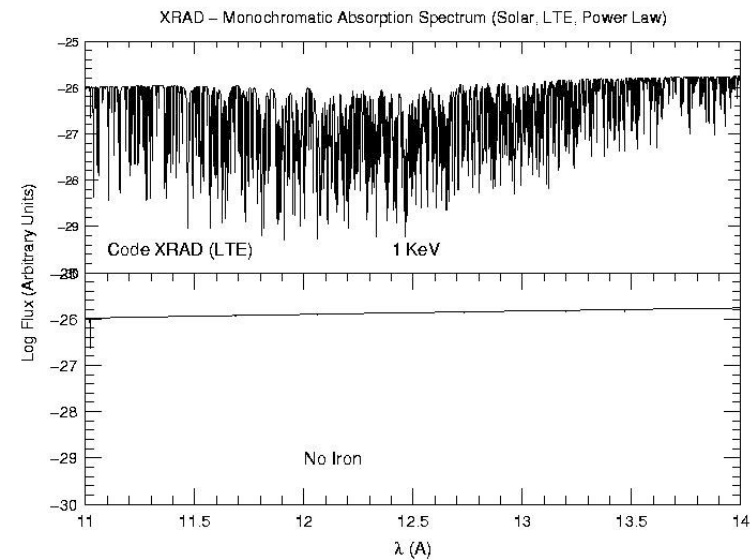
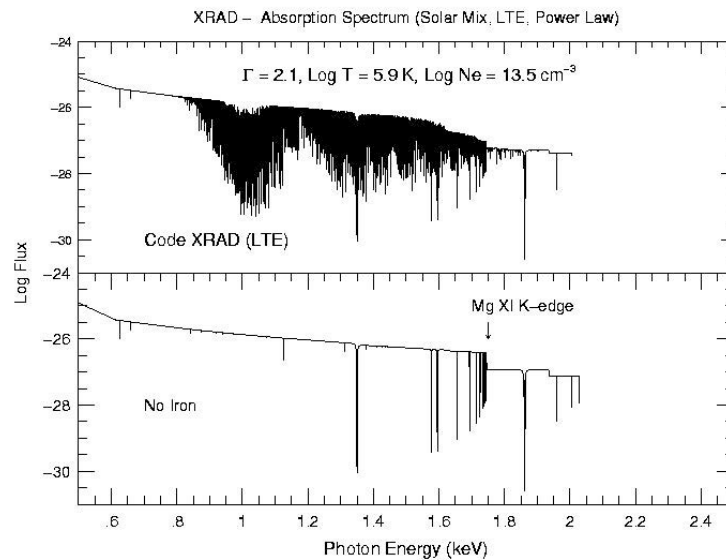
Expt: Savin et.al. (ApJS, 123, 687, 1999)

Monochromatic Opacities

- Experimental verification of
 - Cross sections and transition rates
 - Monochromatic opacity/transmission spectra of elements
- Astrophysical verification with observed spectra

Code XRAD – Theoretical X-ray Absorption Spectrum The Opacity Project and The Iron Project Data

(Pradhan 2004)



**Power-law radiation field (NOT Blackbody),
Monochromatic opacities and spectrum for arbitrary mixtures**

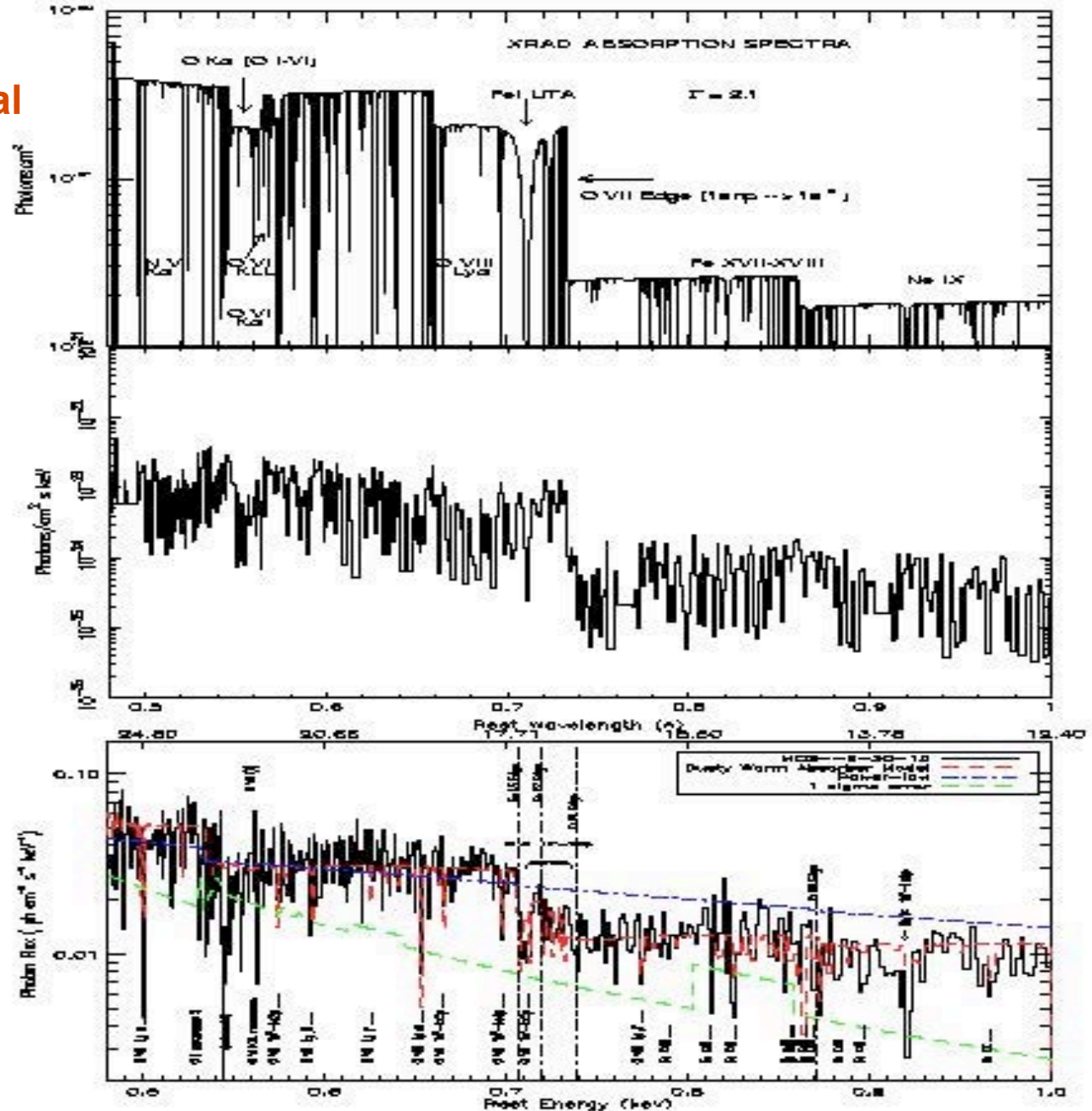
Mono X-ray Opacities: Modeling The Spectrum of AGN MCG-6-30-15

Black Hole Candidate:
Relativistic Gravitational
Broadening ?

Code XRAD
(Pradhan 04)

↓
Convolved with
XSPEC

Chandra Spectrum
(Lee et.al. 2001)

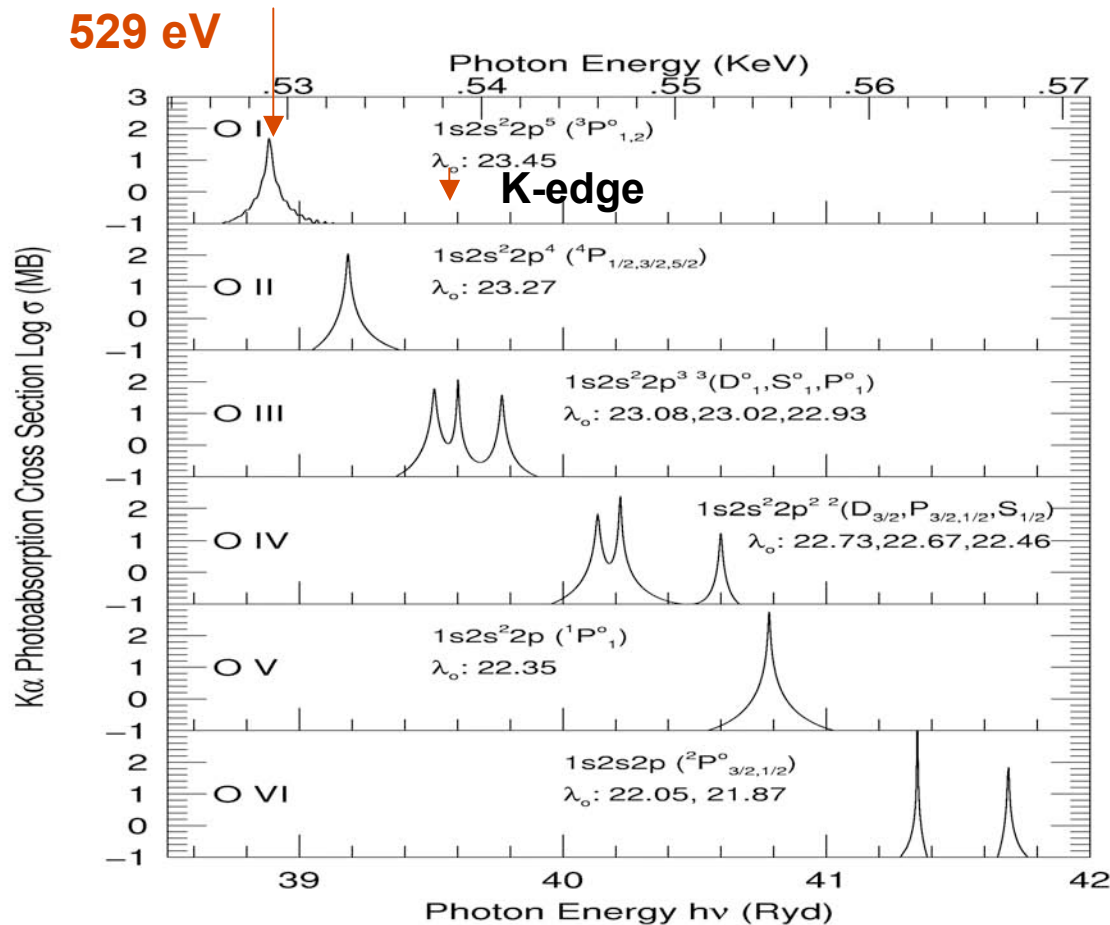


NANOSPECTROSCOPY

Computational Nanoscience at Fundamental Atomic and Molecular Scales (OSU)

- **Nanobiomedicine and Nanomaterials**
- **Broadband (indiscriminate!) imaging yields pictures, but not detailed nanoscopic information**
- **Spectroscopy is the most powerful tool**
 “A spectrum is worth a thousand pictures”
- **Paradigm shift from imaging to spectroscopy, such as occurred in astronomy**
- **Spectroscopy should be far more efficient with reduced radiation exposure by targeting spectral features in atoms and molecules**

Resonance Peaks in X-Ray Photoabsorption By Oxygen



Resonance in neutral O at 0.529keV; X-ray absorption cross section is higher by factor of up to 100 than at other energies

AVOID X-RAYS AT 529 eV → ~ 100 TIMES MORE DAMAGE TO HUMAN BODY !!

Pradhan, Nahar, Delahaye, Chen, Oelgoetz (2003)

Spectral 'Windows' in X-ray opacities

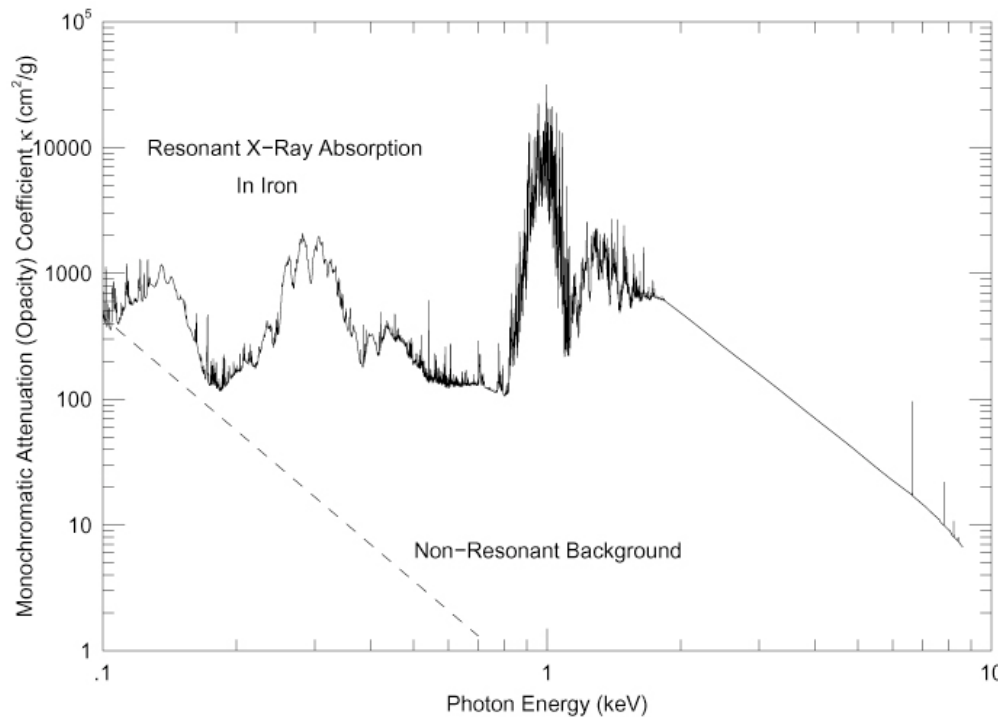
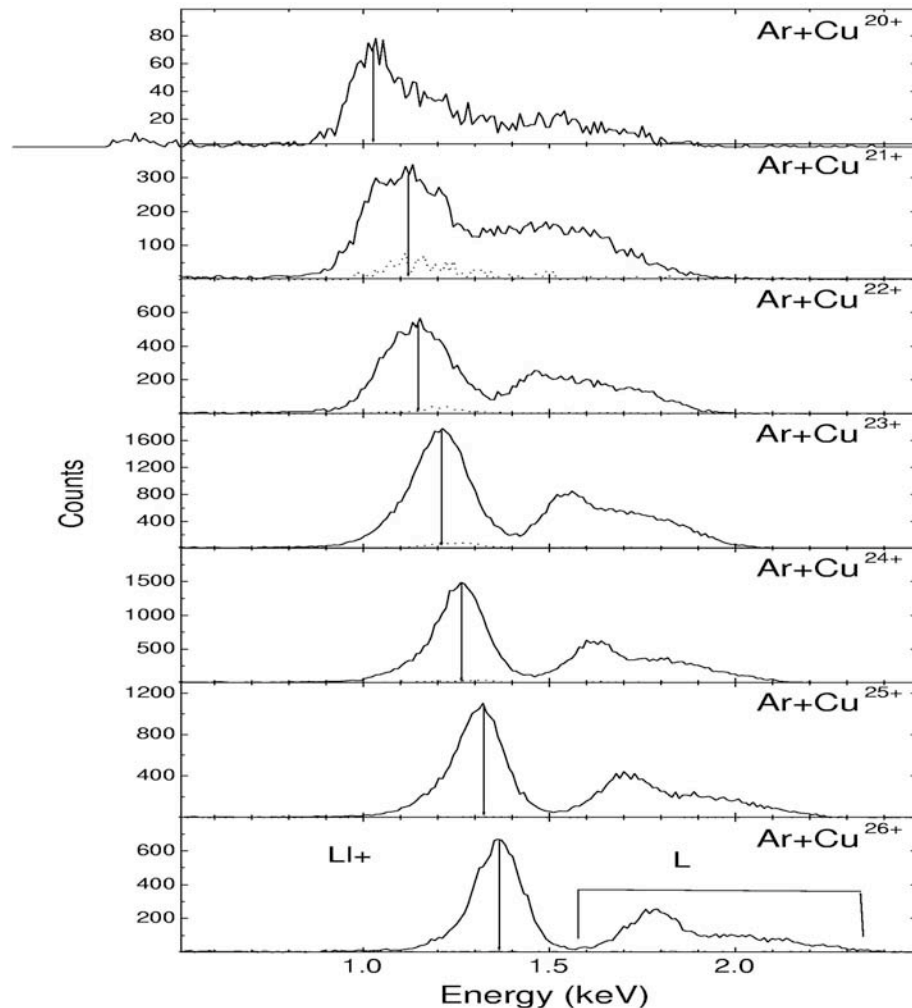


Fig. 1. The enhancement in X-ray photo-absorption in iron due to low energy resonance complexes. Compared to the non-resonant background, the **attenuation coefficients** may be up to several orders of magnitude higher, particularly in specific **'spectral windows'** such as the one at 1 KeV due to L-shell excitations. Heavier elements will have such features at much higher energies.

Lighter 'biogenic' elements (H,C,N,O) have far lower absorption coefficient at high energies; beyond the K-edge, cross section $\sim E^{-3}$. X-rays are absorbed by iron and heavier elements with orders of magnitude higher efficiency at energies of resonance-arrays.

Experiment: X-Ray Fluorescent Emission “Spectral Windows” From Copper



Preliminary results from collaborators using the Pelletron: Heavy ion Accelerator at the Tata Institute For Fundamental Research, Mumbai, India (A. Kumar & L. Tribedi, private communication)

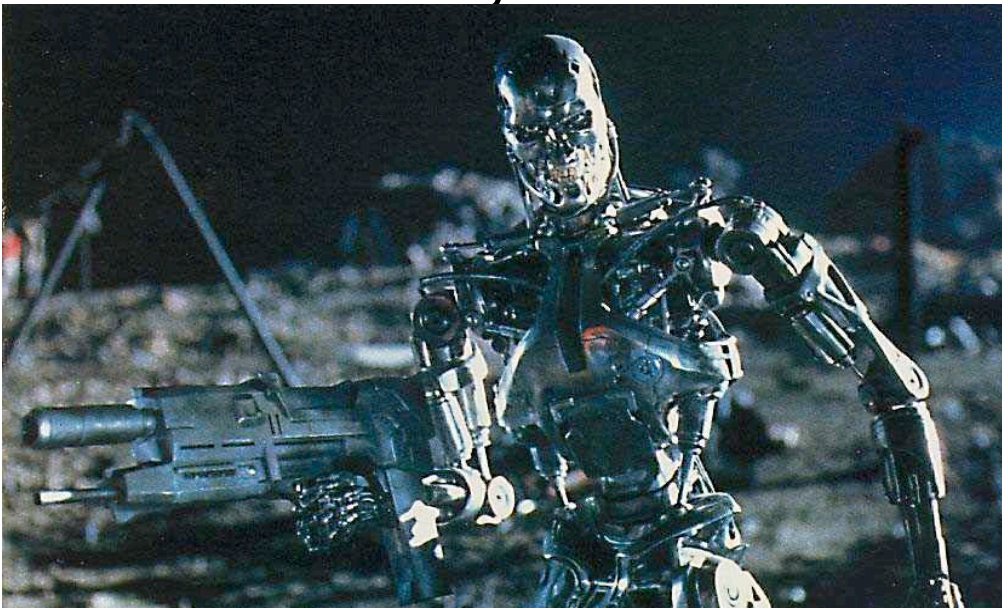
More experiments needed to locate peak emission windows

Conclusion

- Definitive opacities with state-of-the-art atomic physics have not yet been computed (EOS ?)
- Calculations are needed for heavy elements, **Iron and beyond**, including relativistic effects using Breit-Pauli or Dirac R-matrix codes
- Collaboration with LANL, LLNL might be desirable to compare detailed opacities
- Nanotechnology, fusion, and other applications next generation of AM codes

New Computational Technology For Atomic and Molecular Physics

- TENSOR CONTRACTION ENGINE (TCE) for automatic formula derivations and parallel implementation of any given model of wave function theory.
 - Expediency
 - Optimization & Parallelization
 - Maintainability & portability
 - Extensibility



"It doesn't feel pity, or remorse, or fear."

The Terminator

(And has no sense of humor)

Opacity Calculations at Los Alamos

or

Dark Doings on the Mesa

Norman H. Magee

**Los Alamos National Laboratory
Los Alamos, NM 87545**

Opacity calculations have been done at Los Alamos for more than 40 years. This has involved many people and a long series of opacity codes. During this period, there have been many innovations and changes as developers strove to take advantage of new physics models and improved computational facilities. One of the most important lessons learned during this evolution was the need for constant evaluation and comparison of results, especially as new models were included or as calculations were pushed into new physical regimes. Los Alamos has always tried to maintain two or more "independent" opacity codes to monitor all code changes, and while this is a necessary procedure, it is not sufficient to ensure the best opacity calculations. This can only be done by comparisons with experiment and with truly independent codes from other laboratories or groups. In the late 1980's, these both became realities with the start of the Opacity Workshops and the first quality transmission experiments at AWE. All current opacity codes have benefited from both of these developments, but the benefits have been limited because of the relatively small number of elements, temperatures and densities that have actually been compared or measured. While workshop cases are chosen to test critical regions, one or two test points can not predict error bars for the full temperature-density ranges covered by modern opacity tables. The next step forward for verification and validation will have to involve much more extensive comparisons among all of the major opacity codes, and include EOS as well as opacities.

This work has been performed under the auspices of the U.S. DOE.

Atomic Physics, Opacity, Non-LTE and Spectra

Harris Mayer

Art Cox

Don Eilers

John Stewart

Dave Barfield

Doug Sampson

Bob Cowan

Joe Mann

Walter Huebner

Mary Argo

Al Merts

Norm Magee

John Keady

Carlos Iglesias

Bob Clark

Joe Abdallah

Chris Fontes

Honglin Zhang

David Kilcrease

Stephane Mazevet

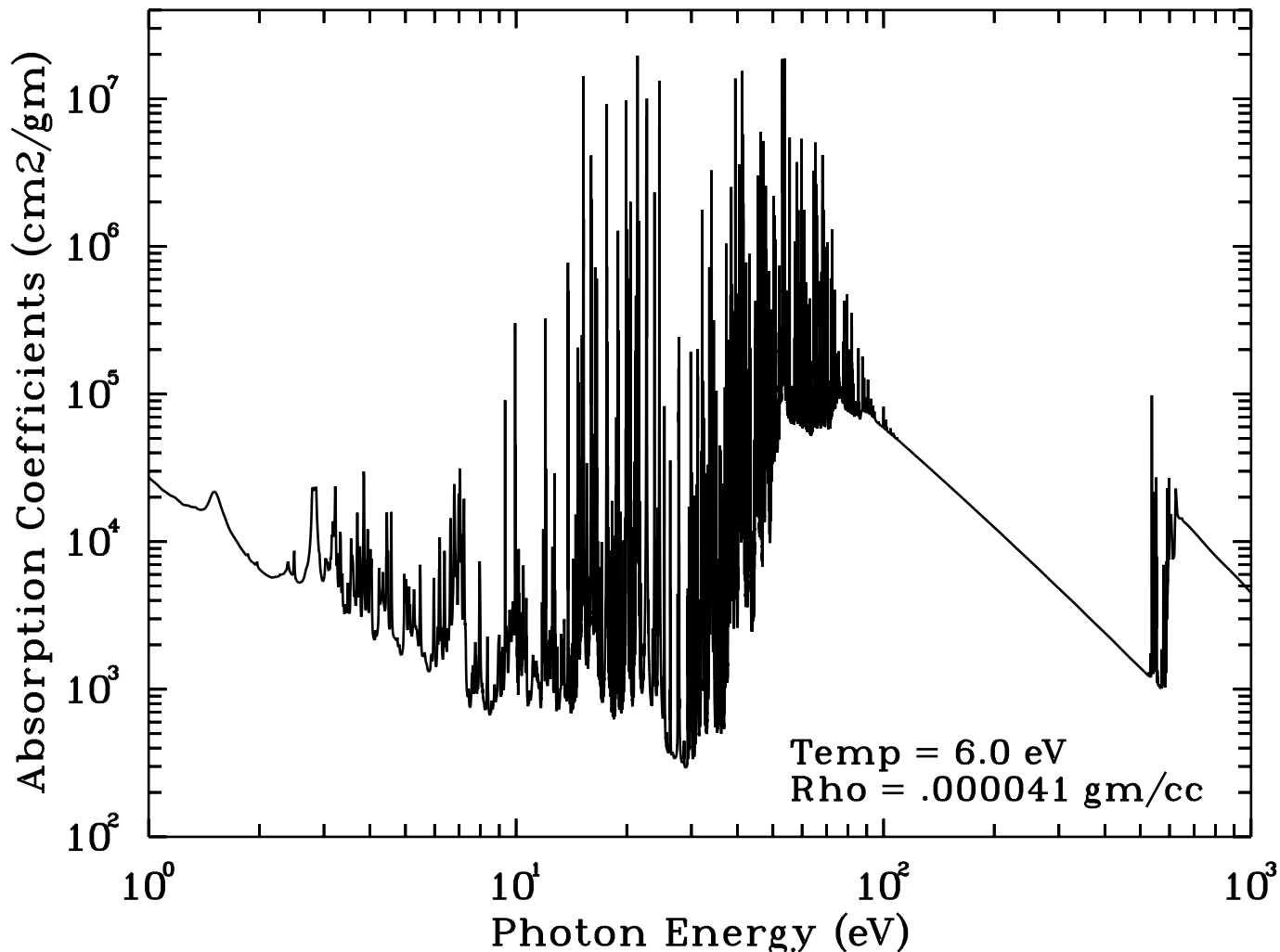
Lee Collins

Manolo Sherrill

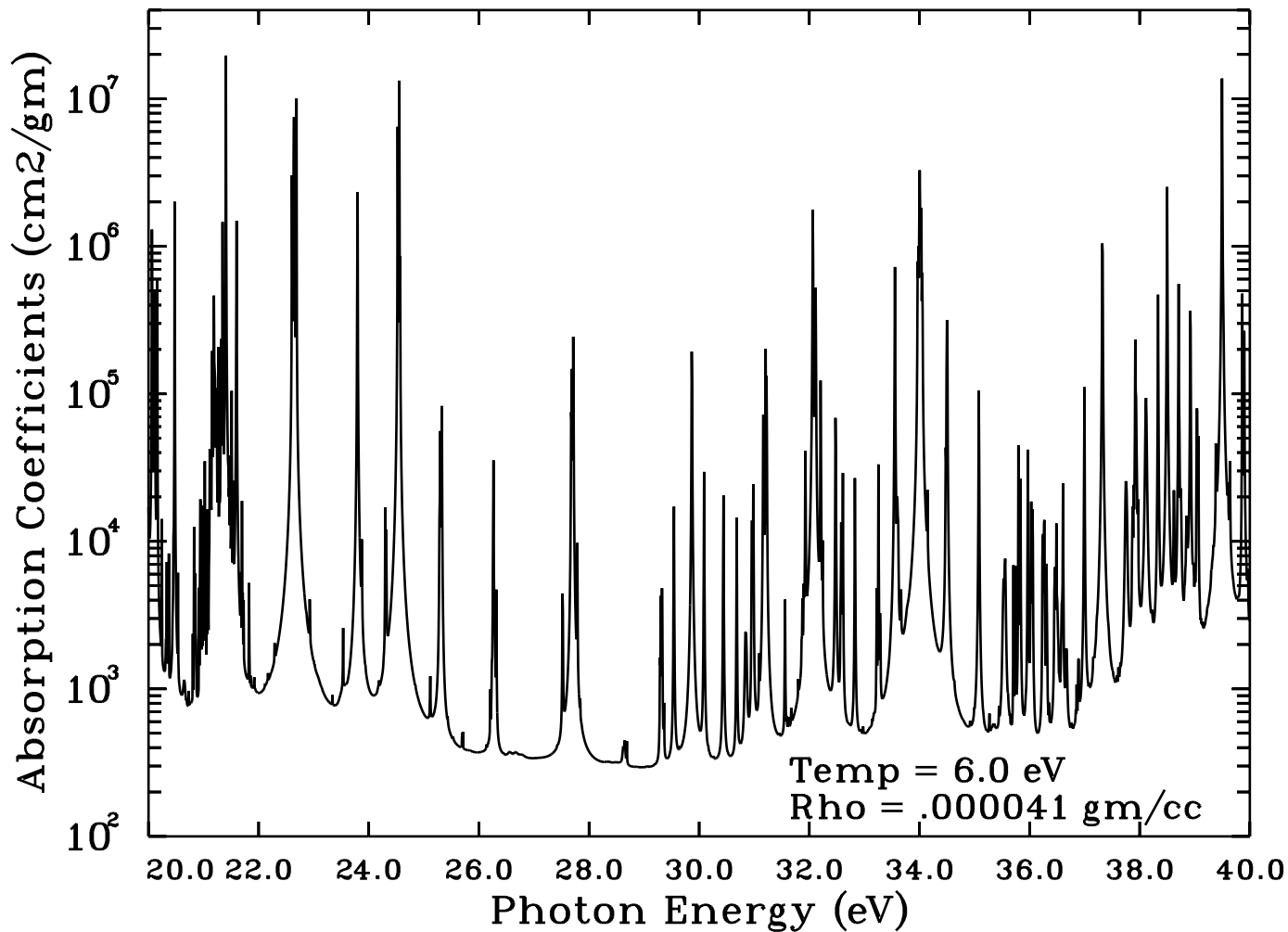
Peter Hakel

James Colgan

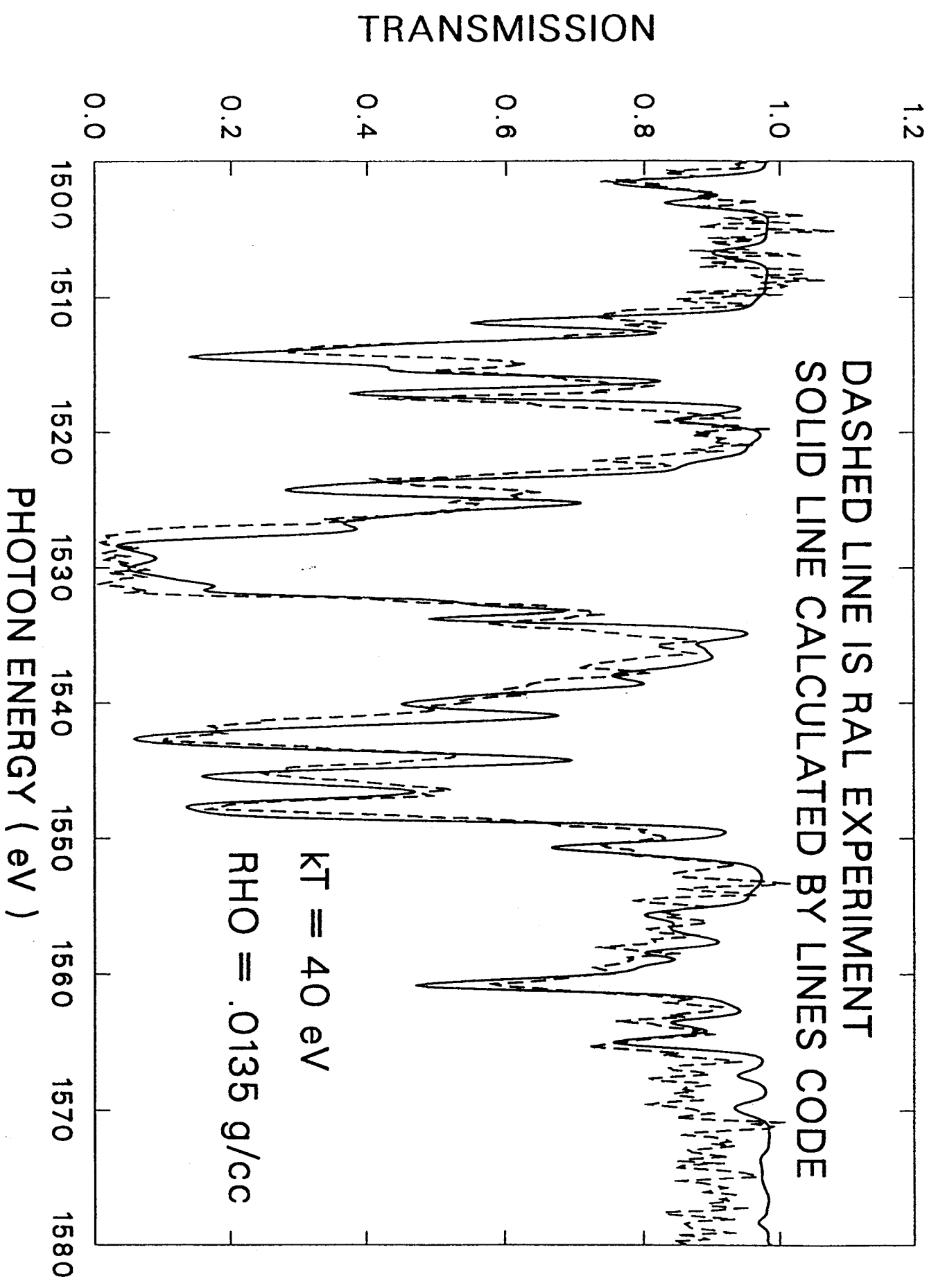
Oxygen Spectra Plot from ATOMIC Code



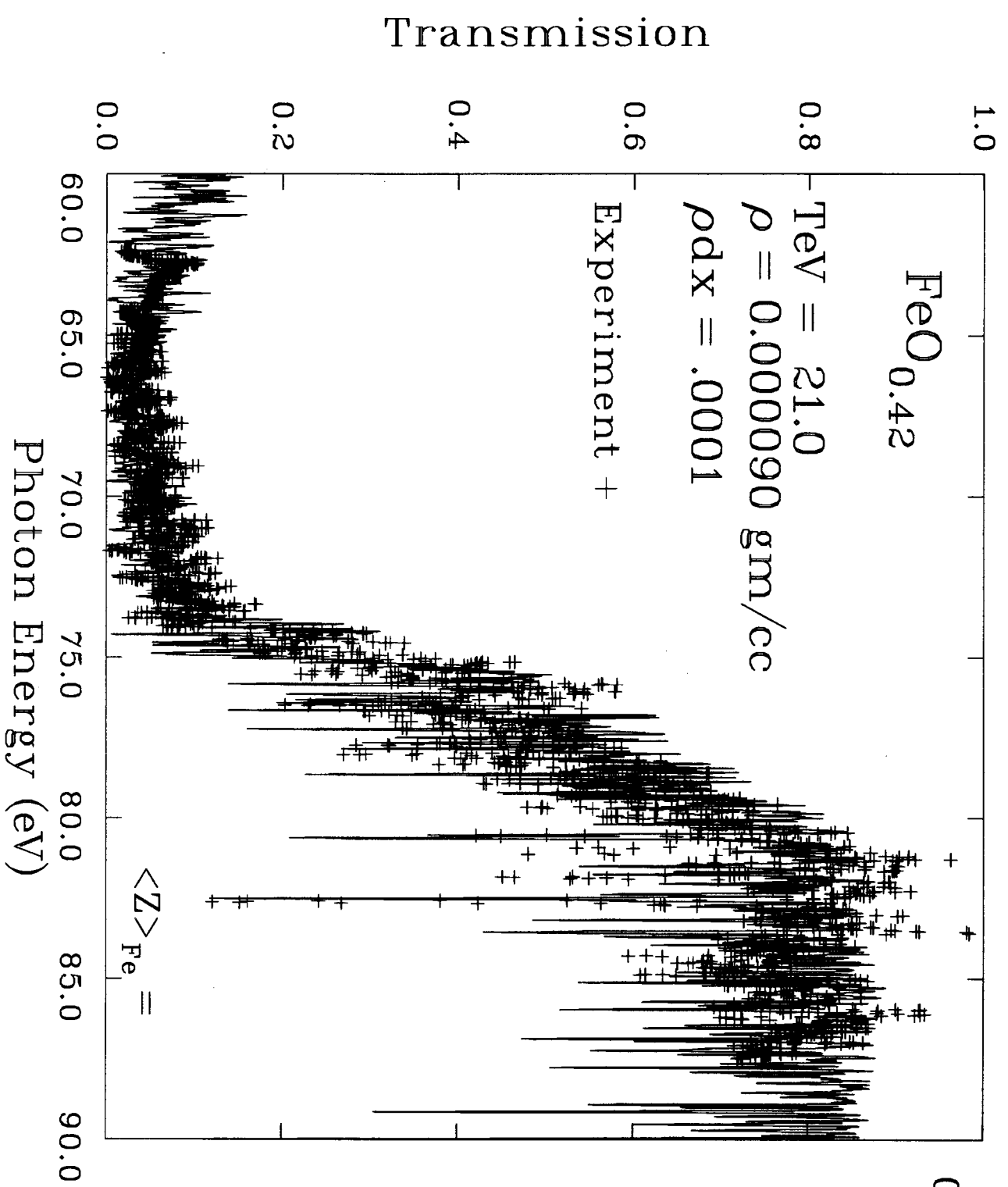
Oxygen Spectra Plot from ATOMIC Code



ALUMINUM X-RAY TRANSMISSION



06/05/98



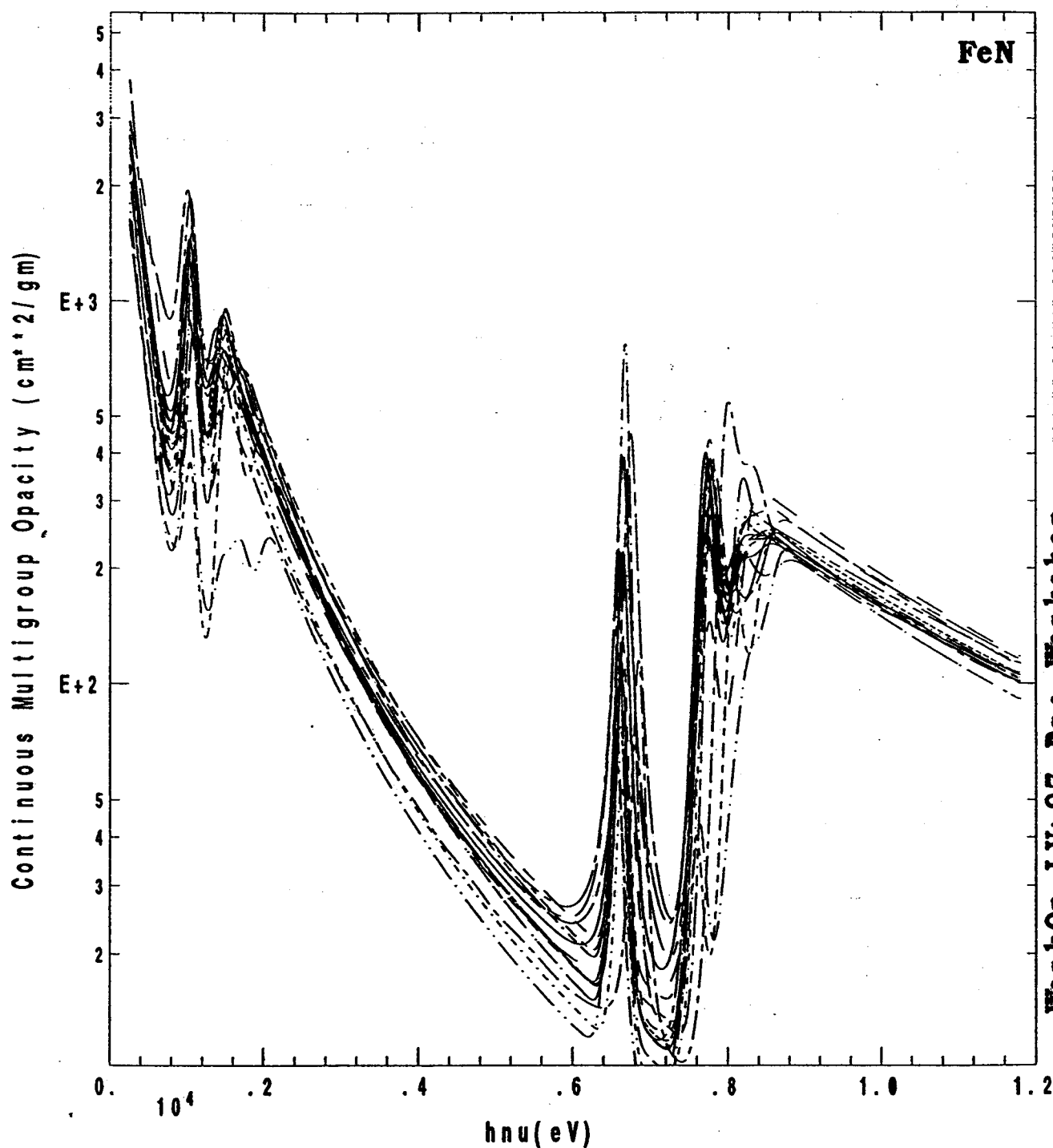
Continuous Multigroup Opacity (group width= $kT/3$) for FeN

$Z=26$ $\text{Rho} = 8.0\text{E}+00 \text{ g/cc}$ $kT = 600. \text{ eV}$

The Rosseland Mean of the Continuous Multigroup Opacity is identical, by construction, to the Rosseland Mean of the submitted total opacity.

*** N.B. The Planck Mean and peak heights are NOT preserved. ***

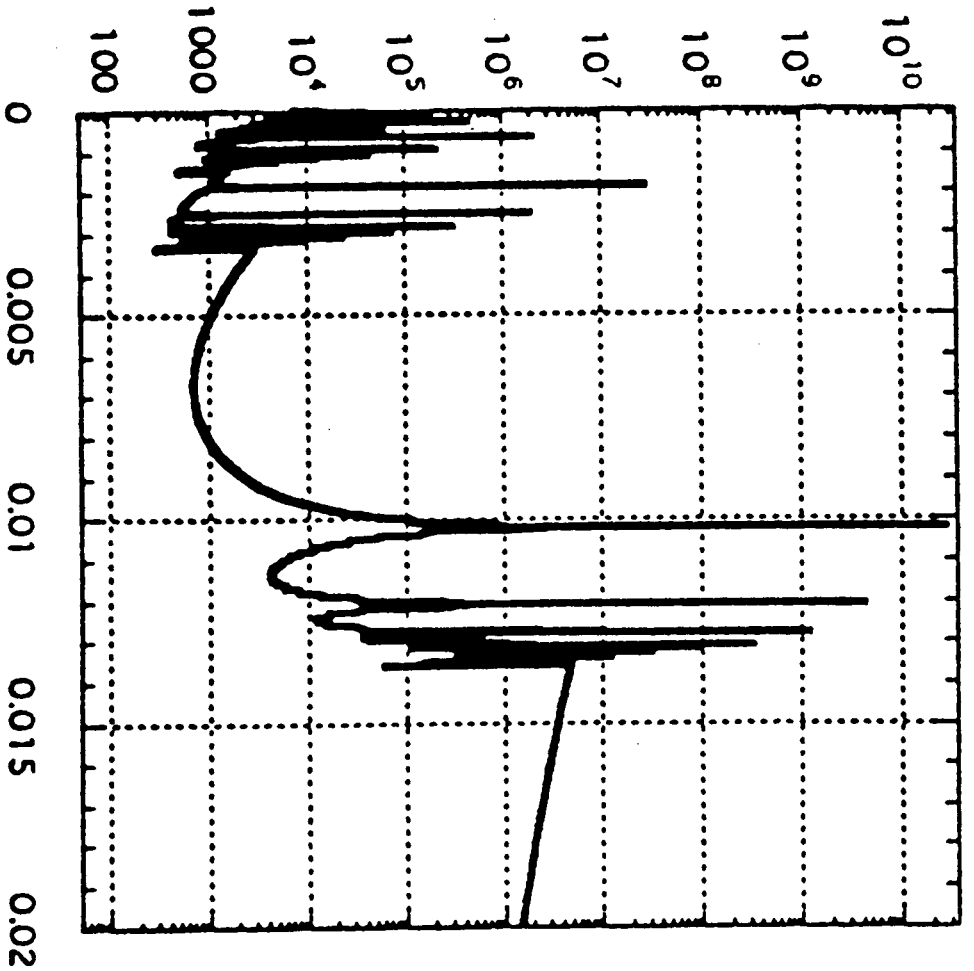
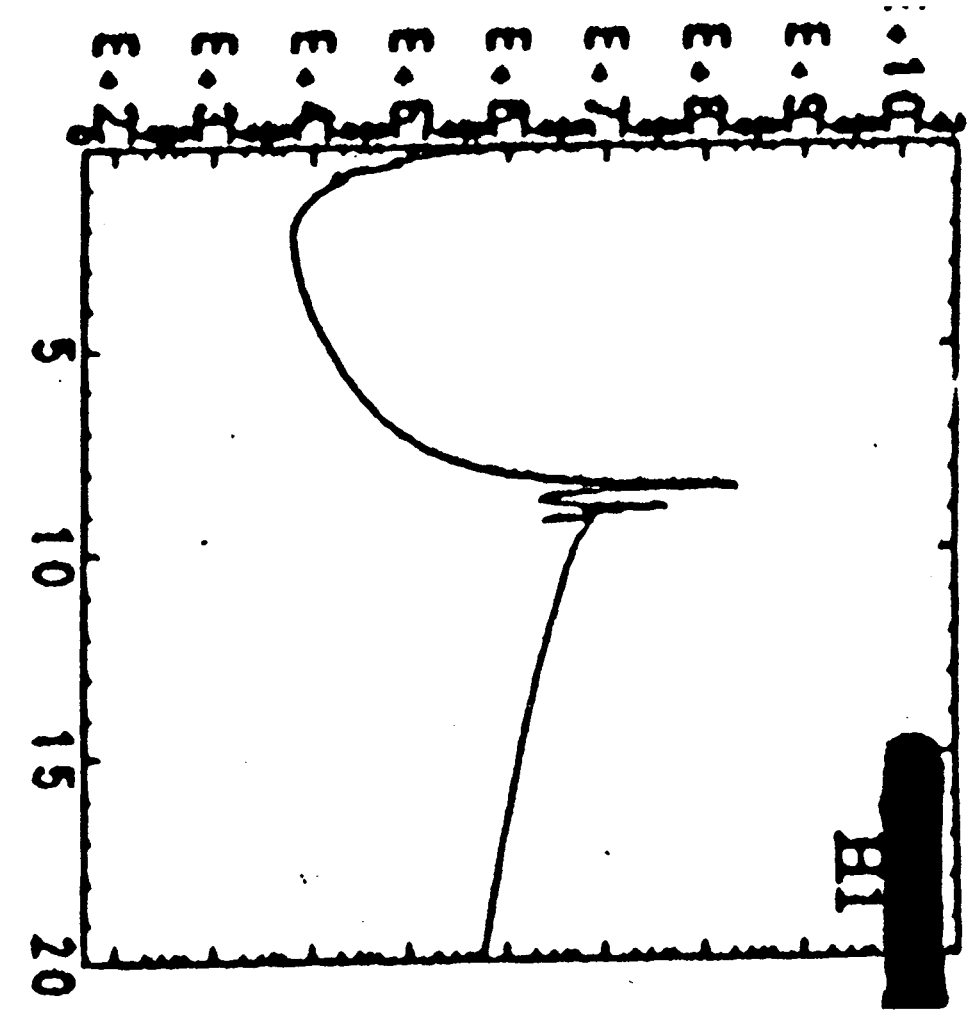
Compare valleys and smooth portions. Disregard absolute peak heights.



PLEASE DO NOT DISTRIBUTE

WorkOp-IV:97 Pre-Workshop

██████████ H1



Los Alamos Opacity Codes

LEO

HEO

VASP

RMOP

**LINES
FINE**



EXOP



MOOP



LEDCOP



ATOMIC



The Making of *ATOMIC*

FINE

Spectral modeling code

Direct access to atomic physics data (*CATS*, *RATS*, *GIPPER*, *ACE*)

Bound-bound & bound-free cross sections

LTE & non-LTE

Low & high Z

+

LEDCOP

Free-free

Scattering

Stark broadening

Conductive opacity

Line shapes

+

new

F90

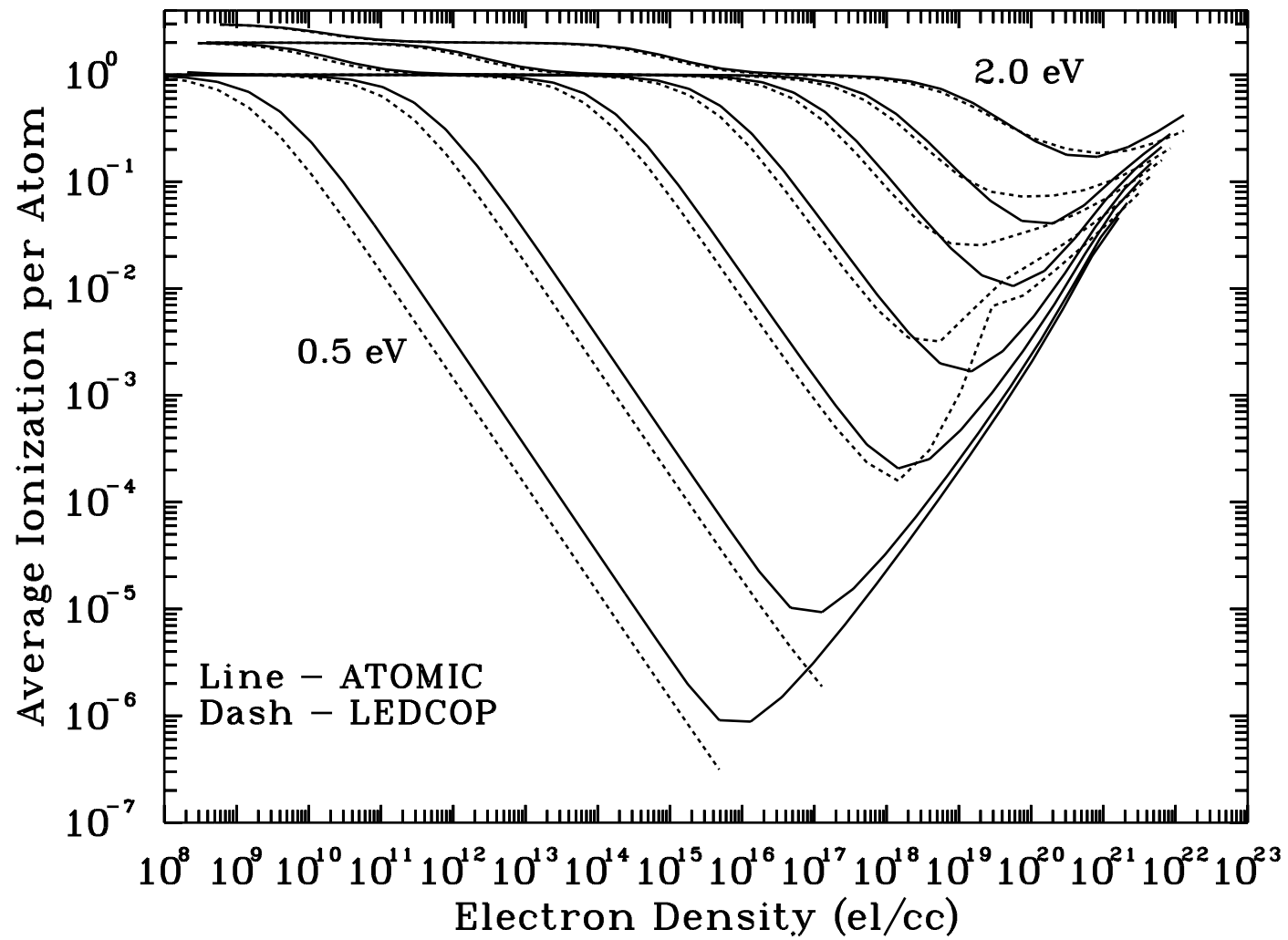
Parallelization

EOS

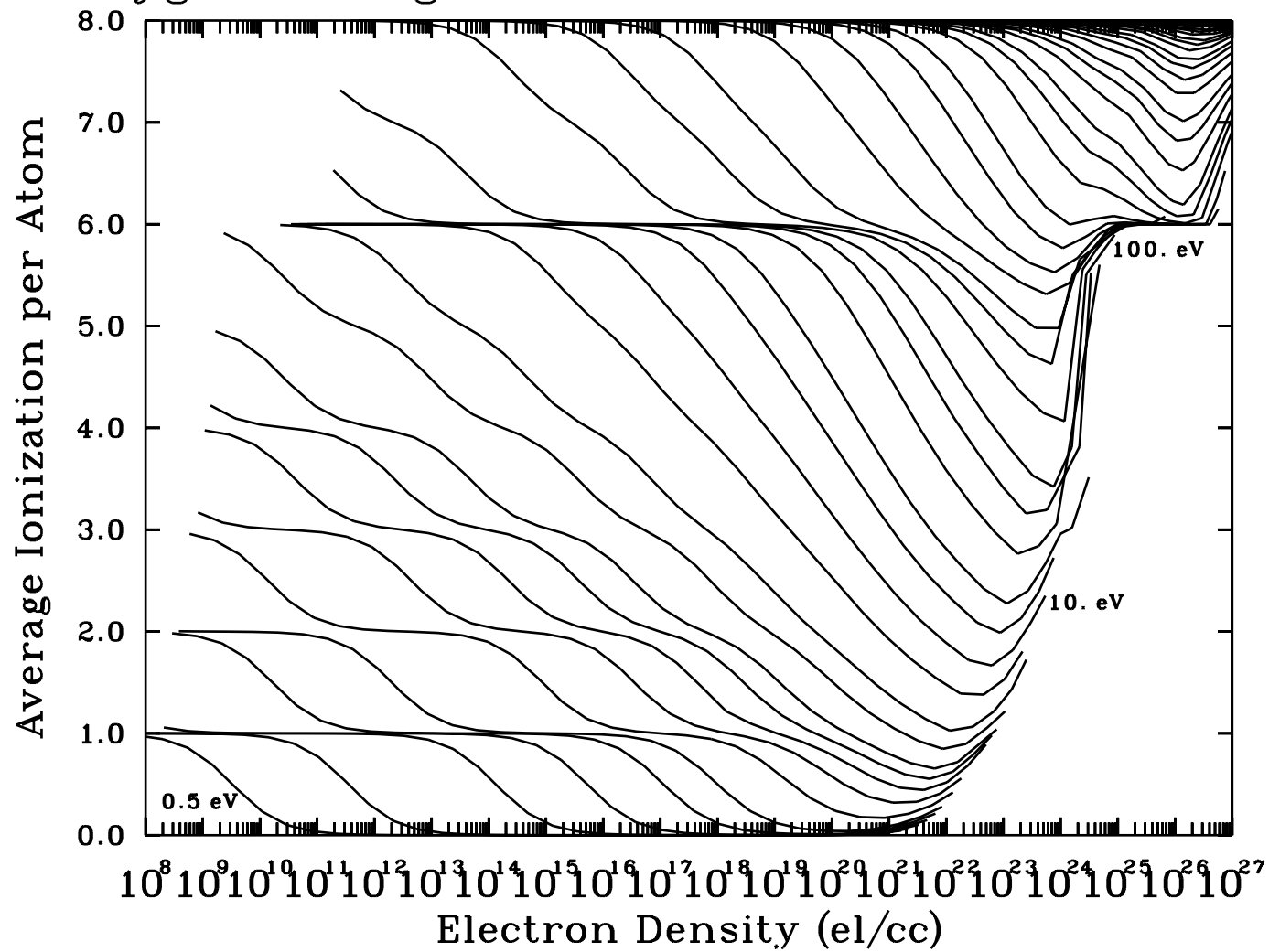
Line-edge merging

Histograms

Oxygen Ionization Comparision



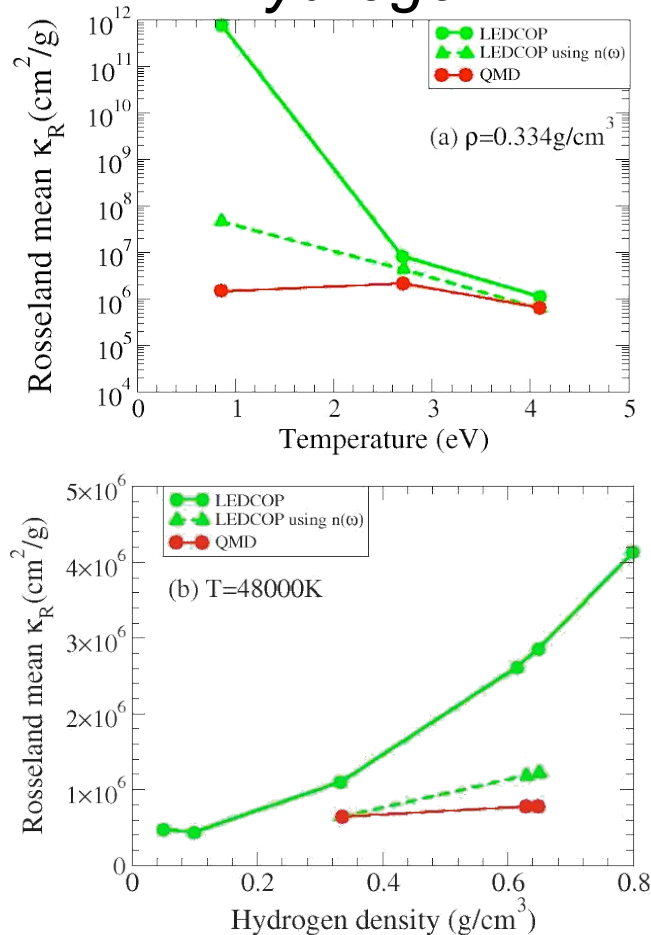
Oxygen Average Ionization from ATOMIC Code



QMD for Opacities

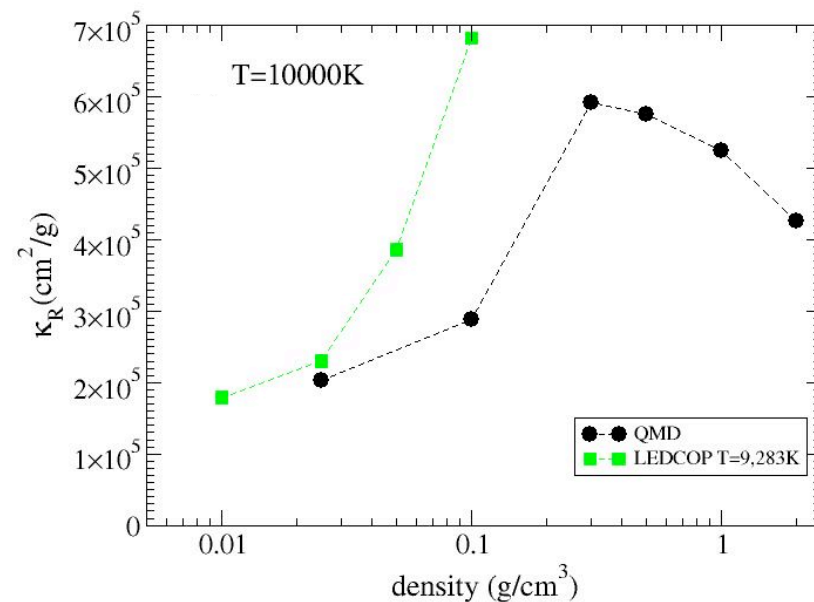
Comparison to *LED COP*

Hydrogen



S. Mazevet *et al*, Astron. Astrophys. **405**, L5 (2003)

Aluminum



S. Mazevet *et al*, Phys. Rev. E **71**, 016409 (2005)

Typical Output Quantities for Comparisons

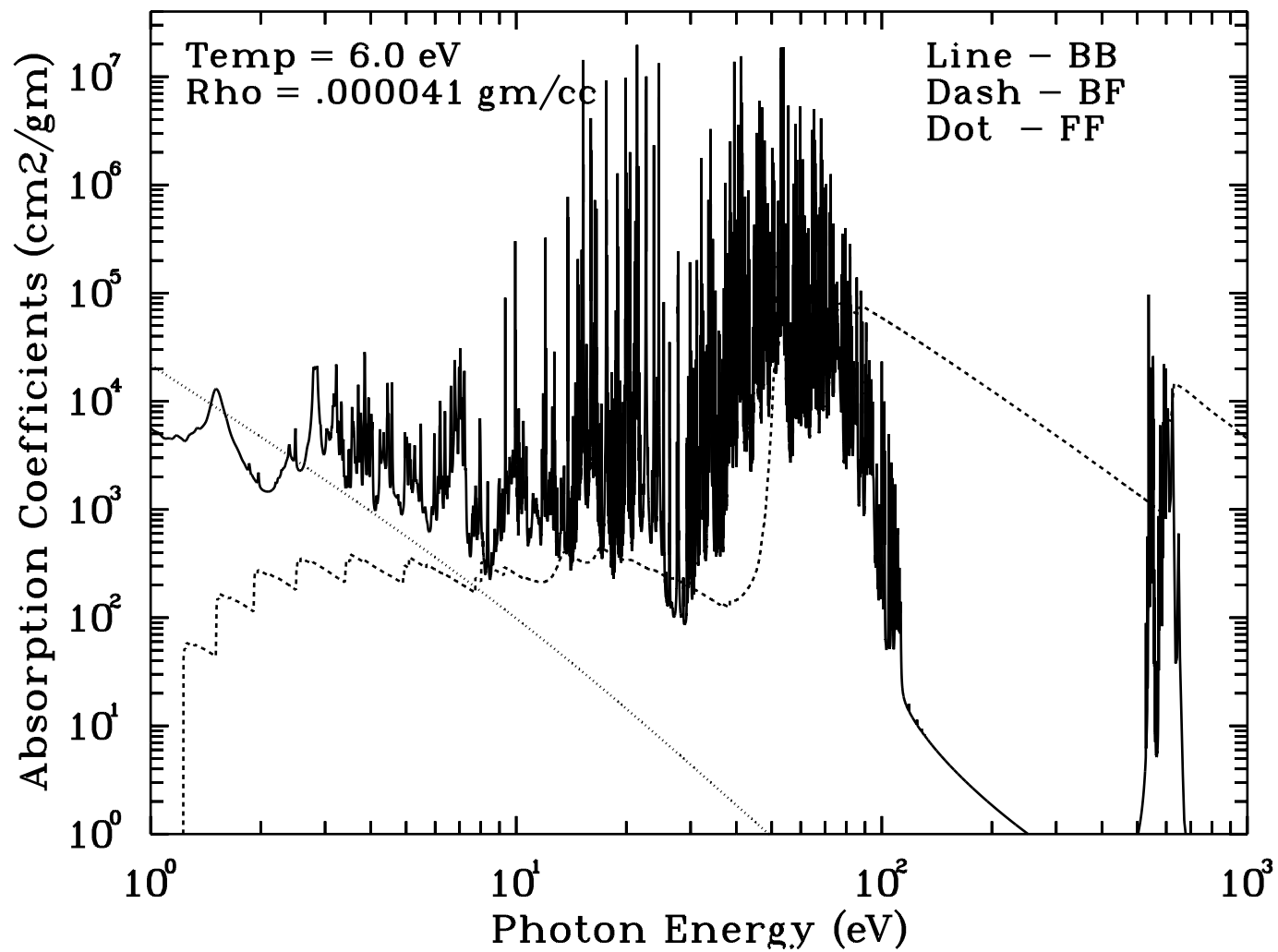
EOS

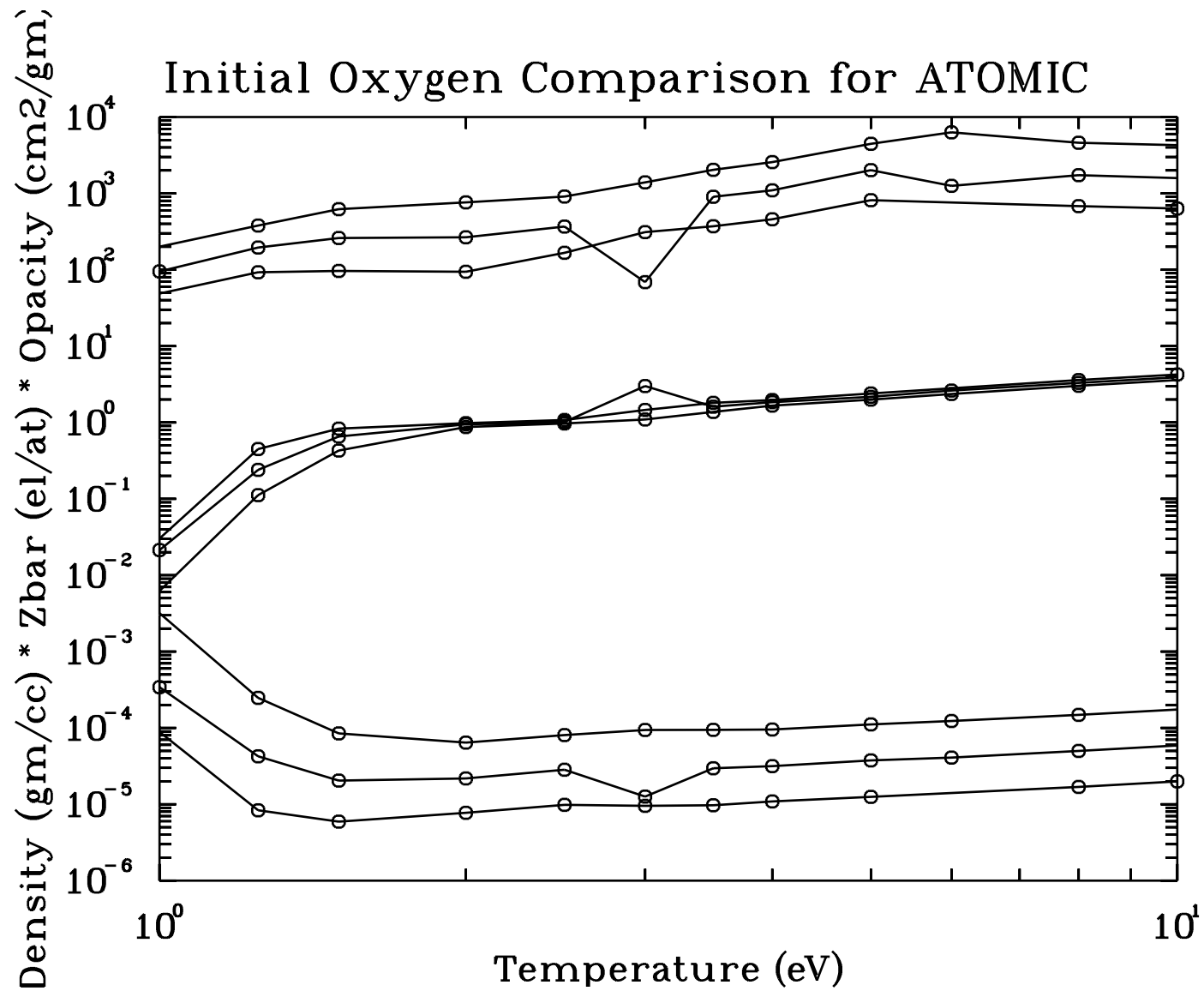
- Zbar**
- Electron Density**
- Ion Density**
- Mass Density**
- Pressure (kinetic, plasma, etc. terms)**
- Energy (kinetic, plasma, etc. terms)**
- Plasma Frequency Cutoff**
- Ion & Configuration Abundances**

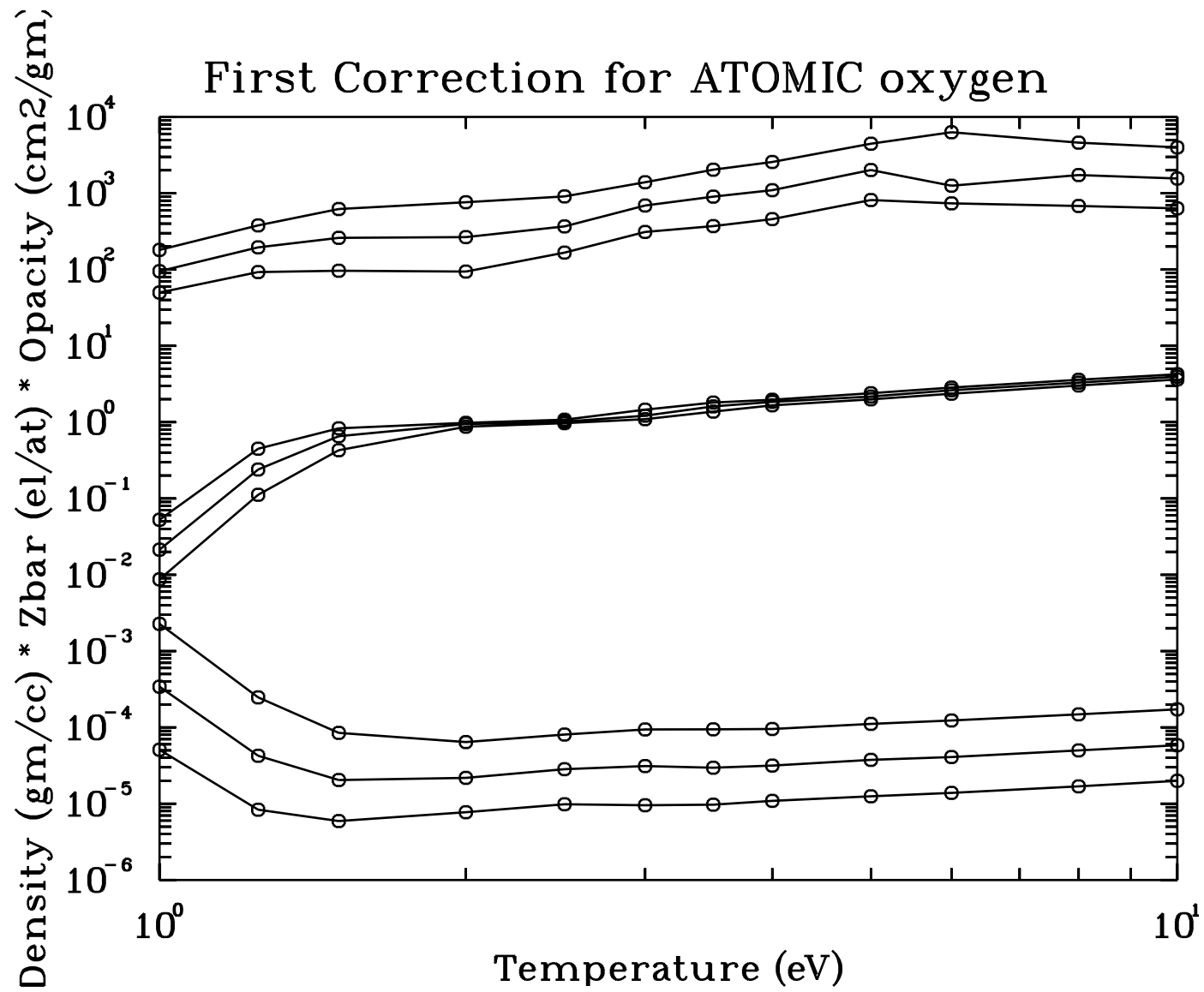
OPACITY

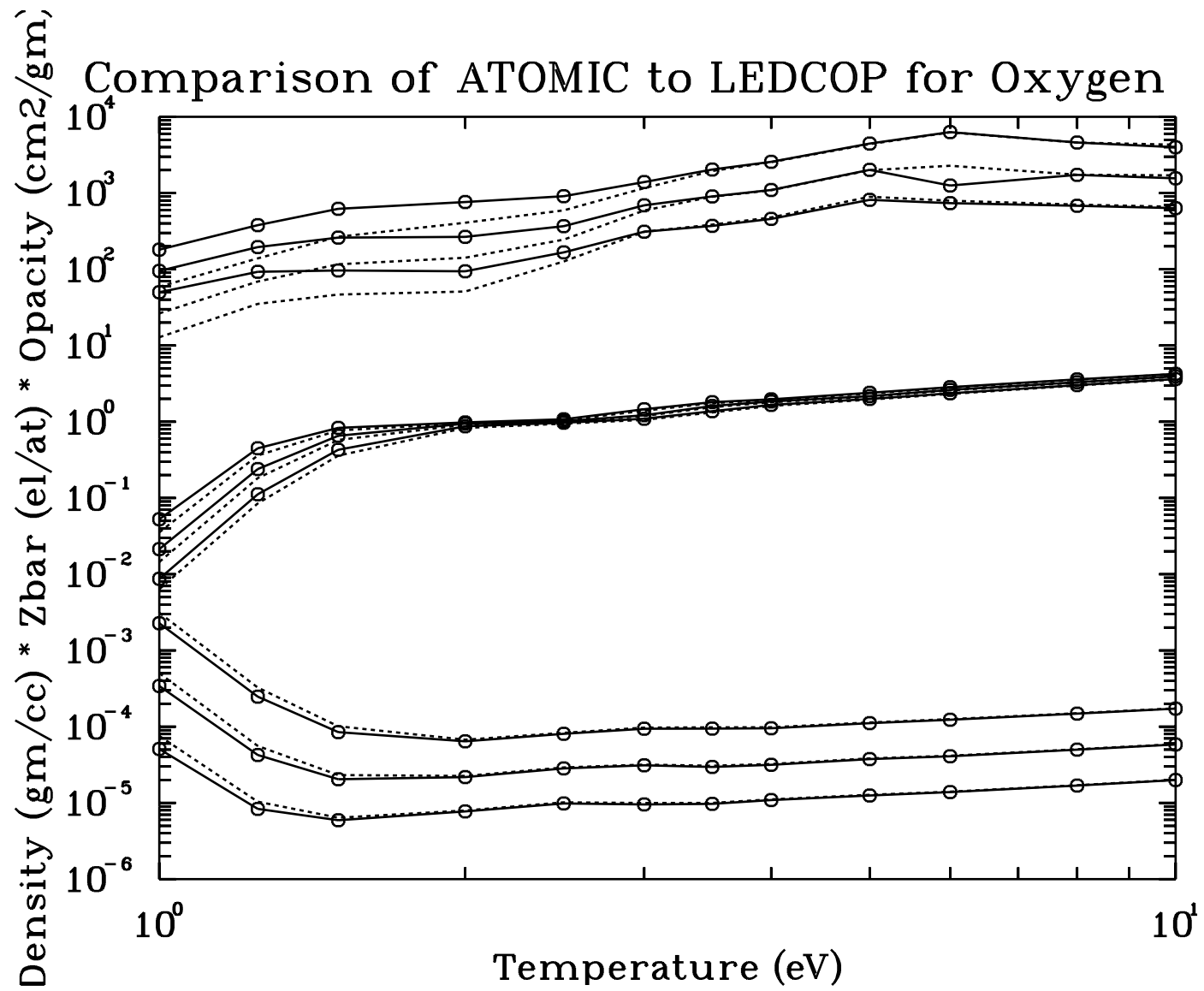
- Continuous & Total Rosseland Opacity**
- Continuous & Total Planck Opacity**
- Conductive Opacity**
- Energy Dependent Opacities**
 - ...Total Absorption**
 - ...FF Absorption**
 - ...BF Absorption**
 - ...BB Absorption**
 - ...Scattering**
- Spectral Identification**

Oxygen Spectra Plot from ATOMIC Code

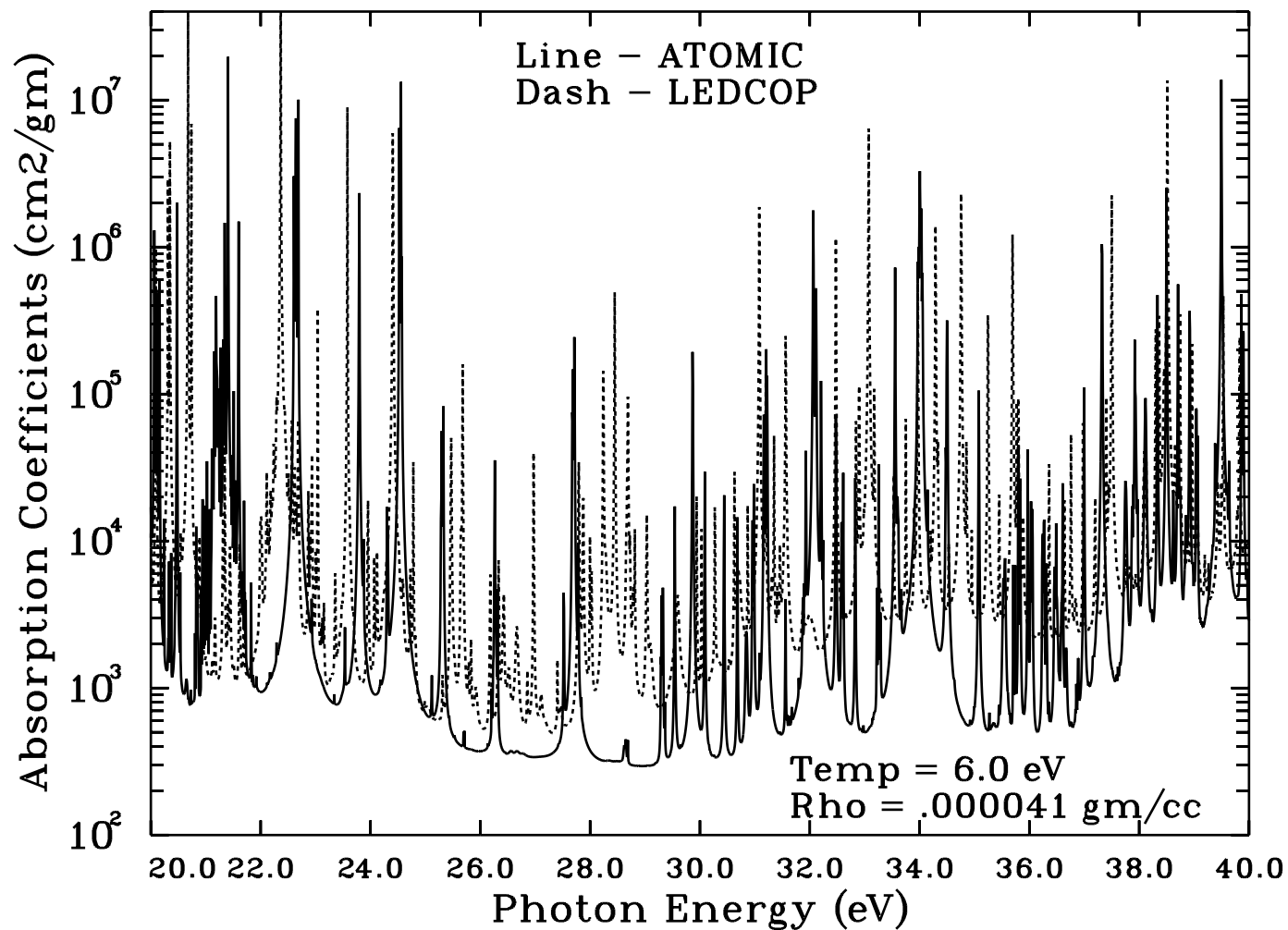




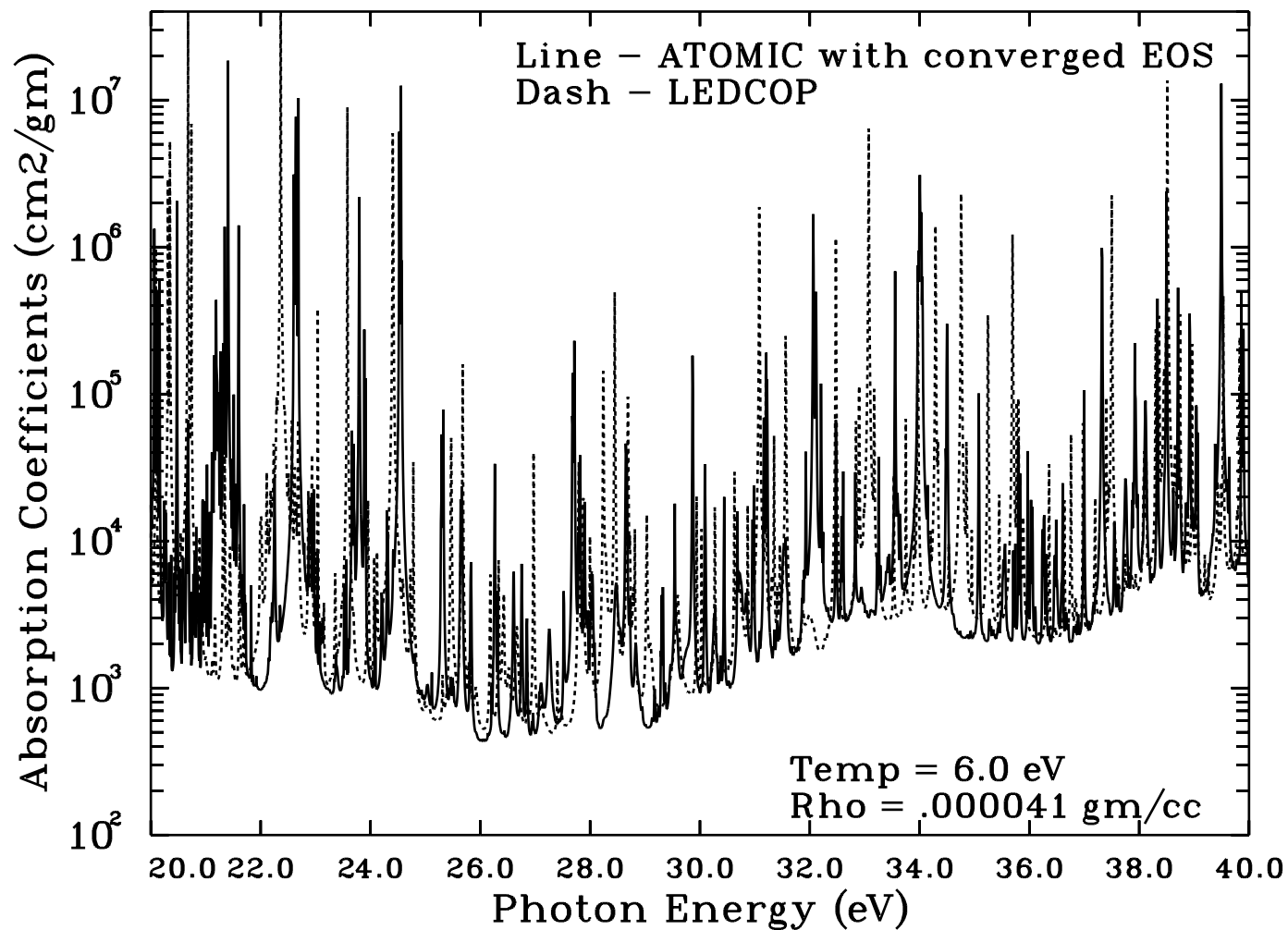


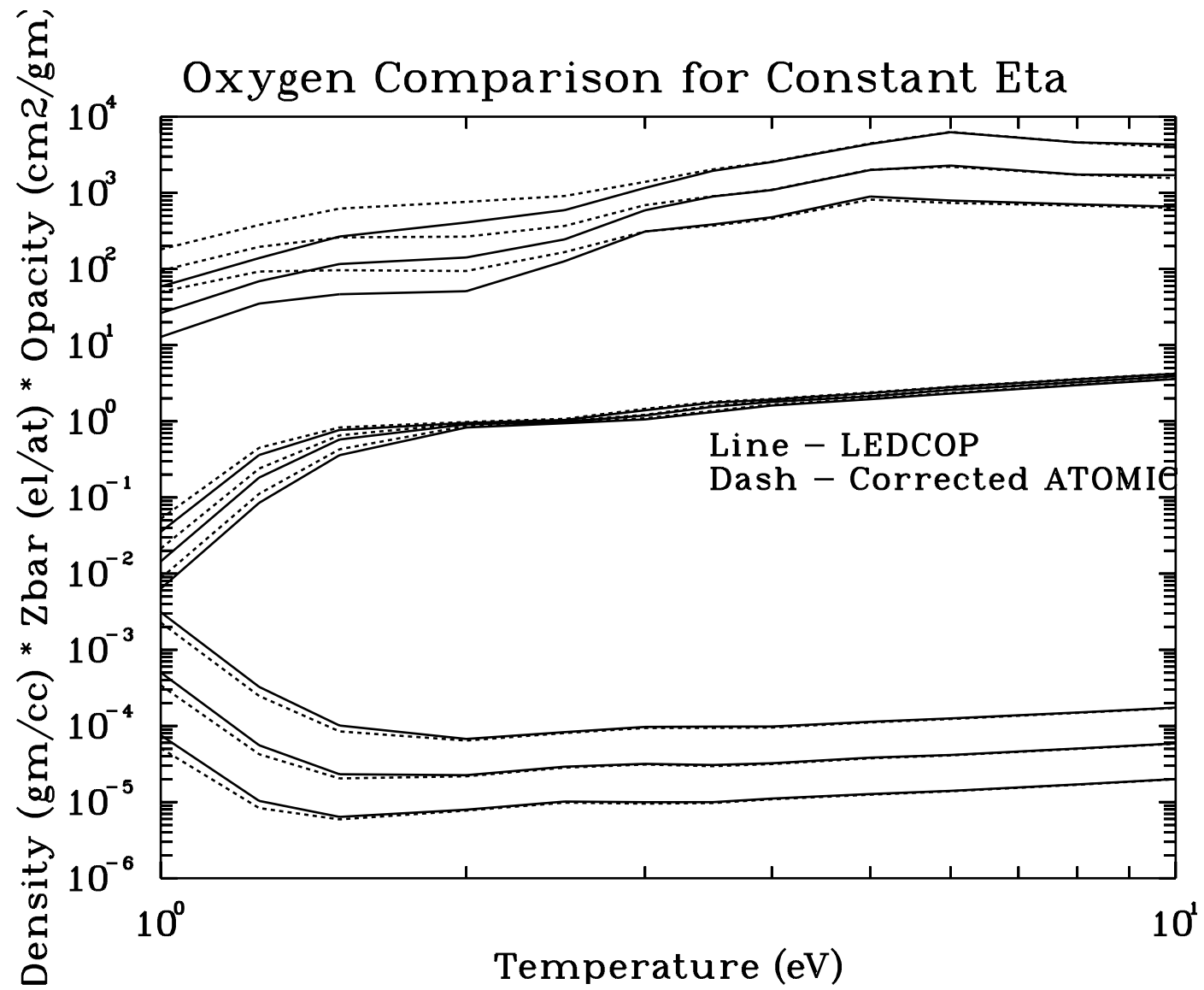


Oxygen Spectra from ATOMIC and LEDCOP



Oxygen Spectra from ATOMIC and LEDCOP





Neglected Opacity Issues

W. F. Huebner

Southwest Research Institute

P. O. Drawer 28510

San Antonio, TX 78228-0510

Neglected Opacity Issues

Conservation and Continuity of Oscillator Strengths

Completeness of Species Considered

Uncertainties in Models, Methods, and Calculations

Completeness of Processes Considered

Justification for the Assumptions of LTE

Special Cases

Designing Opacities to Meet Requirements

Laboratory Experiments

Benchmark Calculations

Oscillator Strengths

Conservation of Oscillator Strength:

The Thomas-Reiche-Kuhn sum rule should be used to check one-electron sequences ($\sum_n f_{nm} = 1$) and Z -electron atoms ($\sum_{nm} f_{nm} = Z$).

Continuity of Oscillator Strength:

In a one-electron sequence the sum rule is continuous from bound-bound to bound-free absorption. See Fano and Cooper Rev. Mod. Phys. **44**, 441 (1968).

Completeness of Species Considered

- Test For the Formation of Molecules:

While it may not be of interest to calculate molecular contributions to opacity at low temperatures, tests should be included to warn the user that the opacity lacks molecular contributions, and list the molecules that may form from the mixture of elements considered.

Completeness of Species Considered (continued)

- Minimization of the Gibbs free energy of formation for species of chemical elements and compounds in their gas and condensed phases is general, elegant, powerful, and guarantees conservation of matter. This method automatically includes reactions of disproportionation and reactions involving condensed phases.

$$G = \sum_{p=1}^{q+s+1} \sum_{i=1}^{m_p} n_{pi} (\Delta G_{pi} R_o T \ln a_{pi}),$$

where p represents a gas phase, q the number of condensed phase solutions, s the number of pure condensed phases, m_p the number of species in each phase, n_{pi} the number of moles of species i in phase p, and a_{pi} the activity of species i in phase p.

Completeness of Species Considered (continued)

- Heavy Element Impurities:

It is absolutely essential that impurities be included in the calculation of mixtures. This is particularly true if the impurities are from elements with a higher Z .

Uncertainties in Opacities

- Uncertainties in Models, Methods, and Calculations:
Arise from the need to know atomic and molecular structure, stages of ionization and dissociation, level populations, spectral line shapes, and plasma interactions.
- Sources of Uncertainties:
 1. Physical process
 2. Chemical (elemental) abundances
 3. Mathematical procedures.

Physical Process

Sources include approximations in the model of the atom or molecule used to describe the absorption and scattering processes:

Configuration interaction

Line broadening

Line shapes and line wings

Pressure balance

Collective effects

Charge conservation

Element conservation in phase transitions

Chemical Abundances

The usual approximation is the abbreviation of the elemental, molecular, and ionic composition of a medium to its “most important” constituents.

Some very underabundant species may have a line or band spectrum in an important region where the extinction coefficients of the most abundant species are very small.

Spectra of major and minor species should always be inspected.

Mathematical Procedures

Primarily iterative convergence procedure, fits to tabular data, limits imposed by electronic computers (e.g., accidentally cancellation of two nearly equal numbers).

Completeness of Processes Considered

Contribution of Plasmons to Opacity (Keady et al., 1990):

Plasmon = quantum of charge-density oscillation in a plasma.

When an x-ray interacts with an electron in a plasma, the recoil energy of the electron may remove it from the collective modes of the plasma, generating density fluctuations and creating plasmons. This influences Compton scattering. From energy conservation

$$h\nu + \gamma mc^2 = h\nu' + h\nu_p + \gamma' mc^2, \quad \gamma = [1 - (v/c)^2]^{-1/2}.$$

ν = incident photon, v = initial velocity of electron, m = electron mass, ν_p = plasma frequency. The plasmon energy is the binding energy of the electron to the plasma.

Plasmons (continued)

From momentum conservation

$$(hv/c) + \gamma m v \cos \theta = (hv'/c) \cos \Theta + \gamma' m v' \cos \theta'$$

$$\gamma m v \sin \theta = -(hv'/c) \sin \Theta + \gamma' m v' \sin \theta'$$

Angles are relative to the incident photon. θ, θ' = initial and final direction of electron, Θ = direction of photon. The plasmon is heavy compared to electron. Momentum transfer to plasma is negligible.

$$hv' = \frac{(hv_p)^2 - 2\gamma hv_p mc^2 - 2hv hv_p + 2\gamma hv mc^2 - 2\gamma hv mc v \cos \theta}{2hv - 2\gamma mc v \cos(\theta + \Theta) - 2hv \cos \Theta - 2hv_p + 2\gamma mc^2}.$$

The differential cross section for excitation is

$$d\sigma_p/d\omega = (e^2/mc^2)^2 [1 - (1/2) \sin^2 \Theta] S(\mathbf{k}), \quad S(\mathbf{k}) = \hbar \mathbf{k}^2 / (8\pi^2 m v_p)$$

$\hbar \mathbf{k} / (2\pi)$ = momentum transfer of photon to electron.

Plasmons (continued)

Substituting $h\nu'$ and integrating gives for $\nu \gg \nu_p$ the total plasma interaction cross section

$$\sigma_p = (8\pi/3) (e^2/mc^2)^2 (h\nu)^2/(2mc^2 h\nu_p) .$$

$$\sigma_p = (2\pi/3) \alpha^6 a_o^2 (h\nu)^2/(h\nu_p) , \text{ in Rydberg units.}$$

For keV x-rays and typical plasma conditions, this cross section is same order magnitude as the Compton cross section.

Plasmon effects can be important at high densities, where, however, free-free absorption may dominate over scattering.

The cross sections must be multiplied by the form factors F_{inc} and F_{coh} for incoherent and coherent scattering, respectively.

Special Cases

- Failure to Attain LTE:

For heavier elements, LTE conditions may not be attainable at high temperatures and low densities because radiative deexcitation may be faster than collisional excitation.

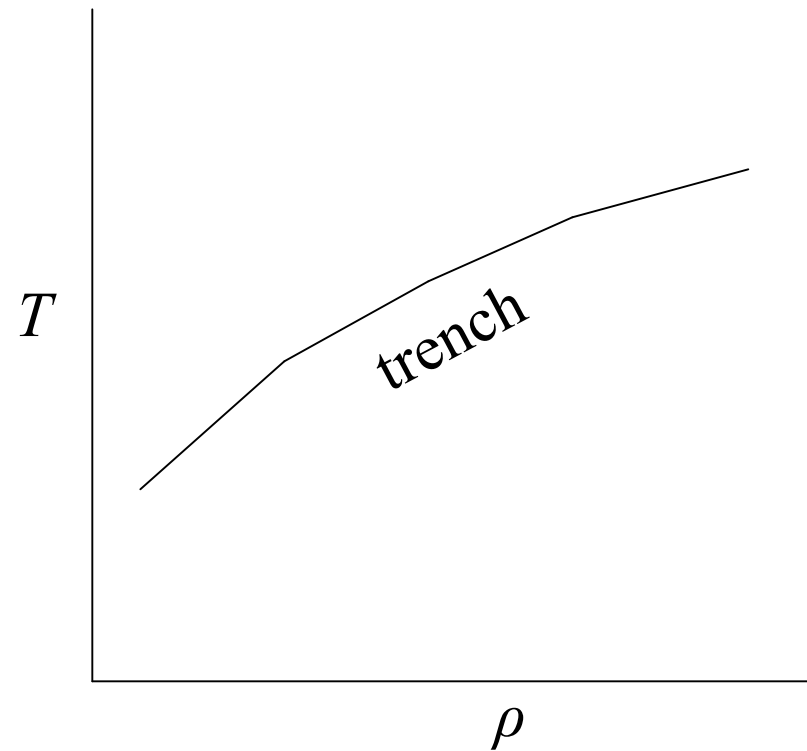
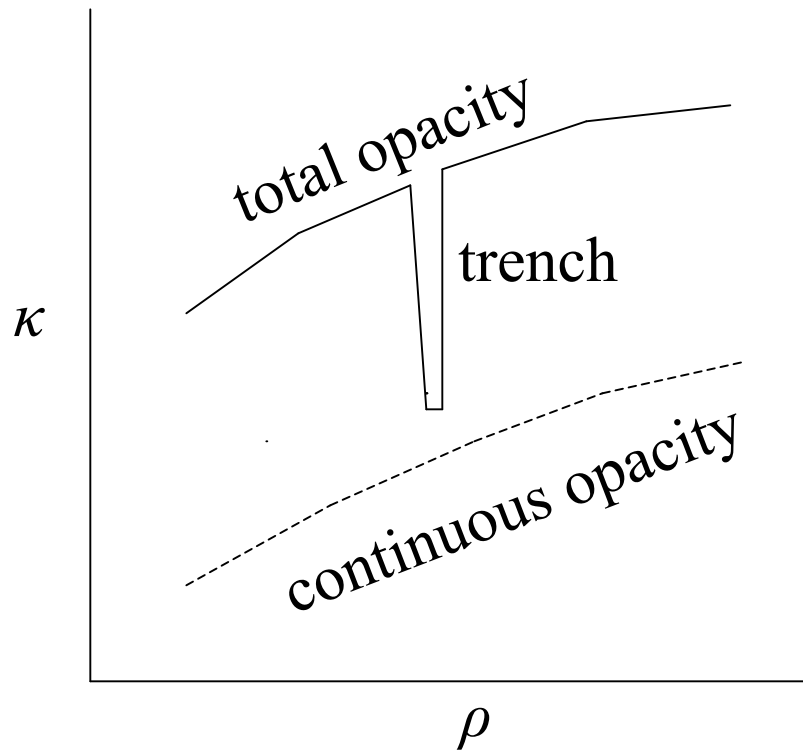
Special Cases (continued)

- Opacity Trenches:

Partially filled shells bring about many electron configurations and many different ways for electrons to couple. The result is a plethora of overlapping spectral lines. For some elements temperature-density regions exist in which the ion structure is dominated by closed shells. There, the number of possible electron configurations and couplings are severely limited when compared to neighboring regions with more than one electron (or electron hole) relative to the closed shells. As a result the line spectrum is sparse and the opacity is drastically reduced. The temperature-density regions where this opacity reduction occurs is very narrow, i.e., like a trench.

Special Cases (continued)

Opacity Trenches:



Los Alamos, 3-5 May, 2005

Designing Opacities to Meet Requirements

Designing materials to meet opacity requirements:

For example:

High opacity from low- Z elements.

Opacities that block a photon energy range over a certain $T - \rho$ range.

Laboratory Experiments

Validation of opacity codes and verification of opacity calculations are very important. One has to keep in mind that opacity calculations are complex, but individual processes can be checked independently. Laboratory experiments are complex, but individual processes cannot be checked independently.

Difficulties with laboratory experiments include:

1. Attainment of LTE
2. T and ρ determination
3. T and ρ gradients
4. Edge effects
5. Back lighting
6. Plasma impurities

Laboratory experiments can provide supporting evidence for opacity calculations.

Benchmark Calculations

Opacity calculations are based on many processes. Most of these processes are calculated using different models, different wave functions, disjointed processes (e.g., line wings vs. underlying continuum, absorption vs. scattering, etc.). Sometimes not even The elemental composition is consistent across phase transitions (e.g., with rising temperature from a dusty atmosphere – molecular gas – atomic gas – plasma).

A detailed benchmark calculation for a pure plasma should be carried out (perhaps in conjunction with an opacity experiment).

Opacities in Astrophysics

Arthur N. Cox

Los Alamos Astrophysics

Group T-6

Los Alamos National Laboratory

Needs for Matter Opacities

- 1. Star Formation
- 2. Stellar Structure
- 3. Stellar Evolution
- 4. Stellar Pulsations
- 5. Stellar Explosions

OP Form for Calculating Stellar Opacities

Abundance Fractions

Hydrogen Abundance (X)
Metal Abundance (Z)

Metal Fractional Composition (default = solar)

Note: metal abundancies are re-normalised to the value of Z which has been set --- it is necessary to specify only the relative abundance for each metal.

C (Z=6)	<input type="text" value="0.2460"/>	N (Z=7)	<input type="text" value="0.0647"/>	O (Z=8)	<input type="text" value="0.5140"/>
Ne (Z=10)	<input type="text" value="0.0815"/>	Na (Z=11)	<input type="text" value="0.00148"/>	Mg (Z=12)	<input type="text" value="0.02636"/>
Al (Z=13)	<input type="text" value="0.00205"/>	Si (Z=14)	<input type="text" value="0.0246"/>	S (Z=16)	<input type="text" value="0.01125"/>
Ar (Z=18)	<input type="text" value="0.0023"/>	Ca (Z=20)	<input type="text" value="0.00159"/>	Cr (Z=24)	<input type="text" value="0.000324"/>
Mn (Z=25)	<input type="text" value="0.00017"/>	Fe (Z=26)	<input type="text" value="0.02244"/>	Ni (Z=28)	<input type="text" value="0.00123"/>

OPAL MIXTURE COMPOSITION

type 2 number fractions

Enhanced element 1: (C-Si only)

Enhanced element 2: (C-Si only)

Metallicity, Z: (0-0.2, input truncated to nearest 0.0001)

Symbol	Z	At. mass (a.u.)	My Fraction	Initial Fraction
H	1	<input type="text" value="1.00790"/>		
He	2	<input type="text" value="4.00260"/>		
C	6	<input type="text" value="12.01100"/>	<input type="text" value="0.245518"/>	0.245518
N	7	<input type="text" value="14.00670"/>	<input type="text" value="0.064578"/>	0.064578
O	8	<input type="text" value="15.99940"/>	<input type="text" value="0.512966"/>	0.512966
Ne	10	<input type="text" value="20.17900"/>	<input type="text" value="0.083210"/>	0.083210
Na	11	<input type="text" value="22.98977"/>	<input type="text" value="0.001479"/>	0.001479
Mg	12	<input type="text" value="24.30500"/>	<input type="text" value="0.026308"/>	0.026308
Al	13	<input type="text" value="26.98154"/>	<input type="text" value="0.002042"/>	0.002042
Si	14	<input type="text" value="28.08550"/>	<input type="text" value="0.024552"/>	0.024552
P	15	<input type="text" value="30.97376"/>	<input type="text" value="0.000195"/>	0.000195
S	16	<input type="text" value="32.06000"/>	<input type="text" value="0.011222"/>	0.011222
Cl	17	<input type="text" value="35.45300"/>	<input type="text" value="0.000219"/>	0.000219
Ar	18	<input type="text" value="39.94800"/>	<input type="text" value="0.002291"/>	0.002291
K	19	<input type="text" value="39.09830"/>	<input type="text" value="0.000091"/>	0.000091
Ca	20	<input type="text" value="40.08000"/>	<input type="text" value="0.001586"/>	0.001586
Ti	22	<input type="text" value="47.90000"/>	<input type="text" value="0.000075"/>	0.000075
Cr	24	<input type="text" value="51.99600"/>	<input type="text" value="0.000329"/>	0.000329
Mn	25	<input type="text" value="54.93800"/>	<input type="text" value="0.000170"/>	0.000170
Fe	26	<input type="text" value="55.84700"/>	<input type="text" value="0.021877"/>	0.021877
Ni	28	<input type="text" value="58.70000"/>	<input type="text" value="0.001293"/>	0.001293

These initial number fractions are set to the solar composition of Grevesse & Noels, 19

Los Alamos TOPS Specification either number or weight fraction

Mix specification

Fraction by ☒ Number *or* ☐ Mass.

Input format is ☒ Fraction, Element *or* ☐ Fraction, Element, Isotopic weight.

In specifying a mix, the fraction represents relative numbers of atoms if the number fraction box is checked. If the mass fraction box is checked, the fraction represents relative masses of the specified elements. The fractions need not be normalized.

The element specification can be the atomic number, the chemical symbol (case insensitive) or the OPLIB matid. Thus aluminum can be specified as Al, al, 13, 113718 or n13718 (for the new [denser photon energy grids](#)).

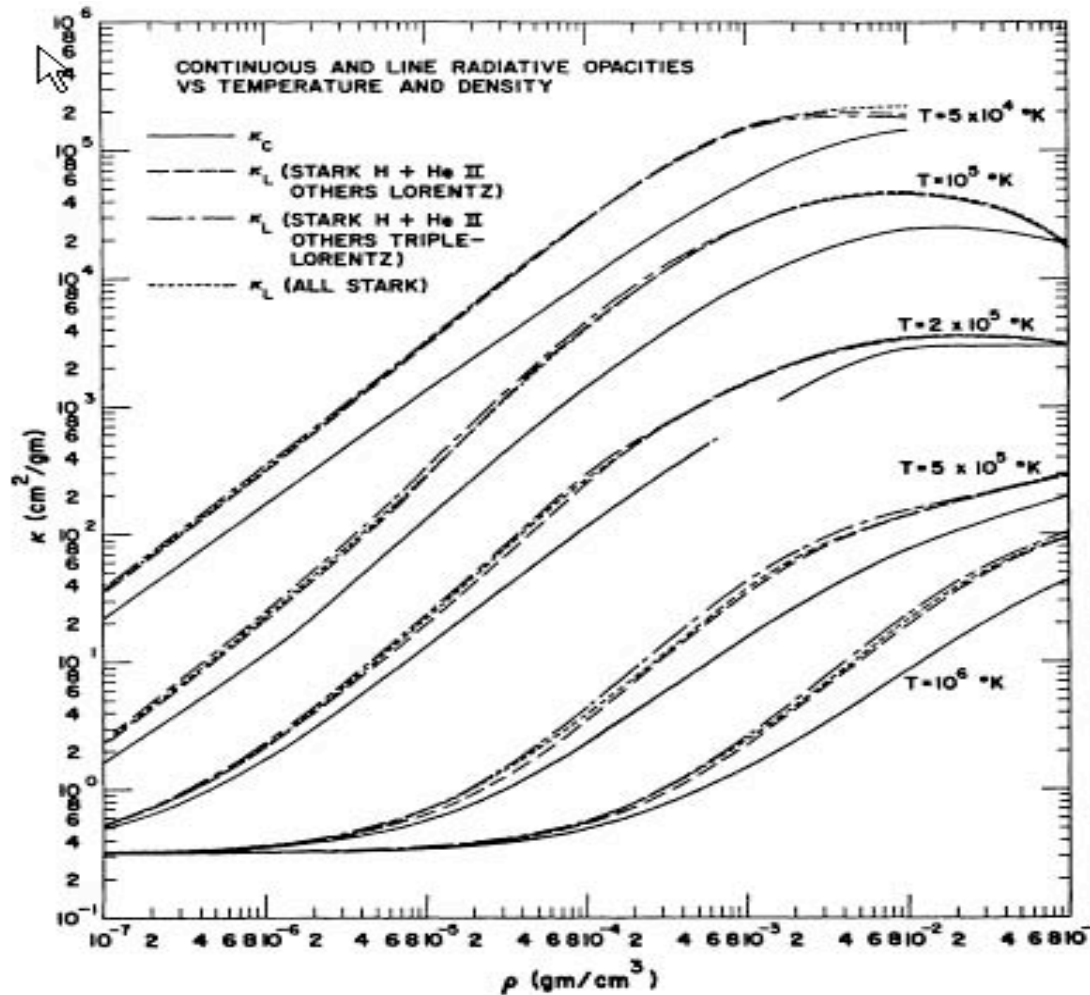
If the "Fraction, Element, Isotope" box is checked, a specific isotopic weight must be entered for each element of the mixture. If this box is not checked, no isotopic weight should be entered, the Web Page will use the normal values.

User specified mixture. Up to 450 characters may be used for the mixture specification. User can choose to supply a name for the mixture, up to 15 characters.

1. al

Optional [Mixture Name](#): (User supplied, maximum of 15 characters)

Effects of Spectral Lines on Los Alamos Opacities, Cox, 1965



Cox and Tabor Astrophysical Journal Supplement 1976, ApJS,31, 271

Abstract

Radiative opacities for **40 mixtures** of hydrogen, helium, and heavier elements are presented which represent the best large set of homogeneous data available for stellar structures. Smaller special tables of opacities are also calculated for specific applications in studies of stellar structure, evolution, and pulsation. Improvements in the computational methods include an **increased iron abundance** in the heavy-element composition, a better allowance for the ion continuum depression, and corrections in several bound-electron energy levels. It is noted that some of the opacities are not realistic because of zero hydrogen abundances or a lack of any possible molecules.

Updated OPAL Opacities

Iglesias, C.A. and Rogers. F.J., 1996, ApJ, 464, 943

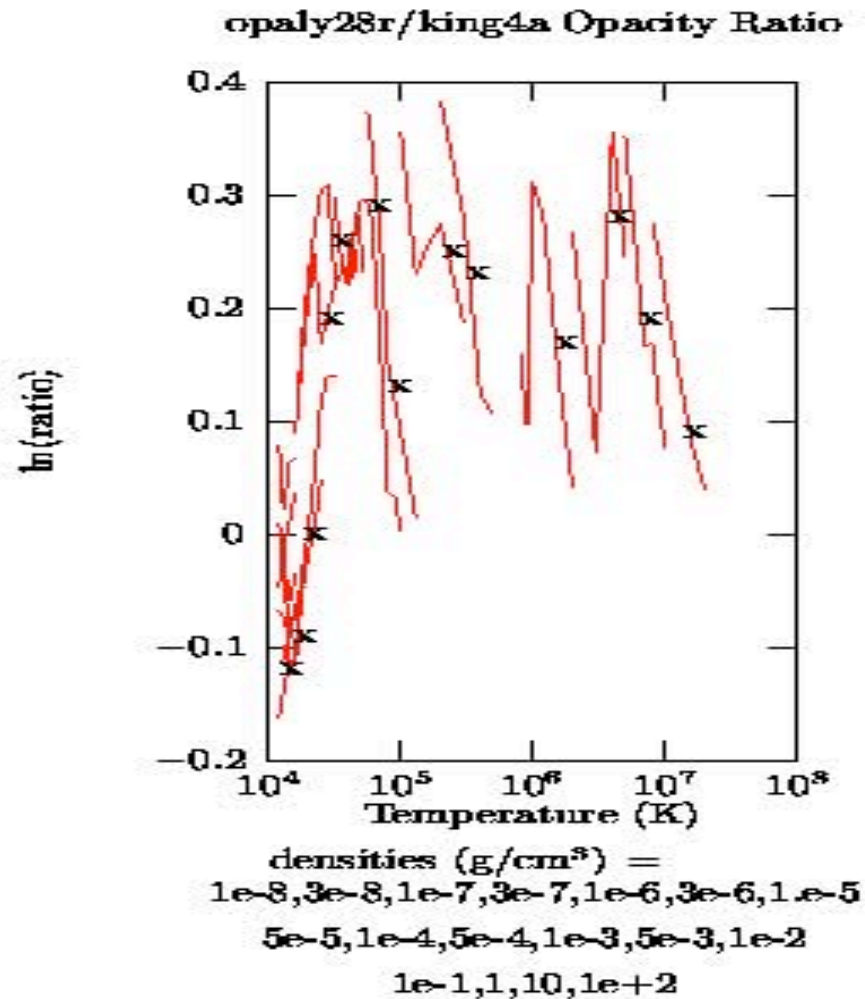
Abstract

The reexamination of astrophysical opacities has eliminated gross discrepancies between a variety of observations and theoretical calculations; thus allowing for more detailed tests of stellar models. A number of such studies indicate that model results are sensitive to modest changes in the opacity. Consequently, it is desirable to update available opacity databases with recent improvements in physics, refinements of element abundance, and other such factors affecting the results.

Updated OPAL Rosseland mean opacities are presented. The new results have incorporated improvements in the physics and numerical procedures as well as corrections. The main opacity changes are increases of as much as 20% for Population I stars due to the explicit inclusion of 19 metals (compared to 12 metals in the earlier calculations) with the other modifications introducing opacity changes smaller than 10%. In addition, the temperature and density range covered by the updated opacity tables has been extended. As before, the tables allow accurate interpolation in density and temperature as well as hydrogen, helium, carbon, oxygen, and metal mass fractions. Although a specific metal composition is emphasized, opacity tables for different metal distributions can be made readily available. The updated opacities are compared to other work.

Subject headings: atomic data — atomic processes — stars: interiors

OPAL Solar Opacity Larger Than Old Los Alamos Opacity



opaly28r Composition Cox-Tabor Z Composition

El	Z	A	N	X
H	1.0	1.00797E+00	9.07156E-01	7.00000E-01
He	2.0	4.00260E+00	9.13793E-02	2.80000E-01
C	6.0	1.20112E+01	2.84436E-04	2.61540E-03
N	7.0	1.40067E+01	8.01664E-05	8.59600E-04
O	8.0	1.59994E+01	6.36796E-04	7.79960E-03
Ne	10.0	2.01830E+01	3.58814E-04	5.54400E-03
Na	11.0	2.29898E+01	1.42048E-06	2.50000E-05
Mg	12.0	2.43120E+01	1.79456E-05	3.34000E-04
Al	13.0	2.69815E+01	1.19090E-06	2.46000E-05
Si	14.0	2.80860E+01	2.27711E-05	4.89600E-04
Ar	18.0	3.99480E+01	2.38377E-05	7.29000E-04
Fe	26.0	5.58470E+01	3.69376E-05	1.57920E-03

COMPOSITION OF Z FOR STANDARD MIXTURES

Element	Number Fraction	Mass Fraction
C.....	0.194250	0.13077
N.....	0.054747	0.04298
O.....	0.434873	0.38998
Ne.....	0.245034	0.27720
Na.....	0.000974	0.00125
Mg.....	0.012256	0.01670
Al.....	0.000810	0.00123
Si.....	0.015552	0.02448
Ar.....	0.016280	0.03645
Fe.....	0.025224	0.07896

Comparison of OPAL and OP Opacities for a Solar Mixture

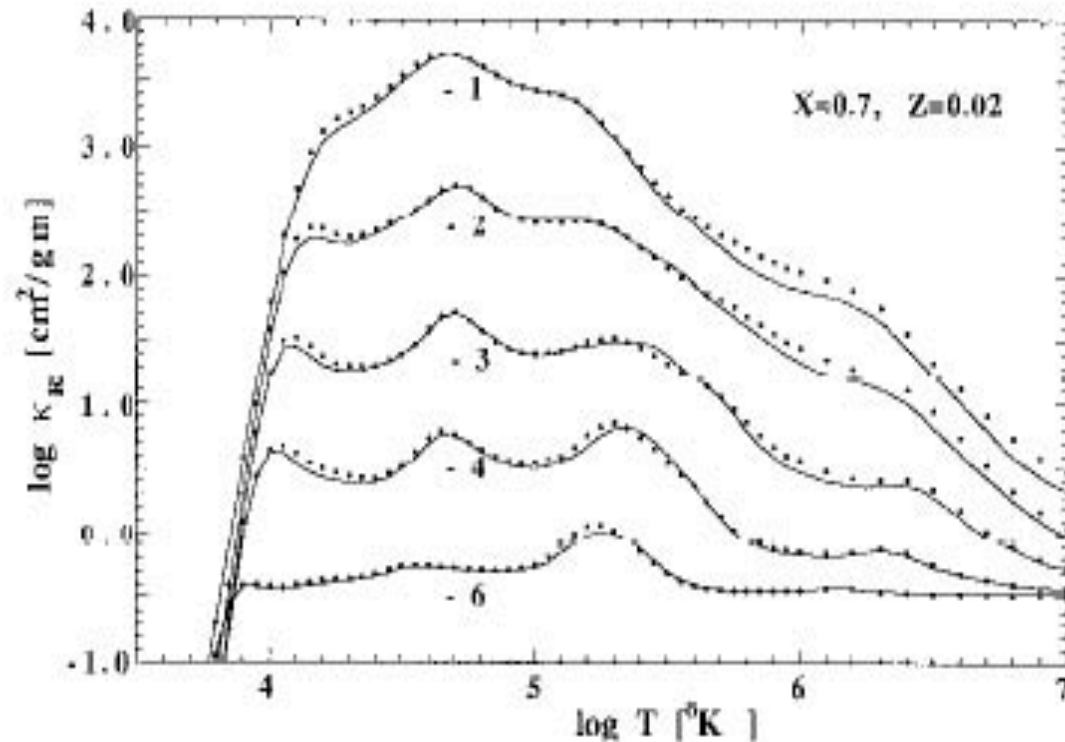
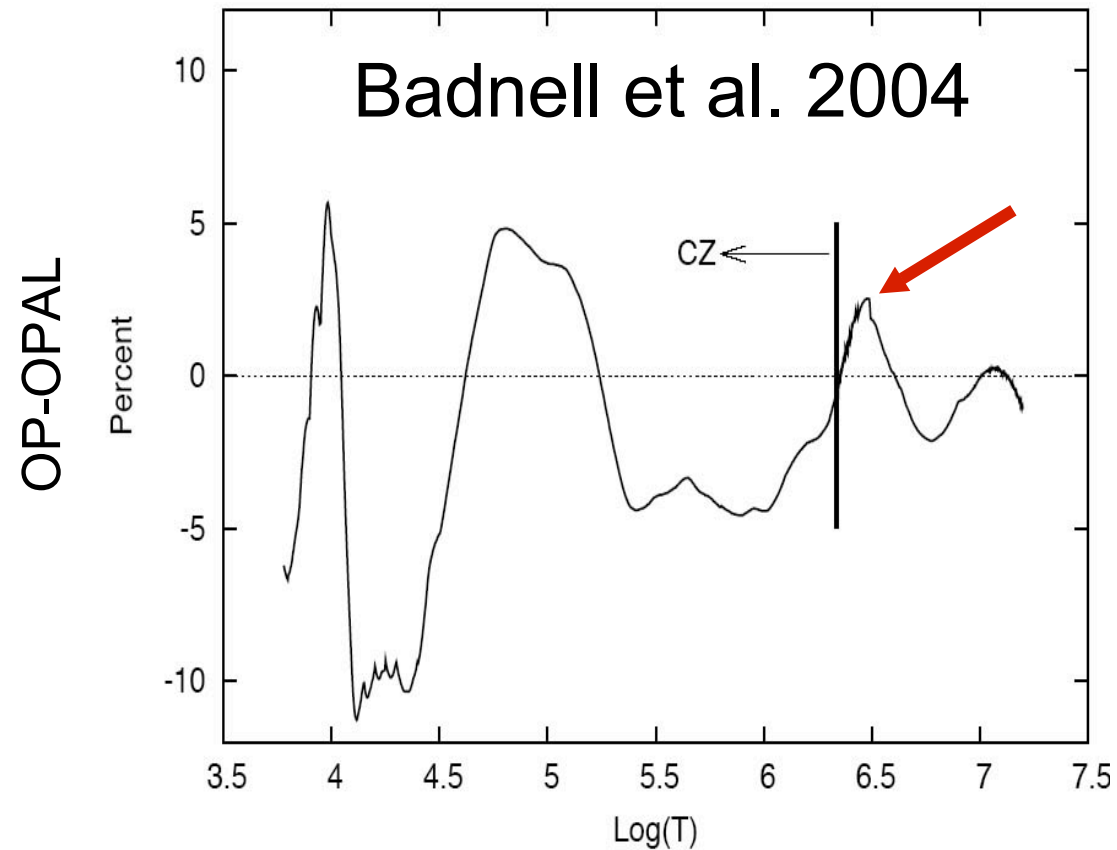


Figure 1. Comparison of OPAL (dots) and OP (solid lines) Rosseland mean opacities at constant values of $\log R$ for the element distribution used by Seaton *et al.* (1994) where X is the hydrogen mass fraction and Z is the metallicity.

The new OP opacities are only slightly larger than the OPAL opacities just below the solar convection zone.



Helioseismic Tests of the New Los Alamos LEDCOP Opacities, 2001,ApJ,561,450

Abstract

We compare the helioseismic properties of two solar models, one calibrated with the OPAL opacities and the other with the recent Los Alamos LEDCOP (Light Element Detailed Configuration Opacity) opacities. We show that, in the radiative interior of the Sun, the small differences between the two sets of opacities (up to 6% near the base of the convection zone) lead to noticeable differences in the solar structure (up to 0.3% in sound speed), with the OPAL model being the closest to the helioseismic data. More than half of the difference between the two opacity sets results from the interpolation scheme and from the relatively widely spaced temperature grids used in the tables. The remaining 3% intrinsic difference between the OPAL and the LEDCOP opacities in the radiative interior of the Sun is well within the error bars on the opacity calculations resulting from the uncertainties on the physics. We conclude that both the OPAL and LEDCOP opacities produce solar models in close agreement with helioseismic inferences, but discrepancies still persist at the level of 0.6% between the calculated and inferred sound speed in the radiative interior of the Sun.

Neuforge-Verheecke, C; Guzik, J.A.; Keady, J.J.; Magee, N.H.; Bradley, P.A.; Noels, A.

Opacity Differences OPAL-LEDCOP versus Solar Model Radius Neuforge-Verheecke, C, et al.,2001

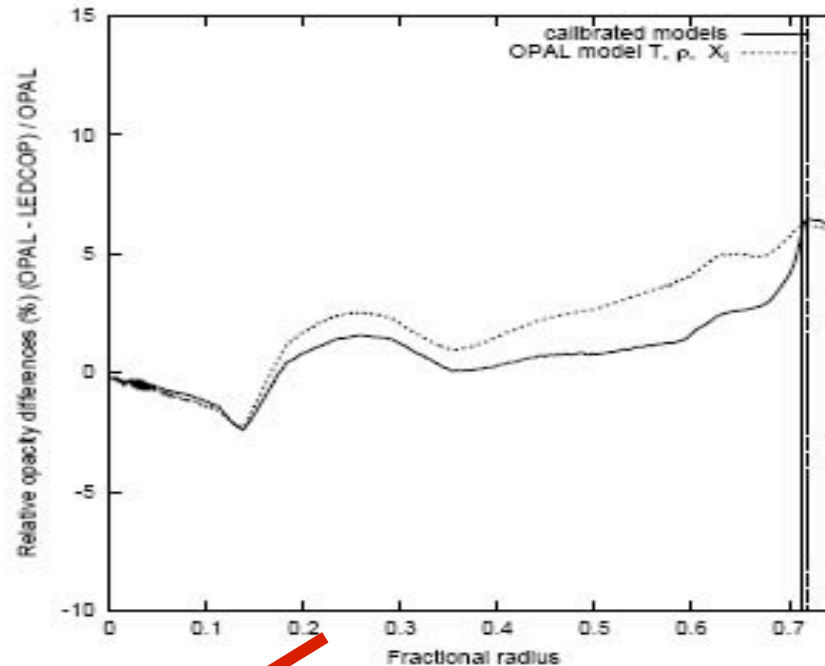


FIG. 1.—Relative opacity differences between the calibrated LEDCOP and OPAL model (solid line), and relative differences between the LEDCOP and OPAL opacities calculated with the temperature, density, and composition profile of the OPAL model (dotted line), as a function of the fractional radius. The opacity differences that we obtain are very similar in both cases. The first way to compare the OPAL and the LEDCOP opacities, i.e., for the actual run of the physical quantities in the different calibrated models, allows us to link the sound speed differences to the opacity differences, since, in each model, the sound speed is calculated for the actual run of the physical quantities. The vertical lines indicate the convection zone base location in the different models.

β Cephei Model Opacity Temperature Derivative versus Lagrange Mass Shell

Cox. Morgan, Rogers & Iglesias, ApJ, 1992

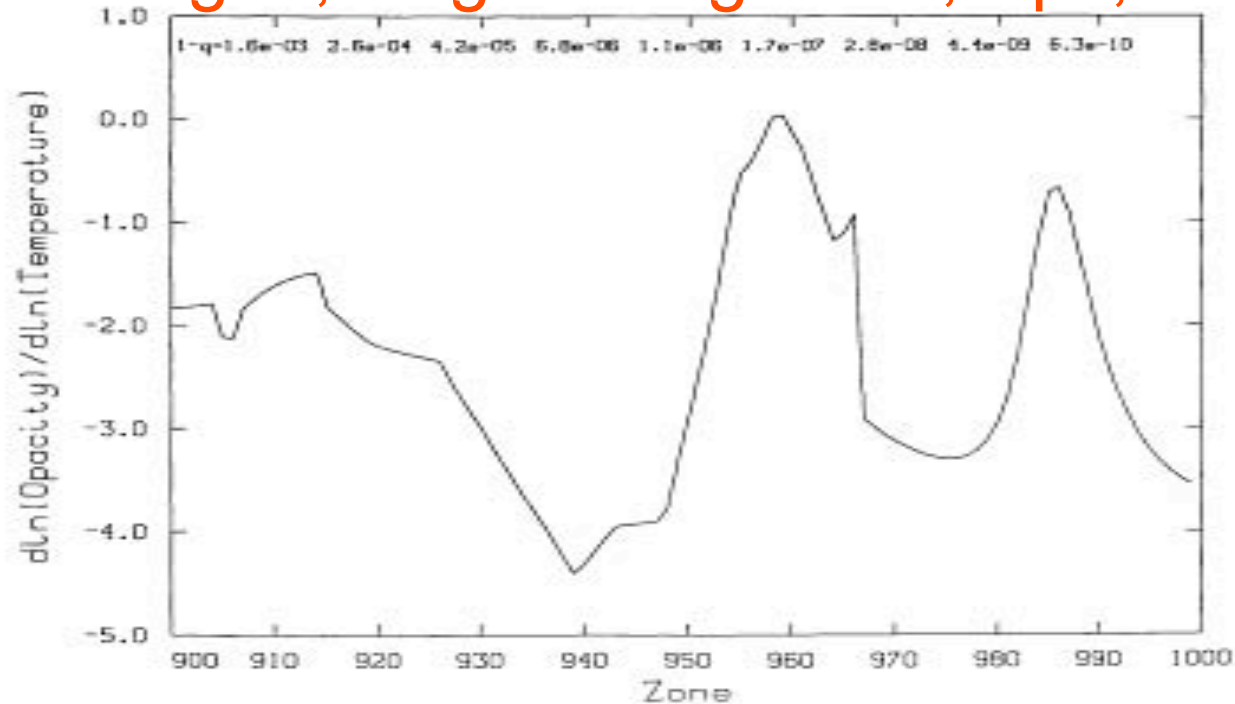


FIG. 1.—The logarithmic derivative of the opacity with respect to temperature vs. zone number is plotted, based on data from Table 1. The surface mass depth for this irregular zoning is indicated at the top. The iron line peak between zones 950 and 970 is in the pulsation driving region. The usual helium ionization region, centered at $\sim 40,000$ K lies between zones 980 and 990.

β Cephei Model Pulsational Driving versus Lagrange Mass Shell

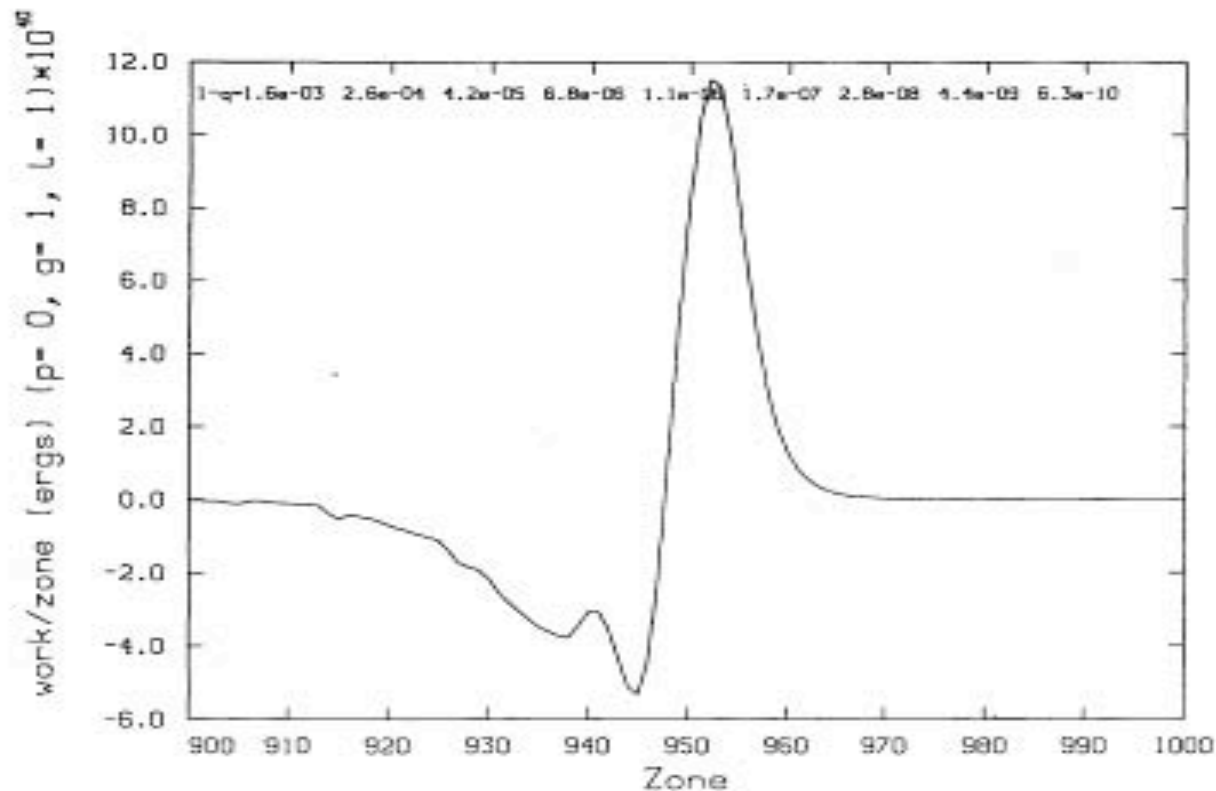


FIG. 2.—The work per zone to drive or damp pulsations is given versus zone number. All the pulsation driving seen is done in the outer 2×10^{-6} of the model mass between temperatures of 100,000 and 250,000 K. The surface mass depth for this irregular zoning is indicated at the top.

Double-Mode RR Lyrae Variable Period Ratios versus Period using OPAL Opacities

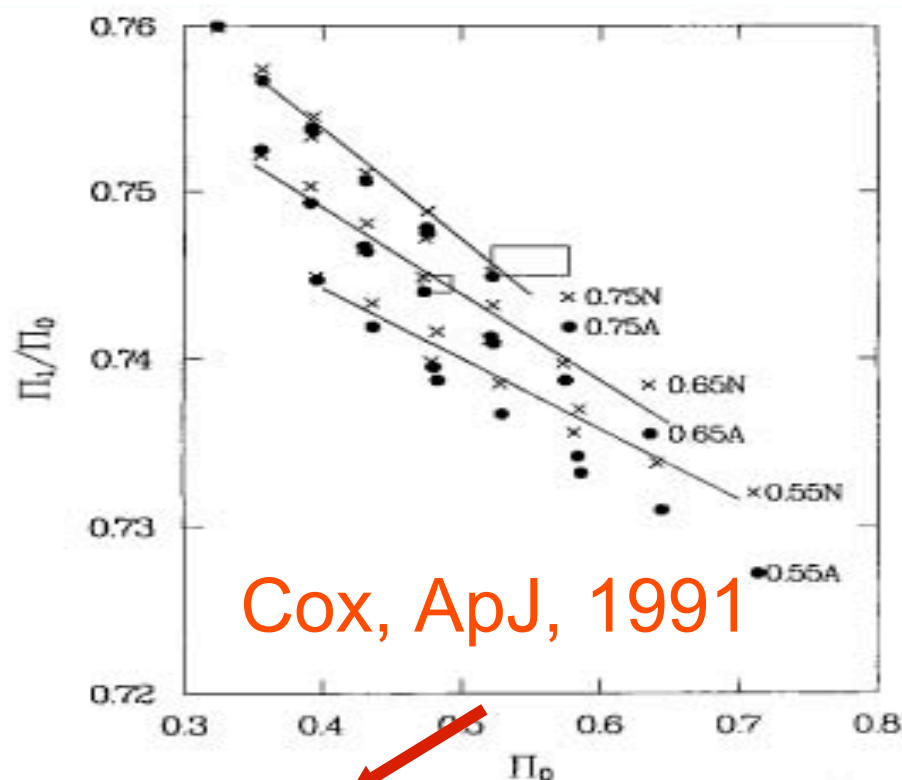


FIG. 1.—Both adiabatic and nonadiabatic period ratios are plotted vs. the fundamental mode periods for the 27 models. A least squares line is plotted for the 0.55, 0.65, and 0.75 M_\odot nonadiabatic cases. The slopes for these lines are -0.0420 , -0.0517 , and -0.0565 day $^{-1}$, and the period ratios at 0.5 day are 0.7400, 0.7438, and 0.7471. The left box encloses the Oosterhoff type I cluster variables, whereas the larger box encloses the Oosterhoff type II cluster variables.

Opacity versus Radius for an RR Lyrae Variable Model at the Evolution Mass

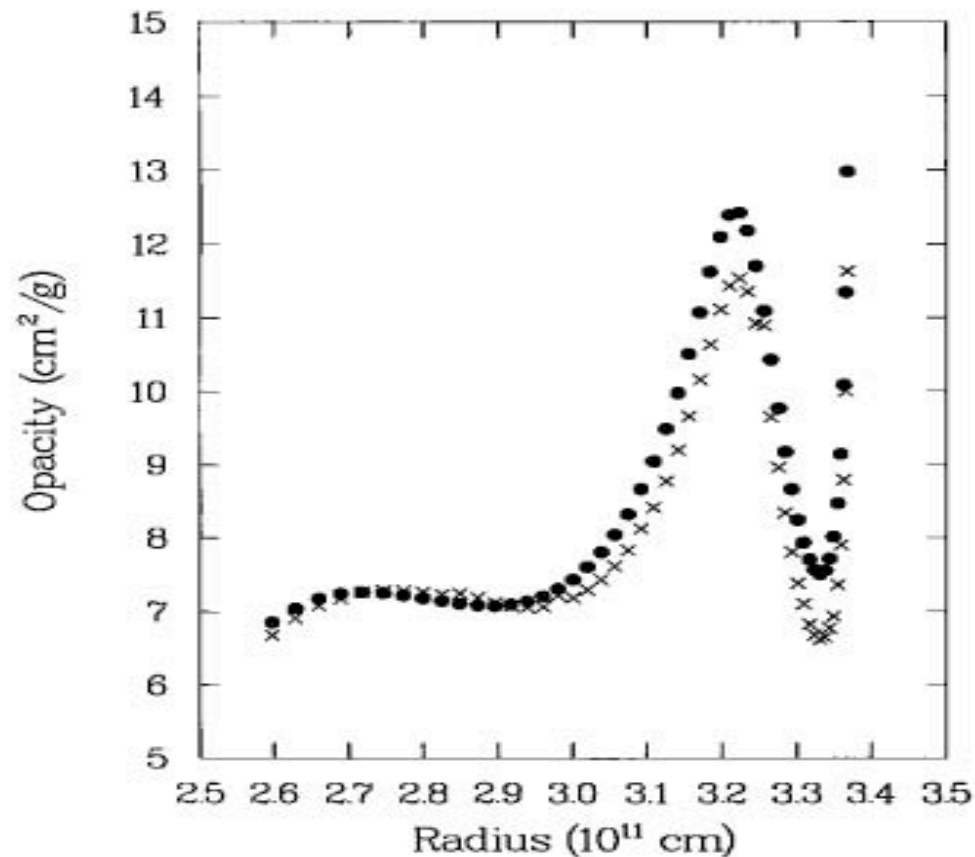


FIG. 2.—Opacity in the two models at $0.65 M_{\odot}$ is plotted vs. radius. The reduced opacity model is represented by crosses (x).

δ Scuti and Cepheid Instability Strip Blue Edges for Different Masses and Helium Abundance

Cox, King, & Tabor, ApJ, 1973

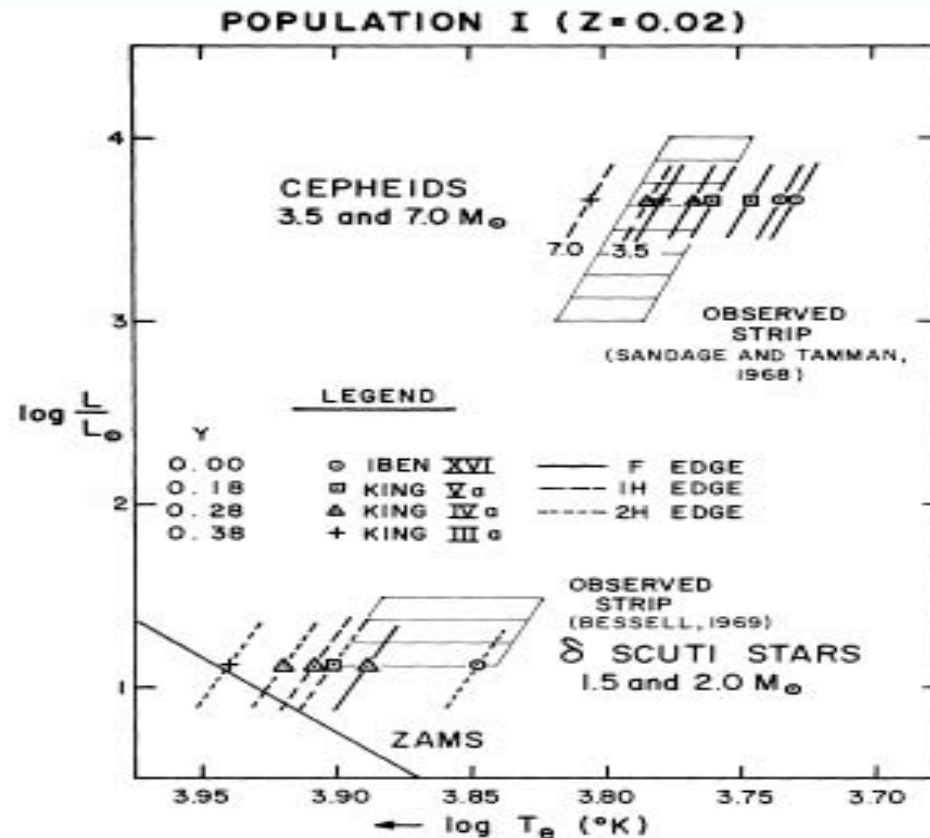


FIG. 5.—Theoretical blue edges for δ Scuti stars and Cepheids in the H-R diagram

Iron Abundance versus Mass Depth for 8 Effective Surface Temperatures for sdB Stellar Models

Charpinet, et al. ApJ, 1997

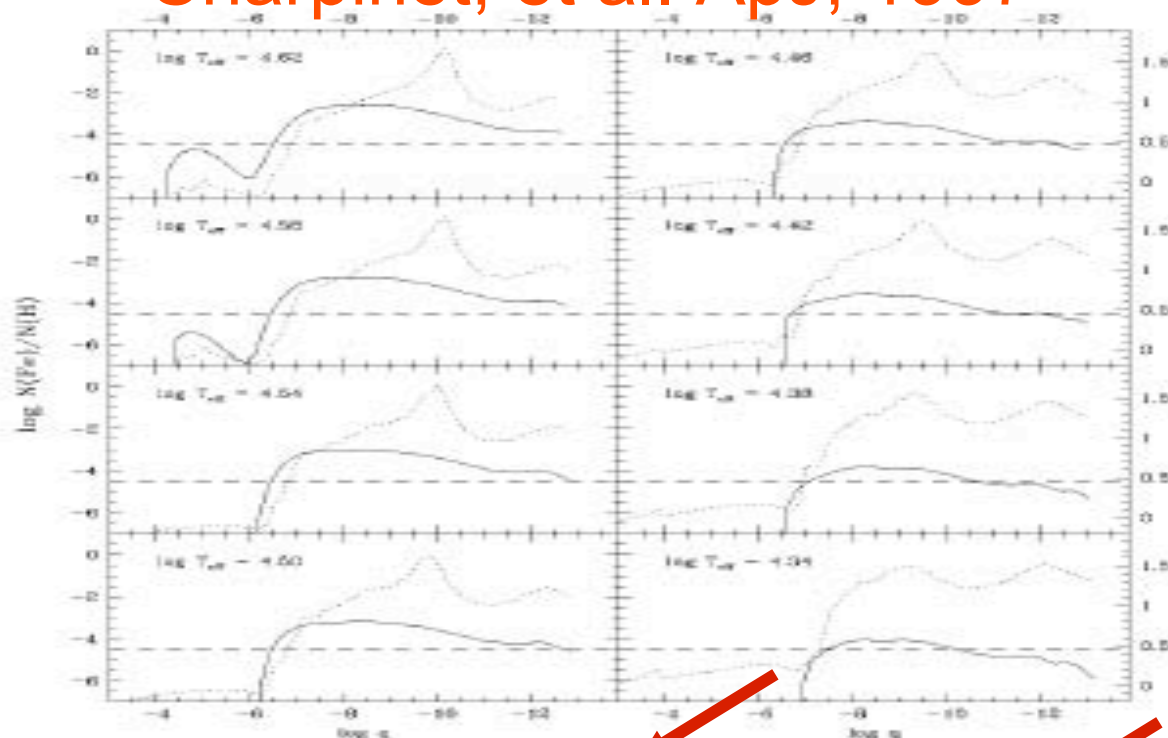


FIG. 1.—Equilibrium abundance of iron (solid curve) as a function of the fractional mass depth $\log q$ [$= \log (1 - M(r)/M_*)$] for a series of representative models of sdB stars with $M = 0.48 M_\odot$, $\log g = 5.8$, and $\log T_{\text{eff}}$ from 4.34 to 4.62 in steps of 0.04. In each panel the tip of the solid curve on the right hand side corresponds to the location of the Rosseland photosphere. The dashed horizontal line gives the normal value of the Fe/H number ratio. Also shown is the profile of the Rosseland opacity (dotted curve); its logarithmic value can be read on the right axis.

Solar Model Observed minus Calculated p-mode Oscillation Frequencies for High Degree

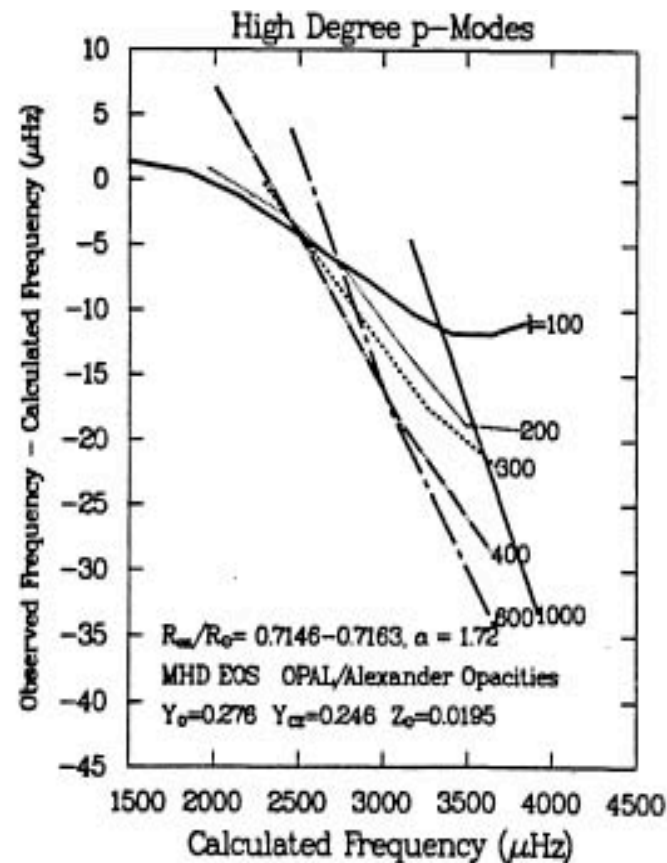


Figure 3. O-C vs. calculated p -mode frequencies of degree $\ell = 100, 200, 300, 400, 600$, and 1000 for MHD EOS solar model described in Fig. 1. Lines connect modes of same degree ℓ and different radial order n . Observations are from Libbrecht et al. (1990).

Solar Model Observed minus Calculated p-mode Oscillation Frequencies for 50% Opacity Increase

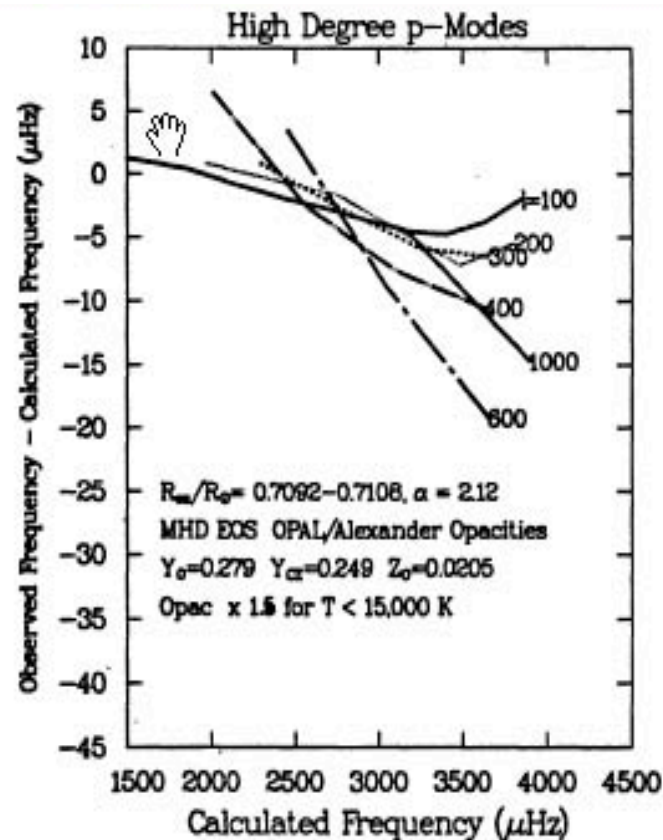


Figure 6: O-C vs. calculated p-mode frequencies of degree $\ell = 100, 200, 300, 400, 600$, and 1000 for MHD EOS model with 50% opacity increase for temperatures $< 15,000$ K. The opacity increase improves the agreement with observation for these high-degree modes (compare with Fig. 3).

Solar Model Observed minus Calculated p-mode Oscillation Frequencies for 50% Opacity Increase and Turbulent Pressure

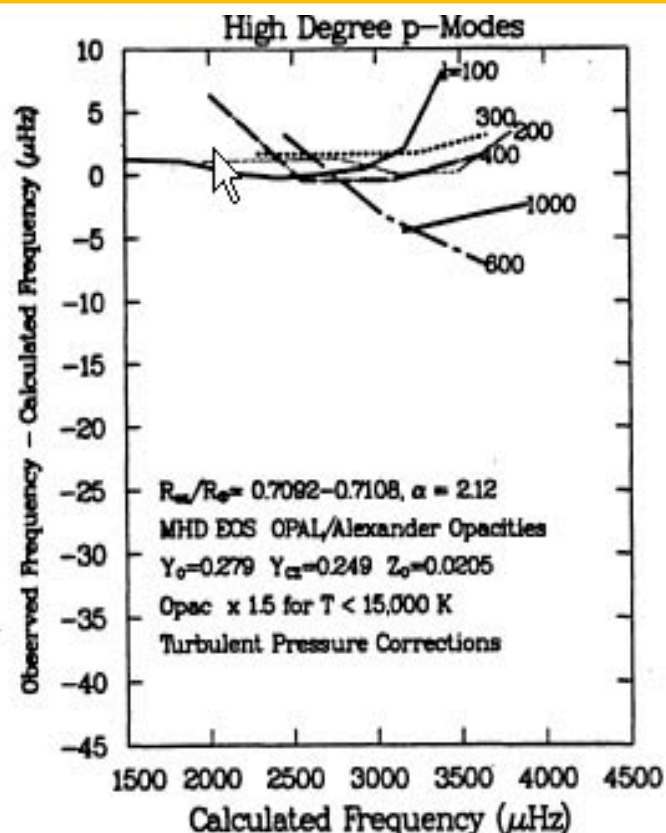
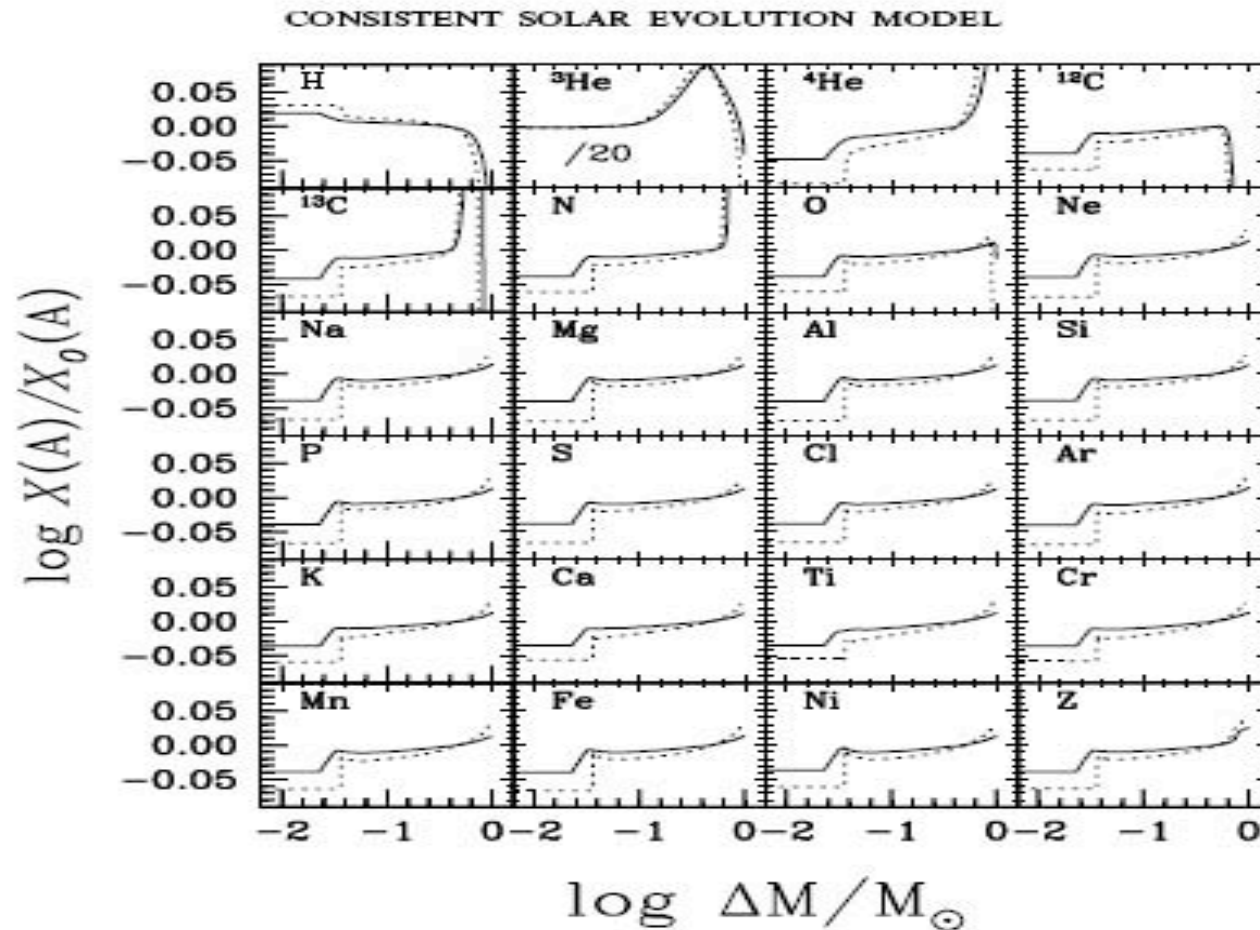


Figure 7. O-C vs. calculated p -mode frequencies of degree $\ell = 100, 200, 300, 400, 600$, and 1000 for MHD EOS model with 50% opacity increase for temperatures $< 15,000$ K, and including frequency corrections due to turbulent pressure as calculated by Guzik & Cox (1992). Turbulent pressure further improves agreement with observation for these high-degree modes.

Settling and Radiative Levitation of Solar Elements Using OPAL Monochromatic Data

Turcotte, Richer, Michaud, Igelesias, Rogers, ApJ, 1998



Surface Mass Fraction Composition of GW Virginis Model

observed $X_{\text{He}}=0.33$, $X_{\text{C}}=0.50$, $X_{\text{O}}=0.17$

$X_{\text{H}} = 0.02057$

$X_{\text{He}} = 0.43601$

$X_{\text{C}} = 0.16904$

$X_{\text{N}} = 0.000000000$

$X_{\text{O}} = 0.040694$

$X_{\text{Ne}} = 0.021265$

$X_{\text{Na}} = 0.00018440$

$X_{\text{Mg}} = 0.0033876$

$X_{\text{Al}} = 0.000016262$

$X_{\text{Si}} = 0.00014687$

$X_{\text{P}} = 0.00004010$

$X_{\text{S}} = 0.000051357$

$X_{\text{Cl}} = 0.0000043391$

$X_{\text{Ar}} = 0.000010271$

$X_{\text{Ca}} = 0.0000035543$

$X_{\text{Ti}} = 0.00000000000$

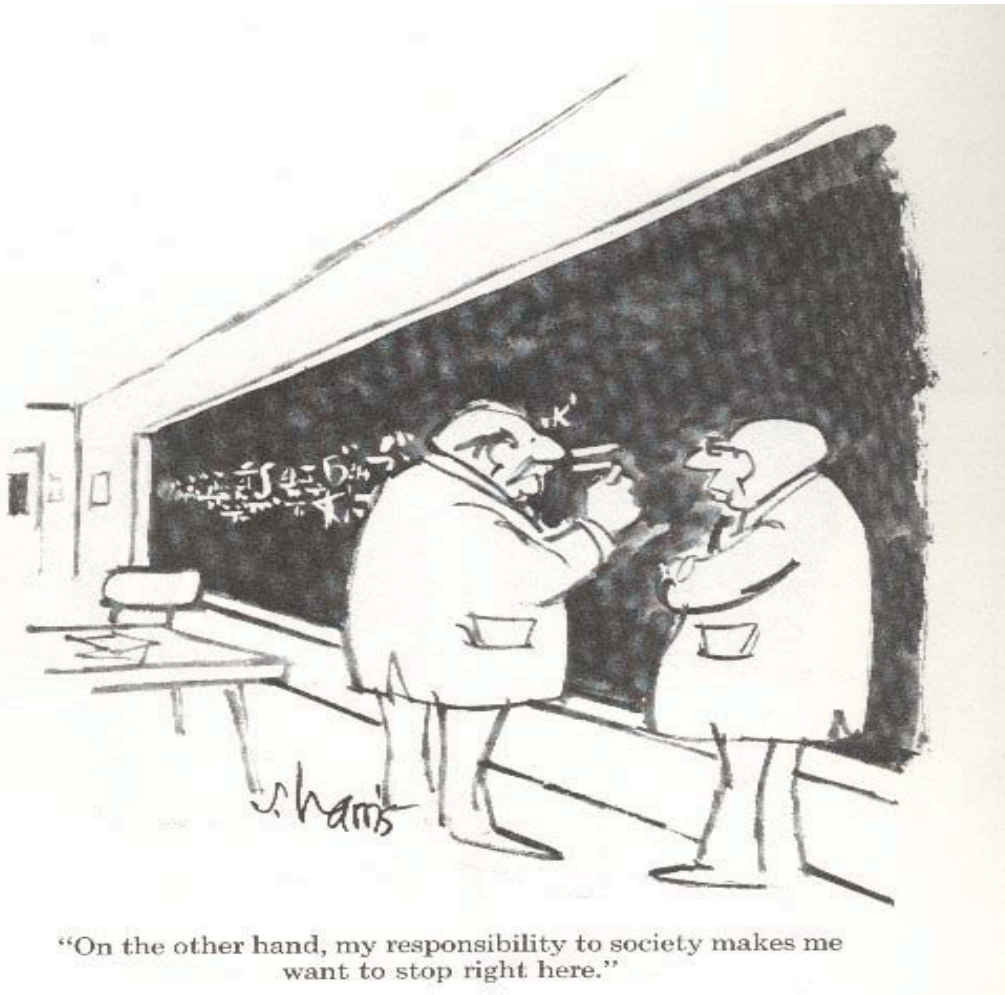
$X_{\text{Cr}} = 0.0000013147$

$X_{\text{Mn}} = 0.00000020743$

$X_{\text{Fe}} = 0.000073255$

$X_{\text{Ni}} = 0.000036881$

On the other hand, my responsibility to society makes me want to stop right here.



QMD Simulations of dense plasmas

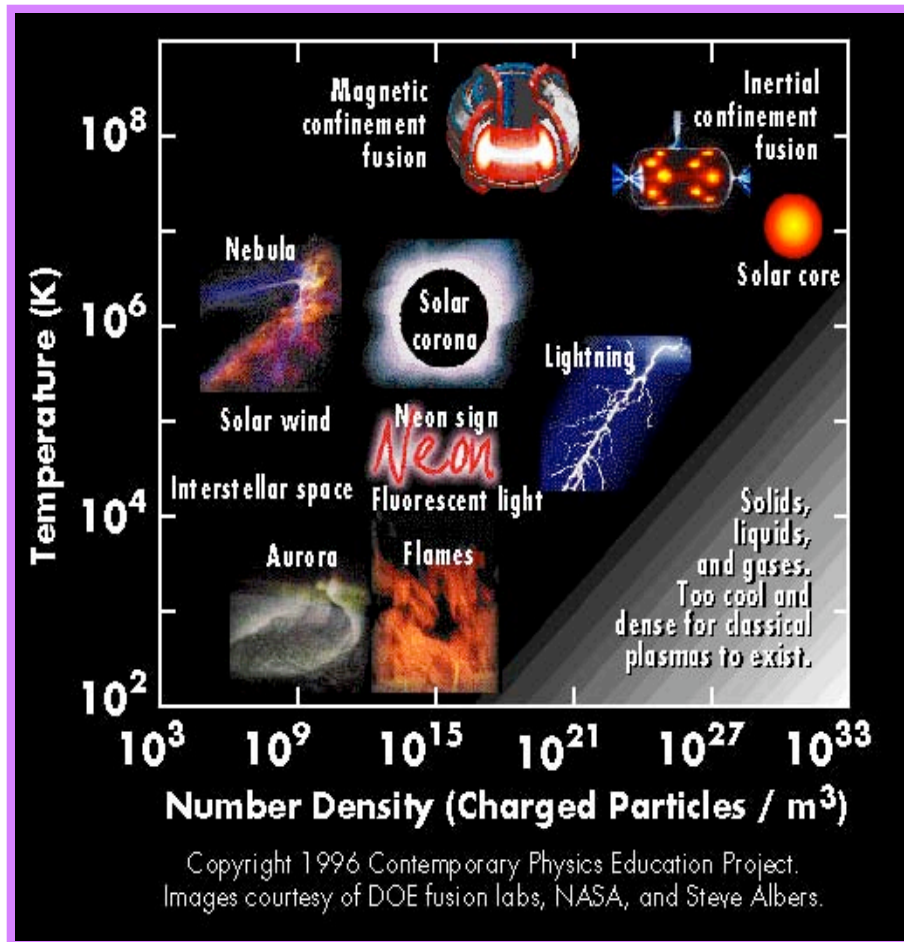
S. Mazevet

*Atomic and Optical Theory group
Theoretical Division
Los Alamos National Laboratory*

LAUR-05-1095



Warm dense matter



- High density

$$\rho = 10^{22-30} \text{ g/cm}^3$$

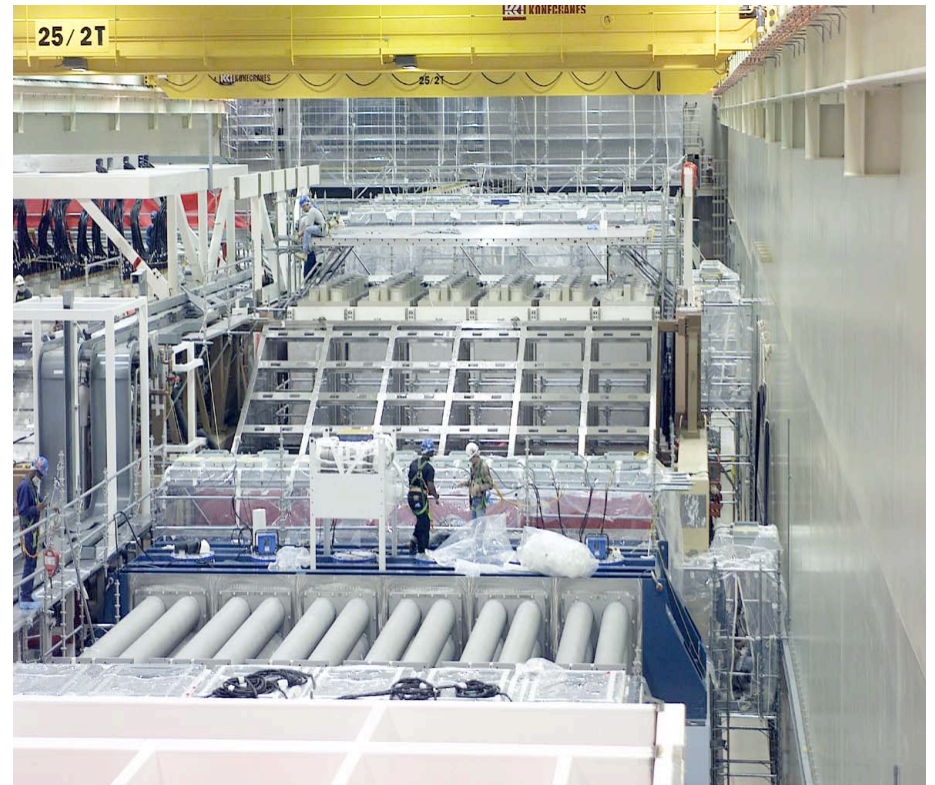
- Low temperature: few eV
- Quantum regime for the e-
- QMD applied to the physical properties of various systems in this regime
- Applications: stellar and planetary modeling, geology, stockpile stewardship

Warm dense matter experiments

2 stages gas-gun, LLNL



NIF, LLNL--Omega (Roch.)



Warm dense matter experiments

Z-pinch, Sandia NL



• **Dynamical experiments:**
Shock

• **Measurable quantities:**
Hugoniot points

$$(U_0 - U_1) + \frac{1}{2}(V_0 - V_1)(P_0 + P_1) = 0$$

**Variation of the internal energy,
pressure and temperature
between the initial and final shock
state**

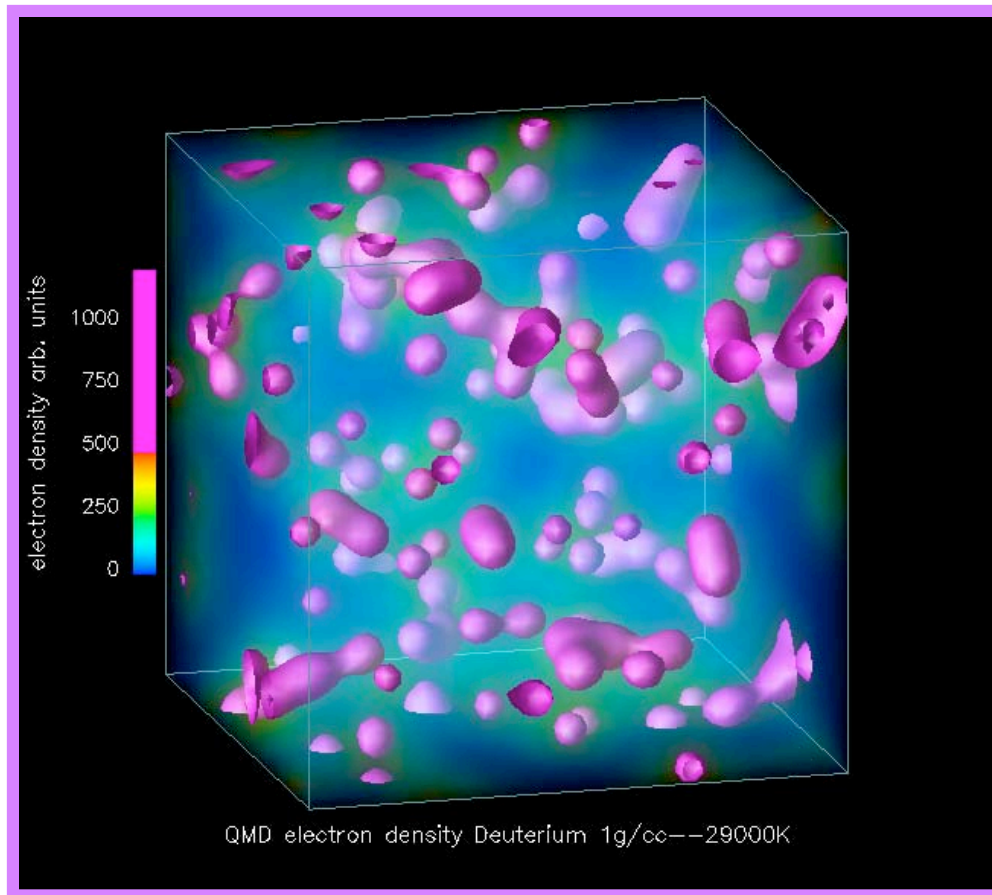
• **Conductivity, reflectivity**

Quantum Molecular Dynamics

- **3-D reference cell of N atoms+periodic boundary conditions**
- **Constant density and volume**
- **Born-Oppenheimer framework**
- **Treat the electrons fully Quantum Mechanically within the Density Functional framework**
- **Nuclei: solve classical equations of motion using the quantum mechanical forces**
- **Canonical and microcanonical ensembles**
- **Temperature effect: Finite-temperature density functional (Fermi-Dirac distribution) $T_e = T_i$**

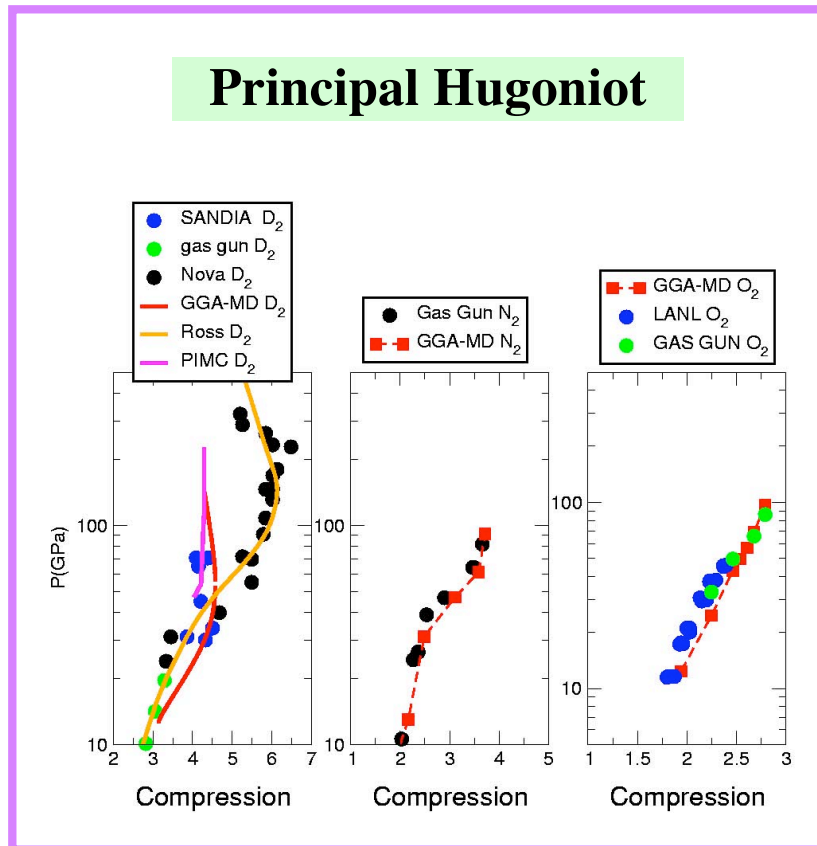


Transient effects



- Describe various species and mixtures
- Include various processes:
 - * ionization-recombination
 - * binding-dissociation of mol.
- Electron density for deuterium at 1g/cm^3 and $T=29000\text{K}$
- Provide a consistent set of optical electrical and material properties from the same simulation: experimental validation of the method

EOS of shocked diatomic fluids

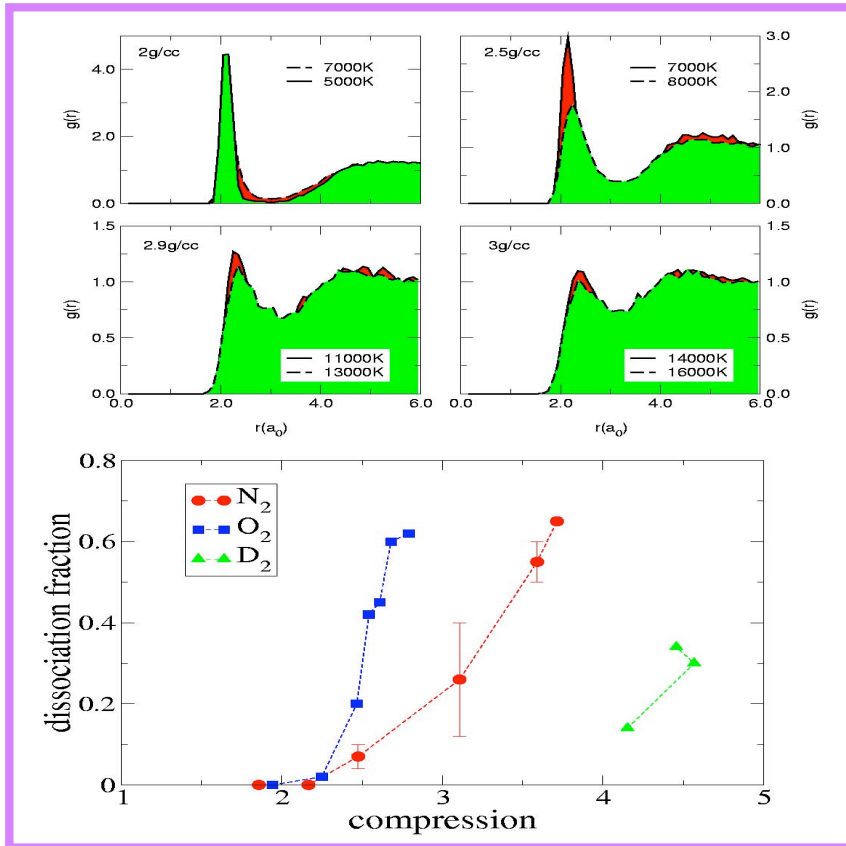


- For hydrogen QMD Hugo. is in good agreement with the SANDIA data but disagree with NOVA. QMD EOS agrees with PIMC EOS.

- Overall fair agreement with experimental data for three similar diatomic fluids.

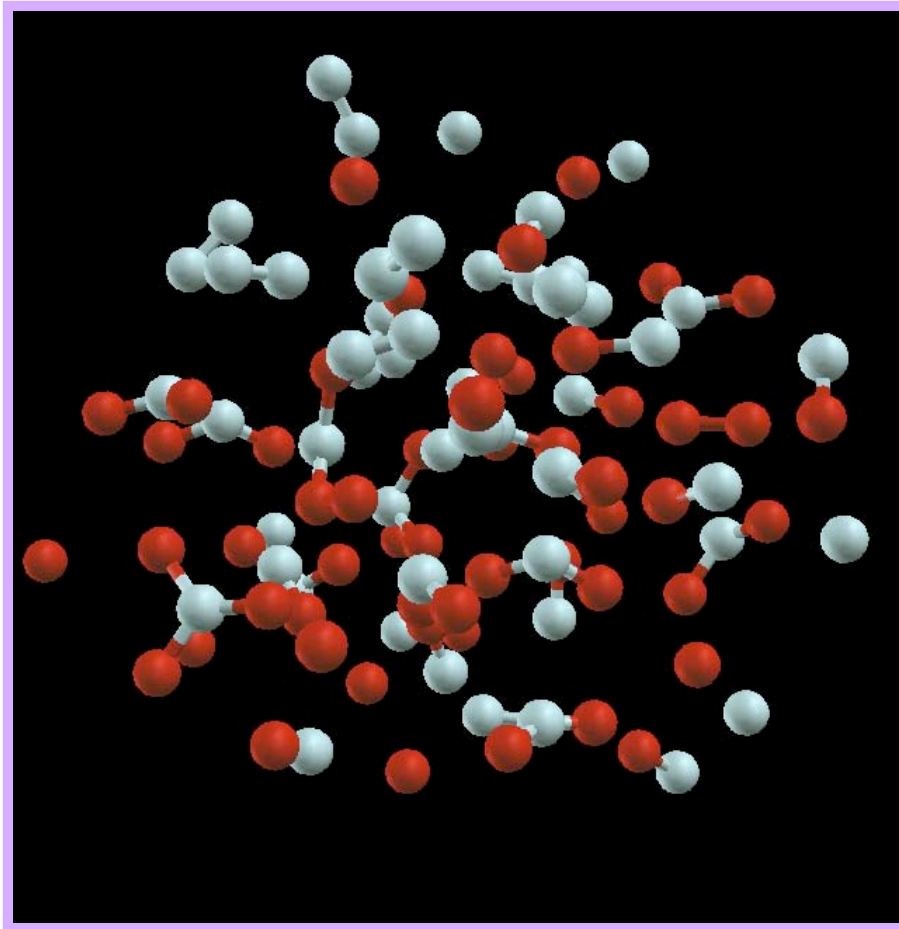
- Three species show inflection in the Hugoniot which relates to the continuous dissociation as the density increases.

$g(r)$ and dissociation fraction



- Dissociation can be quantified using the correlation function $g(r)$ and/or dissociation fraction
- Example: nitrogen $g(r)$ along the principal Hugoniot
- Cluster model where a molecule is defined as 2 atoms closer than a given radius: dissociation fraction (needs to be correlated with lifetime)
- The three fluids completely dissociate along the Hugoniots

Constituency Analysis on Shocked NO



- 2.38g/cm^3 $T=4,000\text{K}$
- Random Snapshot
- Grey: N Red: Oxygen
- Formation of N_2 molecules
- Formation of higher order structures.
- Good agreement between the QMD and exp. data for the Hugoniot

Electrical properties

- **Kubo-Greenwood:**

$$\sigma_1(\omega) = \frac{2\pi}{\Omega\omega} \sum_{ij} F_{ij} |D_{ij}|^2 \delta(\epsilon_j - \epsilon_i - \omega)$$

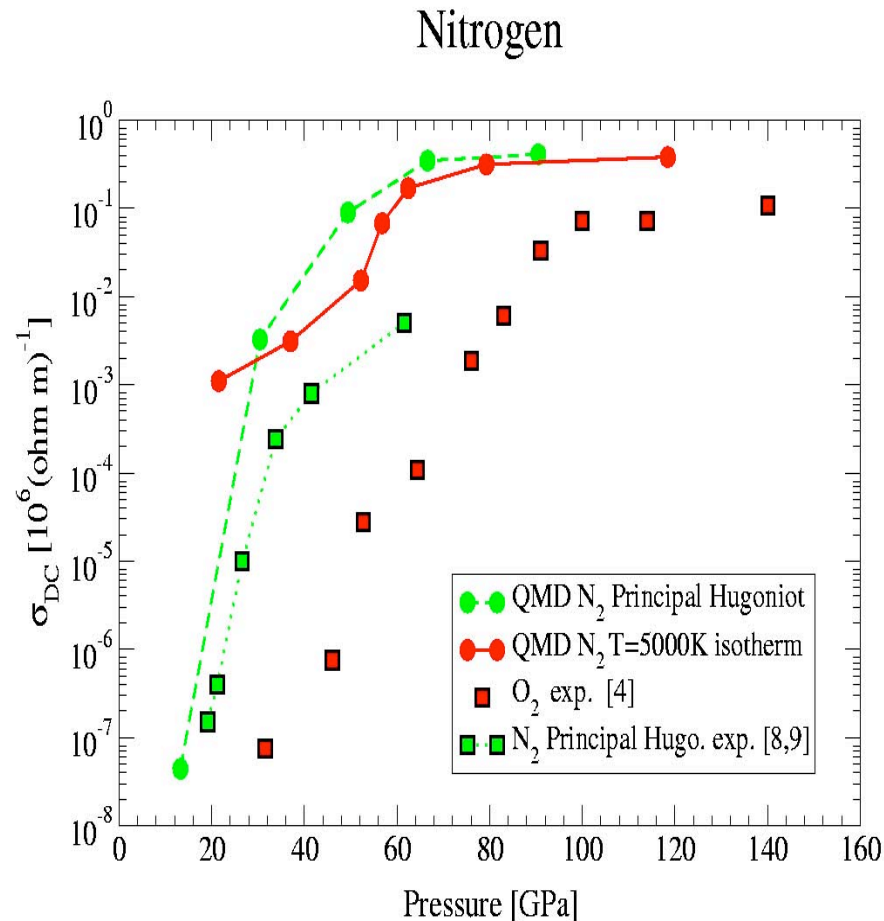
- **DC conductivity :**

$$\sigma_{DC} \equiv \lim_{\omega \rightarrow 0} \sigma(\omega)$$

- **Delta function replaced by a Gaussian**
- **Result depend on the width chosen**
- **Applied for a spatial configuration at a single time step**
- **Trajectory-averaged optical property given by:**

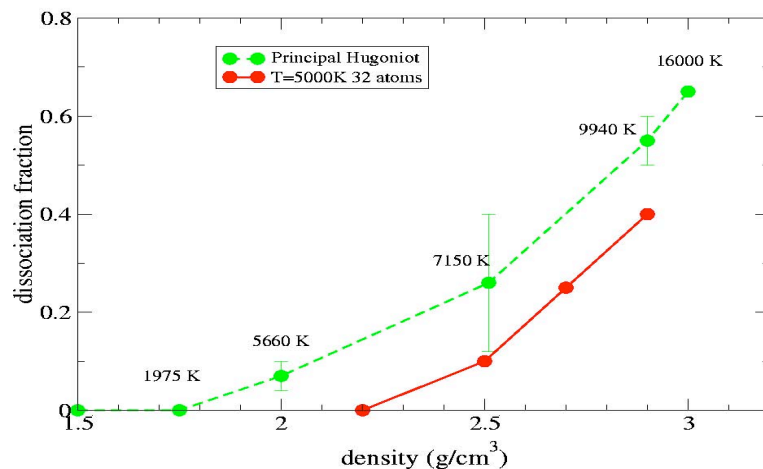
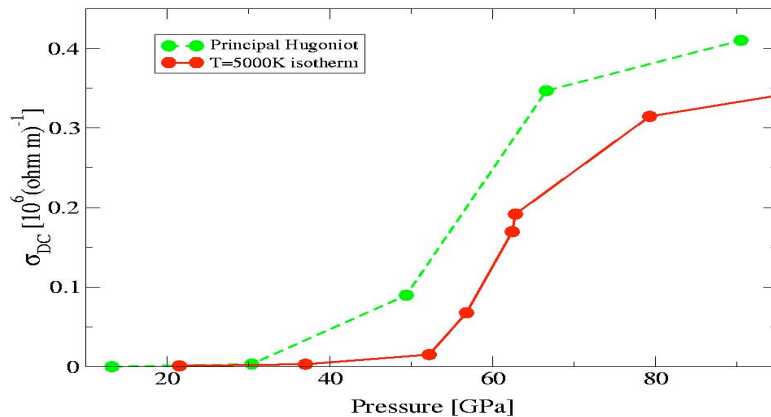
$$\sigma = \frac{1}{n_{\text{snap}}} \sum_{i=1}^{n_{\text{snap}}} \sigma_i$$

Nitrogen DC conductivity



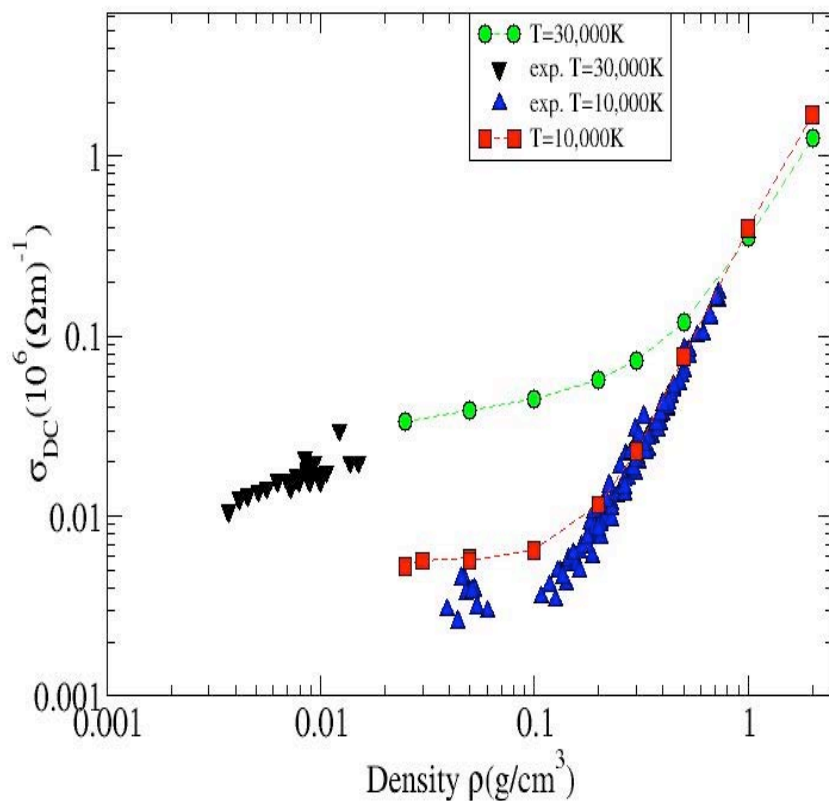
- N_2 exp. along principal Hugoniot
- O_2 experimental data obtained using multiple shock experiment to limit the temperature increase
- QMD along 5000K isotherm is representative of the second shock along the dissociation region and ring up experiment above 100GPa
- Qualitative agreement in the overall variation of the conductivity: non-metal to metal transition

Origin of the rise in conductivity



- Conductivity along the principal Hugoniot consistently higher than along the 5000K isotherm
- The increase in conductivity can be directly associated with the increase in dissociation fraction
- The conductivity “plateau” as soon as the fluid has completely dissociated
- The increase along the 5000K isotherm shows that the effect is driven by pressure where the atoms act as “dopants”

Aluminum Conductivity



- QMD M. Desjarlais PRE (2002)
- Exp De Silva PRE (1998)
- From liquid to dense plasma (2g/cm^3)
- EOS agrees well with SESAME
- Along each isotherms, variation of conductivity is well described
- Z_{bar} varies from 0.1 to 3 in agreement with LEDCOP

Optical properties

- **Kubo-Greenwood**

$$\sigma_1(\omega) = \frac{2\pi}{\Omega\omega} \sum_{ij} F_{ij} |D_{ij}|^2 \delta(\epsilon_j - \epsilon_i - \omega)$$

- **Kramers-Kronig relations lead to**

$$\sigma_2(\omega) = -\frac{2}{\pi} P \int \frac{\sigma_1(\nu)\omega}{(\nu^2 - \omega^2)} d\nu$$

- **Dielectric functions**

$$\epsilon_1(\omega) = 1 - \frac{4\pi}{\omega} \sigma_2(\omega)$$

$$\epsilon_2(\omega) = \frac{4\pi}{\omega} \sigma_1(\omega)$$

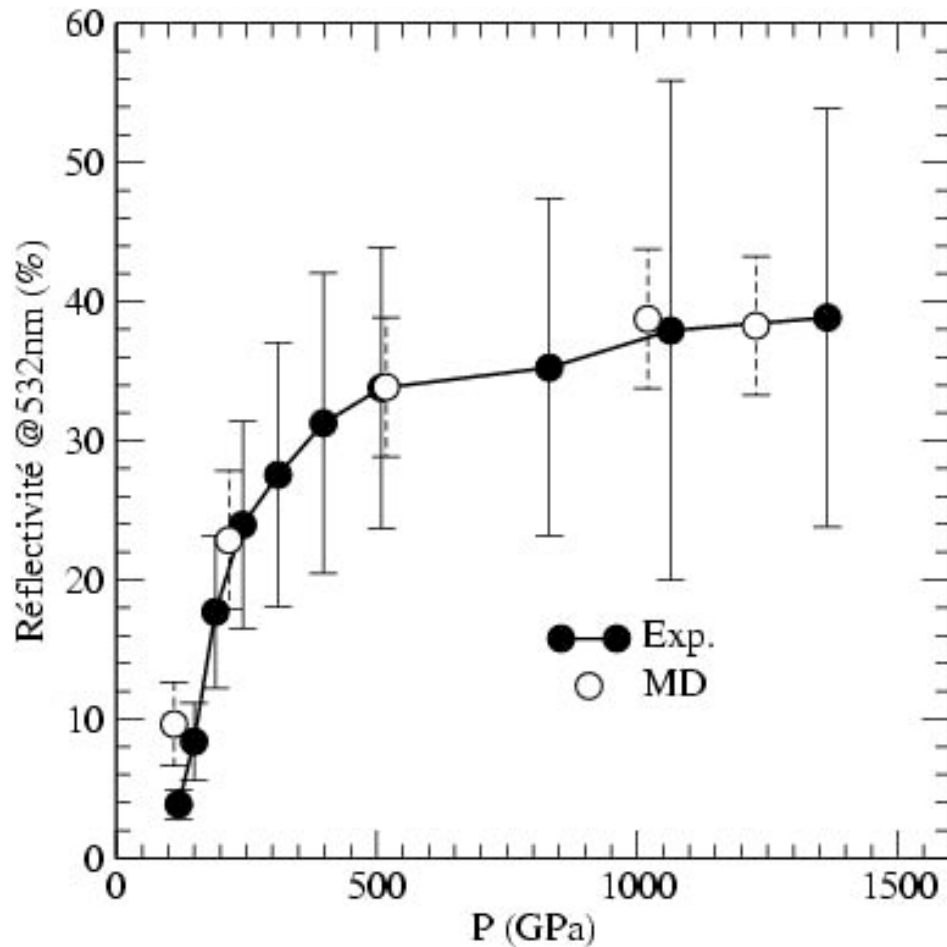
- **Leads to index of refraction, reflectivity and absorption coefficient**

$$\alpha(\omega) = \frac{4\pi}{n(\omega)c} \sigma_1(\omega)$$

$$n(\omega) = \sqrt{\frac{1}{2} [|\epsilon(\omega)| - \epsilon_1(\omega)]}$$

$$r(\omega) = \frac{[1 - n(\omega)]^2 + k(\omega)^2}{[1 + n(\omega)]^2 + k(\omega)^2}$$

SiO₂ reflectivity



SiO₂ among the best known insulator (LiF and Al₂O₃) and important for geophysics

Measurements at omega (Hicks et al.) CEACAM 2003

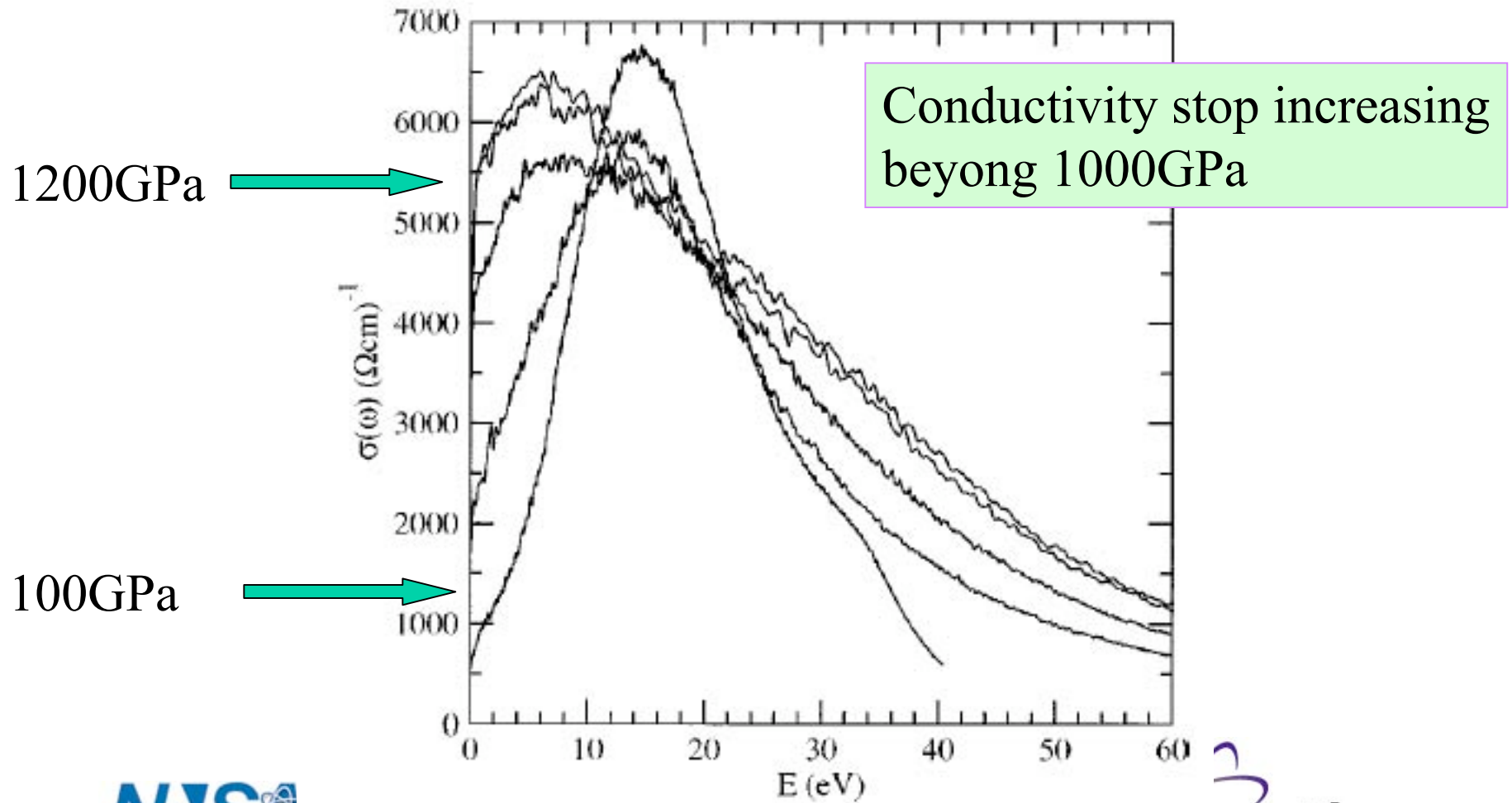
Metallic state above 500GPa

EOS agrees with SESAME and QMD.

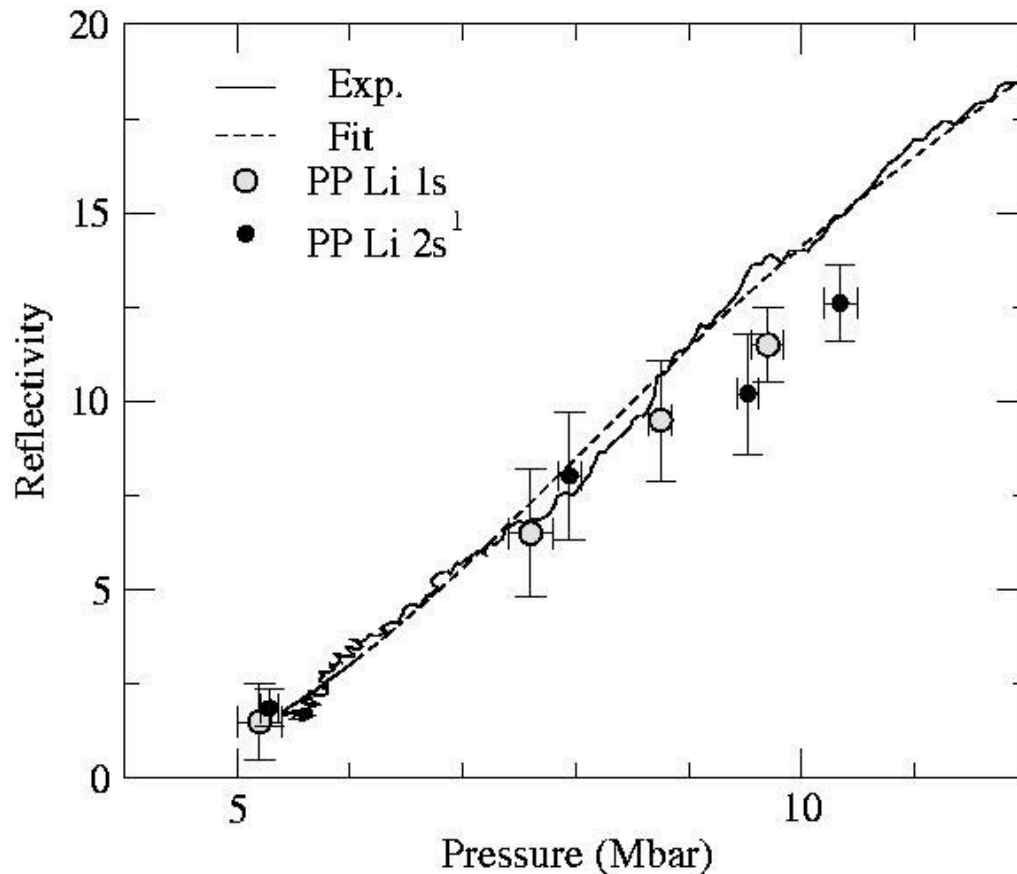
Good agreement with QMD

SiO₂ optical conductivity

Non Drude like up to the highest pressure



Shocked LiF



- LiF is an ionic crystal
- Standard window in shock exp.
- Exp Fe reflectivity upon melt
- Steady increase in reflectivity as the crystal melts
- Thermal excitation across a reducing band gap fails with Hicks model
- Shows that the failure is due to the SESAME EOS

Rosseland mean opacity

- **Rosseland Mean Opacity**

$$\frac{1}{\kappa_{Rosseland}} = \int_0^{\infty} d\nu \frac{B'(\nu, T)}{\alpha(\rho, T, \nu)}$$

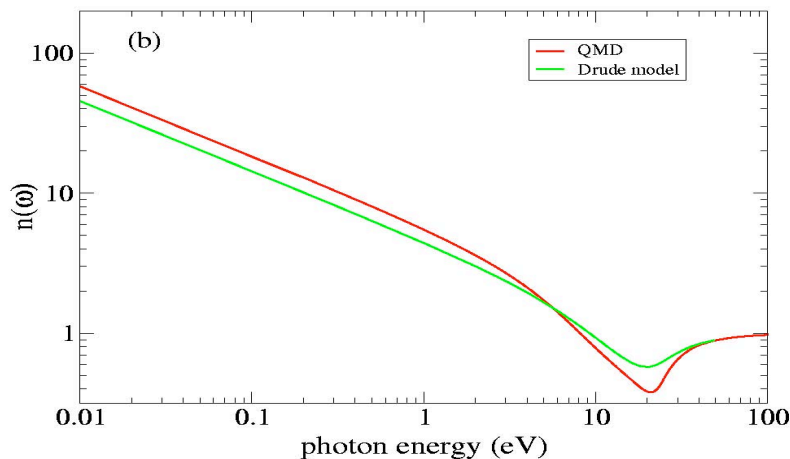
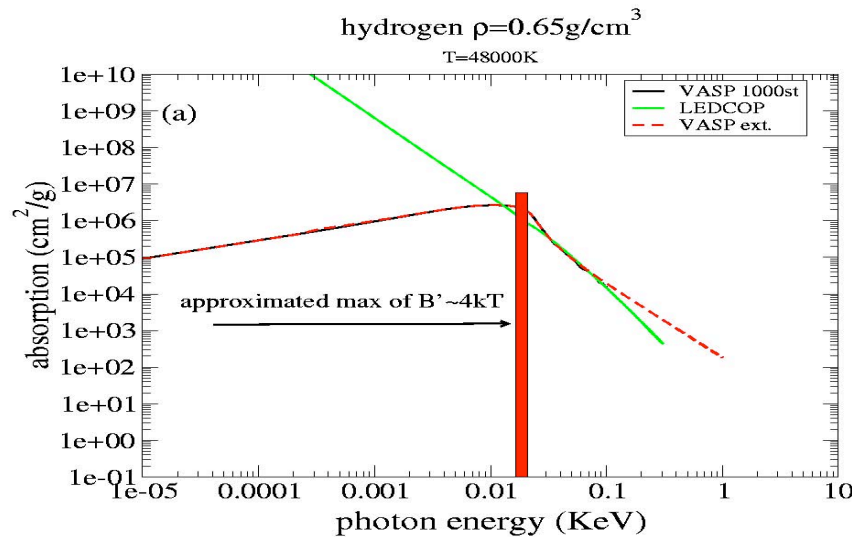
$B'(\nu, T)$ is the derivative of the Planck function

$\alpha(\rho, T, \nu)$ is the absorption coefficient

- **With QMD need to extrapolate the high photon behavior**

- **Various approximations are used: including $n^3(\omega)$ and ω_p**

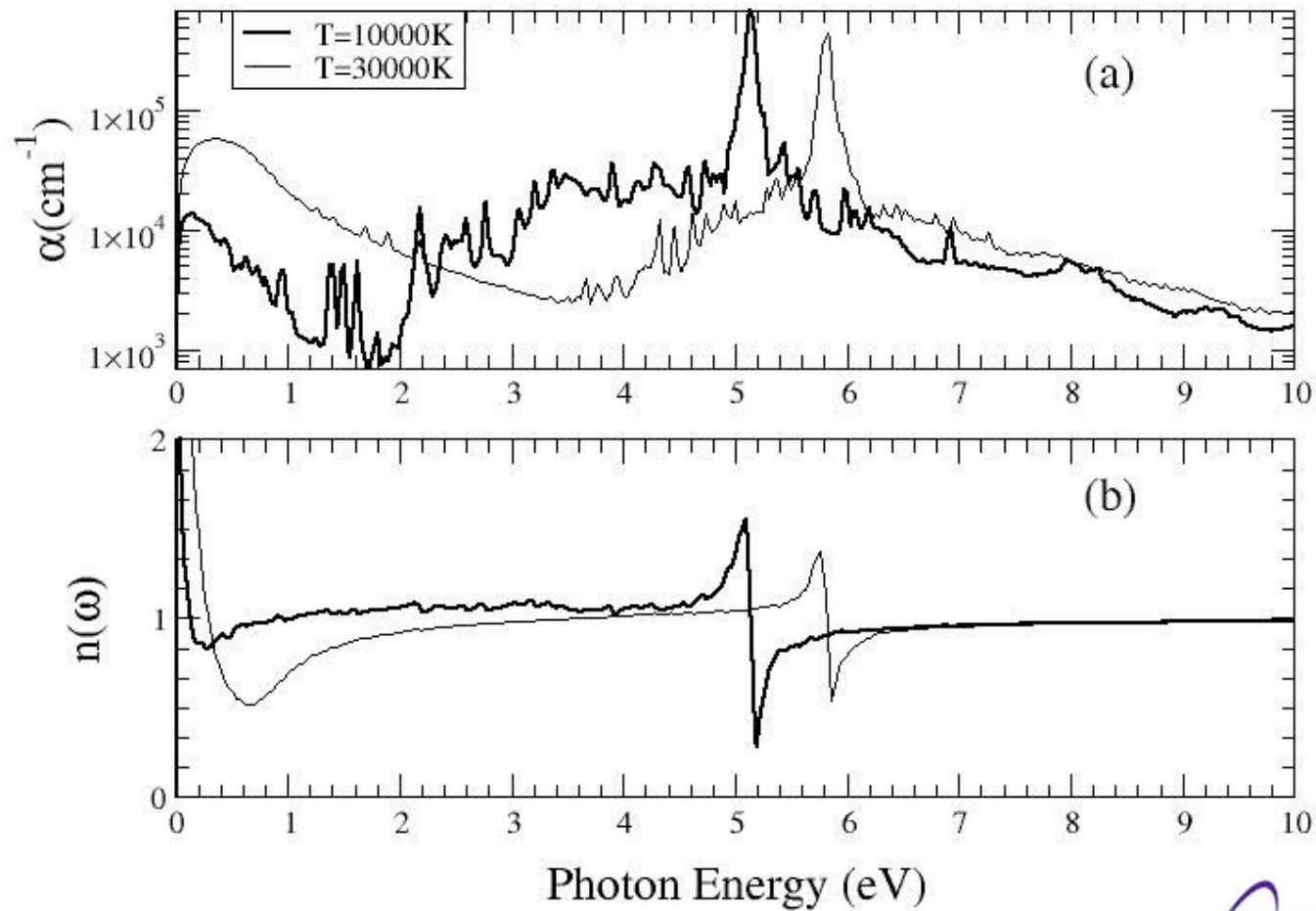
absorption coefficient



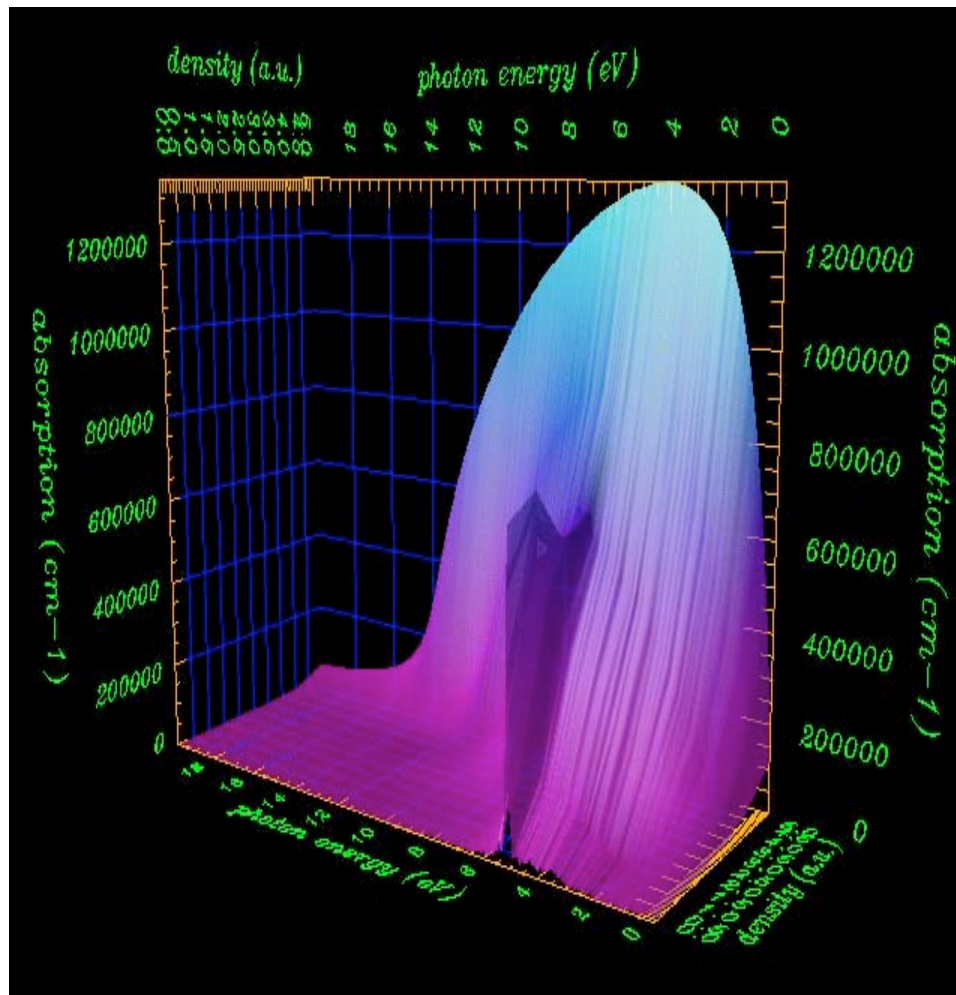
- Regime where hydrogen is a completely ionized plasma
- Absorption compares well to LEDCOP except at low photon energy
- Below 10eV does not agree with the modeling code due to the Kramer's relation for the free-free
- Needs to match the DC conductivity at zero frequency

Al absorption coefficient

$$\rho = 0.025 \text{ g/cm}^3$$

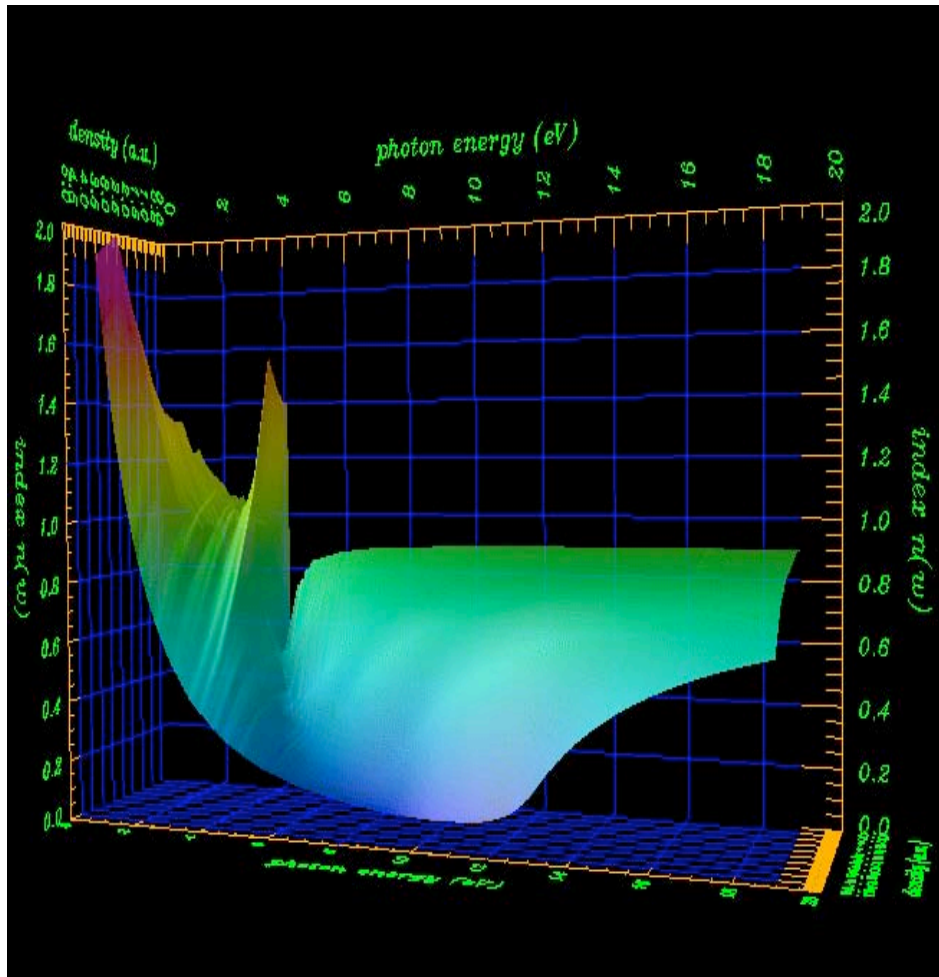


Aluminum absorption coefficient



- Aluminum at fixed temperature $T=10000\text{K}$ and density from 2g to 0.025g/cm^3
- As the density decreases appearance of the 3s-3p inner shell transition of atomic aluminum
- Transition positioned at 5eV
- Average atomic configuration for 3s-3p transition at 5.08eV !

Aluminum index of refraction



- Low density limit

$$\epsilon(\omega) = 1 + \frac{4\pi N e^2}{m} \sum_i \frac{f_i}{(\omega_i^2 - \omega^2 - i\Gamma_i \omega)}$$

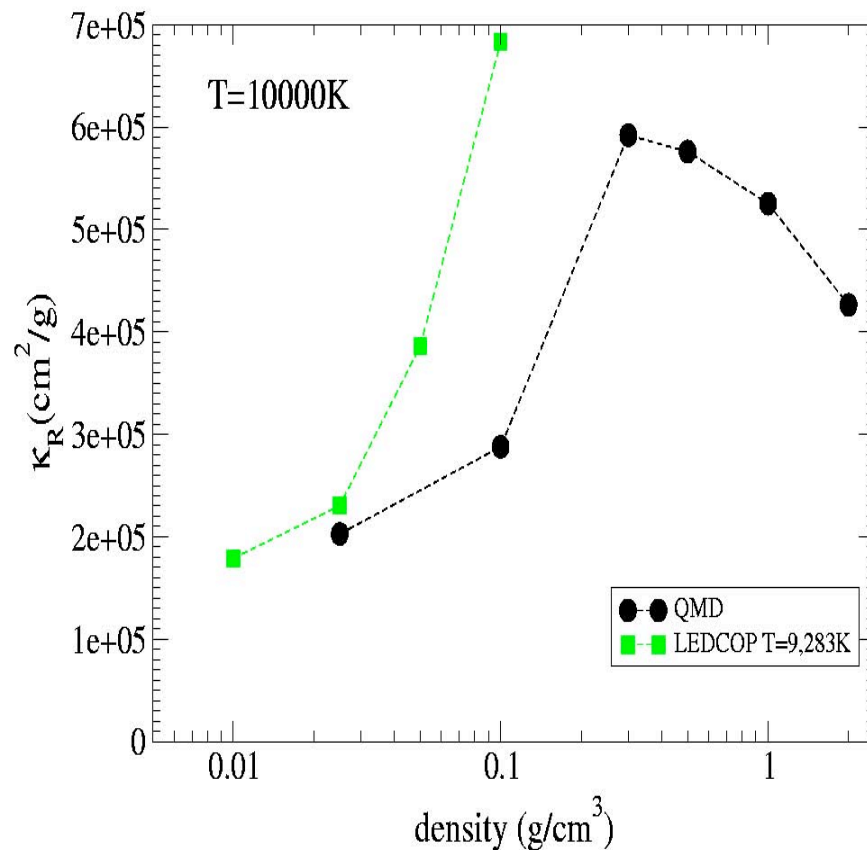
- High density limit

$$\epsilon(\omega) = 1 - \frac{\omega_p^2}{\omega(\omega + i\nu_D)}$$

- Encompass within the same method various regimes from atomic to plasma states
- Bloch functions: bands width Increase as a function of density

Comparison of the Rosseland mean for Aluminum

Pressure ionization



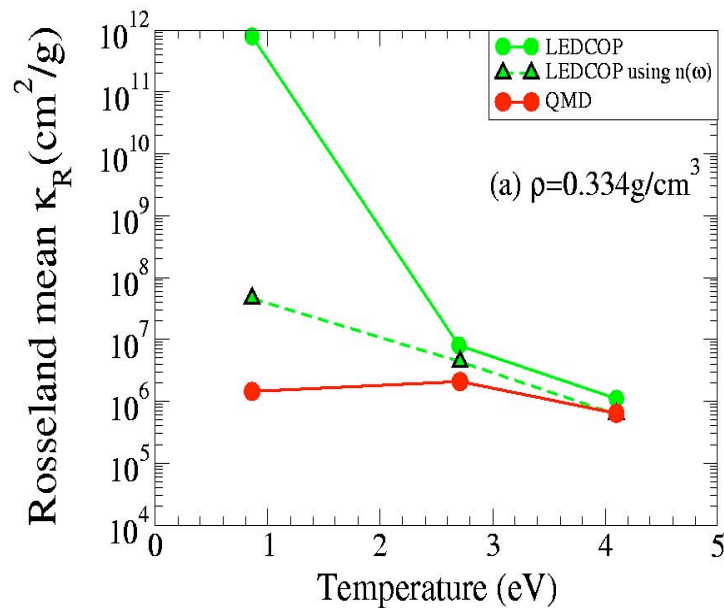
Conductivity data (Desjarlais et al. PRE 2002) in good agreement with experimental data

Divergence in the opacity code LEDCOP due to the pressure ionization model for both the EOS and the bound-free description

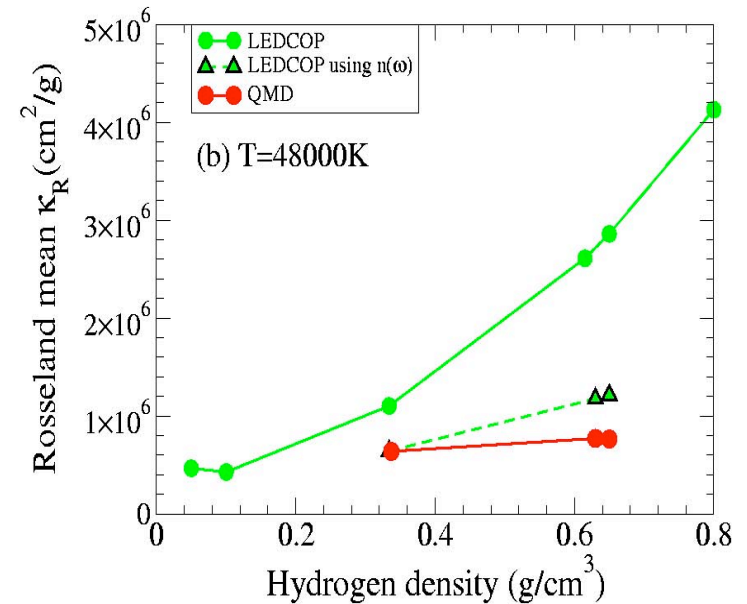
Provide a benchmark for modeling codes

Comparison of the Rosseland mean for hydrogen

Fixed density, increasing temp.

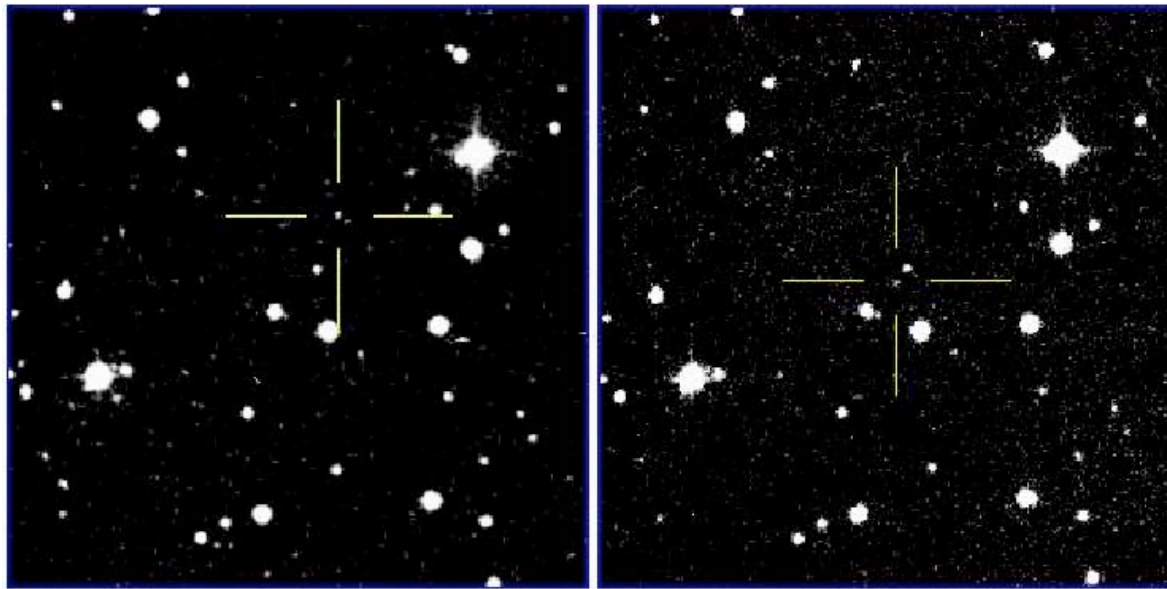


Fixed temp., increasing density



White Dwarf Atmospheres

White dwarf populations could be used for cosmochronology
Biggest uncertainties lie in the optical properties of the outer atmospheres composed of helium and hydrogen-helium mixtures



He:

$$\rho < 2 \text{ g/cm}^3$$

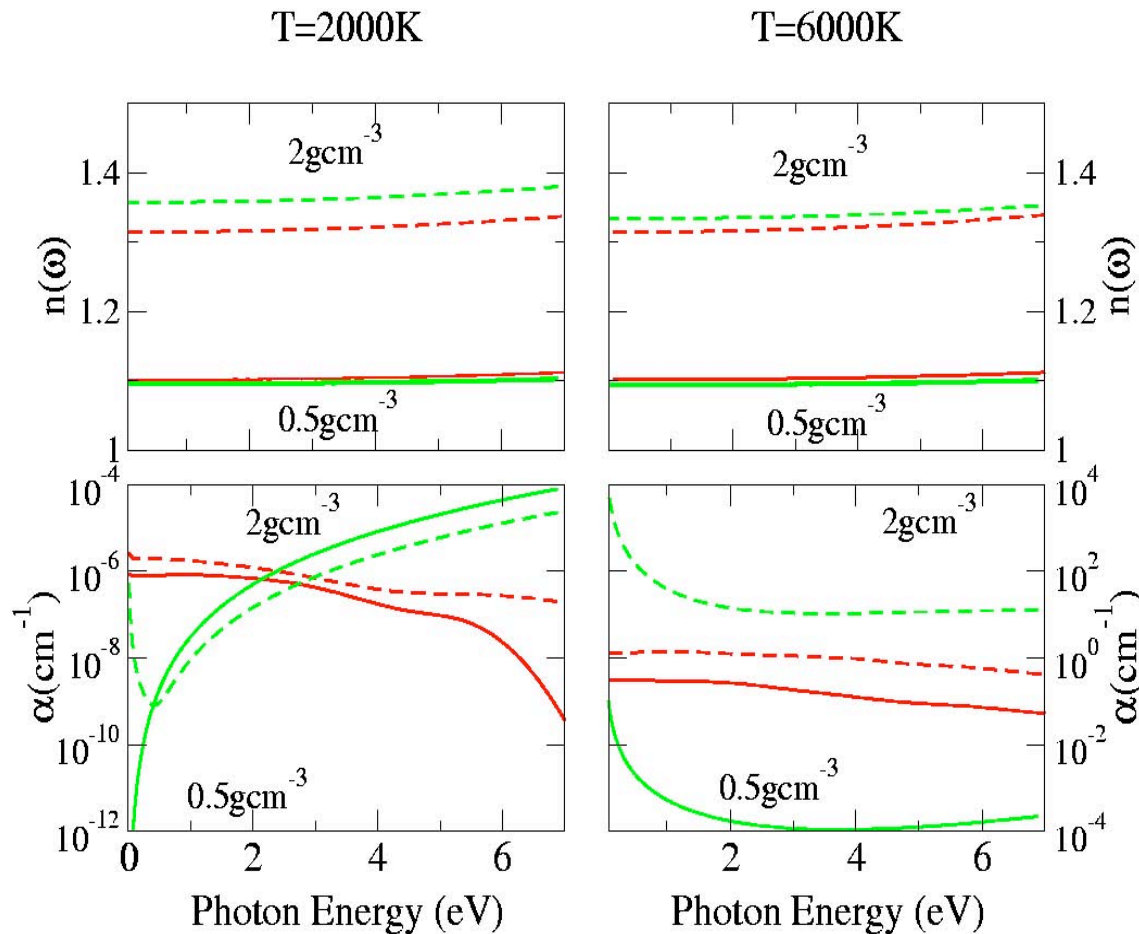
$$T < 1 \text{ eV}$$

1951

1987



Helium opacities



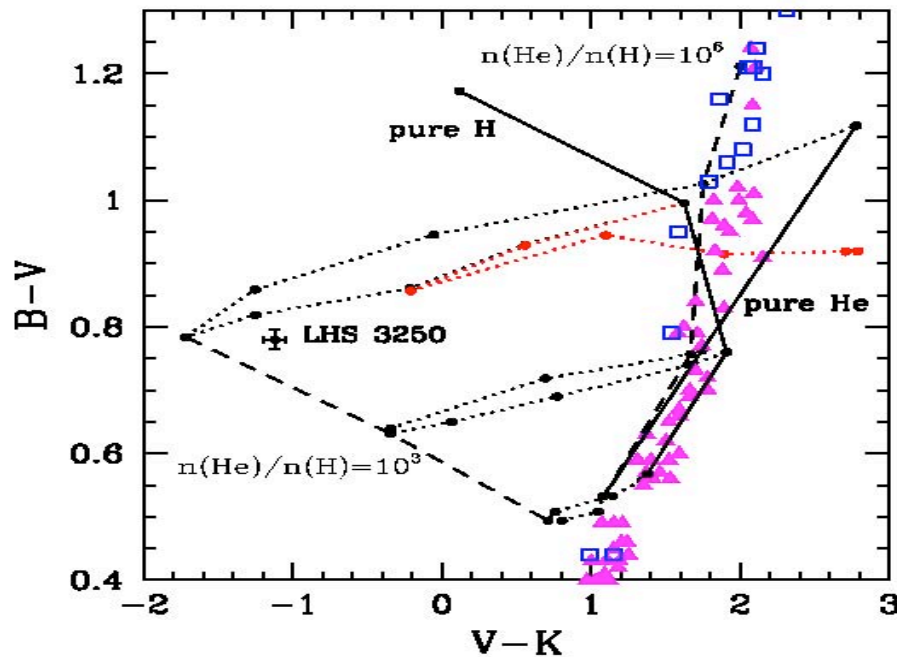
Good agreement with gas gun EOS and chemical model

Good agreement for the index of refraction

Orders of magnitude difference when compared with atomic opacities
Iglesias, Rogers, Saumon
Ast. J. (2002)

White dwarf populations

Preliminary atmosphere calculations indicate that pure helium white dwarfs may not be as common as thought before
Consistent with stellar evolution models



Experiments at Omega and in Russia

Gap underestimated by 2-3eV (10%) using GGA. (hybrid)

Thermal conductivity

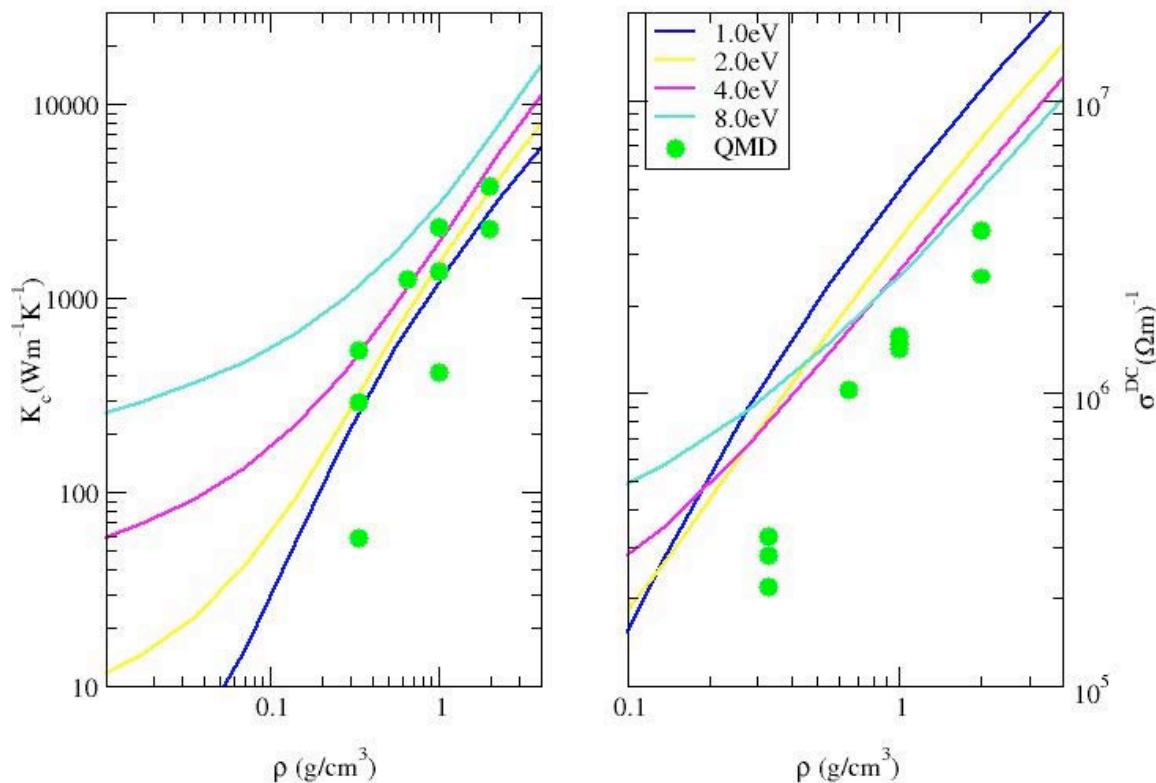
Maybe the most used but less known of the transport properties
Hubbard-Lampe model is used in most opacity codes

$$\begin{aligned} \langle j \rangle &= \frac{1}{e} \left(e L_{11} E - \frac{L_{12} \nabla T}{T} \right) \\ \langle j_q \rangle &= \frac{1}{e^2} \left(e L_{21} E - \frac{L_{22} \nabla T}{T} \right) \\ L_{ij} &= (-1)^{i+j} \int d\varepsilon \sigma(\varepsilon) (\varepsilon - \mu)^{(i+j+2)} \left(-\frac{\partial f(\varepsilon)}{\partial \varepsilon} \right) \end{aligned}$$

Chester-Tellung-Kubo-Greenwood formulation

Thermal conductivity

Sesame tables for hydrogen: model of Rinker



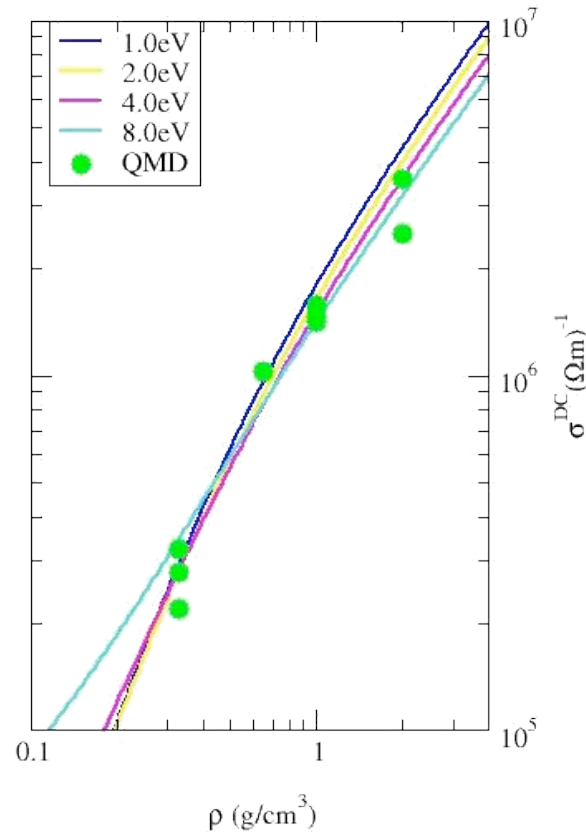
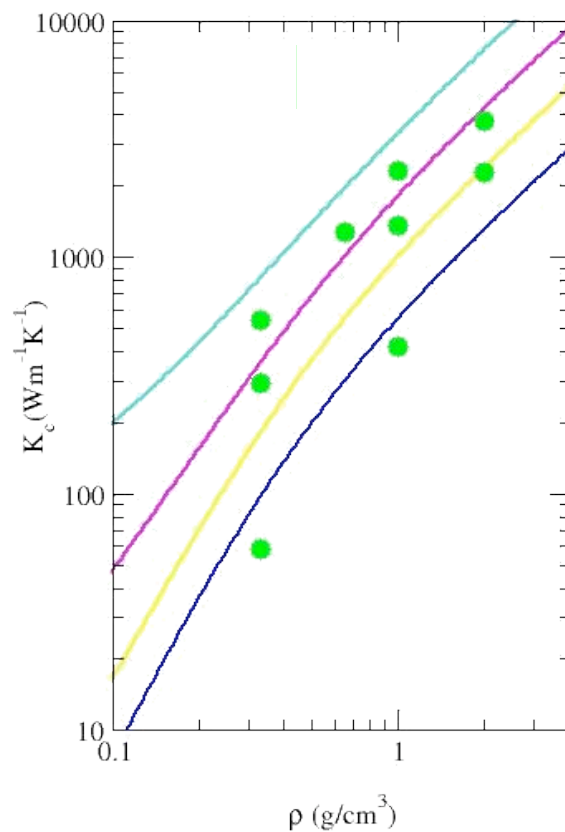
High density low temperature:
Weidman -Franz law

Deviation to the WF
as the temperature
increases

L/L0 increases before
reaching the low
density limit

Thermal conductivity

Model of Kitamura and Ichimaru: fit for $1 < Z < 26$



Overall good agreement with QMD for both the hydrogen electrical and thermal conductivities in the warm dense matter regime

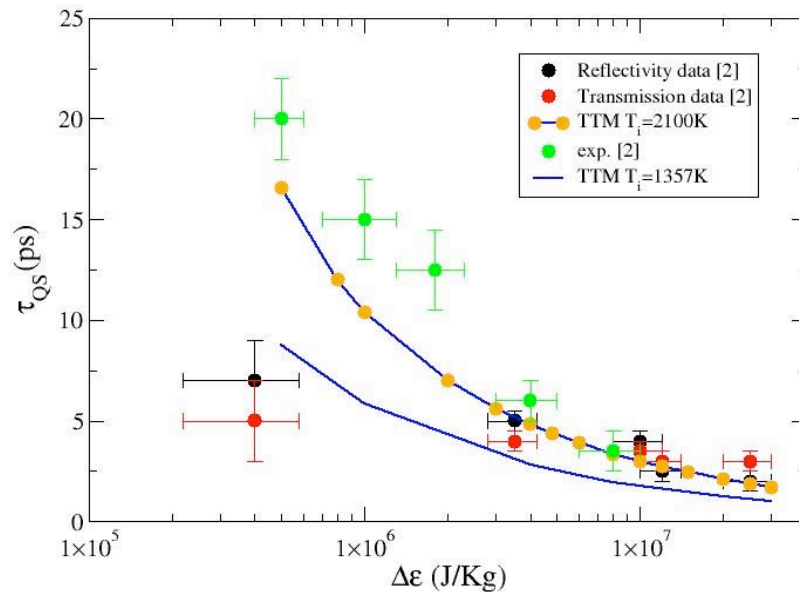
Should be used in opacity code ATOMIC

Optical conductivities of warm dense gold

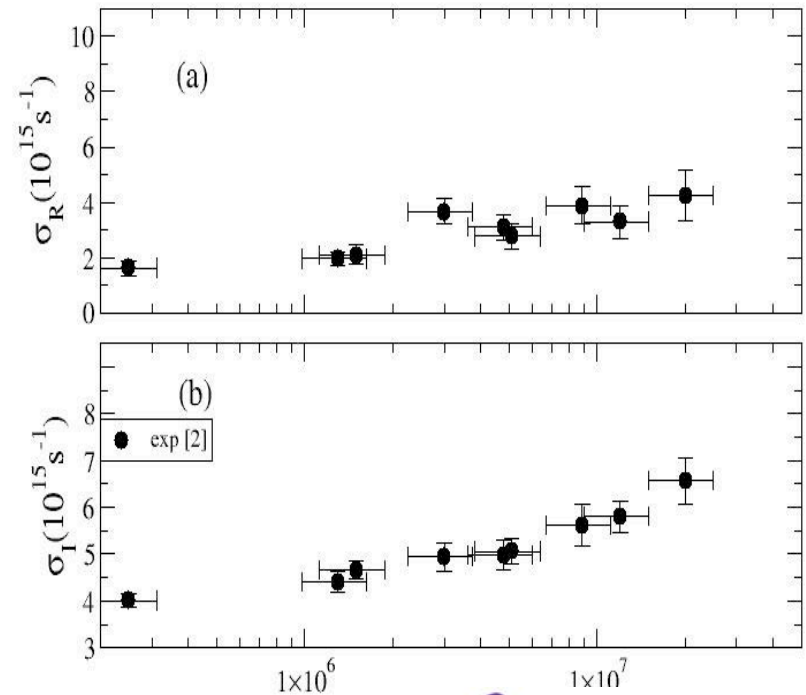
Conductivities of warm dense metal by measuring time resolved optical properties after laser illumination of metallic thin films

A. Ng group LLNL (PRL 2004)

Quasi steady state



Conductivities at 1.54eV



Can ab-initio method be used?

Non-equilibrium situation $T_e > T_i$.

Evolution of the lattice structure: fcc to liquid to expanding system.

Needs to be followed in time for several ps.

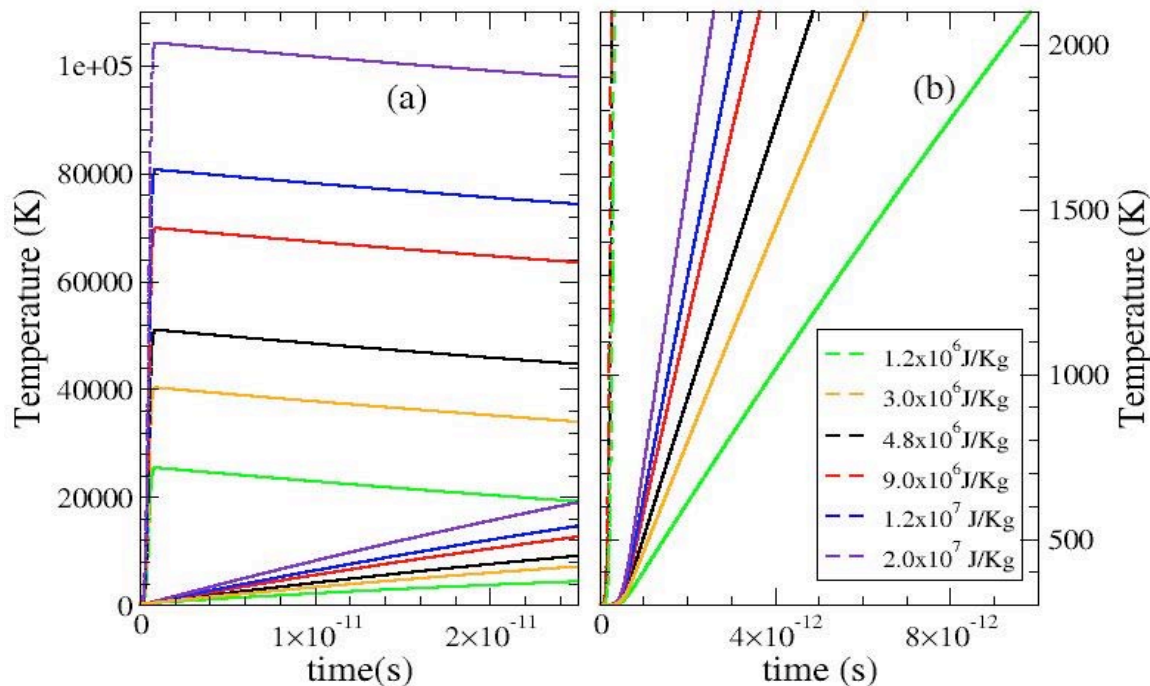
Energy exchange between electrons and ions is purely a non-adiabatic effect. Electron-phonon coupling varies as a function of T_e and time. QMD uses BO

Is the melting caused by change in ion potential as for silicon or e-phonon or both?

Two temperature model

$$C_e(T_e) \frac{\partial T_e}{\partial t} = \nabla [K_e(T_e) \nabla T_e] - g(T_e - T_i) + S(t)$$

$$C_l(T_i) \frac{\partial T_i}{\partial t} = \nabla [K_l(T_i) \nabla T_i] + g(T_e - T_i)$$



$$K_l = 0$$

$$K_e = 0$$

$$C_e = A_e T_e$$

$$A_e = 71 J m^{-3} K^{-2}$$

$$g = 2.1 \times 10^{16} W m^{-3} K^{-1}$$

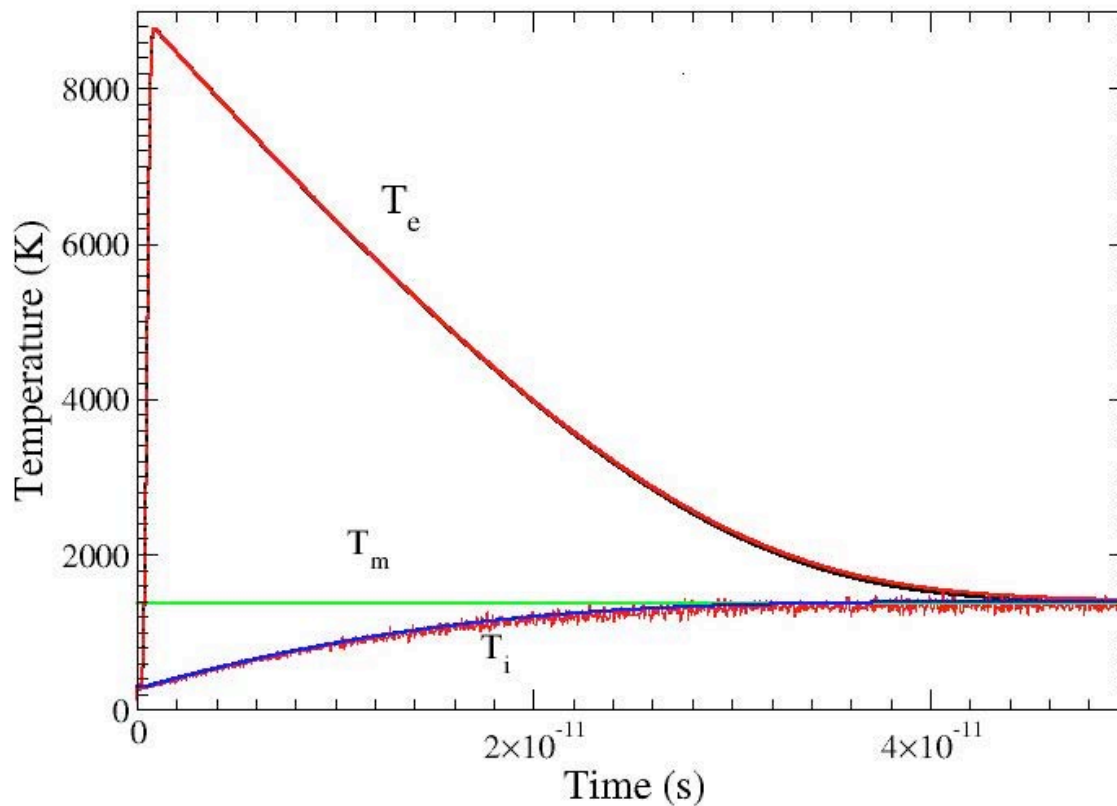
$$C_l = 2.4 \times 10^6 J m^{-3} K^{-1}$$

Hybrid classical MD

Mix the continuum model with MD

Ivanov et al. PRB 2003

Classical glue model for gold



$$m_i \frac{d^2 r_i}{dt^2} = F_i + \zeta m_i v_i$$
$$\zeta = \frac{gV(T_e - T_i)}{\sum_i m_i v_i}$$

T_e and T_i closely follow TTM model

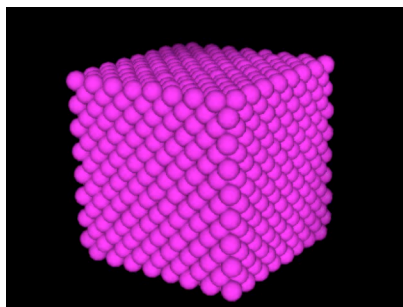
Results no longer depends on C_l

Hybrid Molecular Dynamics

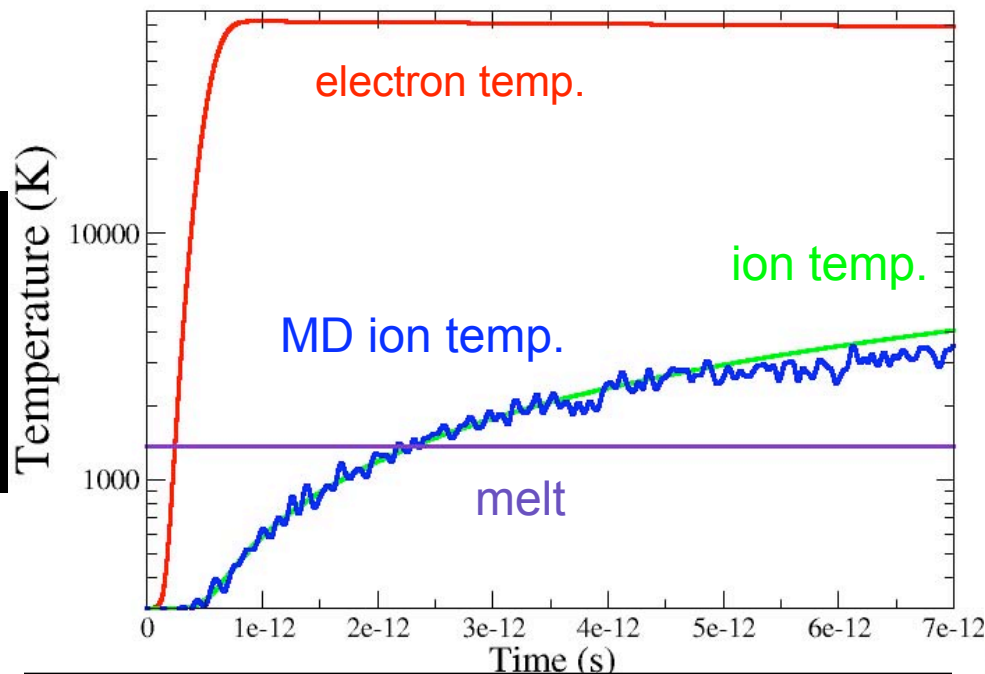
Allows to follow the evolution of the lattice structure as a function of time, temperature and laser energy.

Simulations performed at constant volume

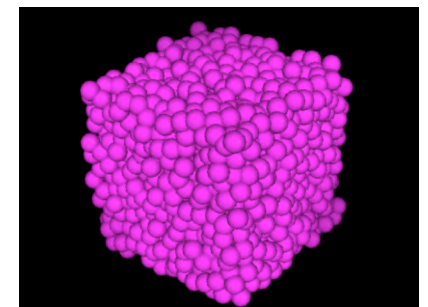
t= 0s:
fcc gold
at T=300K



0<t<5e-13s:laser energy deposited



t=7e-12s:
melted
gold at 3800K



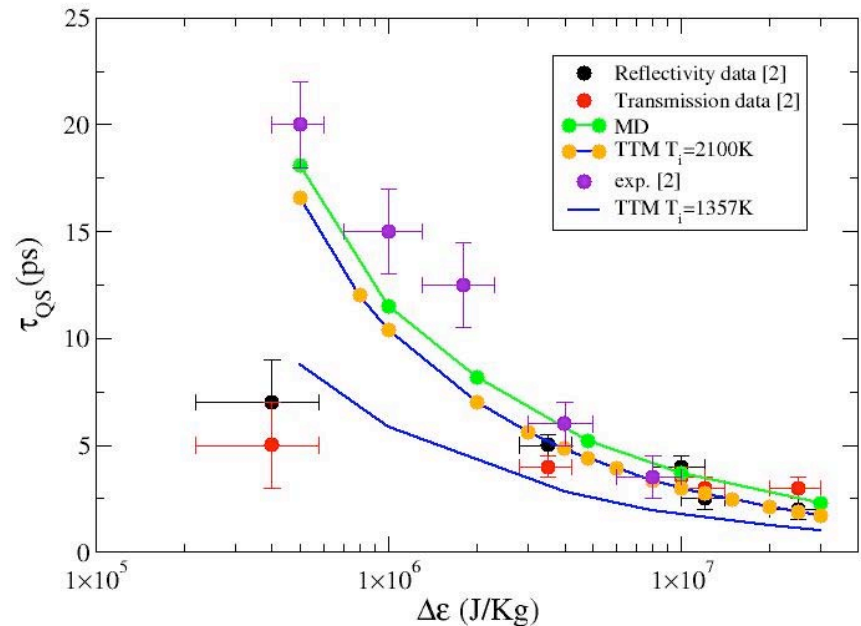
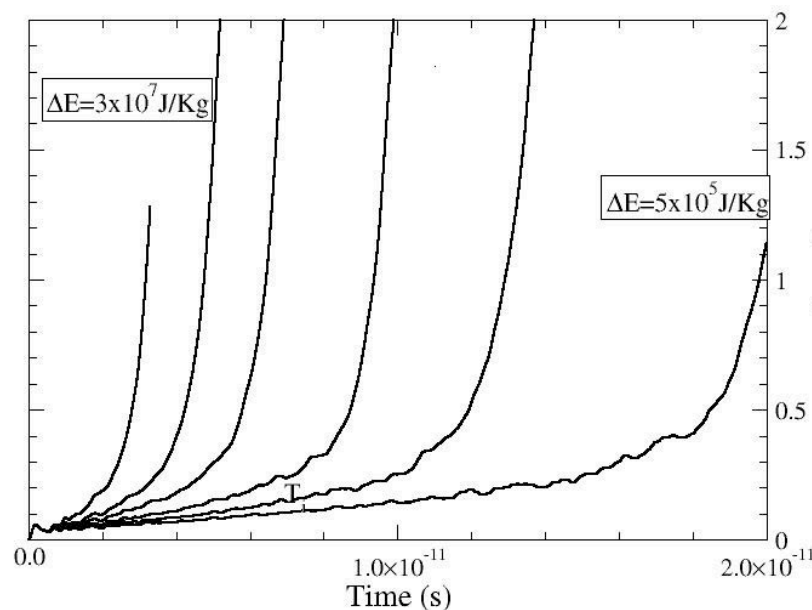
Hybrid MD Results

Mean square displacement as a function of laser energy

Nucleation time from fcc to liquid

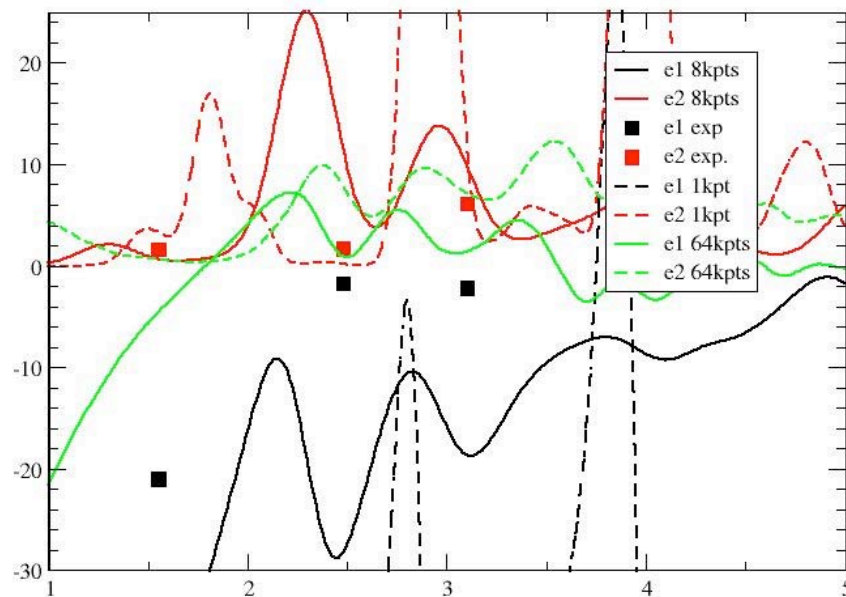
Explains the experimental quasi steady state as the duration of a metastable fcc state.

For high energies, TTM time to reach T_m + nucleation time



Ab-initio MD

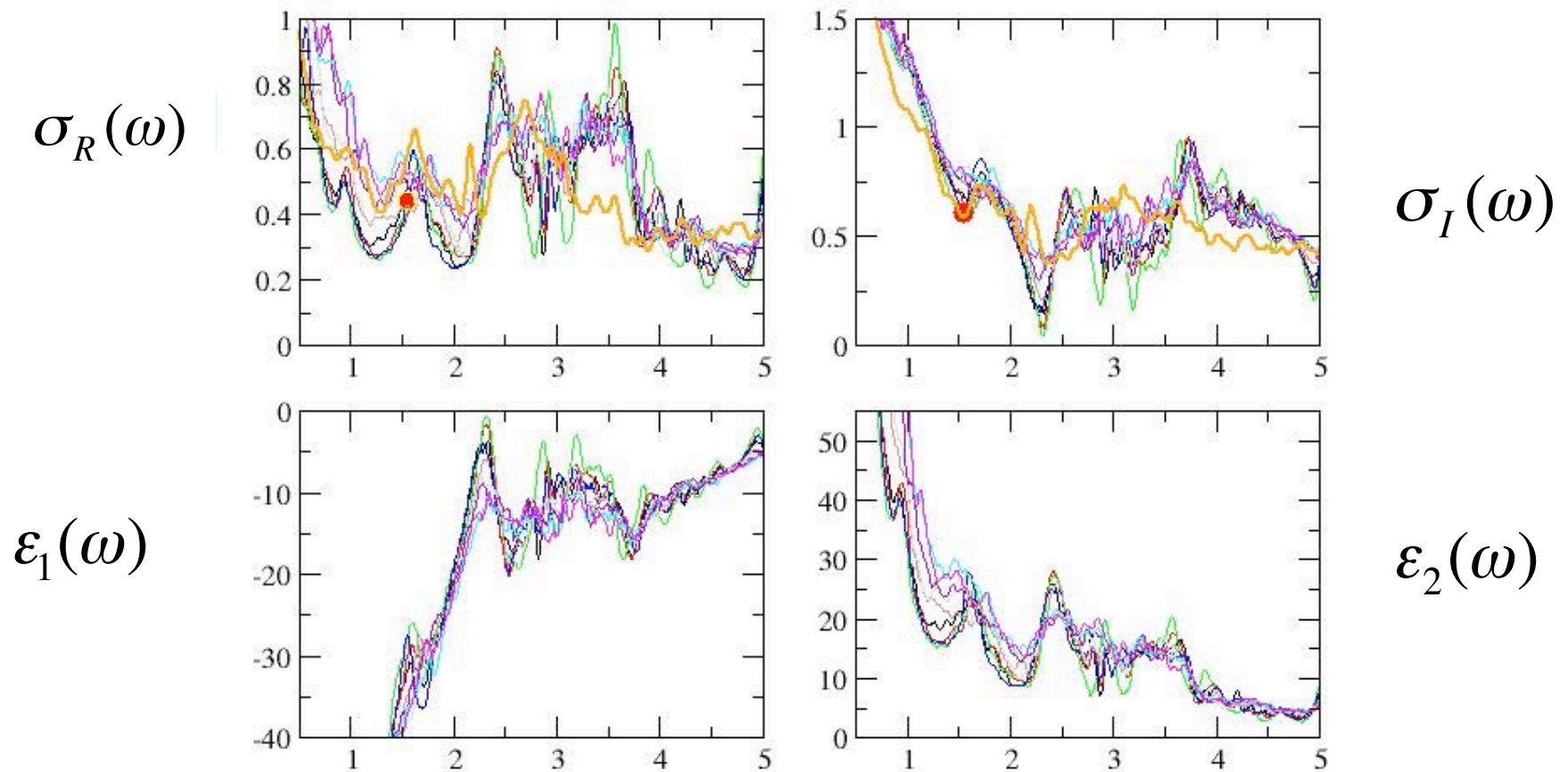
54 atom cell equilibrated at 300K does not melt with $T_e=6\text{eV}$
Melting due to the e-phonon coupling alone as in hybrid MD
Dielectric constant at 300K in quantitative agreement with
exp measurements when using 64 K points



- Performed QMD simulations
1. assuming an fcc structure
 2. increasing T_i to follow TTM
 3. T_e given by TTM

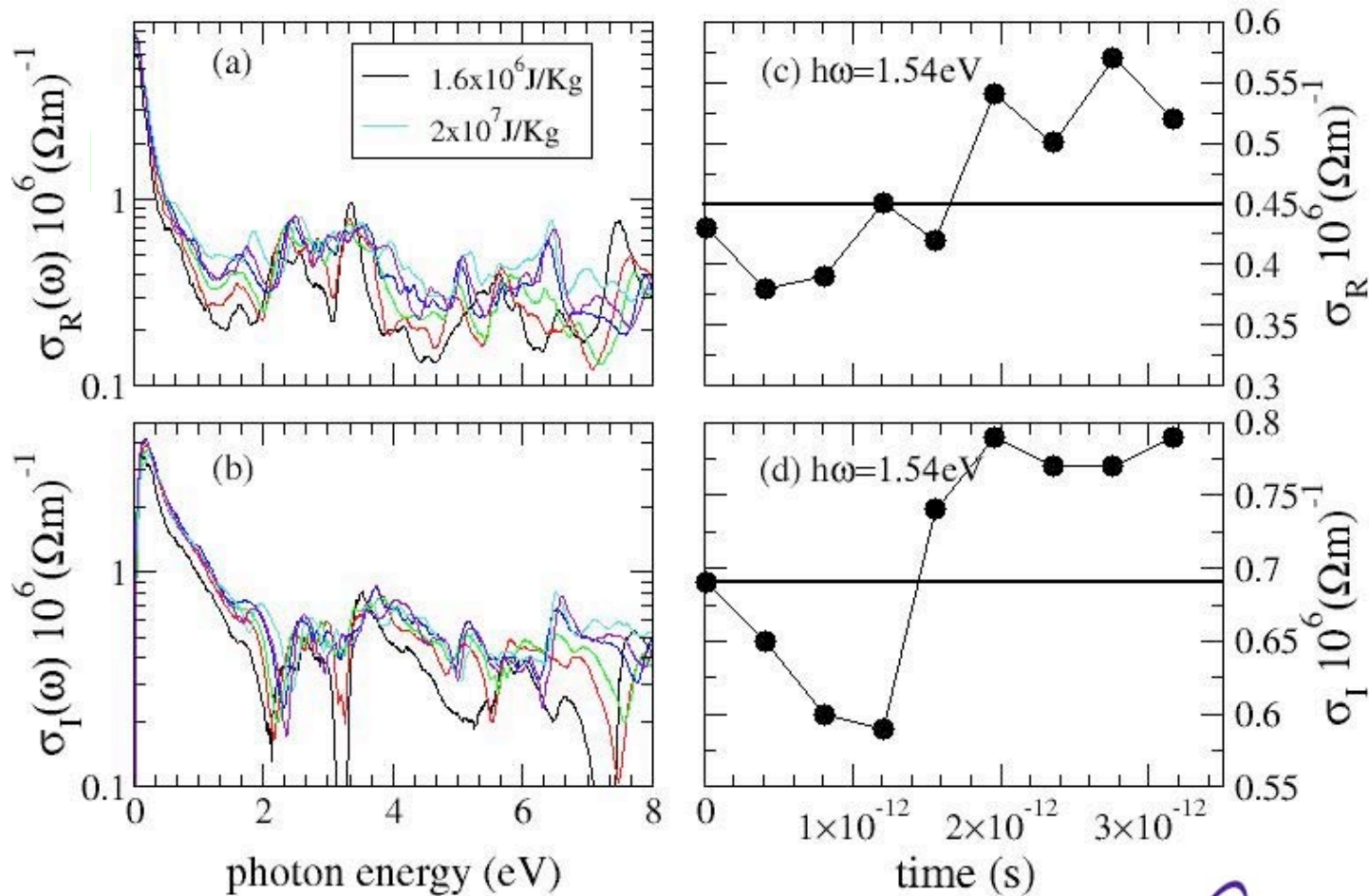
Time resolved optical properties

$9 \times 10^6 \text{ J/Kg}$ $T_e = 5.35 \text{ eV}$ $300 \text{ K} < T_i < 2100 \text{ K}$ in 3.1ps 4kpts



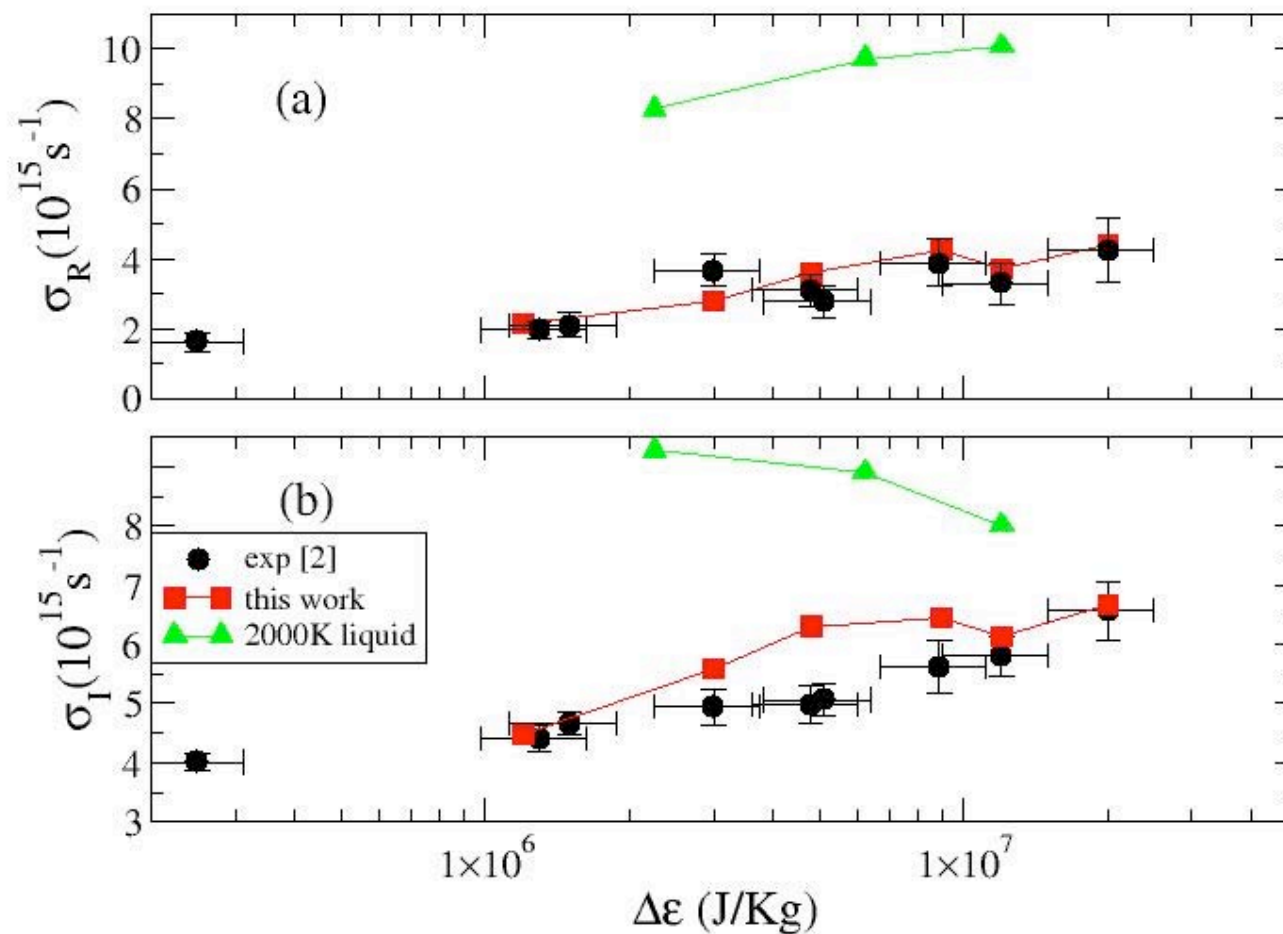
Dependence on laser energy

Conductivity averaged along the quasisteady state



Comparison with experiment

Experimental data compatible with a metastable fcc state
Marked difference with liquid properties



Non-equilibrium calculation conclusions

Good agreement with the measured conductivities for gold

The quasi steady state observed in the optical properties is compatible with the existence of a metastable fcc state.

Hybrid simulations performed at constant volume: abnormal overheating?

Effect of the electron temperature on the hybrid simulation parameters: T_e dependent potential, e-phonon coupling

Scenario: Melting front propagating toward the center of the thin film



Conclusions

QMD allows to calculate electrical and optical properties consistent with the Equation of State (EOS).

QMD provides a valuable tool to test and validate physical models used in modeling codes such as opacities.

Useful for media constituted of various mixtures: electrons, ions, atoms, molecules...

Method currently applied to the modeling of white dwarf atmospheres. Calculate cooling rates.

Calculations of non-equilibrium optical properties



Collaborators

Diatomic fluids and aluminum: L. A. Collins, J.D. Kress, J.D. Johnson (LANL), M. Desjarlais (SNL)

White dwarfs: D. Saumon and P. Kawolsky (LANL)

Comparison with LEDCOP: N. Magee(LANL)

Mixtures (NO, SiO₂, LiF): J. Clerouin, Y. Laudernet, P. Blottiau (CEA-DAM)

Gold: J. Clerouin, V. Recoules, P.M. Anglade, G. Zerah (CEA-DAM)



***Improvements to the Finite
Temperature Average-Atom
Model:
The RPA equations –
A progress report***

*J. Colgan, G. Csanak, L. A. Collins, (T-4)
C. J. Fontes (X-5)*

Los Alamos Opacity Workshop, April 2005

Outline of talk

- Motivation and background to this work
- The average-atom model/equations
- The RPA equations
- Some preliminary results
- Conclusions

Motivation

- At low/intermediate densities it is possible to calculate, at some level of detail, the radiative properties which are needed to describe the atomic processes in a plasma (e.g. current LANL ATOMIC code)
- At high densities more approximate methods must be used. Plasma effects (e.g. pressure ionization) often dominate and must be taken into account in a consistent manner which must also treat the correlations between the bound and free electrons [Blenski, ApJ **127**, 239 (2000)]
- Recent and planned intense laser pulse experiments expect to reach these very high (approaching solid) densities
- Only viable way forward are average-atom type approaches

Background: Average-Atom approach

- The AA approximation is where the charge and excited-state distributions inside a plasma are replaced by a single fictitious ionic species which has the average charge of the ions in the plasma and the average population distribution of the ions among the various excited states
- Fundamental assumption that the plasma can be modeled by a finite temperature electron system in a central potential
- This central potential has contributions from the nucleus, the bound and free electrons, and from the other ions and electrons within the plasma

Background

- The work of Csanak and Kilcrease [JQSRT **58**, 537 (1997)] discussed the AA model and the fact that the orbitals calculated by a standard average atom (AA) approach cannot represent the “excited orbitals” of an atom in a plasma [this was also pointed out by F. Perrot]
- Basically because these “excited orbitals” are calculated in the incorrect potential (V^N , not the correct V^{N-n_j}), due to the non-removal of the self interaction term in the H-F equation for these orbitals
 - [For the ground state, the self interaction term is removed, as pointed out by H. Kelly, but not for the excited states]

Background

- This may not make a significant difference for thermodynamic quantities (such as EOS properties), but for spectral properties, such as photoabsorption, more accurate schemes are necessary
- A promising approach to computing the correct AA excited orbitals is the temperature-dependent Hartree-Fock approximation, or Random Phase Approximation (RPA)
 - This introduces important channel-coupling between excited states into the problem
 - This also removes the self-interaction term from the excited orbitals and so properly describes the “excited states” of an average atom.
- This can be considered a solution to the Latter-tail correction problem as discussed by, e.g. Salzmann et al in their work on photoexcitation and photoionization of hot dense Al plasmas
- In the $T=0$ limit this approach is identical to that pioneered by Amusia for photoionization

Background

- Subsequently, Csanak and Meneses [JQSRT **71**, 281 (2001)] developed these RPA equations and constructed them in a coupled integro-differential form
- They then solved these in the *single-channel approximation*.
- They used the AA orbitals and occupation numbers from the INFERNO code to compute oscillator strengths for a He plasma
- This includes the ion-ion correlations in a fairly crude way, where the ion density is presumed to be zero within the ion (AA) sphere, and constant outside it

Background

- Recently, Csanak and Daughton [JQSRT **83**, 83 (2004)] solved the same *single-channel* RPA equations for He and Li plasmas.
- In this case they used an AA model which included ion correlation, in which the ion density is computed from hypernetted chain (HNC) theory
- They compared oscillator strengths and transition energies with previous calculations of Rozsnyai, where fairly good agreement was found over a range of densities

Background

- In this work, we solve the RPA equations using an improved AA model based on the APATHY code of Bill Daughton. This incorporates a pseudo-atom approach which allows a clear definition of the internal energy of the system.
- We solve the RPA equations using a Linear Algebra (LA) technique pioneered by Lee Collins
- This allows us to solve the coupled-channel equations in a fairly straightforward manner
- Preliminary results are presented

Finite temperature RPA

- Will not derive the RPA equations here!
- Suffice to say for now that the derivation is based on the work of Csanak and Kilcrease using the AA orbitals.
- The RPA approach produces the appropriate potential for the excited electron of the “average-atom” and can incorporate channel-coupling effects

Average-atom eigen-functions

- The AA orbitals $[P_{vl}(r)]$ are eigenfunctions of the AA one-electron problem written in the form

$$H_{l_i}^{AA} P_{v_i l_i}(r) = \varepsilon_{v_i l_i} P_{v_i l_i}(r)$$

- where H^{AA} is the AA radial Hamiltonian with:

$$H_{l_i}^{AA} = -\frac{1}{2} \frac{d^2}{dr^2} + \frac{l_i(l_i + 1)}{2r^2} - \frac{Z}{r} + V^{AA}(r)$$

- Z the nuclear charge
- $V^{AA}(r)$ includes the *electrostatic* plus *local exchange* potential of the AA model. It is temperature and density dependent and depends on the Fermi factor

$$n_i = \frac{1}{1 + e^{\beta(\varepsilon_i - \mu)}}$$

- ε_{vl} is the eigen-energy of the AA orbital $P_{vl}(r)$

- In differential form the *coupled-channel* RPA equations look like:

$$\begin{aligned}
 (H_{l_i}^{AA} - \varepsilon_{v_j} - \omega_n) P_{(v_j l_j) n l_i}^L(r_1) = & \\
 - n_{v_j l_j} \frac{\sqrt{(2l_i + 1)(2l_j + 1)}}{4\pi} \sum_{ll'} \sqrt{(2l + 1)(2l' + 1)} \sum_{v'} \{ & \\
 \beta_{l_i l_j}^L \int_0^\infty dr_4 V_L(r_1, r_4) P_{(v' l') n l}^L(r_4) P_{v' l'}(r_4) P_{v_j l_j}(r_1) & \\
 - \sum_{\lambda} \alpha_{l_i l_j L}^{\lambda} \int_0^\infty dr_4 P_{v_j l_j}(r_4) V_{\lambda}(r_1, r_4) P_{(v' l') n l}^L(r_1) P_{v' l'}(r_4) & \\
 + \sum_{v_i} n_{v_i l_i} P_{v_i l_i}(r_1) \mathfrak{S}_{v_i l_i, v_j l_j}^{n l_i} & \\
 \} &
 \end{aligned}$$

Exchange term

Contribution to the electrostatic potential

Orthogonality term:
Given by

$$\begin{aligned}
 \mathfrak{S}_{v_i l_i, v_j l_j}^{n l_i} = & \beta_{l_i l_j}^L \int_0^\infty dr_3 \int_0^\infty dr_4 P_{v_i l_i}(r_3) P_{v_j l_j}(r_3) V_L(r_3, r_4) P_{(v' l') n l}^L(r_4) P_{v' l'}(r_4) \\
 - \sum_{\lambda} \alpha_{l_i l_j L}^{\lambda} \int_0^\infty dr_3 \int_0^\infty dr_4 P_{v_i l_i}(r_3) P_{v_j l_j}(r_4) V_{\lambda}(r_3, r_4) P_{(v' l') n l}^L(r_3) P_{v' l'}(r_4) &
 \end{aligned}$$

α and β are
angular factors

Finite temperature RPA

- These RPA equations are the proper one-electron equations for the orbitals of an “excited electron” in the plasma
- ω_n is the transition energy of interest
- The 1st and 2nd terms on the RHS remove exactly the electrostatic and exchange pieces of the potential necessary to remove the self-interaction.
- The amount of charge removed is controlled by n_j ; the fractional occupation number of the AA orbital.
- The final orthogonality term controls the overlap between the true excited-states and the AA “excited states”. Again, its importance depends on the occupation number of these AA “excited-states”.
- Finally, $V_L(r_1, r_2)$ is the multipole component in the expansion of the Coulomb potential

Average-Atom approach: APATHY

- To solve the AA equations and to generate a self-consistent set of AA orbitals and potentials we use the *APATHY* code
- Developed by Bill Daughton and collaborators at LANL
- Solves non-relativistic Schrödinger equation for bound/continuum wavefunctions for electron density
- Sophisticated treatment of the ion-ion correlations using a “pseudo-atom” approach along with hypernetted-chain theory
- Has been compared in detail with SESAME database for Al and Si for a range of EOS quantities

Solution of the RPA equations

- Use the Linear Algebra (LA) method [eg: Collins & Schneider, PRA **24**, 2387 (1981)] to solve the RPA equations
- This has previously been used in many other scattering problems and has found to be a robust, reliable method
- Extension of the LA method to treat bound-state problems also made by Lee Collins
- Problem is recast into an integral equation and solved using numerical quadrature
- Equation is converted into integral form by using Green's functions
- Extension to a coupled-channel problem has been made and is currently being tested

Results

- Preliminary calculations so far
- Compare a He plasma at 10 eV at various densities with previous work of Csanak and Daughton, as well as older AA results of Rozsnyai
- Good agreement is found for the single-channel case using the LA method
- Found that inclusion of the orthogonality term makes little difference for these conditions

He plasma oscillator strengths – SCRPA calculations

T=10 eV, $\rho=1.5 \times 10^{19}/\text{cm}^3$

All quantities in atomic units

We compare with the previous
calculations of Csanak & Daughton

		w_{2p}	OS	w_{3p}	OS	w_{4p}	OS	w_{5p}	OS
C & D		1.58	2.70e-2	1.84	5.30e-3	1.94	1.93e-3	1.98	9.00e-4
LA code		1.58	2.70e-2	1.85	5.33e-3	1.94	1.93e-3	1.98	9.01e-4

T=10 eV, $\rho=1.5 \times$

$10^{20}/\text{cm}^3$

		w_{2p}	OS	w_{3p}	OS	w_{4p}	OS	w_{5p}	OS
C & D		1.51	0.109	1.75	2.13e-2	1.82	7.01e-3	1.85	2.57e-3
LA code		1.51	0.109	1.75	2.15e-2	1.82	7.08e-3	1.85	2.64e-3

He plasma oscillator strengths – SCRPA calculations

T=10 eV, $\rho=1.5 \times 10^{20}/\text{cm}^3$

All quantities in atomic units

Convergence of calculations with respect
to the number of points in the LA calculation

		w_{2p}	OS	w_{3p}	OS	w_{4p}	OS	w_{5p}	OS
LA code (60)		1.51	0.109	1.75	2.15e-2	1.82	7.08e-3	1.85	2.64e-3
LA code (80)		1.51	0.109	1.75	2.15e-2	1.82	7.08e-3	1.85	2.64e-3
LA code (90)		1.51	0.109	1.75	2.15e-2	1.82	7.08e-3	1.85	2.64e-3

He plasma oscillator strengths – SCRPA calculations

T=10 eV, $\rho=1.5 \times 10^{19}/\text{cm}^3$

Comparing OS divided by
initial occupation number

We compare our calculations with
previous AA calculations of Rozsnyai

		w_{2p}	OS	w_{3p}	OS	w_{4p}	OS	w_{5p}	OS
Rozsnyai		1.56	3.50e-1	1.83	7.49e-2	1.93	2.72e-2	1.97	1.20e-2
LA code		1.58	3.82e-1	1.85	7.54e-2	1.94	2.74e-2	1.98	1.28e-2

T=10 eV, $\rho=1.5 \times 10^{20}/\text{cm}^3$

		w_{2p}	OS	w_{3p}	OS	w_{4p}	OS	w_{5p}	OS
Rozsnyai		1.73	0.288	1.93	6.00e-2	1.99	2.14e-2	-	-
LA code		1.51	0.337	1.75	6.64e-2	1.82	2.18e-2	1.85	8.12e-3

He plasma oscillator strengths – SCRPA calculations

T=10 eV, $\rho=1.5 \times 10^{20}/\text{cm}^3$

All quantities in atomic units

Effect of including orthogonality term in RPA
equations

		w_{2p}	OS	w_{3p}	OS	w_{4p}	OS	w_{5p}	OS
LA code (no orthogonality)		1.51	0.109	1.75	2.15e-2	1.82	7.08e-3	1.85	2.64e-3
LA code (orthogonality to 3 orbitals)		1.51	0.109	1.75	2.16e-2	1.82	7.12e-3	1.85	2.65e-3

Orthogonality term has a small effect for this system

Conclusions & future directions

- Formulated an RPA approach to properly describe spectral properties of atoms in dense plasmas
- Used the APATHY code to solve the AA equations
- Used the Linear Algebra code to solve the RPA equations
- We are now in a position to solve the coupled-channel RPA equations and apply them to systems of interest

- In differential form the *single-channel* RPA equations look like:

$$\begin{aligned}
 (H_{l_i}^{AA} - \varepsilon_{v_j} - \omega_n) P_{(v_j l_j) n l_i}^L(r_1) = & \quad \swarrow \text{Exchange term} \\
 - n_{v_j l_j} \beta_{l_i l_j}^L \int_0^\infty dr_4 v_L(r_1, r_4) P_{(v_j l_j) n l_i}^L(r_4) P_{v_j l_j}(r_4) P_{v_j l_j}(r_1) \\
 - n_{v_j l_j} \sum_{\lambda=\text{even}} \alpha_{l_i l_j L}^\lambda \int_0^\infty dr_4 [P_{v_j l_j}(r_4)]^2 v_\lambda(r_1, r_4) P_{(v_j l_j) n l_i}^L(r_1) \\
 + \sum_{v_i} n_{v_i l_i} P_{v_i l_i}(r_1) \mathfrak{S}_{v_i l_i, v_j l_j}^{n l_i} & \quad \nwarrow \text{Contribution to the electrostatic potential}
 \end{aligned}$$

Orthogonality term:
Given by

α and β are
angular factors

$$\begin{aligned}
 \mathfrak{S}_{v_i l_i, v_j l_j}^{n l_i} = & \beta_{l_i l_j}^L \int_0^\infty dr_3 \int_0^\infty dr_4 P_{v_i l_i}(r_3) P_{v_j l_j}(r_3) v_L(r_3, r_4) P_{(v_j l_j) n l_i}^L(r_4) P_{v_j l_j}(r_4) \\
 - \sum_{\lambda=\text{even}} & \alpha_{l_i l_j L}^\lambda \int_0^\infty dr_3 \int_0^\infty dr_4 P_{v_i l_i}(r_3) P_{v_j l_j}(r_4) v_\lambda(r_3, r_4) P_{(v_j l_j) n l_i}^L(r_3) P_{v_j l_j}(r_4)
 \end{aligned}$$

APATHY: outline

- The AA approximation is where the charge and excited-state distributions inside a plasma are replaced by a single fictitious ionic species which has the average charge of the ions in the plasma and the average population distribution of the ions among the various excited states
- Fundamental assumption that the plasma can be modeled by a finite temperature electron system in a central potential
- This central potential has contributions from the nucleus, the bound and free electrons, and from the other ions and electrons within the plasma
- A local exchange potential is used which is a function of the electron density [we use a finite-temperature exchange-correlation potential of Perrot and Dharma-wardana]

- Several different AA approaches have been used
- Standard approach is “ion cell” model:
 - Confine each ion to a cell
 - Each cell contains Z electrons and is neutral
 - One solves for a self-consistent potential (for the electrons):

$$\nabla^2 V(r) = 4\pi Ze\delta(r) - 4\pi en_e(r)$$

- More recent approach is ion correlation model
- Statistical distributions of both ions and electrons are computed around the test ion

$$\nabla^2 V(r) = 4\pi Ze\delta(r) - 4\pi e[Z^* n_i(r) - n_e(r)]$$

- Properly adding up the various energy terms is still ambiguous

APATHY: AA model

- Decompose plasma into N identical charge clouds
- One has a central “pseudo-atom” with a statistical distribution of other pseudo-atoms
- Energy of a single pseudo-atom is clearly defined, as is the interaction energy between the pseudo-atom and the rest of the plasma
- Allows the total internal energy of the system to be easily written
- Results in a self-consistent potential for system of the form

$$V(r) = V_{atom}(r) + n_i \int g(r') V_{atom}(r - r') dr' + V_{exc}(r)$$

APATHY: AA model

- In this equation V_{atom} is defined as

$$V_{\text{atom}}(r) = -\frac{Z}{r} + \int \frac{n_e(r')}{|r - r'|} dr'$$

- Where the bound and free electron densities are given as

$$n_{\text{eb}}(r) = \sum_{n,l} f(\varepsilon_{nl}, \mu) \frac{2(2l+1)}{4\pi} \frac{u_{nl}^2(r)}{r^2}$$

$$n_{\text{ef}}(r) = \int_0^\infty d\varepsilon f(\varepsilon_{nl}, \mu) \sum_{l=0}^\infty \frac{2(2l+1)}{4\pi} \frac{u_{\varepsilon l}^2(r)}{r^2}$$

- Where f is the usual Fermi factor and $u(r)$ are the radial atomic wavefunctions for a given state
- A local exchange potential is used which is a function of the electron density [we use a finite-temperature exchange-correlation potential of Perrot and Dharma-wardana]

APATHY: Ion-ion correlation

- Hypernetted Chain Theory (HNC) to compute ion density
- Non-perturbative method, well suited to modeling the long-range interactions
- Uses the Ornstein-Zernike relation to compute the pair correlation function $h(r)$:

$$h(r) = c(r) + n_{io} \int c(|r - r'|) h(r') d^3 r'$$

- The radial distribution function $g(r)$ is then simply given from the closure relation:

$$g(r) = 1 + h(r) = \exp[-\beta u(r) + h(r) - c(r) + B(r)]$$

- The ion density is then given as $n_i(r) = n_{io} g(r)$ with n_{io} the macroscopic ion density for a given canonical ensemble.

ATOMIC opacity calculations using CHEMEOS

Peter Hakel and David P. Kilcrease
Atomic and Optical Theory Group (T-4)
Theoretical Division
Los Alamos National Laboratory

The new ATOMIC code

- Another Theoretical Opacity Modeling Integrated Code
- **ATOMIC = FINE + LEDCOP + CHEMEOS**
- J. Abdallah, J. Colgan, C. Fontes, P. Hakel, D. Kilcrease, N. Magee, S. Mazevet, M. Sherrill, H. Zhang
- low-Z opacity and equation of state code
- both LTE and non-LTE conditions
- plasma effects / continuum lowering

The equation-of-state (EOS) model

- tested against quantum molecular dynamics (QMD) and path-integral Monte Carlo (PIMC) calculations for hydrogen and helium
- application to heavier elements (C, O, Ar)

LTE: free energy minimization

- chemical picture
- ensures thermodynamic consistency of the model
- yields LTE population distribution $\{ N_s \}$
- plasma and EOS characteristics can be obtained as derivatives of the free energy $F(V, T, \{ N_s \})$

- pressure:

$$P = - \left(\frac{\partial F}{\partial V} \right)_{T, \{N_s\}}$$

- energy:

$$E = -T^2 \left(\frac{\partial (F/T)}{\partial T} \right)_{V, \{N_s\}}$$

W. Däppen, L. Anderson, and D. Mihalas: Ap.J. **319**, 195 (1987)

D. Saumon and G. Chabrier: Phys. Rev. A **44** (8), 5122 (1991); **46** (4) 2084 (1992)

G. Chabrier and A.Y. Potekhin: Phys. Rev. E **58** (4), 4941 (1998)

Occupation probability formalism

- models the elimination of bound states by dense plasma effects (e.g., microfields)
 - “gentle” truncation of partition functions (LTE)
 - modified atomic kinetics rate equations (NLTE)
- allows for a smooth merging of bound-bound and bound-free sections of the spectrum (edge lowering/broadening)

D.G. Hummer and D. Mihalas: Ap.J. **331**, 794 (1988)

D. Mihalas, W. Däppen, and D.G. Hummer: Ap.J. **331**, 815 (1988)

I. Hubeny, D.G. Hummer, and T. Lanz: Astron. Astrophys. **282**, 151 (1994)

A. Nayfonov, W. Däppen, D.G. Hummer, and D. Mihalas: Ap.J. **526**, 451 (1999)

Occupation probabilities w

- charged particle (plasma microfield $P(F)$)
perturbations of atomic structure

$$w_{mf} = \int_0^{F_c} P(F) dF \quad ; F_c - \text{critical microfield}$$

- finite-size effects

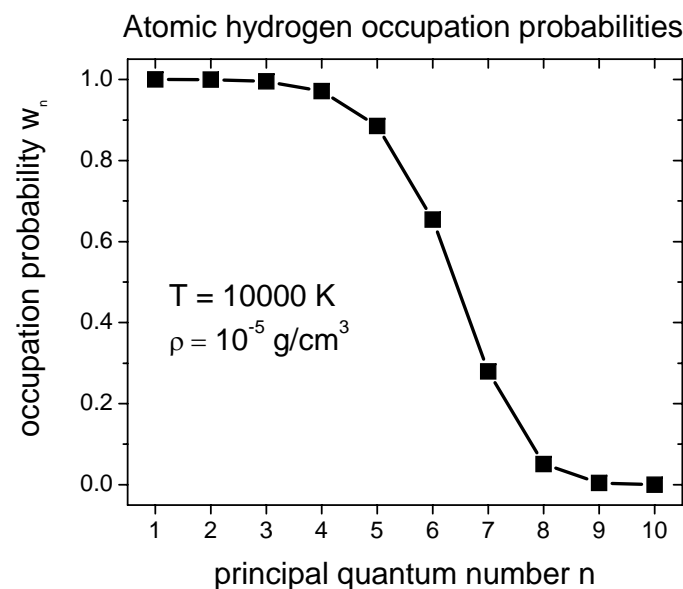
$$w_{hs} \propto \text{excluded volume}$$

- convergent partition function

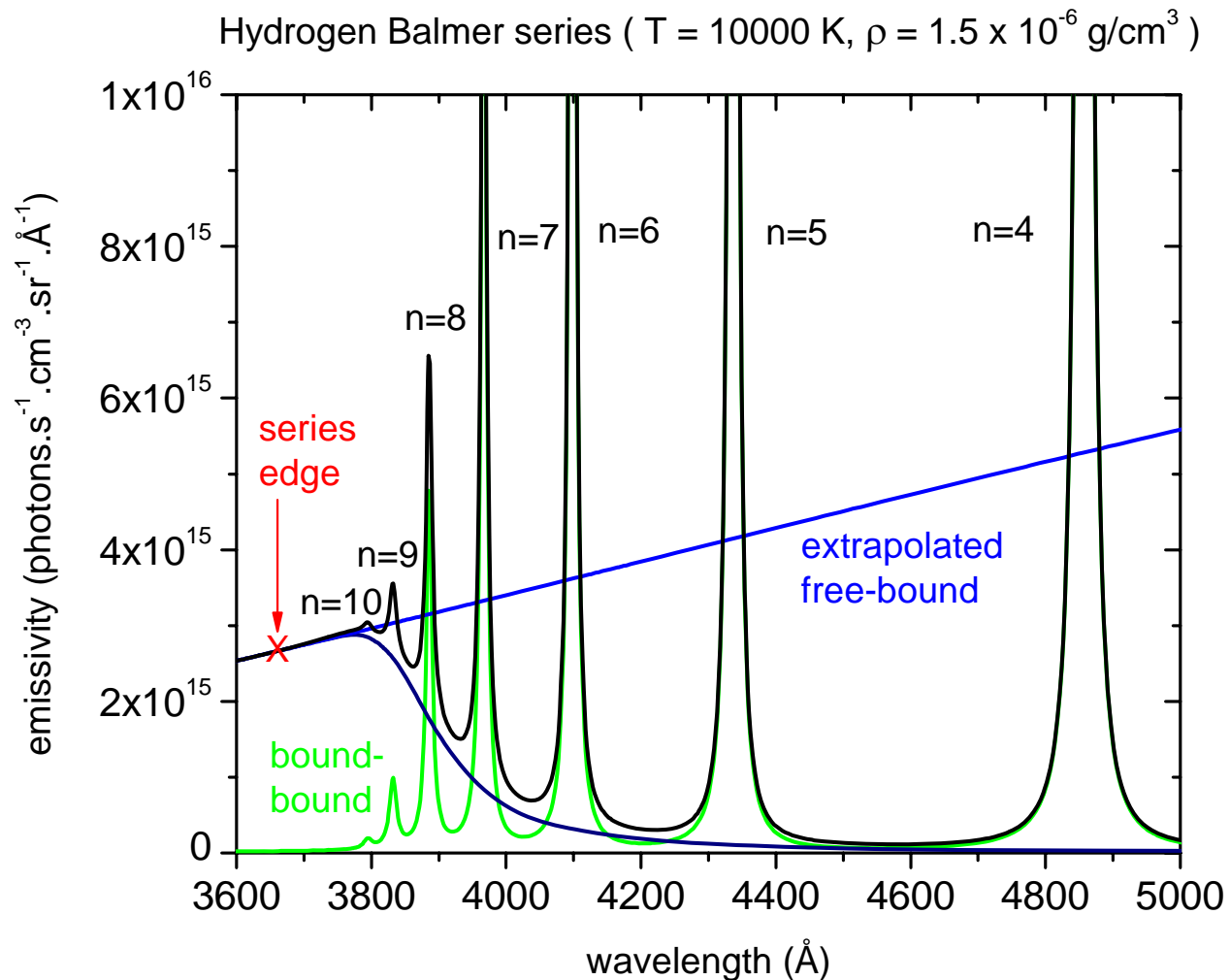
$$\tilde{Z} = \sum_j w_j g_j \exp(-E_j/kT)$$

- LTE level populations N_j

$$N_j/N_T = w_j g_j \exp(-E_j/kT) / \tilde{Z}$$



Spectral line series edge broadening



W. Däppen, L. Anderson, and D. Mihalas: Ap.J. **319**, 195 (1987)

I. Hubeny, D.G. Hummer, and T. Lanz: Astron. Astrophys. **282**, 151 (1994)

Helmholtz free energy contributions

$$F = -kT \ln Z$$

- chemical picture \leftrightarrow partition function factorization

$$F = F_1 + F_2 + F_3 + F_4 + F_5$$

- F_1 - ions, translational (classical)
- F_2 - ions, internal (partition functions \tilde{Z})
- F_3 - electrons, with degeneracy effects
- F_4 - Coulomb interaction plasma term
- F_5 - finite atom size effects (pressure ionization)

Free energy contributions, cont.

- F_1 - ions, translational (classical ideal gas)

$$F_1 = kT \sum_{s \neq e} N_s \left[\ln \left(\frac{N_s \Lambda_s^3}{V g_s} \right) - 1 \right] \quad \Lambda_s = \sqrt{\frac{2\pi \hbar^2}{m_s kT}}$$

- F_2 - ions, internal (excited states)

$$F_2 = \sum_{s \neq e} N_s \left(E_{s1} - kT \ln \tilde{Z}_s \right) \quad \tilde{Z}_s = \sum_j w_{sj} g_{sj} \exp \left(-\frac{E_{sj} - E_{s1}}{kT} \right)$$

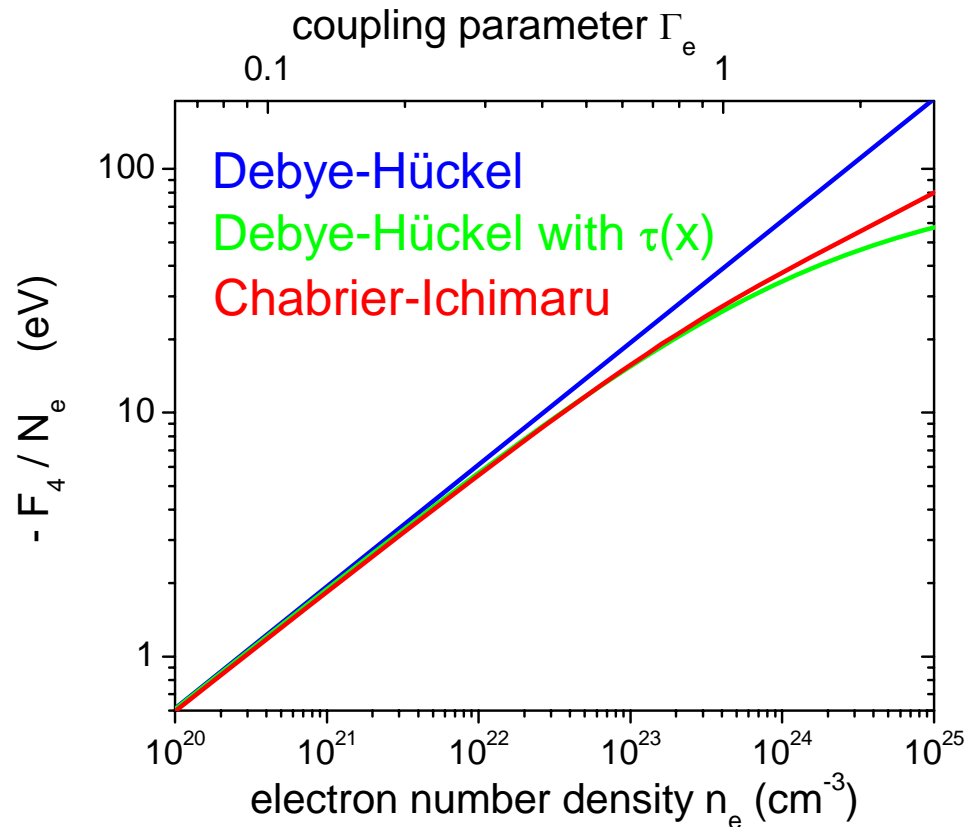
A.Y. Potekhin, G. Chabrier, and D. Gilles, Phys. Rev. E **65**, 036412 (2002)

- F_3 - electrons: ideal, partially degenerate Fermi gas

$$F_3 = kT N_e \left(\eta - I_{3/2}(\eta) / I_{1/2}(\eta) \right) \quad I_{1/2}(\eta) = \frac{N_e \Lambda_e^3}{2V}$$

Free energy contributions, cont.

- F_4 - Coulomb interaction plasma term



example:

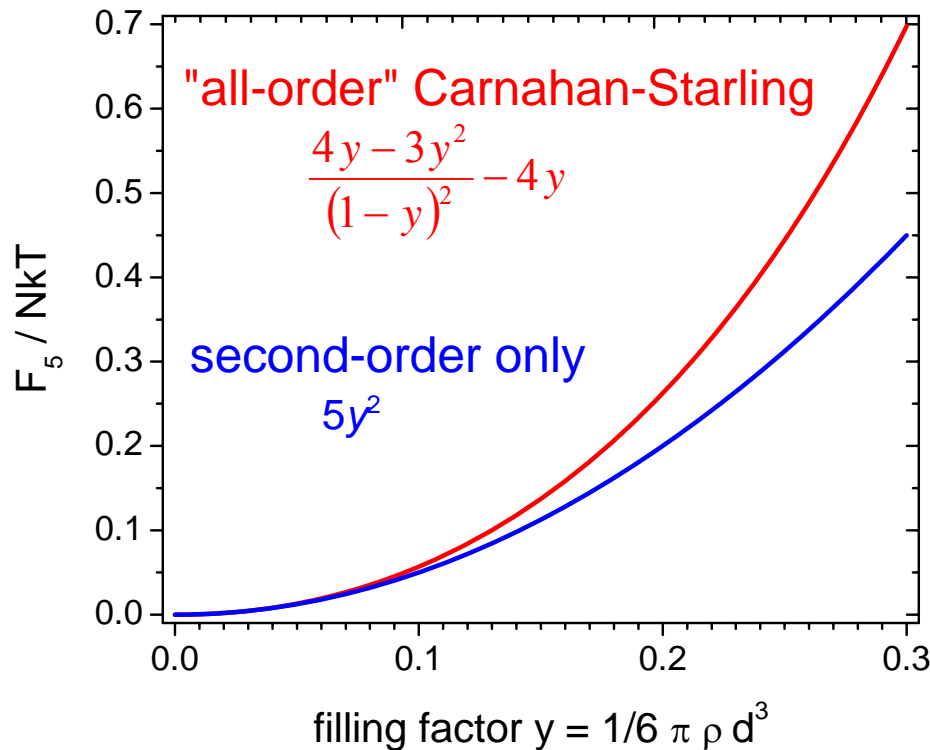
fully ionized hydrogen
 $T = 200,000 \text{ K}$

G. Chabrier and A.Y. Potekhin, Phys. Rev. E **58** (4), 4941 (1998); **62** (6) 8554 (2000)

S. Ichimar, H. Iyetomi, and S. Tanaka, Phys. Rep. **149** (2&3), 91 (1987)

Free energy contributions, cont.

- F_5 - finite atom size effects (pressure ionization), mixture of hard spheres



example:

one-component
hard-sphere system:
 d – hard-sphere diameter
 ρ – particle number density

N.F. Carnahan and K.E. Starling, J. Chem. Phys. **51** (2), 635 (1969)

Free energy contributions, cont.

- simple hard-sphere description becomes inadequate at high densities
- liquid perturbation theories: known reference system plus corrections (Barker-Henderson, and Weeks-Chandler-Andersen, ...)

$$F_5 = F_5^{ref} + \frac{N^2}{2V} \int d\vec{r} g_{ref}(r) u_{attract}(r) + \dots$$

- soft-sphere model = hard-sphere reference system with density- (and temperature-) dependent radii
- effective radii values calibrated by comparisons with *ab initio* calculations such as QMD, PIMC

Minimizing F : initialization

- solve a system of Saha-type equations derived from stoichiometric constraints:

$dF = 0$ for process $A^{m+} \leftrightarrow A^{(m+1)+} + e^-$ yields,

$$\frac{n_{m+1}}{n_m} = \frac{\tilde{Z}_{m+1}}{\tilde{Z}_m} \exp\left[-\left(\chi_{m,m+1} - \phi_m + \mu_e^{(0)}\right)/kT\right]$$

- analogous equations for molecular dissociation
- closure provided by:

- total mass conservation

$$N_{total} = \sum_{m \neq e} a_m N_m$$

- charge neutrality condition

$$N_e = \sum_{m \neq e} z_m N_m$$

Helmholtz free energy contributions in the Saha-based initialization model

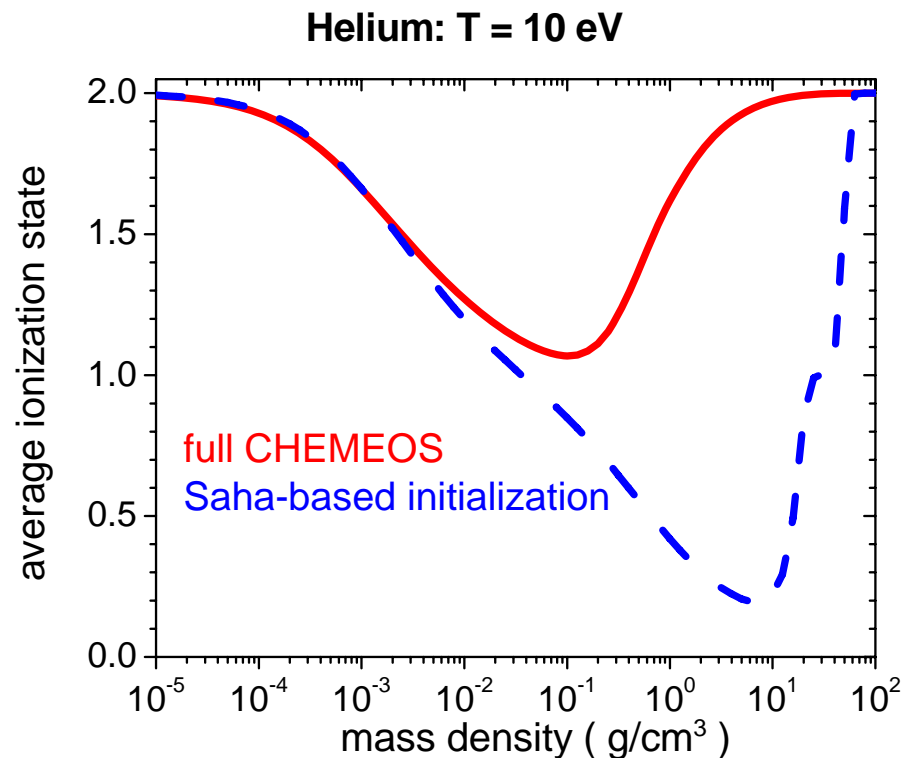
$$F = -kT \ln Z$$

$$F = F_1 + F_2 + F_3 + F_4 + F_5$$

- F_1 - ions, translational (classical): full account
- F_2 - ions, internal: ground-states only (see also F_5)
- F_3 - electrons, with degeneracy effects: full account
- F_4 - Coulomb interaction term:
Stewart-Pyatt continuum-lowering formula
- F_5 - finite atom size effects (pressure ionization):
density-dependent occupation probabilities of
ground states in F_2

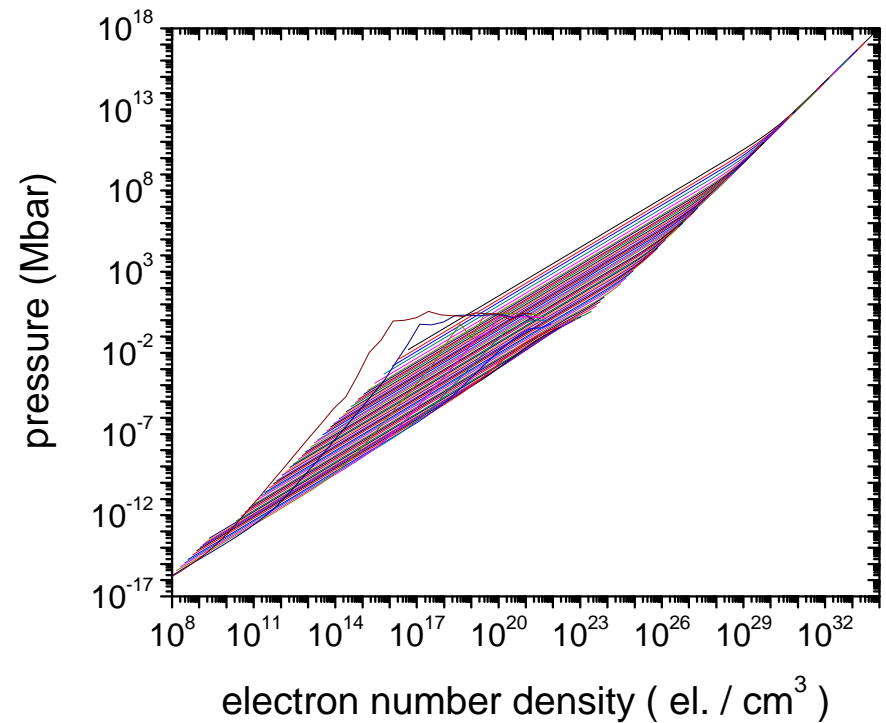
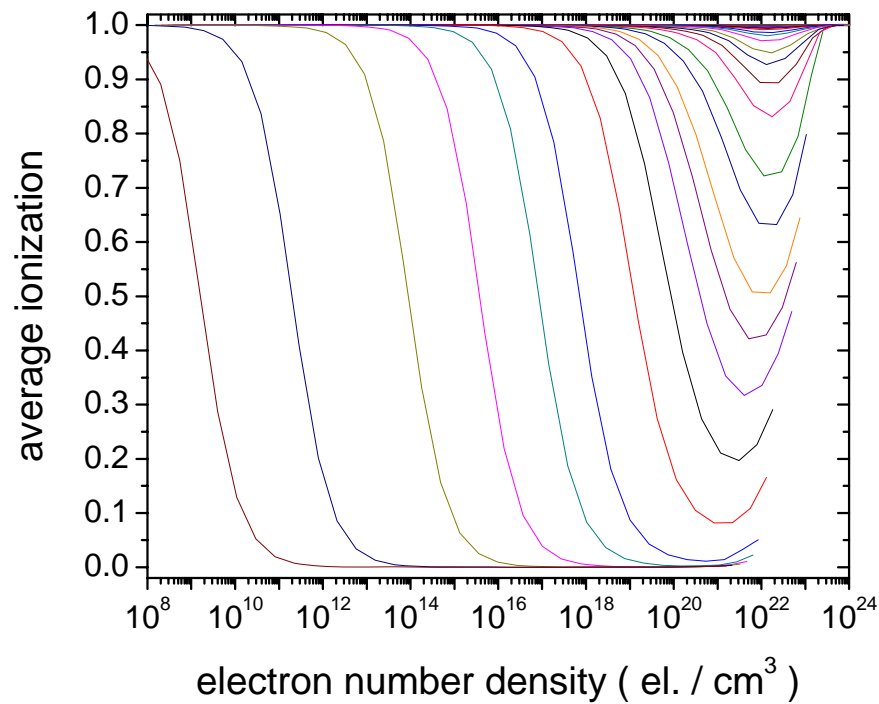
Minimizing F : continued...

- Powell method (no use of gradients) with the “Saha-based solution” providing the initial guess
- truncated-Newton algorithm (Stephen Nash); use of gradients should speed up code (future work)



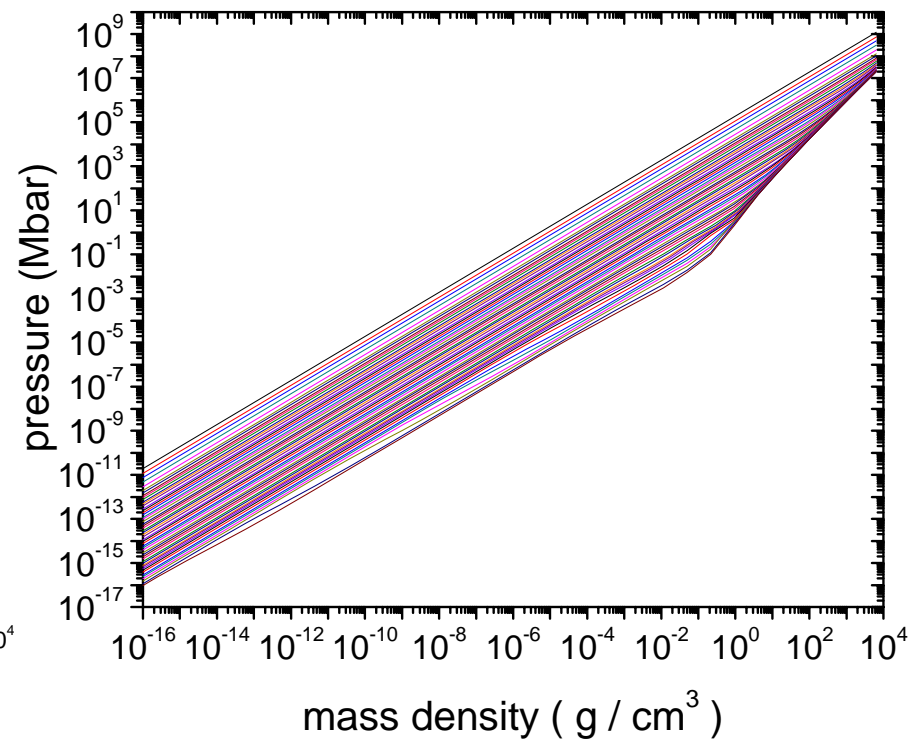
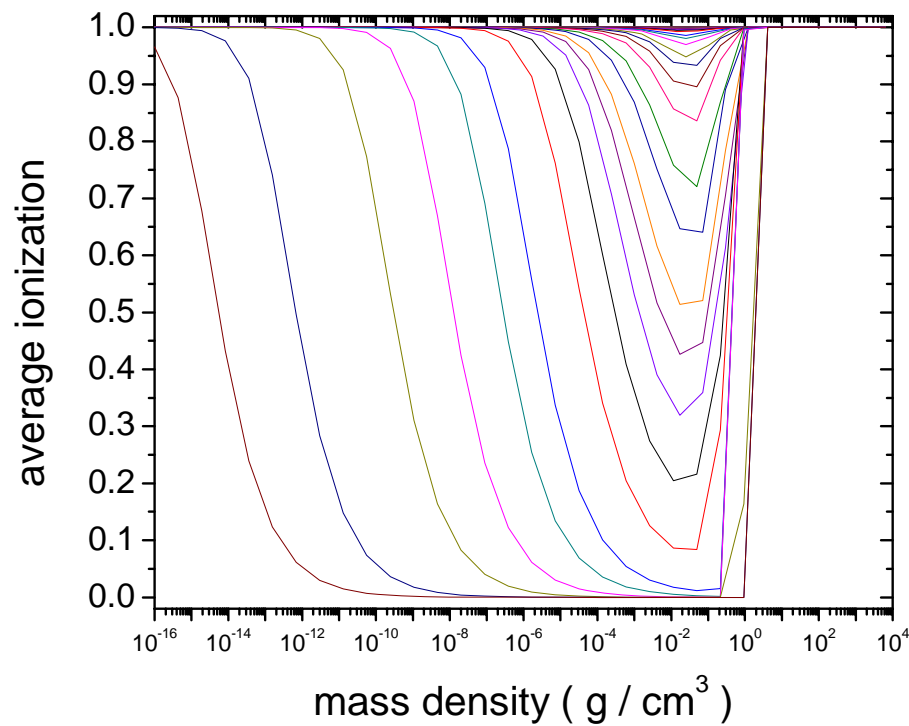
Hydrogen table

electron number density on input



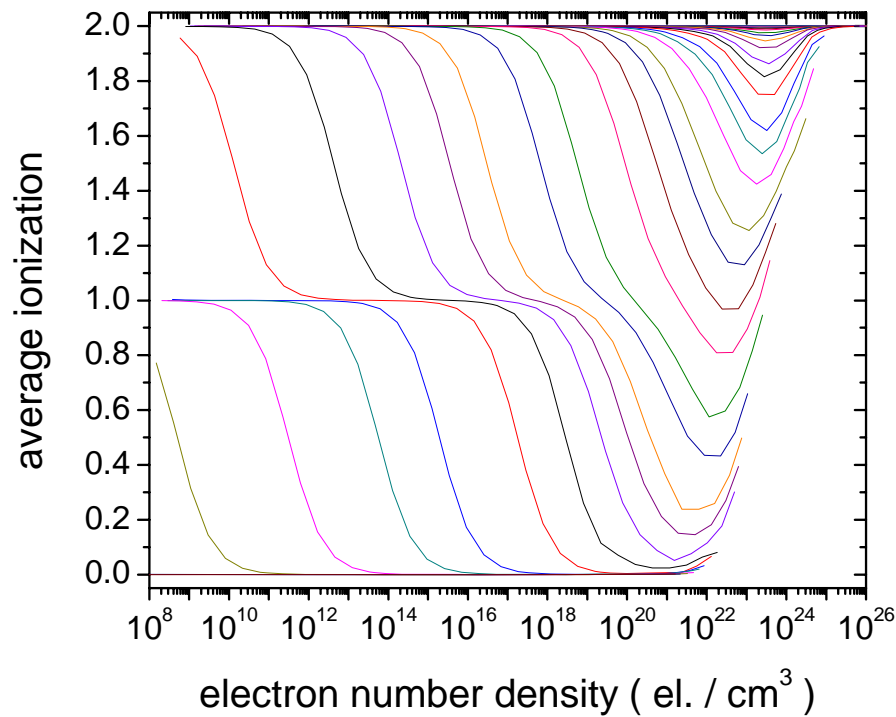
Hydrogen table

mass density on input

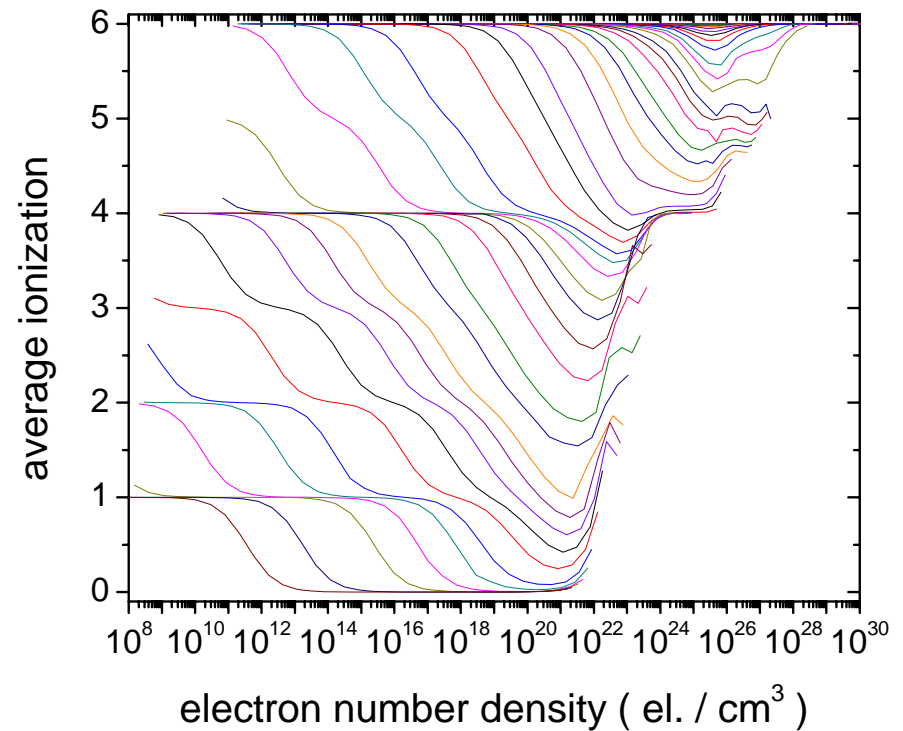


Helium and Carbon tables

electron number density on input



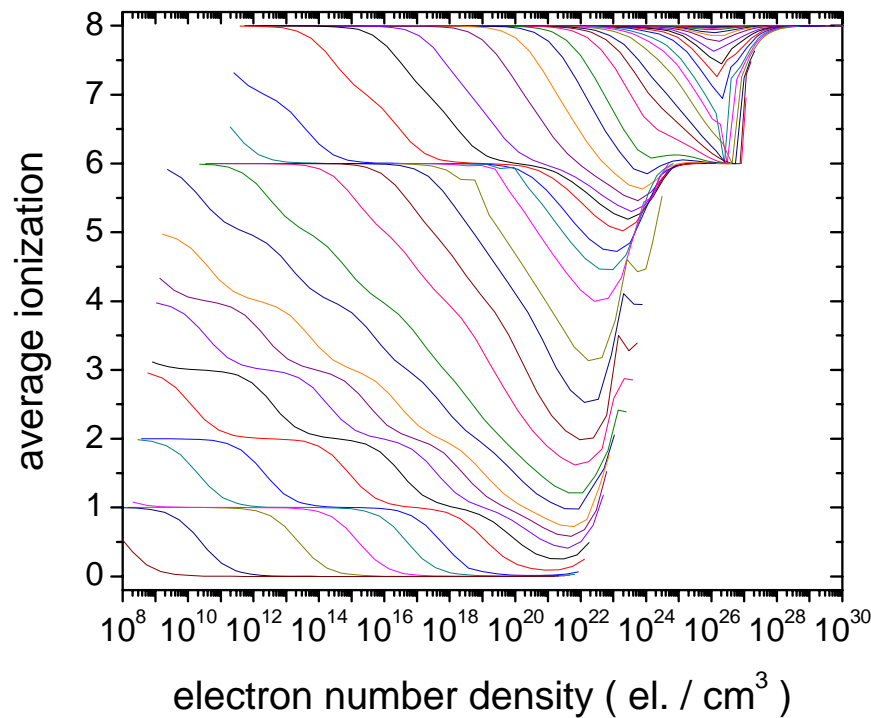
Helium



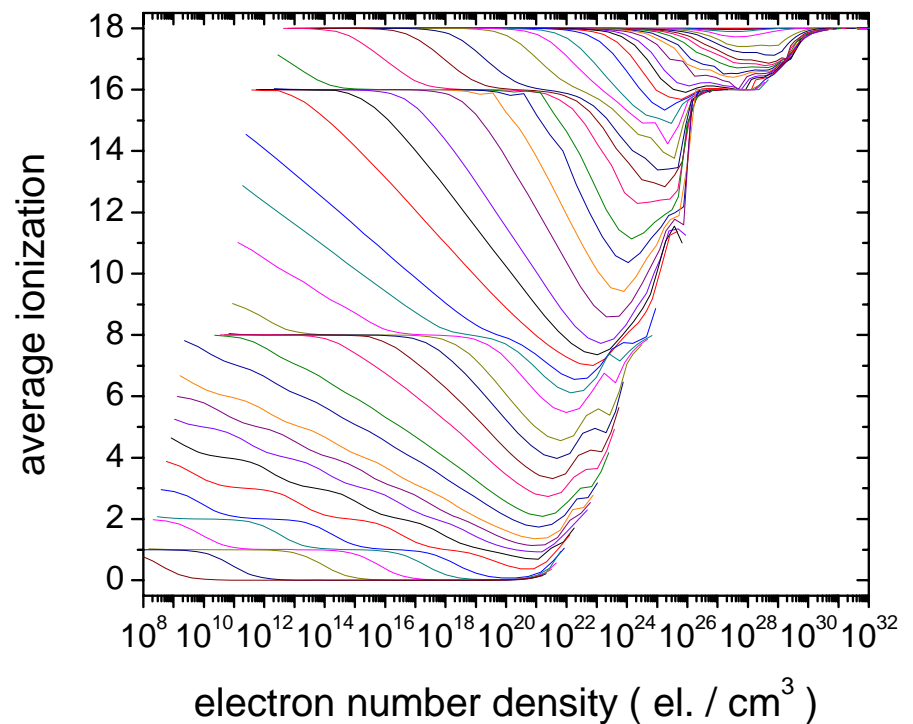
Carbon

Oxygen and Argon tables

electron number density on input

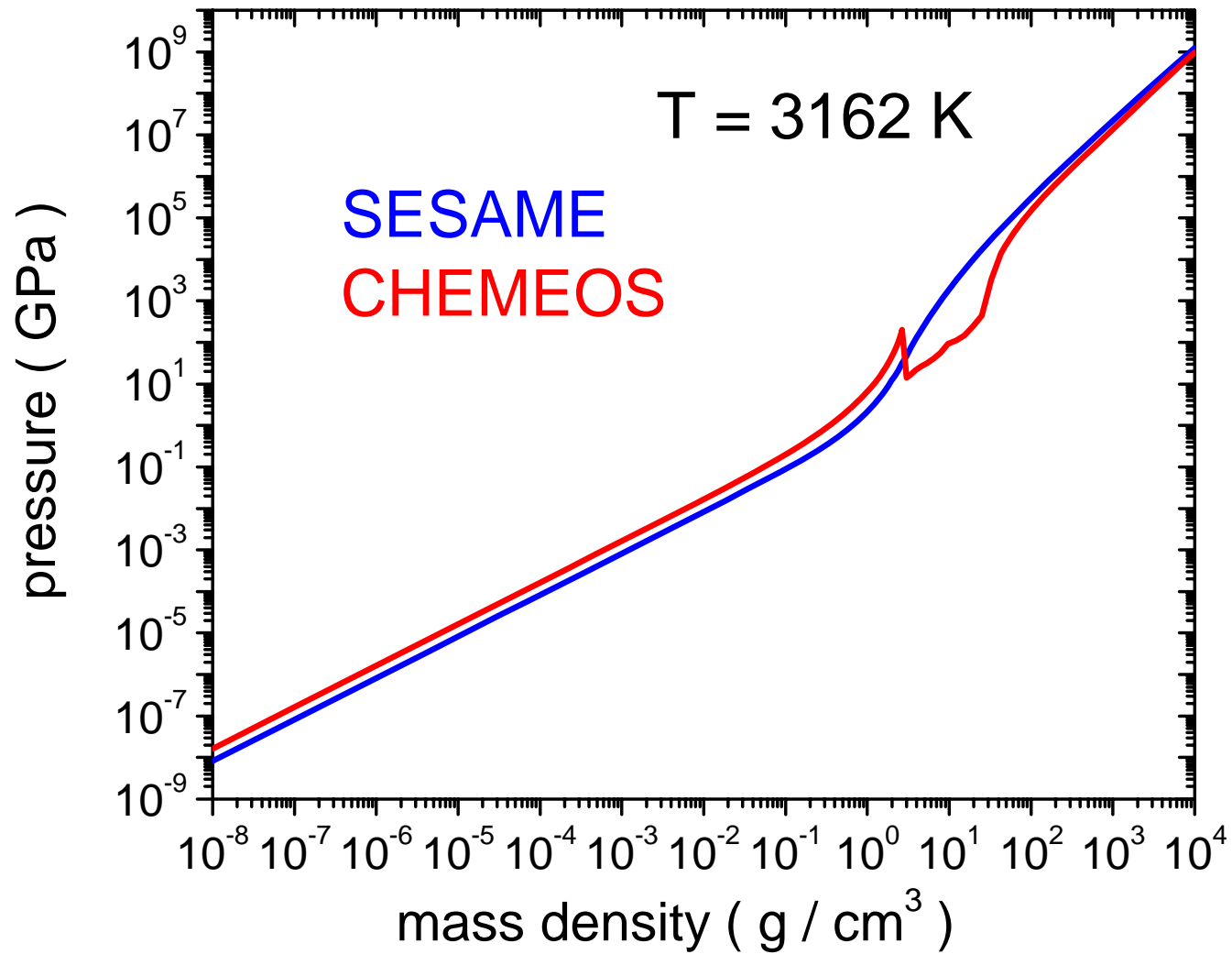


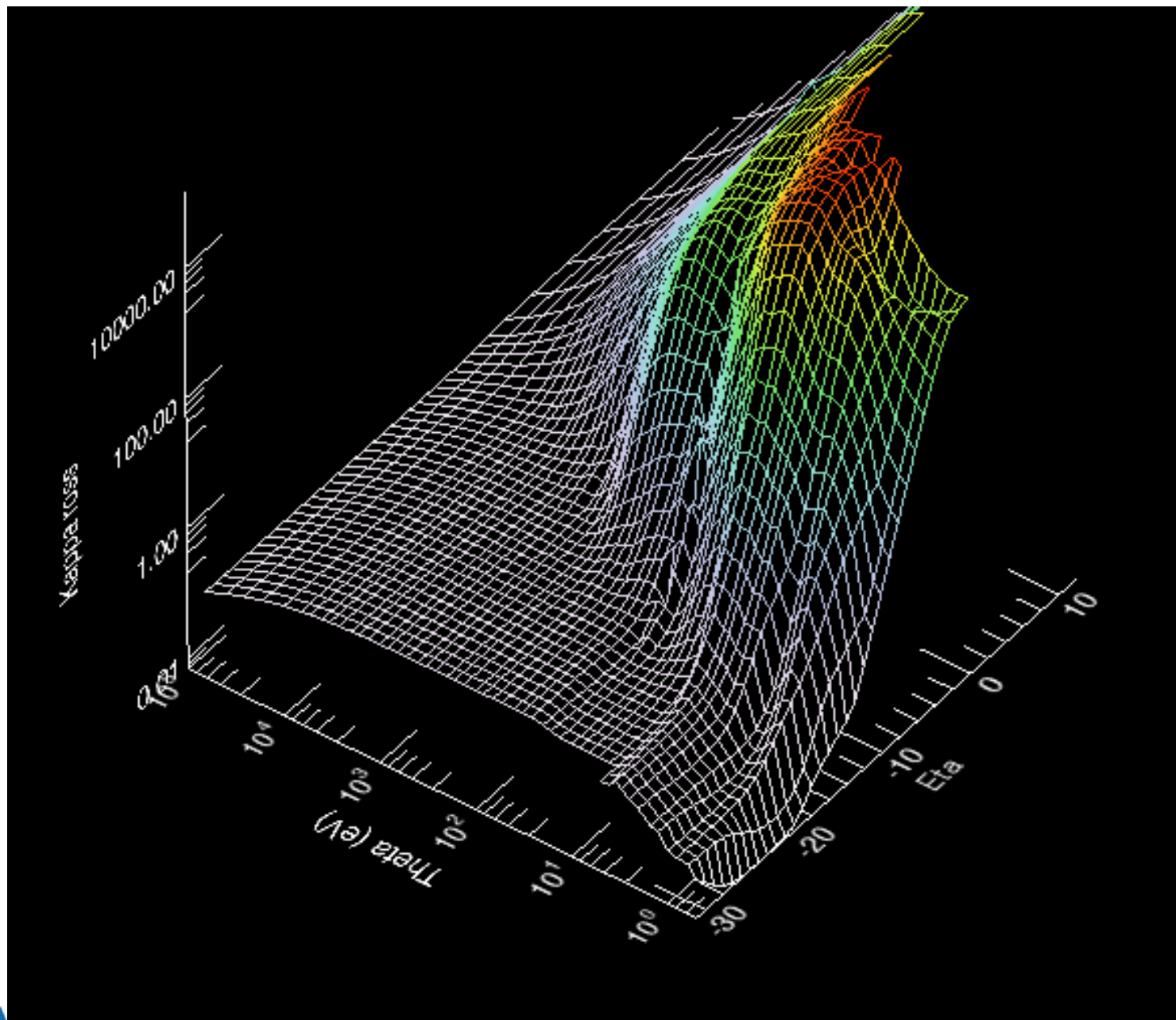
Oxygen



Argon

OXYGEN





Occupation probabilities

H-like CARBON: $T = 10^6$ K, $\rho = 0.01$ g / cm³

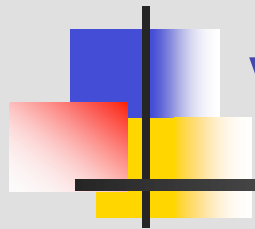
n	CHEMEOS [†]	Holtmark*	OP*	APEX*	OPAL*
1	1.00	1.00	1.00	1.00	1.00
2	1.00	9.97E-1	9.91E-1	9.98E-1	9.96E-1
3	9.87E-1	9.50E-1	9.06E-1	9.76E-1	9.95E-1
4	7.08E-1	4.90E-1	4.95E-1	7.20E-1	9.95E-1
5	1.25E-1	5.25E-2	3.62E-2	1.76E-1	9.14E-1
6	1.14E-2	4.63E-3	6.33E-6	2.21E-2	5.27E-1
7	1.04E-3	5.19E-3	2.96E-16	2.46E-3	1.62E-1
8	9.58E-5	7.79E-5	4.76E-41	3.66E-4	2.37E-2
9	7.63E-6	3.19E-6	1.06E-94	6.75E-5	2.23E-3

[†] A.Y. Potekhin, G. Chabrier, and D. Gilles, Physical Review E **65**, 036412 (2002)

* C.A. Iglesias and F.J. Rogers, Astrophysical Journal **443**, 460-463 (1995)

Summary and future work

- new low-Z opacity and EOS code *ATOMIC*
- chemical picture
- free-energy minimization method
- occupation-probability formalism
- analytic equations of state
- self-consistent opacity and EOS data
- application to non-LTE
- better microfields (unscreened → screened)
- application to heavier elements



Visualization Tools for Opacity Analysis

Leslie Welser

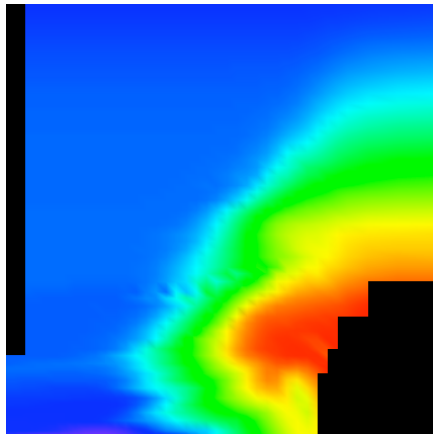
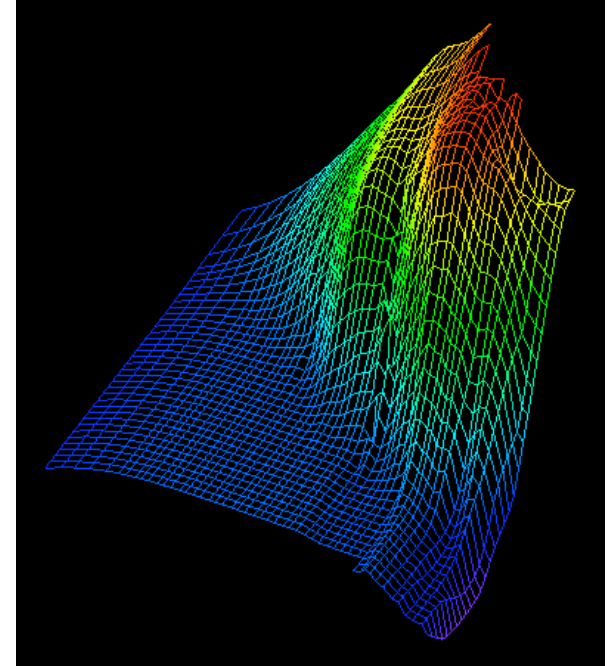
Graduate Research Assistant, LANL T-4 and X-2
University of Nevada, Reno

LANL T-4 Collaborators:

Joe Abdallah, David Kilcrease, Norm Magee, Manolo Sherrill,
Peter Hakel, Stephane Mazevet, James Colgan,
Chris Fontes (X-5), Honglin Zhang (X-5)

Introduction to Opacity Visualization

- The need for opacity visualization
 - investigation of new opacity tables (ATOMIC)
 - comparison of codes
 - reduce the learning curve
 - graphical user interface will facilitate studies into the deep details of opacity code output
 - IDL Virtual Machine allows anyone to run the program without having to purchase IDL



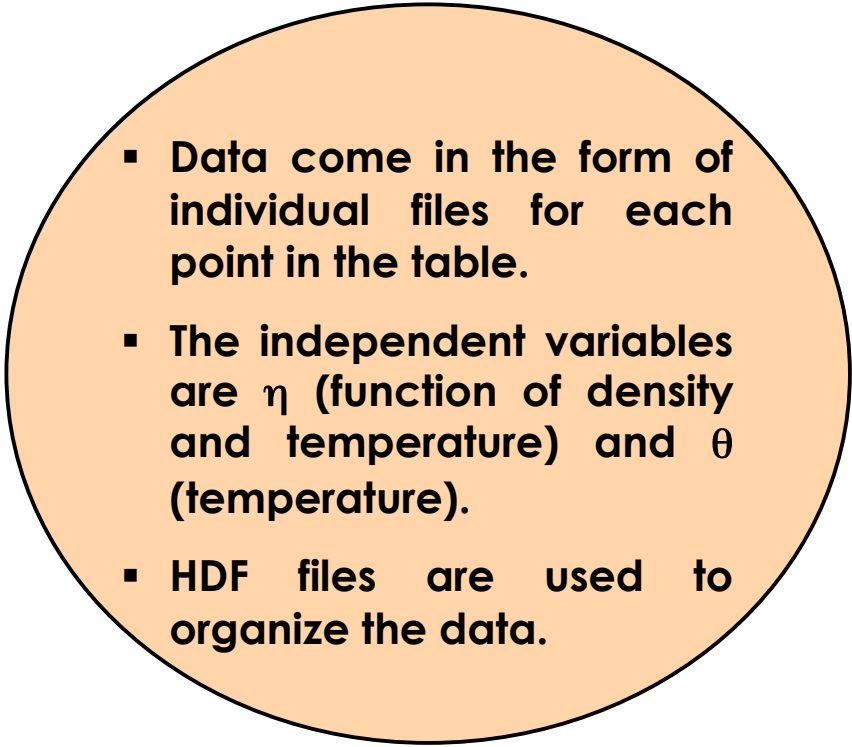
Main goal of this opacity visualization project:

Build an easy-to-use yet sophisticated tool to allow the T-4 opacity group to 'diagnose' their opacity tables.



Data for Visualization

- Many physical quantities are output from ATOMIC
 - Opacities
 - Rosseland
 - Planckian
 - Conductive
 - Rosseland + Conductive
 - Planckian + Conductive
 - Z-bar
 - Ion density, electron density
 - Mass density
 - Total internal energy
 - five individual contributions
 - Total pressure
 - five individual contributions
 - Debye radius
 - Plasma frequency

- 
- **Data come in the form of individual files for each point in the table.**
 - **The independent variables are η (function of density and temperature) and θ (temperature).**
 - **HDF files are used to organize the data.**



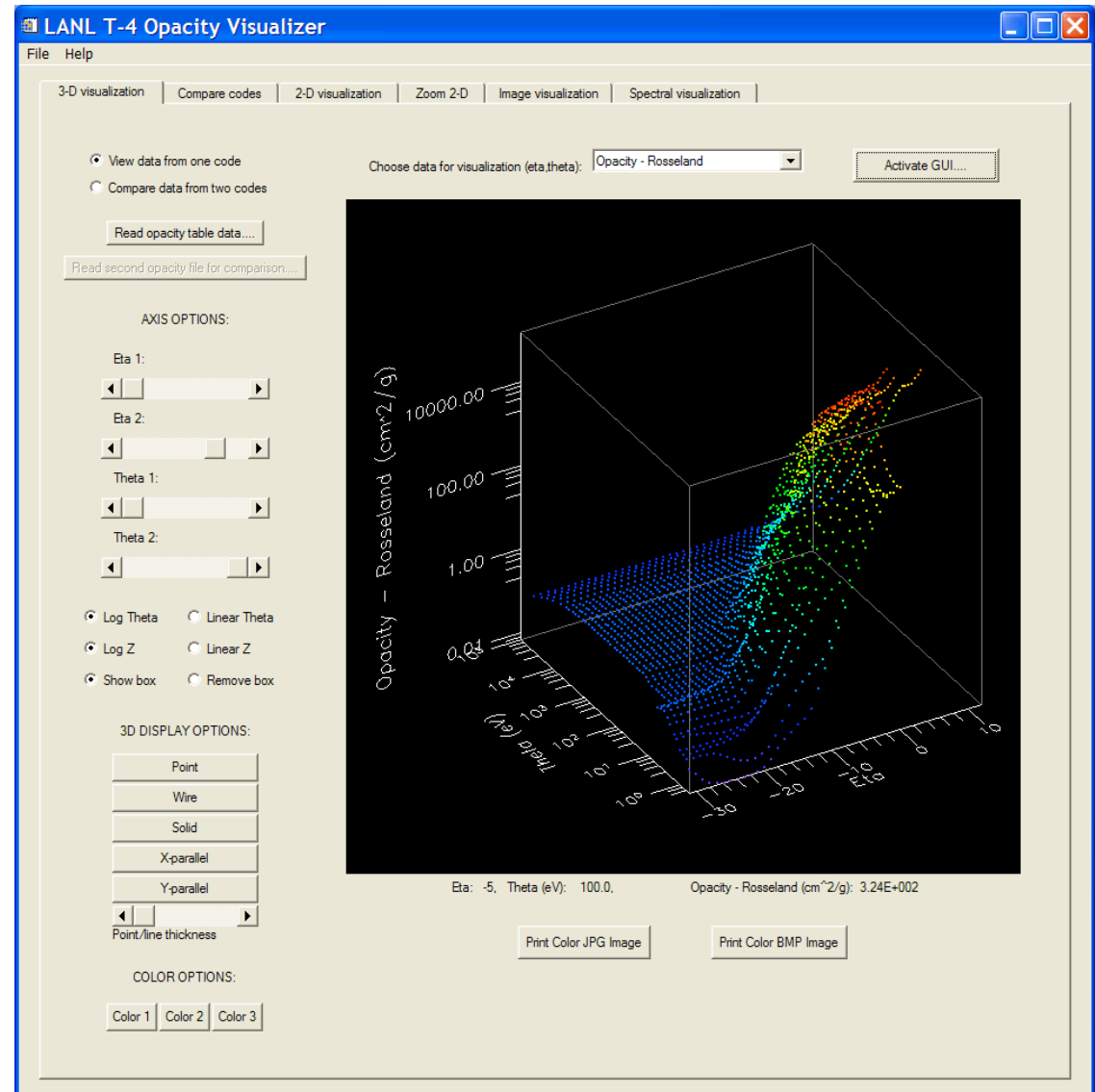
Important Needs

- Graphical user interface built in IDL (Interactive Data Language)
 - tab layout: simple straightforward interface with room for later additions and improvements
 - 'crash-proof': buttons, droplists, slider bars, and windows become active only when the input data becomes available
 - no set order of operations: users can flip between tabs and change previous choices
- 3-d capability
 - visualization of surfaces as a function of η and θ
 - object-oriented programming allows plot rotation and manipulation
- 2-d capability
 - selection of regions of interest for 2-d representation
 - zooming and printing possibilities
- Capability to visualize spectra
 - allows comparison of three spectra from specific points in the table

3-d Visualization of Opacity Table Output

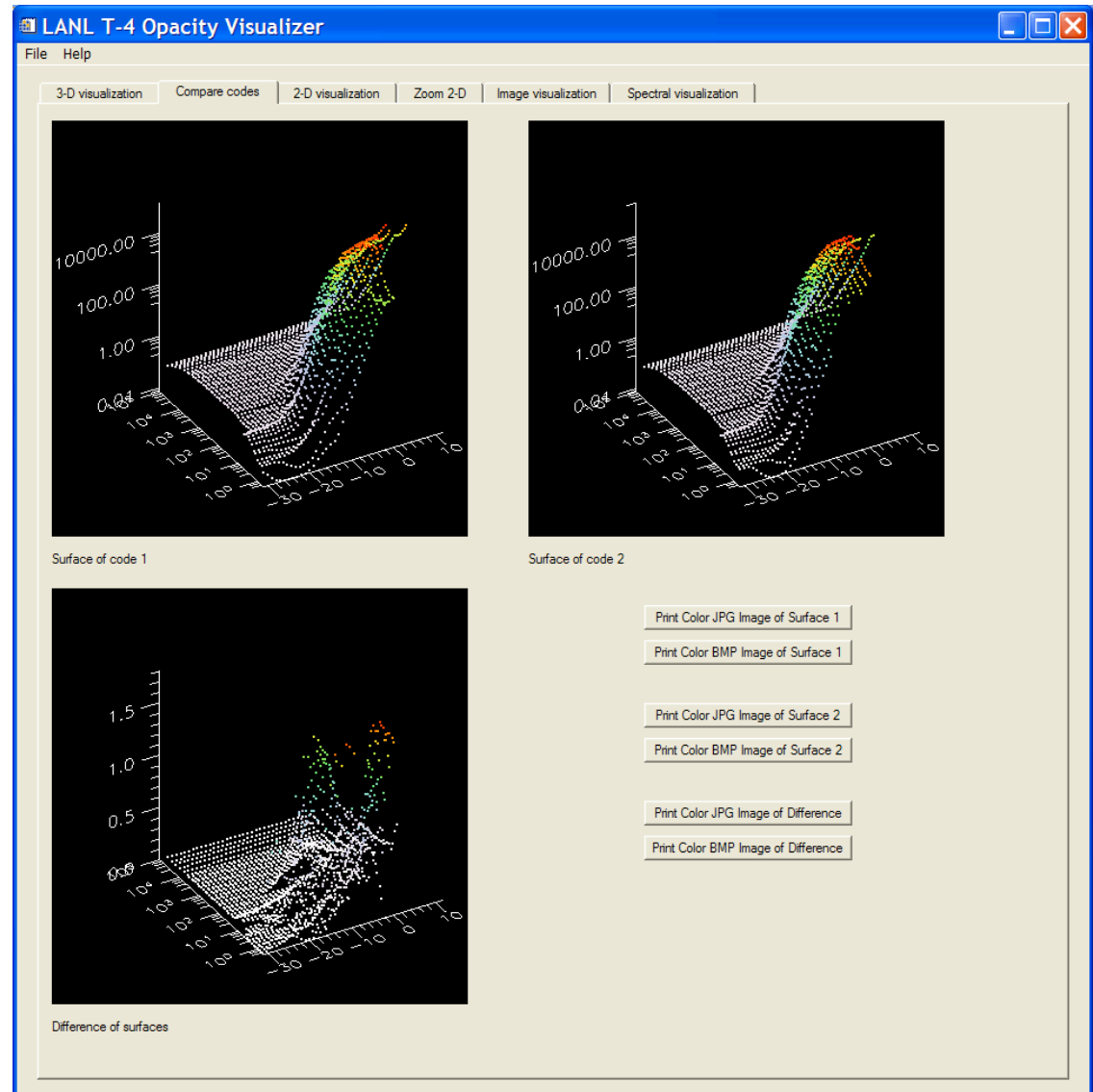
■ Main 3-d tab

- read in data (from 1 or 2 codes)
- data selected in droplist is the 'active' dataset
- rotate 3-d surface
- mouse position on surface gives data point
- change η and θ range
- specify log or linear axes
- show or remove 3-d box
- options for display
- color options
- example: Rosseland opacity as a function of η and θ



Comparison of Codes

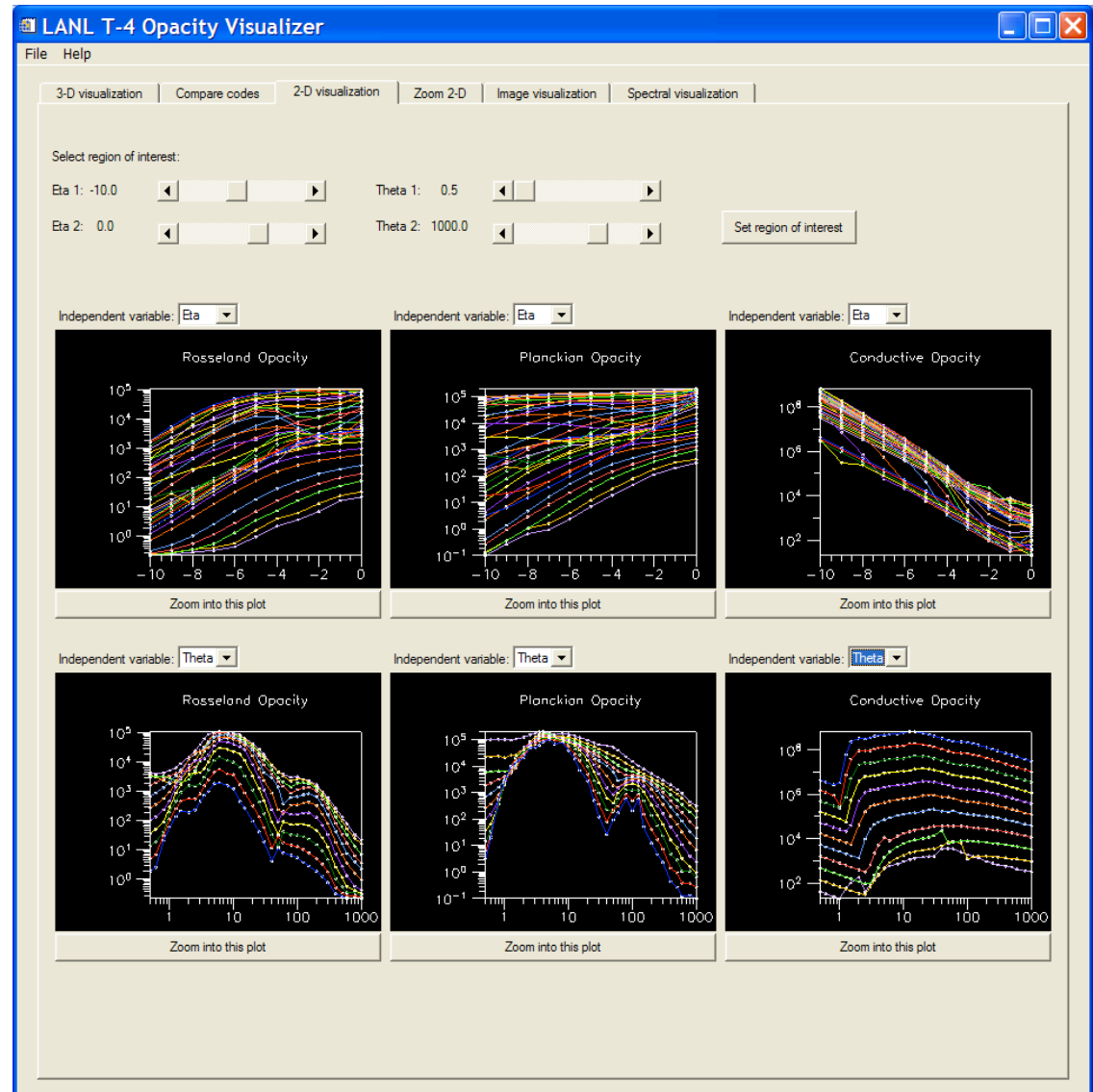
- Code comparison tab
 - view 3-d surfaces of two datasets side-by-side
 - view surface which represents difference between the two codes
 - print color JPG and BMP images



2-d Visualization of Opacity Table Output

■ 2-d tab

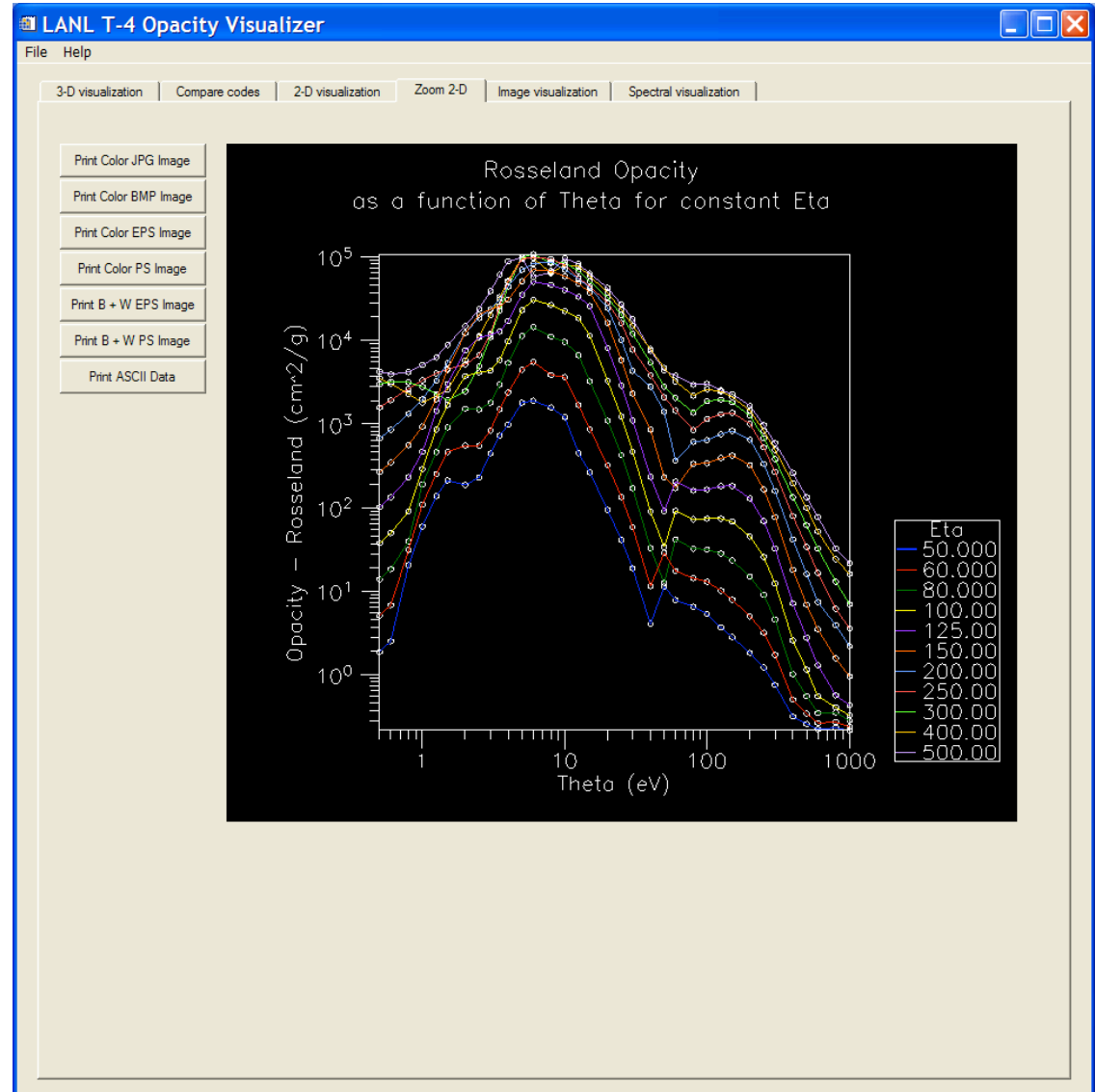
- select a 'region of interest' with η and θ slider bars
- six small 'snapshots' allow active dataset to be displayed
- best used for a quick survey of the data
- each snapshot can be zoomed into
- example: different opacities as a function of either η or θ for constant θ or η



Zooming and Printing Capability

■ Zoom 2-d tab

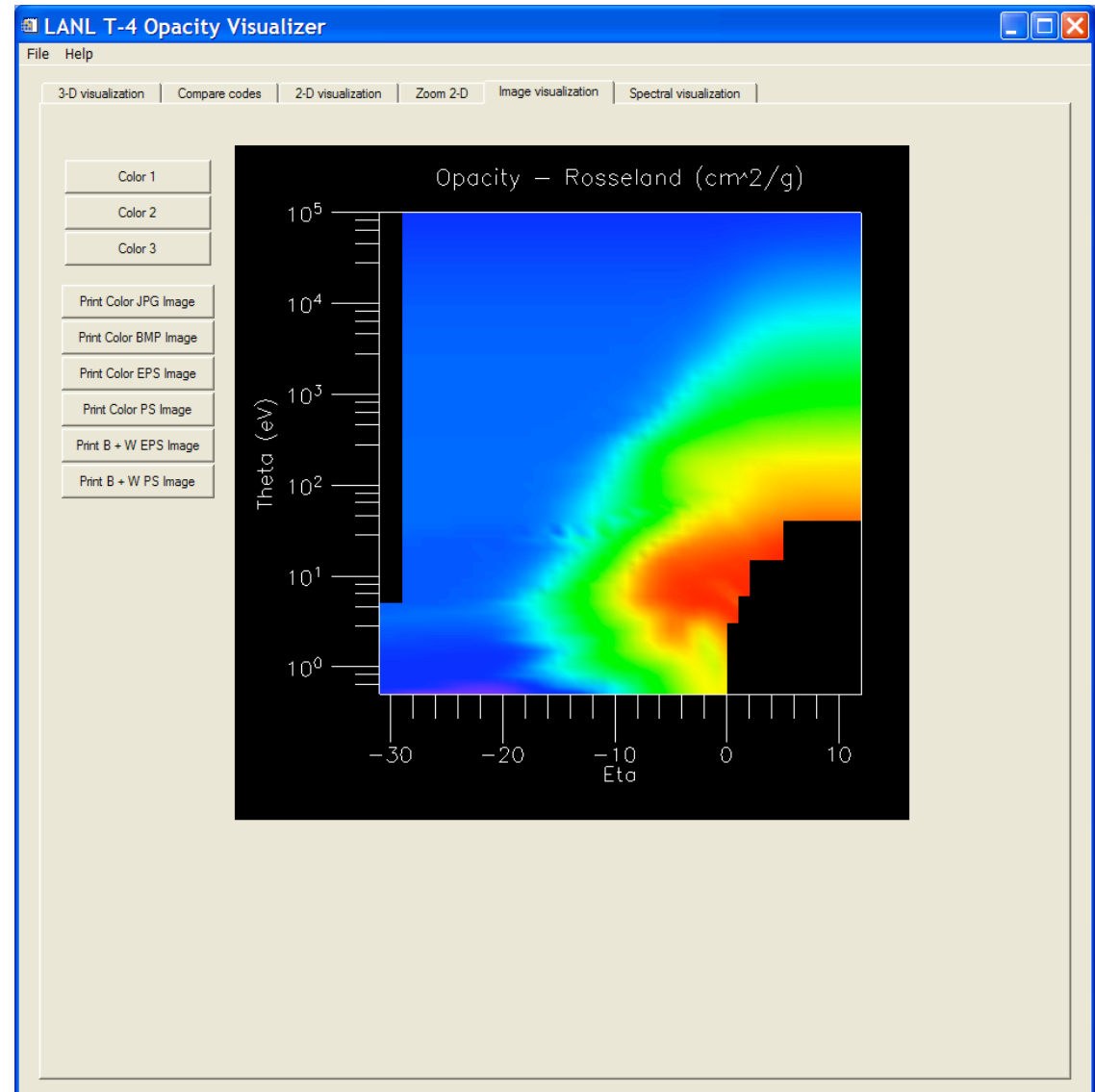
- larger and better quality plots
- axis range is same as on 2-d tab
- legend provides info on iso- η or iso- θ
- printing capability for JPG, BMP, EPS, and PS files (white background)



Surface Image Visualization

■ Image tab

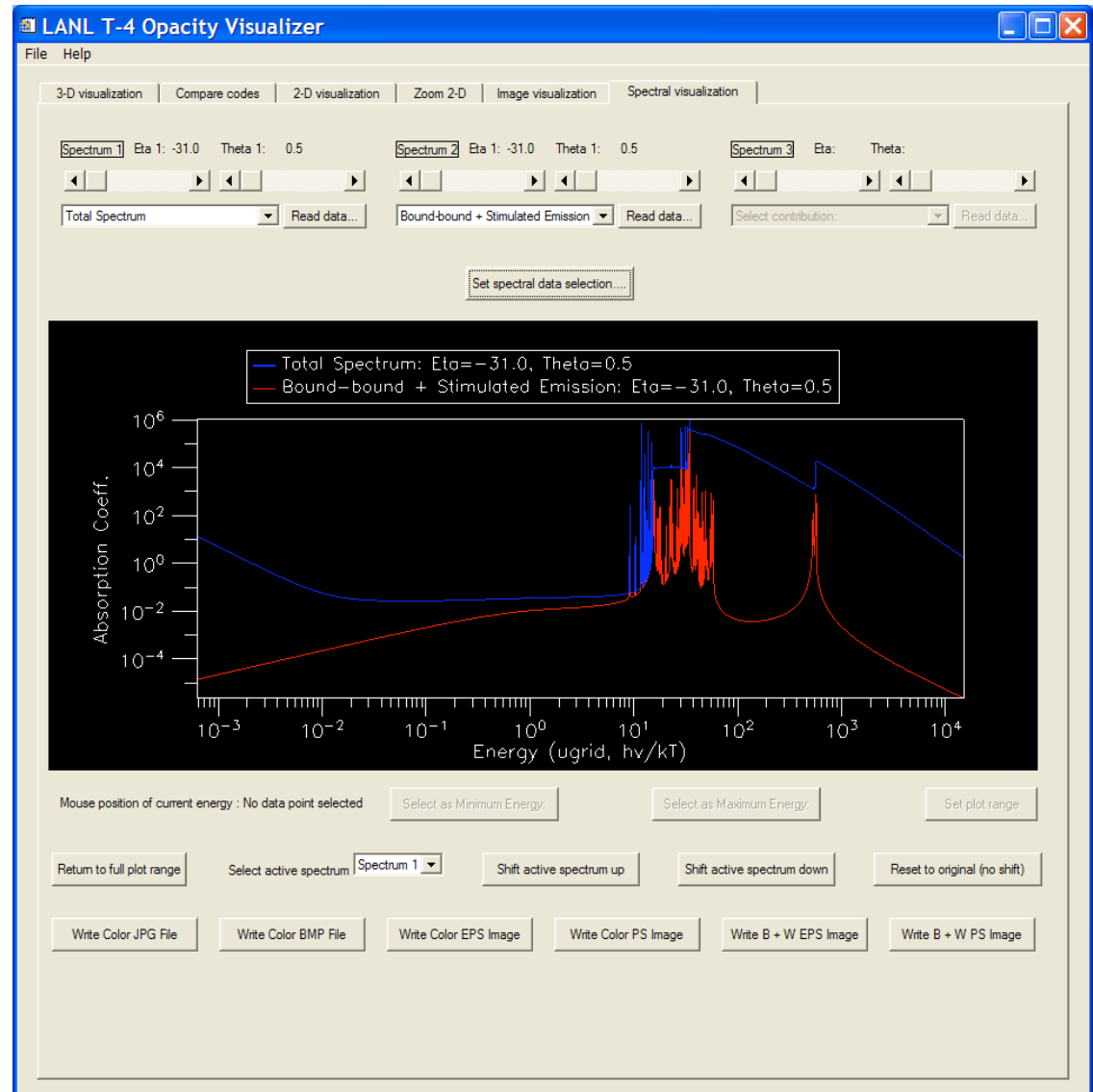
- visualization of active dataset (looking down on surface)
- helps to see missing points in the table
- color scheme can be changed
- printing capability for JPG, BMP, EPS, and PS files



Visualization of Spectra

■ Spectra tab

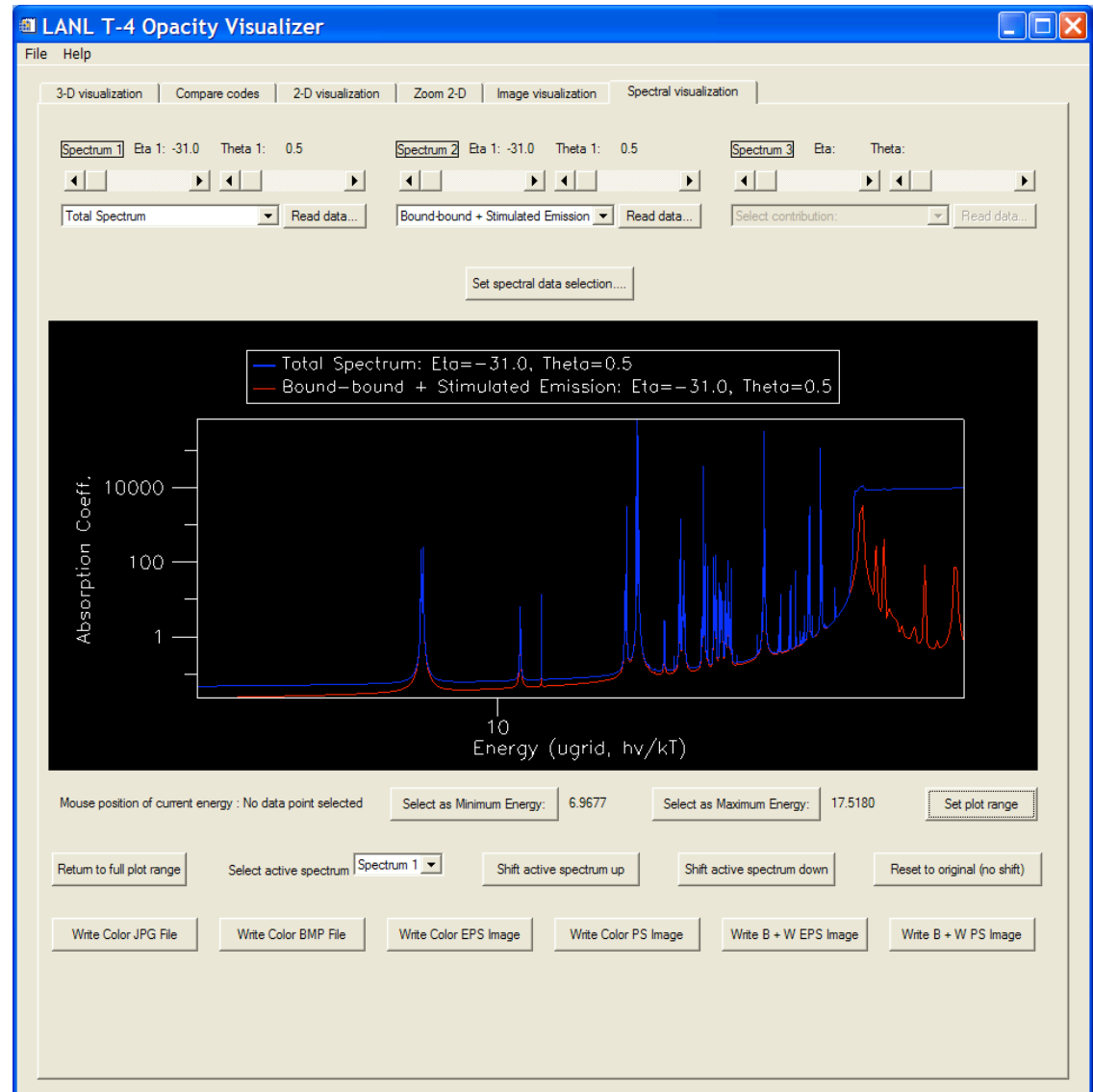
- choose up to three individual data points with associated spectra
- can compare spectral contributions from the same point, or the same contribution from different points
- capability to compare spectra generated by other codes
- printing capability for JPG, BMP, EPS, and PS files



Visualization of Spectra

■ Spectra tab

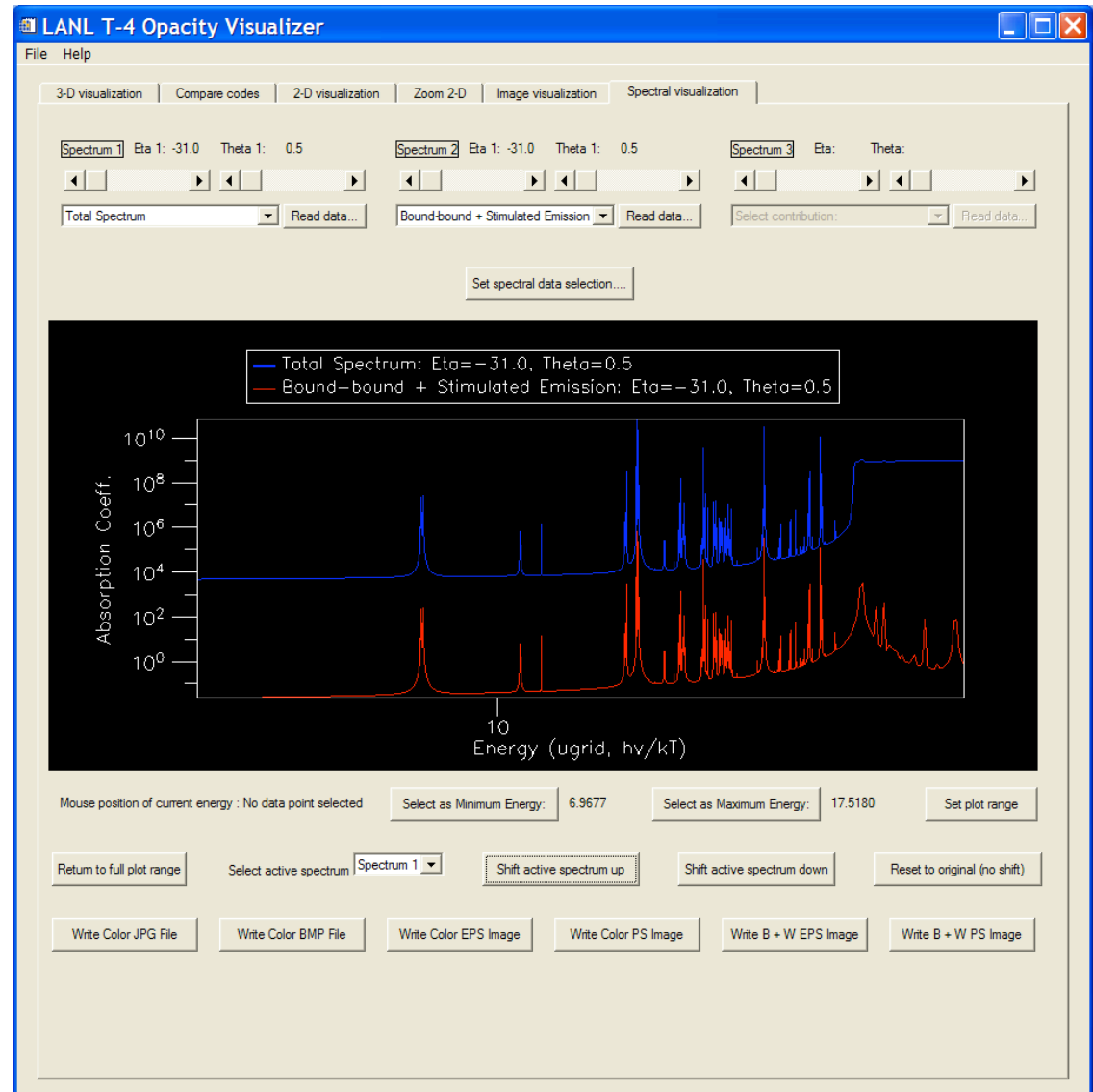
- example: zoom into region of interest
- can reset to full plot range



Visualization of Spectra

■ Spectra tab

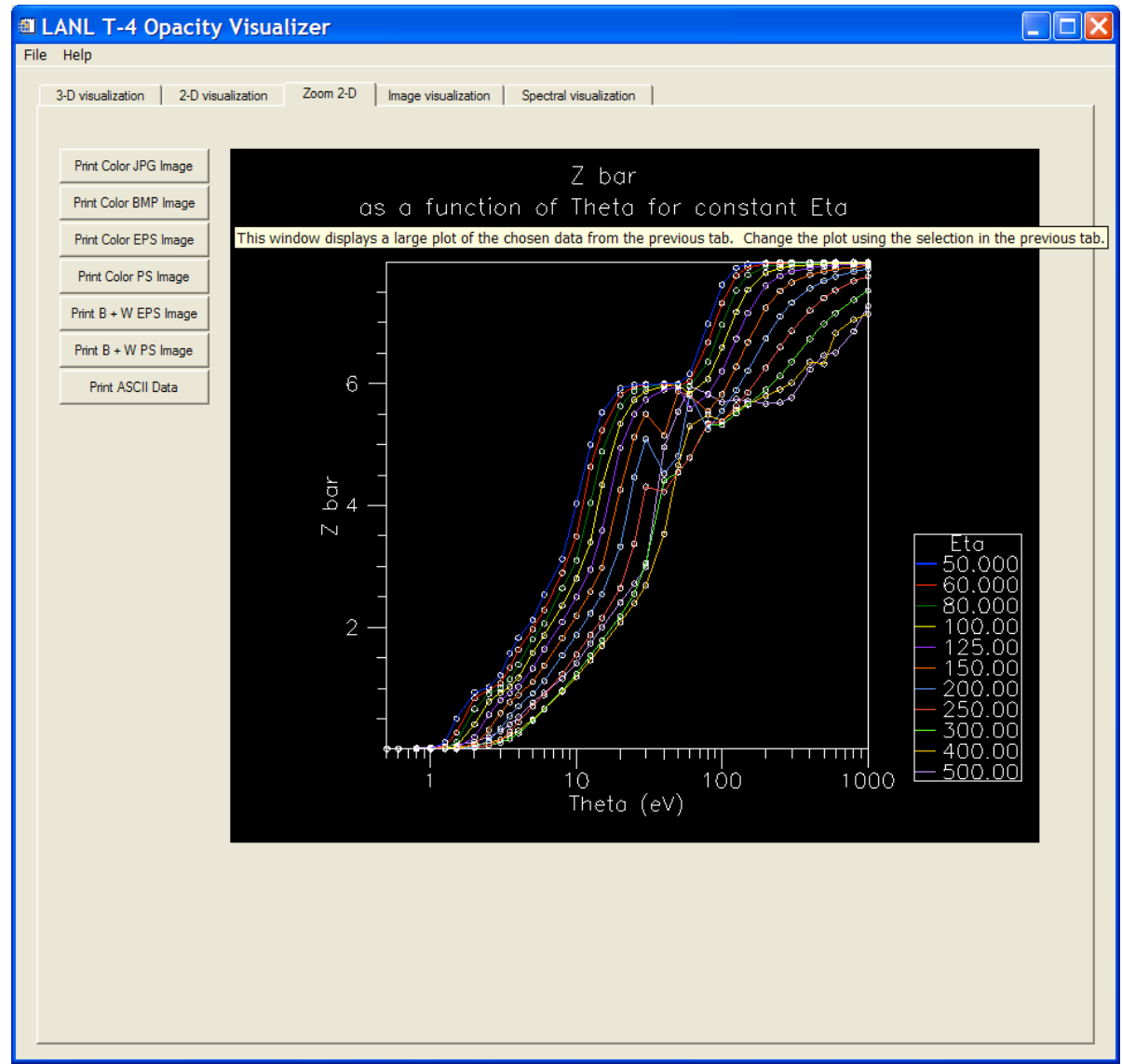
- example: select active spectrum and shift it up or down for easier comparison
- can reset to original case with no shift



Documentation and Help

■ Help options

- documentation in the form of a PDF file
- tooltip tutorial
- contact information
- version information





Conclusion and Future Work

- Capabilities to expand
 - expand ability to compare two datasets from two different codes
 - improve printing ability with more options
 - create interactive help menu

Main goal of this opacity visualization project:

Build an easy-to-use yet sophisticated tool to allow the T-4 opacity group to 'diagnose' their opacity tables.

Adapt the tool for outside use on the T-4 opacity webpage.

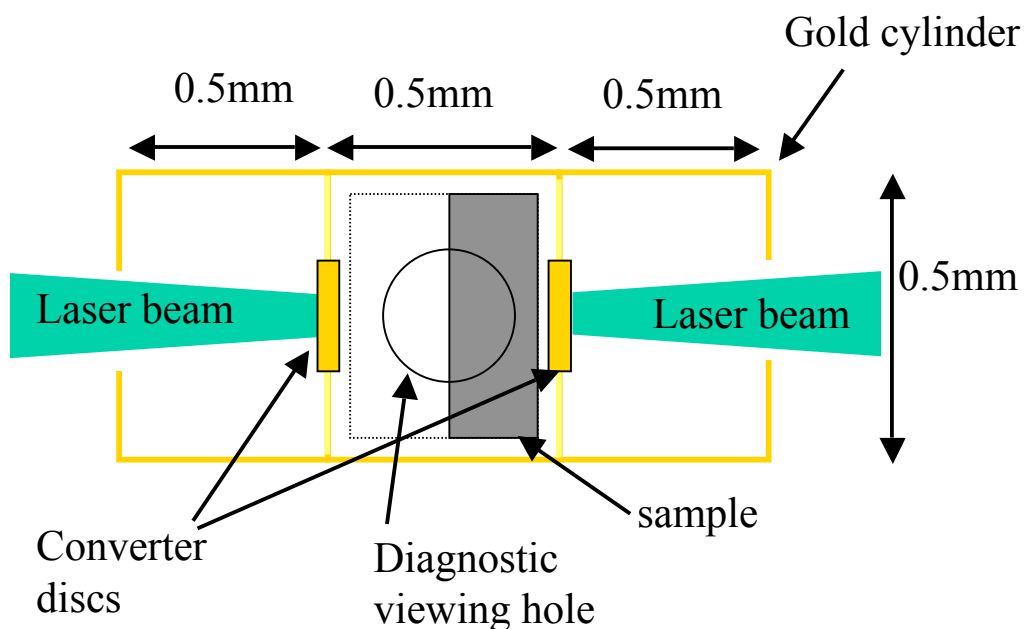
Recent and proposed opacity experiments at the AWE HELEN laser.

D J Hoarty, E L Clark, B J B Crowley, S J Davidson,
J W O Harris, L Upcraft, P Graham, S F James, S G Gales,
C D Bentley, C C Smith.

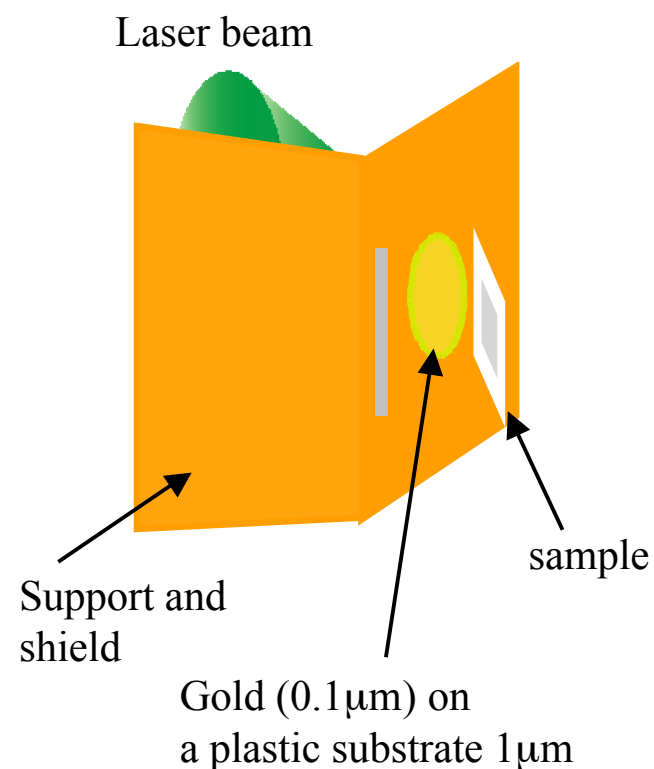
HELEN experiments-creating the opacity sample by X-ray heating of thin foils

Two methods :

1. Hohlraum

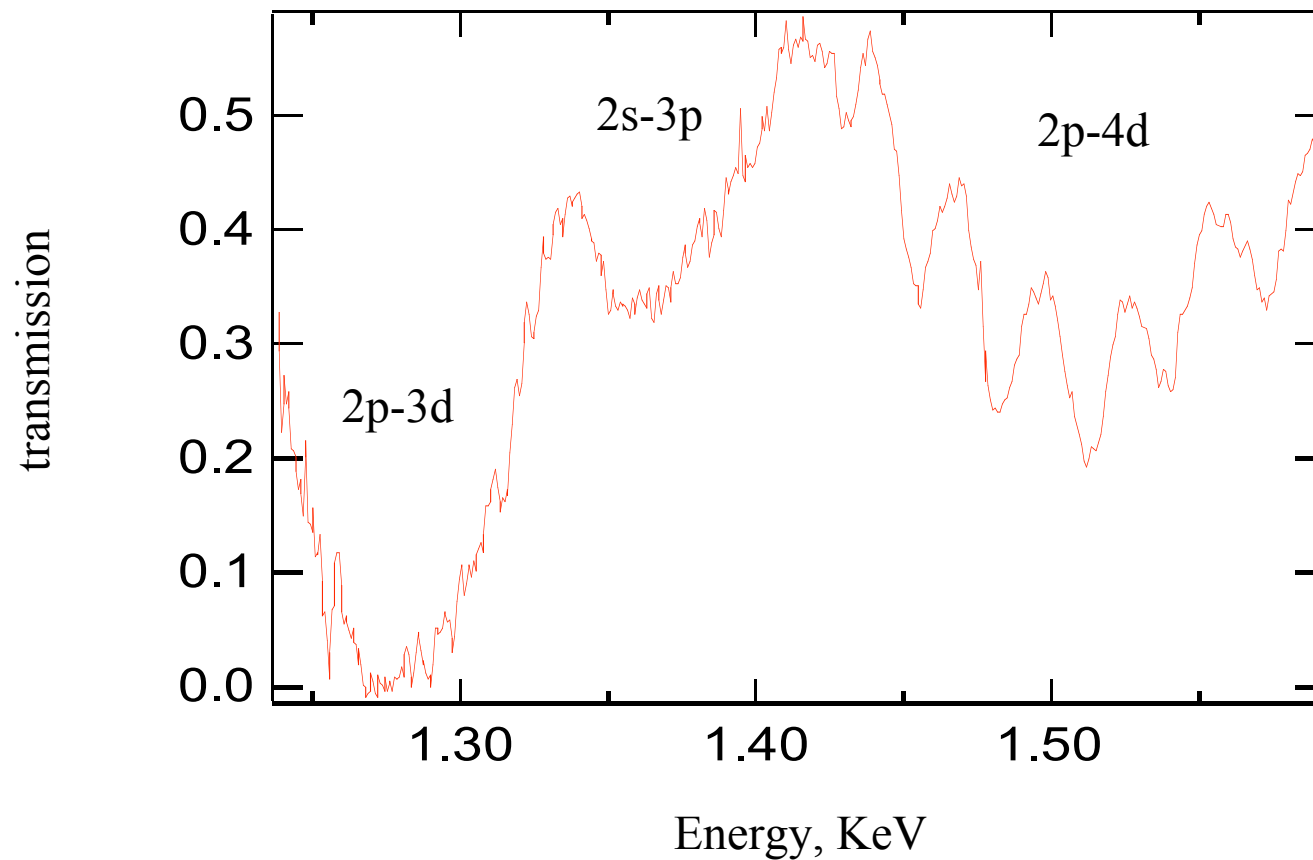


2. Burnthrough foil

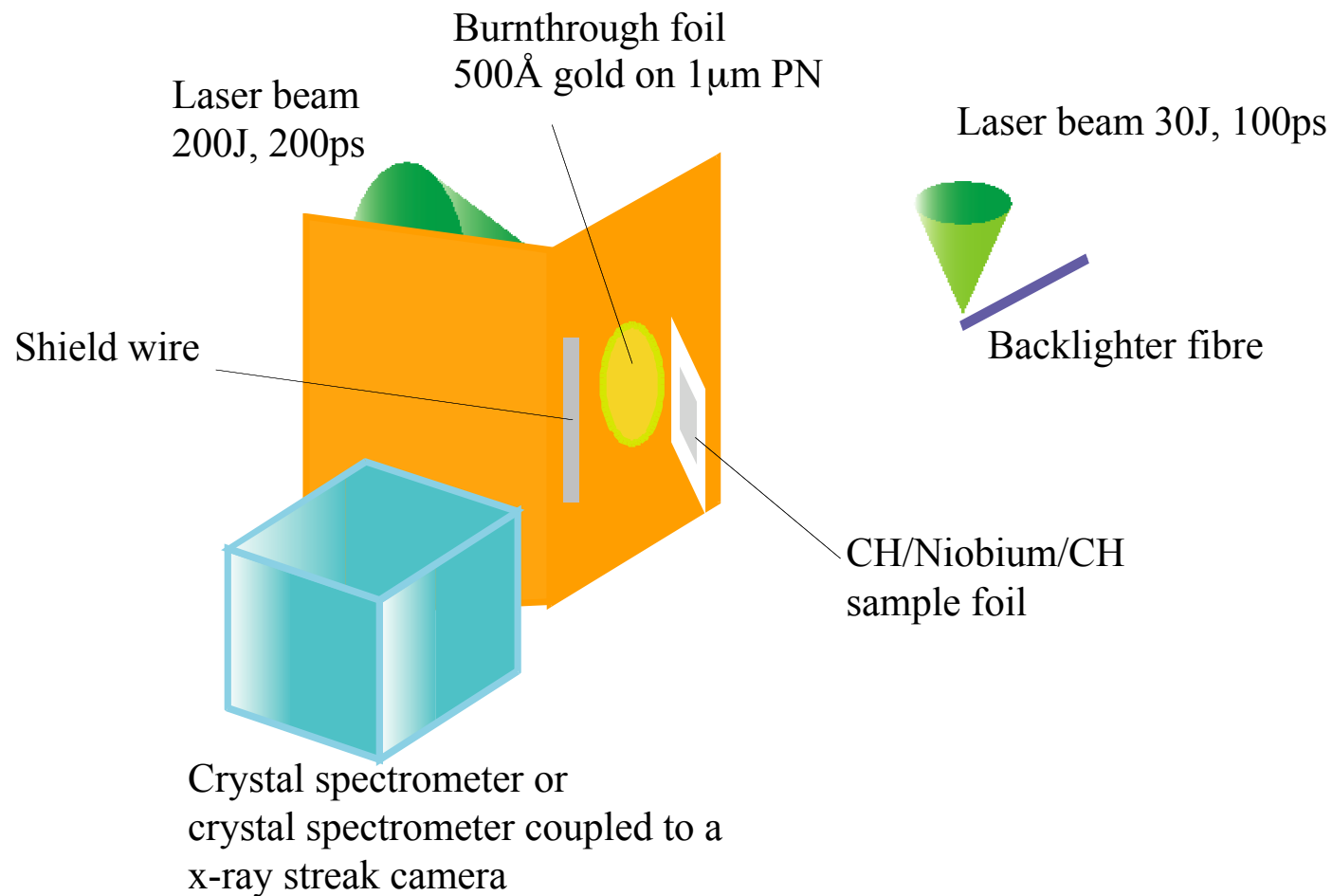


Past HELEN experiments have measured absorption in open M-shell configurations using germanium samples heated in hohlraums.

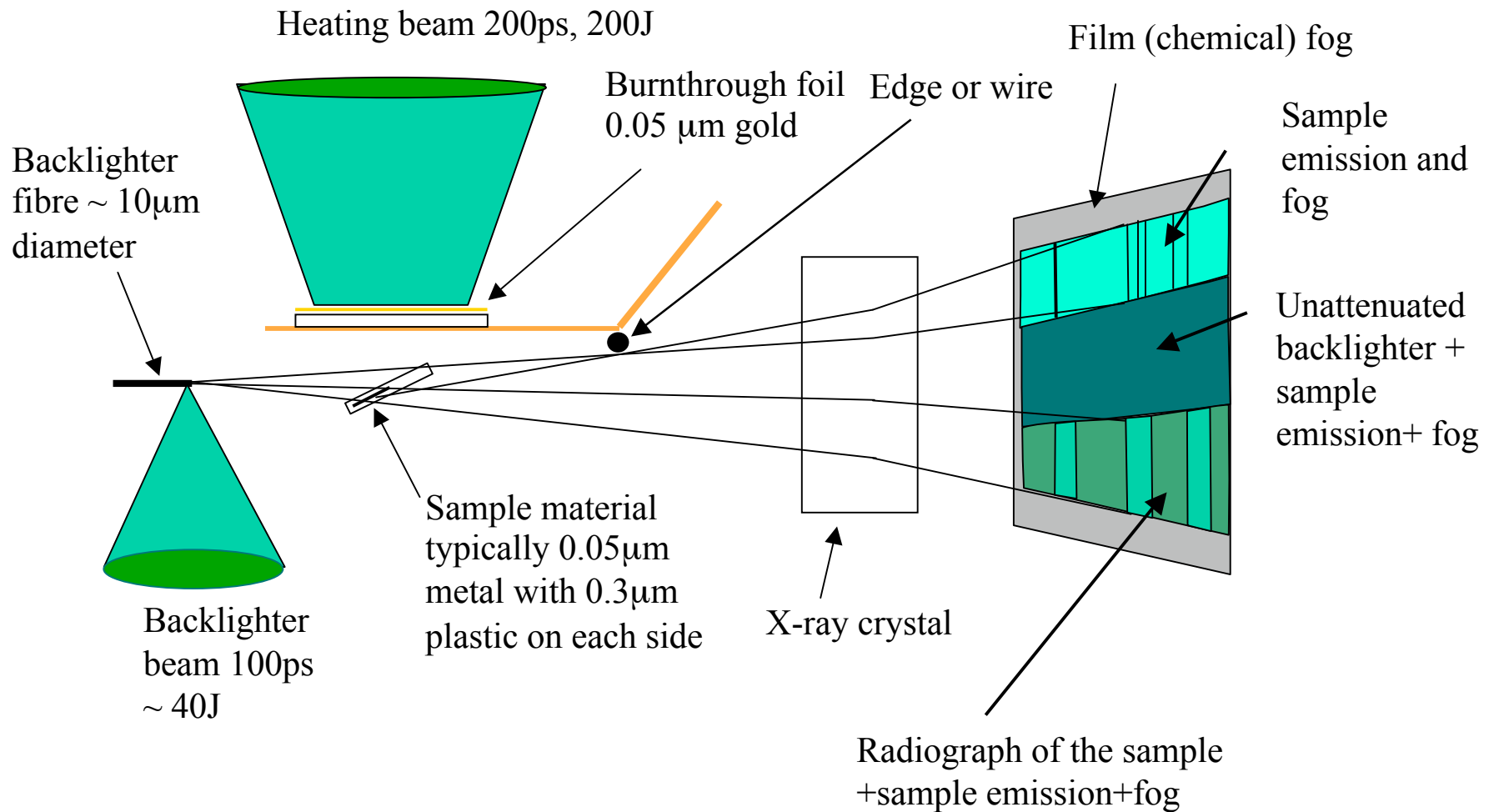
Germanium absorption 0.05g/cc, 76eV



Niobium experiments used point projection spectroscopy and samples heated by burnthrough foils.

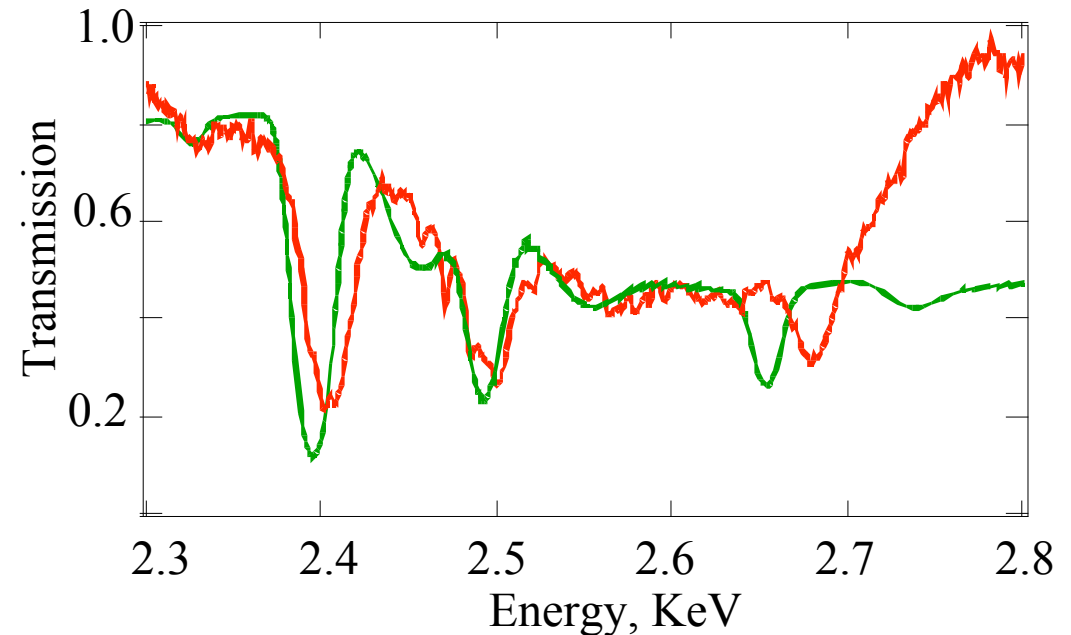


Diagnosing the sample with point projection spectroscopy

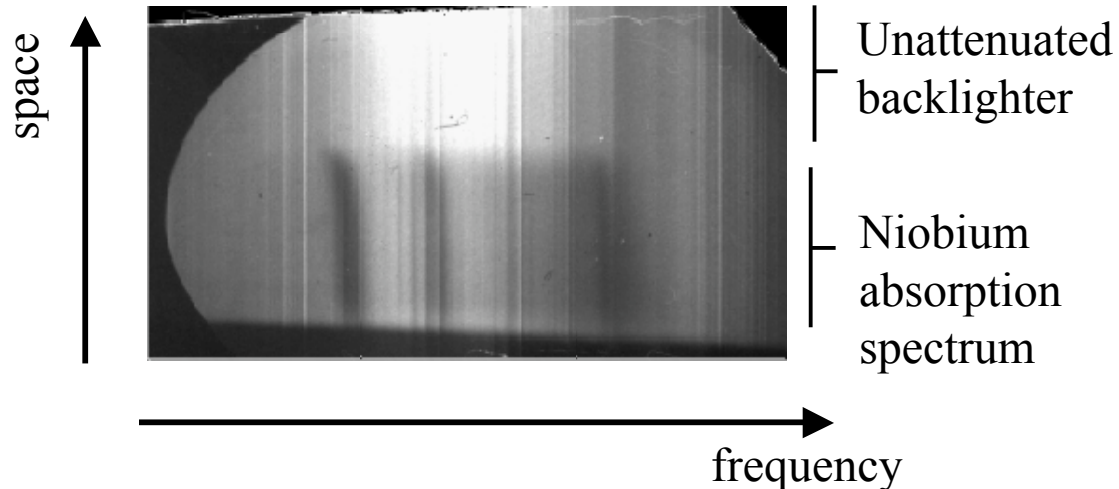


Absorption spectra are rich in detailed information to compare to calculation predictions.

- Data give information on: -
 - the position and width of transition arrays.
 - the positions of absorption edges
 - the transmission of arrays
 - the transmission between arrays

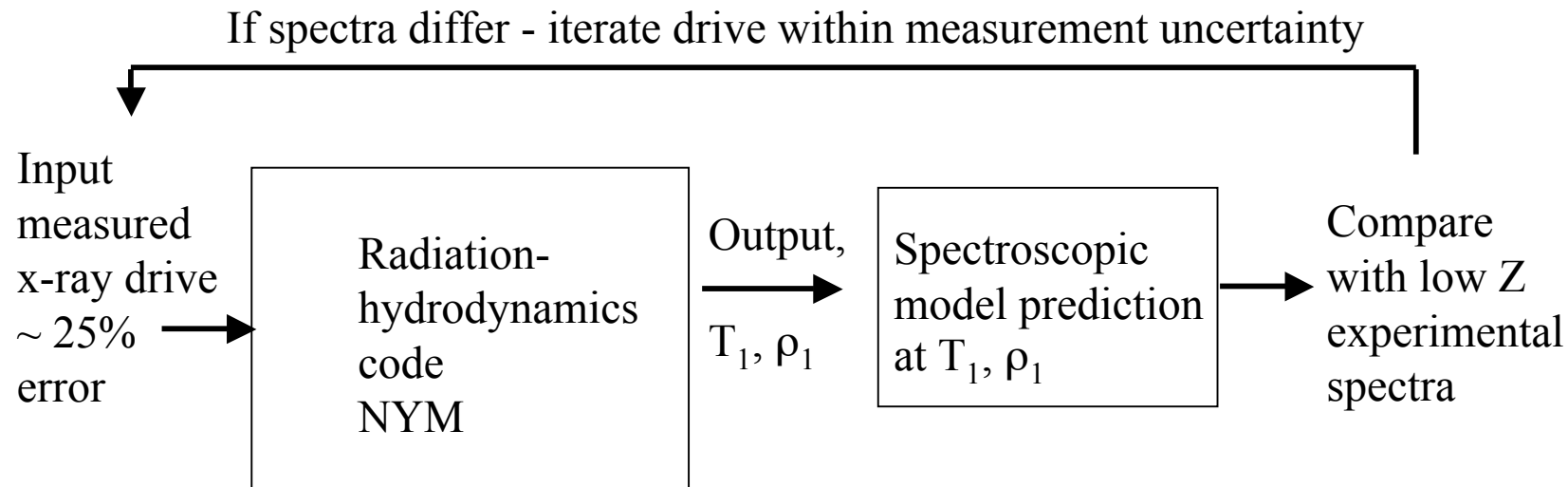


Dispersed radiograph



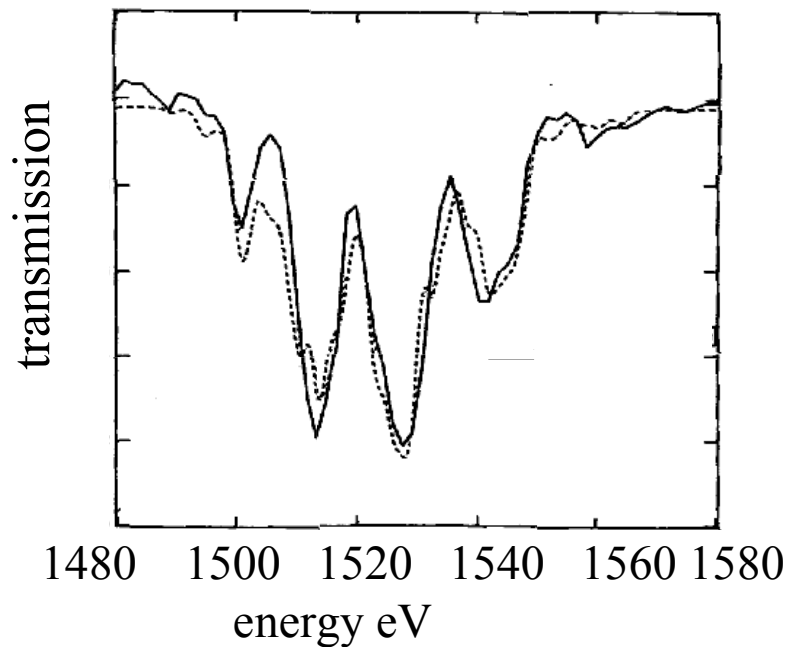
Diagnosing the sample conditions.

- Not enough to measure an absorption spectrum, the sample conditions must be known.
- The conditions are constrained by a combination of measurements and two-dimensional radiation hydrodynamics modelling.
- Measurements include x-ray flux measurements of the hohlraum x-rays using flat response x-ray diodes and x-ray spectroscopy of low Z materials (Al or Mg).
- Recent experiments have used mixtures of low and high Z materials.

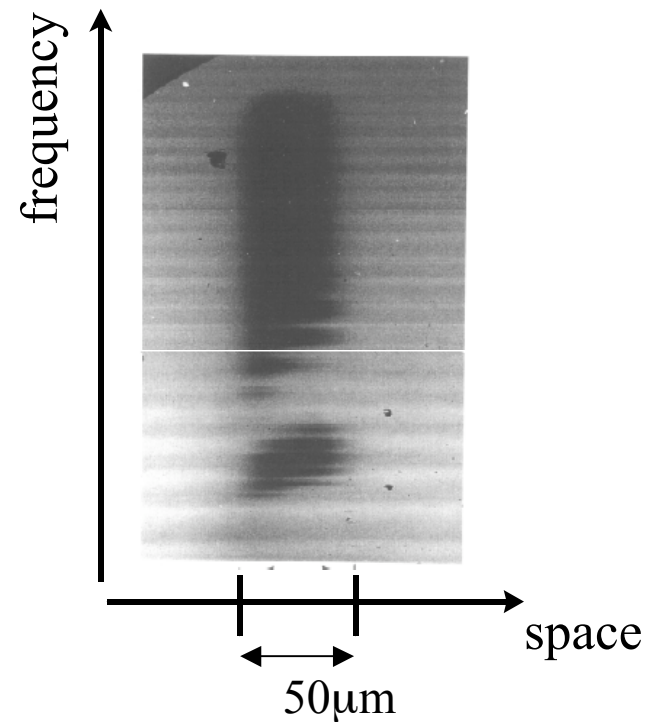


Drive and sample characterisation - expansion and ionisation measurements.

Modelling of the 1s-2p transitions in LTE ionised aluminium samples to infer the heating effect of the burnthrough foils



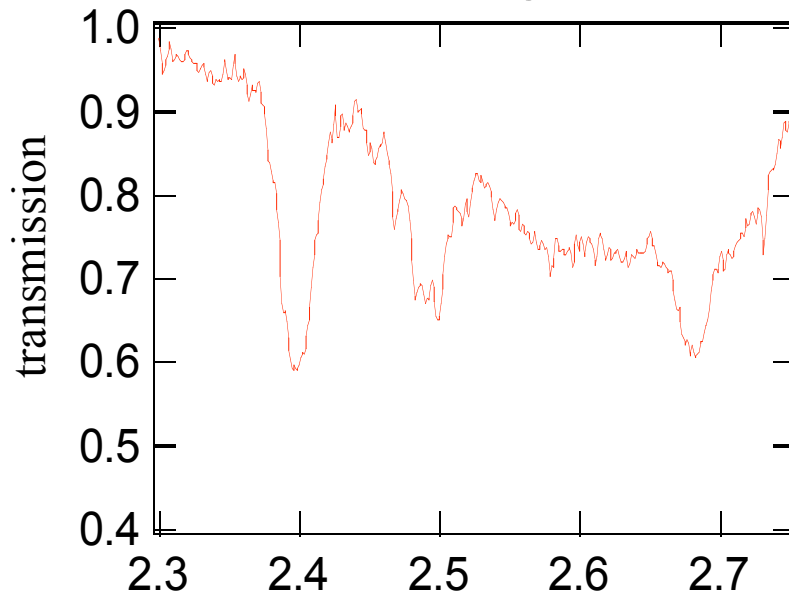
Side-on radiographs of expanded Al samples



The L-shell absorption spectrum in plasmas with a near full M-shell changes dramatically over a small temperature range.

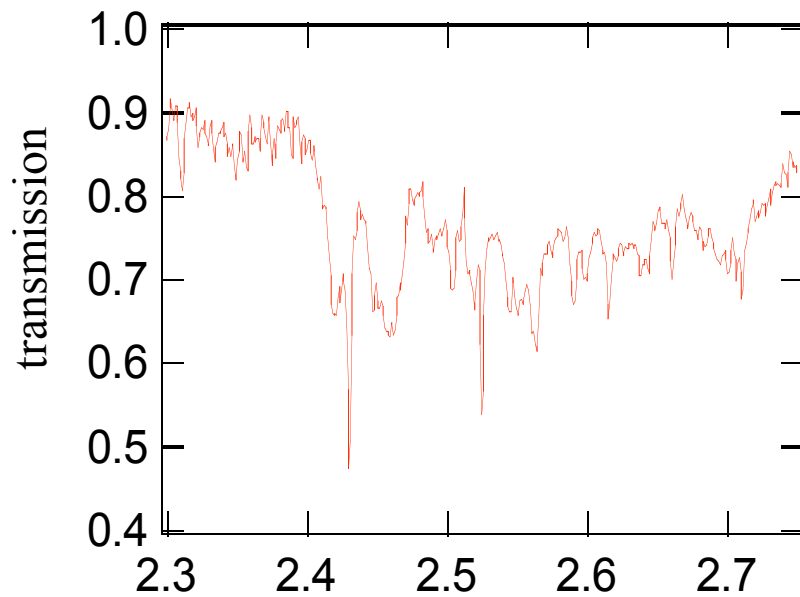
Niobium absorption spectra in the region of 2p-4d transitions

32eV, 0.05g/cc



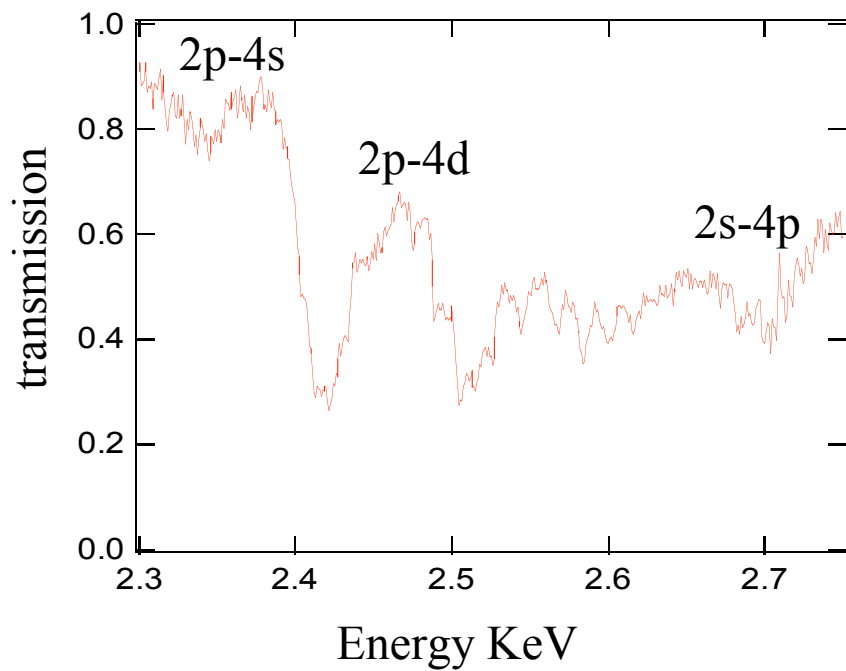
Energy KeV

42eV, 0.03 g/cc

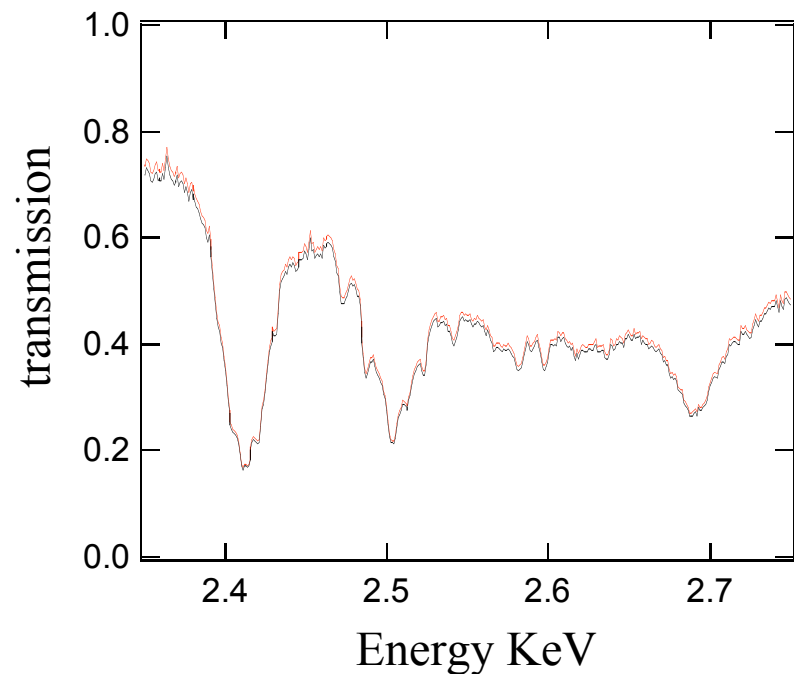


Energy KeV

The experimental data were obtained at slightly different conditions by varying the backlighter delay with respect to the heating beam.

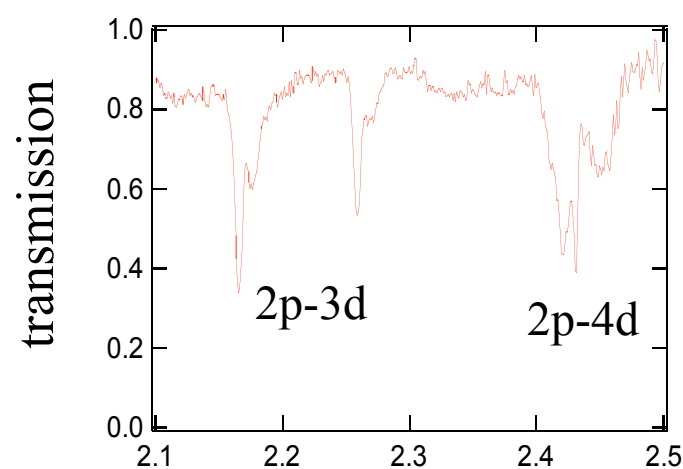
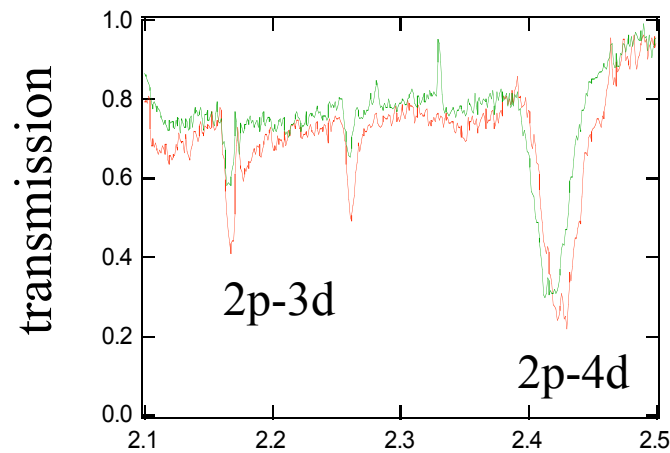
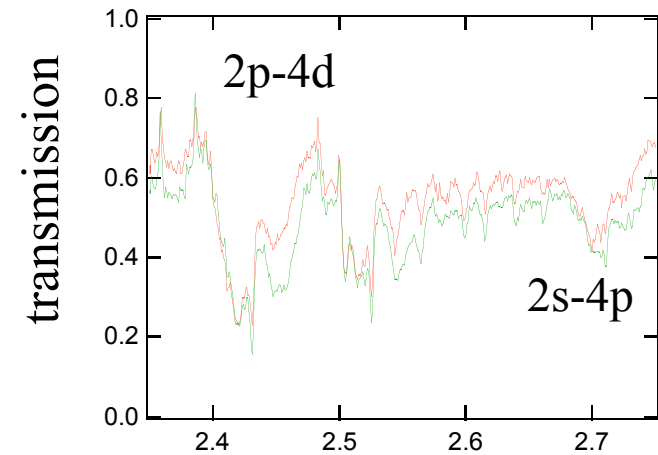
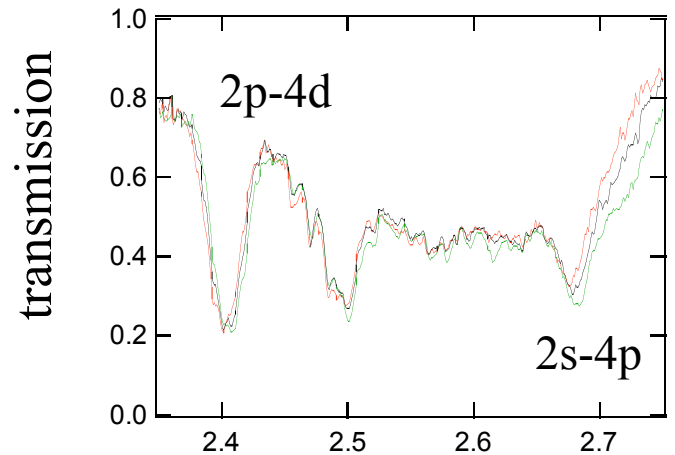


~Te 38eV, density 0.05g/cc



~ Te 34eV, density 0.06g/cc

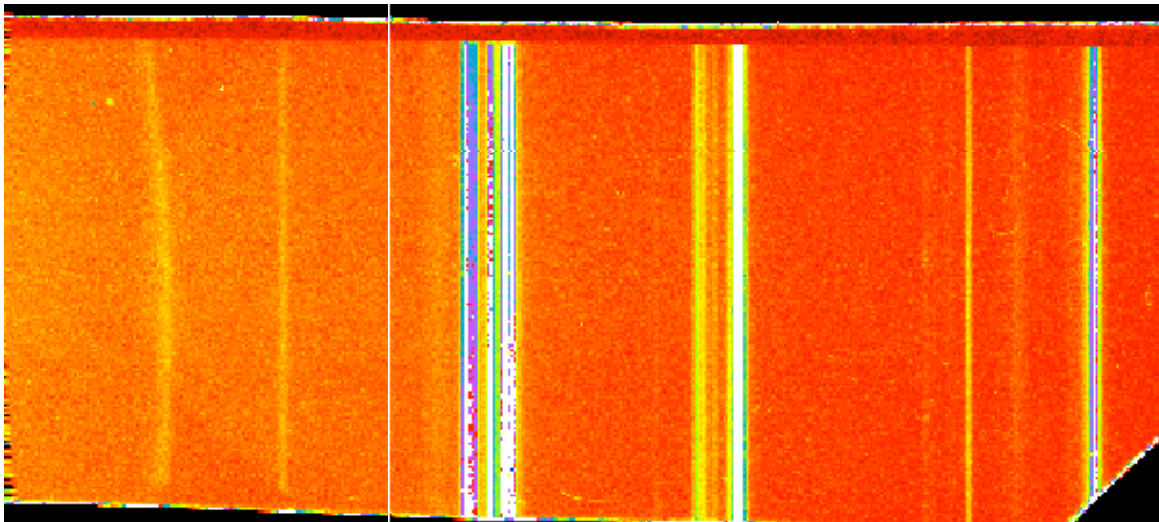
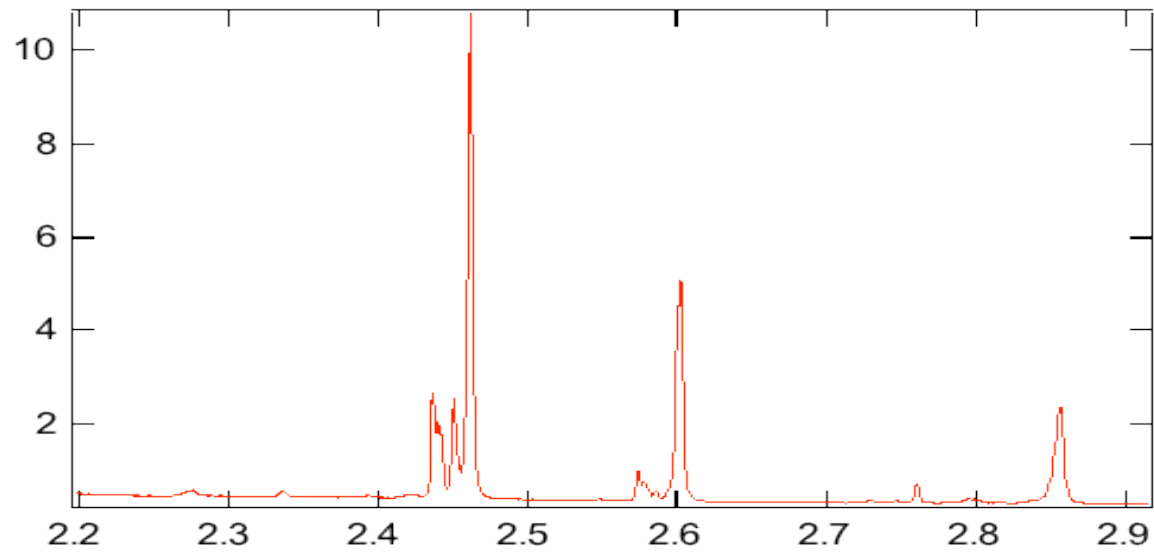
Measurements of niobium L-shell transitions were made at conditions where the M-shell average occupancy changes from zero to one.



Energy KeV

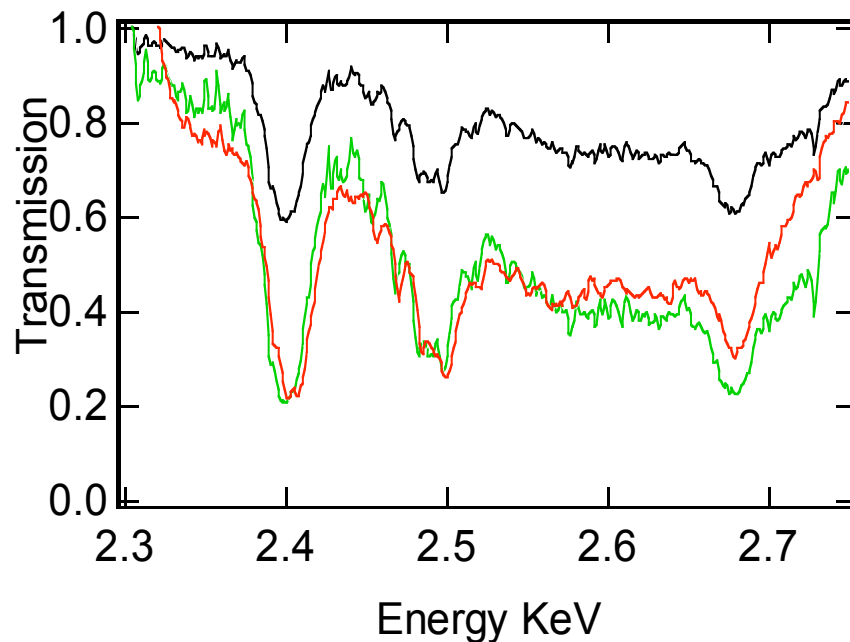
Energy KeV

Spectrometer spectral calibration using low Z (Sulphur) K-shell line emission

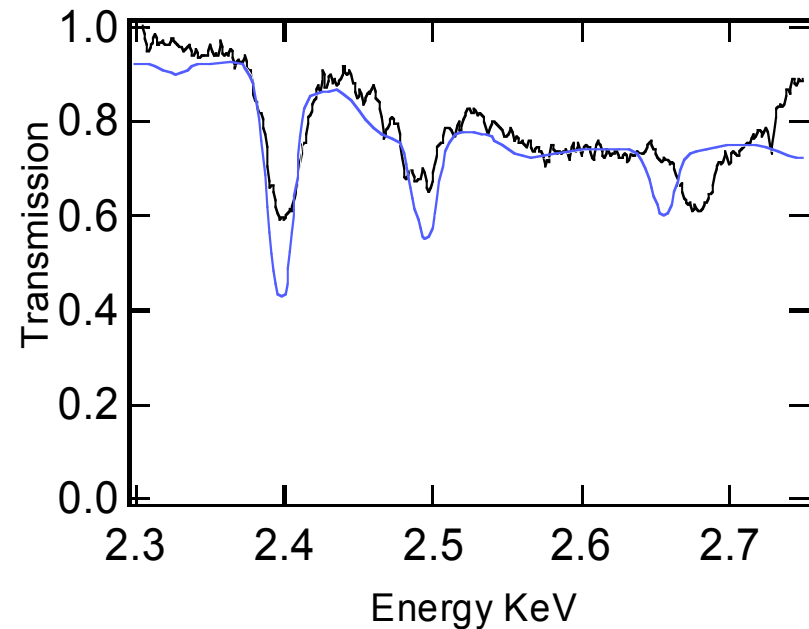


Helen experiments on different thickness samples suggest arrays are not porous. However a discrepancy with the calculations remains.

Experiments on thick and thin samples suggest there is no significant unresolved structure.

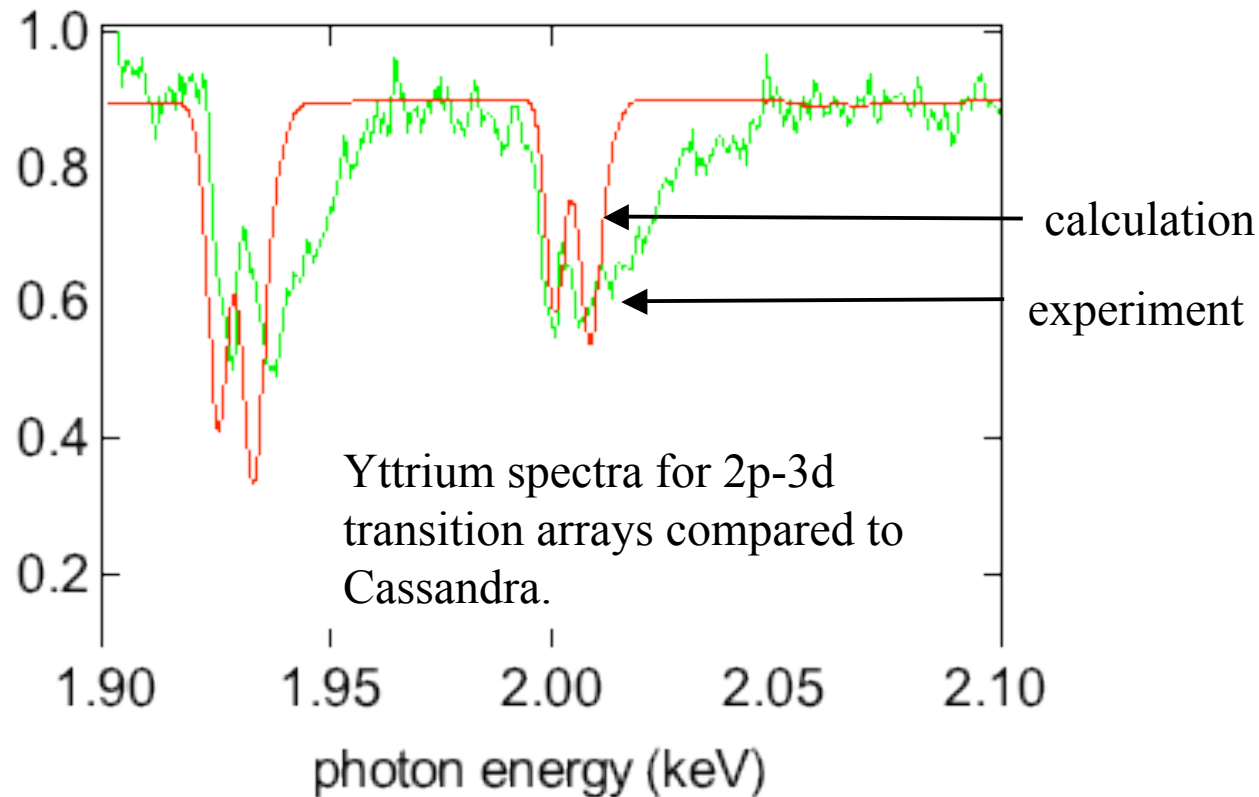


However calculation and experiments disagree on the transmission in the centre of transition arrays.

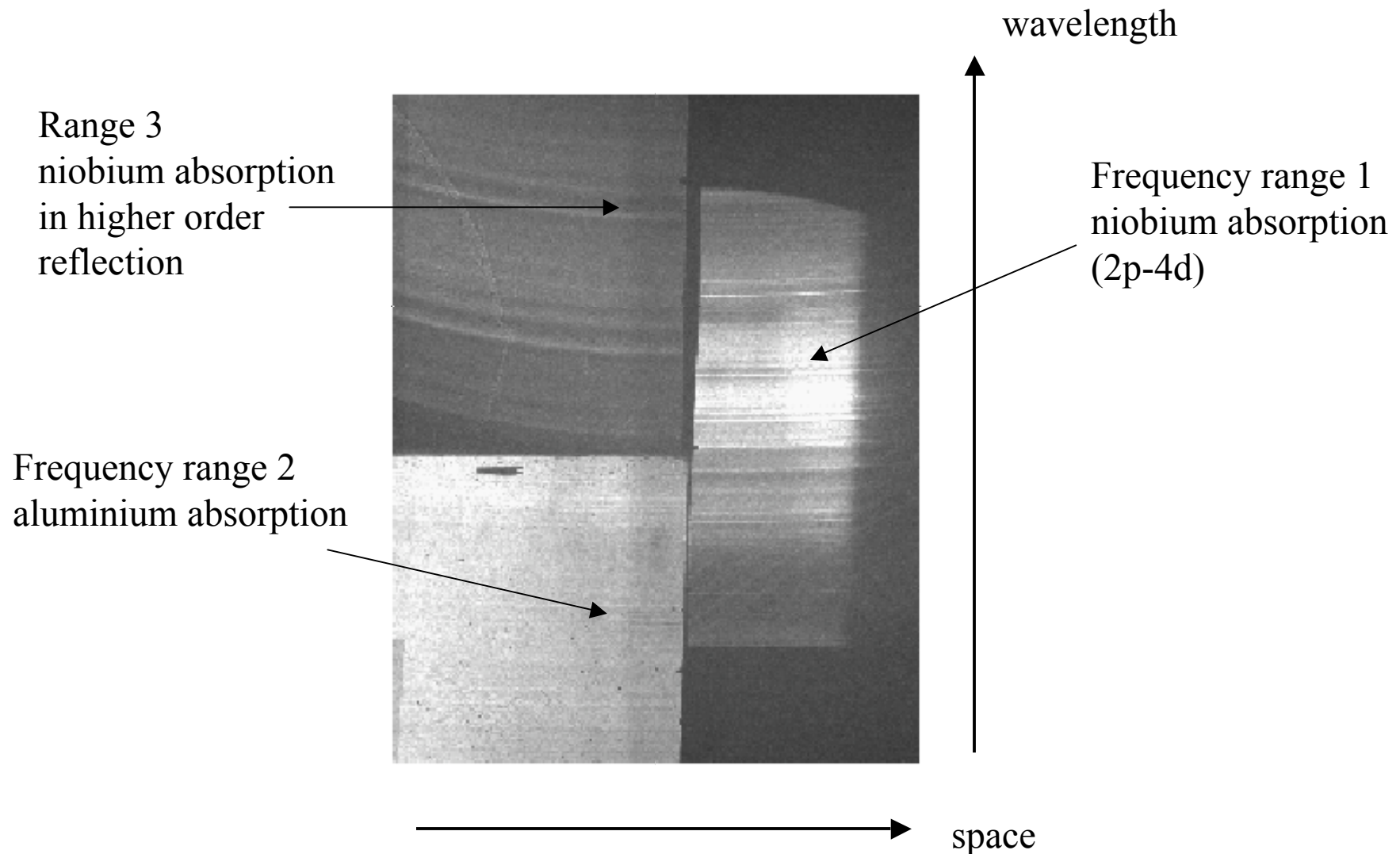


Some experimental findings still remain unexplained - transition array porosity in mid-Z elements and transition array wings.

- HELEN experiments showed blue wings on transition arrays for near full M-shell configurations. These were not predicted by Cassandra.

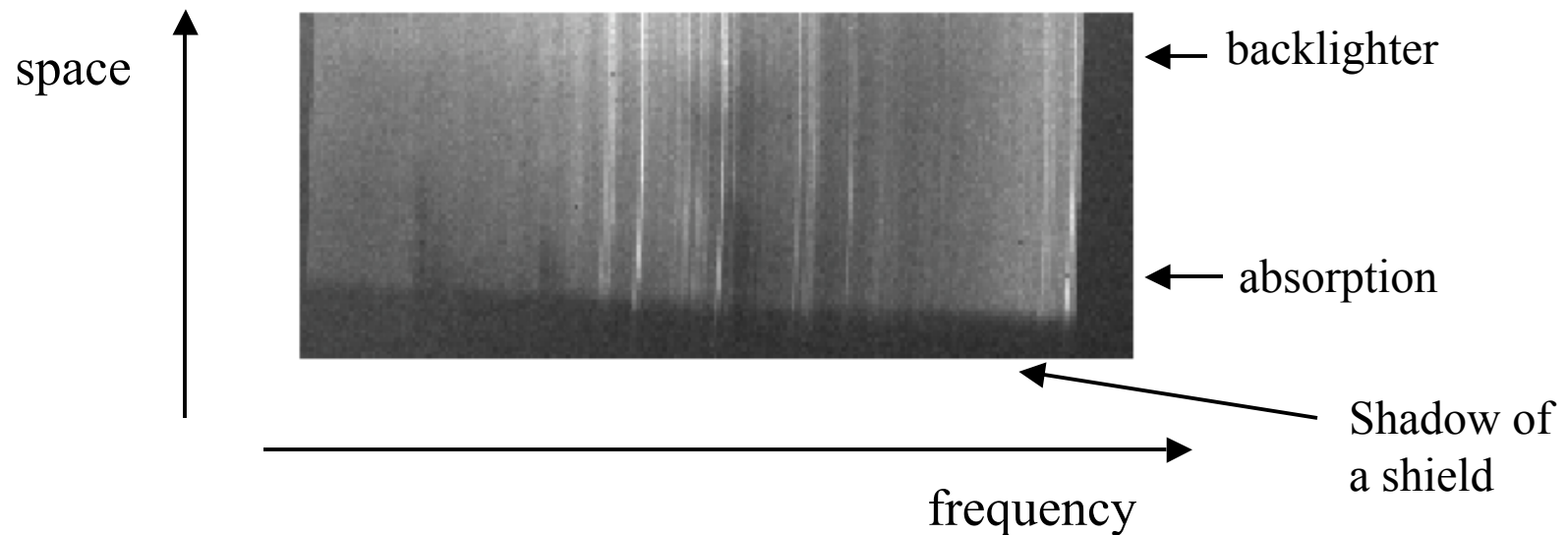


Spectra from mixtures of niobium and aluminium have been measured to help fix the conditions in the earlier experiments.



Yttrium measurements have been repeated with different backlighter spectra to try to resolve the blue wing discrepancy

Yttrium spectra in the region of the 2p-3d transitions
backlit by a gold spectrum



Summary

- Absorption data has been taken in the spectral range of 2.1-2.8KeV, covering 2p-4d and 2p-3d transitions arrays in niobium, under conditions where the niobium ions have full or almost full M-shell occupancy and the spectra change very rapidly as a function of temperature.
- The data show transition array positions, structure, widths, bound-free absorption, high-lying lines and transmission both in transition arrays and between arrays.
- Additional data was taken on Yttrium samples with slightly higher M-shell vacancies than the niobium.
- Some more shots are planned in 2005 using hohlraum heating and short pulse (CPA) back lighting.

High density opacity experiments



D.J. Hoarty, J. W. O. Harris, B.J. B. Crowley, S. James, S. Gales, C. Bentley,
C. C. Smith, S. J. Davidson P. Graham, S. J. Rose, M. Stevenson,
E. L. Clark, L. Upcraft.

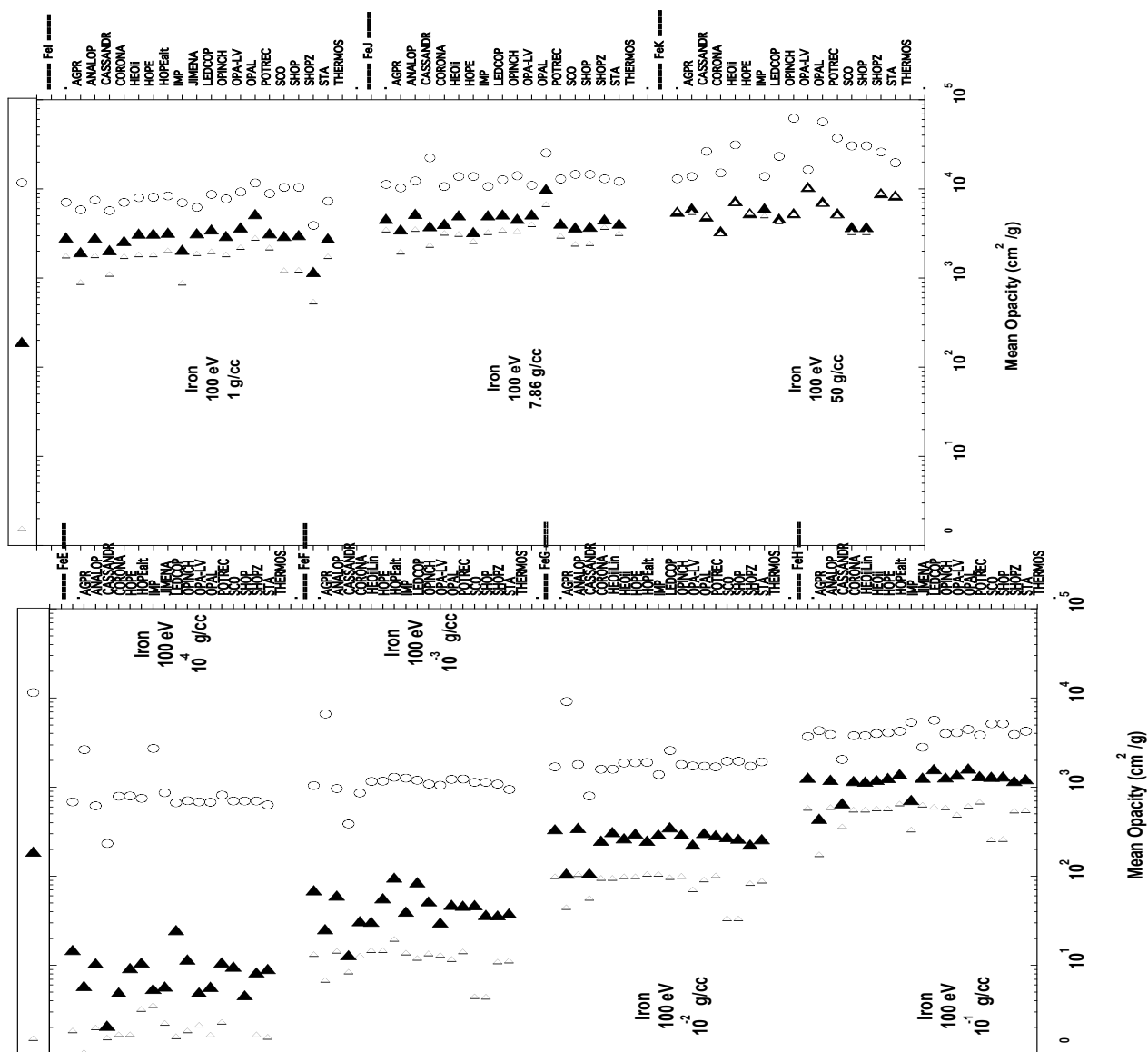
AWE plc, Reading, RG7 4PR United Kingdom.

Code comparisons reveal disagreements between models

Open circles
Planck mean

Black triangles
Rosseland mean

Open triangles
Rosseland mean
continuous opacity



**Iron
100eV,
10e-05
- 50g/cc**

Extension of opacity measurements to high density strongly coupled plasma

- At high density ion-ion interactions are strong.

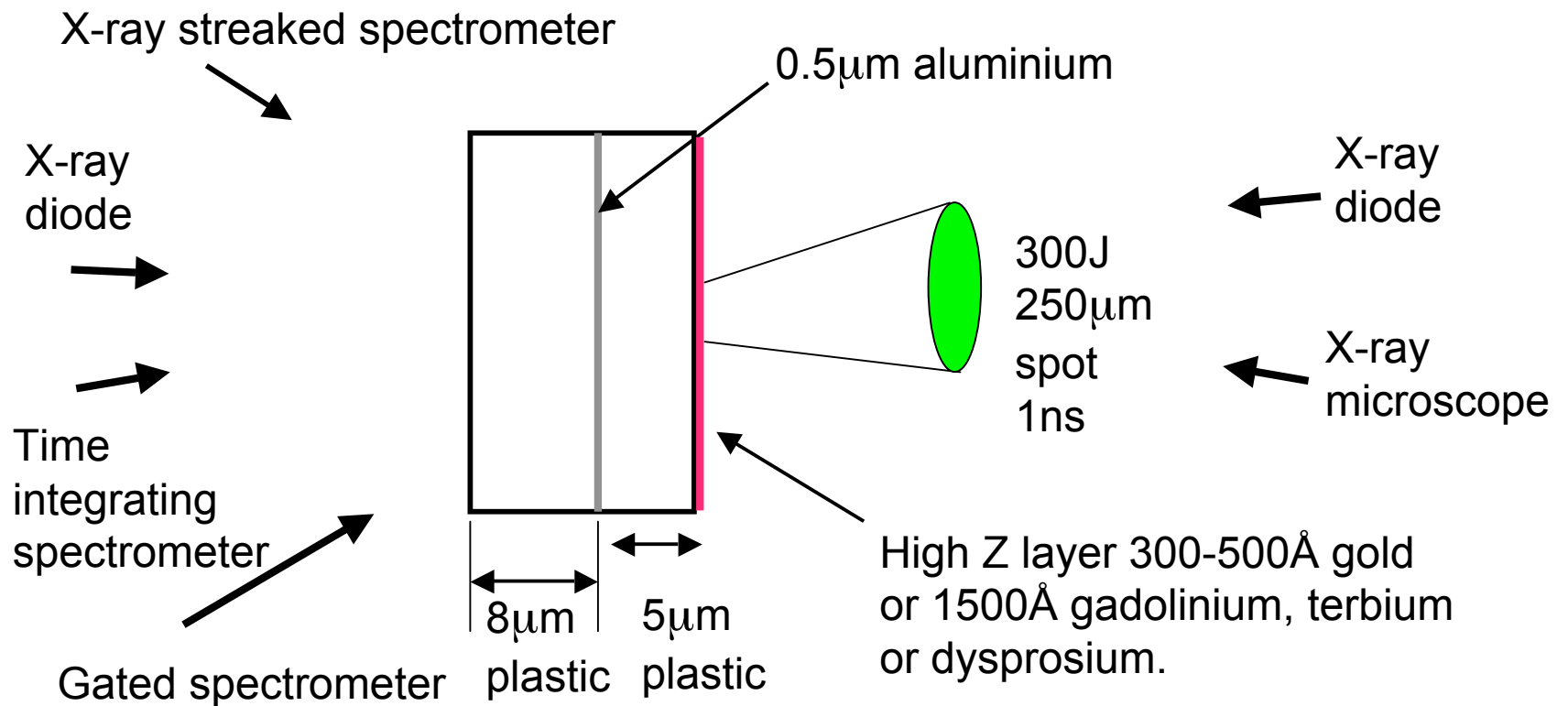
A **strongly coupled plasma** is defined by the plasma coupling constant: -

$$\Gamma = \frac{Z^2 e^2}{R_i T}$$

The plasma is strongly coupled when $\Gamma > 1$

- High density effects include :-
 - lowering of the ionisation energy (ionisation potential depression)
 - merging of high series lines
 - Stark broadening (quasi-static, electron impact broadening)

Experimental Setup

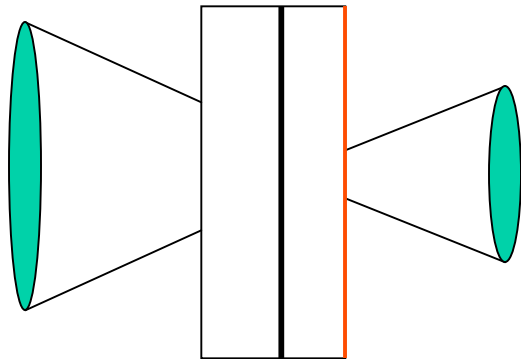


The buried layer is heated and shocked to create a high density open L-shell aluminium plasma.

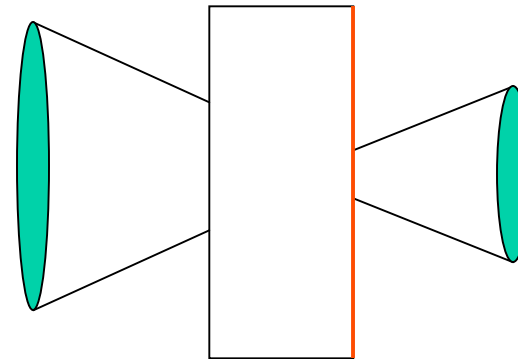
**There was a range of different irradiance conditions in the study.
Targets with no buried layer gave the high Z emission spectrum.**



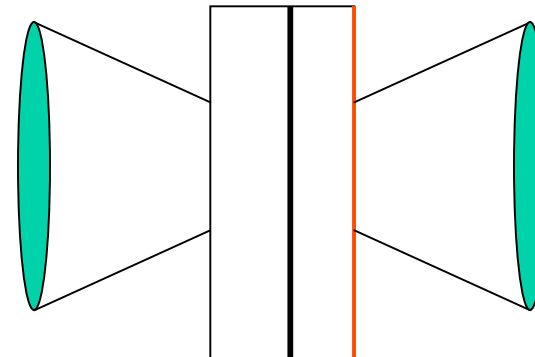
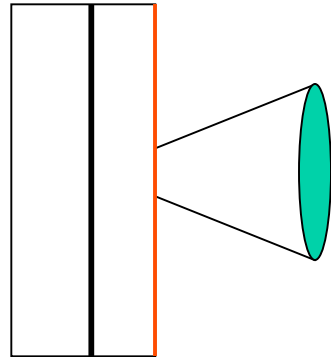
Double sided unequal irradiance.



Targets without the buried layer

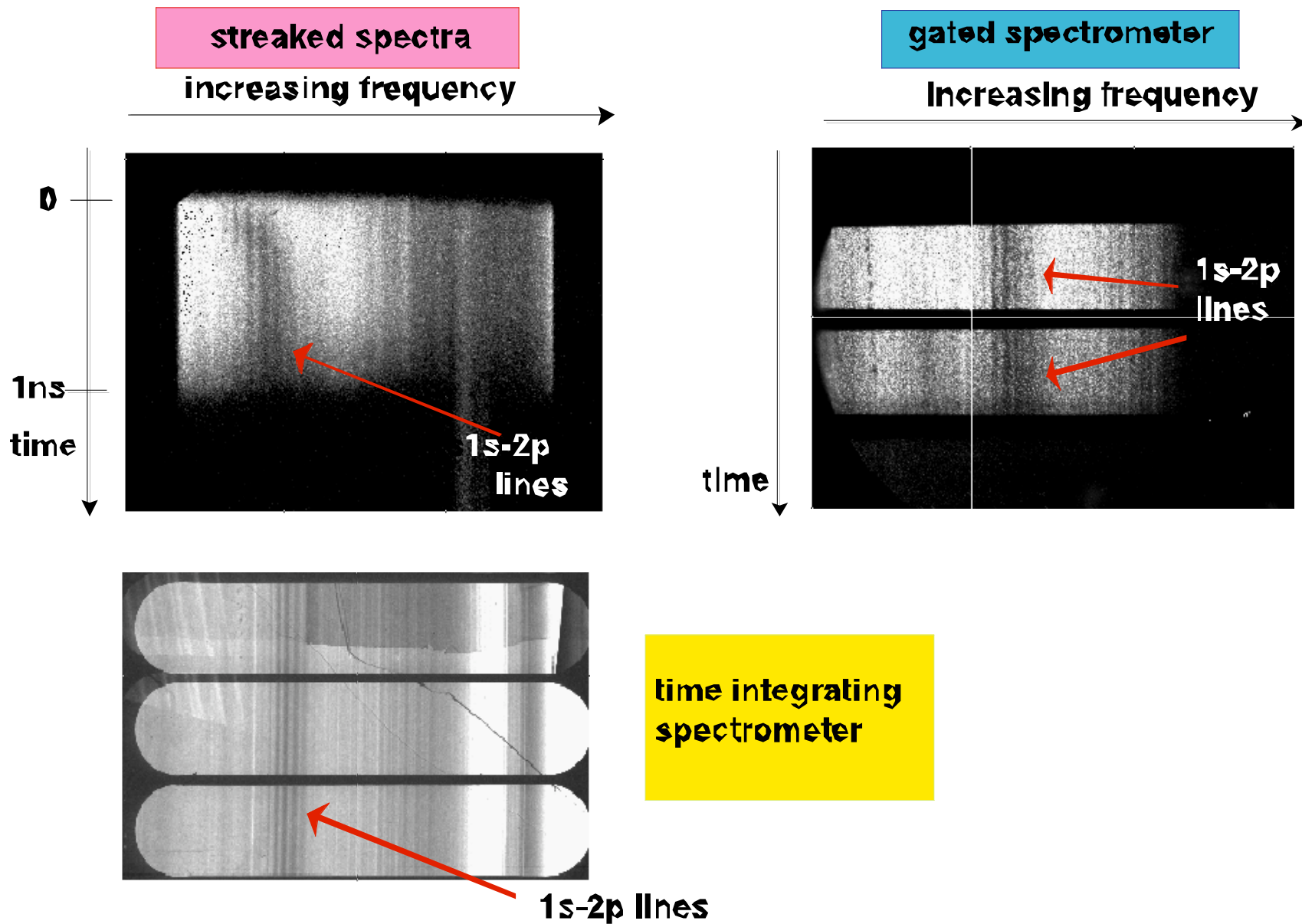


Single sided



Double sided equal irradiance.

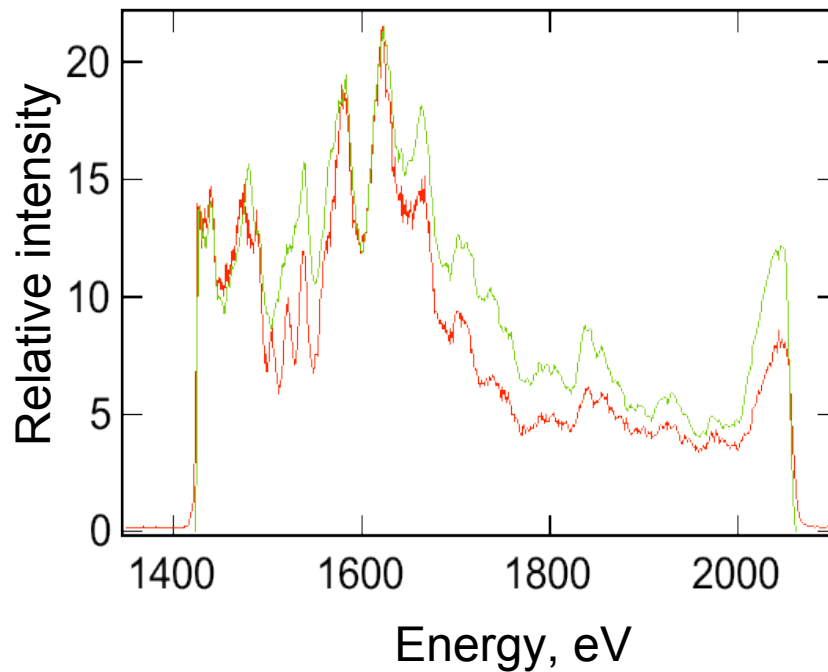
Absorption spectra were measured time resolved and time integrated on the same shot



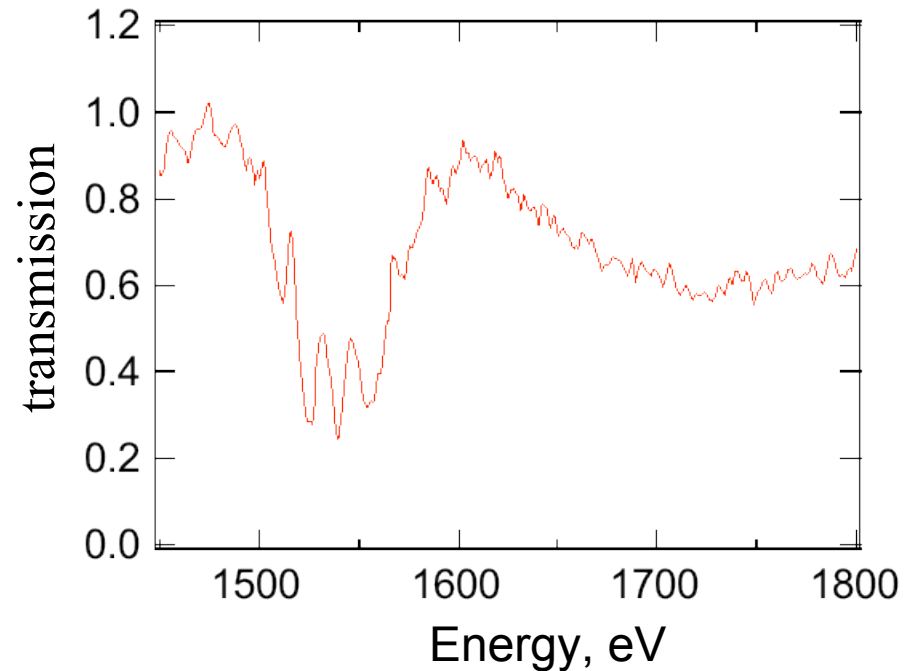
High Density transmission spectra

Line-outs through the backlighter (no Al sample) and absorption spectra (0.5 μ m Al sample)

— Gd backlighter
— Al absorption



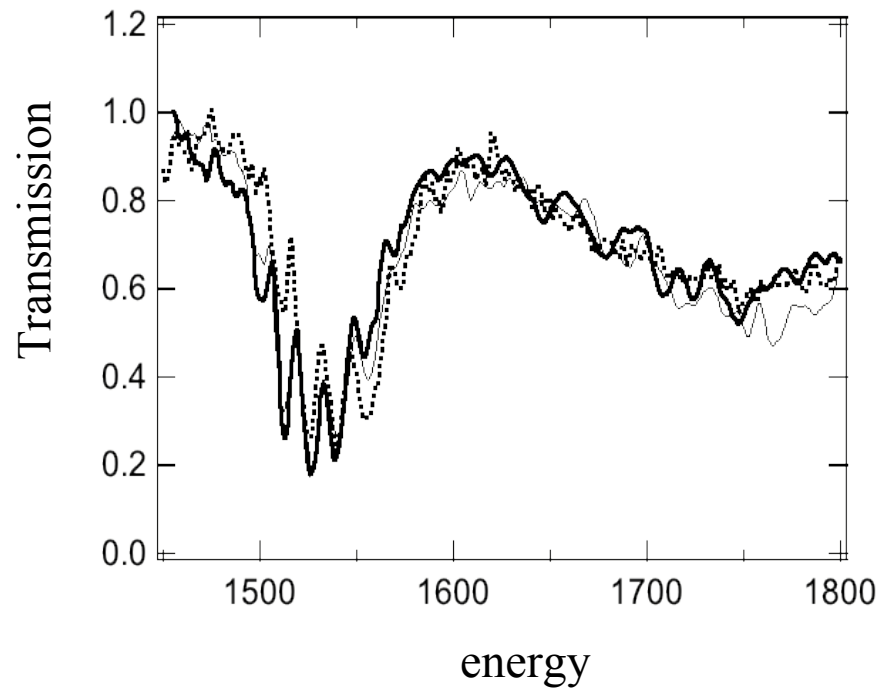
Al Transmission spectra backlit by Gadolinium.



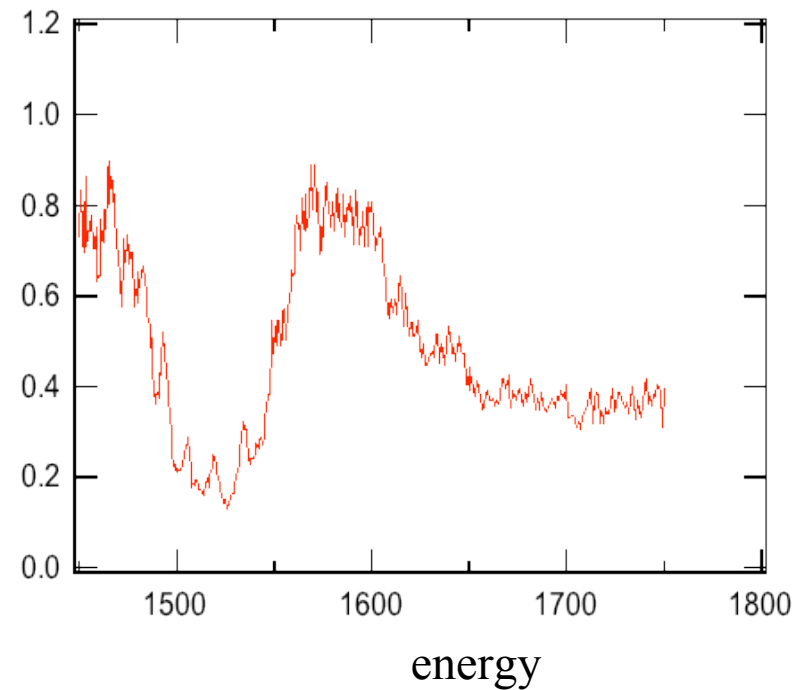
High density Al transmission spectra were reproducible

Spectra were checked for reproducibility using different back-lighters, crystals and photo-cathodes.

- Gadolinium backlighter
- Gadolinium backlighter
- Gold backlighter



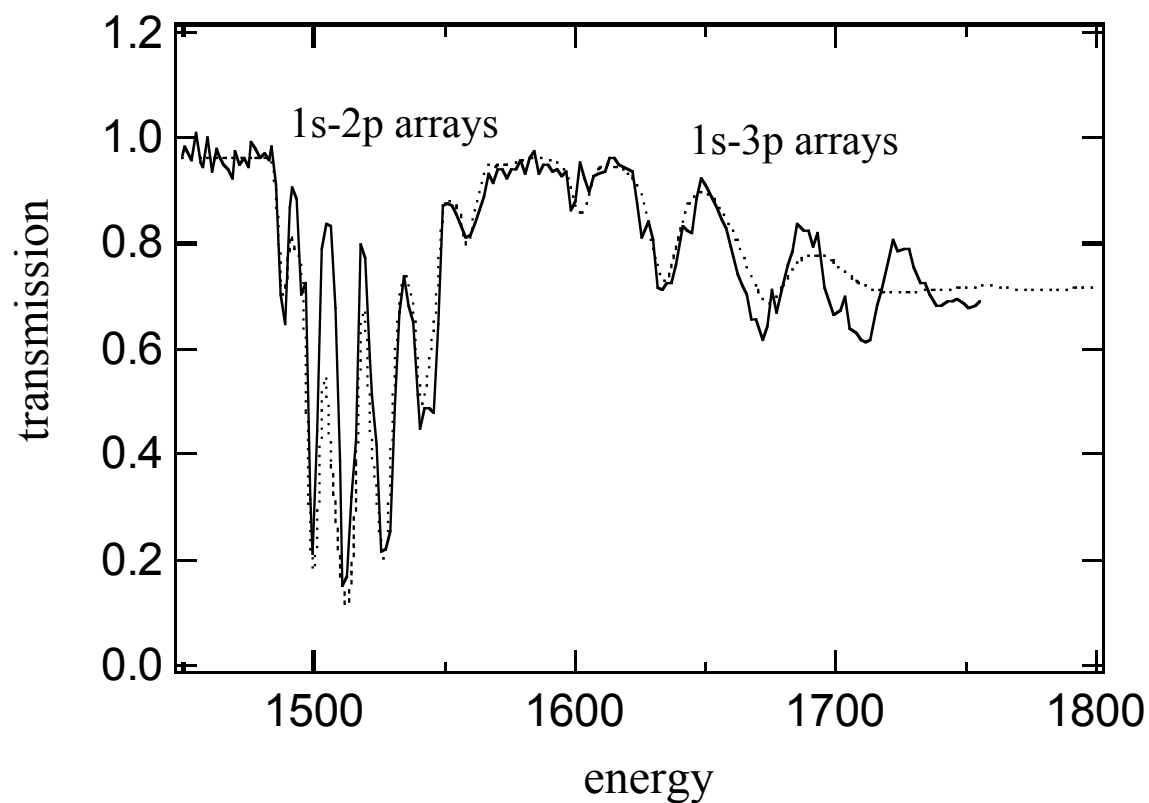
1 micron thick aluminium sample
(backlit by terbium).



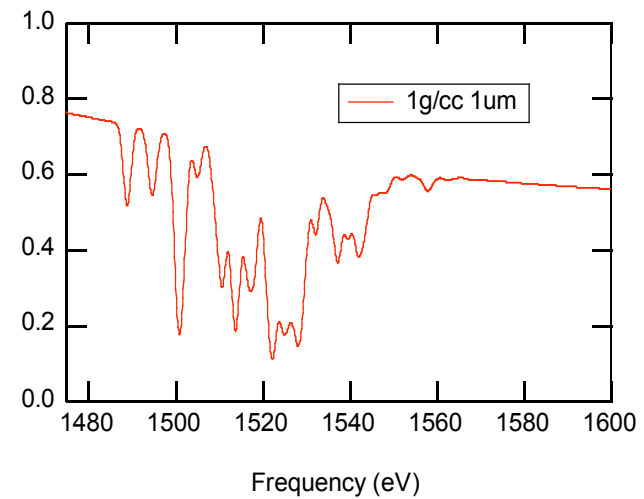
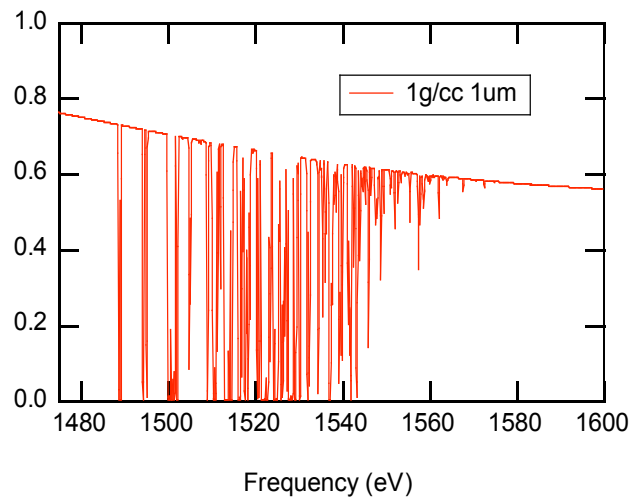
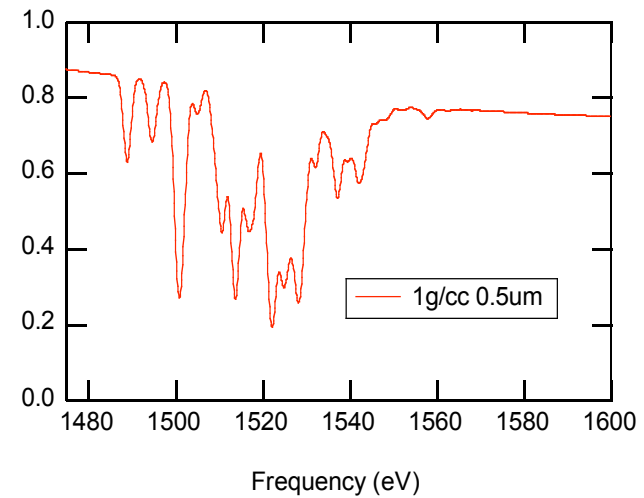
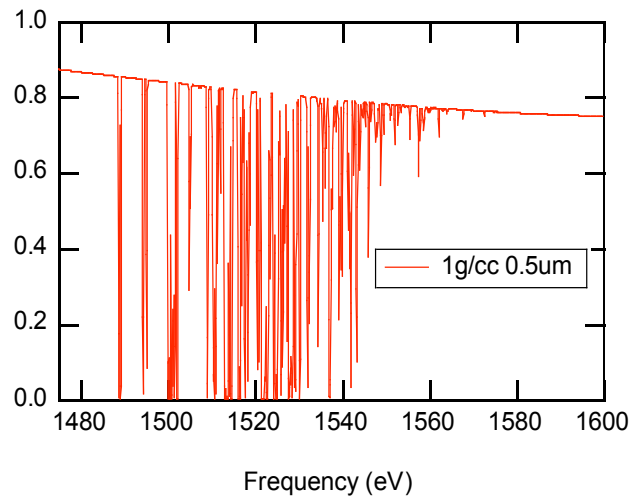
Low density 0.5 μ m aluminium foil transmission spectra exhibit clear 1s-3p array absorption.

— experiment

..... Calculation - sepsaha code



Effect of instrumental broadening



Absorption spectrum Doppler
broadened

With instrumental broadening

Effect of instrumental broadening

- Instrumental broadening puts a limit on the optical depth of material that can be measured. Beyond this limit (typically $\tau \sim 3-4$) further increases in optical depth cannot be measured in the transmission spectrum. The absorption is said to be **saturated**.
- Transmission in a spectrum with large unresolved transition arrays (UTA's), in which lines wholly or partially overlap, may be poorly approximated by modelling with statistical methods using continuous envelopes. If there are gaps between lines in these arrays they may be more transmitting than calculation predicts. Such arrays are said to be **porous**.
- UTA's may be more transmitting than calculated due to spectral structure below resolution limit of the spectrometer leading to **array porosity**. This is so-called **unresolved structure**.

Tests for saturation and unresolved structure

- If the absorption spectrum is saturated (or has unresolved structure) then the spectrum will no longer scale with thickness according to Beer's law.
- Test by taking measurements at different thicknesses.

$$T_1 = \exp(-\rho\kappa x_1)$$

$$T_2 = \exp(-\rho\kappa x_2) \quad \text{Let } x_2 = 3x_1$$

Then in the absence of unresolved structure $T_2 = T_1^3$

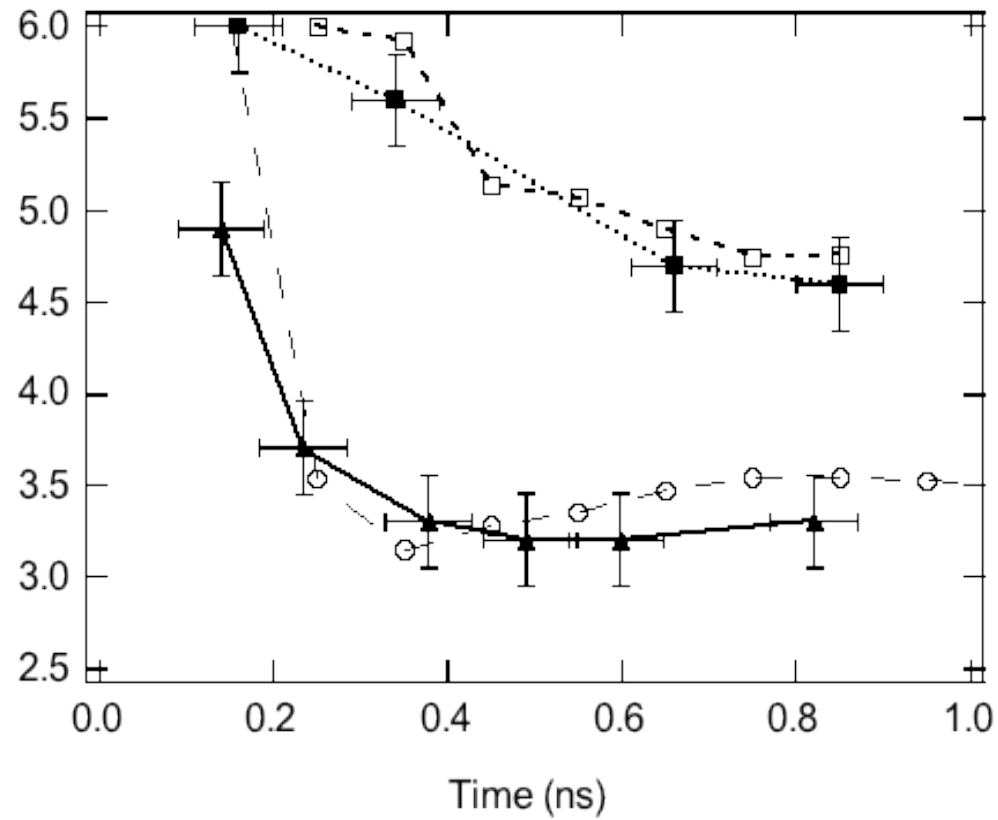


The experimental conditions were obtained from radiation hydrodynamics simulations. The simulations were constrained by experimental measurements.

To infer the experimental conditions simulations were compared to measurements of :-

- The ionisation history of the buried layer.
- The target mass ablation rate
- The X-ray flux emitted from the target.

Time dependent plasma conditions - 2p occupancy

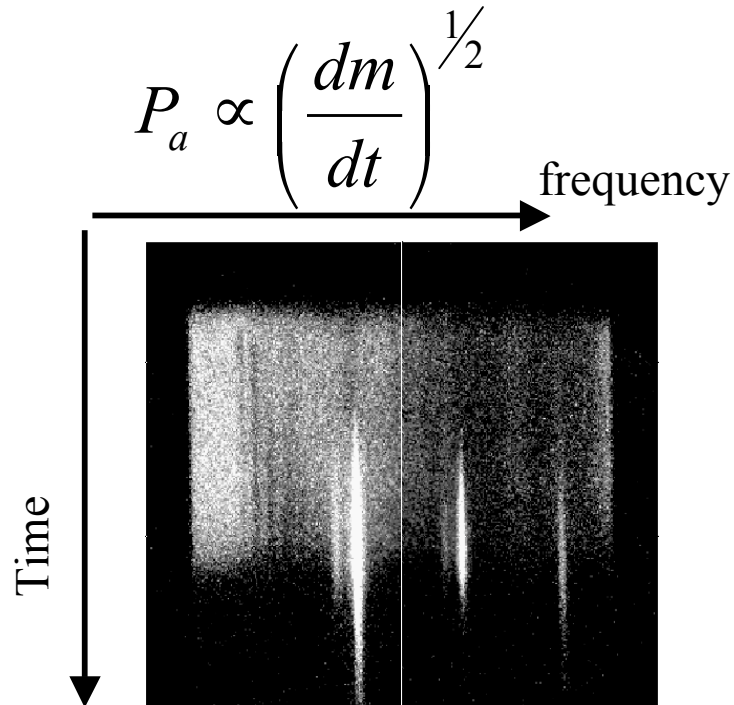


—— Solid lines are ionisation inferred from the experiment

..... Dashed lines are ionisation inferred from predicted conditions

Plasma conditions - mass ablation rate

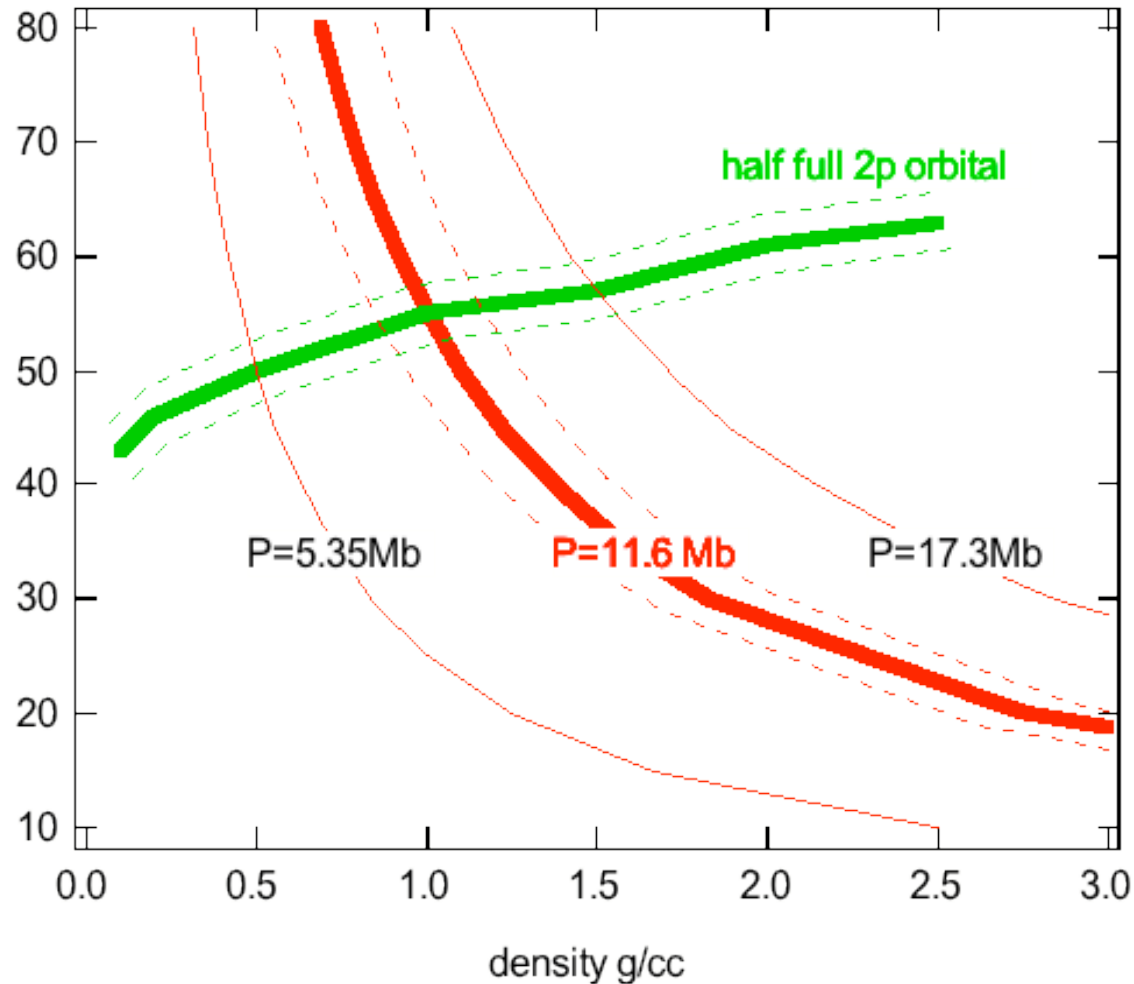
- Pressure and density were constrained by target mass ablation rate. This was measured by the onset of bright He and H-like emission from the buried layer, and compared to hydro simulations
- The mass ablation rate is directly related to the ablation pressure and hence the sample pressure



Pressure variations for aluminium
with a half full 2p orbital

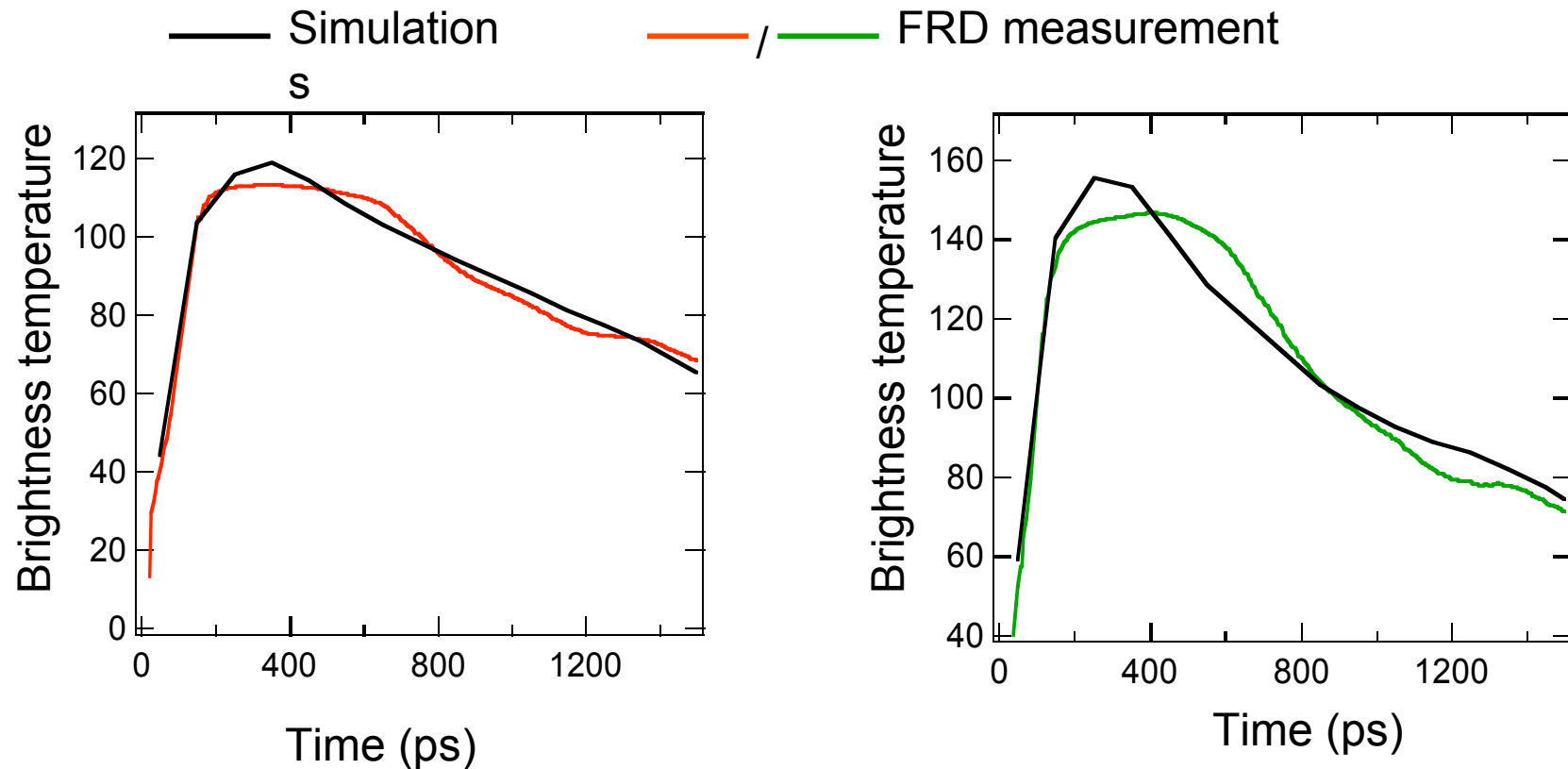
ρ g/cc	Te eV	p Mbar
0.1	43	0.98
0.2	46	2.03
0.5	50	5.35
1.0	55	11.6
1.5	57	17.3
2.0	61	34.3
2.5	63	42.5

The range of ablation pressure and 2p occupancy, taken together, constrain the plasma conditions.

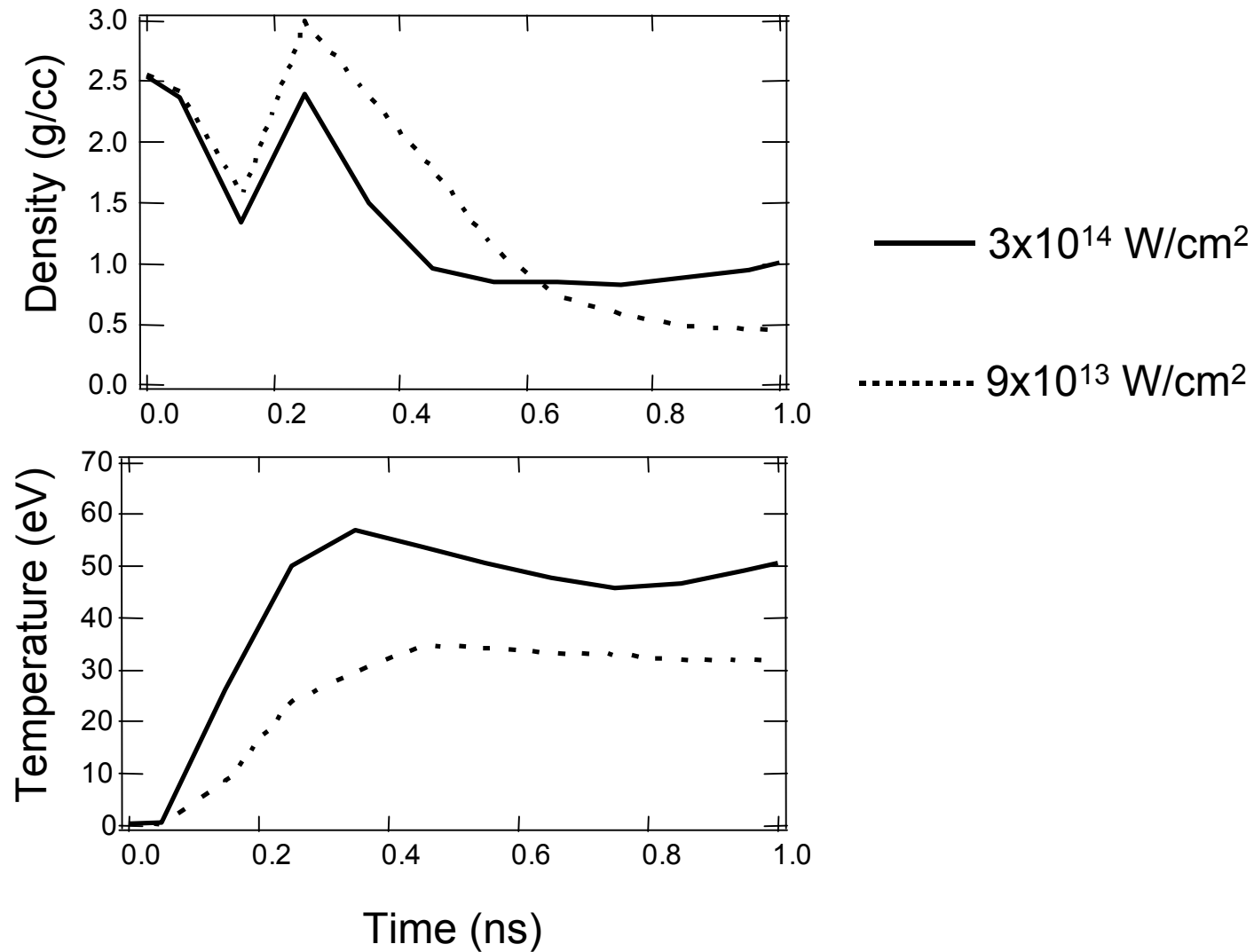


X-ray flux measurements

Flat response x-ray diode measurements of the flux from the high Z (back lighter) layer were compared to the flux from radiation-hydrodynamics predictions.

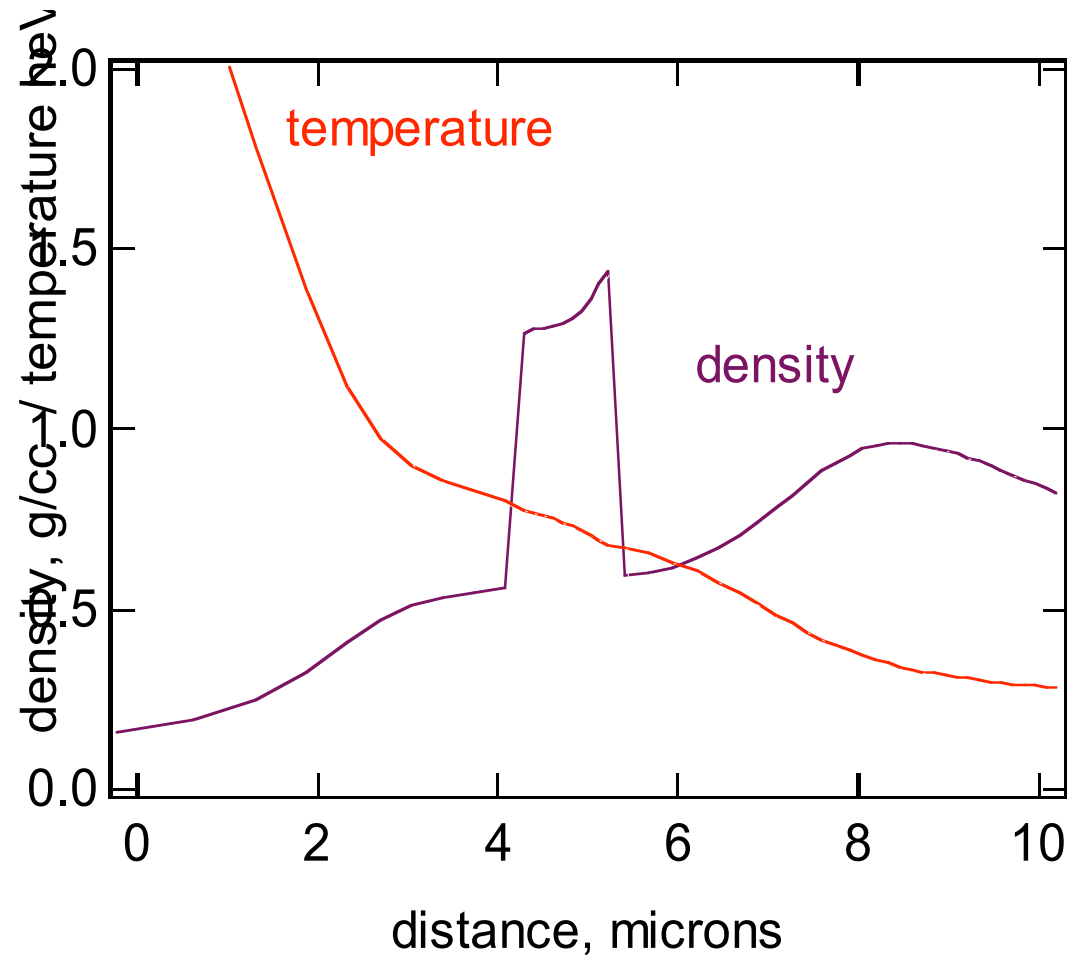


Time dependent density and temperatures in the sample

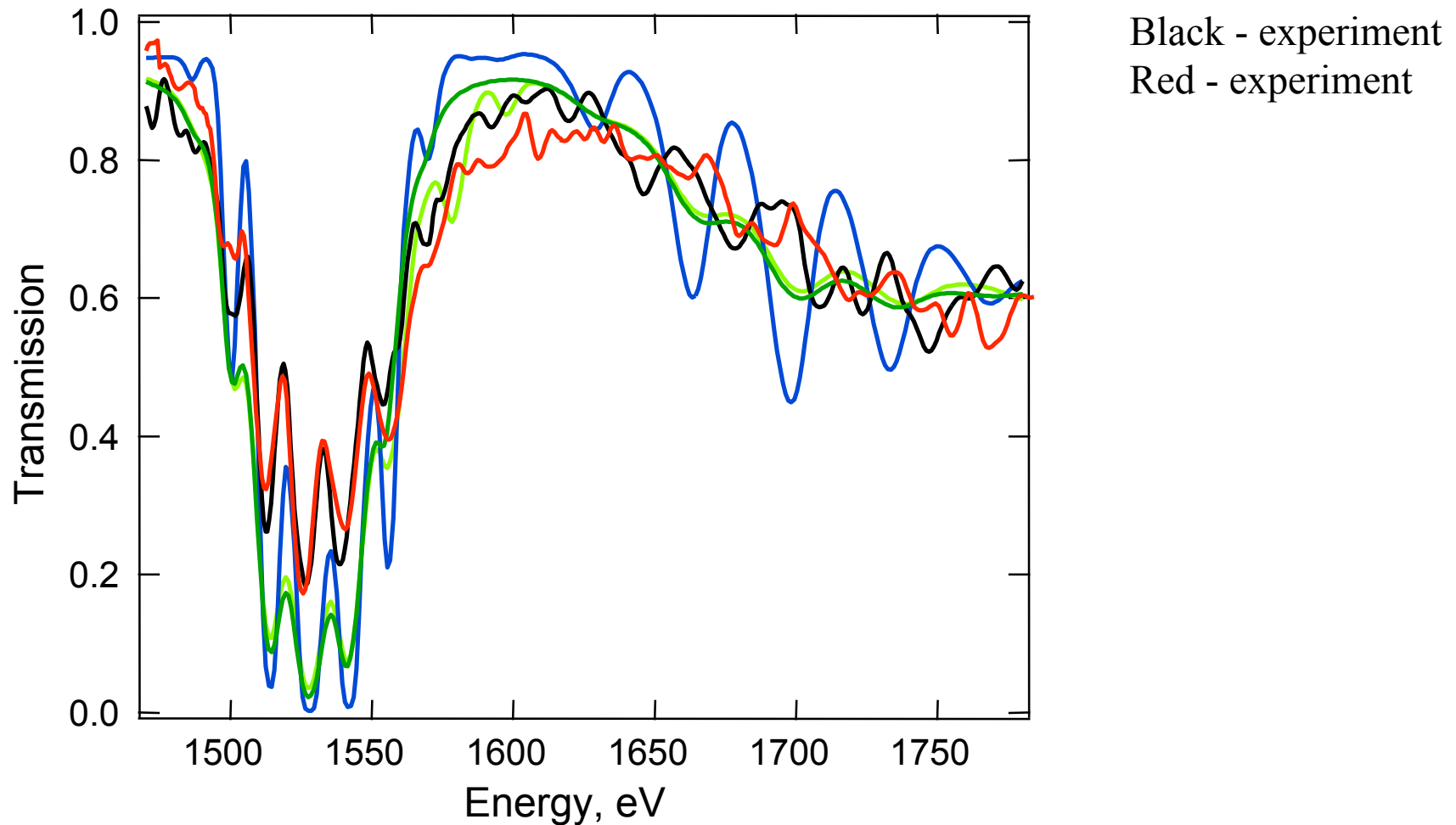


Spatial gradients

The buried layer is predicted to have reasonably small temperature and density gradients after the initial shock reverberation.



Comparisons with simulations show the effect of broadening on the absorption spectrum. In these experiments electron impact broadening is the dominant effect. 1s2p transmission differs from calculation due to porosity and saturation.



Summary/conclusions



- HELEN experiments have started to measure X-ray absorption at high material density ($\sim 1\text{g/cc}$) and electron densities $\sim 10^{23}/\text{cc}$.
- Comparisons with opacity simulations suggest it is important to include line broadening due to electron impact at high densities.
- The 1s-2p transition arrays are more transmitting (porous) than predicted if term structure is treated as a UTA.
- Note the electron impact width $w \propto \frac{n_e}{\sqrt{T_e}}$

In a high temperature, high Z plasma the electron density, at a similar material density, may be much higher than in this experiment and the electron impact width could be similar to that used here.

This effect is currently being investigated with CASSANDRA.

Future high density opacity experiments

- Long pulse direct drive opacity experiments are difficult!
- Experiments using short pulses represent a still more difficult challenge.
 - Short pulse lasers have a different interaction with matter compared to long pulse systems.
 - LTE is more difficult to establish.
 - fast particle heating poorly understood.
 - Diagnosis of rapidly changing plasma conditions much more difficult.
- Further diagnostic development is needed.
- Initial experiments will be carried out between $10^{17} - 10^{18} \text{W/cm}^2$ where fast particle production is low.

HELEN CPA high density opacity experiments

- Foils irradiated with short pulse lasers to give high temperature and high density data . (Emission and possibly absorption experiments.)
 - Fe near solid, $\sim 500\text{eV}$ - expect $Z^* \sim 23$, Li-like ions predominate
 - We can measure line widths in emission to further investigate electron impact broadening in a relatively simple plasma.
 - Investigate higher Z more complex spectra at high electron densities and high ion densities to compare to CASSANDRA.
- Studies of very strongly coupled plasmas (warm dense matter).

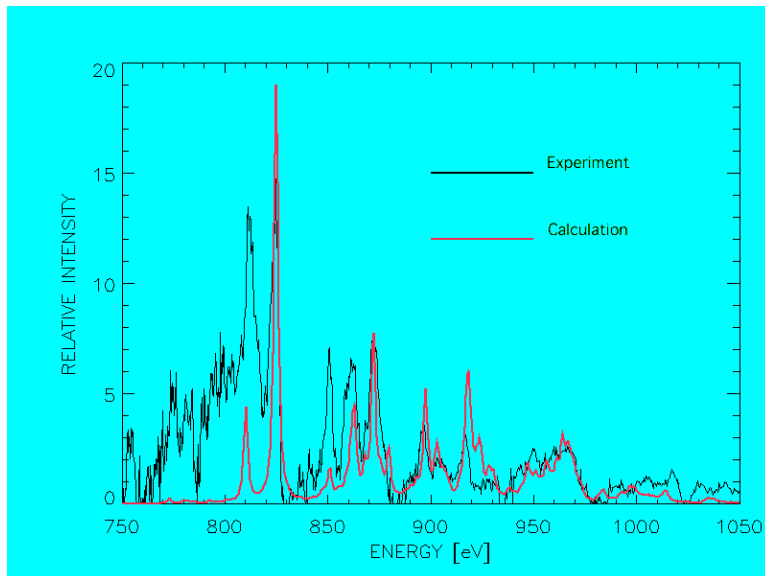
Aims of the proposed HELEN experiments

- To measure emission spectra at near LTE conditions from high density and high temperature buried layers in plastic foils irradiated with the CPA, to compare to predictions of the CASSANDRA code and other state of the art opacity codes.
- To establish the uniformity of the buried layer heating as a function of time.
- To better understand the mechanisms of production and heating of buried layers at 10^{18} - 10^{19} W/cm².
- To assess the feasibility of performing such experiments using the ORION laser.

Thermal conduction heating experiment is based on the work of K. Nazir et al.

Conditions - Solid density, 700eV with gradients

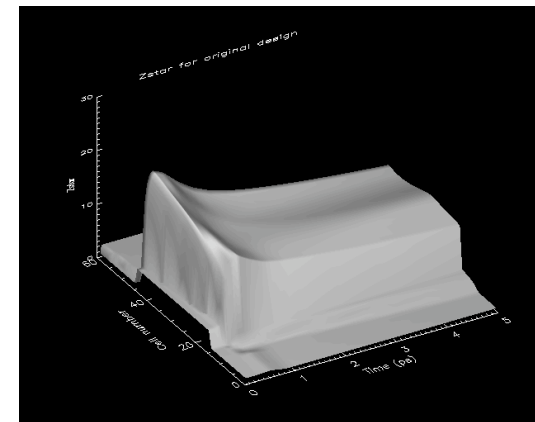
Nazir et al, Appl Phys Letts 69 (24) 1996



Ion stages from
time when buried
layer is cooler, before
and mainly after
peak emission

Ion stages from
near the peak
of the emission

20000Å plastic
1000Å plastic
 10^{17} W/cm²
300 fs
249 nm
1000Å iron

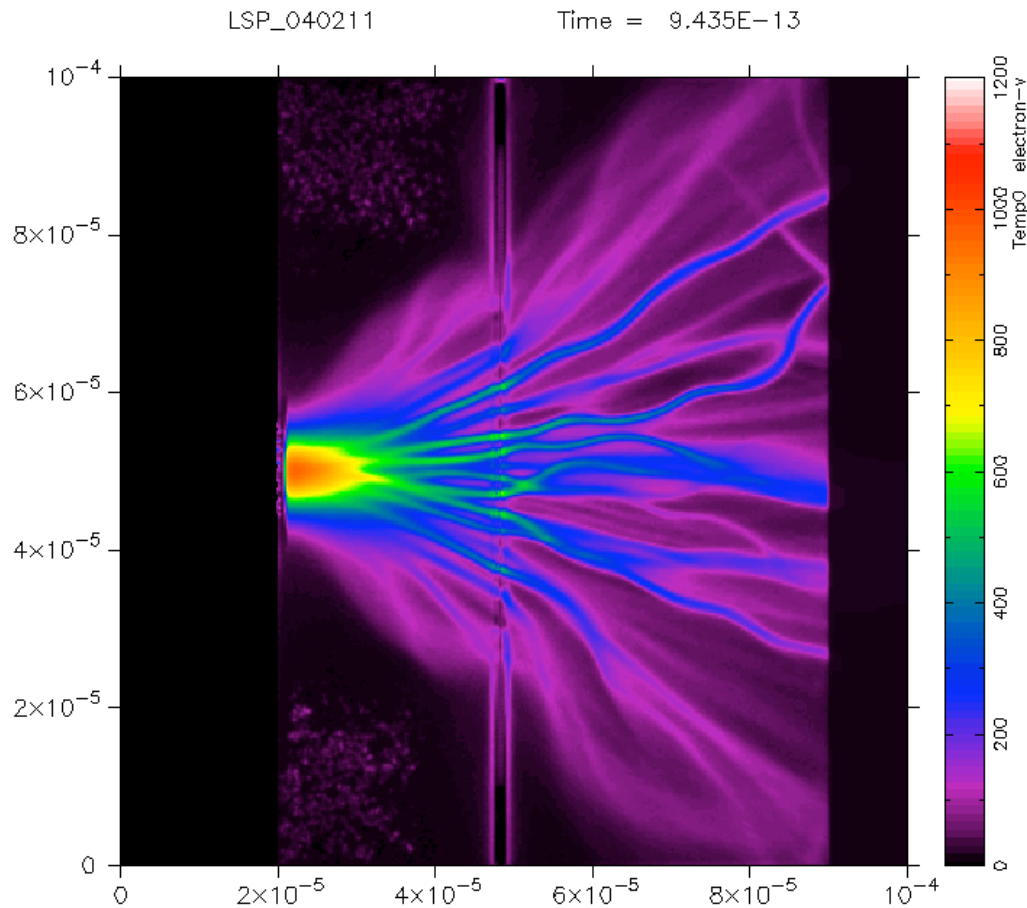


Z^* as a function of time and space

Two buried layer experiments combined

- Thermal conduction heating of a layer near the surface of a plastic foil irradiated at $10^{17}\text{W}/\text{cm}^2$ - emission measurements time resolved and time integrated. Imaging measurements.
- Fast electron and return current heating of more deeply buried layers - up to $25\mu\text{m}$ into the foil. Emission measurements and imaging measurements at 1 and 2ω .
- Measurements will be split in two:-
 1. Spectral measurements for both types of foil using streak cameras and time integrating spectrometers.
 2. Imaging measurements for both types of foil using the spherical multilayer and spherical crystal imaging system

X-ray imaging using spherical multilayer and crystal mirrors will study the temperature uniformity of the buried layers



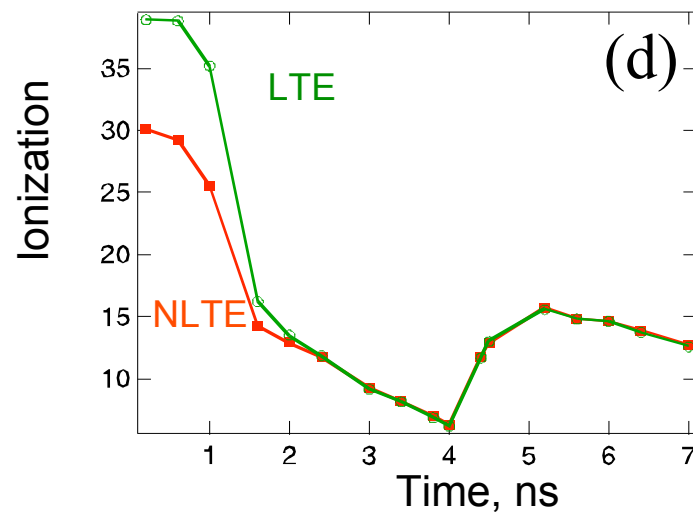
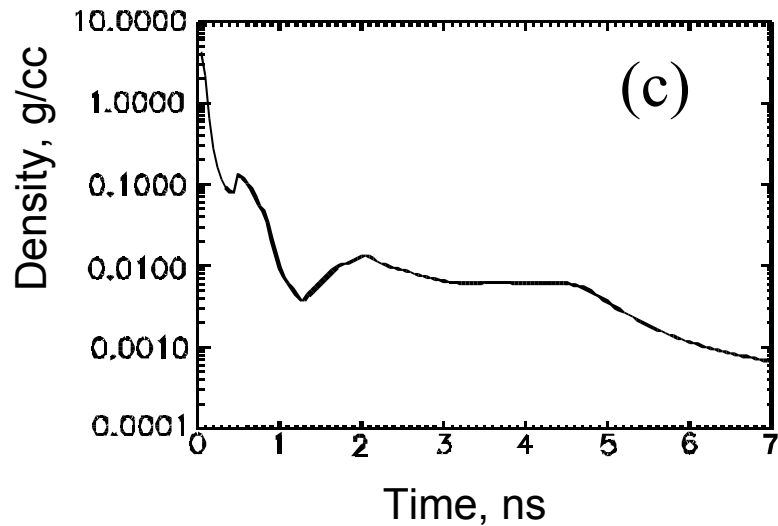
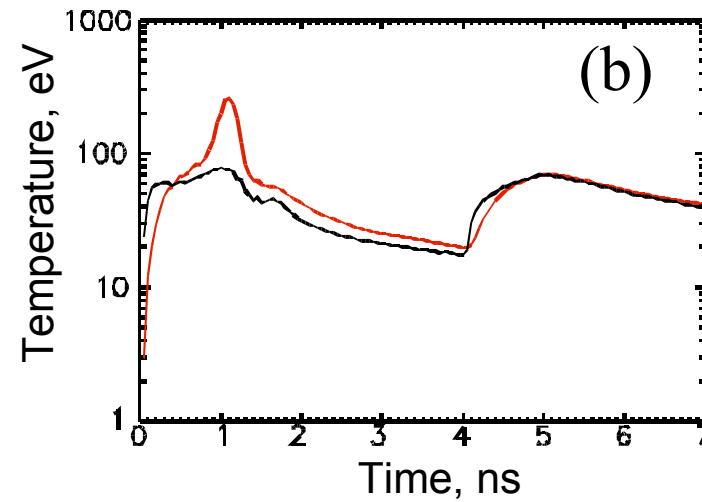
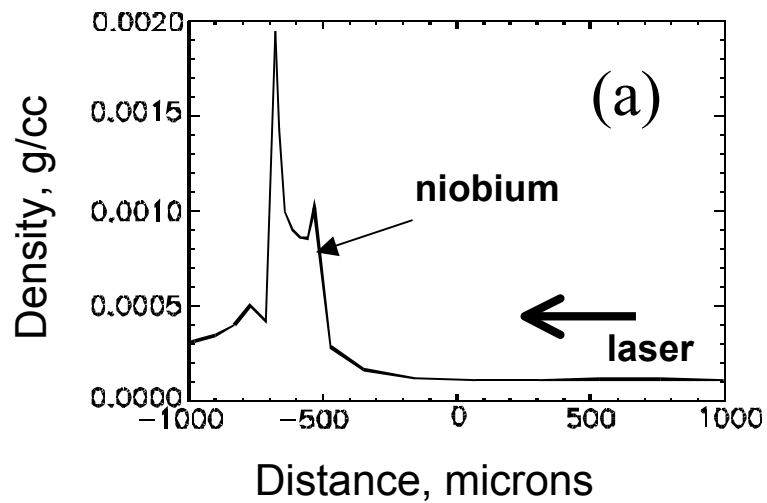
Filamentary structures in the electron temperature for a fast electron heated buried layer

The simulation box is 100 micron square

Low density experiments to measure UTA break-up.

- Low density opacity samples created by exploding thin foils with direct laser irradiation and after a delay reheating them inside a hohlraum.
- Absorption spectra to be diagnosed with high resolution spectrometers.

Exploding foils reheated by a X-ray drive are predicted to give LTE low-density samples.



Summary

- Opacity experiments on HELEN will attempt to measure spectra in temperature/density regimes in which there is presently little or no data.
- High density - Stark effect, continuum lowering
 - buried layer targets irradiated with CPA pulses.
- Low density - UTA break- up
 - exploding foil targets
 - combination of direct and indirect laser heating
 - higher resolution spectral measurements.

UNCLASSIFIED

Possibilities for Opacity Experiments Using TRIDENT Laser Laboratory: and interesting observations at the OMEGA laser

Tom Tierney
(an opacity novice)

P-22: Hydrodynamics and X-ray Physics

Acknowledgements to contributors to this talk

- P-24 Folks: Jonathan Workman, Juan Fernandez, Robert Gibson, Tsutumo (Tom) Shimada, Randall Johnson, Jim Cobble, Damian Swift, Dennis Paisley, ShengNian Luo, Bjorn Manuel Hegelich
- And X-1 people: Nelson Hoffman, Barbara DeVolder, Dave Tubbs, Bob Goldman

Outline of talk

- Current TRIDENT capabilities
- Future TRIDENT design
- Possible opacity+EOS experiment designs for TRIDENT
- An opportune example from OMEGA

TRIDENT is one of the world's most flexible high-fluence laser facilities

- 3 Nd:glass beams
- Four colors: **1054** / **527** / **351** / 265 nm
- 13 element pulse shaping
- Short pulse ~500 fs to UltraLong pulse ~20 μ s
- typical spot sizes: ~10 μ m to 8.0 mm
- ~12 shots / day at energies >40 J or
~20 shots / day at energies < 40 J

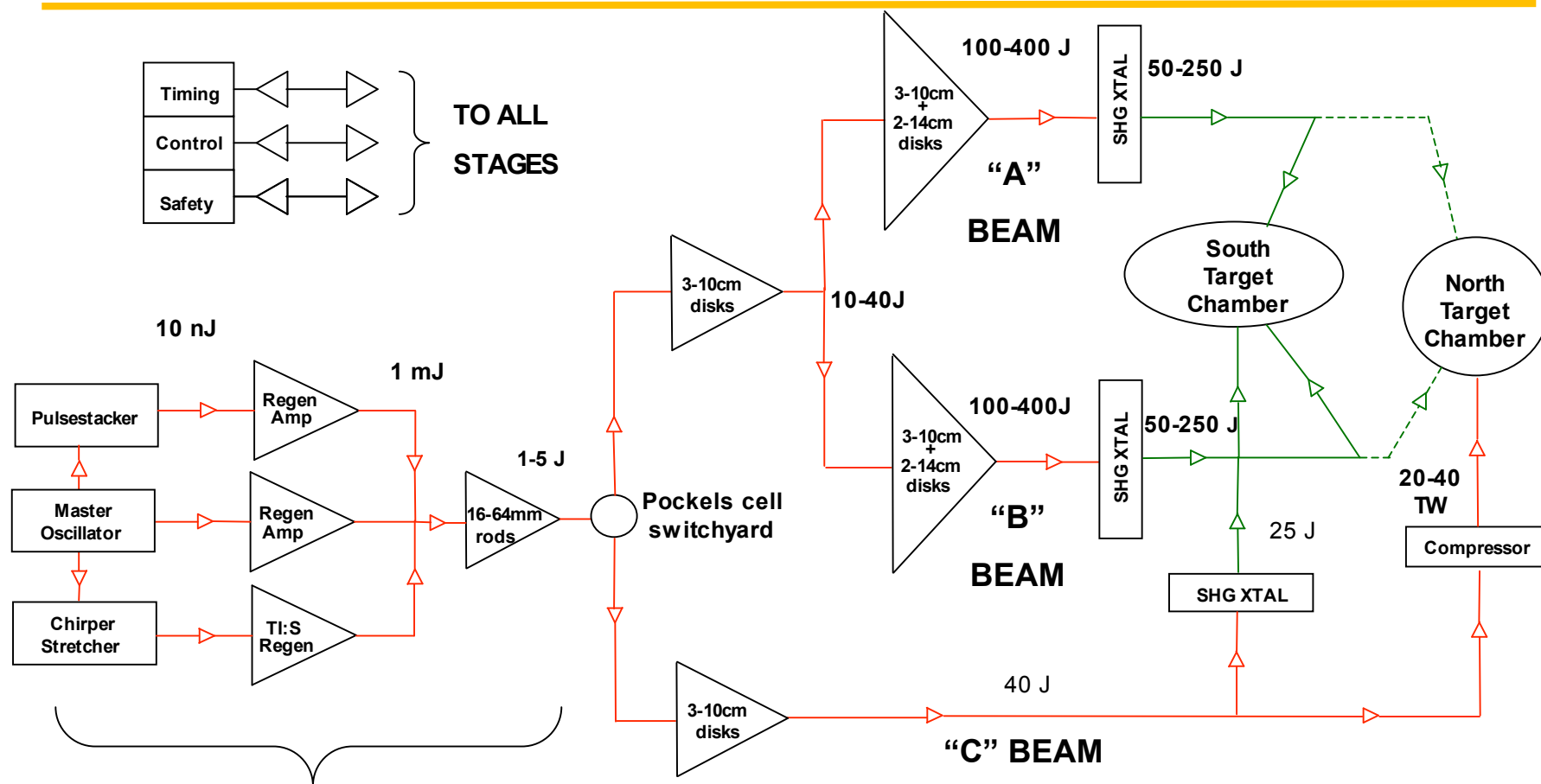


Driver output covers wide parameter space

<u>Parameter (units)</u>	A & B Beams		C Beam		
	<u>Normal</u>	<u>Long-pulse</u>	<u>Normal</u>	<u>SHS</u>	<u>Sub-ps</u>
Wavelength (nm)	527	1053	1053/527 351	1053/527 351/263	1053
Pulse length (ns)	.08-5.0	.08-20000	0.1-2.0	0.1-2.0	0.6 ps
Energy/beam (J)					
100 ps	50	100	50/30/20	5/3/1.5/0.5	30
1-2 ns	250	400	100/60/40		
100-2000 ns		300			
Spot dia. (μm)	100	100	50	5	20
Irradiance (W cm⁻²)	10^{16}		10^{16}	10^{16}	$>10^{19}$
Number of beams	2	1	1	1	1

UNCLASSIFIED

TRIDENT has “2½” beams using an Nd:Glass master oscillator, power amplifier (MOPA) laser and 2 target areas



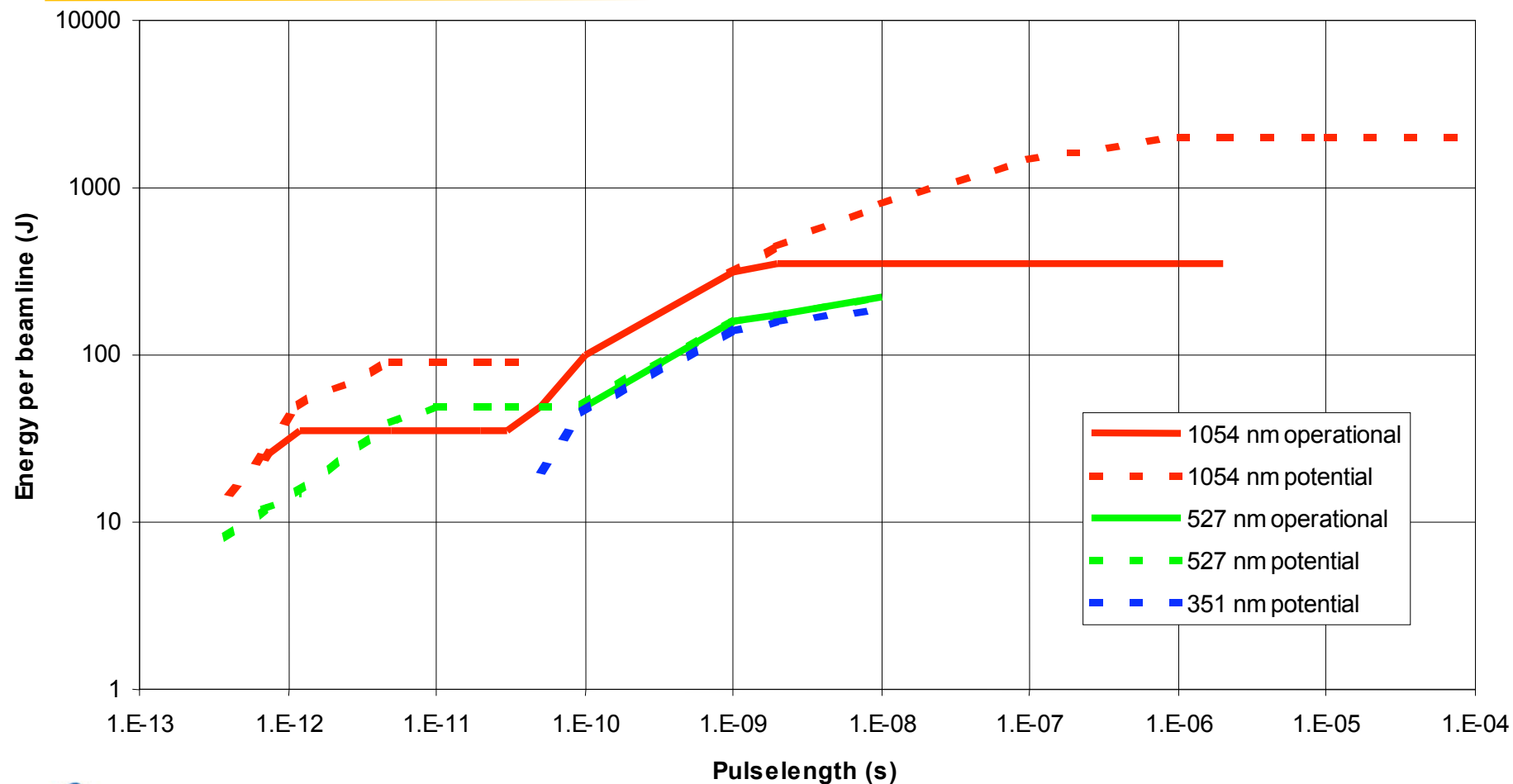
FRONT END

Energies shown are for pulse length range of 1-2 ns

UNCLASSIFIED

UNCLASSIFIED

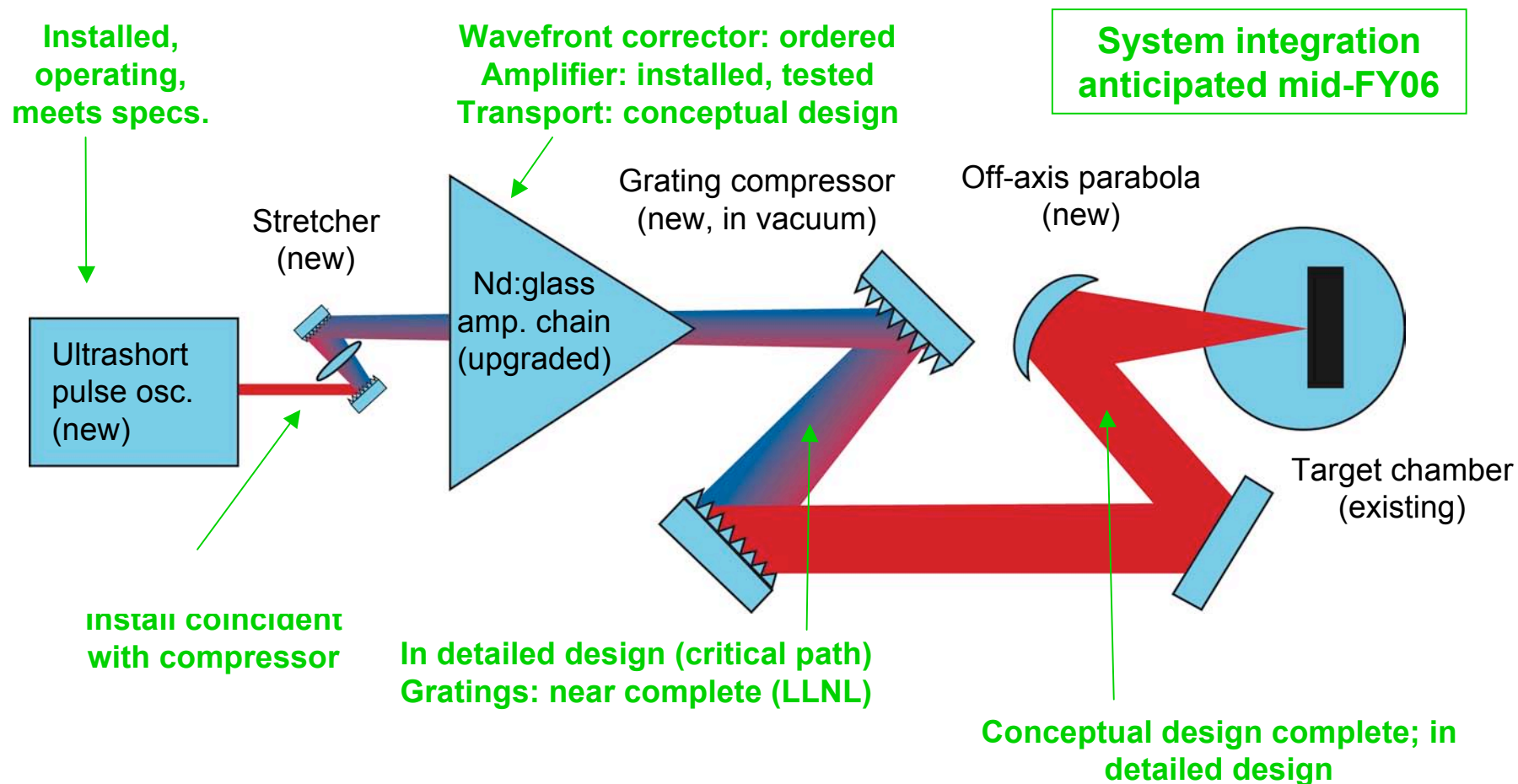
TRIDENT produces energetic pulses over 6.5 orders of magnitude in pulse length.



UNCLASSIFIED

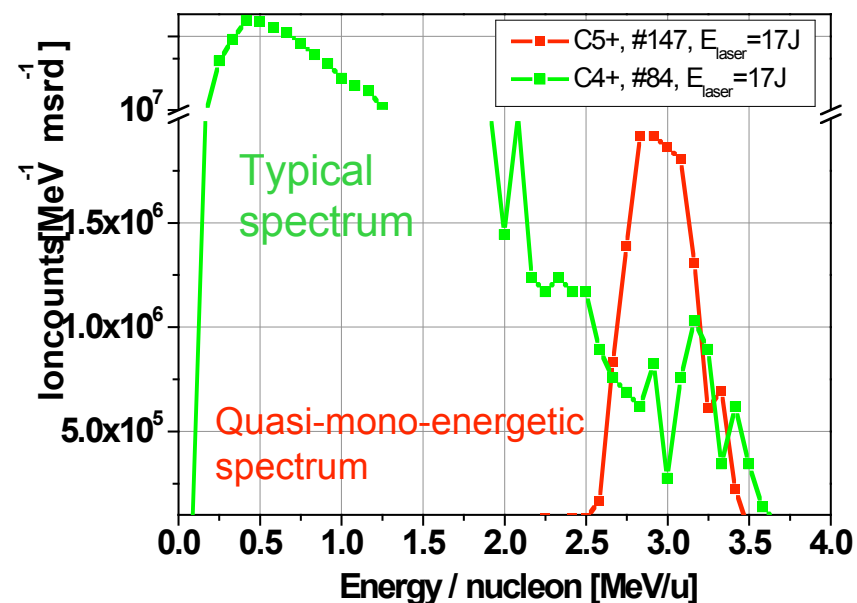
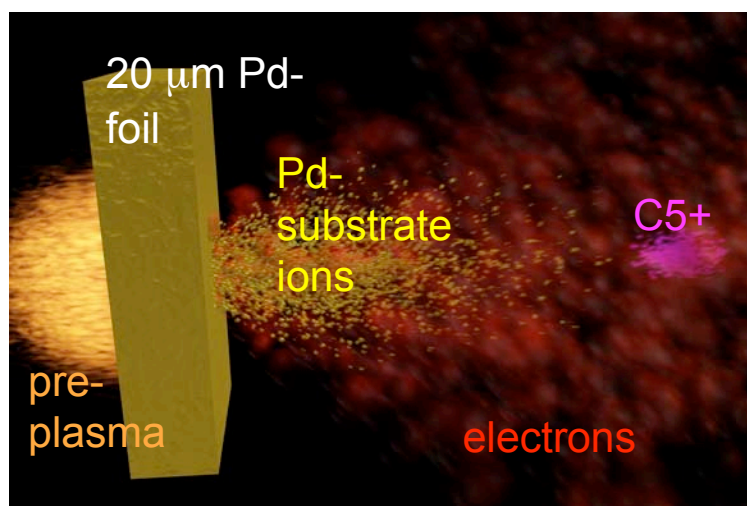
UNCLASSIFIED

TRIDENT enhancement project is progressing towards a FY06 completion.



UNCLASSIFIED

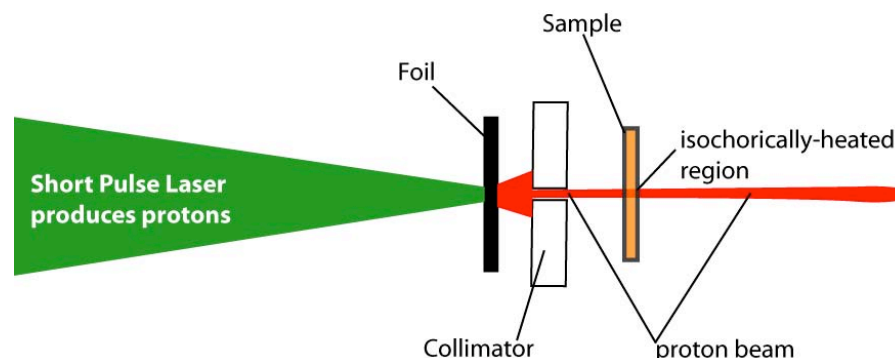
First observation of laser-accelerated quasi-mono-energetic ions*



- 2× increase in number of high-energy ions
- 2.5× increase in energy and conversion efficiency
- 3× increase in beam current

Laser-produced proton beams can be used to quasi-isochorically heat a sample to eV temperatures.

- Short pulse laser accelerates ions (protons and heavier particles).
- Ions impact target (mostly transmissive).
- Sample heats ~uniformly if ions penetrate deeply.
- Measurements must be made quickly (possibly NLTE)

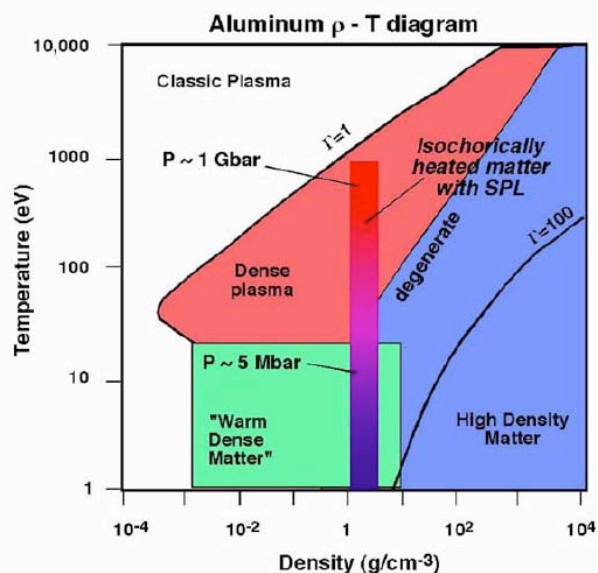


Example:

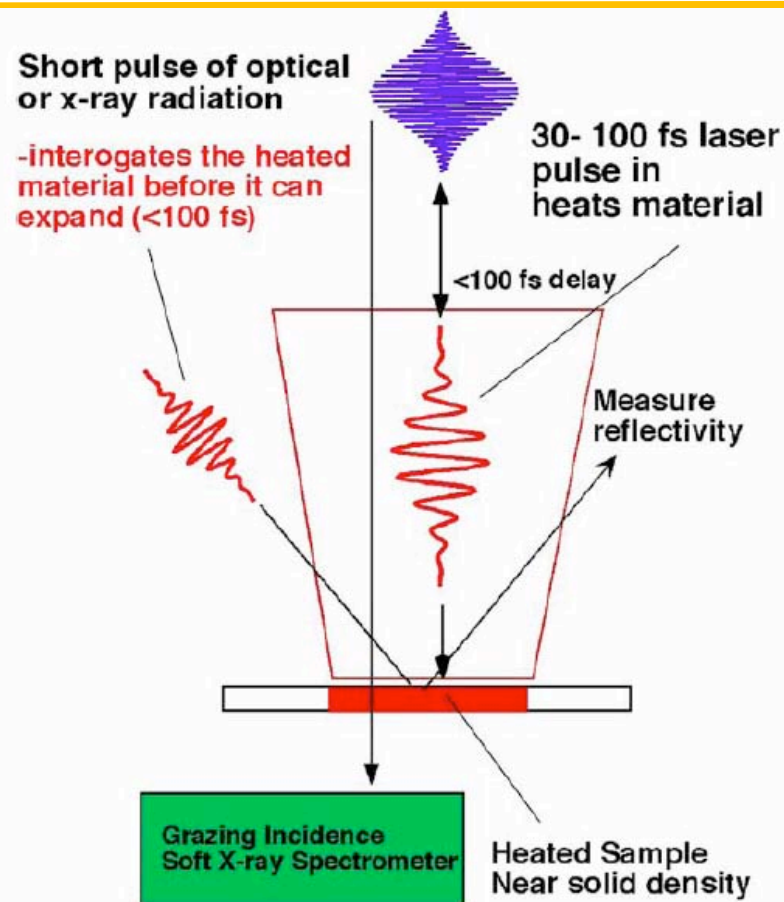
A 25- μm long, 50- μm diameter aluminum slab can be brought to ~ 10 eV by a proton beam produced with less than 1-J laser energy in short pulse.

This can be done at TRIDENT

Direct illumination by short pulsed lasers can probe a wide range of pressures along isochors.



- Near Gbar pressures
- Measurements must be made quickly before expansion.
- Likely NLTE.



T. Ditmire et al., Rad. Phys. and Chem., **70**, 535 (2004).

Laser-produced protons can also be used for radiography of samples

Example: LULI experiments

- Up to 10 MeV proton beam produced by 350 fs, 3×10^{19} Wcm⁻².
- 5 Mbar shock produced by 80 J, 0.5 ns beam.

M. Koenig et al., Nucl.Fusion **44**, S208 (2004)

Proton radiography has been performed at TRIDENT by J. Cobble et al, LA-UR-01-6521

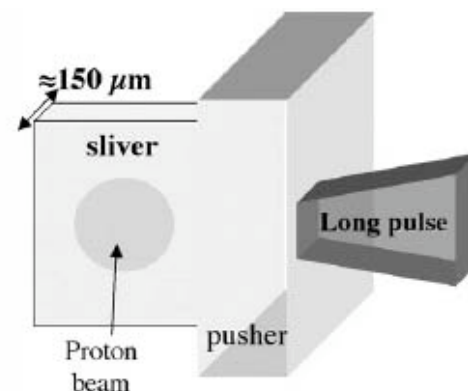


Figure 10. Proton radiography target scheme.

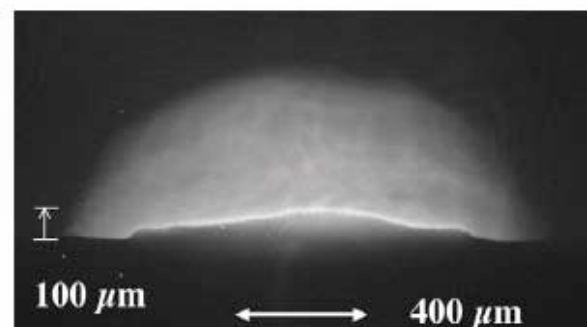


Figure 11. Proton image of an aluminium foil 7 ns after the long pulse beam.

Hot electron generation of K- α emission is a very efficient source for hard x-ray production^a

- Irradiances of $\sim 1.4 \times 10^{18} \text{ Wcm}^{-2}$ would produce tin, Sn, K- α at $E_k = 29.2 \text{ keV}$.
(assuming 1- μm wavelength)
- With a 100-TW laser, a 100- μm spot is adequate for producing Sn K- α .

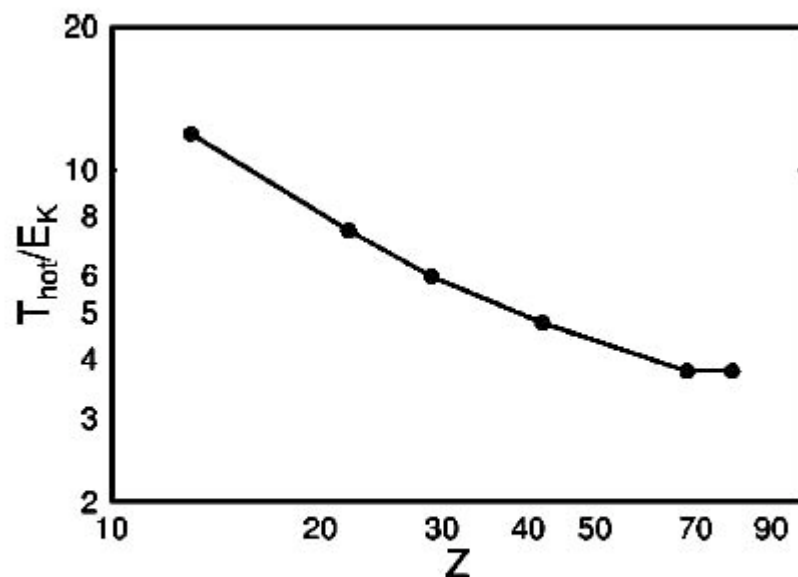


FIG. 5. Optimal ratio of hot-electron temperature to K-shell ionization energy for different target materials Z.

$$T_{\text{hot}} \approx \left(\sqrt{1 + \frac{I \lambda_{\mu}^2}{2.8 \times 10^{18}}} - 1 \right) 511 \text{ keV}$$

^aJonathan Workman, internal memo, P-24-03-086

Previous short pulse laser experiments found high efficiencies and yields in high-Z, K- α x-ray production

- Laser irradiance = 3×10^{17} W/cm², with 1 J in 100 fs^a
- Conversion efficiency to ⁵⁰Sn K- α (~25 keV) was $\sim 10^{-5}$.

- **For TRIDENT:**
 $\sim 10^{11}$ photons at 100 J^b

^aAndersson et al., J. Quant. Elec., **33**, 1954 (1997)

^bJonathan Workman, internal memo, P-24-03-086

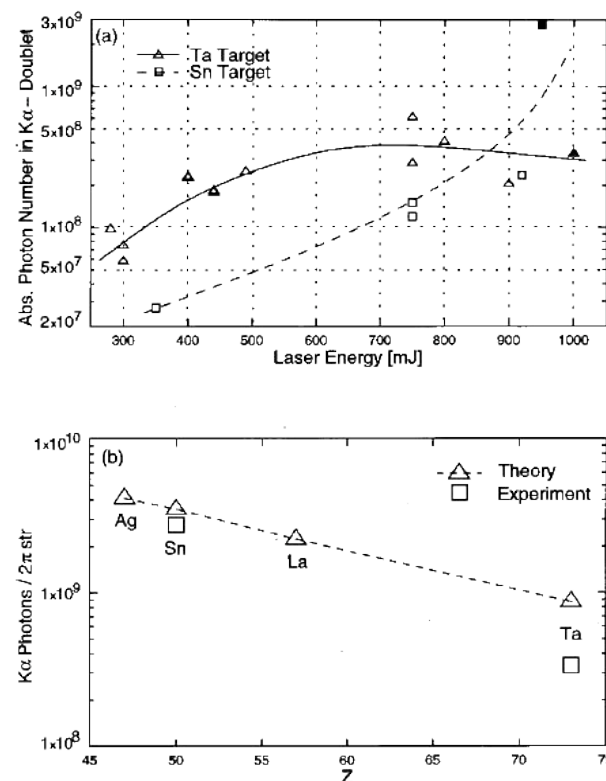
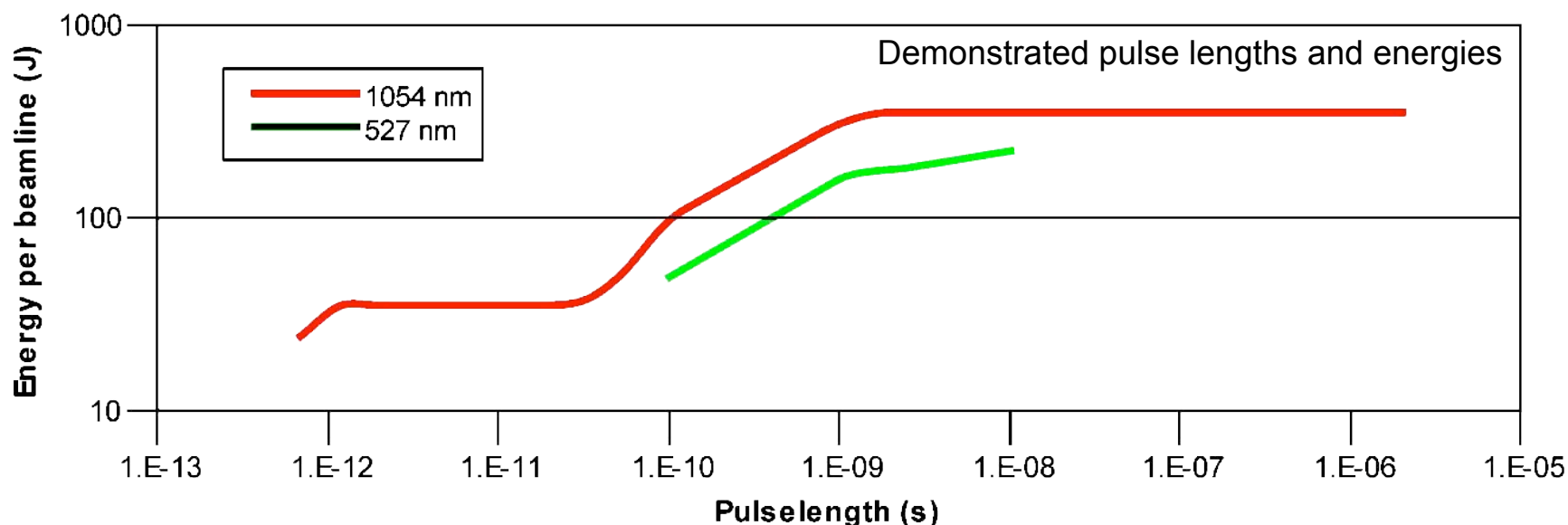


FIG. 10. Comparison of theoretical and experimentally determined K α yield as a function of target material (a) and experimentally determined absolute numbers of photons in K α doublet (b). The curves depict yields calculated using an initial plasma density gradient of $L/\lambda = 1/\lambda[\rho/(d\rho/dz)] = 0.3$. The experimental data in (a) corresponds to the filled points in (b).

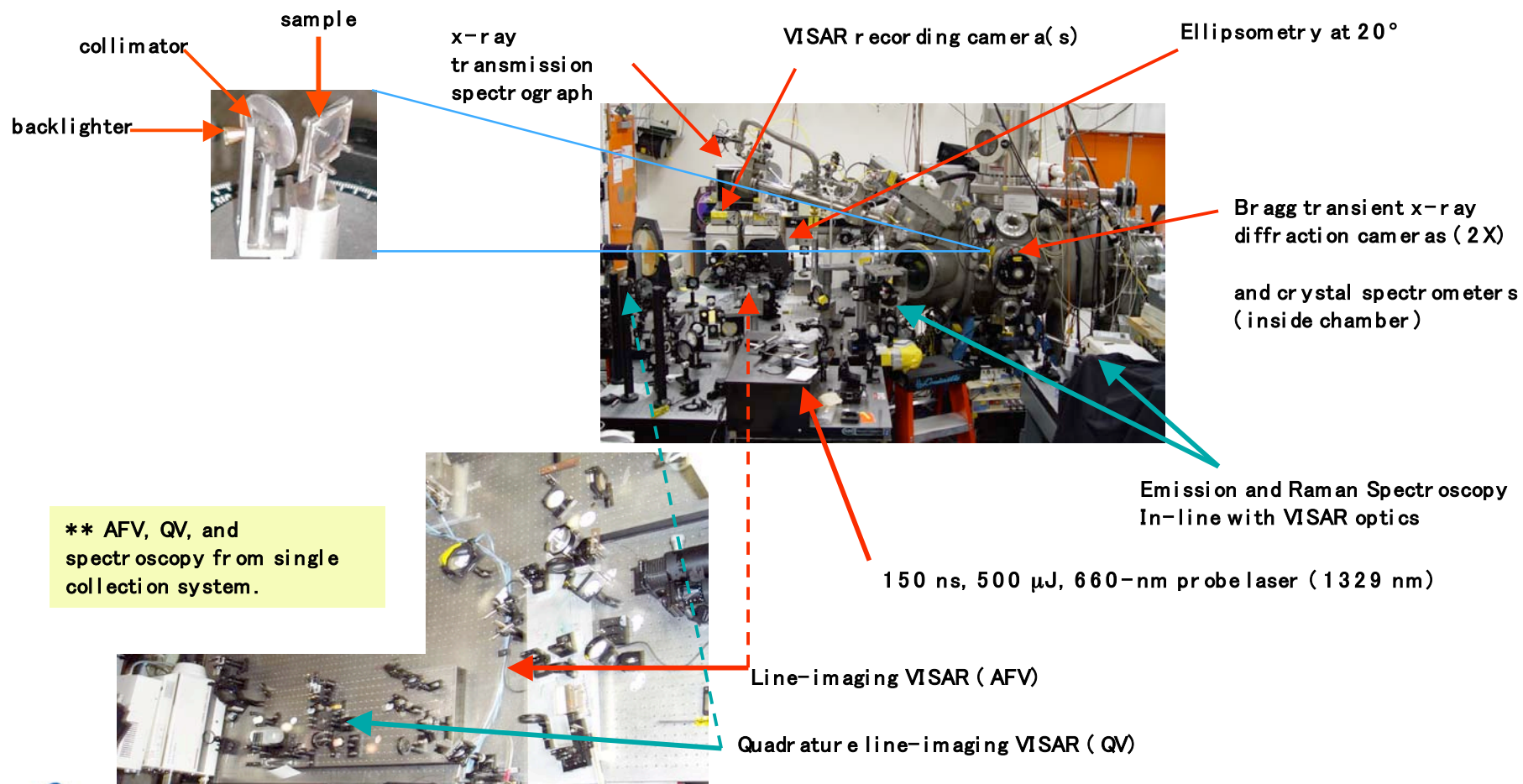
TRIDENT has demonstrated a wide temporal range for dynamic materials experiments.



While short pulses are advantageous to producing high energy photons and particles, **shaped** long pulses are ideal for probing a wide range of equation of states for dynamic materials experiments

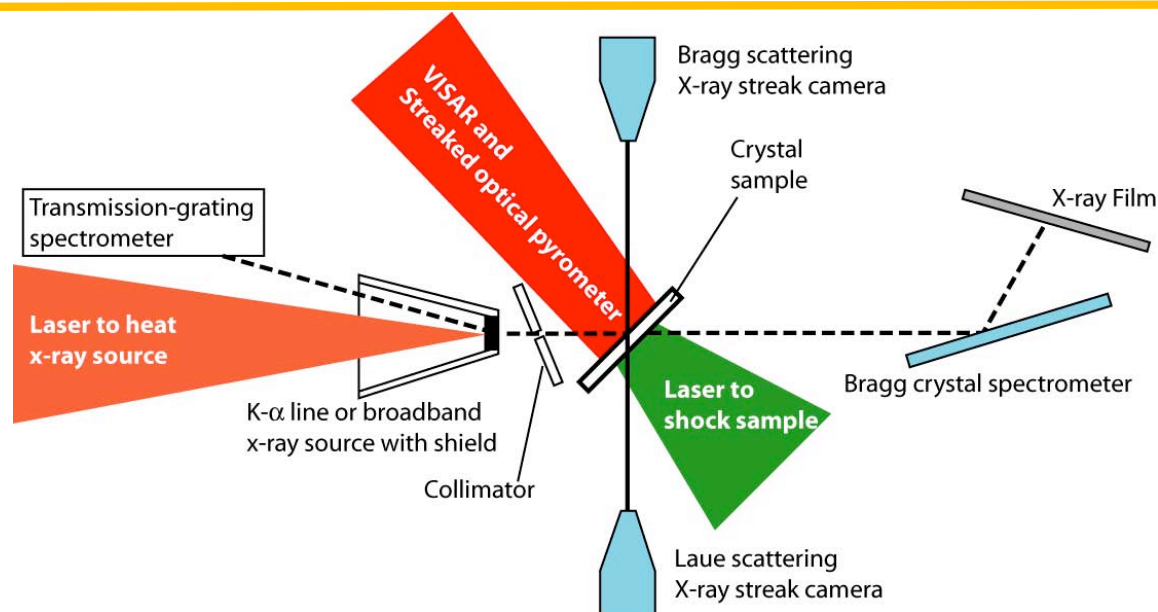
UNCLASSIFIED

Many simultaneous diagnostics are used in TRIDENT experiments



UNCLASSIFIED

Direct laser illumination produces Mbar shocks that compress a crystal.

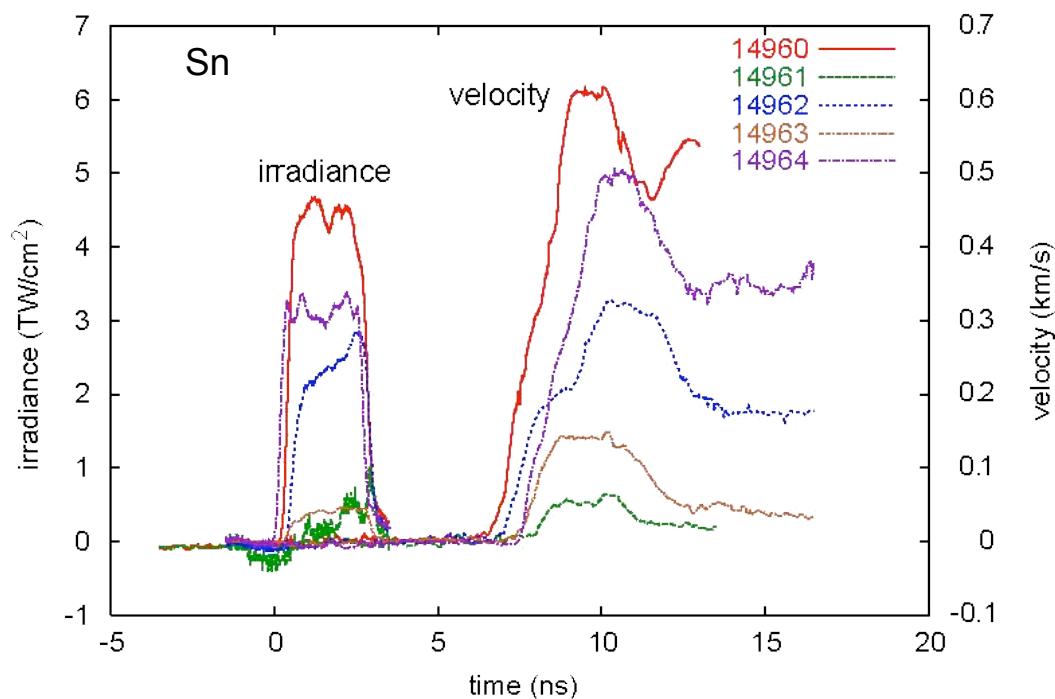


- Either long pulse shock with short pulse x-ray source or short pulse shock with long pulse backlighter
- Sample may include a low-Z “anvil”
- Source spectrum measured during each shot
- Time-resolved spectroscopy is possible

Types of measurements that would be made on a direct-drive compression experiment

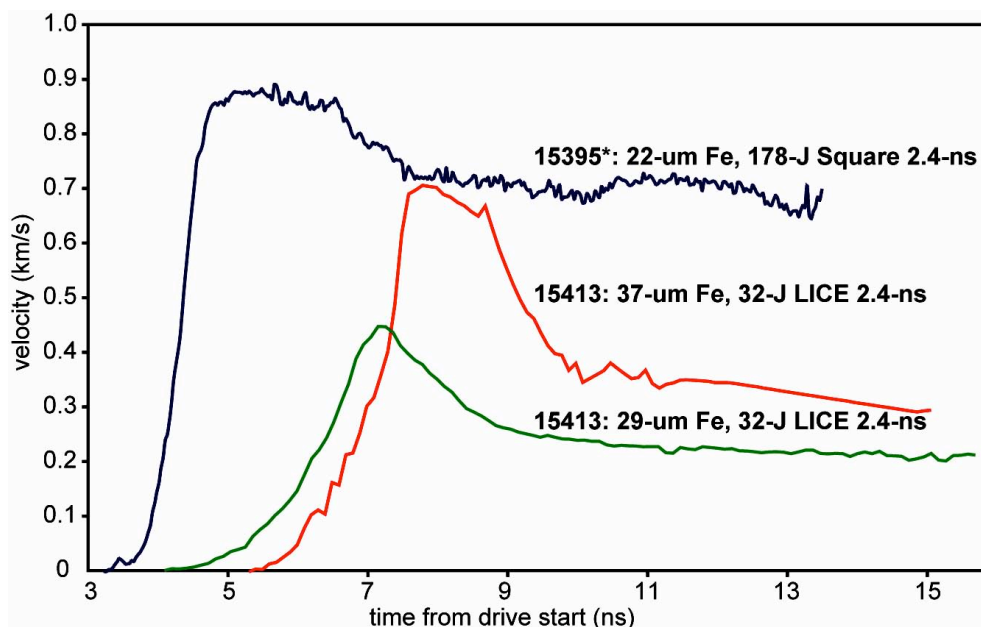
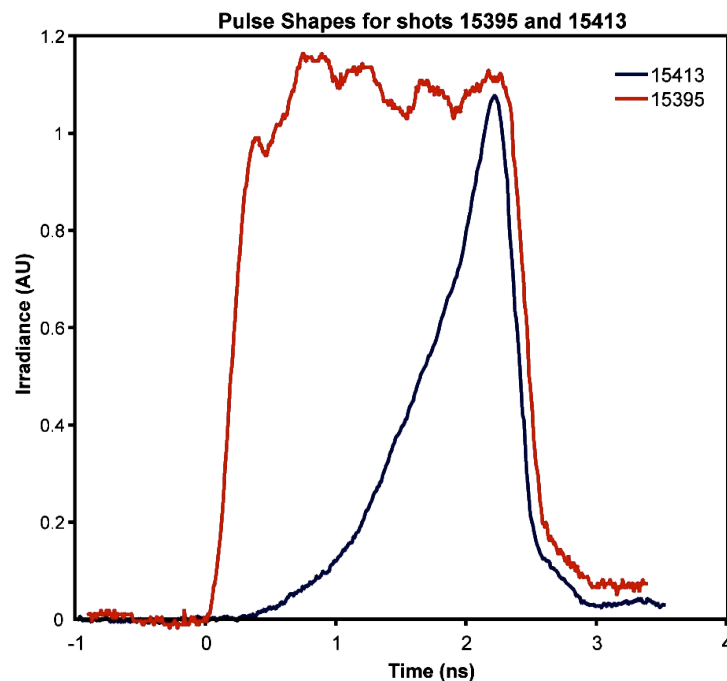
- Line and broadband transmission measurements prior to or at breakout.
- Simultaneous dynamic materials measurements characterize material state(s) and pressure history
 - Velocimetry
 - Pyrometry
 - Ellipsometry
 - Transient x-ray diffraction

Varying the laser irradiance produces different compression histories.



- 13-element pulse stacker
- Automated feedback for “dial-a-pulse”
- Predictive modeling to compensate for amplification

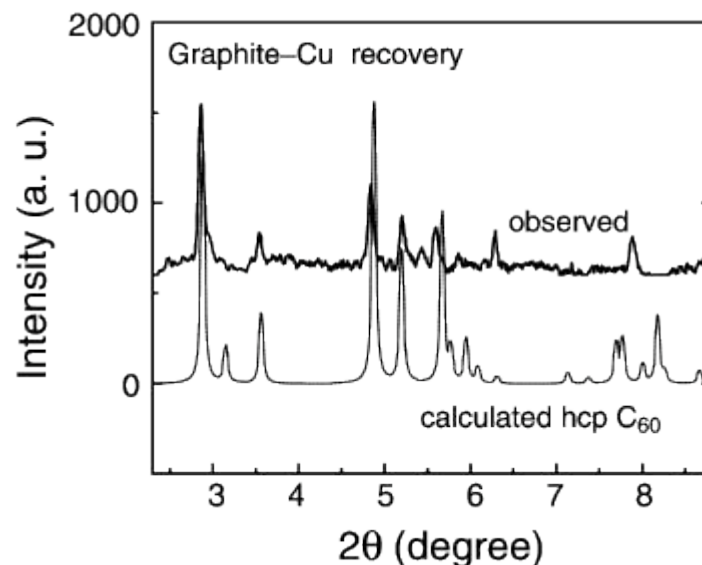
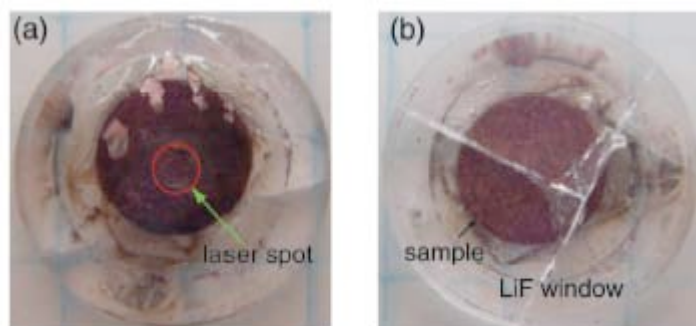
Laser irradiance shaping produces distinct loading profiles: e.g. (Shocks and LICE)



**Example of pulse shaping pressure profiles:
VISAR for shocked iron and quasi-isentropic drives on two iron samples.**

LICE = “Laser quasi-Isentropic Compression Experiments”

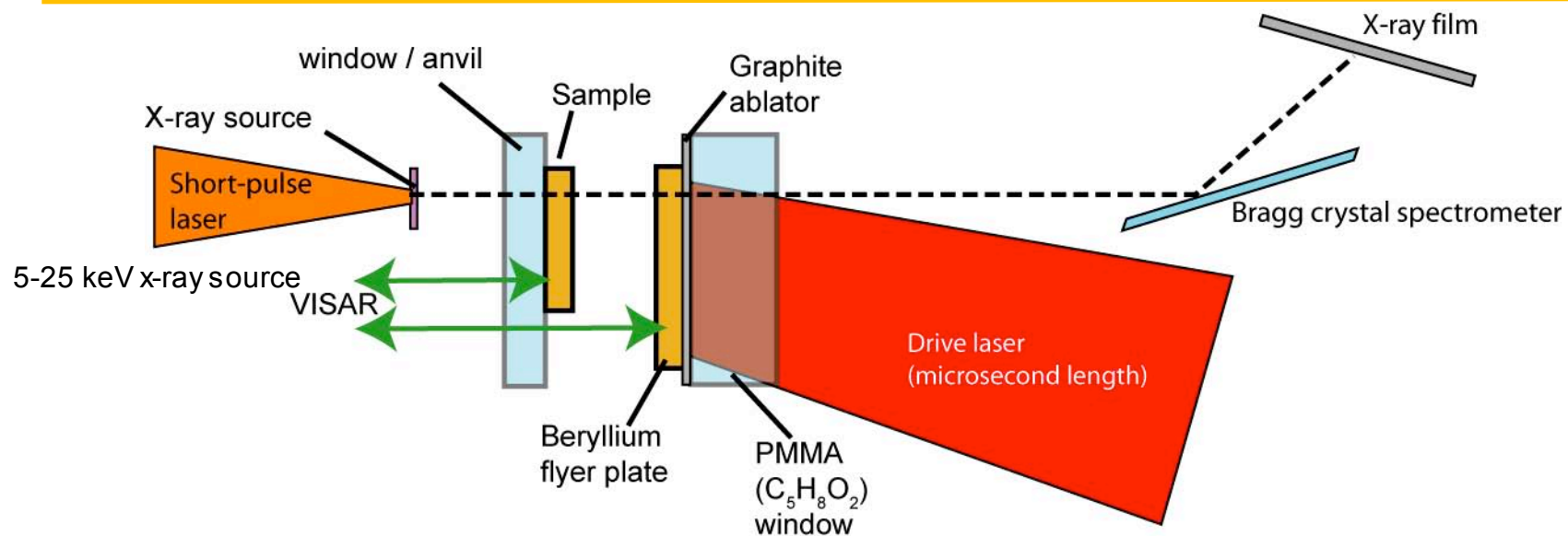
Sample recovery allows for “post-mortem” analysis.



Synchrotron X-ray diffraction pattern (refined) of shocked graphite-Cu mixture (Trident #16726), indicating a hexagonal crystalline phase of two-dimensional polymerization.

O. Tschauner, S. N. Luo *et al.*, High Pressure Research, vol. 24, No. 4, pp471-479 (2004).

Flyer-plate impact can create steady shocks in sample materials (10-700 kbar depending upon materials used)



Shock pressures and duration are dependent upon flyer plate speed and thickness.

We have launched 2-mm thick aluminum flyers to greater than 400 m/s.

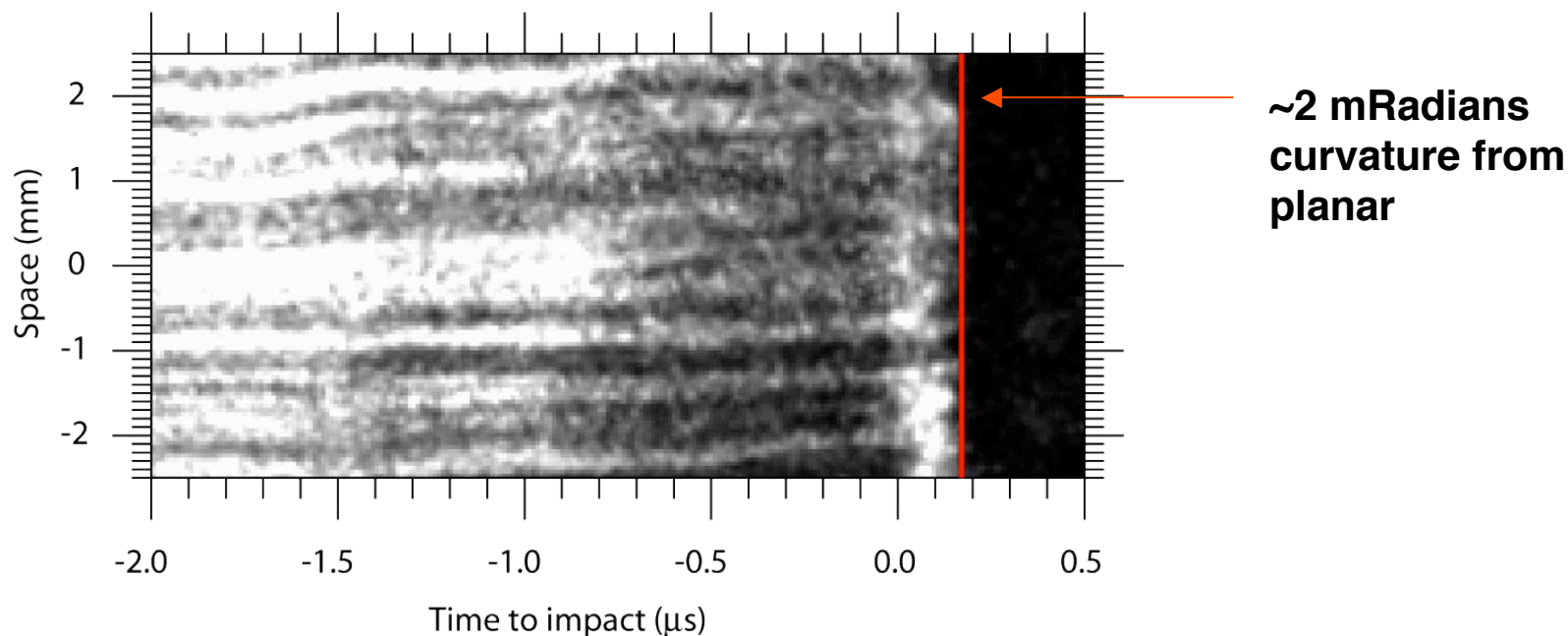
Modeling indicates 25-micron beryllium flyers in excess of 4 km/s

Many measurements are possible on these experiments

- Source spectrum on all shots
- Spectrum thru Be flyer and Be sample (symmetric impact)
- Spectrum thru Be flyer and target sample
- Breakout surface measurements:
 - Velocimetry
 - Emission spectroscopy
 - Raman spectroscopy

Laser-plasma-accelerated flyers have high planarity.

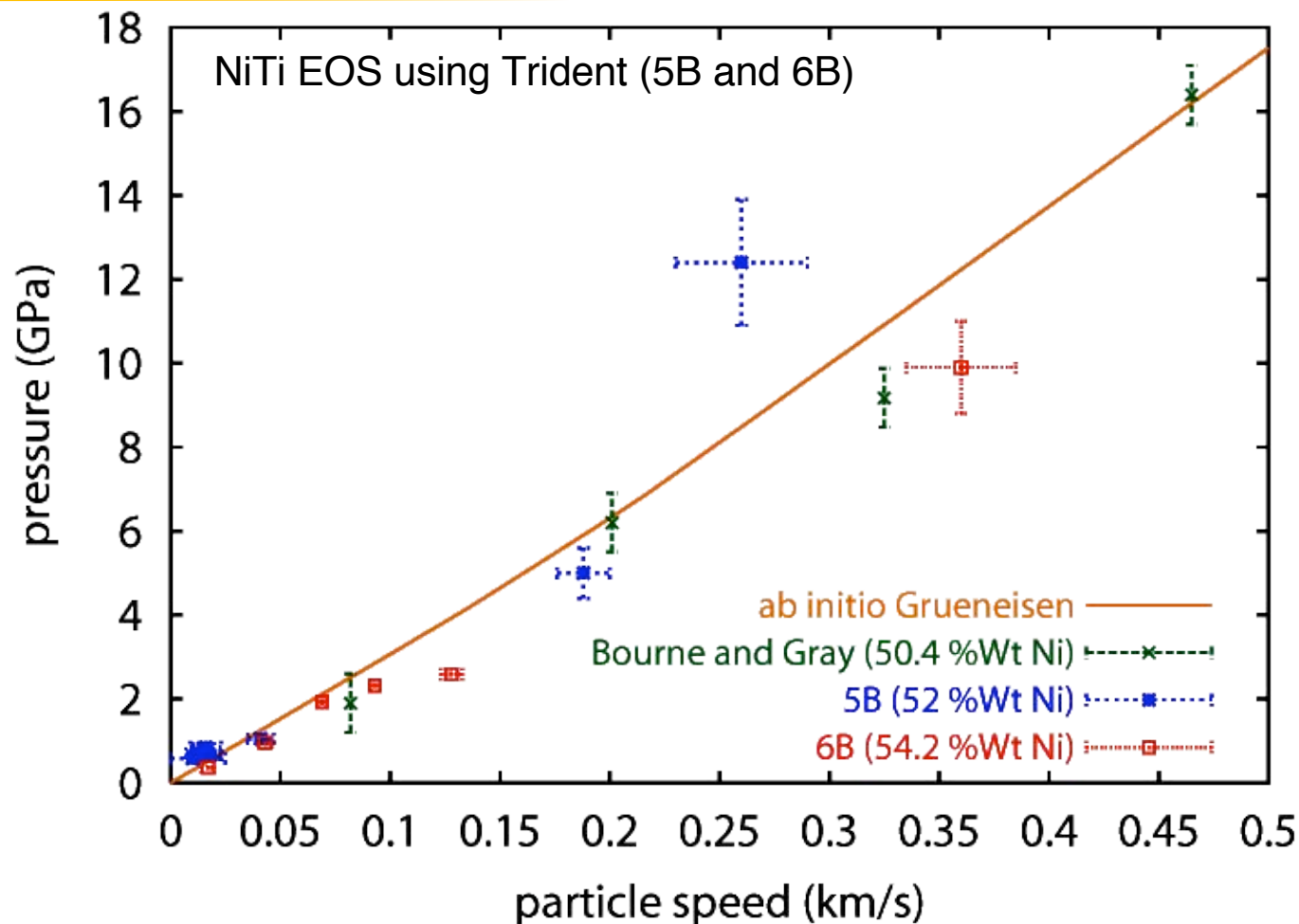
Trident shot 16831 Al flyer with Al target



- Laser reflectivity for planarity measurements with high temporal-spatial resolution
- Typical planarity 2-10 mRadians for flyer velocities 0.1-1.0 km/s.

UNCLASSIFIED

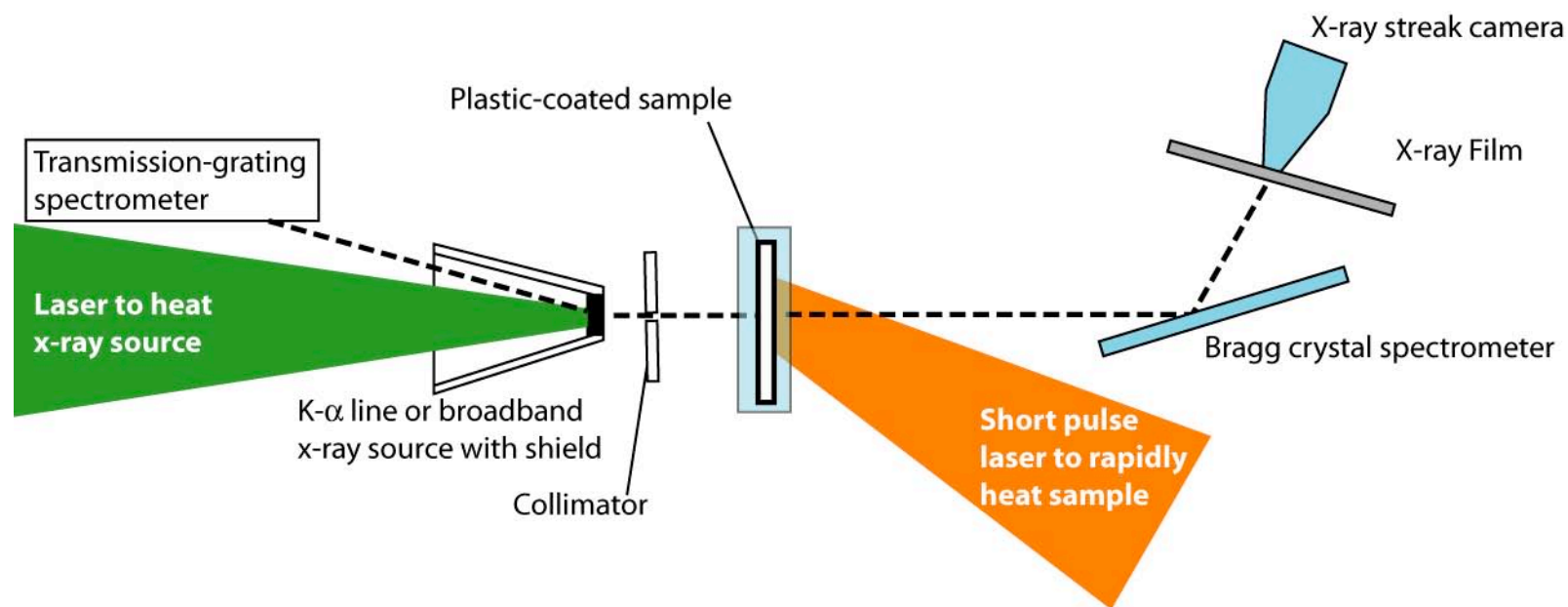
Laser-based flyer-plate experiments can produce data of adequate quality data for equation of state



UNCLASSIFIED

UNCLASSIFIED

The short pulse system can rapidly heat a material isochorically



UNCLASSIFIED

Conclusions for TRIDENT

- TRIDENT's pulse length and shape flexibility allow us to study EOS (and possibly LTE Opacity too).
- Available diagnostics will permit in-depth characterization of material properties during opacity measurements.
- TRIDENT's new Short Pulse Laser capabilities may permit opacity studies of isochorically heated samples
- Laser-produced proton radiography at TRIDENT can be developed as a diagnostic capability.

Example of opacity effects in ICF conditions

Experimental goal:

Define a microstructural specification for NIF's Be-Cu ablators.

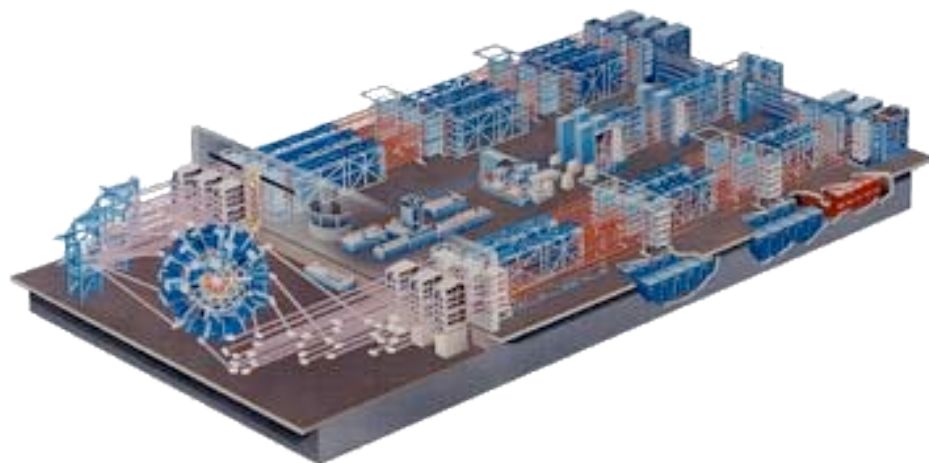
- Grain-seeded Rayleigh-Taylor instability measurements
- Characteristics of NIF's first shock (80-eV hohlraum): shock velocity and temperature.

Disclaimer:

- The “BAMS” OMEGA experiments were not designed to be true opacity measurements.

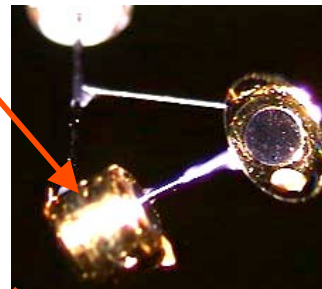
UNCLASSIFIED

Omega laser experiments can closely simulate the expected conditions for BeCu ablators.

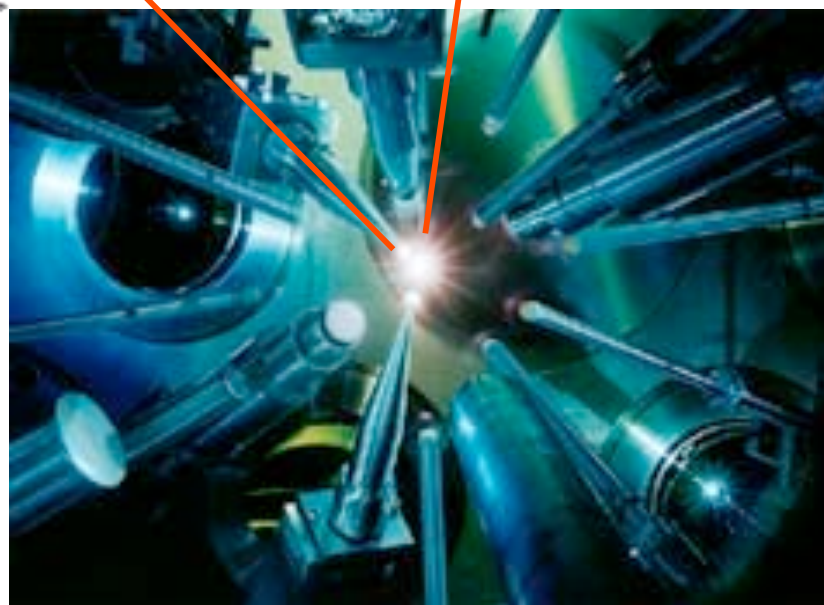


60 beams for total of ~30 kJ

Hohlraum

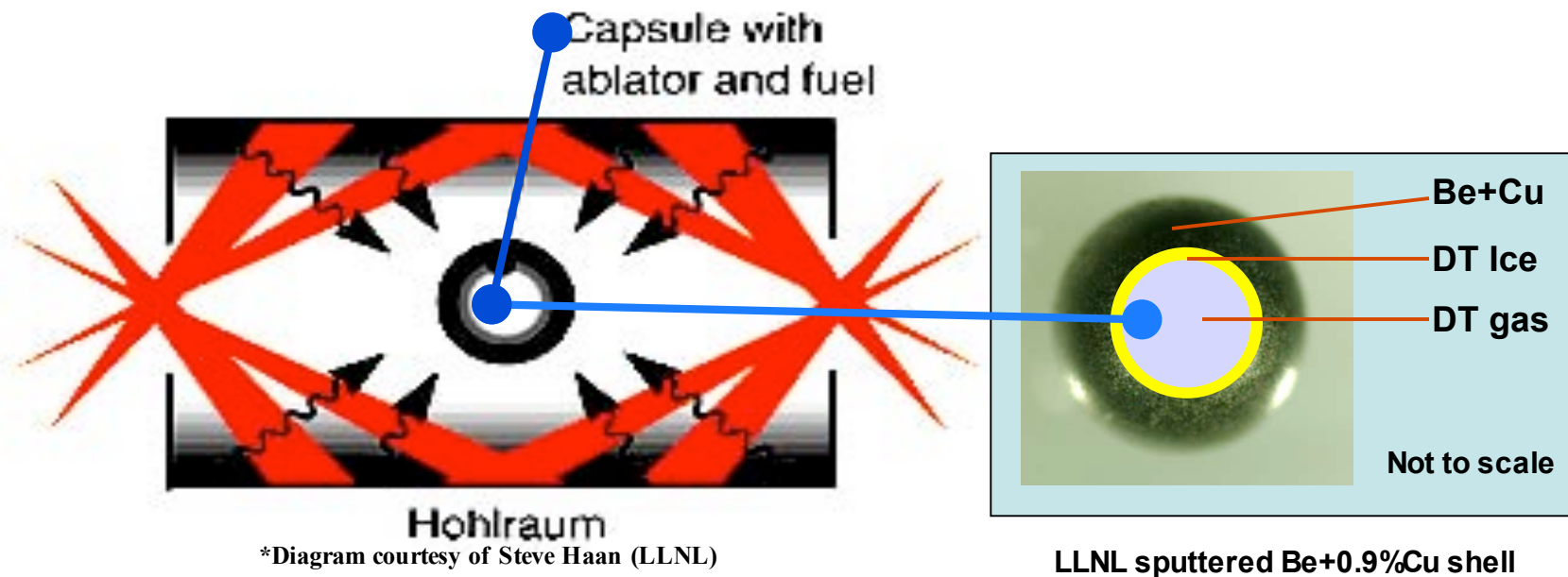


A target that was fielded at Omega



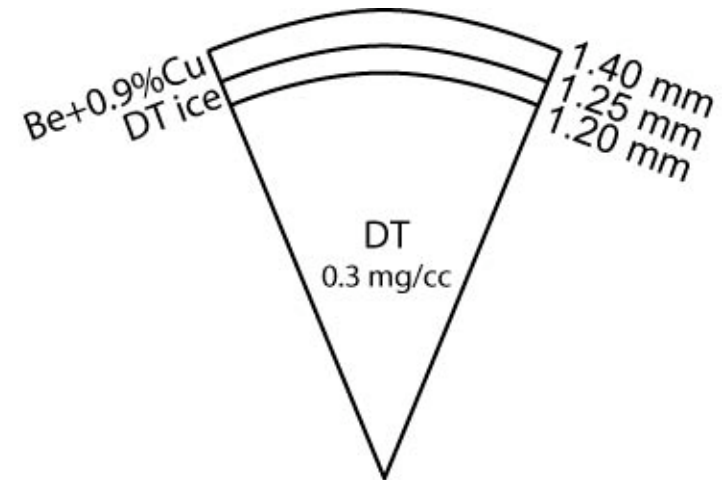
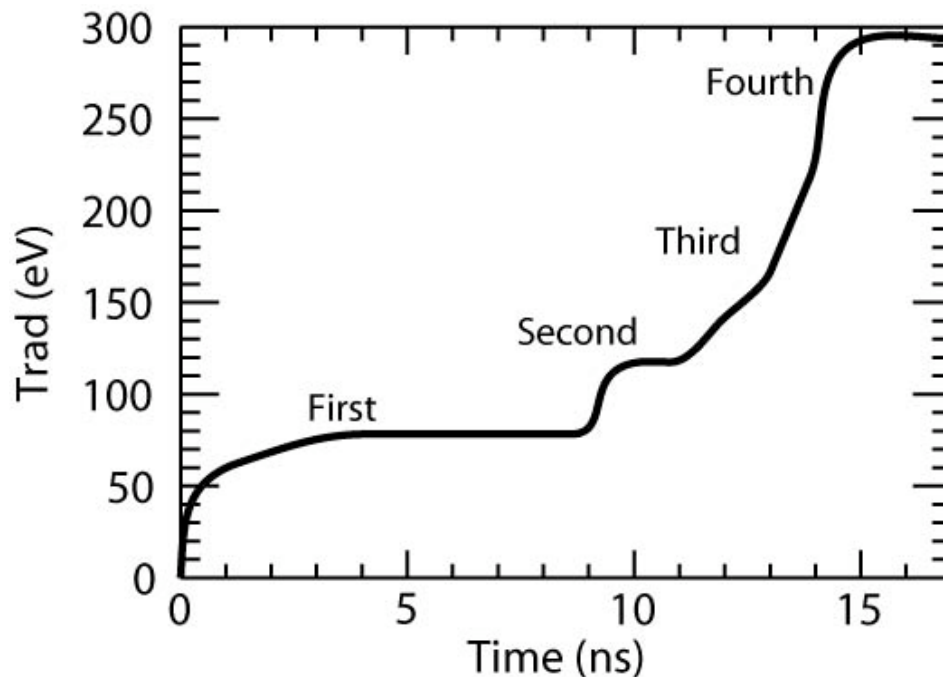
UNCLASSIFIED

Indirect drive uses soft x rays and thermal radiation to heat ablators that surround fuel



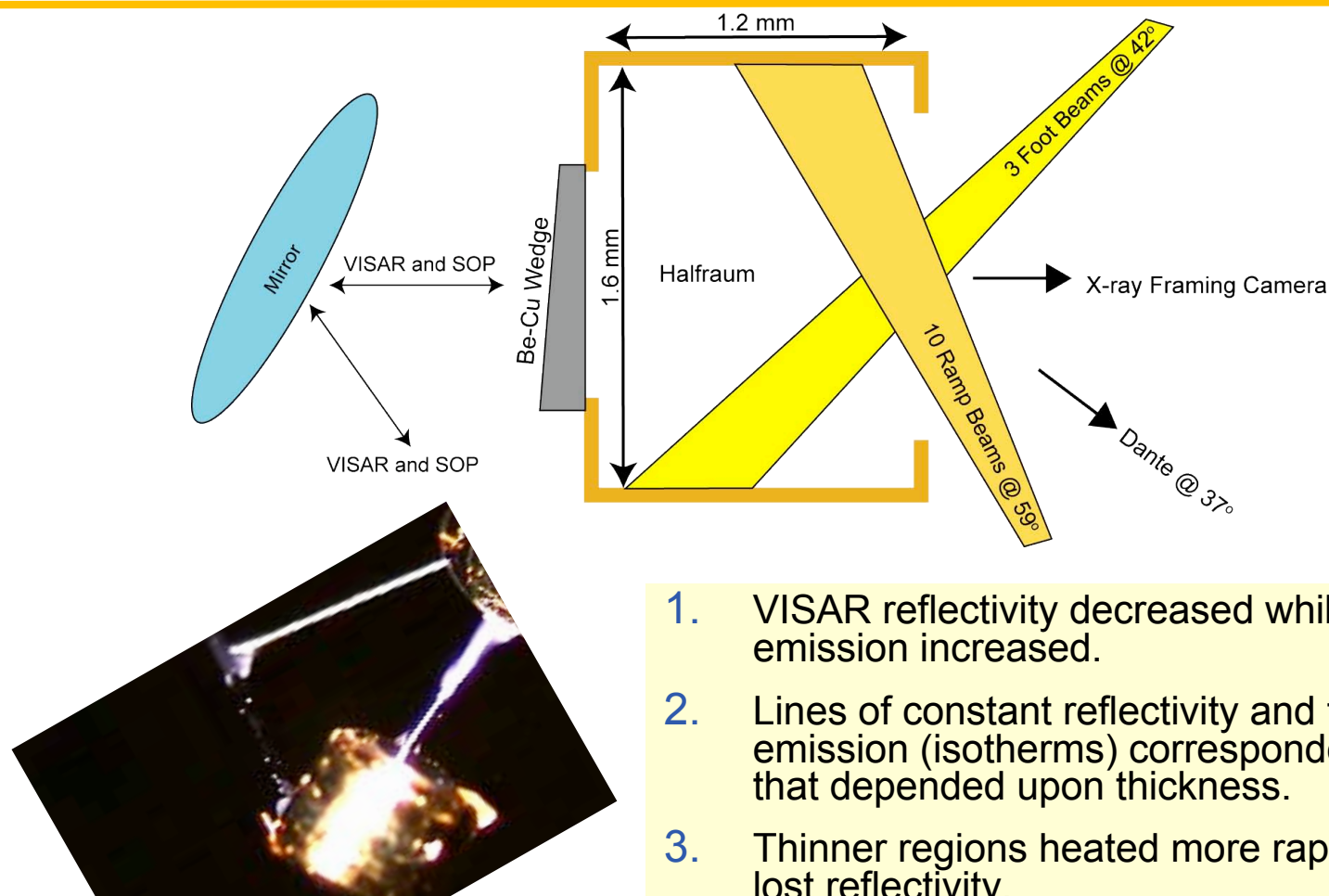
- The National Ignition Facility (NIF) will use up to 192 beams to heat the hohlraum and produce soft x rays.
- Some ablator materials being considered:
 - Be+0.9%Cu, CH+0.6%O+0.23%Br, and $C_{22}H_{10}N_2O_4$

The radiative drive is designed to produce a series of shocks that compress the capsule



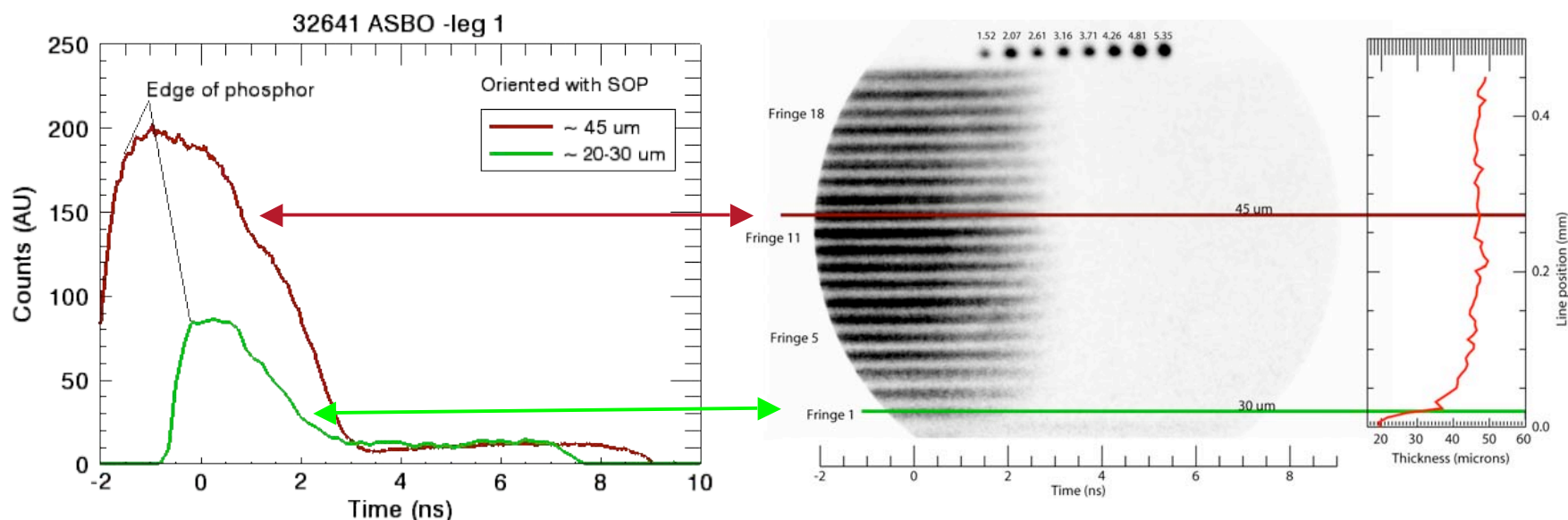
- Iterative 2D and 3D modeling is required to design a laser pulse shape that produces the desired loading profile (temperature history).
- The shocks coalesce within the beryllium-- prior to breaking out into the DT.
- We focus on the first shock, where microstructure effects are most pronounced.

Shock experiments on Be-Cu ablators revealed a preheating source in hohlraum



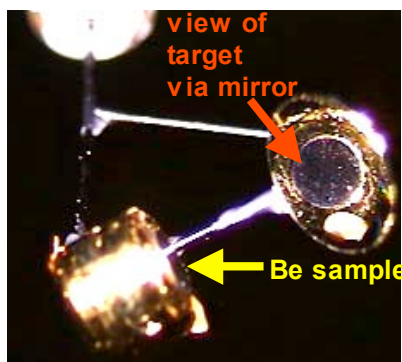
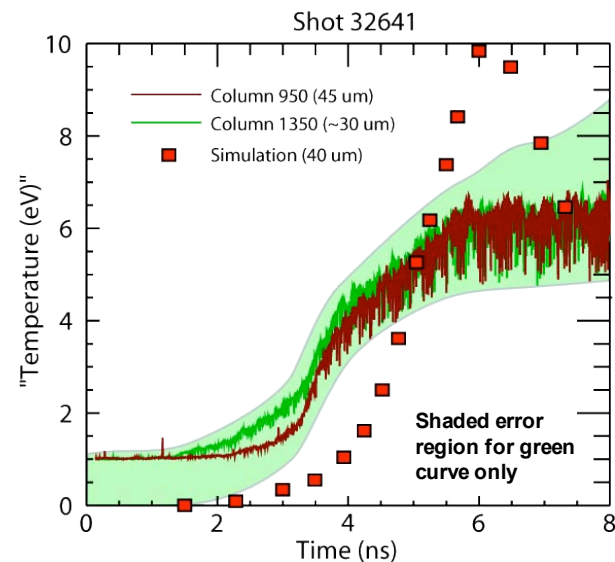
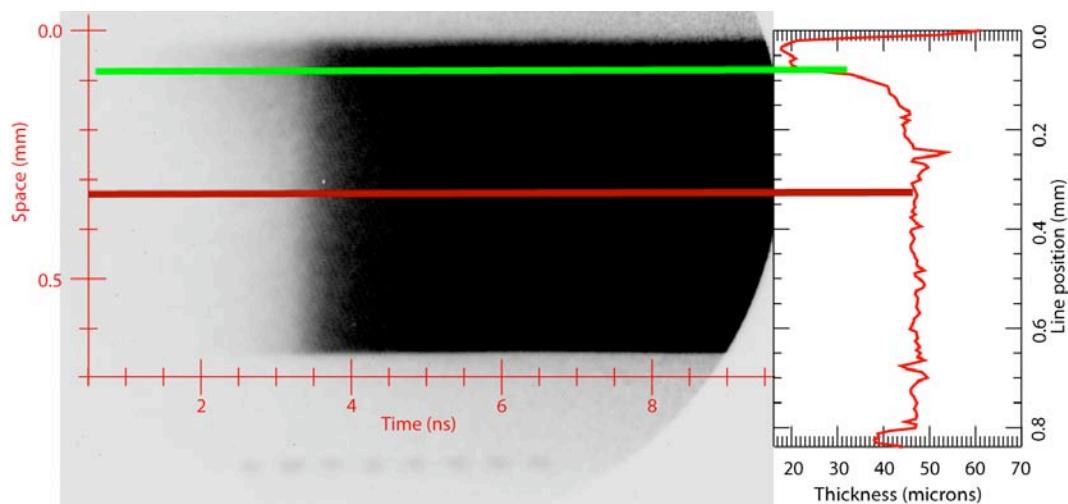
1. VISAR reflectivity decreased while surface emission increased.
2. Lines of constant reflectivity and thermal emission (isotherms) corresponded to times that depended upon thickness.
3. Thinner regions heated more rapidly and lost reflectivity.

VISAR reflectivity drops to zero at $t \sim 3$ ns-- near shock breakout time.



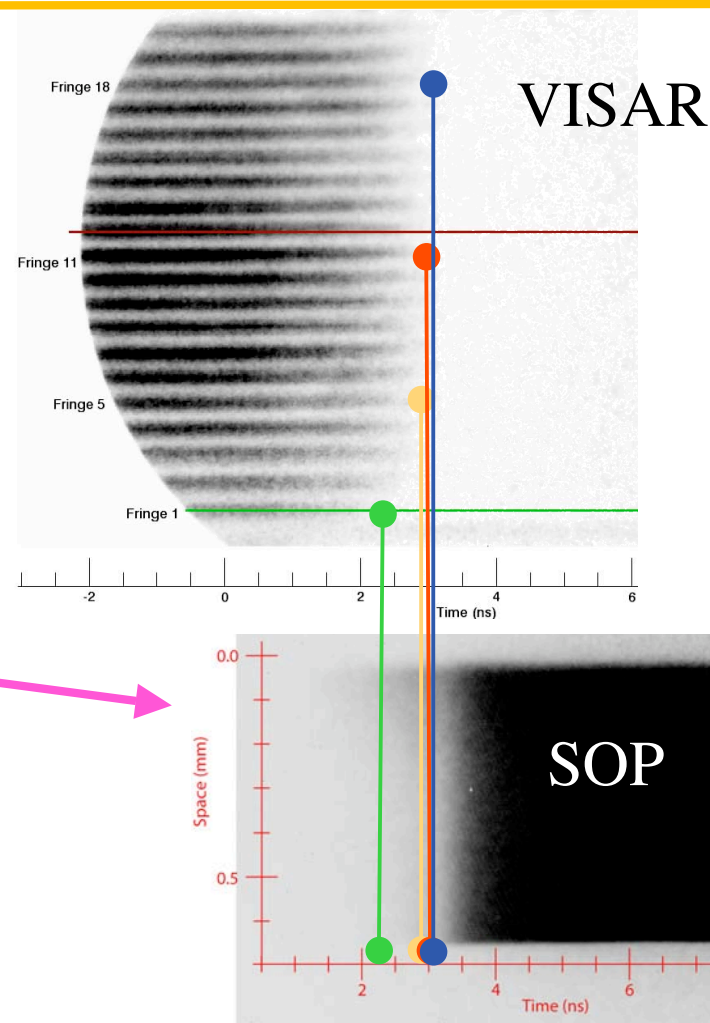
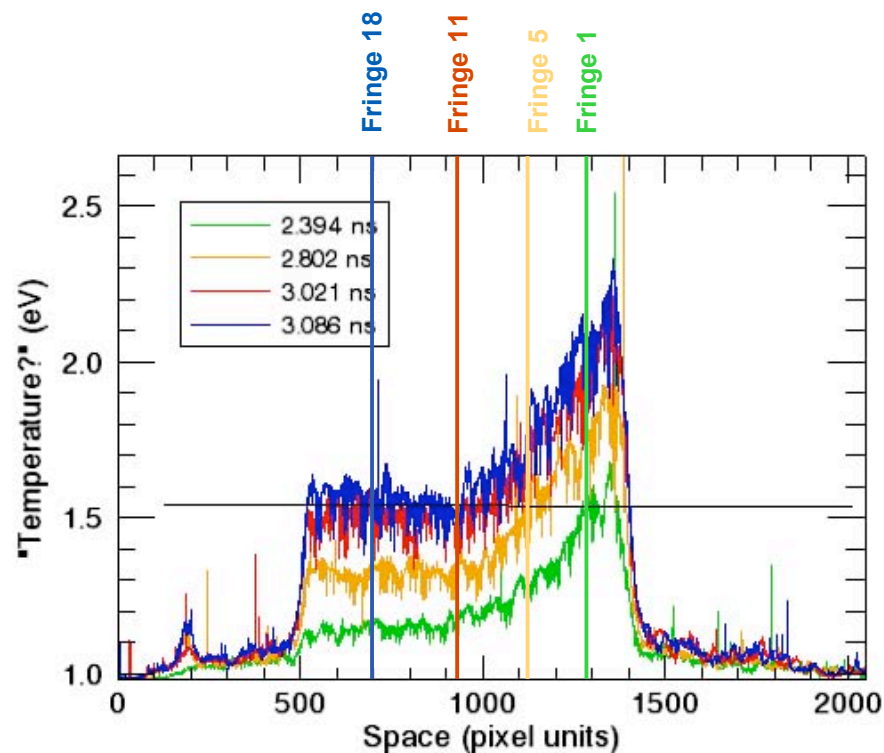
Lineouts along fringes with 50-pixel averages show reflectivity decreasing—more rapidly with thinner regions.

Streaked optical pyrometry observed more preheat than predicted



- Simulations are being refined to include laser "hot spots"
- Spectrum driving preheat appears to be between M and N band. Laser intensity too low for Nickel-like gold lines.

Timing of VISAR's reflectivity disappearance is consistent in temperature.



Analysis technique for the preheat using “isotherms”

We calculate the heating due to absorbed x-rays:

$$\frac{\partial T(x, t)}{\partial t} = \int \frac{\rho(x, t) \kappa(\lambda, T) \varphi(\lambda, x, t)}{c_v(T)} d\lambda$$

Where φ is the x-ray flux at time t and position x with wavelength T is temperature, λ is the x-ray wavelength, ρ is mass density, κ is opacity, and c_v is the specific heat capacity.

We invert this equation to find,

$$u_{eff} \equiv \left. \frac{\partial x(t, T)}{\partial t} \right|_T$$

Assuming opacity changes in soft x-ray regime do not change much for a few eV sample,

$$\kappa(\lambda, T) = \kappa(\lambda) \longrightarrow \kappa_\lambda$$

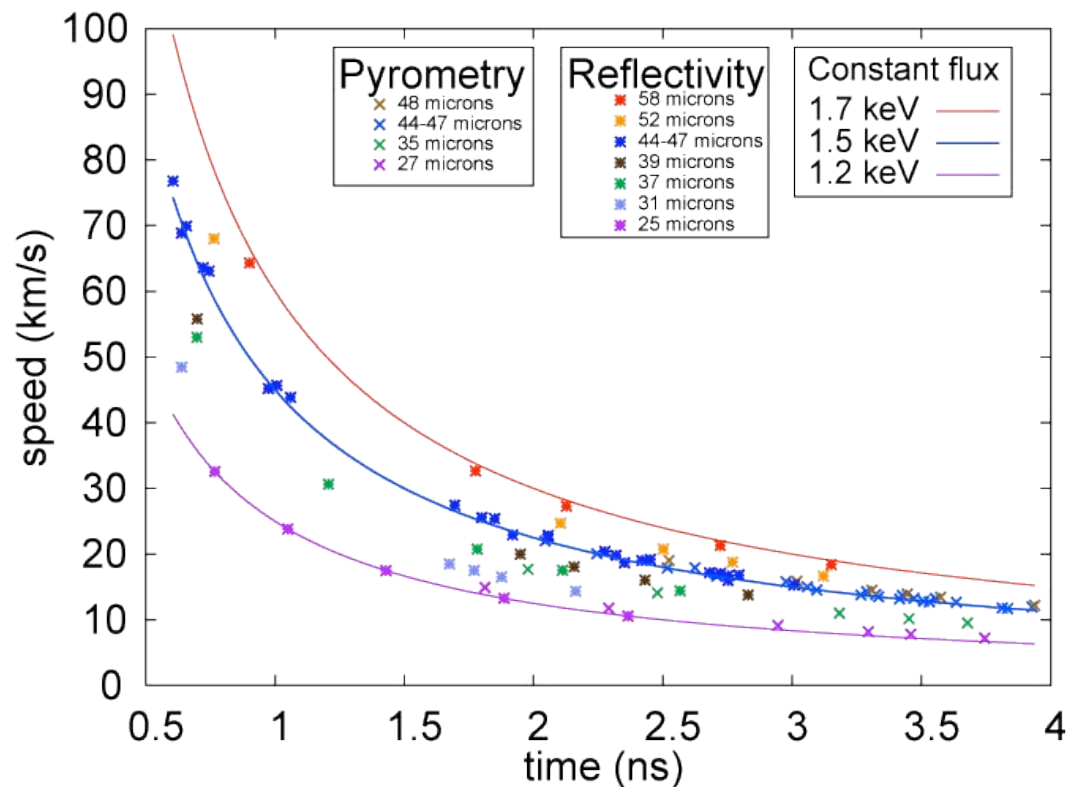
-As an initial assumption*, we then simplify using constant flux to find:

$$u_{eff} = \frac{1}{\rho \kappa_\lambda t}$$

*For the conditions considered here, the “real” flux history can be well approximated as nearly constant for ~3 ns.

Reflectivity decreases and isotherms corresponded well to a broadband source

- “Iso-reflectors” chosen for reflectivity points
 - related to isotherms.
- Isotherms chosen for pyrometry points
- Absolute temperature is not necessary for this analysis technique!



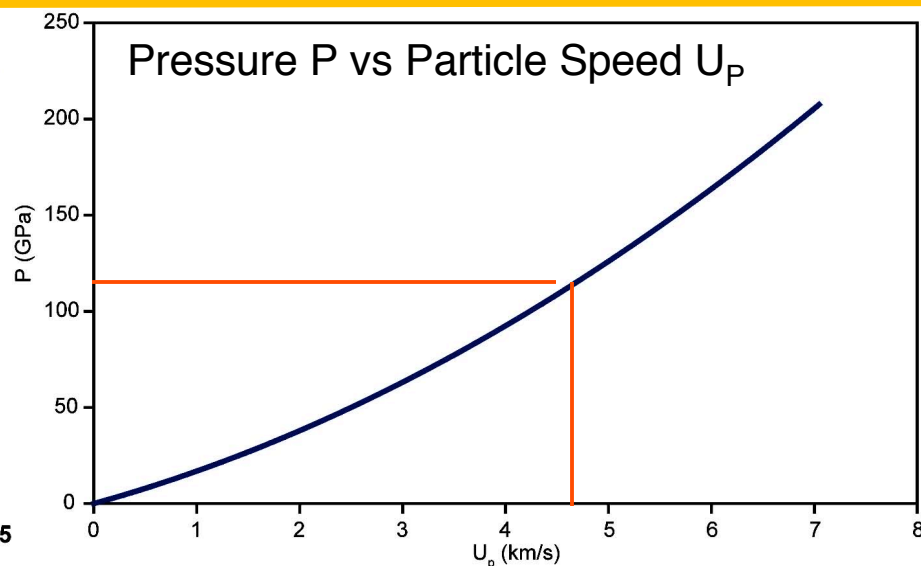
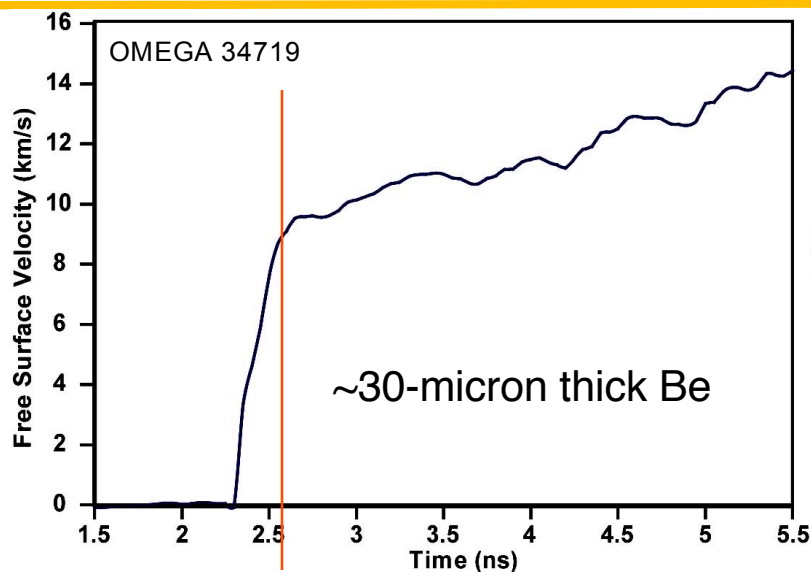
What needs to be done to *really* study opacity of this ablator material?

- Time-resolved transmission spectroscopy thru the sample and out the laser-entrance hole.
- 1-D spatially-resolved spectrum.
- 2-D spatially-resolved soft x-ray images with narrow transmission bands.
- A more complete model needs to be developed.

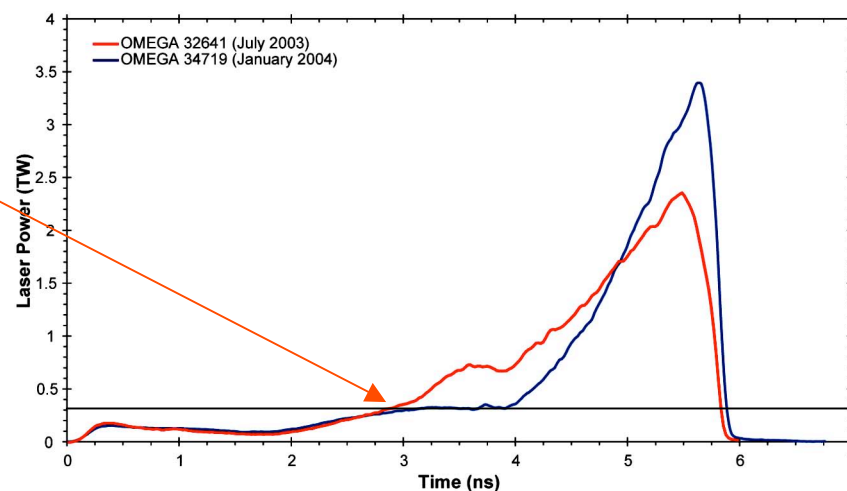
Final Conclusions

- TRIDENT's recent short pulse addition affords access to new material conditions.
- OMEGA is a good platform for studying ICF-related opacities
- Opacity measurements can be made during well-characterized materials experiments.

VISAR shows Be-Cu free surface velocities when laser drive is kept below 0.3TW.

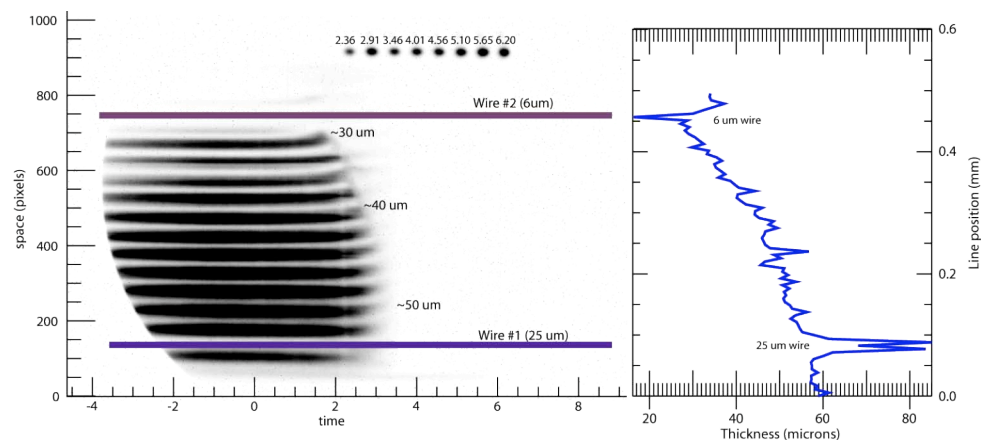
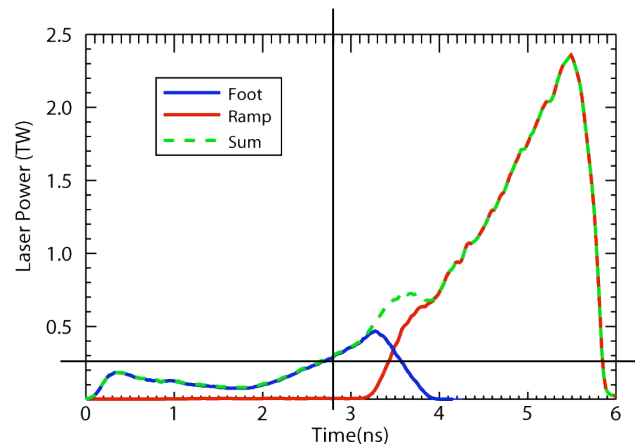
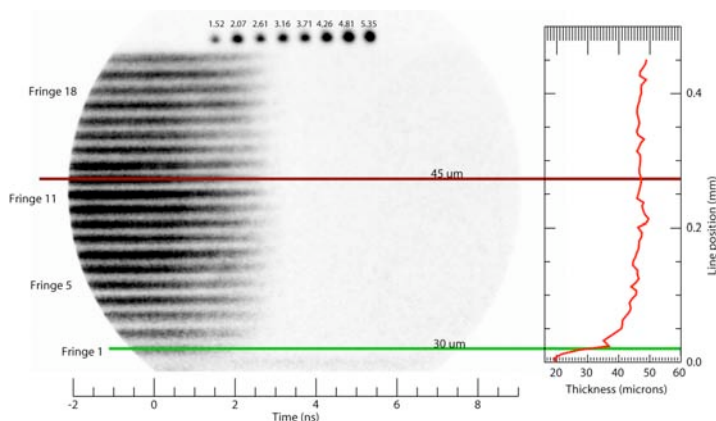


- Last half of foot drive was kept below 0.3 TW.
- Free surface velocity measurements consistent with a 1.2 Mbar shock.
- Predicted breakout at ~3.0 ns.

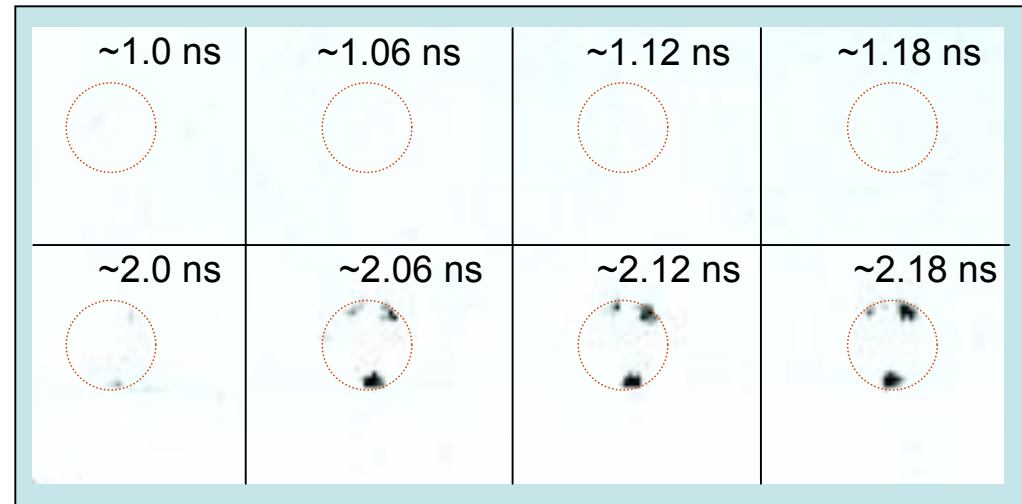
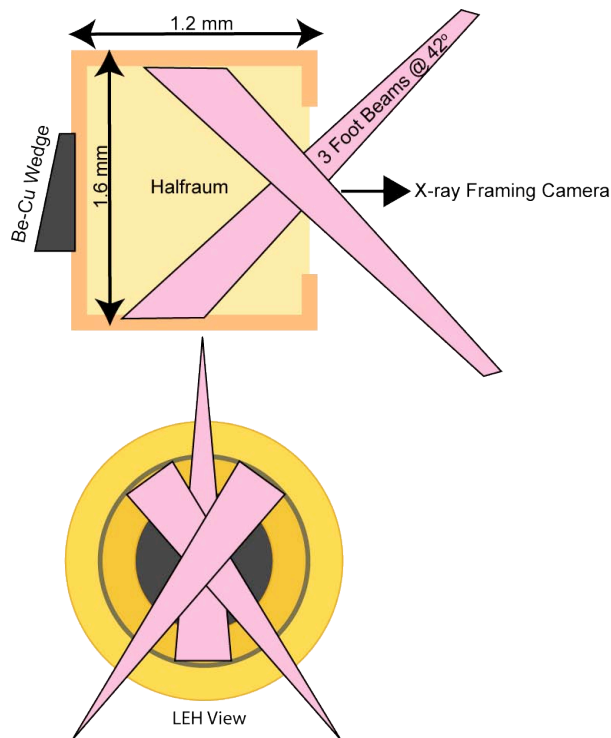


Reflectivity disappeared prior to clear shock breakout.

- Vacuum holhraum example #32641
- Powder-pressed Be-0.9%Cu.
- Breakout was expected in range of $t \sim 3.2\text{--}4.0$ ns.

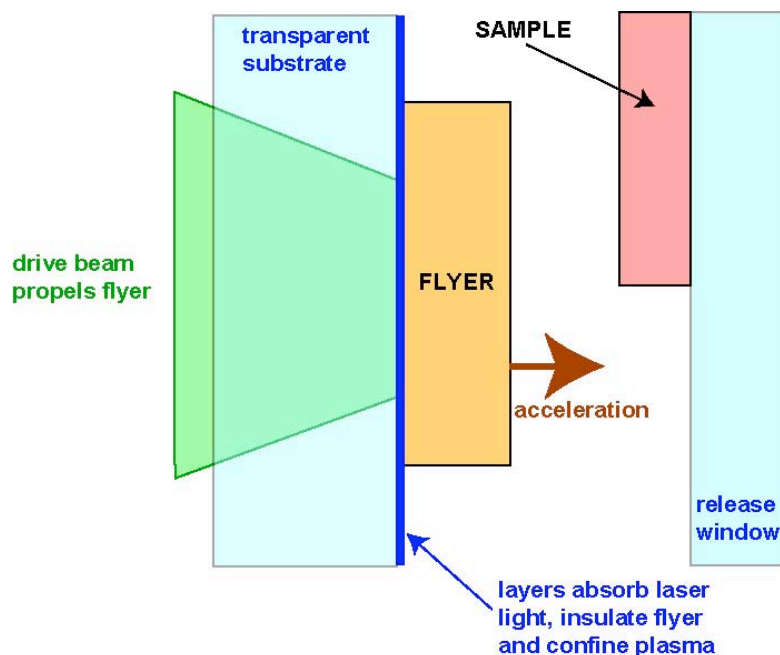


A soft x-ray (> 1 keV) framing camera (XRFC) observed gold ablation and emission



- Gold plasma from wall has ablated to within radius of laser entrance hole (LEH)
- The spots are radiating at energies above 1 keV (0.005" Be filter).

Confined laser plasmas can accelerate flyer plates for dynamic materials experiments.



TRIDENT Drive Characteristics:

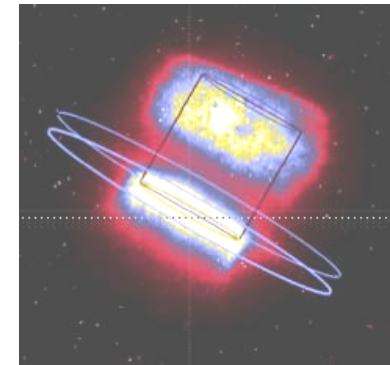
- 0.6-20 μs pulse, 1054-nm
- 0.025 to 2.5 GW/cm^2 (0.5-cm dia. target)
- Sample thickness: hundreds of μm

An Overview of LLNL Experiments Relevant to Opacity Code Validation

Presented to
Los Alamos Opacity V&V Workshop



Physical Data Research Program
Nuclear•Atomic•Condensed Matter Physics



Robert F. Heeter

May 4, 2005

Work performed under the auspices of the U.S. Department of Energy by the Lawrence Livermore National Laboratory under Contract No. W-7405-ENG-48.

UNCLASSIFIED

Heeter-Opacity-V-V slide 1

LLNL has revitalized its opacity experimental efforts in anticipation of breakthroughs on NIF and PWs



2. “Long-Pulse” experiments at Omega and NEL (“NIF Early Light”)

- **Design** Calculations + Theory: hot hohlraums, **opacity targets**, **foil samples**
- Capability Development Experiments:
 - **Spectrometers**, **Backlighters**, NEL commissioning & Hot Hohlraums
- **Code Physics Validation Experiments**: Gd-Al transmission measurements
- **Rosseland Mean Experiments**: working towards T_a (etc.) at $T_r > 100$ eV
- One long-range goal: very high T_r , high-Z LTE experiments on NIF

1. “Short-Pulse” experiments at LULI, COMET, JanUSP, Vulcan-PW...

- Absorption spectroscopy of fs-heated warm dense matter
- Emission spectroscopy of ps-heated hot dense matter
- High-intensity laser-matter coupling studies (backlighters, ps hohlraums)
- Pushing proton heating to higher T for, e.g., solar opacity experiments
- One long range goal: high density, high-Z LTE experiments on PW's

**This talk presents a (non-representative) sample of our unclassified work:
Short-pulse, NIF and NEL, Hot Hohlraums, Omega capability development**

We are currently collaborating with LULI in measuring transmission in low temperature, high density short pulse laser heated matter



Research Team

P. Audebert¹, P. Renaudin², S. Bastiani-Ceccotti¹, S. Tzortzakis¹, C. Chenaïs-Popovics¹, V. Nagels¹, S. Gary², **R. Shepherd⁵, F. Girard², C. Blancard², I. Matsushima⁴, J.-C. Gauthier³,**

**1 Laboratoire pour l'Utilisation des Lasers Intenses,
Ecole Polytechnique, Palaiseau, France**

2 Commissariat à l'Energie Atomique (CEA), Bruyères-le-Châtel cedex, France

3 Université Bordeaux 1, Talence, France

4 NIAISR 1_1_1, Umezono, Tsukuba, Japan

5 Lawrence Livermore National Laboratory, Livermore, Ca., 94551 USA

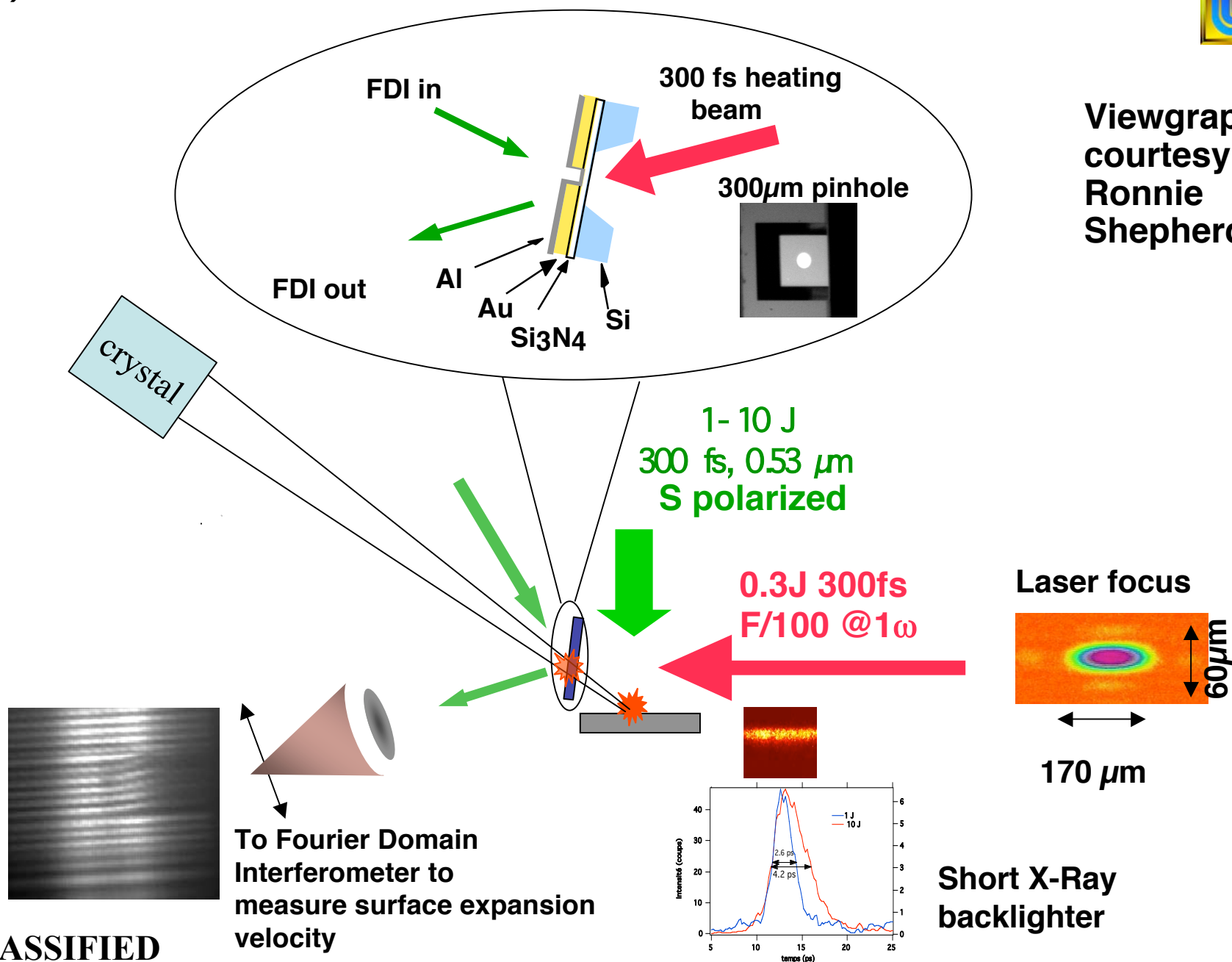
Summary follows; for more details: *Phys. Rev. Lett.* 94, 025004 (2005)

Conceptual layout of the experiment

UNCLASSIFIED



Viewgraph
courtesy of
Ronnie
Shepherd

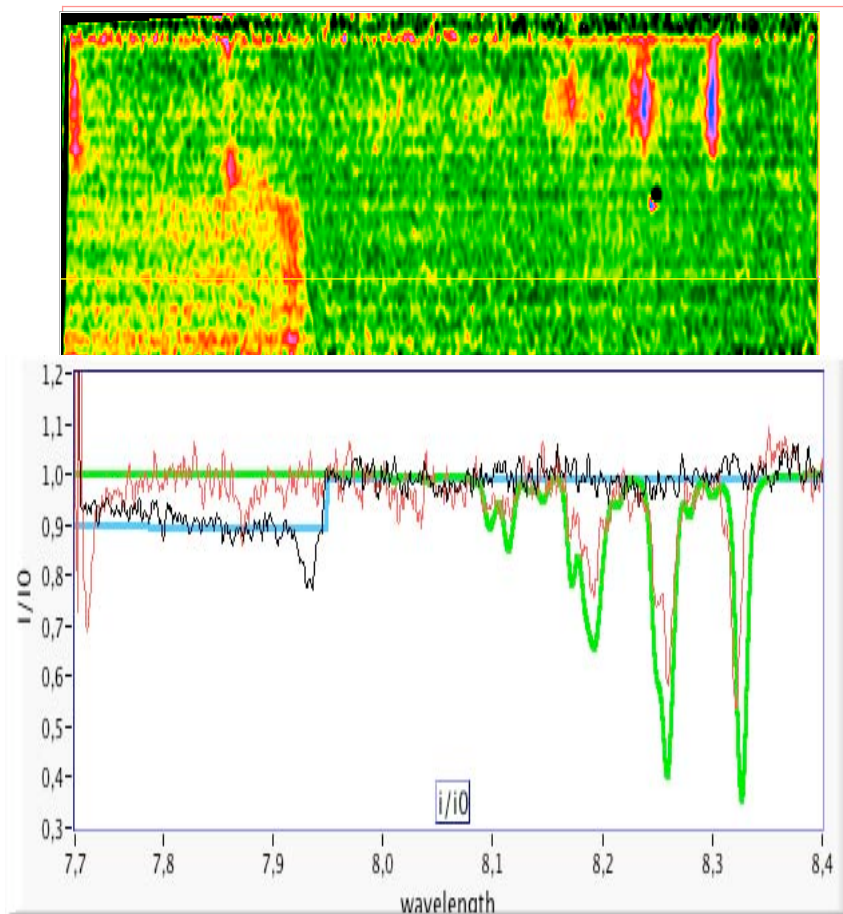


UNCLASSIFIED

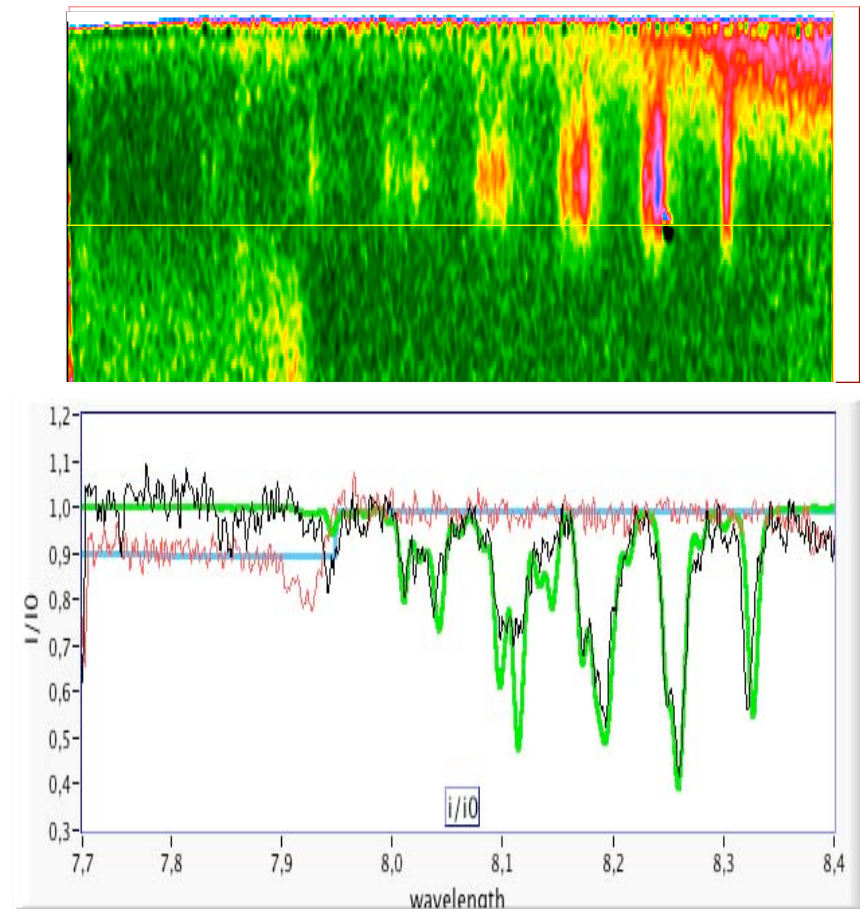
Short-pulse (3 of 4):

UNCLASSIFIED

Data suggest the absorption spectra can be fit using two calculated LTE spectra, keeping the experimental ρ constant



$I=3 \cdot 10^{15} \text{ W/cm}^2$, $x=830 \text{ \AA}$ Al, $t=t_0+7\text{ps}$



$I=3 \cdot 10^{15} \text{ W/cm}^2$, $x=830 \text{ \AA}$ Al, $t=t_0+3\text{ps}$

Well-characterized isochorically-heated matter is an increasingly promising direction for opacity validation experiments

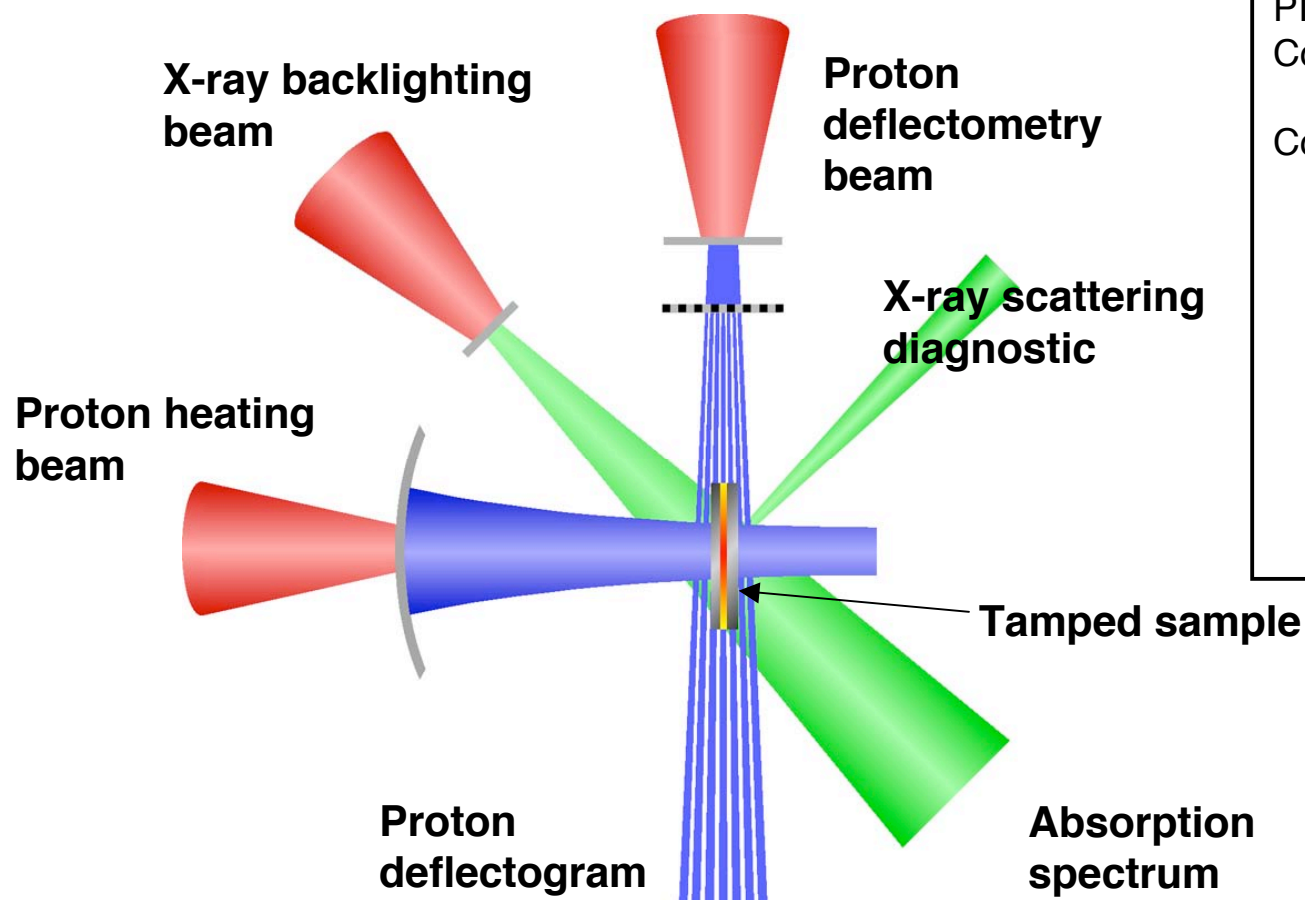
UNCLASSIFIED

Heeter-Opacity-V-V slide 5

Viewgraph courtesy of Ronnie Shepherd



An LDRD effort seeks to build a new platform for Opacity on PW-class lasers, using proton heating



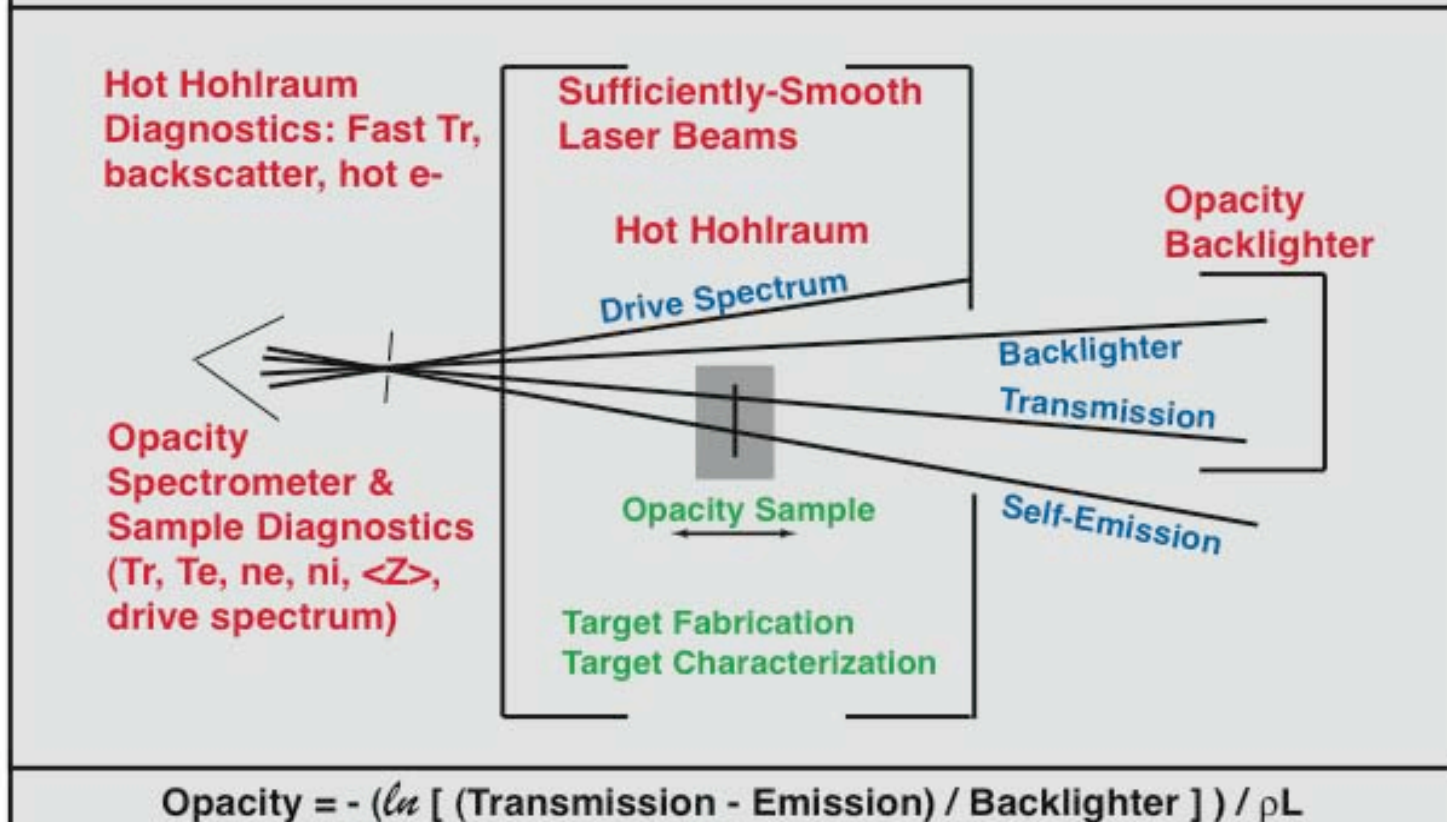
PI:	Prav Patel (PAT)
Co-Pis:	Richard Town (DNT), Andy Mackinnon (NIF)
Co-Is:	Bob Heeter, Carlos Iglesias, Mark Foord, Ronnie Shepherd, Scott Wilks (PAT); Gianluca Gregori, Rich Snively (NIF); Marco Borghesi (Queen's Univ., Belfast, UK)

Plan is to apply an array of old and new short-pulse techniques to tackle the challenge of measuring opacities in high energy density plasmas

Capability Development efforts derive from elements of a large-laser Rosseland mean experiment



Anatomy of typical hohlraum-based opacity experiment (not to scale)



These are extremely challenging experiments - many high-performance components must work simultaneously

NIF will revolutionize LTE transmission opacity experiments... eventually

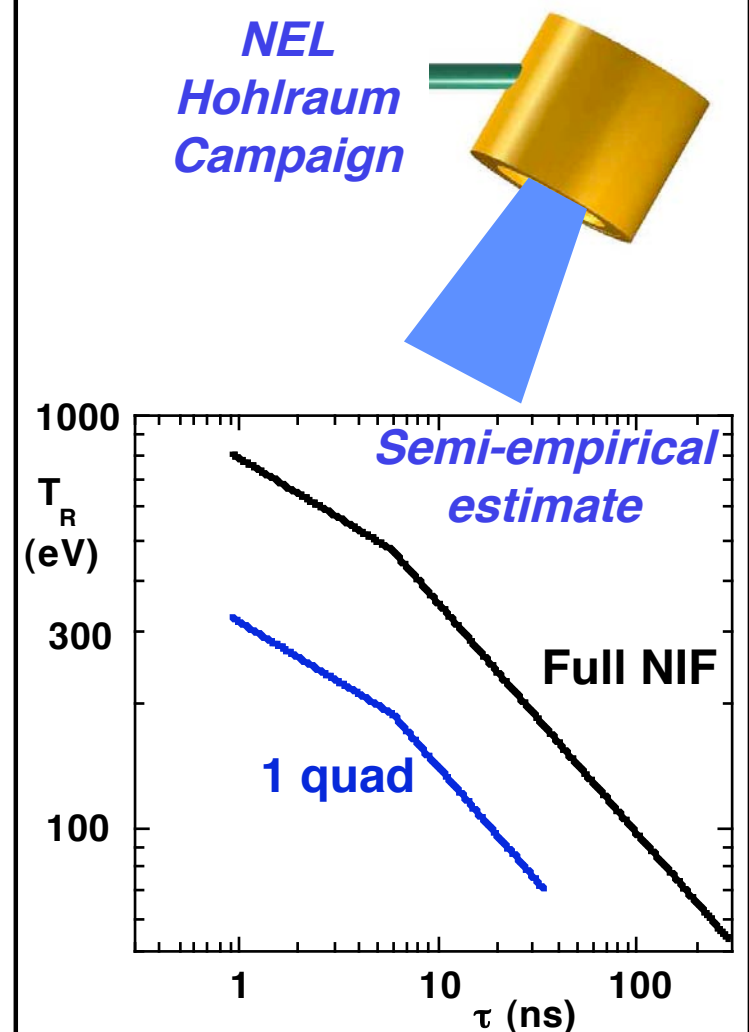


- The NIF Basics:

- 192 beams (48 “quads”)
- GOOD: 1 quad deployed in FY04:
 - NIF Early Light (NEL) experiments
 - Max power ~ 9 TW/quad (9 kJ in 1 ns)
 - Scales to 432 TW; expect ~ 750 TW (Omega: 30 TW)
- Core diagnostics deployed (Dante, framing cameras, backscatter...)
- Results coming up on following slides...
- BAD: No user shots in FY05-FY09
- UGLY: No HED experiments until FY11 (ICF ignition campaign in FY10)

- Utility for Opacity Experiments:

- Scalings suggest very high T_r is possible
- At lower T_r , can do larger, better experiments

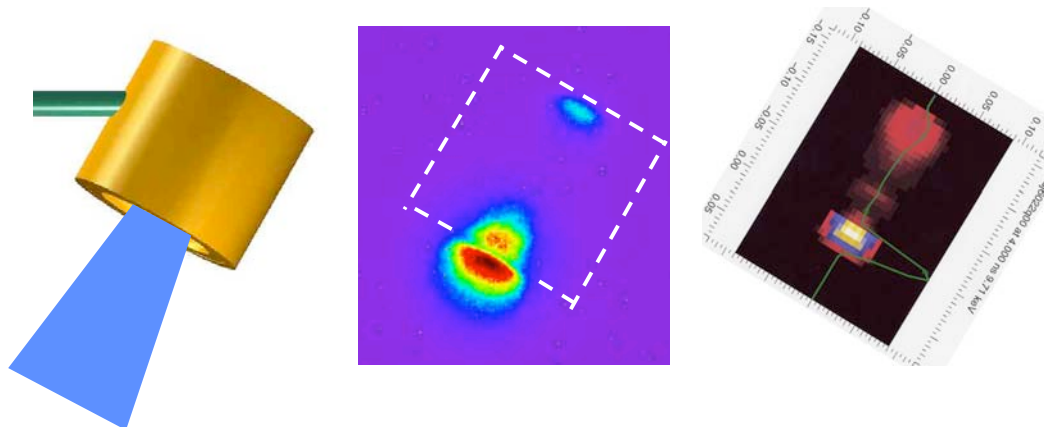


Our Plan: establish NIF-portable capabilities at Omega; much to do by FY11!



First hohlraum experiments on NIF

-Long Pulse Vacuum Hohlraum Performance on NIF



E. Dewald, O. Landen, L. Suter, K. Campbell, J. Schein, M. Schneider, J. Holder, C. Niemann, S. Glenzer, B. Young, J. McDonald, R. Turner, F. Weber, D. Lee, M. Landon, A. MacKinnon, D. Froula, S. Dixit, C. Haynam, B. Hammel, R. Kauffman, J. Celeste, J. McDonald, R. Wallace



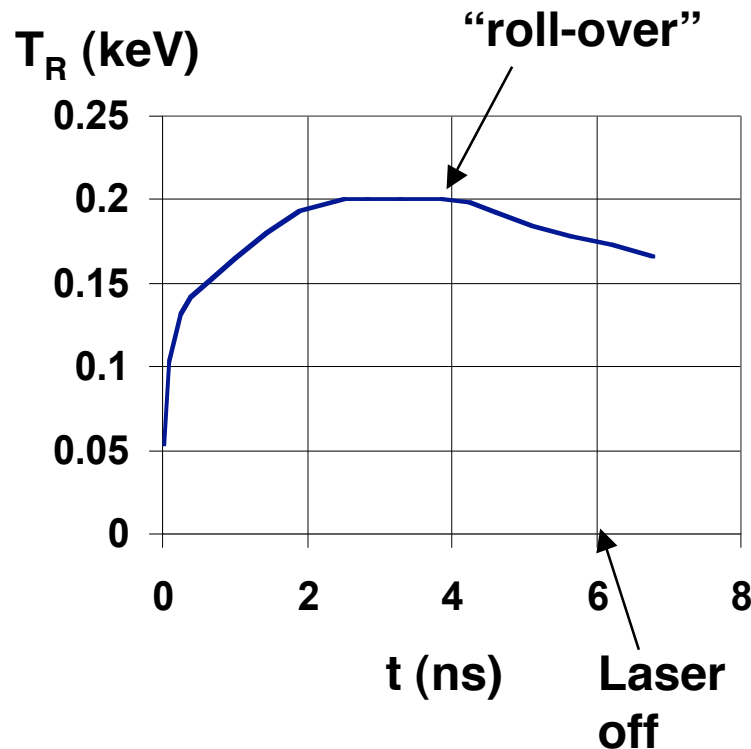
Lawrence Livermore National Laboratory, Livermore, CA

J. Foster (AWE), B. Thomas (AWE), D. Chambers (AWE), R. Stevenson (AWE), M-C Monteil (CEA), J. Fernandez (LANL), J. Kline (LANL), R. Olson (SNL), R. Leeper (SNL), G. Rochau (SNL)

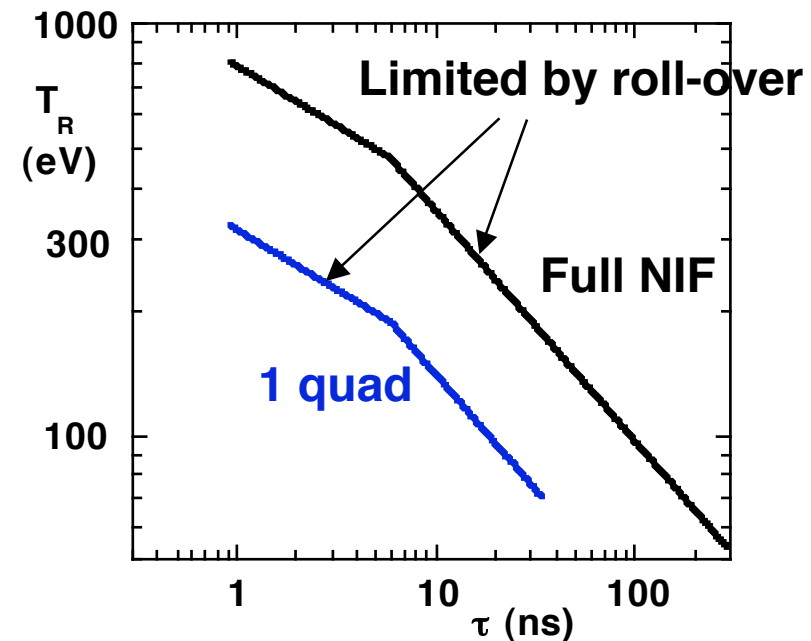


In 1995 Brian Thomas (AWE) developed a “ T_R - τ ” metric for assessing a laser’s utility for HEDS

Basic idea: plasma filling leads to a maximum time that a given hohlraum, irradiated at a given power, will work



Semi-empirical estimate

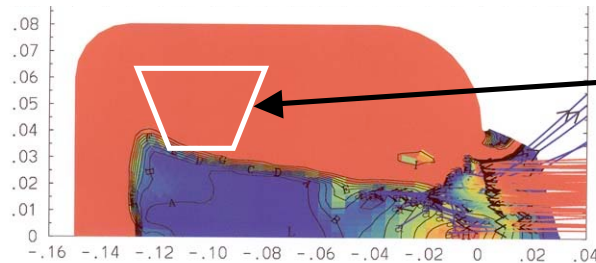


The T_R - τ plot allows estimates of potential HEDS experiments

- However, what physically limits maximum time is debatable
- School 1: LPI fiasco when can fills such that $n_e > 0.1 n_c$
- School 2: Roll-over when can fills so laser depo moves to LEH

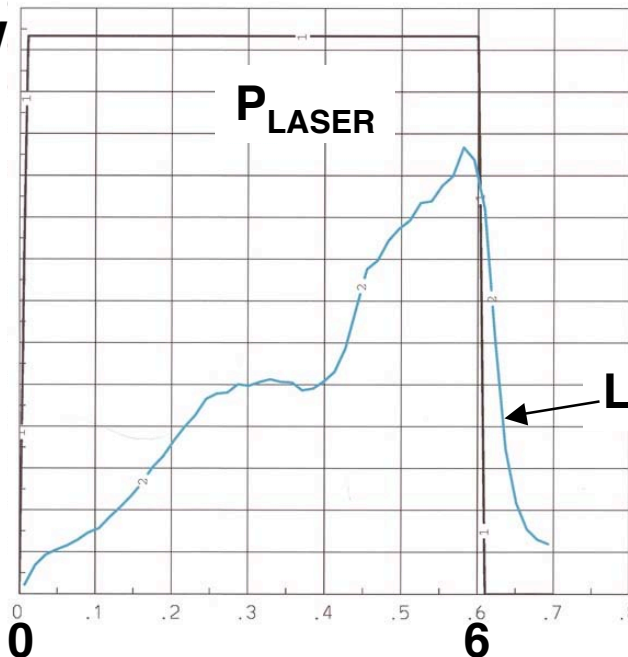


The internal T_R in our simulated experimental volume rolls-over for two reasons



1- Experimental volume's view of source becomes obscured by blow-off
(can be fixed to some degree)

2.7TW



2- Plasma evolution causes laser deposition and rad production to move toward LEH
Rad losses from LEH rise

LEH rad losses

t (ns)

Objectives of Sept. 2004 NEL shots: Establish NEL as hohlraum physics facility, at ignition relevant T_R 's, and understand T_R - τ limits (Thomas plots) for halfraums

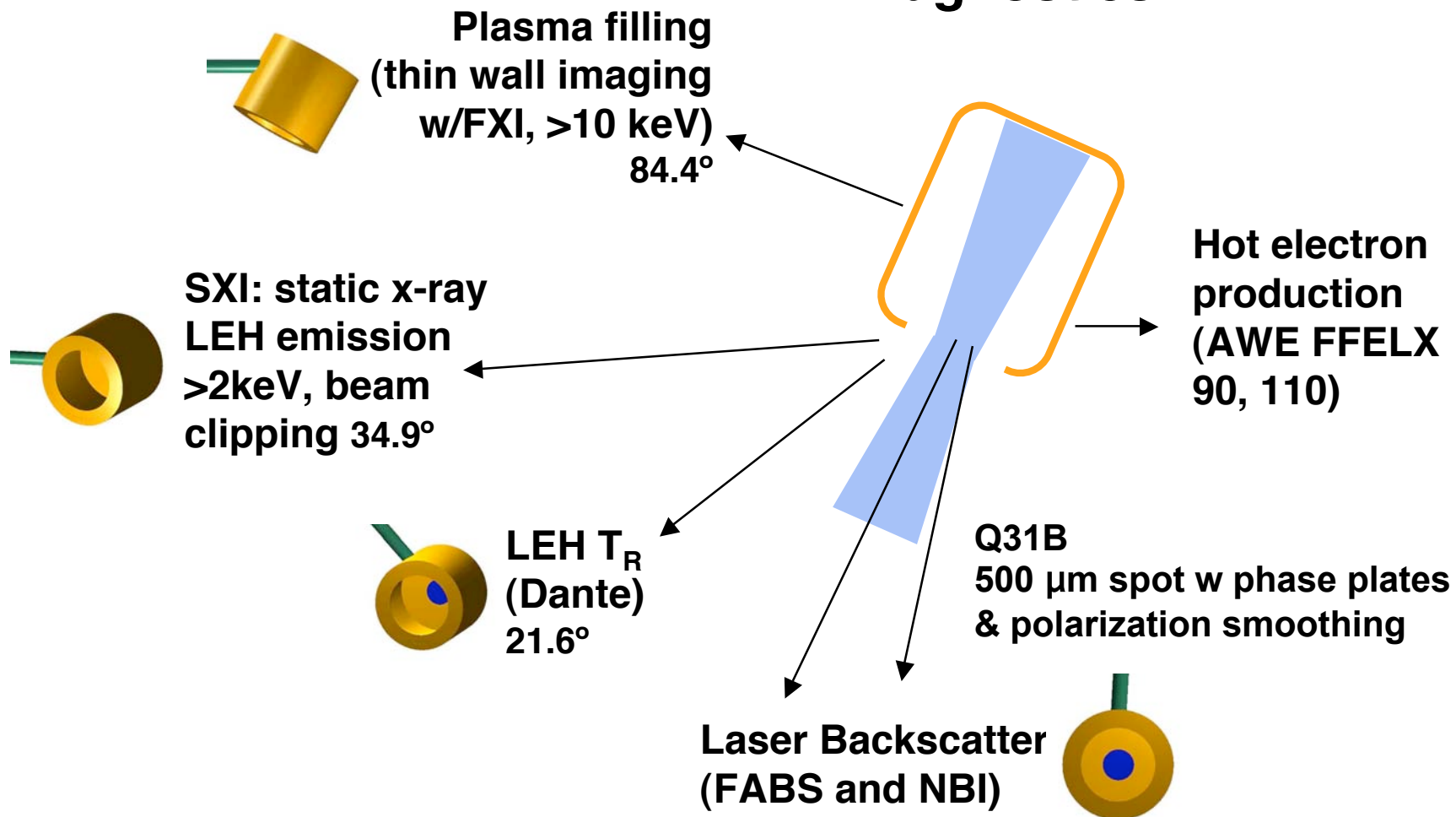
We shot 7 Vacuum hohlraums (5 μ m Au backed by 100 μ m CH) and studied plasma filling via hard x-ray imaging

UNCLASSIFIED

NIF
The National Ignition Facility



Diagnostics:



Hohlraum size: scales $\frac{3}{4}$ (1.2 mm diameter) – 1.5 (2.4 mm diameter)

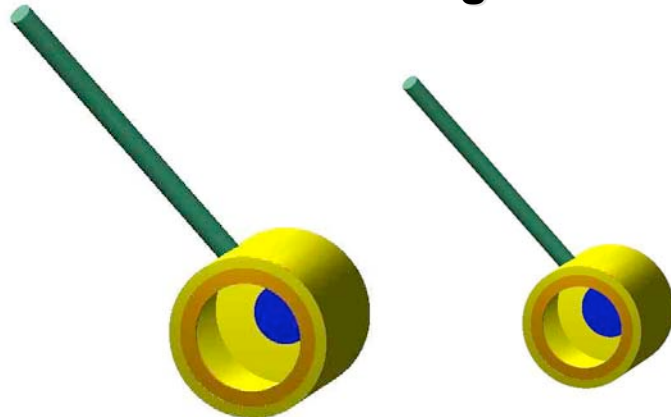
UNCLASSIFIED

Heeter-Opacity-V-V slide 12

We really did two series; a power scaling with 2ns flattop pulses and a filling series with 6 to 9ns flattop pulses



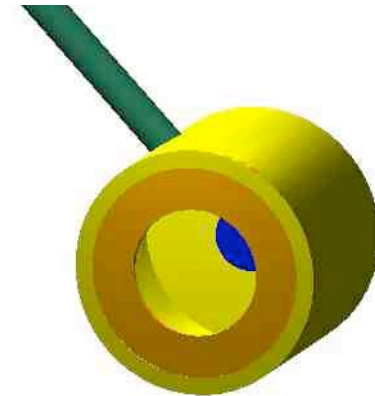
2ns POWER SCALING these provided the best “contact” with Nova and Omega



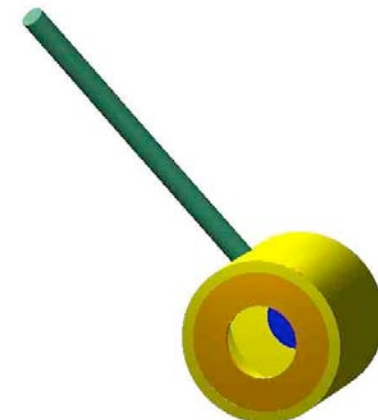
Scale 1 (3/4), 75% LEH; ~5, 9 & 13kJ

All used a 500um diameter spot smoothed by CPP+PS

LONG PULSE EXPERIMENTS (6-9 ns) provided “very filled” info



Scale 1.5 with a 1.4 mm LEH

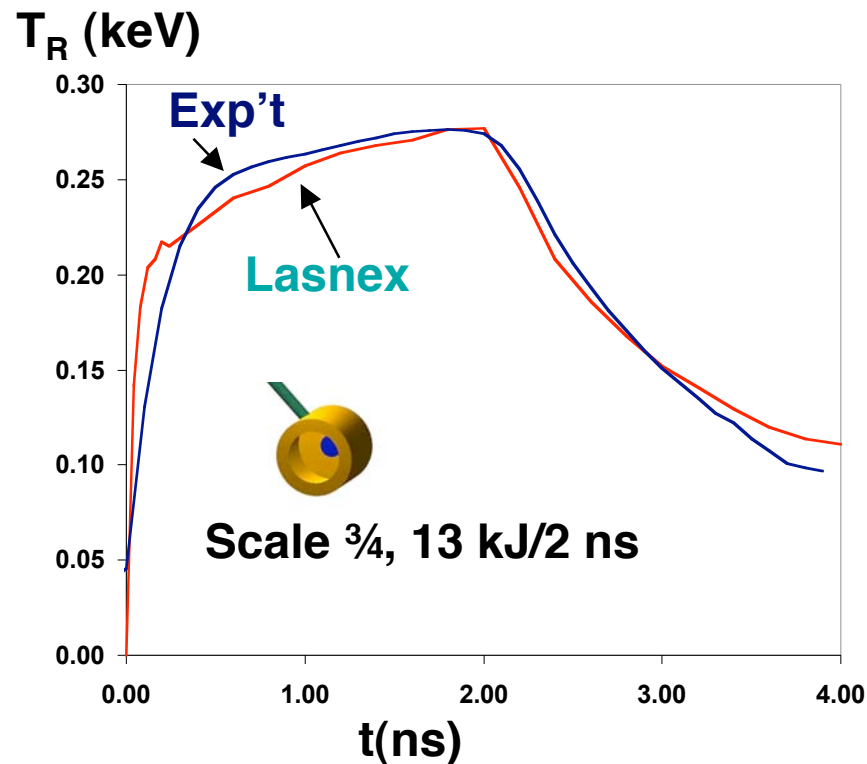


Scale 1, 50% LEH

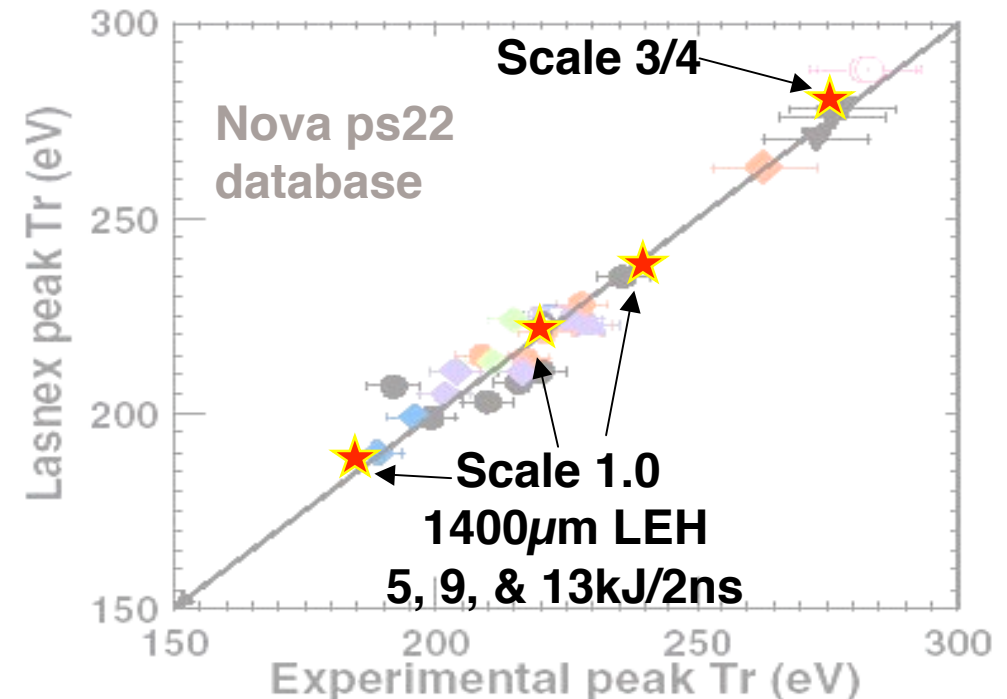
The 2ns power scaling showed hohlraum T_R essentially follows predictions

UNCLASSIFIED

NIF
The National Ignition Facility



2ns power scaling: peak T_R Lasnex vs. Experiment



- Low laser backscattering - scale 1: $<0.05\%$ SBS, negligible SRS, scale $3/4$: $<0.5\%$ SBS, $\sim 0.05\%$ SRS
- ρ hot very low ($<0.2\%$ for scale 1, $\sim 1\%$ for scale $3/4$)

UNCLASSIFIED

Heeter-Opacity-V-V slide 14

The longer pulse hohlraums explored the T_R - τ limits (Thomas plots) for halfraums

UNCLASSIFIED



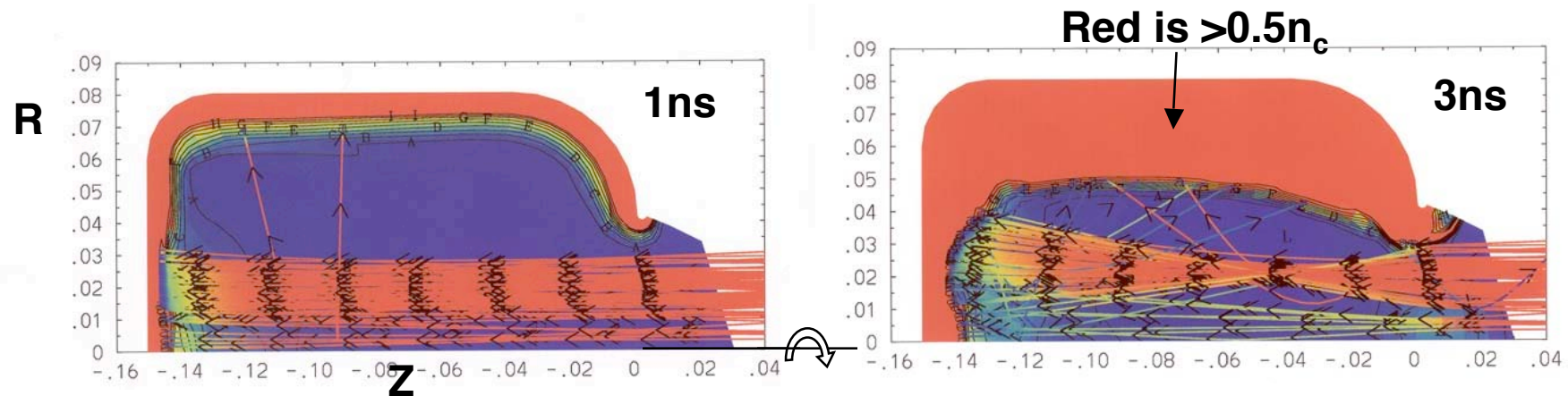
NIF

The National Ignition Facility

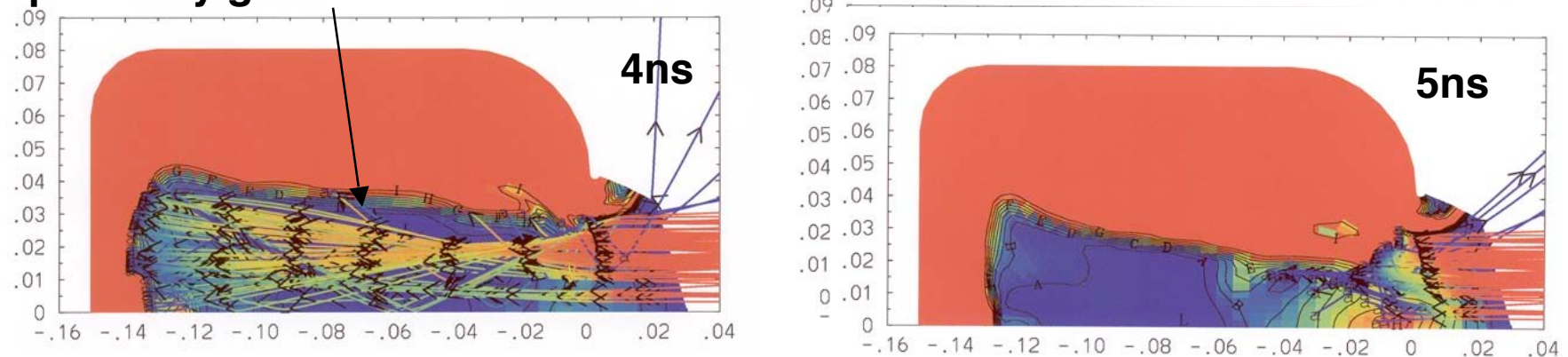


This shows the dynamics of a scale 1.0 heated by a 6ns pulse

- The high pressure of the laser heated channel keeps it open



Steep density gradient between red and blue



UNCLASSIFIED

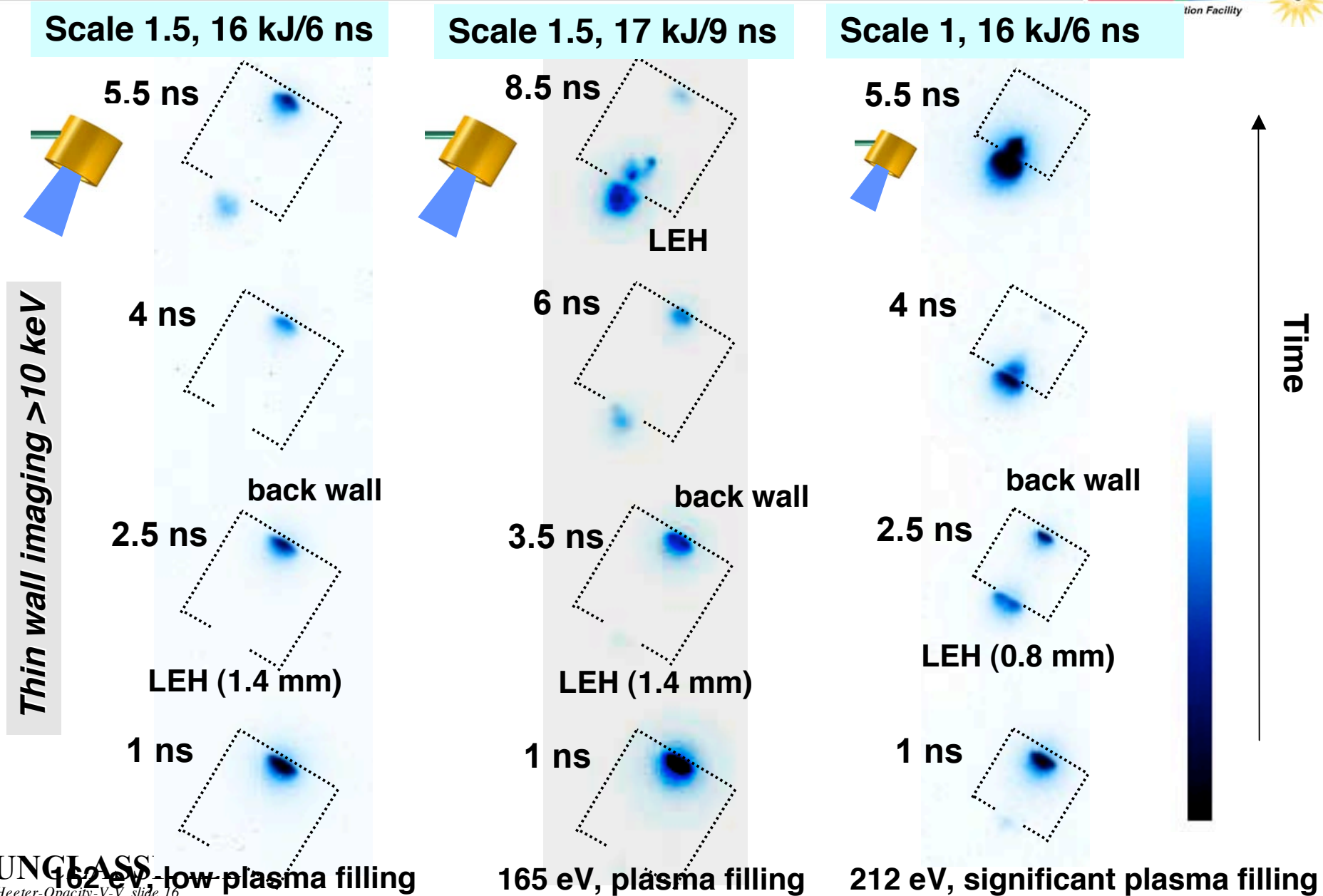
Heeter-Opacity-V-V slide 15

Color indicates electron density: Red=high Blue=low

Thin wall imaging clearly shows laser deposition moving to the LEH with longer pulses as the hohlraum fills with plasma

NIF

tion Facility



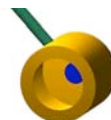
The temporal behavior of x-ray flux, as well as thin-wall imaging, is consistent with our predictions of late time filling

NIF

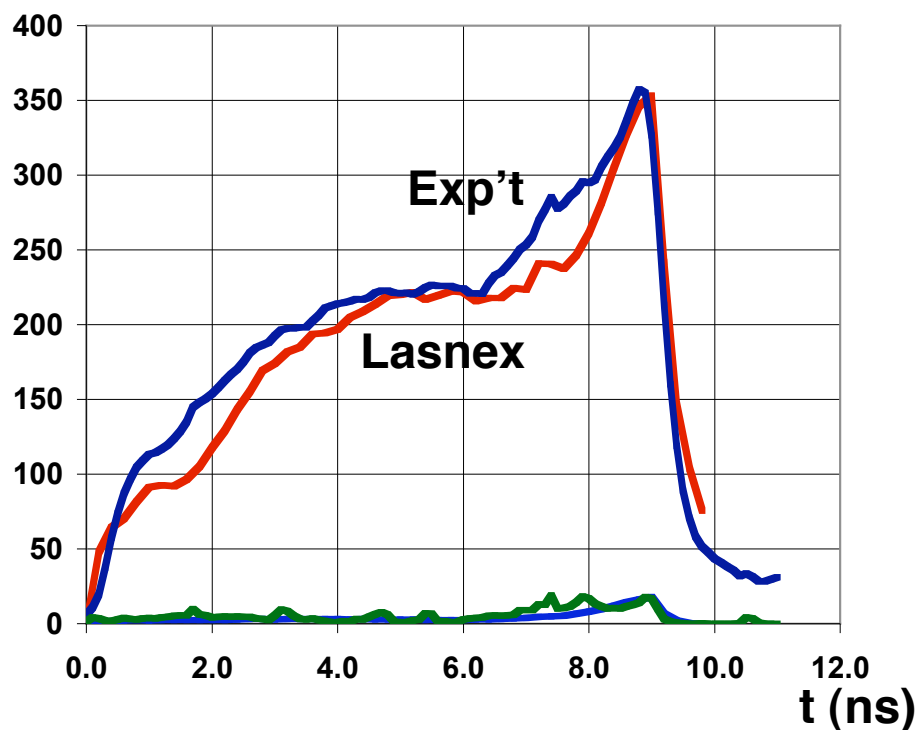
The National Ignition Facility



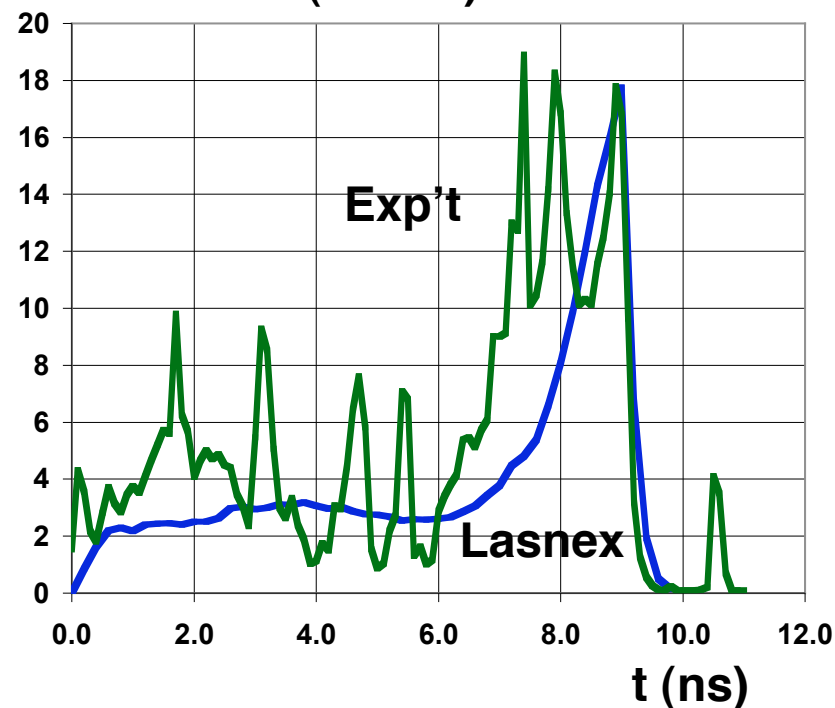
Scale 1.5, 17 kJ / 9 ns



Total flux (GW/sr)



M-band flux (GW/sr)



- The marked rise in total x-ray flux and M-band occurs when the deposition moves to the LEH

- Low laser backscattering - $<0.5\%$ SBS, $<0.05\%$ SRS
- fhot very low ($<0.3\%$)

UNCLASSIFIED

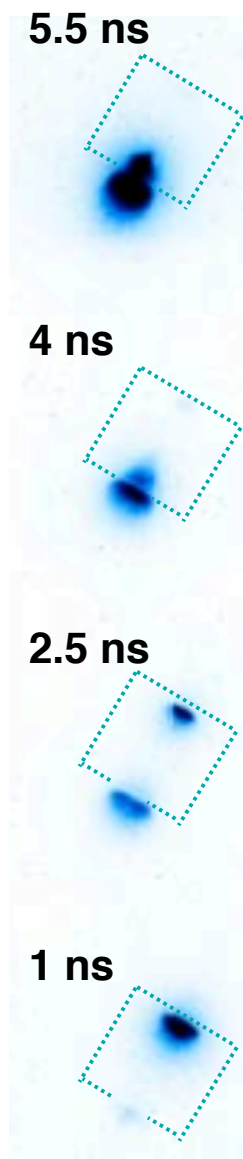
Heeter-Opacity-V-V slide 17

Final NEL ICF Hohlraum Slide

UNCLASSIFIED

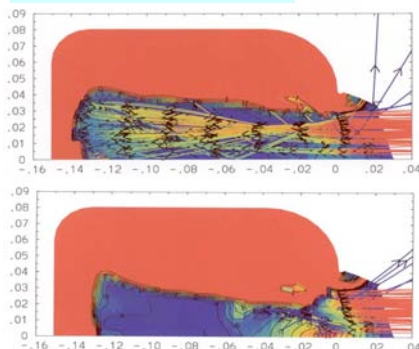
Late rise in Dante flux, correlated w/ hard x-ray emission shift to LEH, supports models of extreme plasma filling

NIF
The National Ignition Facility



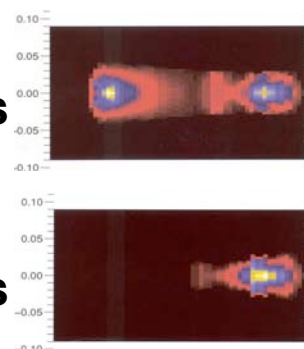
Simulation

Scale 1, 16 kJ/6 ns

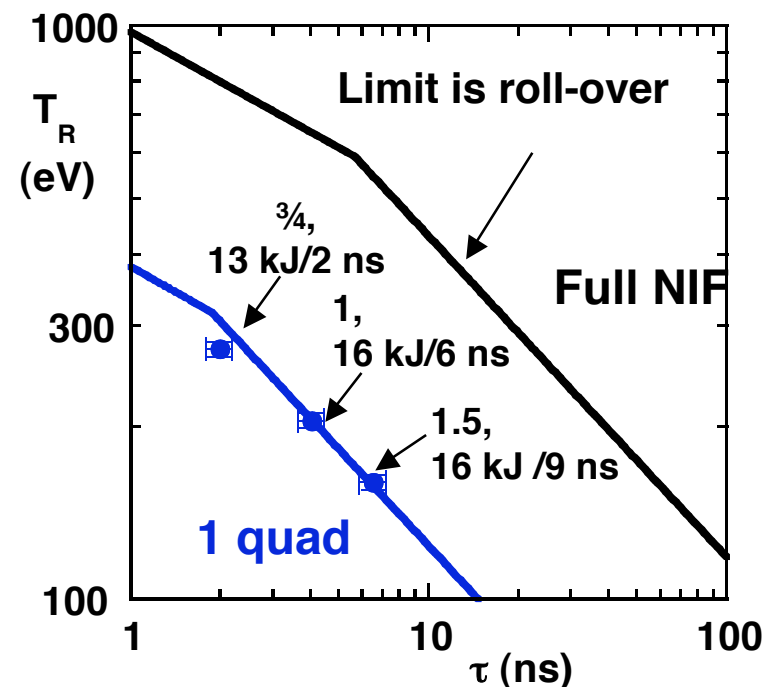
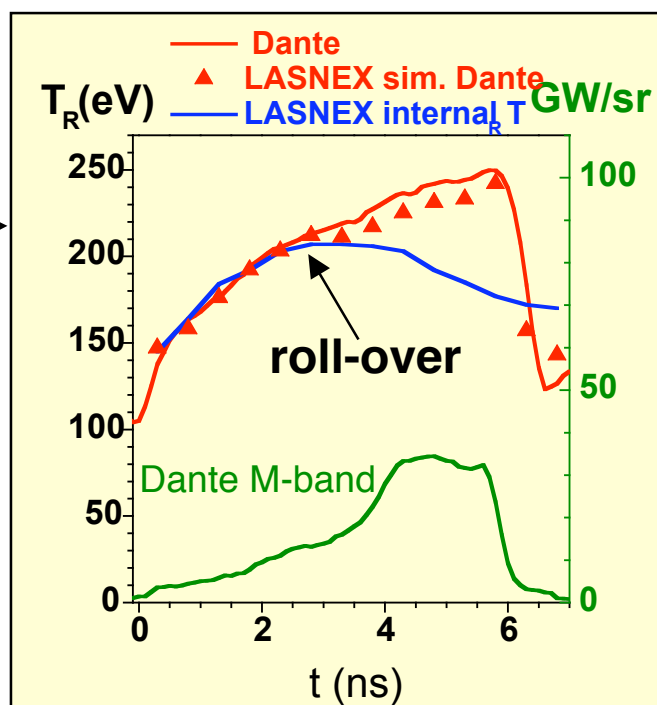


4ns

5ns



Data



• NEL hohlraum data

This work is now in Review-Release for submission to PRL (E. Dewald et al.)

UNCLASSIFIED

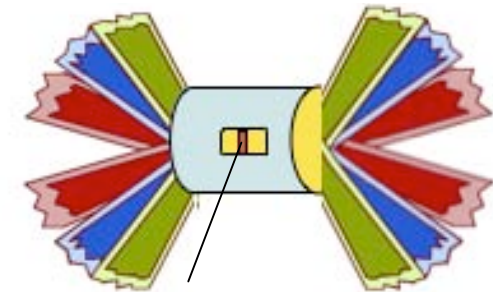
Heeter-Opacity-V-V slide 18

The Hot Hohlraum (HTH) campaign seeks to produce hot radiation environments for weapons physics studies



- Weapons physics at full NIF requires high T_{rad}
 - Different physics regime than ICF
 - Ongoing HTH campaign at OMEGA laser
- The NIF experiments were a collaboration with ICF
 - Simple geometry helped HTH
 - Extended parameter space helped ICF and NIF
 - Diagnostics • Pointing/Positioning • Timing

$$T_{\text{rad}}(\text{HED}) > T_{\text{rad}}(\text{ICF})$$



physics package

NIF Hohlraum and Gas-Tube Campaign

Principal Investigator, Experiments:

Nino Landen, *Associate Program Leader for Ignition Physics Experiments,*

Principal Investigator, Theory:

Larry Suter, *A/X Division (DNT) and Ignition Target Leader, ICF (NIF)*

21 shots into Target Chamber in 11 days

NIF Project Diagnostic Division Leader: Brian MacGowan

**HTH helped collaboration by exercising NIF's performance in several areas
NOT reached by the other early-NIF campaigns**

The 5 NEL Hot Hohlraum shots were truly a team effort



Lead Theorist: **D.E. Hinkel** (*invited talk at APS DPP***)

Lead Experimentalist: **M.B. Schneider**

Co-Leads at NIF: B.K. Young, J.P. Holder

Thanks to M.J. Eckart for guidance and support

Theory Team (A/X Division):

D.E. Hinkel, A.B. Langdon (leaders)

L.J. Suter, E.A. Williams, C.H. Still,

D.H. Munro, M.J. Edwards

Laser Science Team:

S.N. Dixit, J.R. Murray,

C. Haynam, K. Jancaitis

BLIP group

Target Fab:

R. J. Wallace

J. Ruppe

PLUS

E. Moses

and NIF Program

Experimental Team :

M.B. Schneider, O.L. Landen, J.P. Holder, B.K. Young,
D. Bower, K.M. Campbell, J.R. Celeste, S. Compton, R. Costa,
E.L. Dewald, D.C. Eder, A. Ellis, J.A. Emig, J.M. Foster,
D.H. Froula, S.H. Glenzer, R. Griffith, D. Hargrove, G. Holtmeier,
D.H. Kalantar, R.L. Kauffman, J. Kimbrough, R.K. Kirkwood,
A.E. Koniges, D.L. James, G. Jones, J. Kamperschroer, M.R. Latta,
A.P. Lee, F.D. Lee, M. Landon, B.J. MacGowan, A.J. Mackinnon,
K. Manes, T. McCarville, J.W. McDonald, C. Niemann, D. Pellinen,
K. Piston, G.D. Power, I. Reinbachs, V. Rekow, M.A. Rhodes,
J. Schein, M.S. Singh, G. Slark, R.E. Turner, P.A. Waide,
A. Warrick, P. Watts, F.A. Weber, P.E. Young,
H.A. Baldis, M.J. Eckart, R.F. Heeter, M.J. May,
R. Shepherd, P.T. Springer

Funding for smoothing/diagnostics

C.P. Verdon (AX Division Leader)

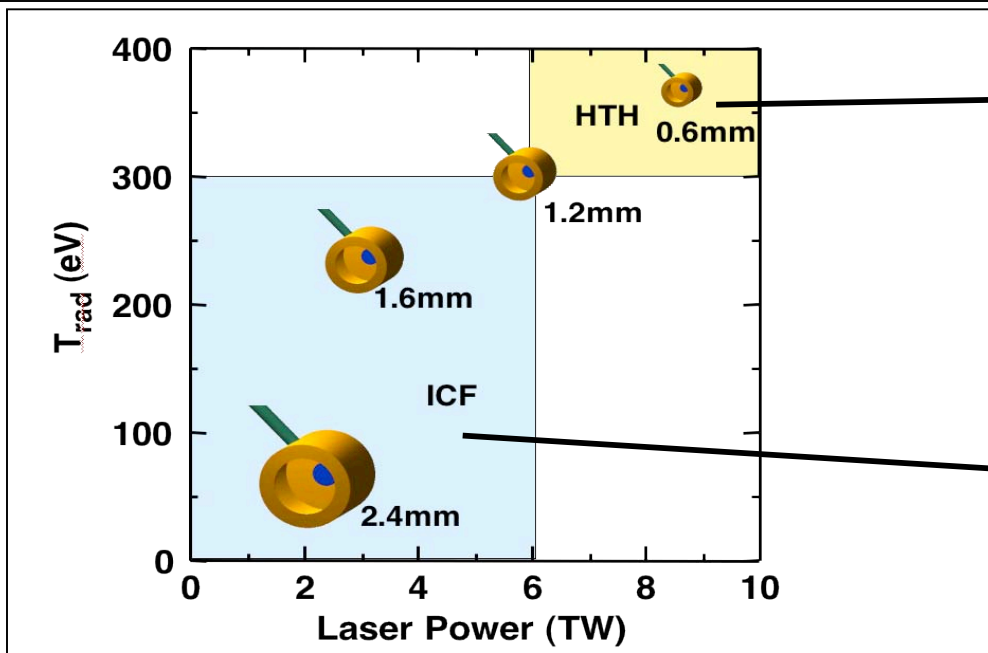
HTH was honored to be part of this great team at NIF

Hot Hohlraums seek to extend hohlraum radiation performance to higher radiation temperatures (T_{rad})

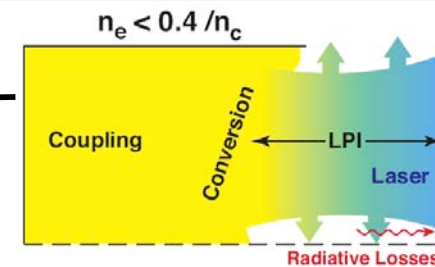


How to get hotter? • small targets • high intensity • short times

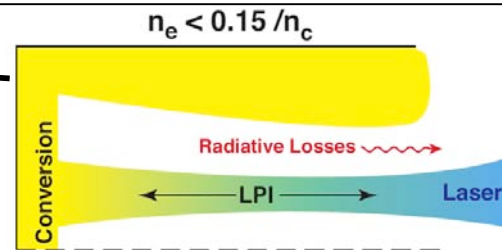
HTH targets are smaller, use higher laser power, and could reach $T_{\text{rad}} > 300\text{eV}$ at NEL



HTH: Laser-plasma interactions occur at or outside the target



ICF: Laser-plasma interactions occur inside the target

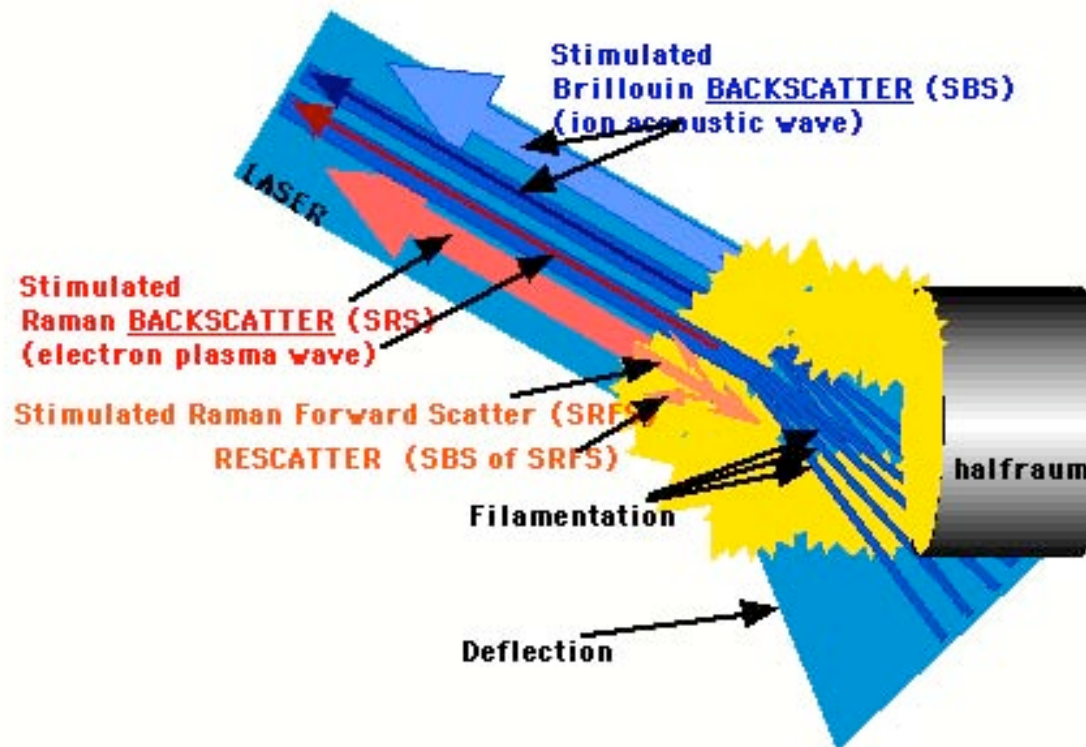


The Hot Hohlraum shots extended the physics regime achievable at NIF Early Light (NEL) *[into territory relevant for NIF opacity]*

At the higher intensities typical in HTH experiments, Laser-plasma interactions can limit laser/hohlraum coupling



Plasma filling and angled, non-ideal beams
result in complex laser-plasma interactions

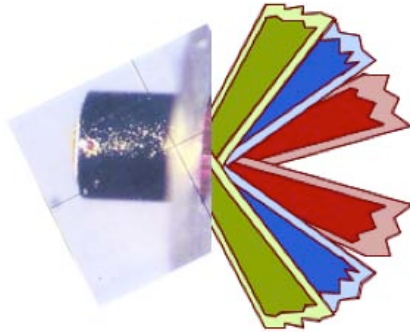


A simple experimental geometry helps one test these complex models

NEL geometry is simpler than OMEGA

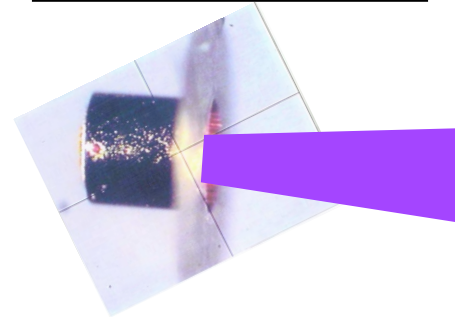


OMEGA setup



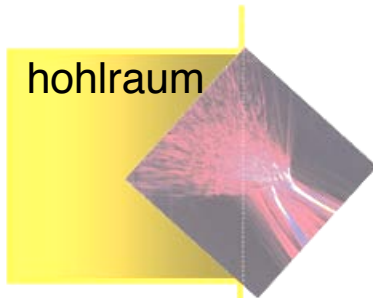
- 19 beams
- oblique angles

NIF setup



- 1 quad of beams
- normal incidence

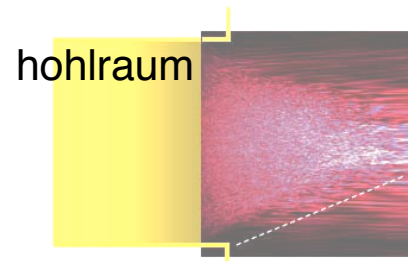
PF3D simulation



- filamentation
- deflection
- cross-beam energy transfer

D.E. Hinkel (A/X Div)

PF3D simulation

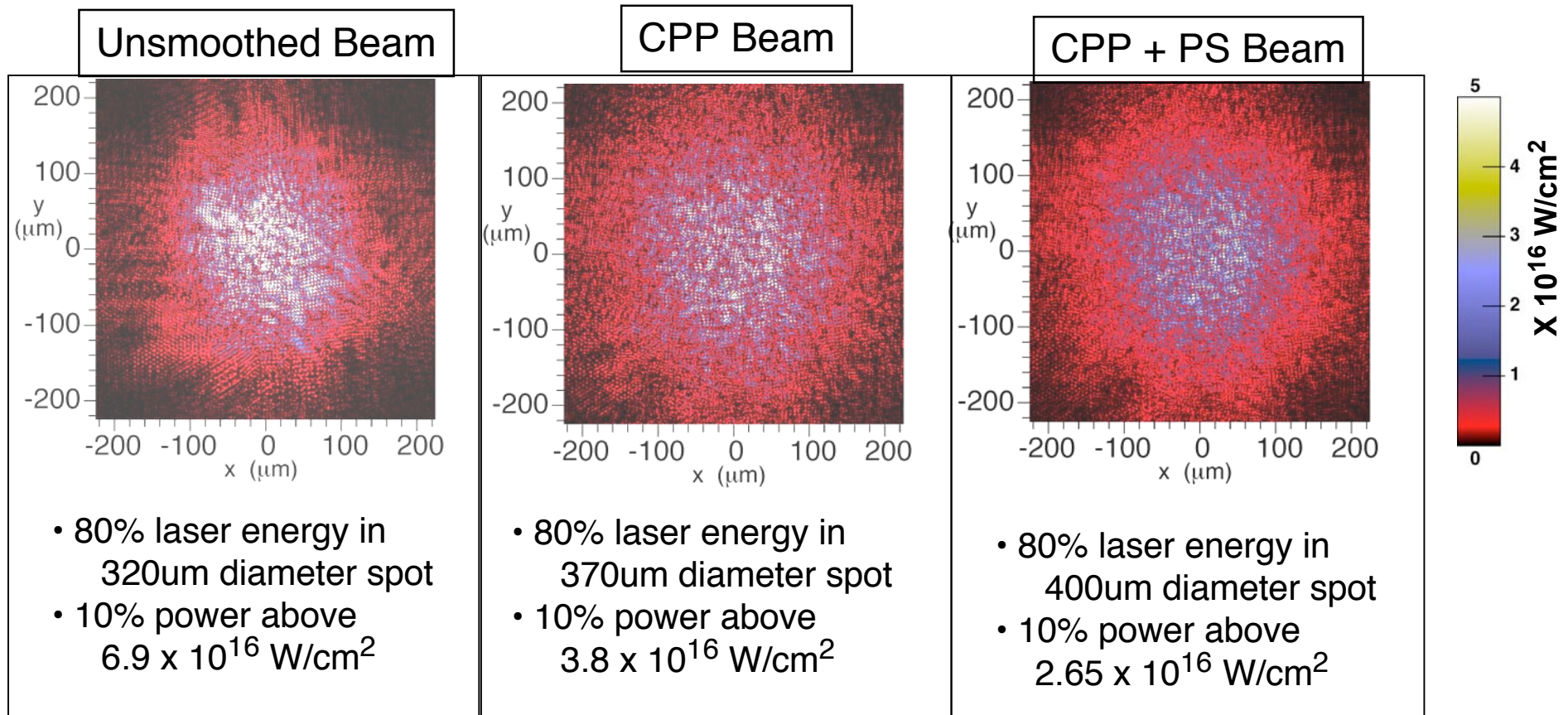


- filamentation

D.E. Hinkel (A/X Div)

Laser-hohlraum coupling at NIF was expected to be better than at OMEGA

The NEL laser beams were conditioned with both spatial and polarization smoothing



**V Division and ICF shared PS crystal costs;
HTH group led effort to get PS crystals fielded**

NEL beam simulations, CPP design: S. N. Dixit, K. Jancaitis PS crystal design: D. H. Munro, S. N. Dixit, A. B. Langdon, J. R. Murray

UNCLASSIFIED

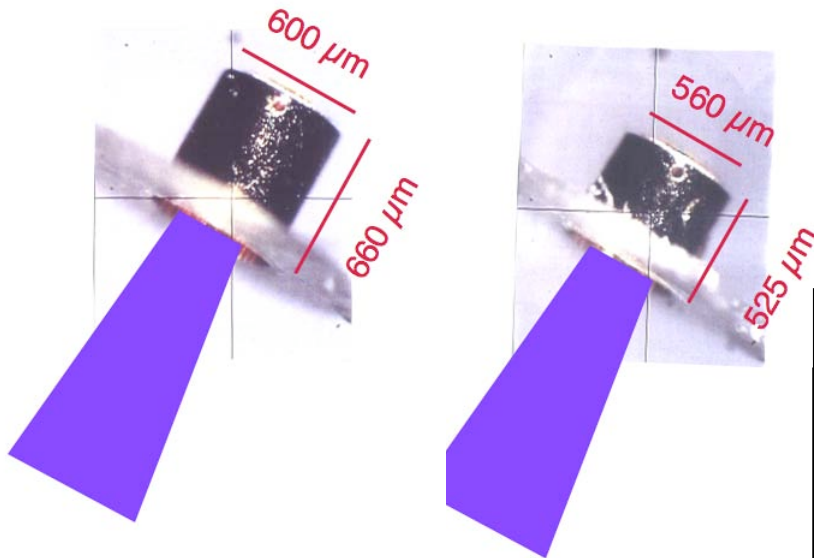
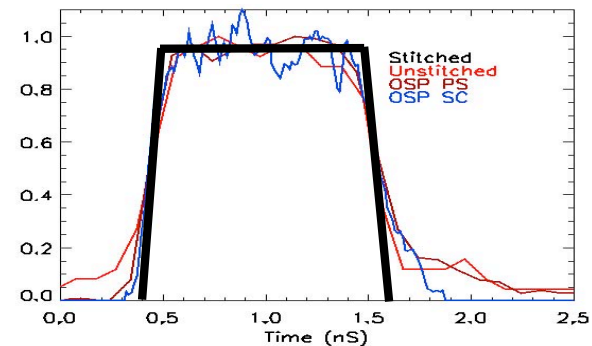
Heeter-Opacity-V-V slide 24



HTH experimental conditions and shot matrix

Targets were halfraums with different aspect ratios

Pulse shape was flattop, 1.1 nS FWHM



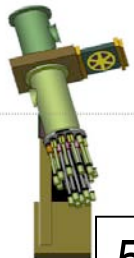
• 3.5 μm Au walls

The 5 HTH shots at NIF

Target	Energy	Smoothing
560um	6 kJ	CPP+ PS
560um	9.5kJ	CPP+ PS
600um	9.5kJ	CPP+ PS
560um	9.5kJ	CPP
600um	9.5kJ	CPP

Good data was obtained on every shot

The measured radiation flux showed very good coupling



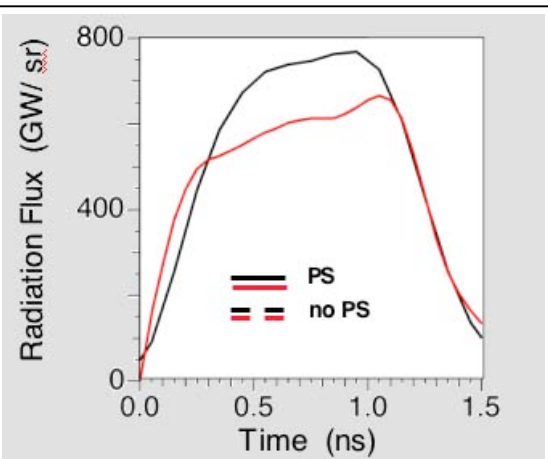
21.8°

DANTE: absolutely calibrated x-ray spectrometer

- Eighteen-channels •Mirror+filter / XRD •Filter /XRD
- All elements pre-calibrated to 5keV •Filters checked after EVERY shot

ICF: K.M. Campbell, J. Schein, O.L. Landen, R.E. Turner, E.L.Dewald; M Div: F.A. Weber

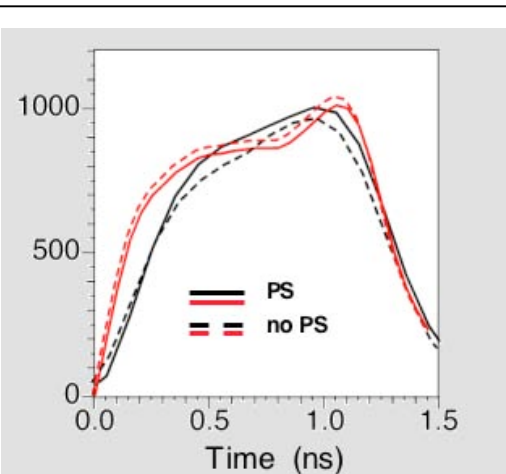
560 um 6kJ



— PS Exp: $T_{\text{rad}} \sim 318 \text{ eV}$
 — Lasnex: $T_{\text{rad}} \sim 307 \text{ eV}$

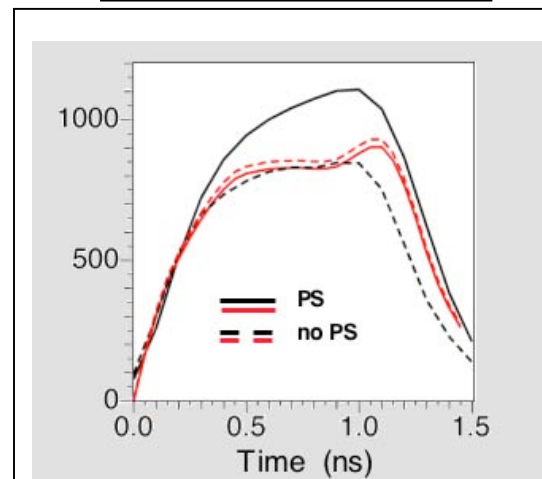
LASNEX: D.E. Hinkel (A/X Div)

560 um 9.5kJ



— PS Exp: $T_{\text{rad}} \sim 340 \text{ eV}$
 — Lasnex: $T_{\text{rad}} \sim 337 \text{ eV}$
 --- No PS Exp: $T_{\text{rad}} \sim 340 \text{ eV}$
 --- Lasnex: $T_{\text{rad}} \sim 343 \text{ eV}$

600 um 9.5kJ



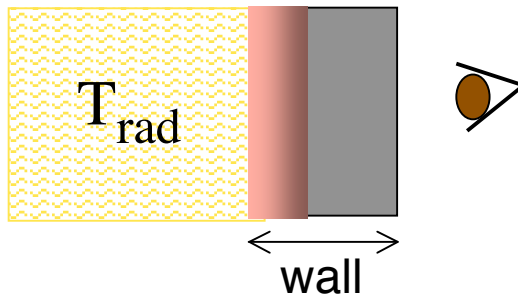
— PS Exp: $T_{\text{rad}} \sim 337 \text{ eV}$
 — Lasnex: $T_{\text{rad}} \sim 320 \text{ eV}$
 --- No PS Exp: $T_{\text{rad}} \sim 315 \text{ eV}$
 --- Lasnex: $T_{\text{rad}} \sim 322 \text{ eV}$

Coupling is better than predicted by LASNEX and is improved with PS

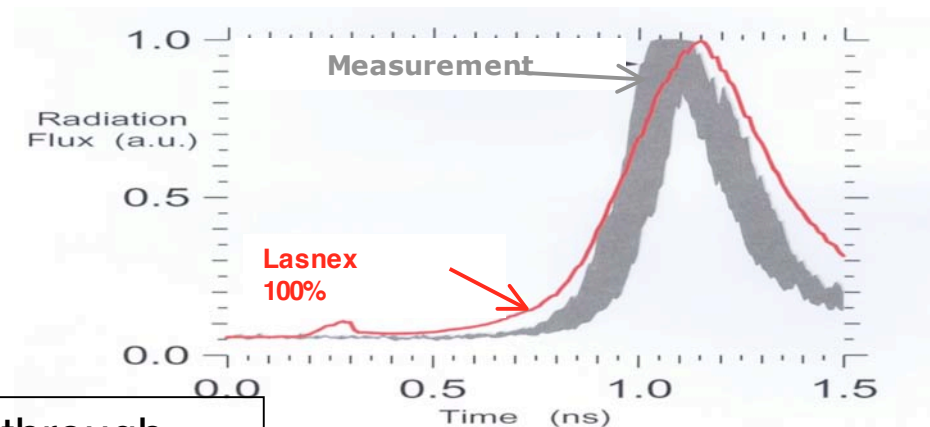
The Hot Hohlraum campaign implemented a second method of measuring radiation drive



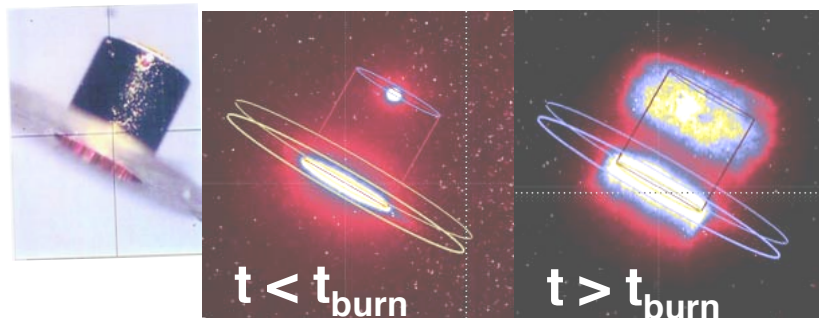
Intense radiation flux inside hohlraum heats wall



Radiation flux from outside wall increases when it gets hot

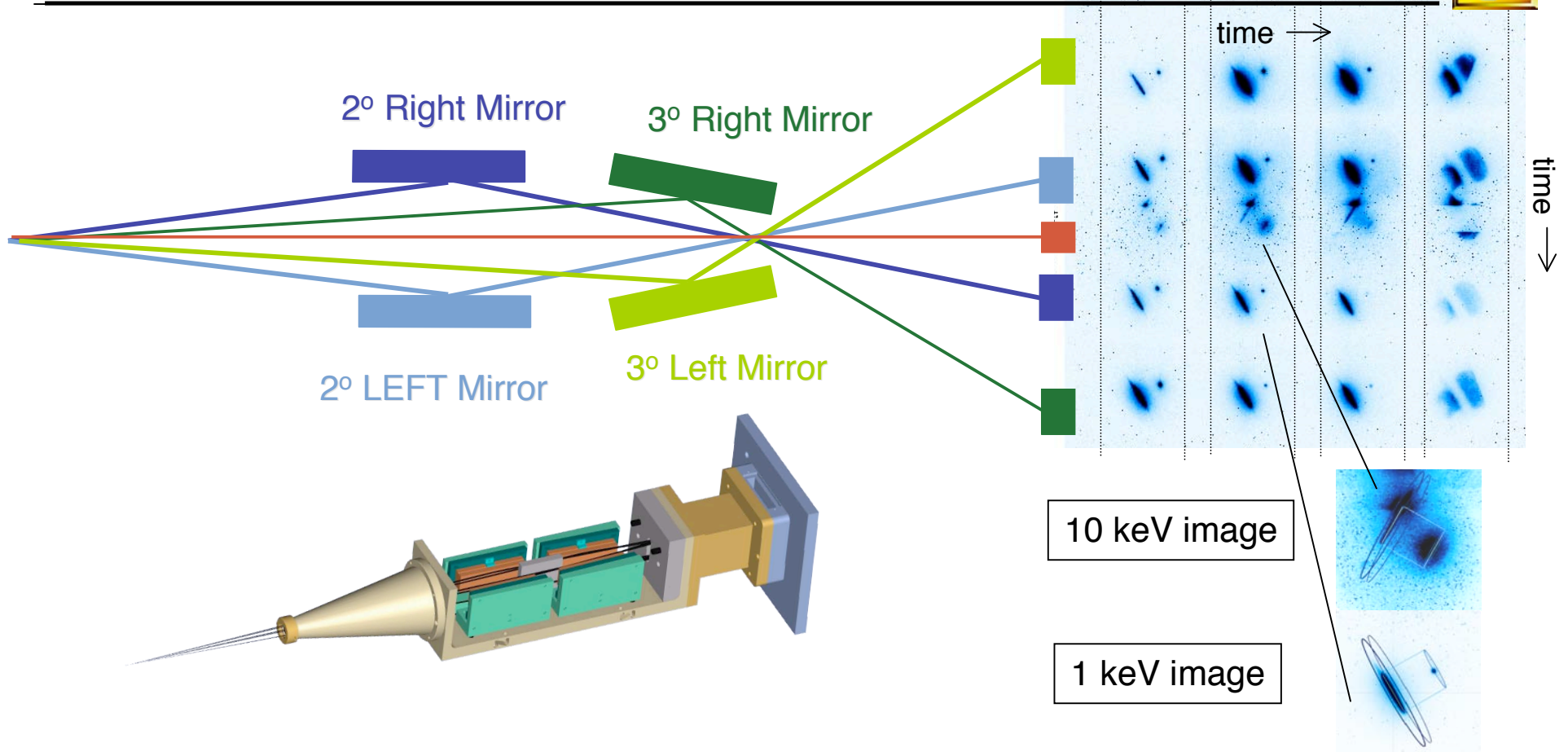


Soft x-ray images show x-ray burnthrough



The x-ray burnthrough diagnostic measures the internal radiation field

The x-ray burnthrough diagnostic (built by V Division) was the SXRI snout mounted on the FXI framing camera



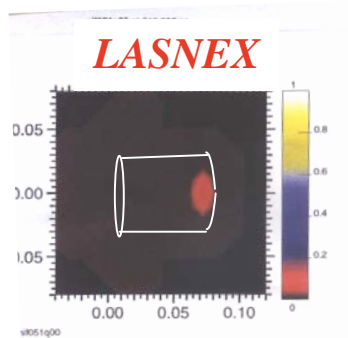
FXI: J.P. Holder (V Div), V. Rekow (ICF) SXRI: M.B. Schneider, D.L. James, J.P. Holder, J.A. Emig, H.C. Bruns, J. Celeste, G.D. Powers, B.K. Young, Filters: A. Ellis (V Div), J. McKenney, O. Garcia (SNL)

**This instrument produced 16 soft x-ray images at 50pS intervals,
and 4 hard x-ray images**

Hard x-ray images show laser deposition region and soft x-ray images show x-ray burnthrough

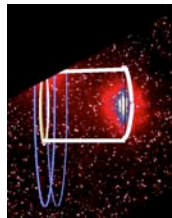


Early in time, images at 10 keV show laser deposition region is at back of can.



DATA (with PS)

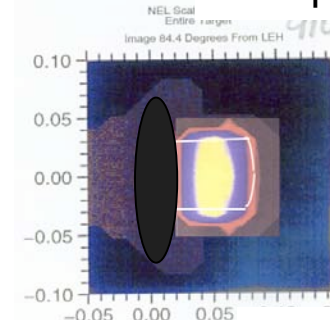
~75ps



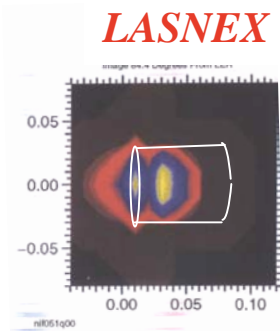
1keV images: burnthrough starts at back of can, but LASNEX predicts in the middle.

LASNEX ~880ps

DATA (with PS)

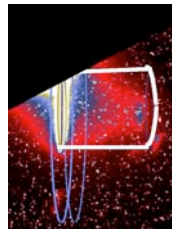


Late in time, 10keV images do not see LASNEX prediction of deposition region near can front.



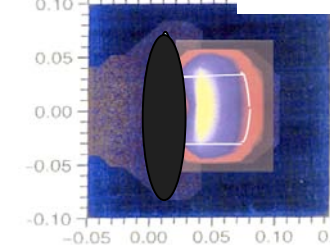
DATA (with PS)

~775ps

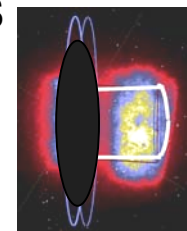
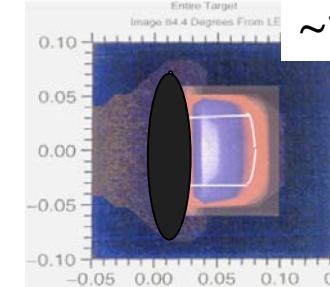


LASNEX: D.E. Hinkel (A/X Div)

~1080ps



~1280ps

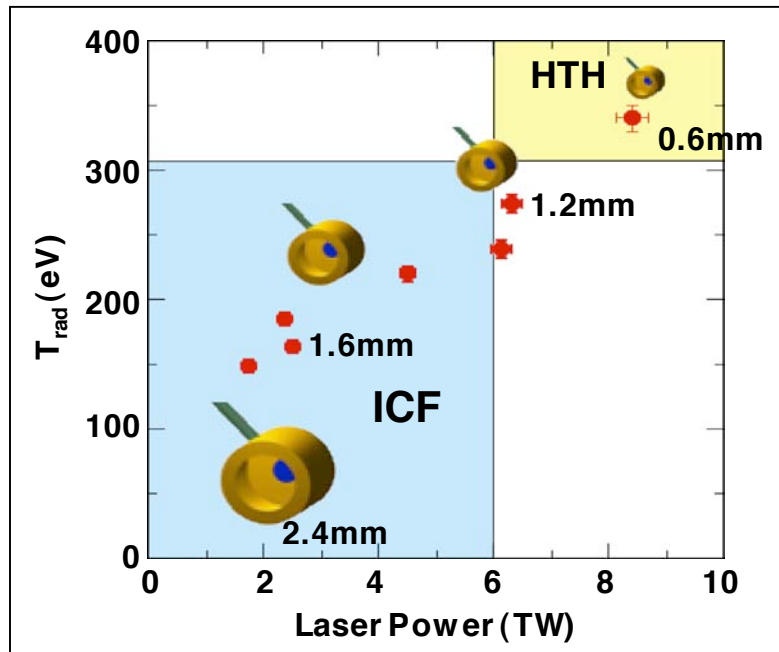


These experiments showed slower hohlraum filling than LASNEX predicts

All five hot hohlraum shots at NIF showed excellent laser coupling to target ($T_{\text{rad}} > 300\text{eV}$)



HTH shots DID extend NEL physics regime



Hot hohlraums coupled best (better than expected)

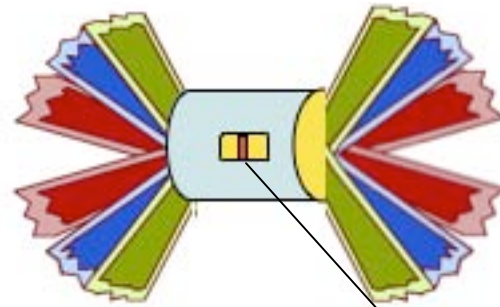
- with smoothed beams
- less extreme conditions
 - larger hohlraum at full energy
 - smaller hohlraum at reduced energy

HOHLRAUMS did not fill with plasma as fast as expected, thus reaching the higher radiation temperature -- not sure why, many ideas...

Other results (backscatter, hard x-rays) give some insight, more physics (not discussed here)

The NIF Hot Hohlraum campaign opens the door for performing hot radiation experiments on real targets

Future: Use High Temperature Hohlraums as x-ray drivers for real experiments . . . at OMEGA laser



Physics package

LDRD (PAT-ER):

Development of Hot, LTE-tunable Radiation Sources Enabling:
Material Science Studies

and

Radiation Transport Simulations in Astrophysical Plasmas

Co-Investigators:

Hector Baldis (UC Davis, V Division)
Duane Liedahl (V Division)
Klaus Widmann (V Division)
Stephanie Hansen (V Division)
Carmen Constantin (UC Davis post-doc)
Steven Ross (UC Davis Ph.D. Student)

Collaborators:

Denise Hinkel (A/X Division)
Peter Beiersdorfer (V Division)
Hyun-Kyung Chung (V Division)
Mark May (V Division)
Bruce Young (V Division)

These experiments add physics to existing OMEGA NLUF shots in collaboration with Hector Baldis

Omega Opacity experiments required development of multiple gated imaging spectrometers



Status Quo 2 years ago:

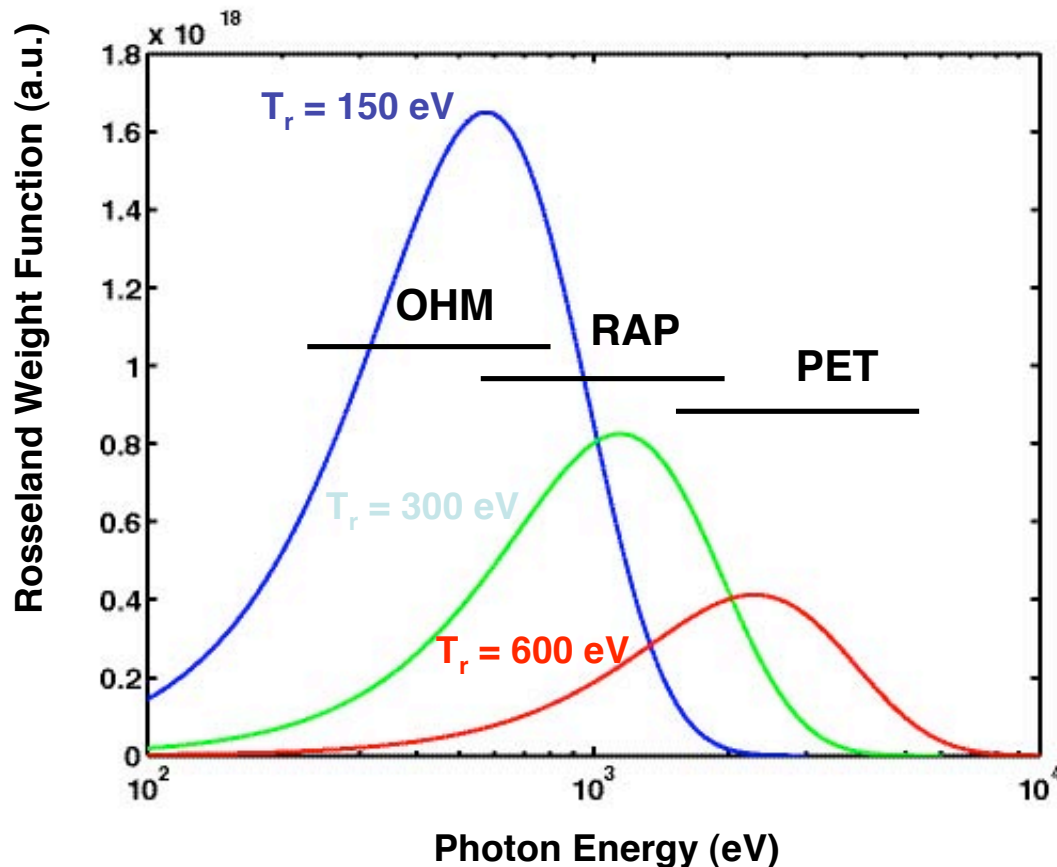
Omega had >5 general-use framing cameras, but only one spectrometer of value for opacity (the old Nova TSPEC, which we'd ported for Non-LTE Au experiments. But TSPEC clips beams.)

New Multipurpose Spectrometer snout (MSPEC)

- 1st unit deployed June 2003
- Goes on XRFC/FXI-class 4-strip (6x34 mm) cameras
- Non-interfering in any laser/target configuration so far
- Now have 4 interchangeable units; all have been deployed
- 4 crystal configurations in use at present
 - Convex (2.0-4.5 keV with RAP)
(M. May et al., RSI 75, 3740 (2004))
 - Elliptical (1.0-1.9 keV with RAP; also PET, OHM)
(R.F. Heeter et al., RSI 75, 3762 (2004))
 - 2 different Flats (RAP 1.5-1.85 keV; PET 3.9-4.6 keV)

MSPEC-Elliptical provided technical foundation for the new “OZSPEC”

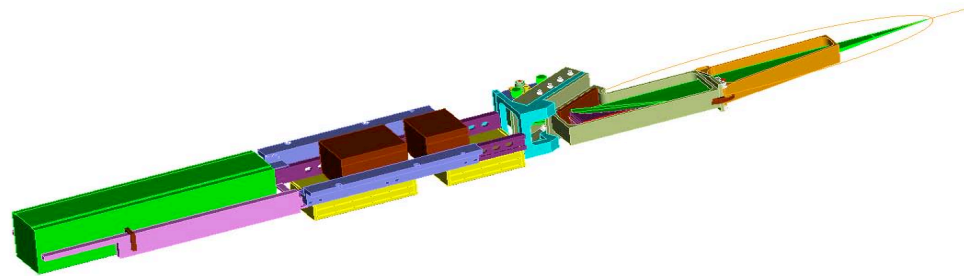
Rosseland Mean Opacity experiments at the higher temperatures anticipated on NIF require new instrumentation



- Need broad spectral coverage
250 eV to > 5000 eV
- Desire resolution $E/\Delta E > 500$
- Crystals scale to higher T_r ;
gratings do not
- New-ish OHM crystal
 - 63.5 Å 2d, $E/\Delta E \sim 1000$
 - opens up soft X-ray range
down to 240 eV
 - can be bent to 25 mm radius
- Broadband and high resolution:
need many pixels: Zipper

A broadband, high-resolution crystal spectrometer would enable validation of opacity codes in regimes of highest impact.

Opacity Zipper SPECTrometer (OZSPEC) design satisfies requirements and makes advances in key capabilities



- “Zipper” detector + elliptical crystal spectrometer = OZSPEC
 - 200 ps gated large format multi-channelplate (MCP) detector
 - Broad spectral range and high resolving power; 2.5x better than previous spectrometers
 - high spatial resolution; required for 800 μm diameter hot hohlraum opacity experiments
 - Compatible with Omega TIM carts
- Diagnostic is development of B. Young’s concept (JOWOG-37 Jan. 2002); motivated by HED experimental requirements

Design results in 2-3 times more data in 200 ps than other framing camera instruments

OZSPEC development was a team effort



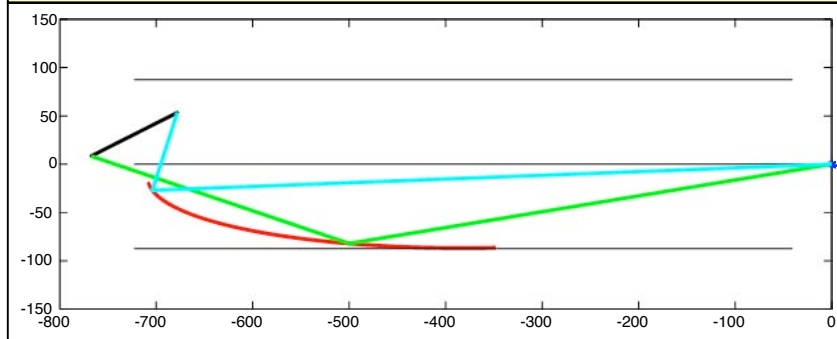
- Instrument is work of many:
S. Anderson, R. Heeter, B. Young, T. McCarville, J. Emig, R. Booth, M. Schneider, D. Norman, I. Reinbachs, L. James
- Immediate application is opacity measurement/code validation at LLE
 - Difficult measurement; requires spatial /spectral /temporal resolution, precision calibration, etc.
- Stepping stone to NIF diagnostics
- Supported by \$1.1M from AX-division (Feb. 2004 - Nov. 2004)
 - PDRP added ~\$300k to finish prototype instrument

Spectrometer design achieves broad bandwidth and high resolution

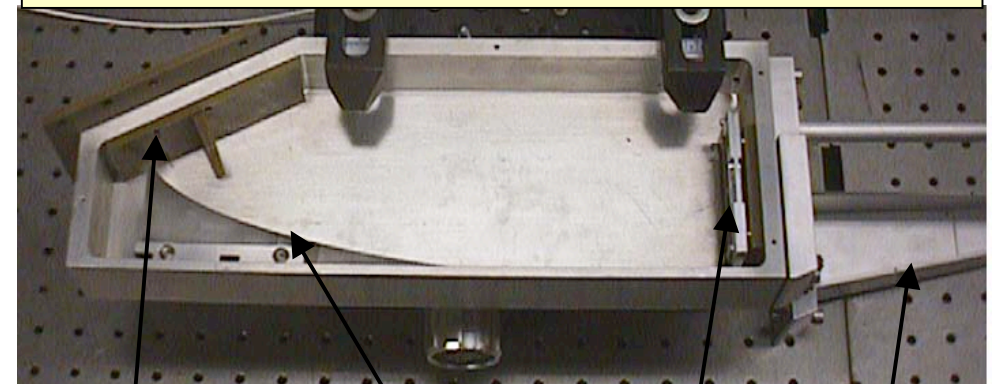


- Uses OHM, RAP, PET ($2d = 63.5, 26.1, 8.7 \text{ \AA}$) xtals with Bragg angle to overlap spectral coverage (14-55°)
 - OHM: 238-807 eV, RAP: 579-1962 eV, PET: 1729-5862 eV
- Ray tracing design optimized resolution/sensitivity given TIM space constraints
- Elliptical geometry allows shielding at second focus

Ray-tracing design output



Fabricated spectrometer body



Focus slit

Xtal mount

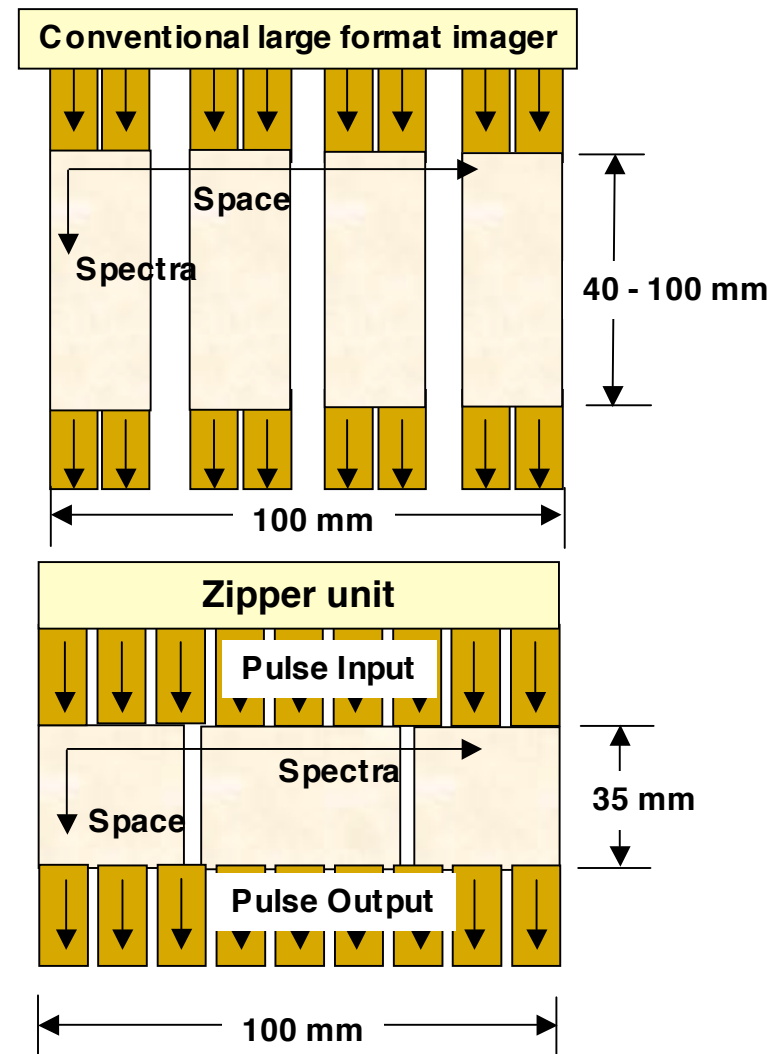
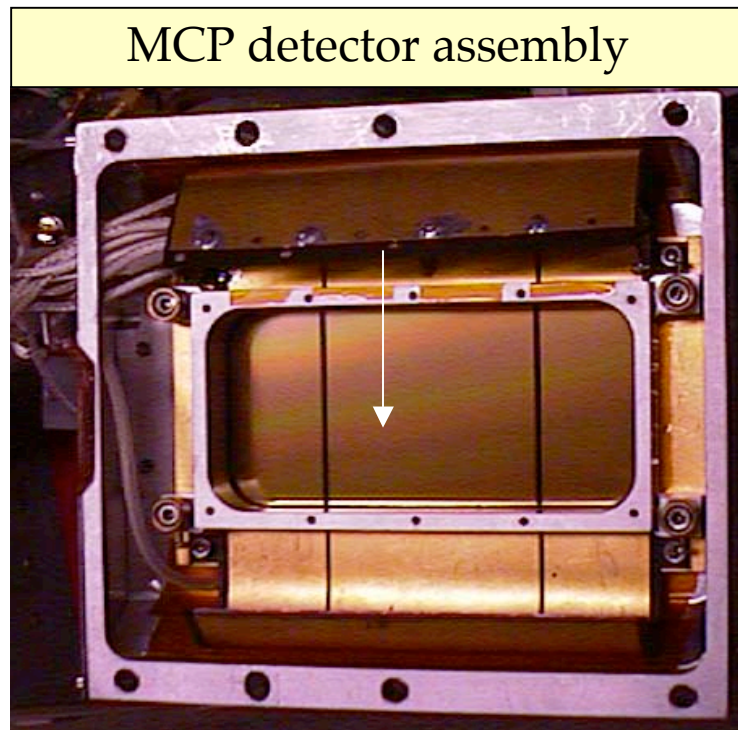
Filters

6x snout

A new large-format, gated “Zipper” detector provides the required increase in image area



- Records spectra distributed over a large area within ~ 200 ps
- Uses same pulser & electronics as standard Nova / Omega framing cameras



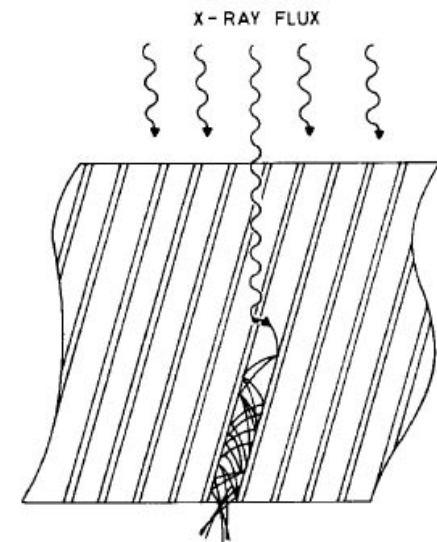
- Major development effort; paper by Tom McCarville et al. submitted to Rev. Sci. Inst.

Detector modeling is required for precision measurements



- Experiments demand ~ few percent level calibration of instrument; opacity error bars, temperature determination.
- Need good models of component response
 - Film
 - Crystal reflectivity, dispersion
 - Filter attenuation
 - *MCP response*

Complicated function of incoming photon energy/angle, plate material, end spoiling, gain model, etc.



Schematic diagram of a microchannel plate*

*J.E. Bateman, *Nucl. Instrum. Methods*, **144**, 537 (1977).

We have coded a detailed MCP response model which agrees well with earlier experiments



- MCP model based on Landen paper:

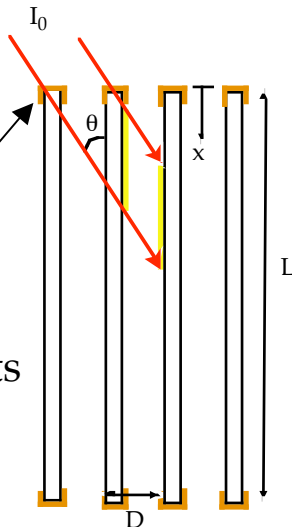
Landen, et al., Rev. Sci. Instrum., Vol. 72, pp. 709-712, (2001).

$$Q = S(E) \left[\frac{R(E)}{\text{mfp}(E) \sin \theta} \right] \cos \theta \sum_n^{\# \text{ pores}} \int_{\text{pore}} I_n(x) G_n(x) dx$$

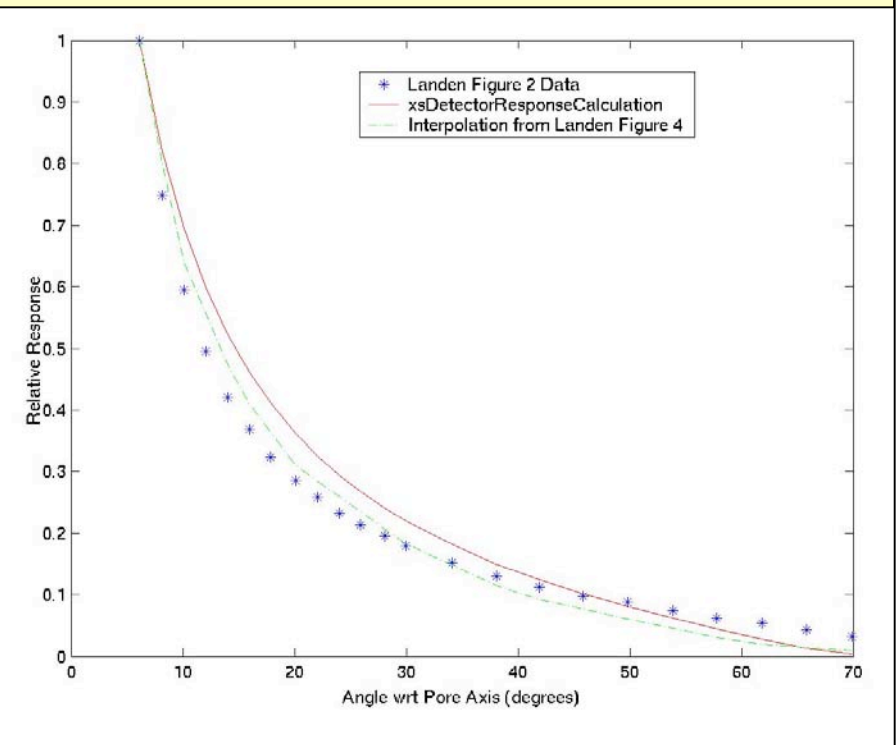
$$I_n(x) = I_0 \exp \left(- \frac{l_{\text{atten}}(\theta, n, x)}{\text{mfp}(E)} \right)$$

$$G_n(x) = \left(\frac{V}{V_0} \right)^{\frac{L}{4D} \left(1 - \frac{x}{L} \right)}$$

Includes end spoiling effects



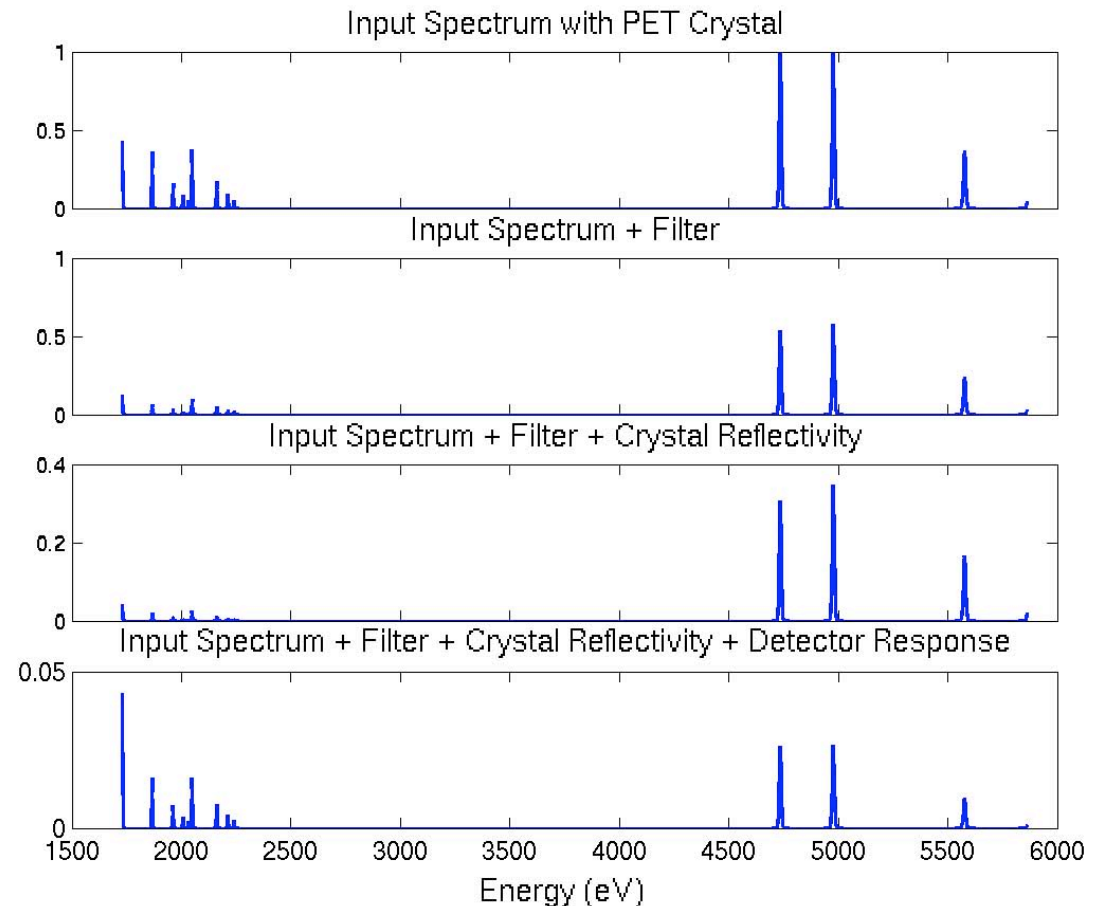
Model and experimental MCP response versus X-ray incidence angle



Full system model is used to balance intensities at ends of spectra

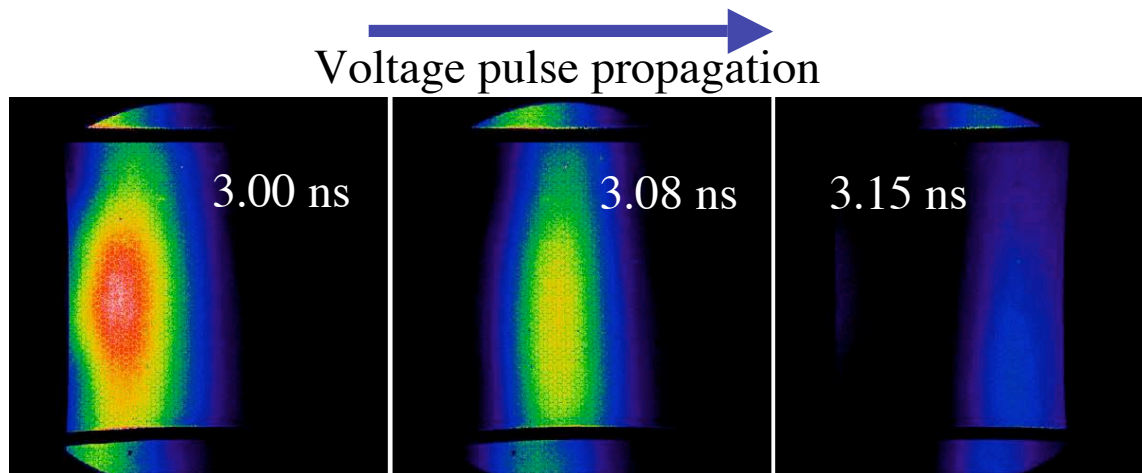


- Simulated response of the PET channel of the spectrometer.
- FAC generated K shell emission lines of H- and He-like Ti and Al (Alumina+Ti target for Janus shots)
- Cumulative effects of the filters, crystal reflectivity, and MCP response.

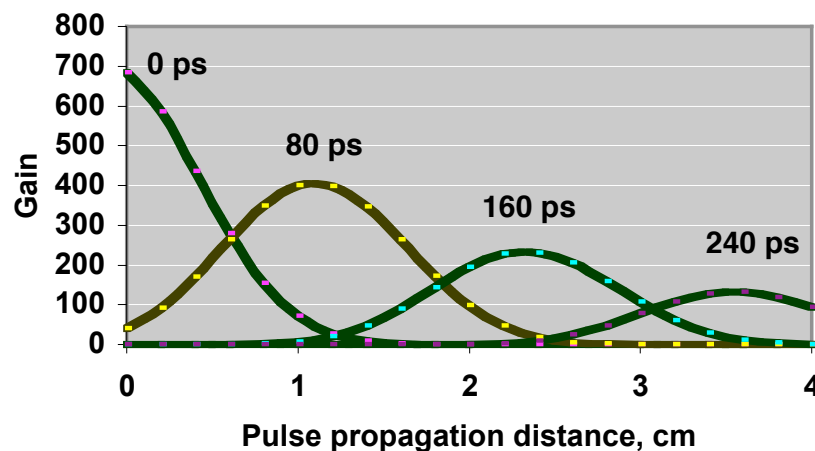
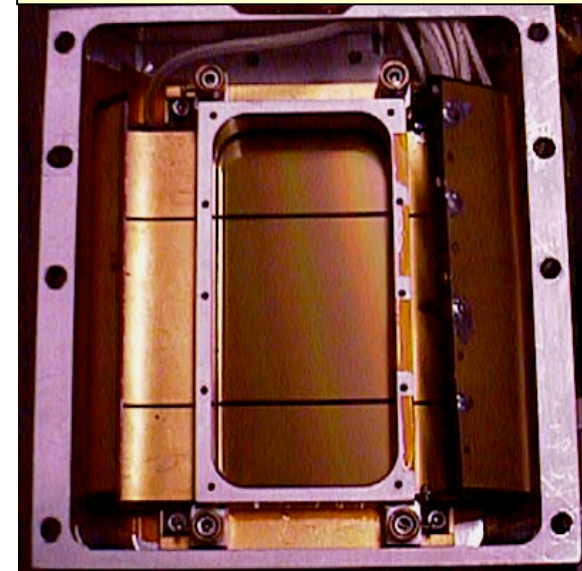


Instrument model facilitates immediate analysis and/or trouble-shooting of data during experiments

The Zipper was tested in gated mode using an ultra-short pulse laser in February



Zipper detector as installed



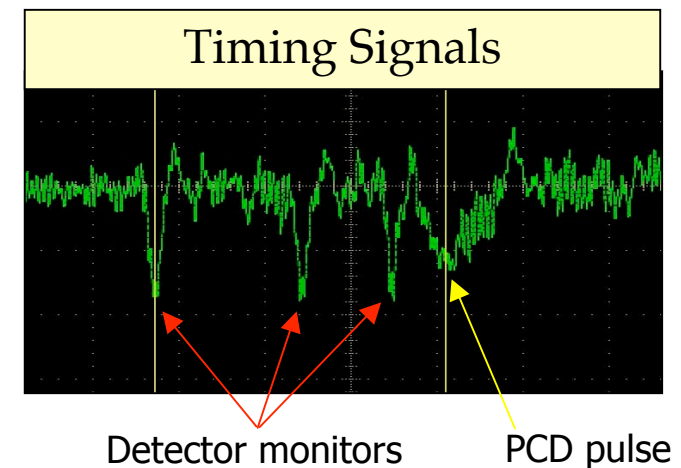
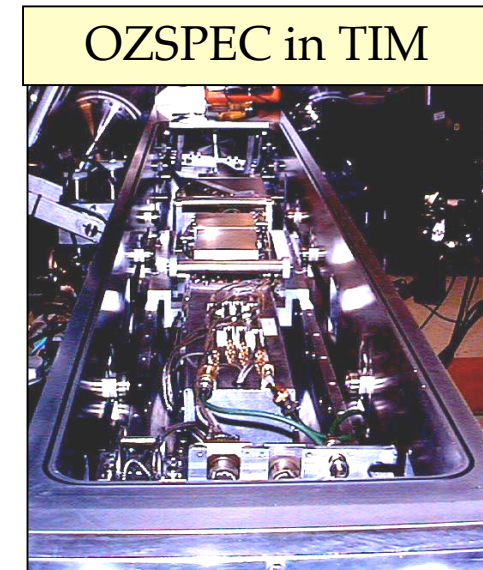
- DC and pulsed mode observed x-rays
- PCD and HV pulse monitor timing set
- USP x-rays allow direct measurement of gain pulse in MCP
- Usual factor of ~5 drop in gain across plate
- Optical gate FWHM < 100 ps

Zipper pulsed response is comparable to conventional cameras in direction of pulse

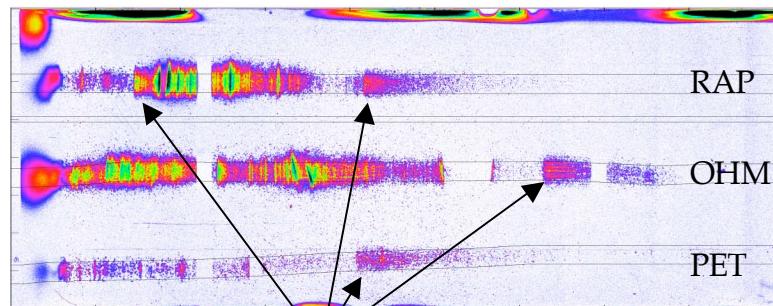
The full OZSPEC instrument was successfully tested at JANUS (180J in 1 or 3 ns) in March



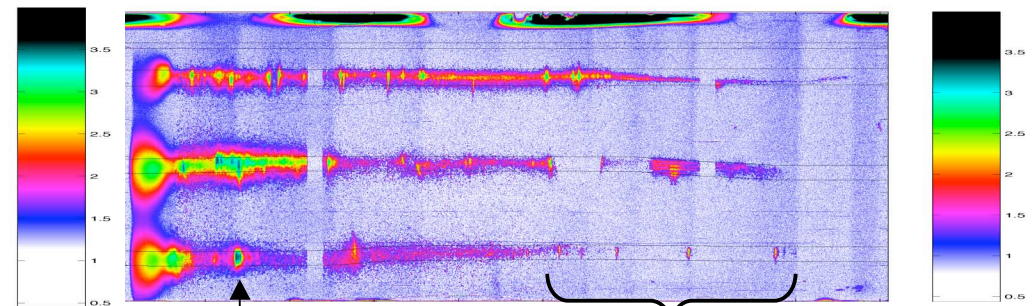
- Zipper + TMAX3200 film pack + elliptical spectrometer in an Omega-class TIM
- Gated spectra obtained on all 3 crystals (0.24-5.8 keV)
- Timing tuned in (for 1-3 ns laser pulses)
- Filter absorption edges and target line emission used to calibrate spectra
- Spatial resolution checked (60 μm slits)
- Channel-plate DC bias issues identified - prior to Omega shots



Gated spectra from JANUS runs provided a wealth of calibration data



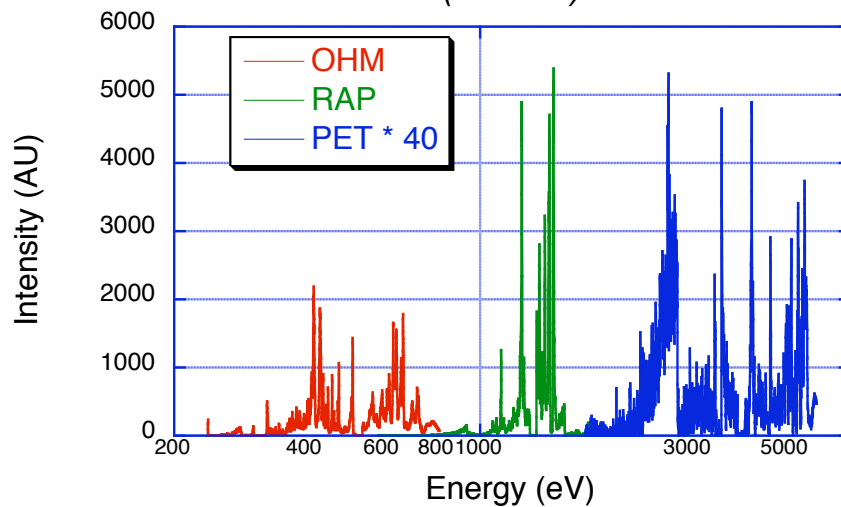
Filter absorption edges



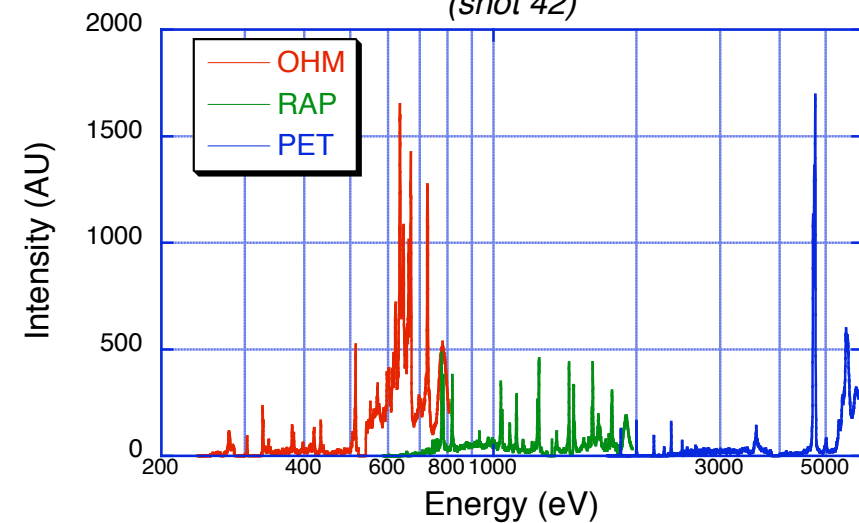
Ti

Si lines

*Cu Spectrum
(shot 36)*



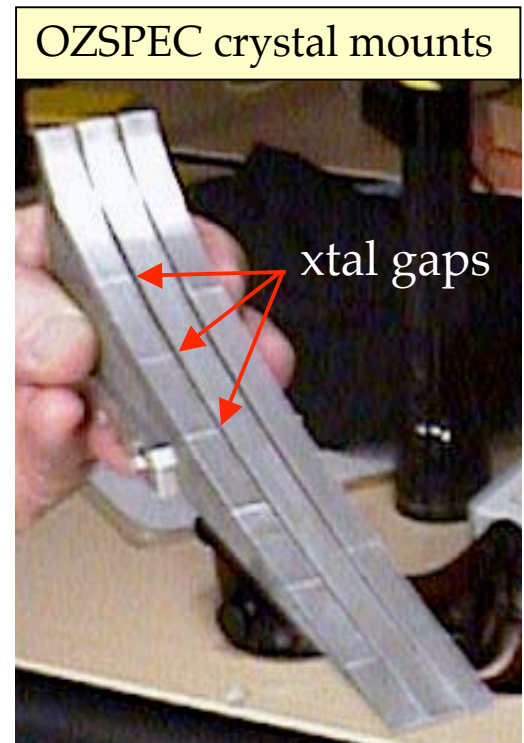
*Pyrex + Titanium Spectrum
(shot 42)*



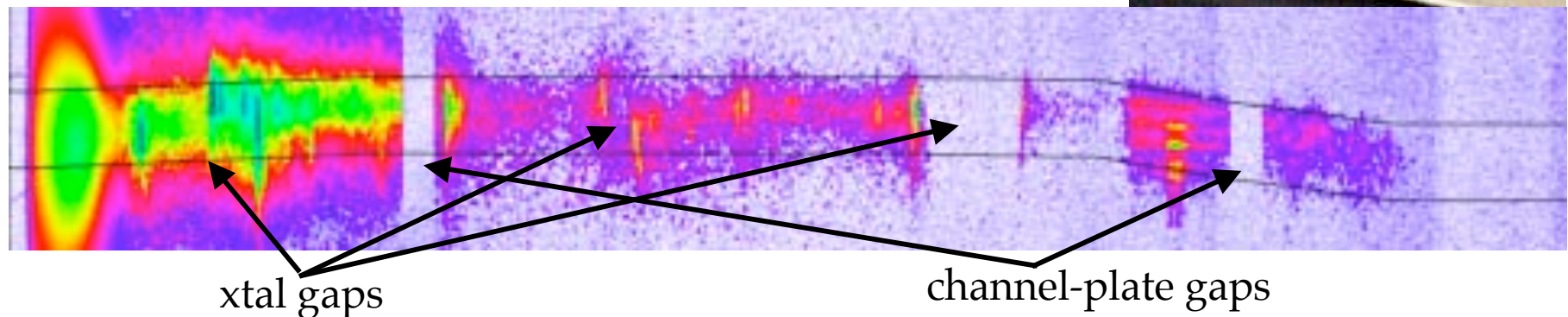


Early analysis has focused on quantifying and reducing the gaps in the spectral coverage

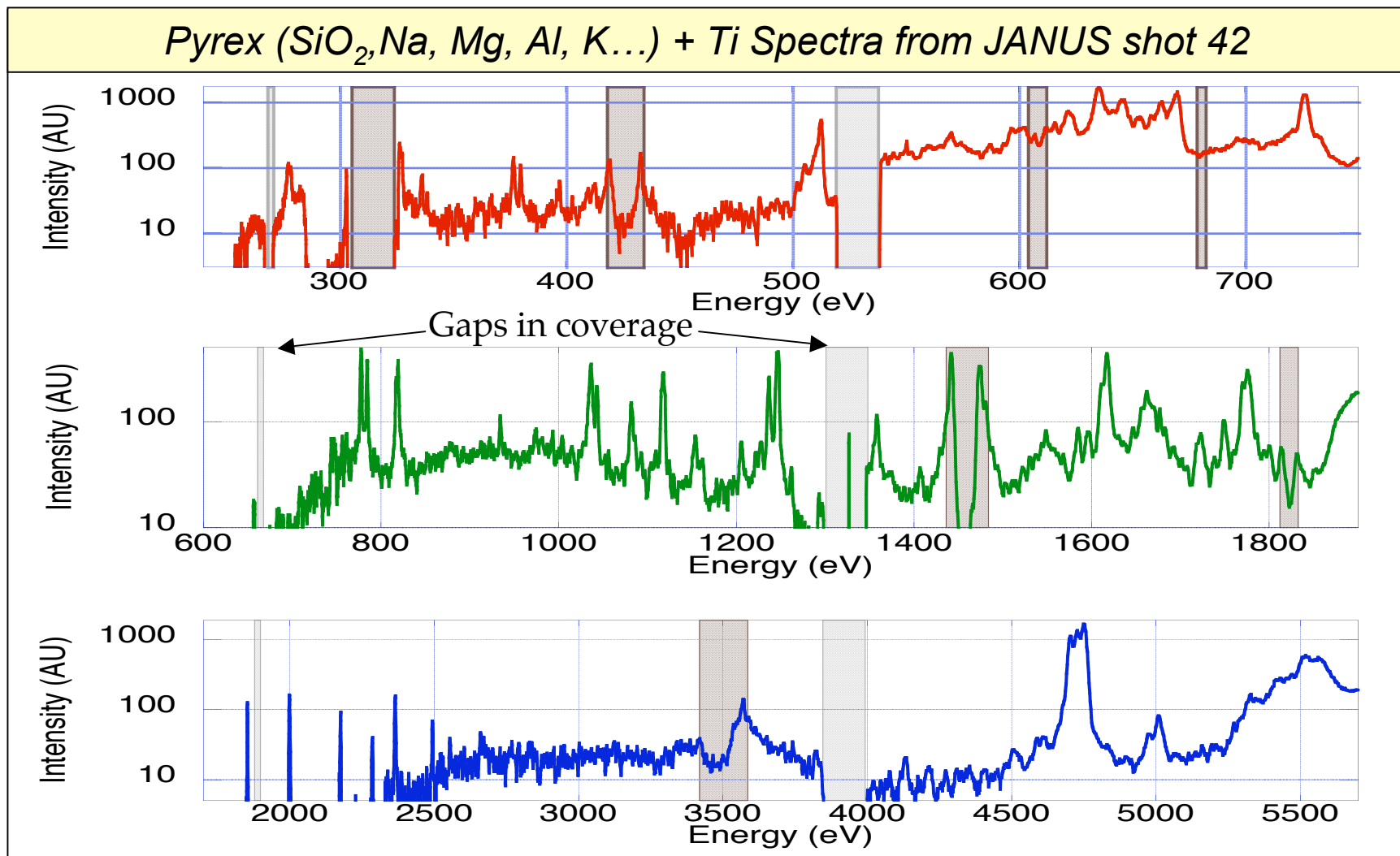
- **Discontinuities in spectrum from:**
 - 2 mm gaps between MCP strips
 - Edges of crystal pieces
- **Use instrument model to align crystal gaps with MCP gaps**
 - Done for Omega shots
 - Works well for RAP, PET;
 - OHM challenging (3 cm strips)
 - Mitigate: duplicate mounts with offset tiling



OHM (240-800 eV) channel of Ti+pyrex spectrum



OZSPEC has the broad spectral coverage and high resolution ($E/\Delta E > 500$, crystal permitting) for which it was designed

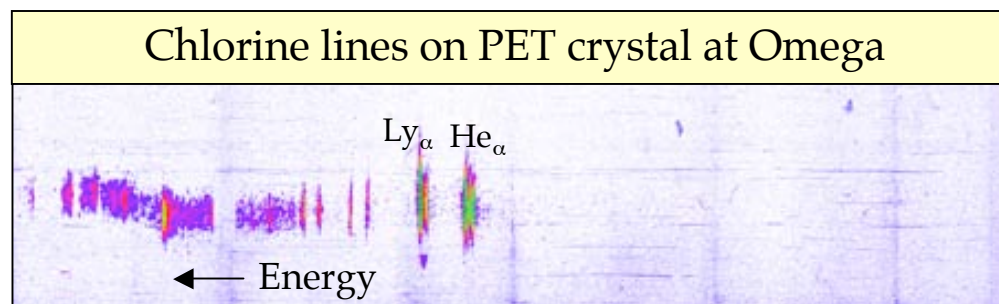


UNCLASSIFIED

OZSPEC was commissioned at Omega from April 4-8



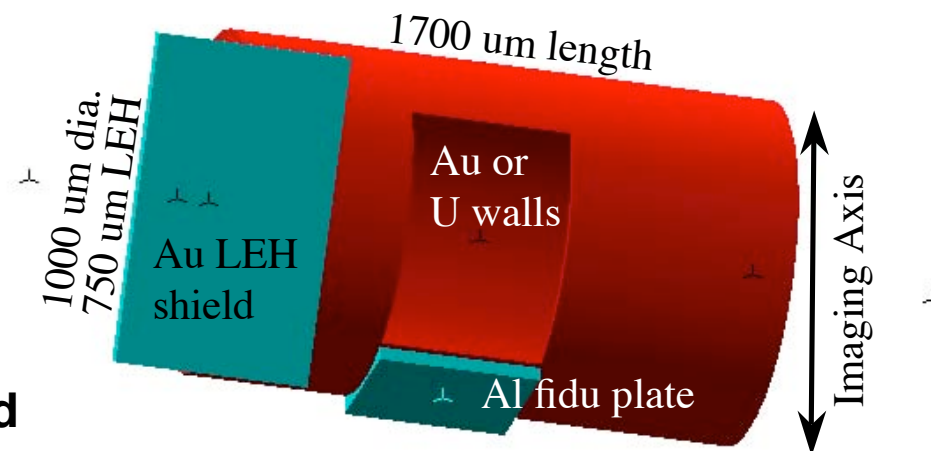
- JANUS and USP experience led to success at LLE
 - Had already resolved several issues that could not have been fixed on-the-fly at LLE: slit apertures, Zipper hardware, pulser supplies, negative biasing, etc.
- April 5-7: 24 “ride along” shots
 - Gated spectra acquired on very first shot; various targets viewed:
 - Polyimide ablaters (C, N, O lines)
 - Hohlraum LEH M-bands (gold, cocktails)
 - Ti backlighter foils
 - Ag targets; Cl calibration shots
 - Timing tuned to ± 100 ps
 - OZSPEC data helping to resolve some unexpected mysteries



OZSPEC is now the workhorse instrument for LLNL's large-laser opacity experiments



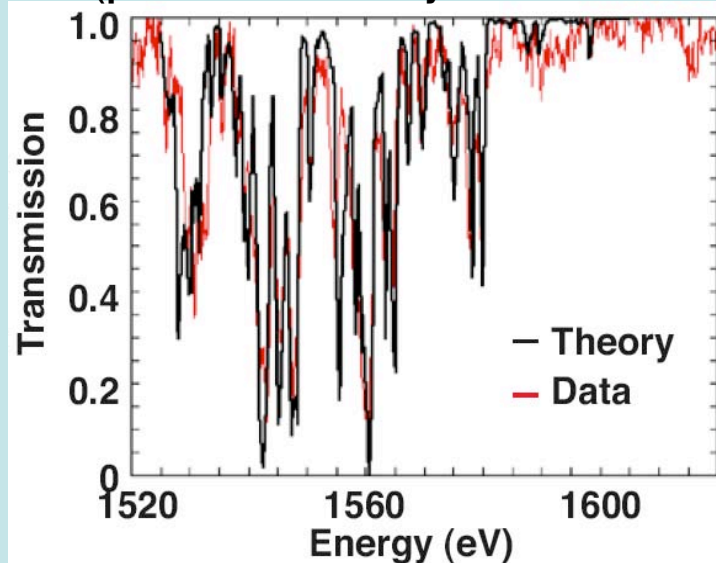
- April 8: Backlighter Development
 - Primary Diagnostic
 - **7 shots (6 expected)**
 - **Excellent data from first shot**
 - OHM/RAP/PET: 250-5500 eV
 - Entire spectrum in each shot
 - Balanced signal levels
 - Film classified, was just scanned
 - Will show sample tomorrow
- June: OZSPEC to characterize point-projection “thermometer” backlight fibers (U, Sm...)
 - In conjunction with next Gd:Al (40 eV) experiments (talk tomorrow)
- Sept.: Possible 1st attempt at Rosseland Mean opacity measurement
 - Ta:Sc at > 100 eV in support of AGEX programs



April shots: our other objective was to establish the n=1-to-2 point-projection absorption method at Omega



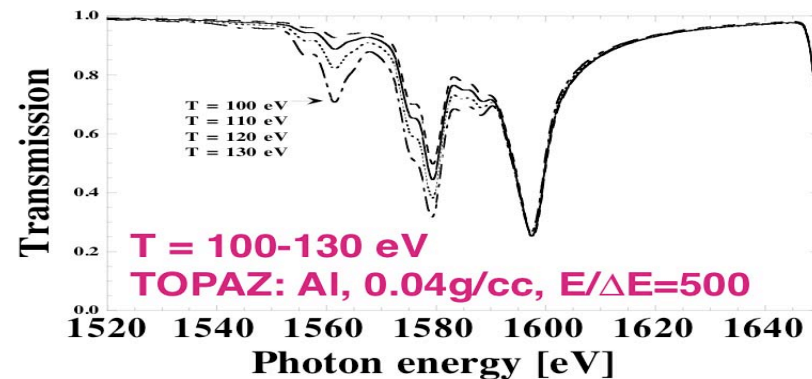
Perry *et al.* PRL 67, 3784 (1991)
(plus much work by AWE & others...)



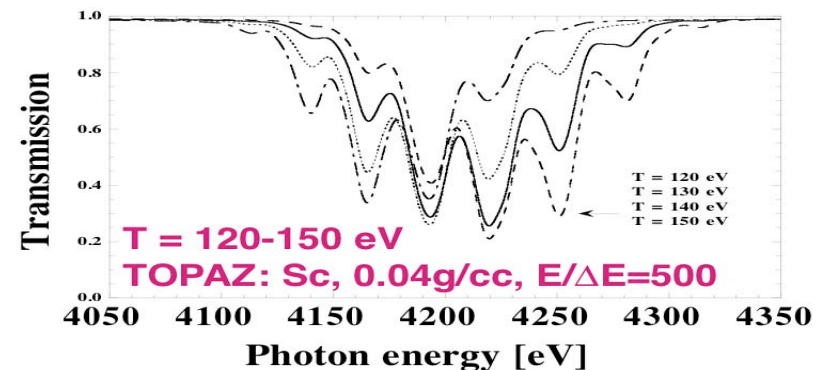
K-shell absorption features
of L-shell ions are strongly
temperature-dependent

We are indebted to Dave Hoarty and others at
AWE for providing us their latest “recipes”.

Extensions to Higher Tr (Carlos Iglesias)



Above 100 eV, Al has only a weak signature

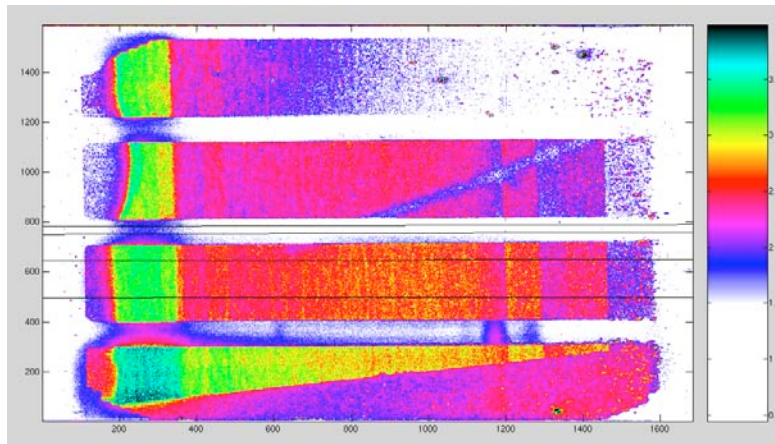


Higher-Z materials are possible (e.g. Sc)

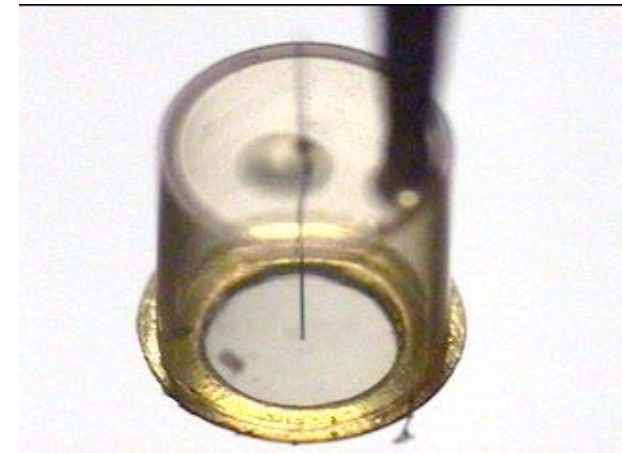
We are beginning to digest the point-projection data for both the Al and Sc 1-2 spectral bands



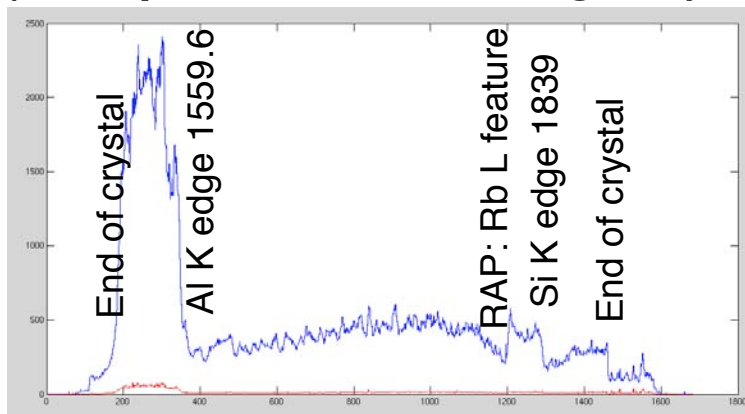
**Image for flat RAP spectrometer,
Sm fiber backlighter**



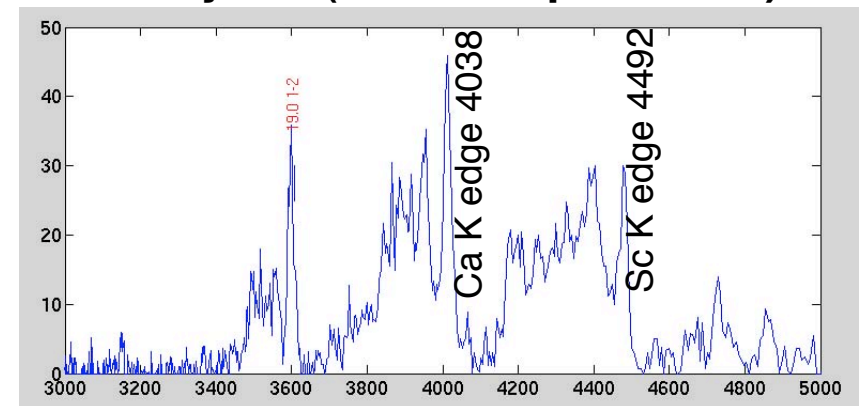
Fiber; epoxy can; Au washer



**Lineout: Sm fiber, flat RAP crystal
(as expected, nice backlighter)**



**Spectrum: Indium-Tin fiber, elliptical
PET crystal (flat PET: poor data)**



Need more work on this one...

Conclusion

UNCLASSIFIED

LLNL's revitalized opacity effort is delivering both near-term V&V data and capabilities needed for NIF



Experiment	Capabilities Required	Status
FY04 Gd:Al 1.1-1.7 keV "Rosseland Style"	40 eV hohlraum design simulations Tamped Samples Design & Fabricate Gated Imaging Spectrometer Bright Uniform Area Backlighter (U/CH foil) <i>Data was acquired May & August 2004</i>	<div></div> Limiting factor
FY05 Gd:Al, Ge:Al 1.1-1.7 keV "Perry Style"	Point-projection spectrometer Al 1-2 range Sm fiber backlighter Al 1-2 range Point-projection spectrometer Gd-Al range U fiber backlighter Gd-Al range	Minor tuning needed Looks reasonable MSPEC-Ellipse point-proj. Must check below 1.5 keV
ASAP Ta for AGEX Rosseland Mean	>100 eV hohlraum design simulations Tamped sample design & fabrication Opacity Zipper Spectrometer Bright backlighter over Rosseland band Point-projection spectrometer for Tr Fiber backlighter for Tr measurement	<div></div> demo unit in fab flat-field needed... <div></div> demonstrated already needs more development
Future Omega Max Tr	Hot hohlraum design based on HTH shots Many more items...	LDRD in progress
FY11+ NIF High Tr	Understand NIF beam coupling for HTH Many more items...	NEL shots promising!
Blue: discussed in the unclassified presentation Purple: discussed in the classified presentation		

UNCLASSIFIED

Heeter-Opacity-V-V slide 50

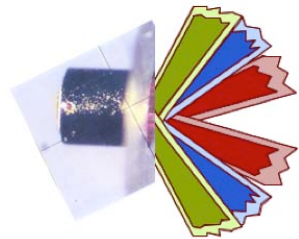
UNCLASSIFIED

Backup Materials

UNCLASSIFIED

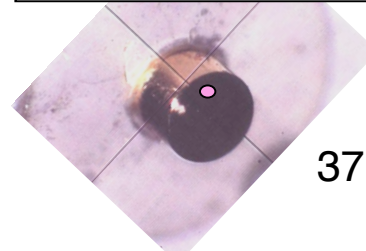
Heeter-Opacity-V-V slide 51

OMEGA experiments show x-ray burnthrough and laser deposition region near FRONT of can



- 19 beams
- 9.5 kJ
- ~1nS flattop

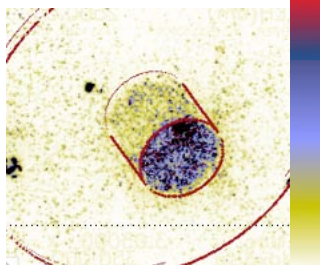
Diagnostic view of target



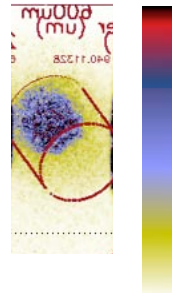
37.4° view of back wall

10 keV images see a laser deposition region move from back wall to front of can

~150 - 200 pS

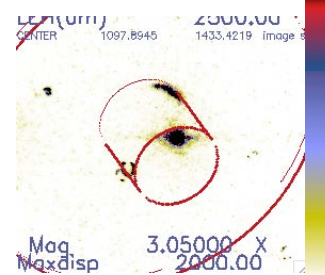


~600-650 pS

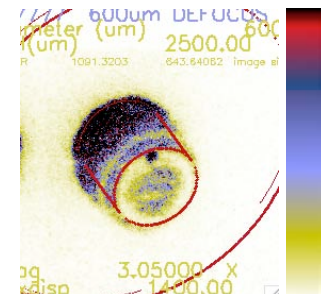


1 keV images see timing hole at early time and, at later times, burnthrough occurring first near front of can.

~150 - 200 pS



~600-650 pS



The OMEGA hohlraums filled faster and were cooler than the NIF hohlraums

Summary of HTH NIF experimental results



Results

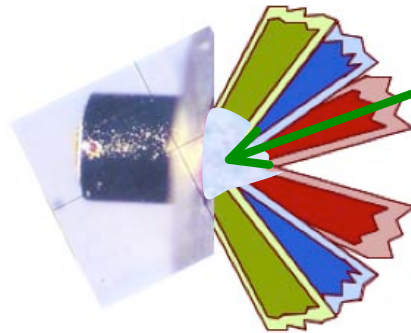
- Radiation temperature was measured showing very good laser coupling to target
- Backscatter: mostly Stimulated Brillouin outside lens
 - filamentation causes beam spray
- Polarization smoothing
 - enhances coupling
 - affects Raman spectra
- Radiation drive higher than predicted
 - images of x-ray burnthrough and hard x-ray region show laser deposition region moves to front of can at slower rate than predicted
- Linearly polarized drive beam produces 20% depolarized backscatter
 - Exercised NIF diagnostics
 - Extended NIF capability for AGEX

HTH success is due to an excellent collaboration between multiple groups: V Division , A/X Division, NIF Facility, ICF Program, NIF Diagnostics Group, AWE, A Program, M Division, UC Davis . . .

NLUF collaboration led by H. Baldis measures plasma conditions at LEH (laser entrance hole)



NLUF interest is high-energy density plasma

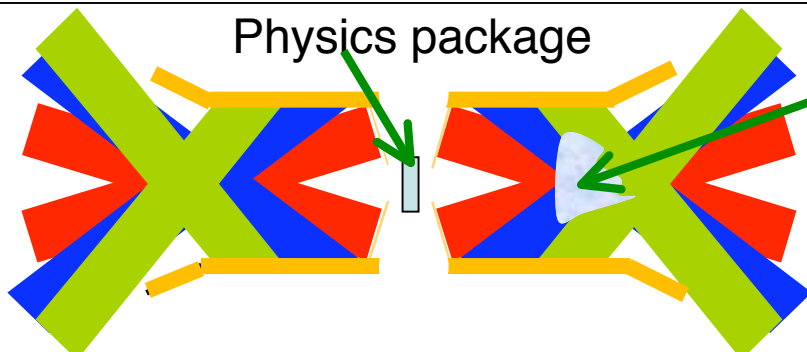


Plasma parameters:

n_e , $\langle Z \rangle$, T_e

Thomson scattering, Optical spectroscopy (Raman backscatter, Brillouin backscatter, Self-Thomson scattering, $3/2-\omega$ spectroscopy), Au M-band X-ray spectroscopy, Time-integrated X-ray spectroscopy

Physics package can be developed in center of hohlraum without disturbing NLUF experiments



Plasma parameters:

n_e , $\langle Z \rangle$, T_e

We propose to add an experimental package in center of hohlraum, and add x-ray diagnostics for T_e , T_{rad} (“(n)LTE-meter”)

Application of Stark-broadened Line Shapes to the Analysis of Line Absorption Spectra

R.C. Mancini*

Sandia National Laboratories, Albuquerque, New Mexico

*On Sabbatical Leave from Physics Department, University of Nevada, Reno

Los Alamos Opacity Validation and Verification Workshop, May 3-5, 2005

Outline

- Ti line absorption model including opacity and line self-emission.
- OMEGA implosion experiment with Ti-doped tracer layer embedded in the shell.
- Absorption line shapes in He- and Li-like Na.
- Z experiment with NaBr layer tampered in a plastic slab.
- Summary.

Ti line absorption model

- The optical depth is written as:

$$\tau_\nu = \pi e^2 / mc (\sum f_{ij} \phi_\nu F_i) N \Delta R$$

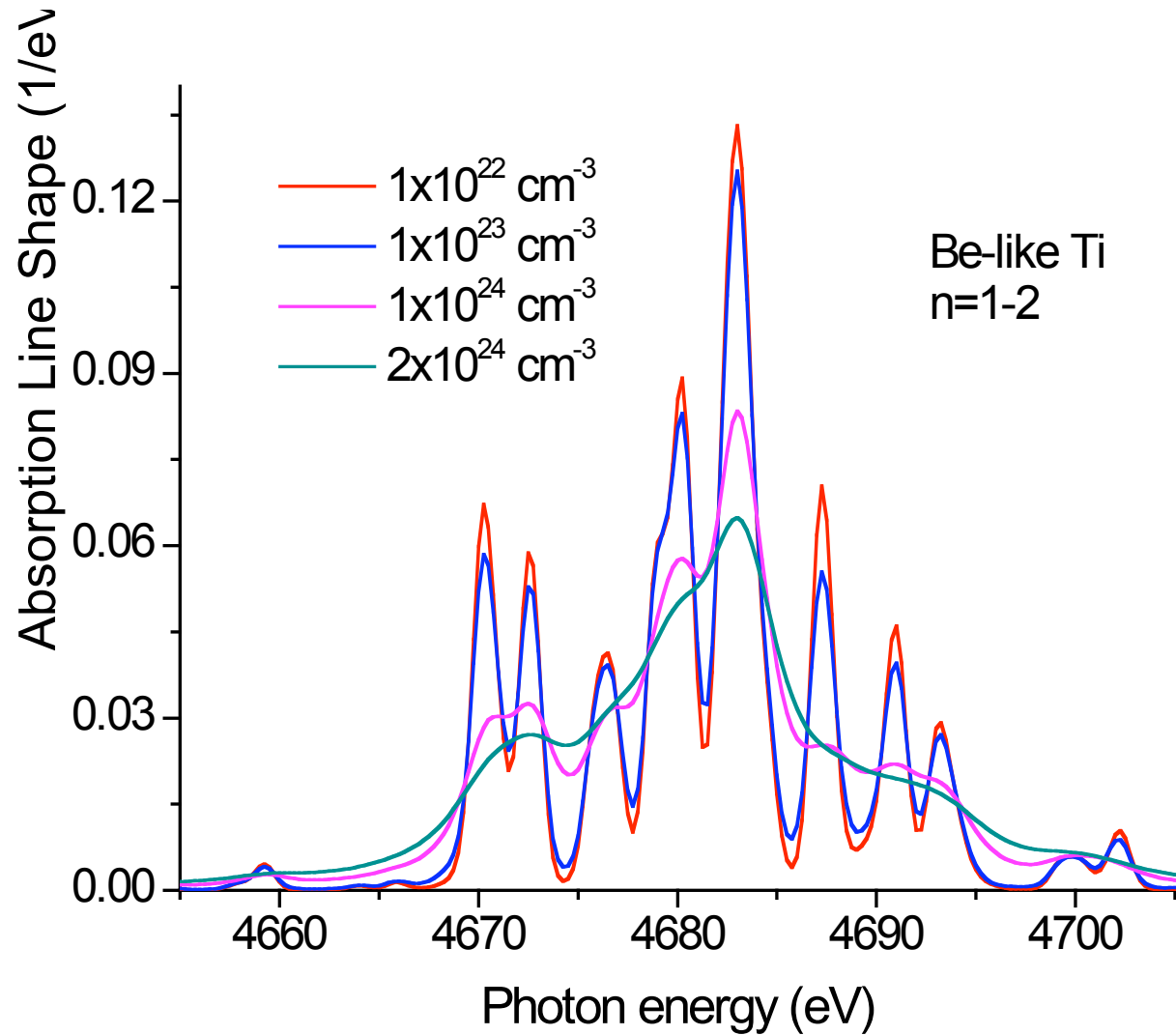
- The sum over line transitions includes all contributions from $n=1$ to $n=2$ transitions in F- to He-like Ti ions.
- The optical depth is density and temperature dependent through the temperature and density dependence of the fractional populations, and the density dependence of the Stark-broadened absorption line shapes.
- Transmission model: $I_\nu = I_o e^{-k_\nu L}$, $L = \Delta R$.

Ti ions: energy levels and line transitions

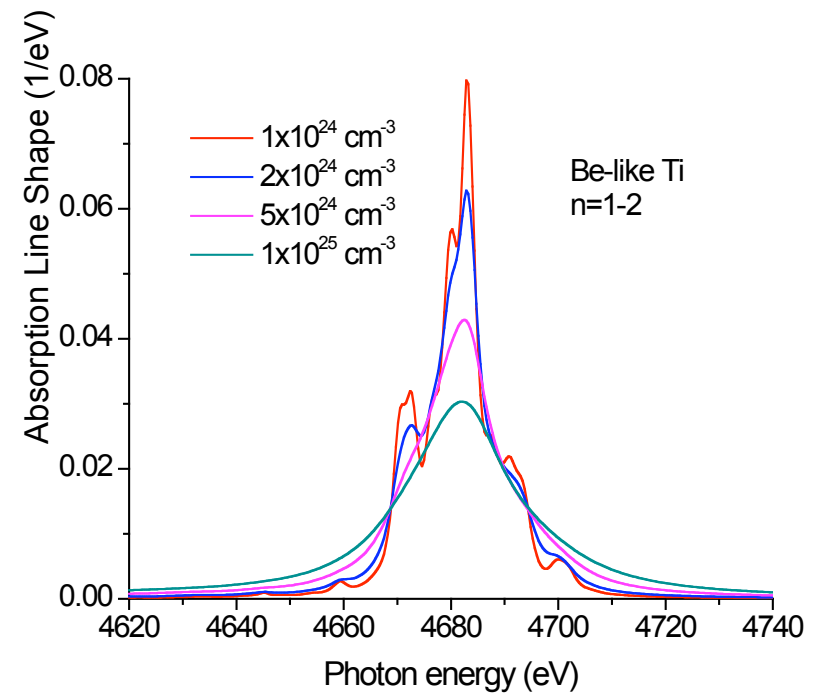
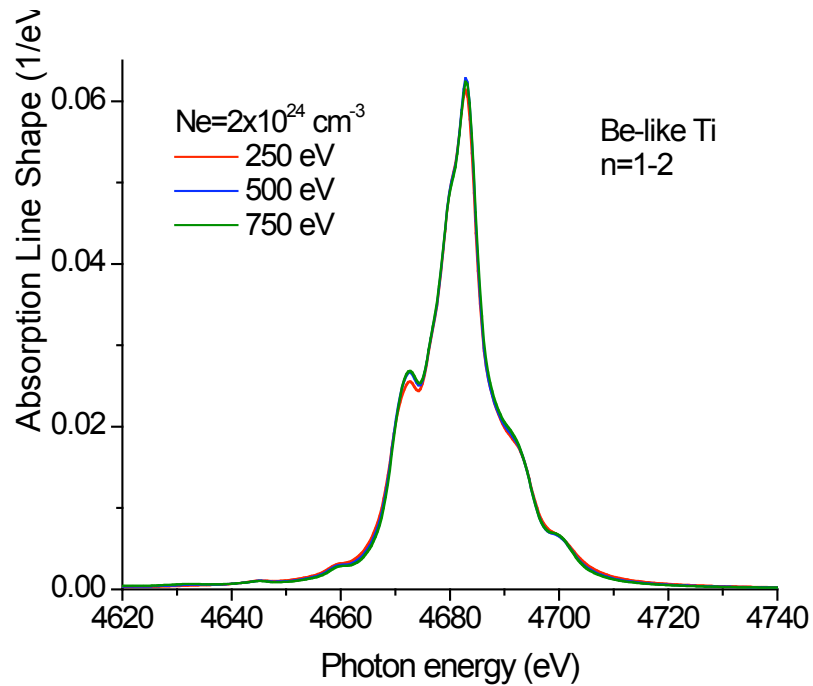
- In each ion, all J-levels and fine-structure line transitions involving configurations with electrons in $n=1$ and $n=2$ are included.
- e.g., for Be-like Ti relevant configurations are:
 $1s^2 2s^2$
 $1s^2 2s 2p$
 $1s^2 2p^2$
 $1s 2s^2 2p$
 $1s 2s 2p^2$
 $1s 2p^3$
- Line transition shapes are broadened and blended by the Stark effect.

ion	Number of lower J energy levels	Number of upper J energy levels	Number of line transitions
He	1	6	2
Li	3	16	21
Be	10	30	85
B	15	35	165
C	20	30	169
N	15	16	169
O	10	6	22
F	3	1	2

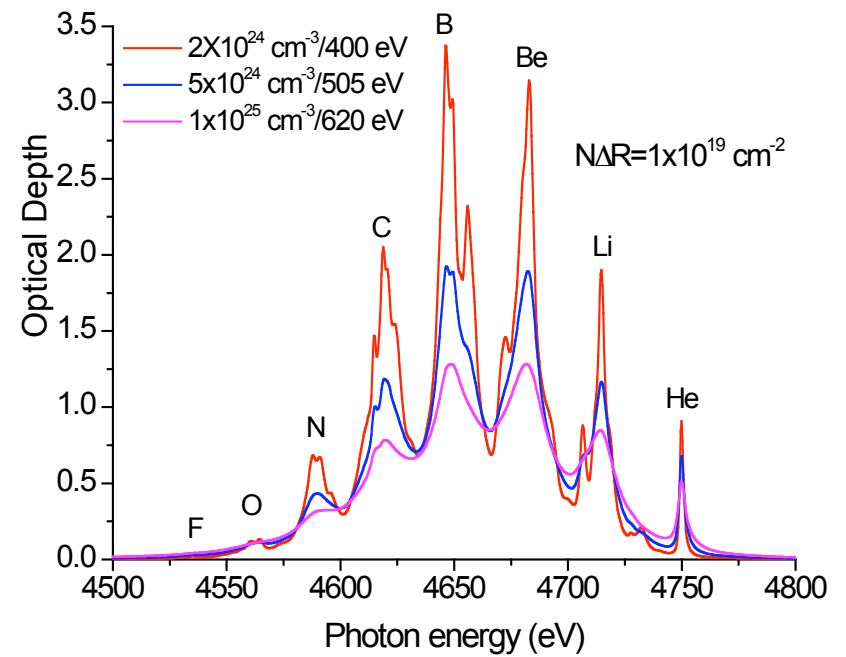
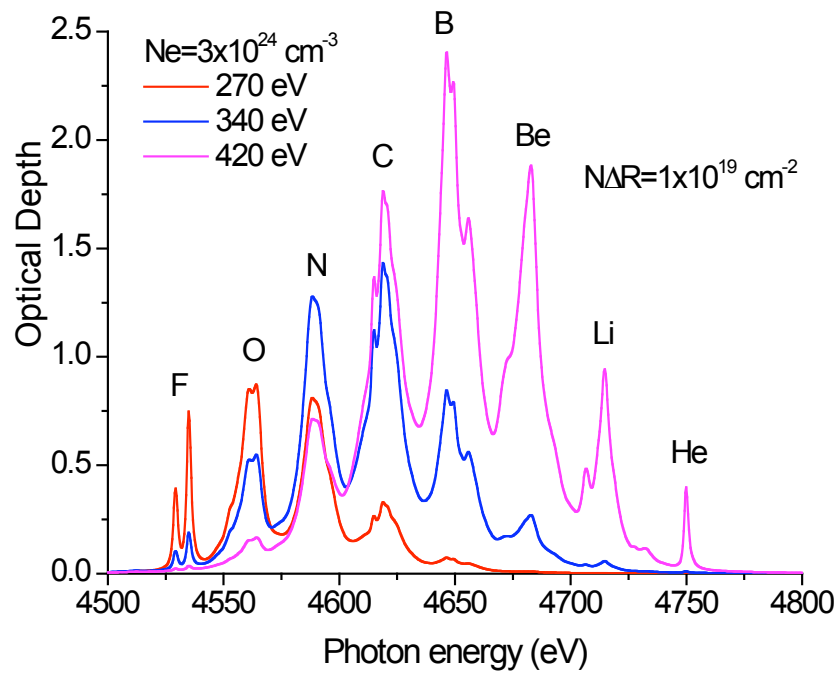
Be-like Ti n=1-2 Stark-broadened line shapes (1)



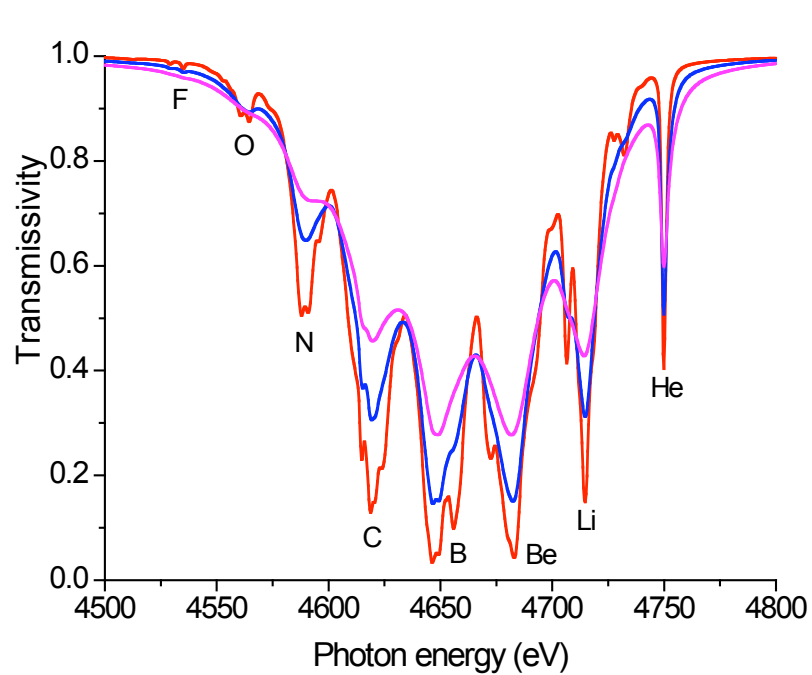
Be-like Ti n=1-2 Stark-broadened line shapes (2)



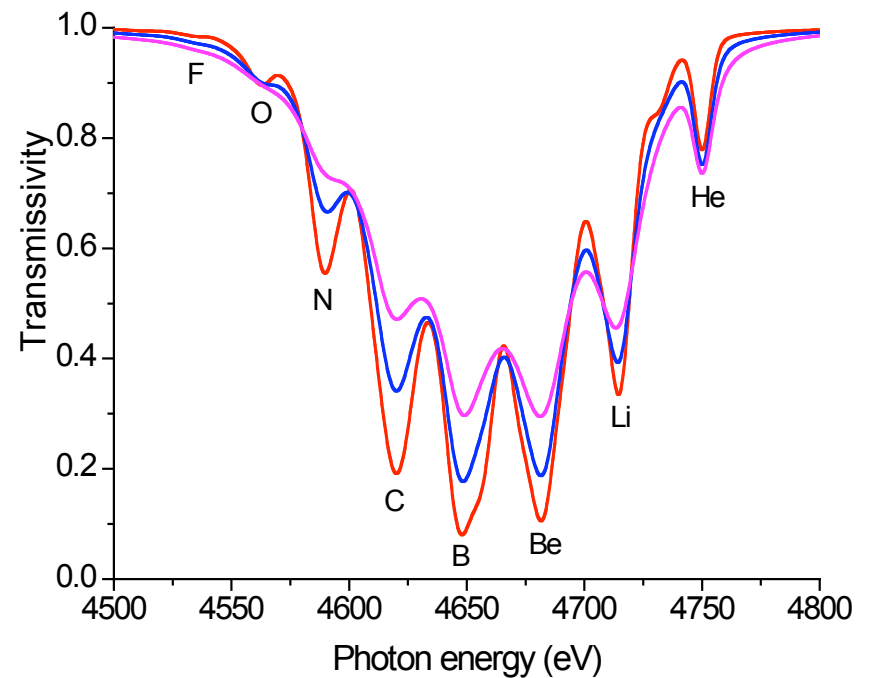
Te and Ne sensitivity of optical depth



Te and Ne sensitivity of transmission



No instrum. broadening



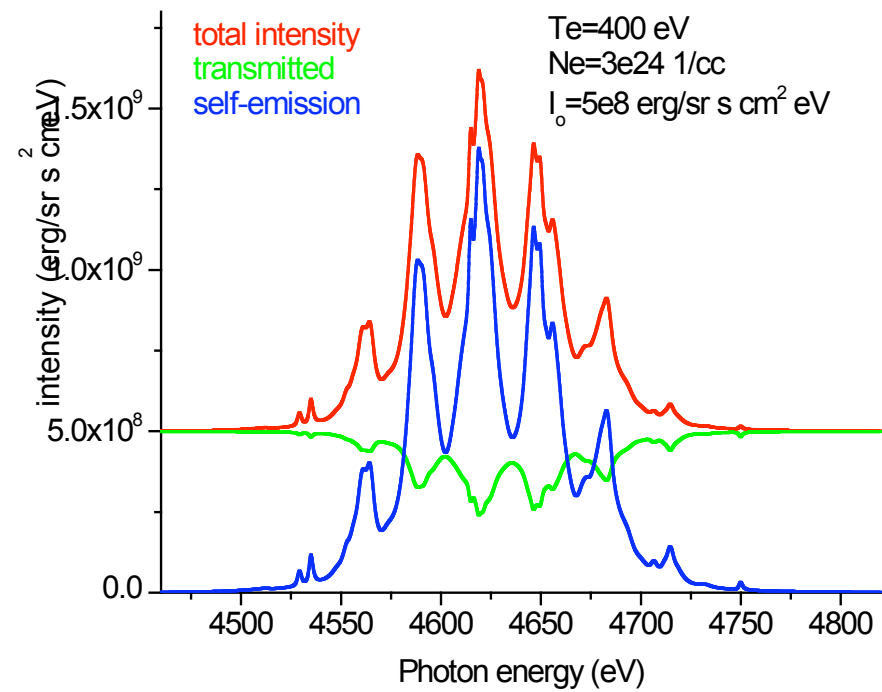
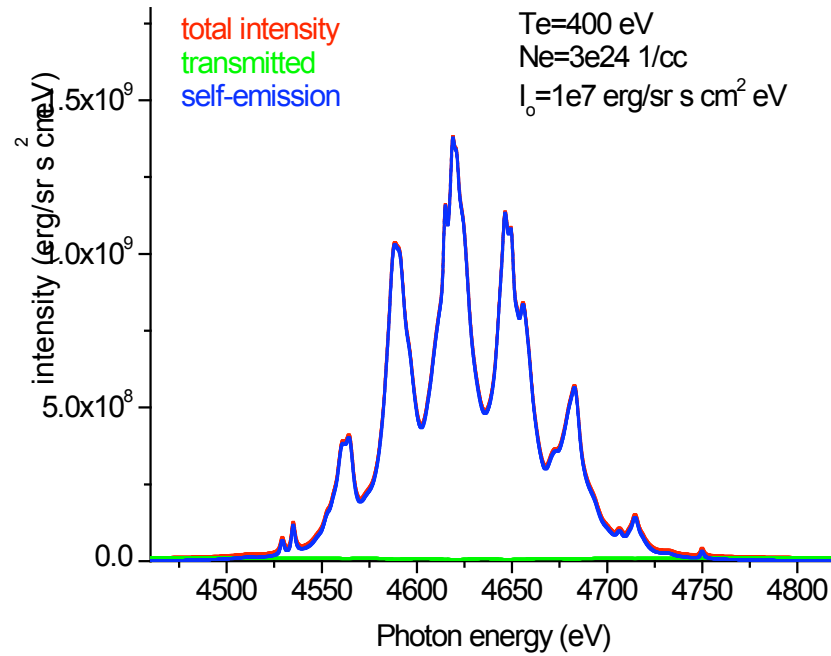
With instrum. broadening
FWHM = 8 eV

Model extension: include line self-emission

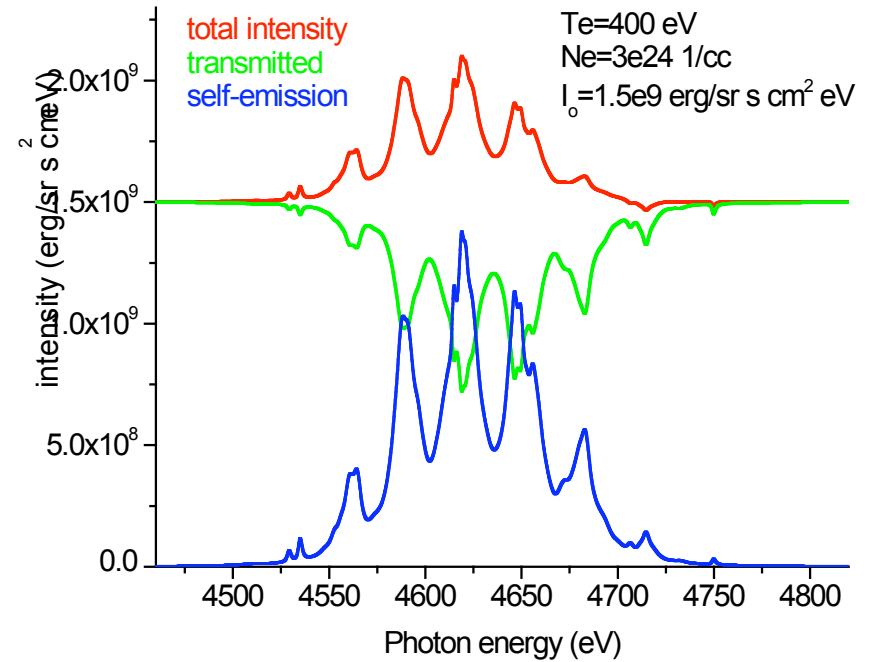
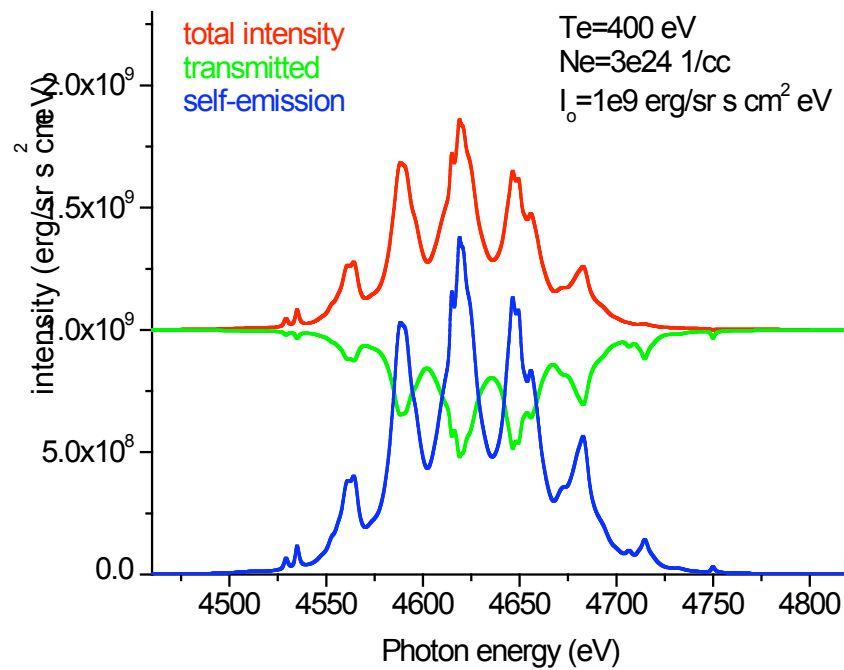
- Solve collisional-radiative atomic kinetics model for level populations including both non-autoionizing and autoionizing levels.
- Atomic data computed with Los Alamos suite of codes: CATS, ACE and GIPPER.
- Include all Ti ionizations stages from Ne- to H-like Ti.
- Model transmitted intensity according to:

$$I_{\nu} = I_o e^{-k_{\nu}L} + j_{\nu}(1 - e^{-k_{\nu}L})/k_{\nu}$$

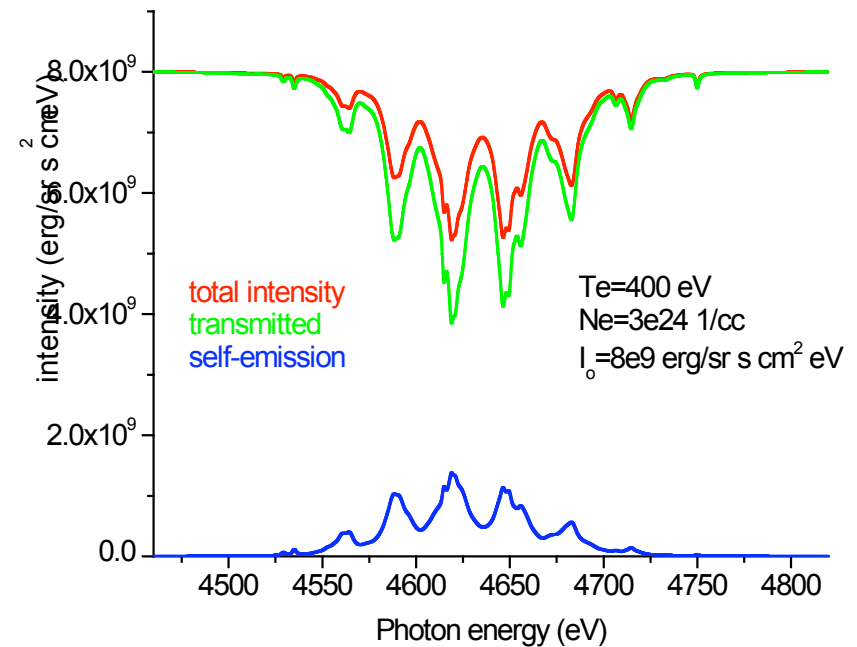
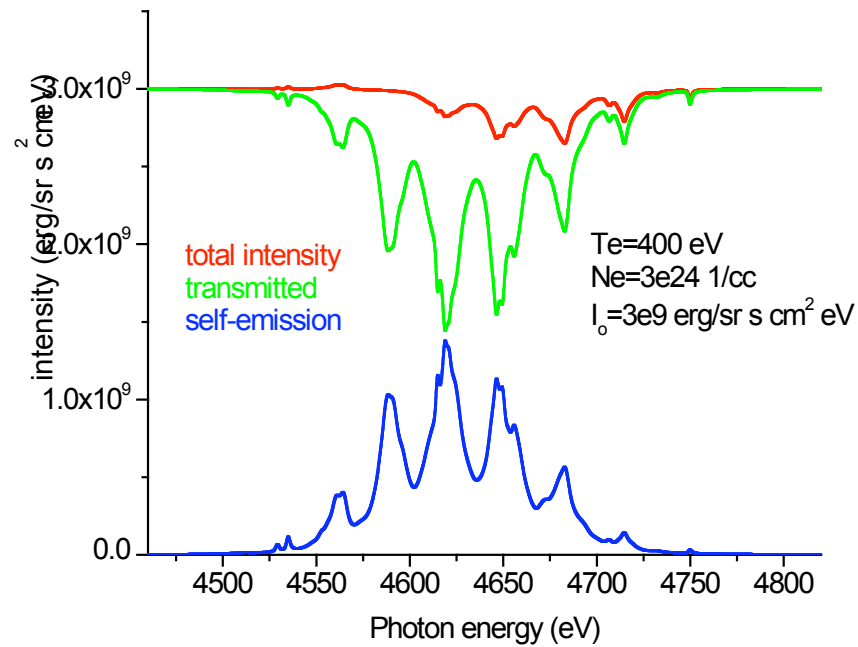
Transmission results (1)



Transmission results (2)



Transmission results (3)



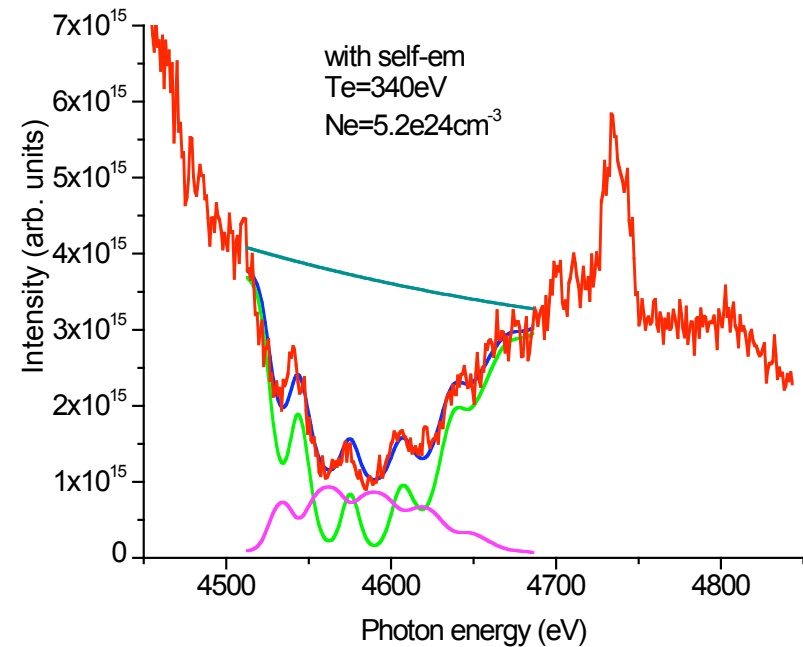
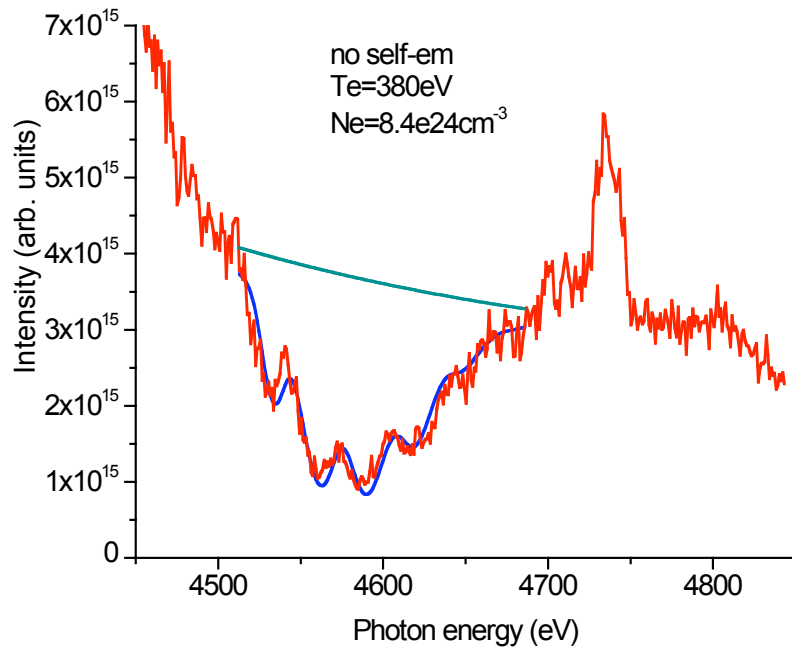
OMEGA implosion experiment (V. Smalyuk, LLE)

- OMEGA direct-drive implosions, 23kJ UVOT.
- Plastic shells, 20 μm wall thickness.
- Ti-doped (2% atomic) CH tracer layers, 1 μm thick, placed at 1, 3, 5, 7 and 9 μm from shell inner surface.
- Core continuum backlights tracer layer, Ti n=1-2 line absorption recorded with streaked spectrometers.
- Resolution power ~ 700 .

Analysis with/without self-emission effect

- No self-emission: $I_\nu = I_o e^{-k_\nu L}$
- L is obtained from least-squares-minimization fit.
- With self-emission: $I_\nu = I_o e^{-k_\nu L} + a j_\nu (1 - e^{-k_\nu L}) / k_\nu$
- L and a are obtained from least-squares-minimization fit.
- Note: for a given set of I_ν^{exp} , I_o , k_ν and j_ν there is a unique solution for L and a .
- I_o is determined from the data.

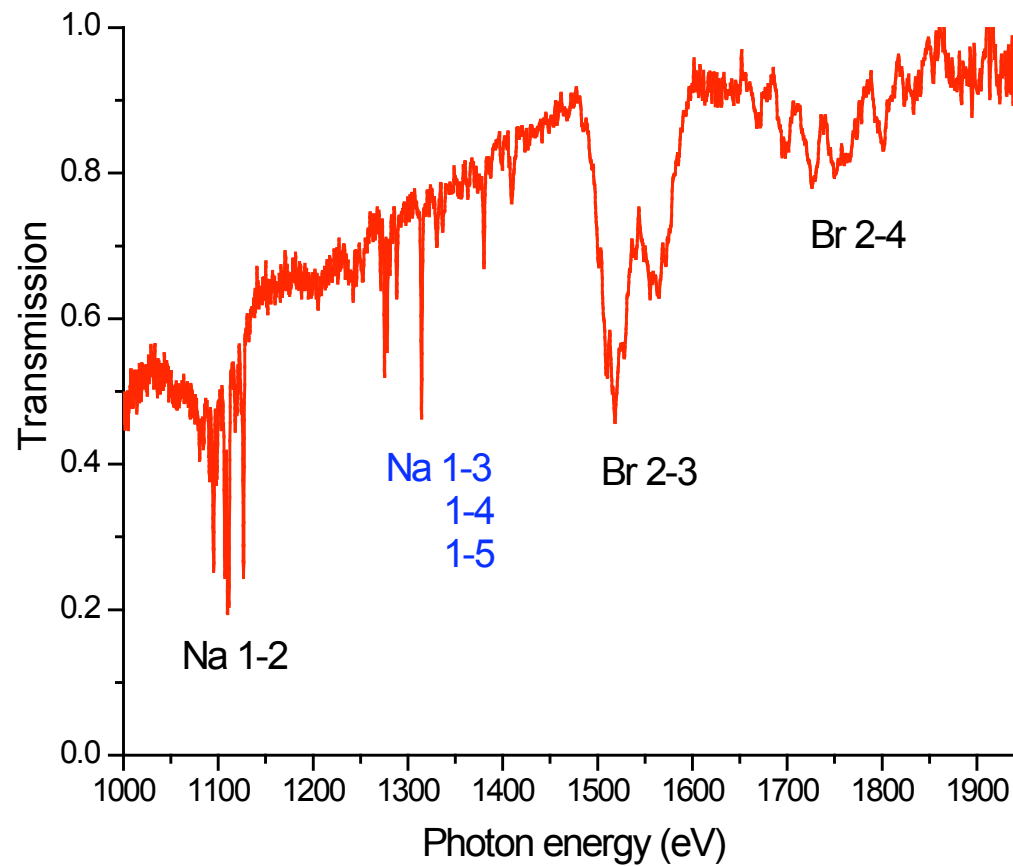
Ti self-emission effect on analysis results



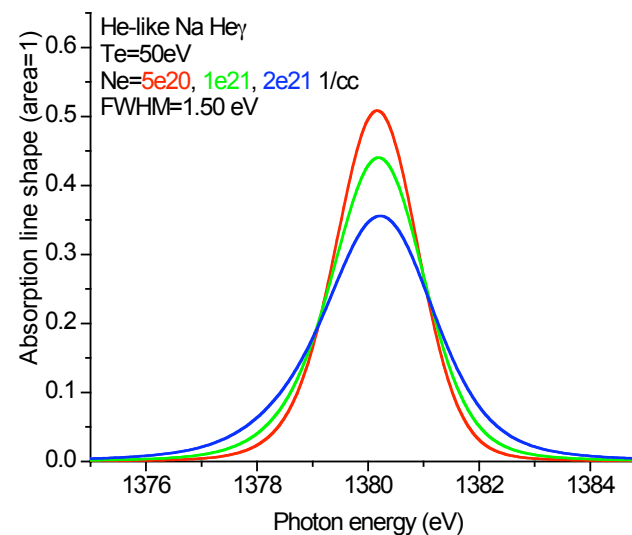
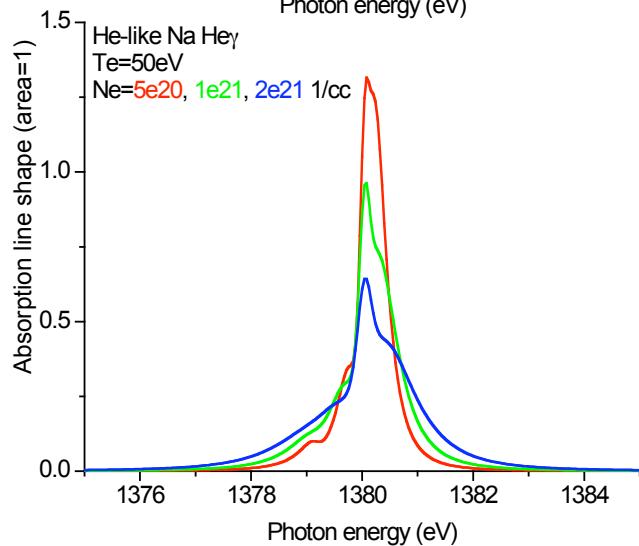
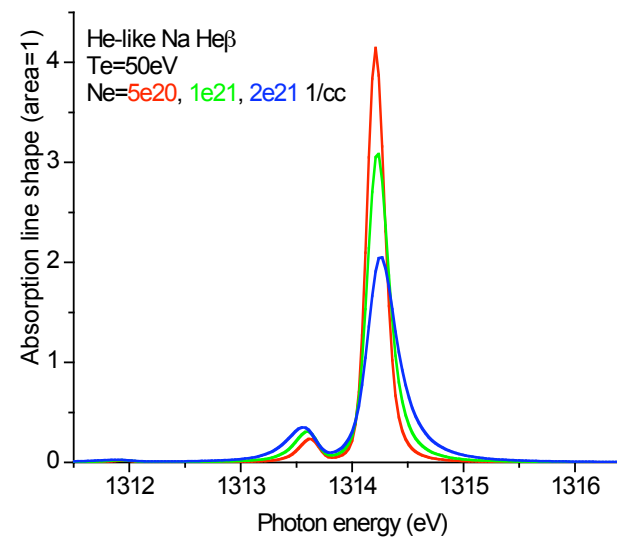
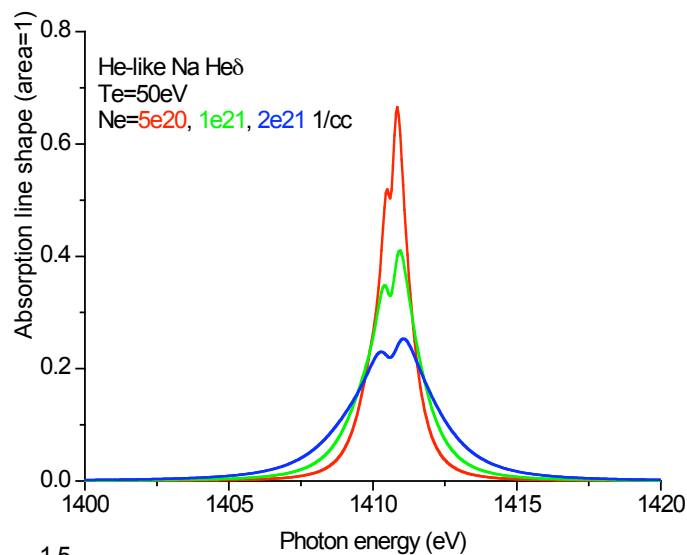
NaBr experiment at Z (J. Bailey, SNL)

- 1500 Å NaBr layer embedded in a 1.96 μm / 2.07 μm plastic (CH) slab
- Radiatively heated and backlighted by z-pinch, located at 42 mm from z-pinch axis.
- $T_e = 50\text{eV}$, $Z_{\text{bar}}(\text{Na}) \approx 9$, $Z_{\text{bar}}(\text{Br}) \approx 10.5$.
- Observation of Na K-shell and Br L-shell, $n = 2 - 3$, absorption lines.
- Time-integrated, spectral resolution power ~ 1000 .

Z shots z535/z536 NaBr absorption spectra

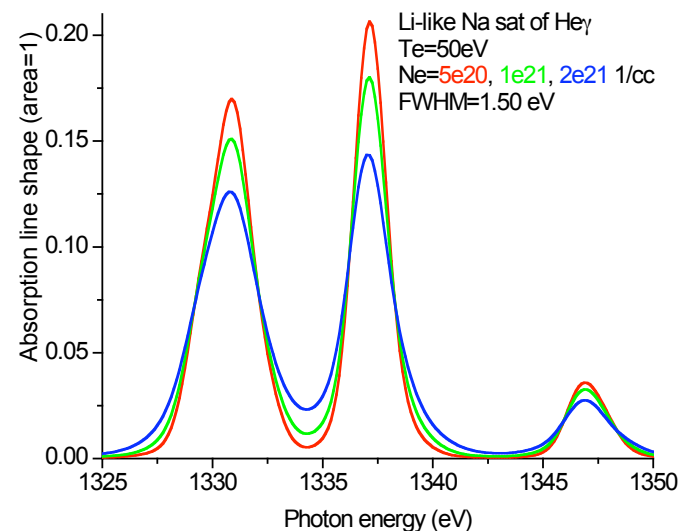
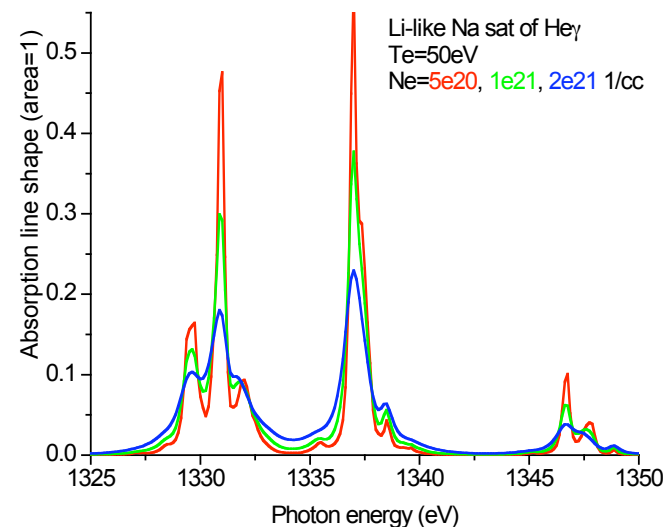


Stark-broadened He-like Na line shapes

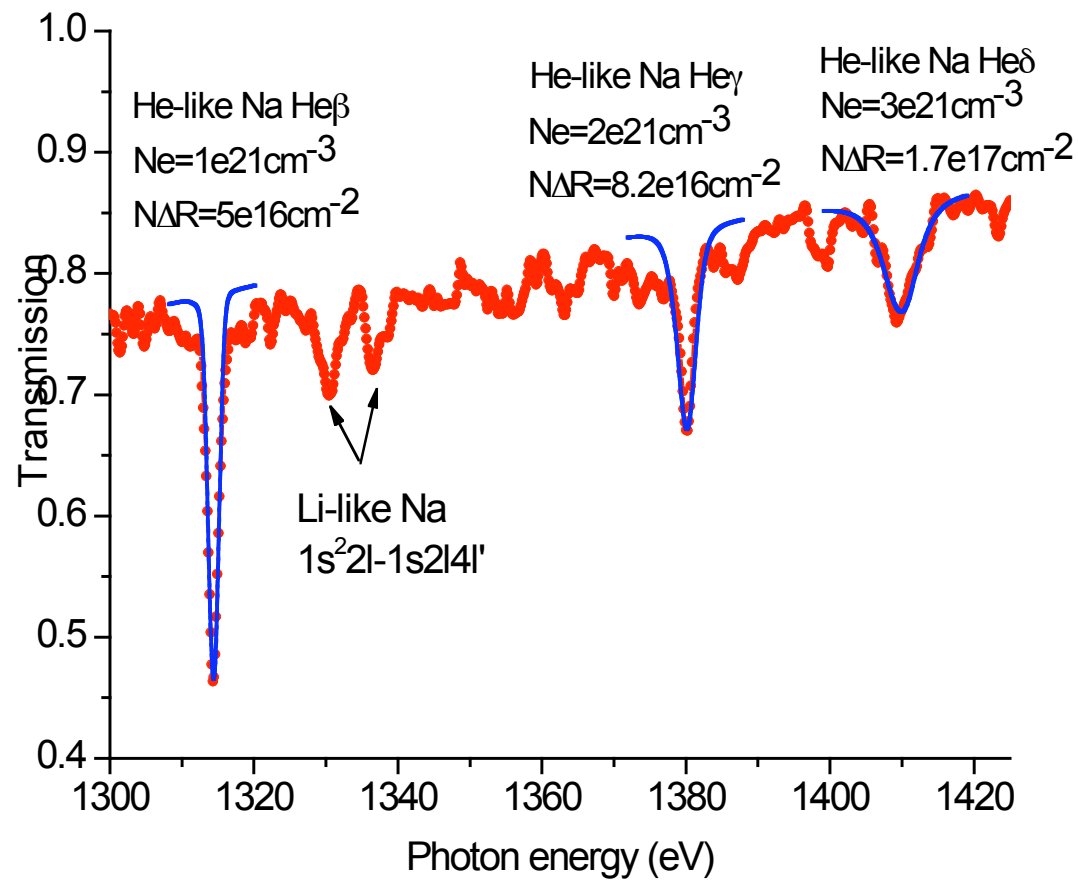


Stark-broadened Li-like Na line shapes

- Li-like Na satellites of He γ line.
- $1s\ 2l\ 4l' - 1s^2\ 2l$
- $l = s, p$
- $l' = s, p, d, f$
- 3 lower J energy levels.
- 98 upper J energy levels.
- 64 fine-structure line transitions.
- Line transition shapes are broadened
are blended by the Stark effect.



Preliminary results: He-like Na absorption lines



Summary

- Application of Stark-broadened line shapes to analysis of line absorption data.
- Dependence of Stark-broadening on density can provide information on density of sample.
- Two application cases:
 - Ti 1-2, Ti-doped tracer layer in plastic shell,
 - He-like Na 1-3, 1-4 & 1-5, and Li-like Na sat of He γ , NaBr layer embedded in plastic slab.
- Preliminary results are encouraging.

Quantum Molecular Dynamics

Simulating Warm, Dense Matter

Lee A. Collins, Joel D. Kress, and Stephane F. Mazevet

Regions of warm, dense matter abound—from the interiors of giant gaseous planets, such as Saturn, and the atmospheres of white dwarf stars to laboratory plasmas in high-energy density generators and inertial confinement fusion capsules. Warm, dense matter, a sizzling “soup” of atoms, molecules, ions, and free electrons, is difficult to describe by standard techniques because it harbors multiple species and processes simultaneously—from ionization and recombination to molecular dissociation and association. Recently, quantum molecular dynamics (QMD), which can predict static, dynamical, and optical properties from a single, first principles framework, has been used to accurately predict properties of hydrogen, oxygen-nitrogen mixtures, and plutonium in the warm, dense state.

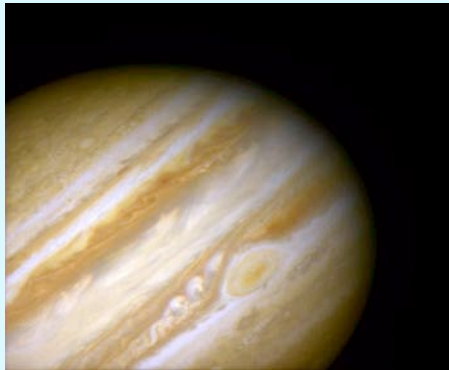


At the core of Saturn,
there is warm, dense matter,
ranging between 5000 and
6000 kelvins in temperature.

Abstract: QMD

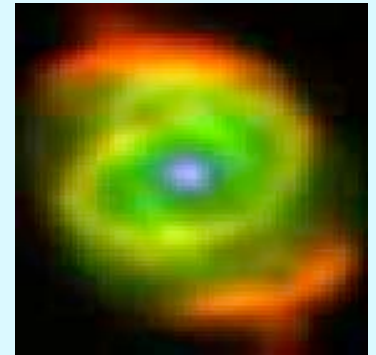
The need to better model the regimes of warm, dense matter [10^2 - 10^6 K; $0.01 - 100$ g/cm³] in which quantal behavior, especially for the electrons, becomes important, has received new impetus from many areas including weapons science and planetary modeling as well as shock-compression and high-energy-density physics. To meet these needs, we have applied quantum molecular dynamics (QMD) methods, which join the latest flavor of Density Functional Theory for the electrons to the classical equations of motion for the nuclei, to a variety of systems and conditions. Examples include static (EOS), dynamical, and optical properties of 1) mixtures [H/He, N/O, Ti/H, SiO₂, Li/F]; 2) shocked materials [Ga, Sn, Fe]; and 3) temporally-evolving samples [e.g. Au] after short-pulse laser irradiation. In addition to providing a basic understanding of the interaction mechanisms, the exploration of mixtures also tests popular models for mixing the properties of the pure species to obtain those of the composite. For the shocked materials, we also examine possible signatures in the optical properties of various phase changes. The third example highlights a push into new physical realms by extending the method to non-equilibrium conditions for coupling of the electron and ion components.

We have developed larger-scale classical and quasi-classical molecular dynamics techniques to treat ultracold multi-component plasmas and Rydberg gases in external fields. Such systems, produced by traps using similar technology as for Bose-Einstein Condensates, can serve as effective laboratories to explore many basic plasma processes. In addition, with an added magnetic field, we have studied the conditions within the ATOM and Athena antihydrogen experiments at CERN with the goal of devising mechanisms to de-excite the high Rydberg states currently produced to low-lying levels that can be spectroscopically probed to determine possible deviations from CPT symmetry and to discriminate among different gravitational theories

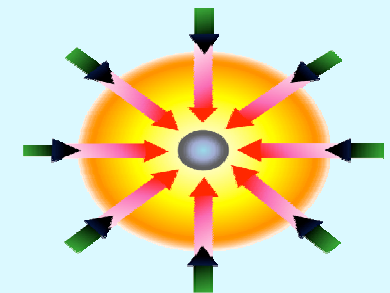
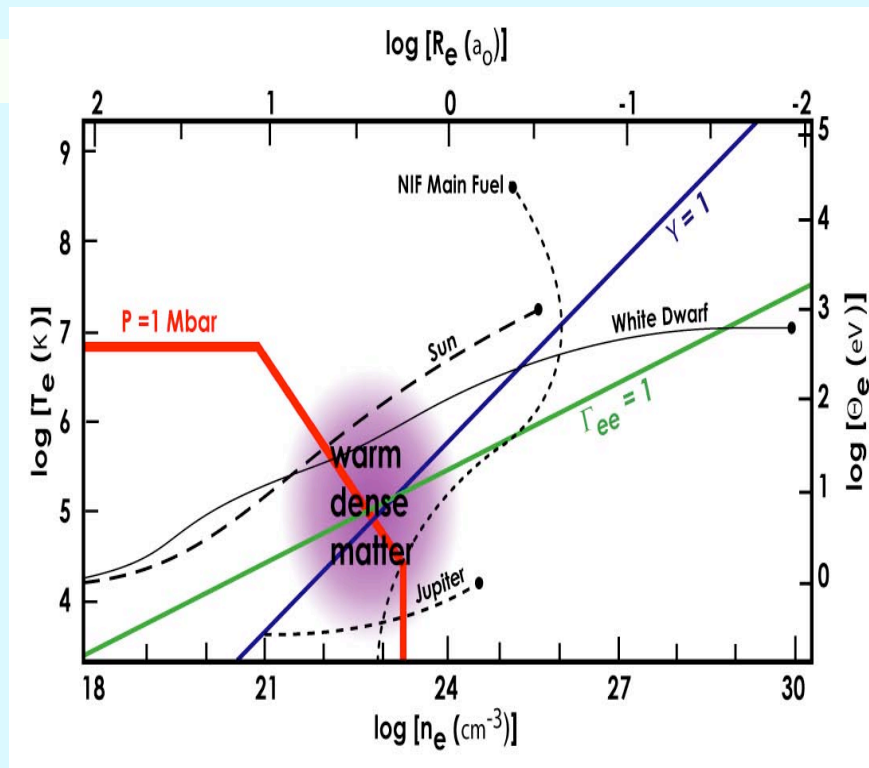


Giant & Extrasolar Planets

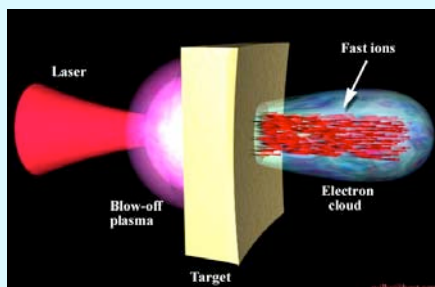
Applications



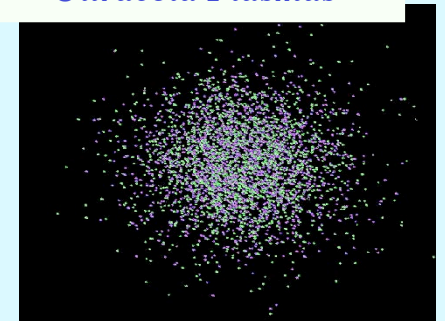
Stellar Atmospheres



High-energy Density Media



Ultracold Plasmas



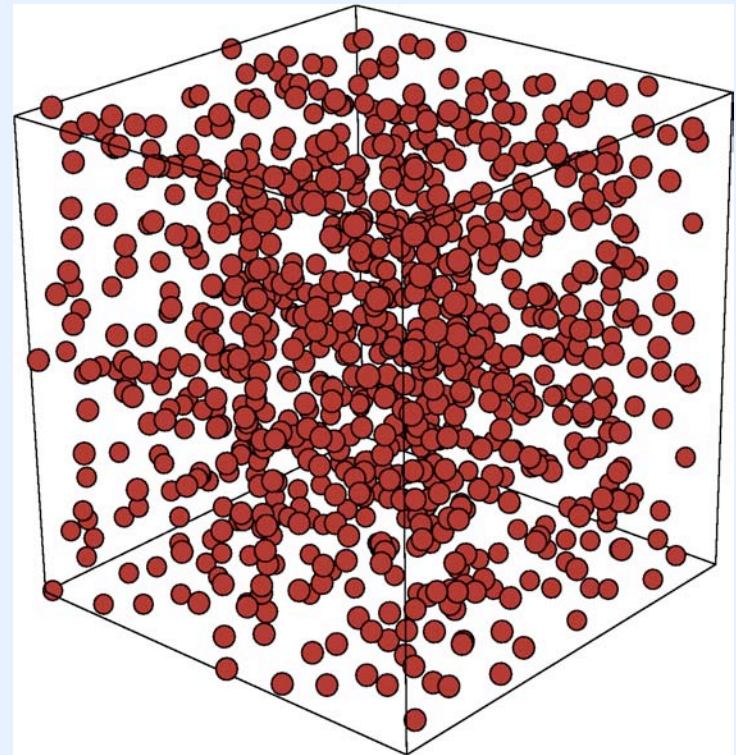
Quantum Simulations

snapshot

- **3D Periodic Cell: N atoms**
- **Born-Oppenheimer**
- **Electrons: Quantum mechanical treatment:**

$$H\Psi = E \Psi$$

*dissociation, association, ionization,
recombination*



Nuclear Motion: $F = ma$

Quantum Molecular Dynamics

Consistent set of Properties: $\{R_i, P_i\}$, $\Psi(r_i; R_i)$

- **Static:** EOS, pressure, internal energy
- **Dynamical:** Diffusion, thermal conductivity, viscosity
- **Optical:** Electrical conductivity, opacity, reflectivity

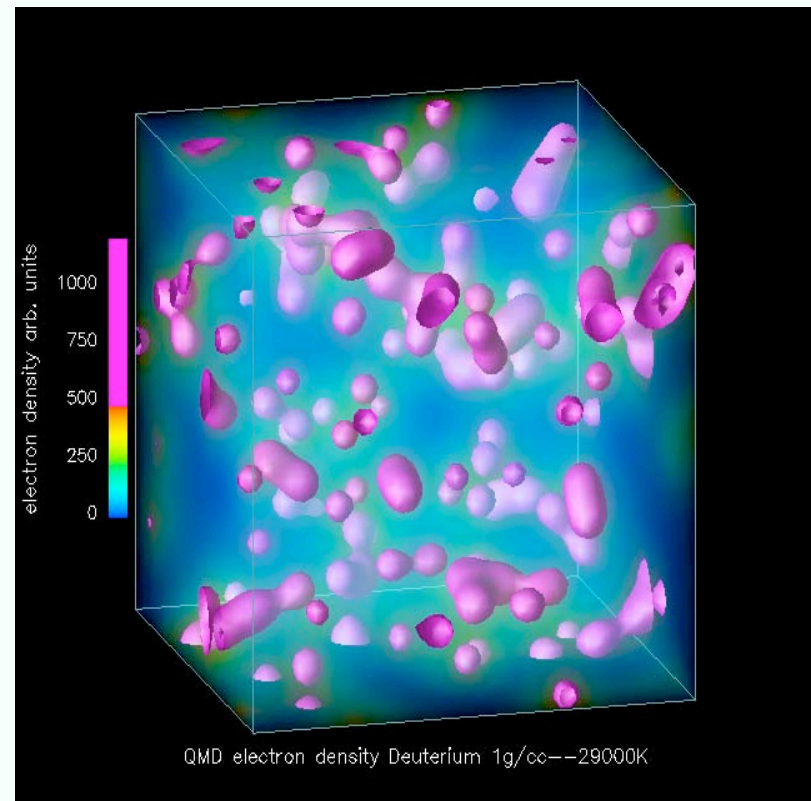
Quantum Simulations

- **Tight-Binding Molecular Dynamics (TB):**
Semi-empirical
- **Density Functional MD:** “ab initio” (DFT)
Local density (LDA),
Generalized Gradient Approximation (GGA),
Hybrid
- **Path Integral Monte Carlo (PIMC):**
Quantum statistical mechanic

Theory & Computation

Finite-Temperature Density Functional Theory

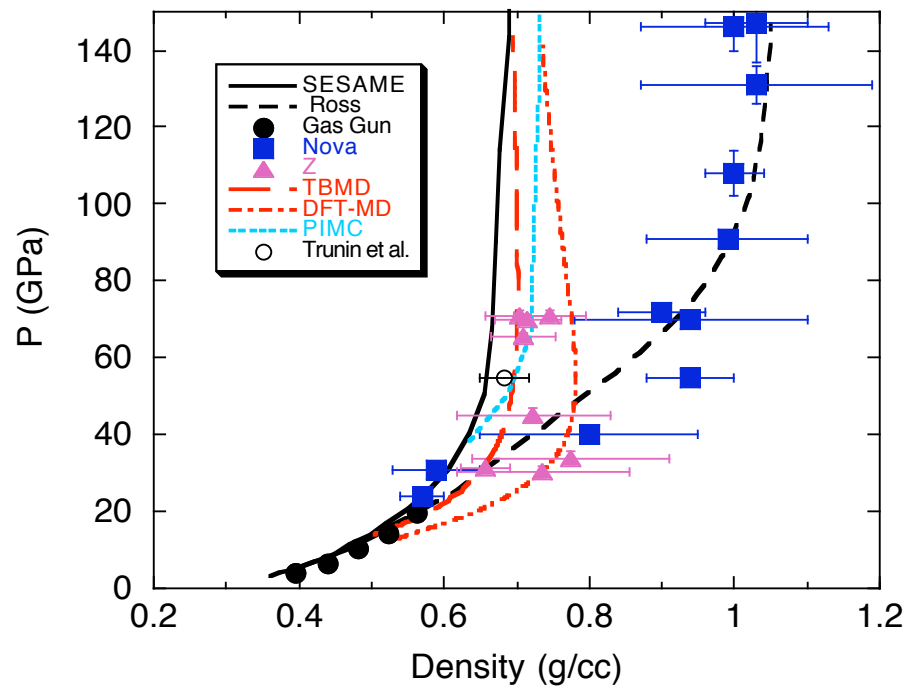
- Generalized Gradient Approximation (GGA)
- Plane-Wave Basis
- Pseudopotential (TM/Ultrasoft)
- Projector Augmented Wave (PAW)
- K-point integration
- LTE ($T_e = T_{ion}$)
- $N \sim 100 - 1000$



Natural Limits

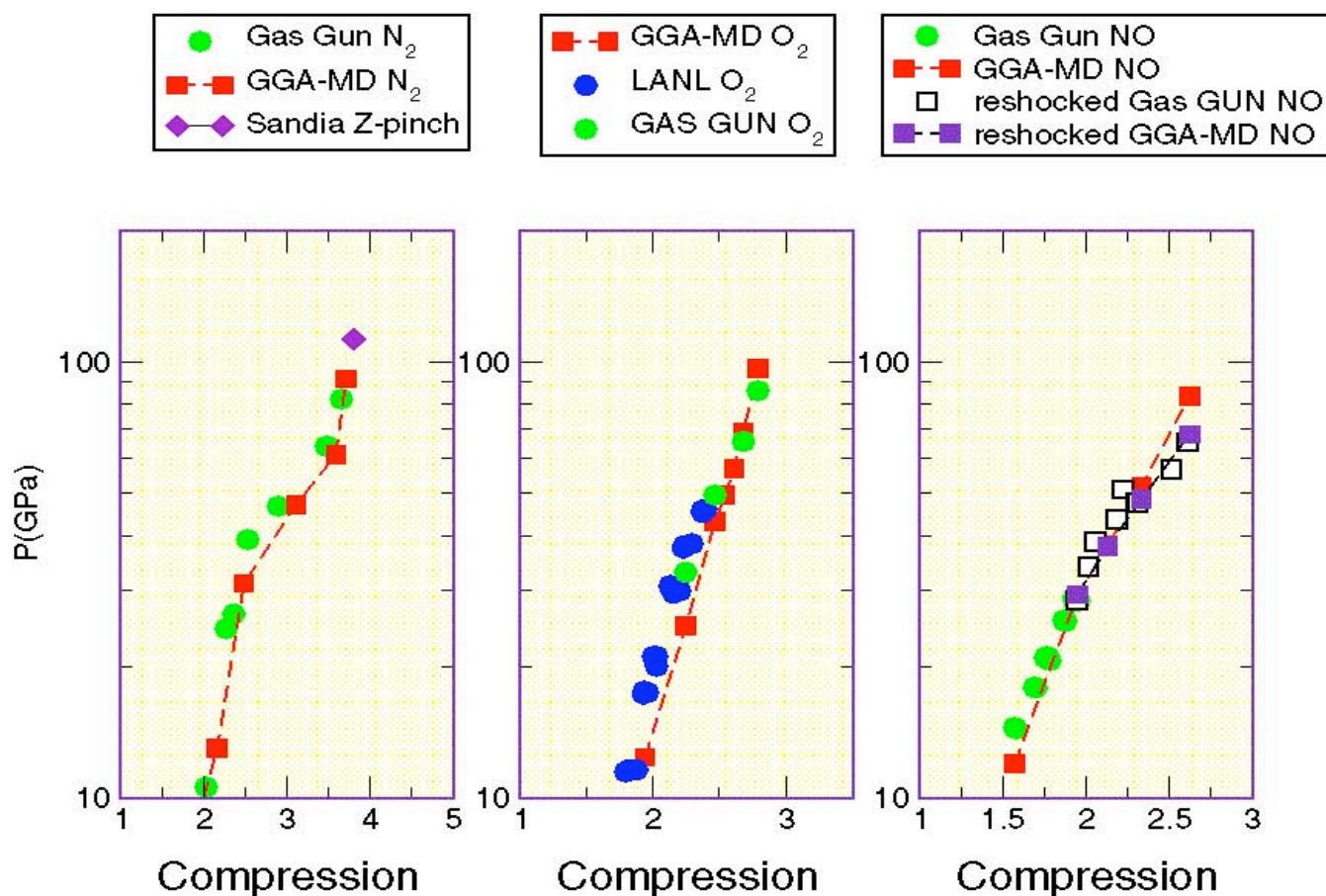
Static Properties

Deuterium Hugoniot

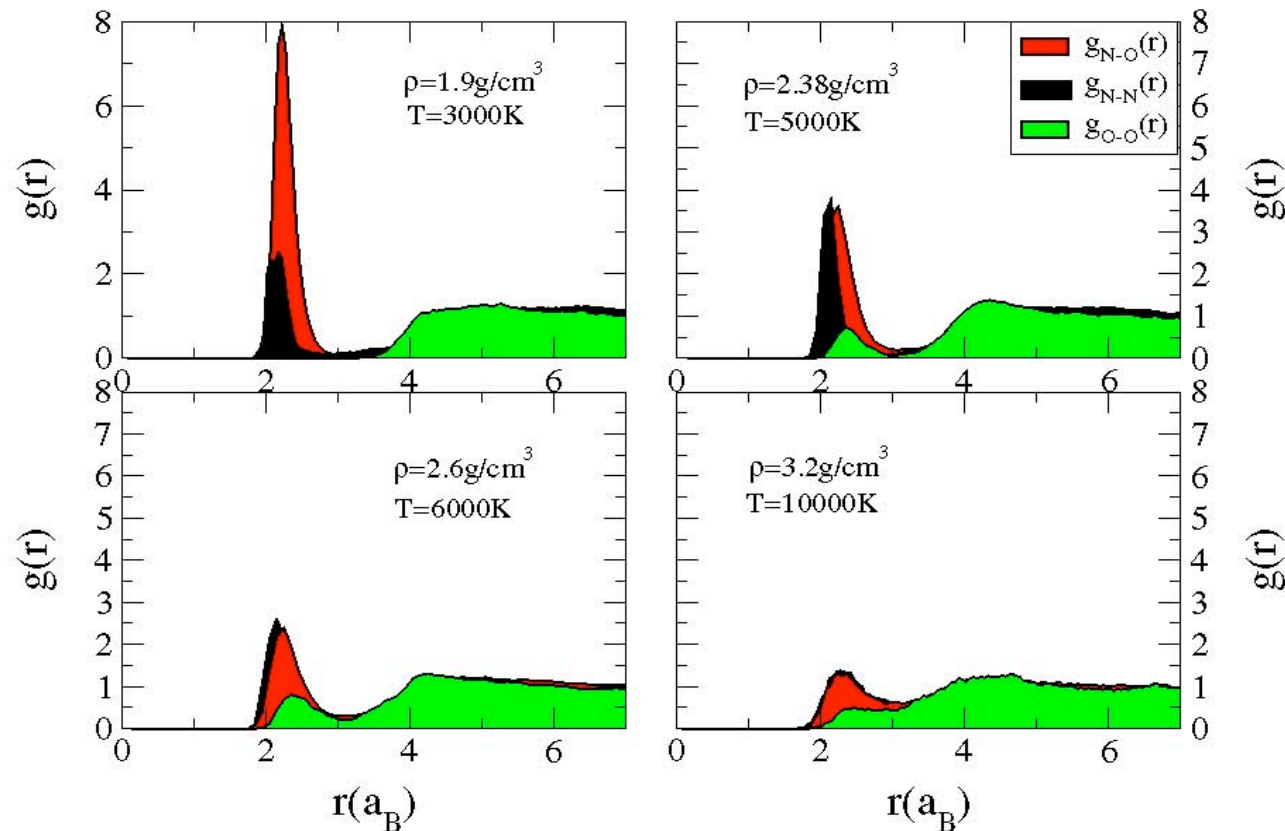


Hugoniot: N_2 , O_2 , NO

Validation: MD-DFT(GGA) and Experiment

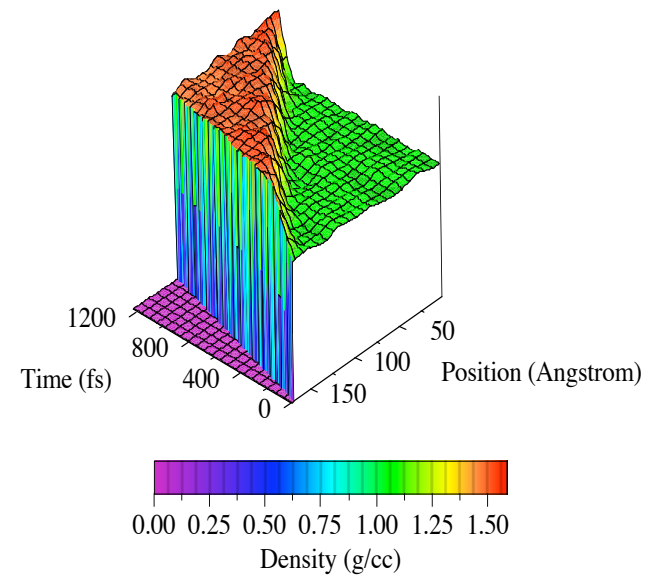
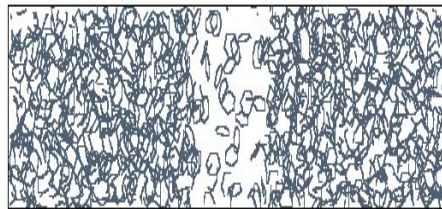
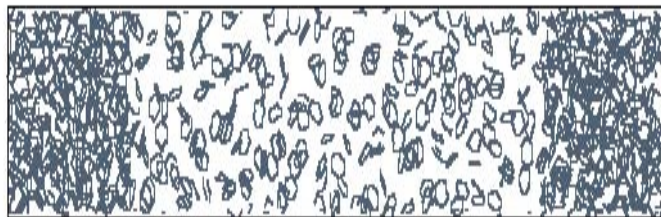
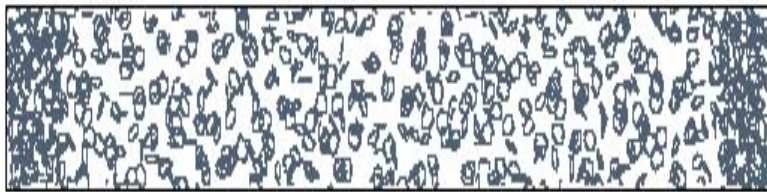


Composition along Principal Hugoniot

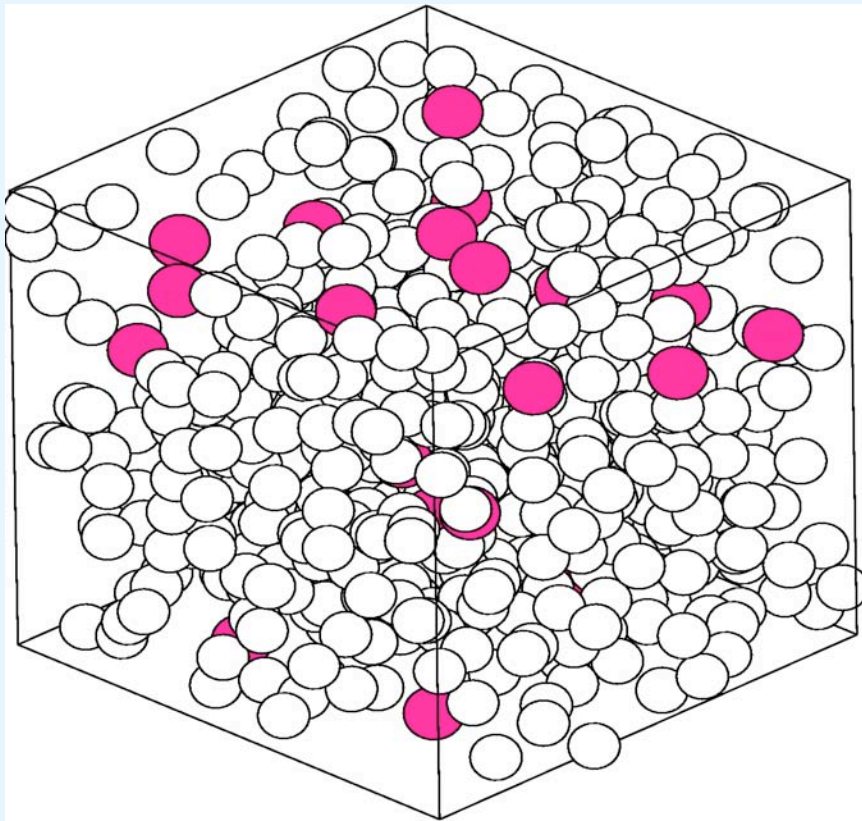


Mazevet, Blottiau, Kress, & Collins, Phys. Rev. B **69**, 224207 (2004)

Dynamical Properties:



Hydrogen/Titanium Mixtures



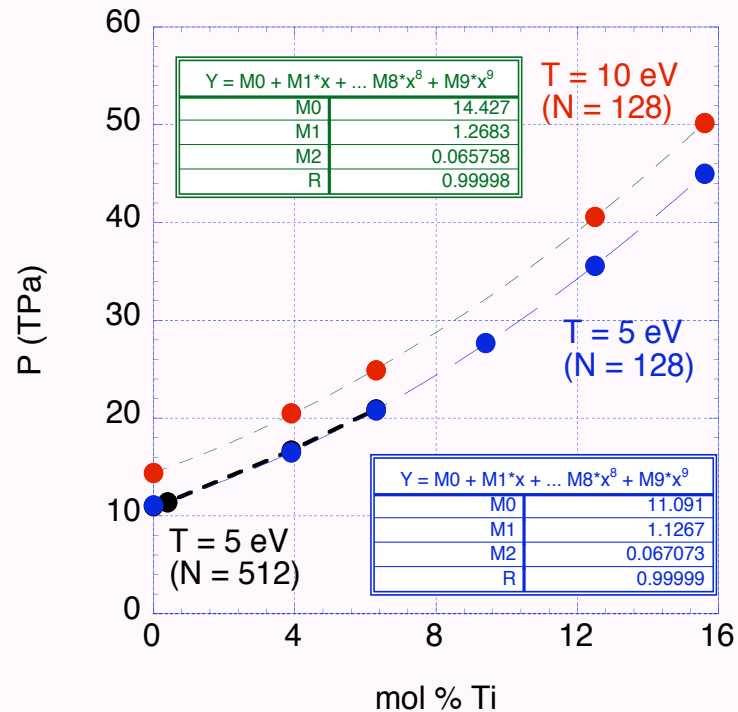
Density = 5g/cc

$\text{H}_{492}\text{Ti}_{20}$ (3.9% Ti)

Hydrogen/Titanium Mixtures

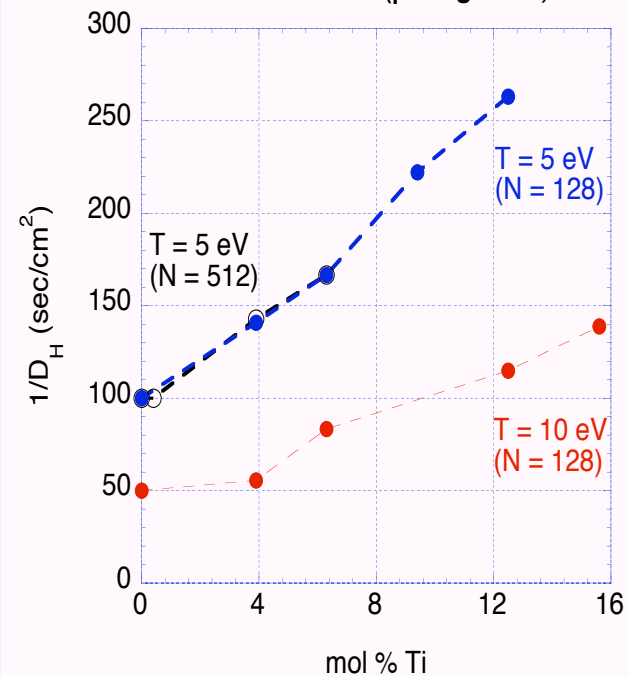
Equation of State

H/Ti "Plasma" ($\rho = 5 \text{ g/cm}^3$)



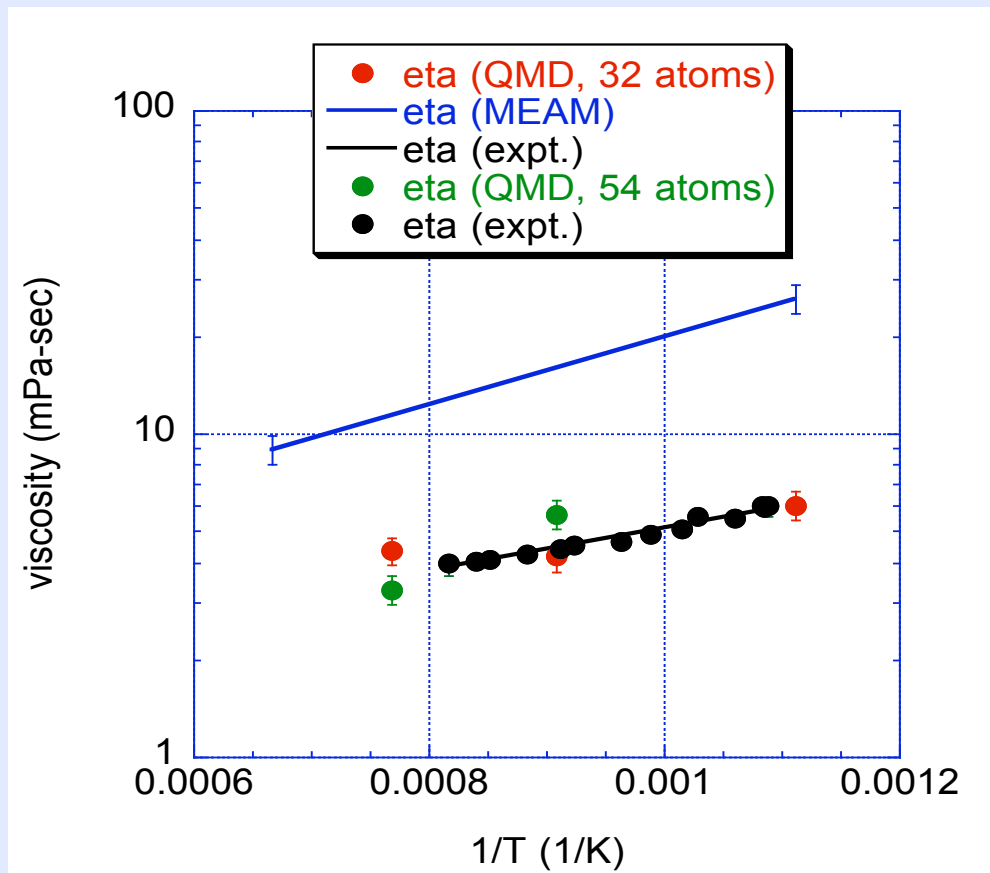
Inverse Hydrogen Self-Diffusion Coefficient

H/Ti "Plasma" ($\rho = 5 \text{ g/cm}^3$)

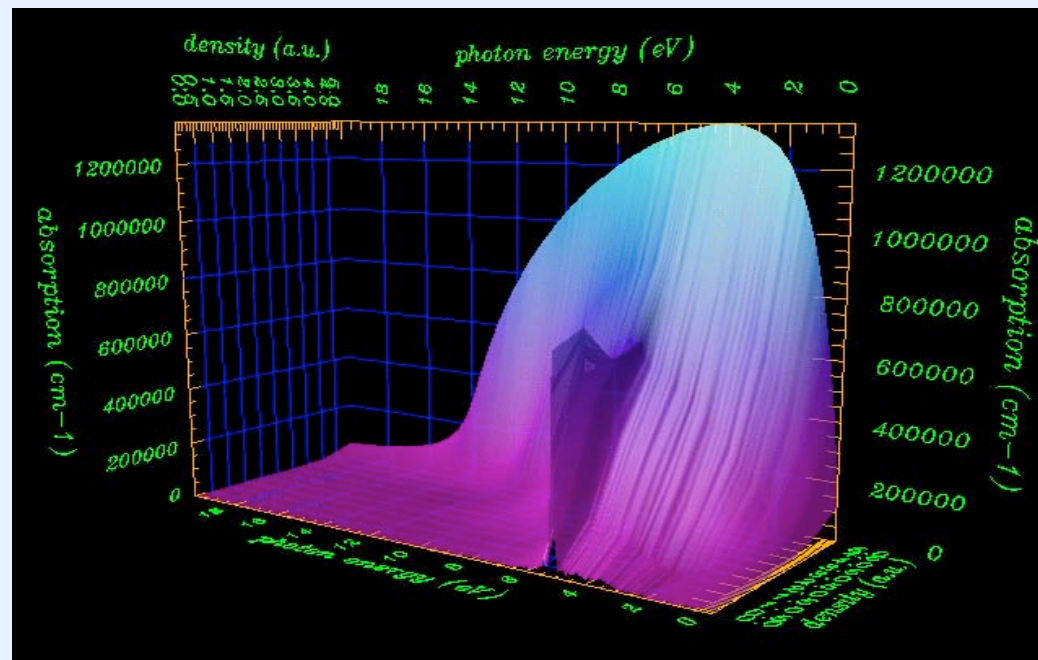


QMD: Pu Viscosity

$$\eta(T) = \frac{k_b T}{D(T) d} \times \text{constant}$$

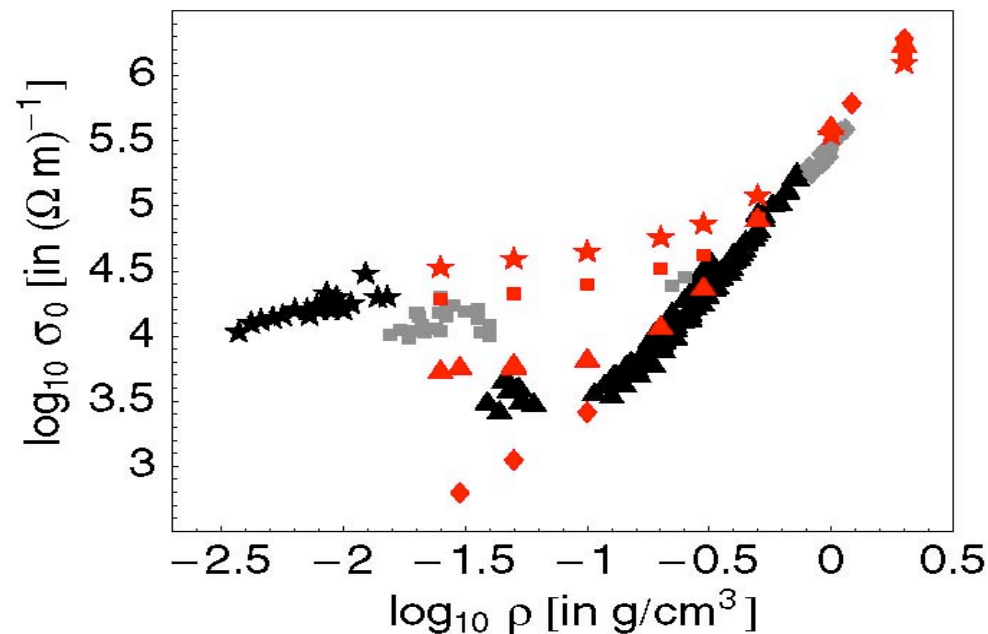


Optical Properties:



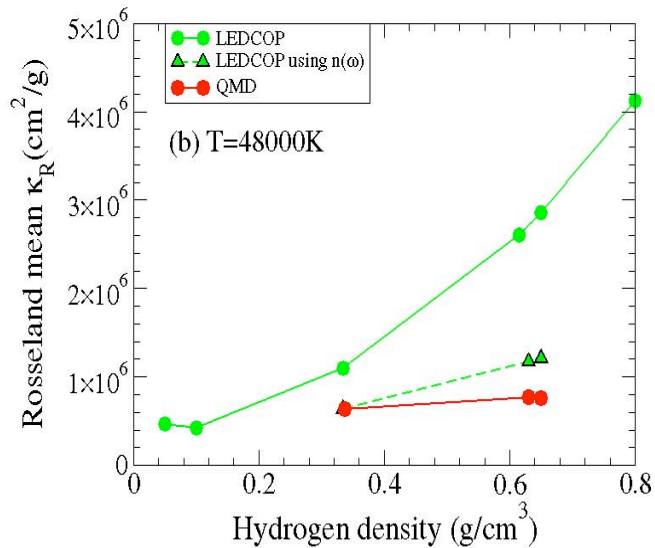
Aluminum: Electrical Conductivity

QMD vs Experiment



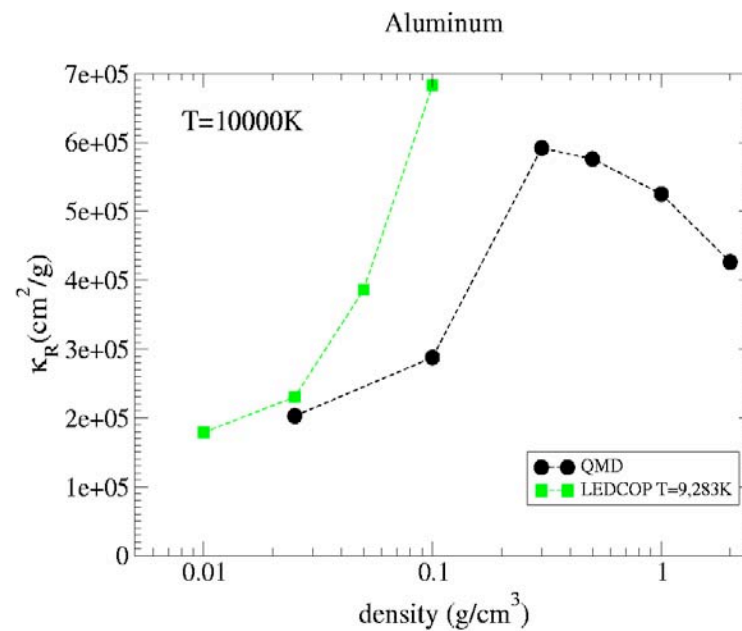
Mazevet , Desjarlais, Collins, Kress, & Magee, Phys. Rev. E **71**, 016409 (2005)

Rosseland Mean Opacity: QMD & LEDCOP



Hydrogen (H)

Aluminum (Al)



Mazevet, Collins, Magee, Kress, & Keady *Astron. Astrophys. Lett.* **405**, L5 (2003)

Future Directions:

- **Non-equilibrium**
[ion-electron coupling]
- **Optical properties**
[TDDFT/RPA]
- **External Fields**
- **Experimental Validation**
- **Predictive capabilities:**
new regimes

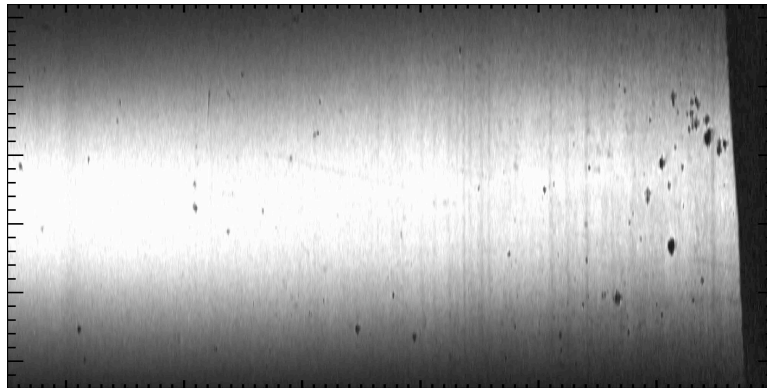




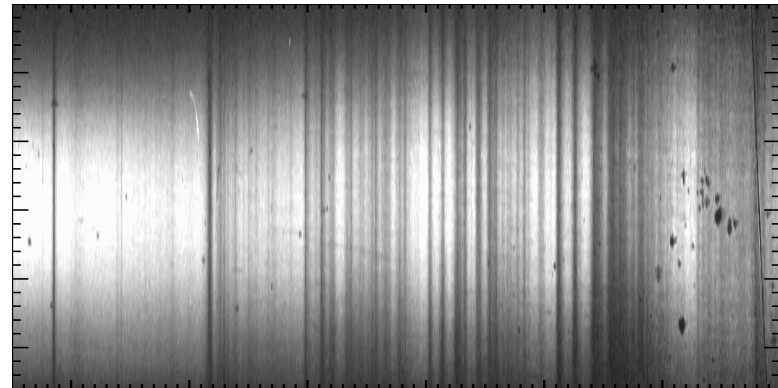
Opacity measurements at Z

Opacity Workshop
Los Alamos National Laboratory
May 5, 2005

without Fe



with Fe + Mg



J. E. Bailey (jebaile@sandia.gov)



Many people contribute to this work

G.A. Rochau, R.B. Campbell, G.A. Chandler, J. McKenney, and T.A. Mehlhorn

{Sandia National Laboratories, Albuquerque, New Mexico}

J.J. MacFarlane, P. Wang, I.E. Golovkin D. Haynes

{Prism Computational Sciences, Madison, Wisconsin}

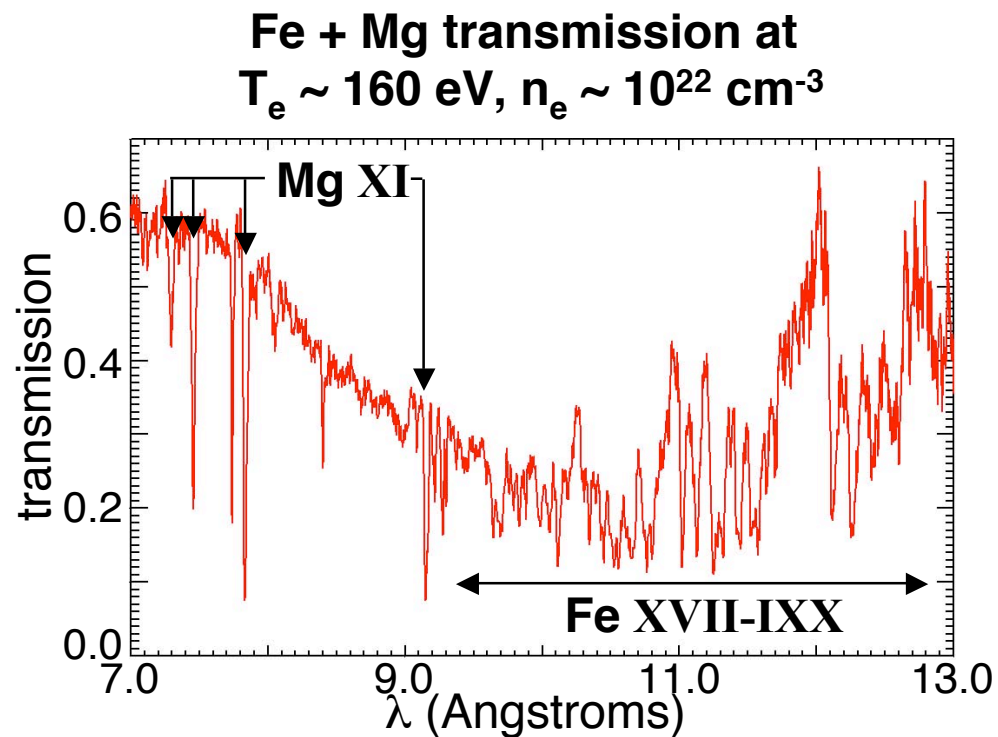
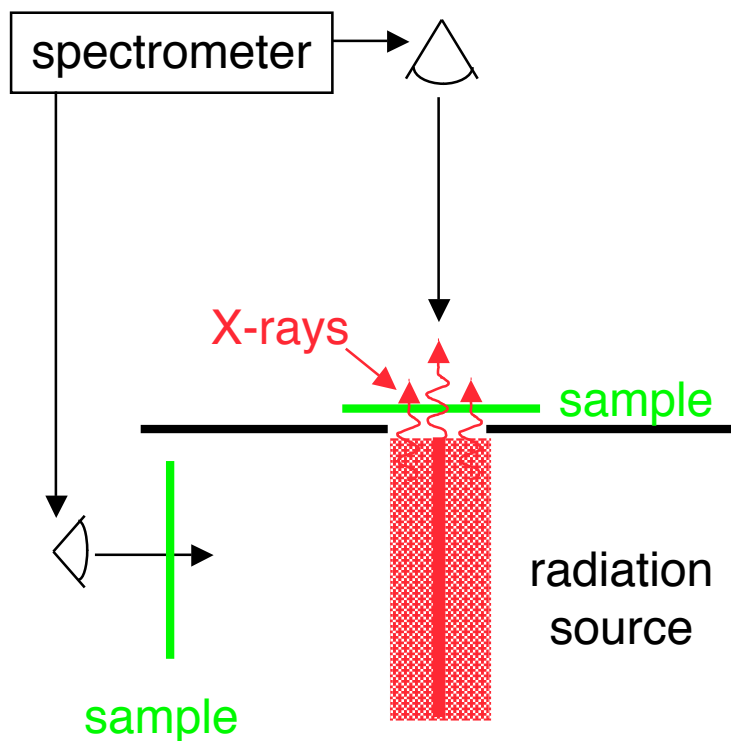
R.C. Mancini

{University of Nevada, Reno, Nevada}

M. Bump, O. Garcia, J.M. Lucas, T.C. Moore

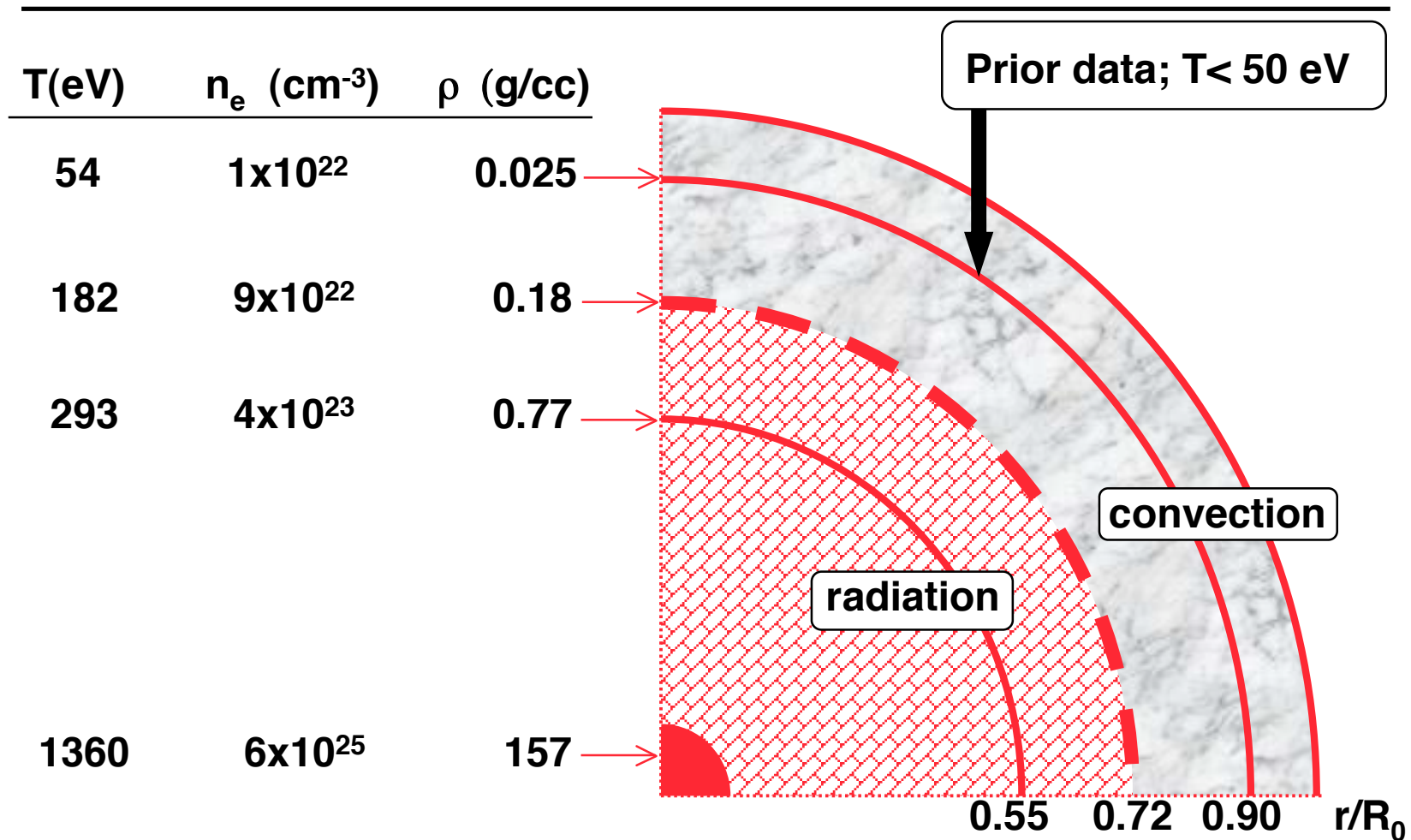
{K-Tech Corp., Albuquerque, New Mexico}

Z opacity experiments strengthen existing database and extend measurements beyond $T \sim 150$ eV





Laboratory opacity measurements at stellar interior conditions are not presently available



Solar model : J.N. Bahcall et al, Rev. Mod. Phys. 54, 767 (1982)



Mid-Z and high-Z opacities are important for many HEDP physics problems

- **ICF ablaters, e.g., Cu-doped Be or Ge-doped CH at T_e up to 300 eV**
- **Z-pinch radiation, e.g., tungsten at $T_e > 100$ eV**
- **Published laboratory opacity measurements at $T > 70$ eV are unavailable (non-existent?)**

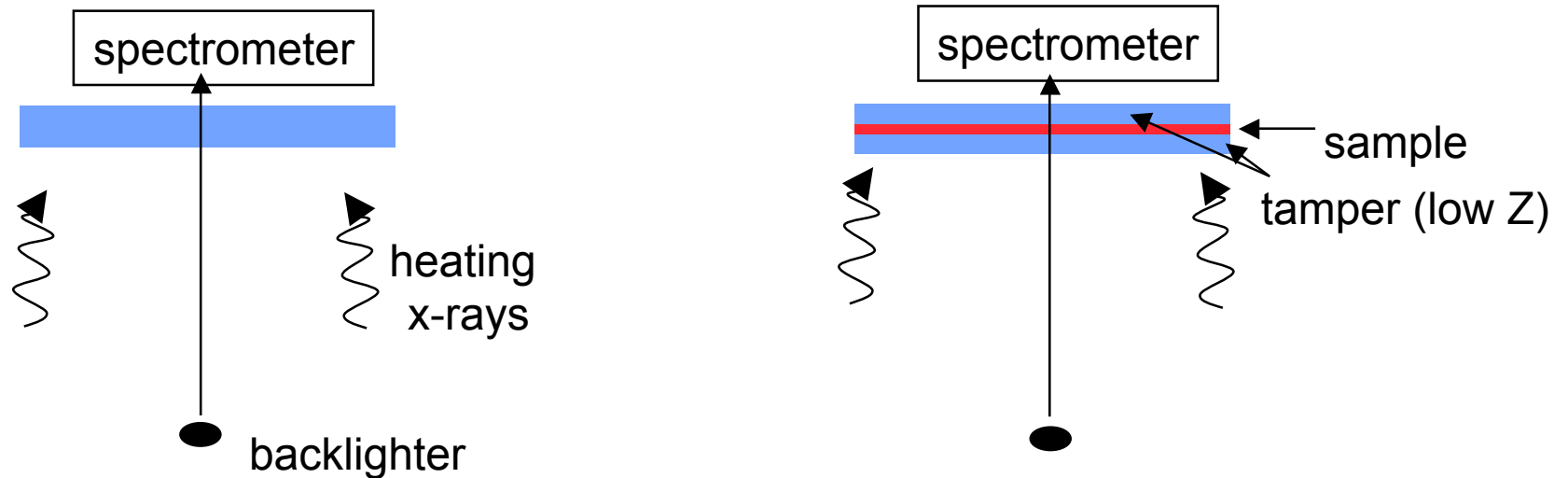


Mid-Z elements pose a challenge for opacity calculations

- Charge state distribution (spectroscopic accuracy)
- What transitions must be included?
- What approximations for configuration and transition grouping?
- What line broadening?



Anatomy of an opacity experiment



Comparison of unattenuated and attenuated spectra determines transmission
 $T = \exp -\{\mu\rho x\}$



Desirable features of an opacity experiment

- **Sample spatial uniformity (thin, large lateral size, thick tamper)**
- **Minimal temporal variations during probe time (backlight short compared to heating x-ray variation)**
- **Steady state (long duration heating x-rays)**
- **Temperature and density measurements (large wavelength range to enable simultaneous low Z and high Z measurements)**

Characteristics of Z x-ray source can promote quality measurements



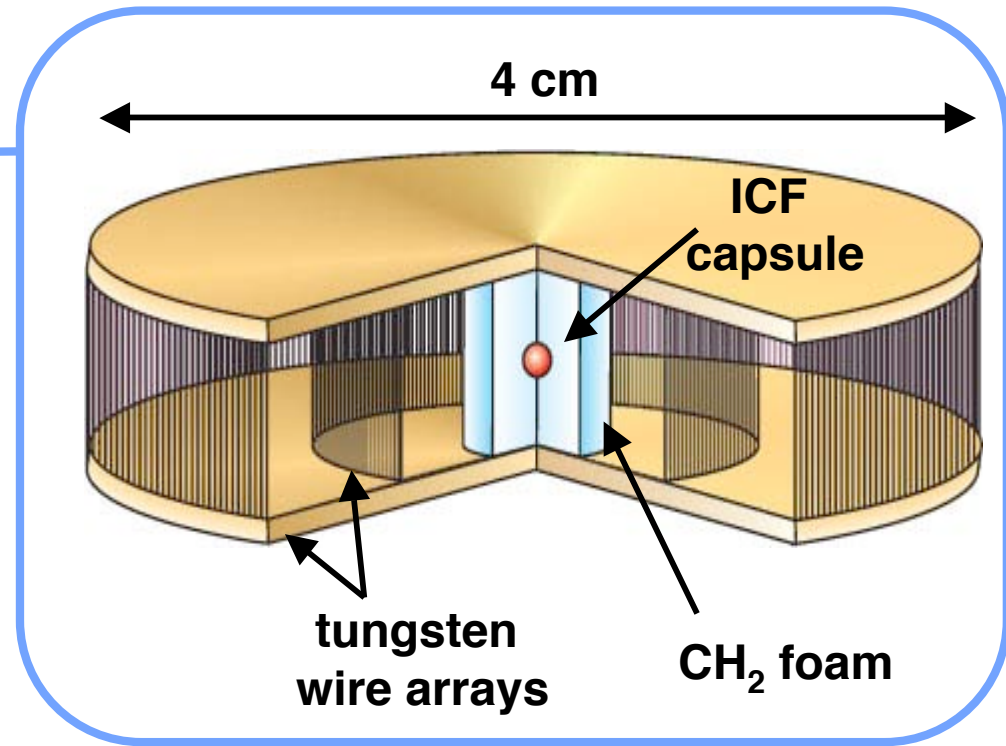
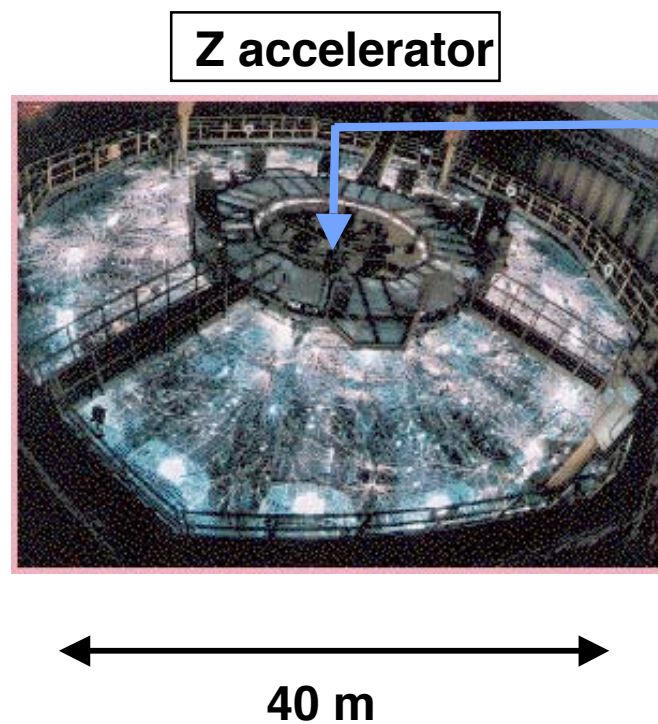
Possible experiment flaws can be evaluated from the scaling of transmission with sample thickness

Potential experiment problems:

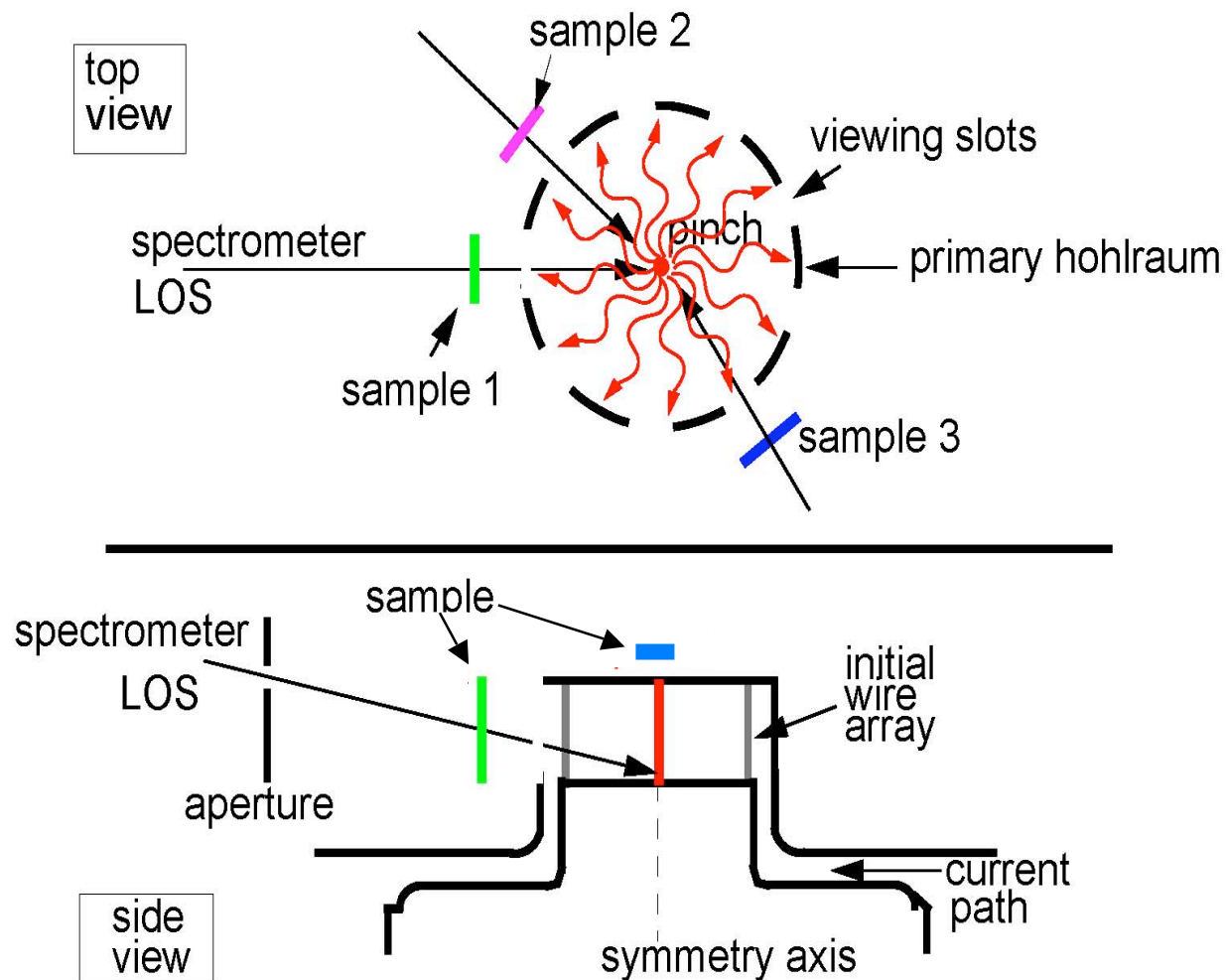
- Sample may not be cartoon-like (pinholes, columnar structure)
- Sample composition or areal density may not match specifications (oxidation, contamination)
- Sample self emission may alter apparent transmission
- Conversion of film density to film exposure may be inaccurate
- Background subtraction incorrect
- Crystal defects may introduce artificial spectral features or mask actual features
- Lines may saturate

All of these problems cause transmission to deviate from expected scaling with thickness : $T_1 = T_2^{(x1/x2)}$

Opacity experiments can exploit the intense radiation provided by the Z accelerator



We have used two different opacity experiment configurations at Z





Each opacity experiment configuration offers advantages and disadvantages

Side-on:

- Multiple large samples exposed in a single experiment
- Many opportunities for ride alongs
- Temperature limited to ~ 50 eV or less

End-on:

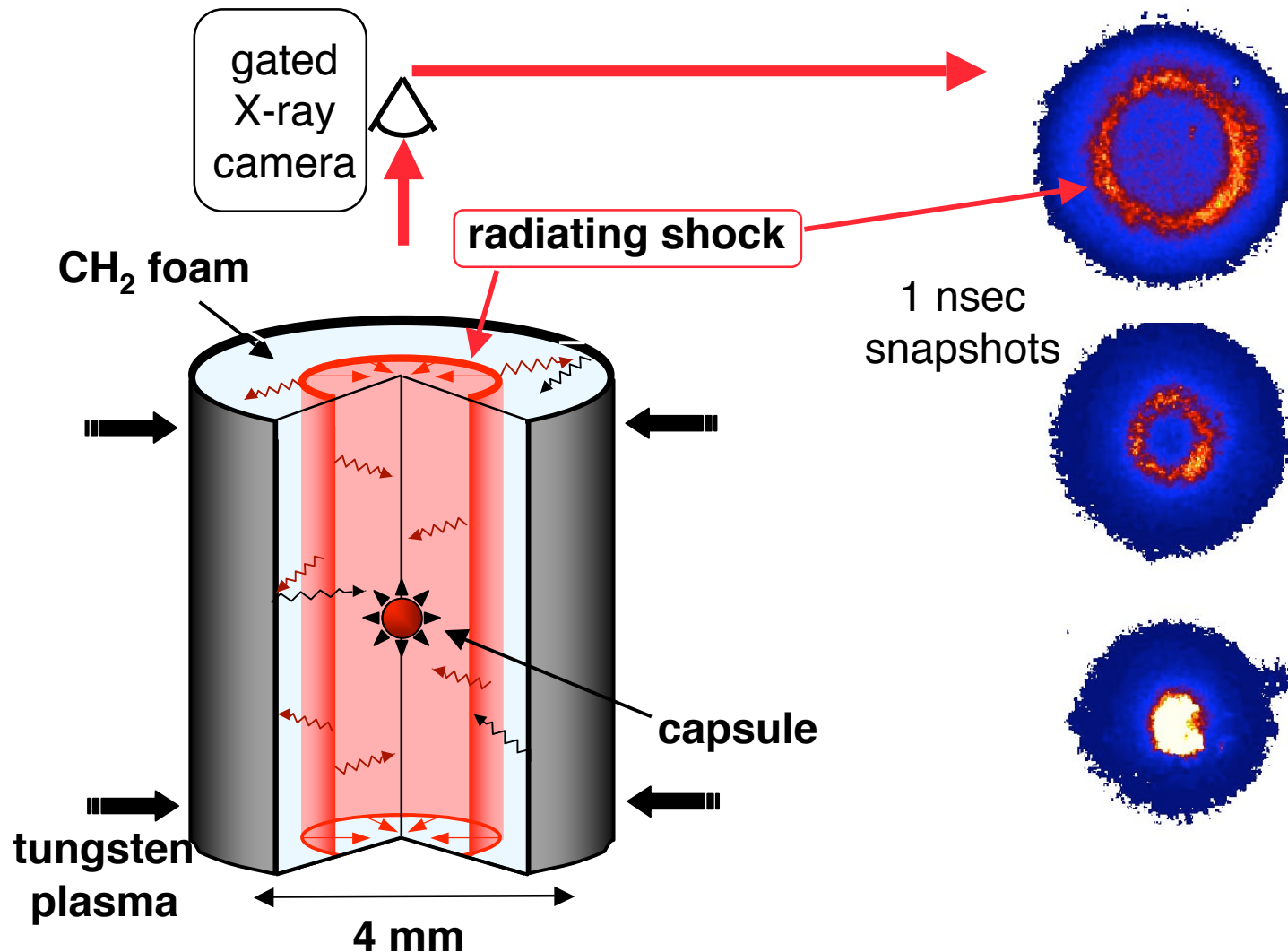
- Single sample exposed in each experiment
- Relatively rare opportunities for ride alongs
- Temperatures above ~ 150 eV can be reached

Other configurations are feasible, but not yet demonstrated on Z

- External hohlraum (Springer et al., JQSRT 58, 927 (1997))
- Interior of dynamic hohlraum (Bailey et al, 2005)

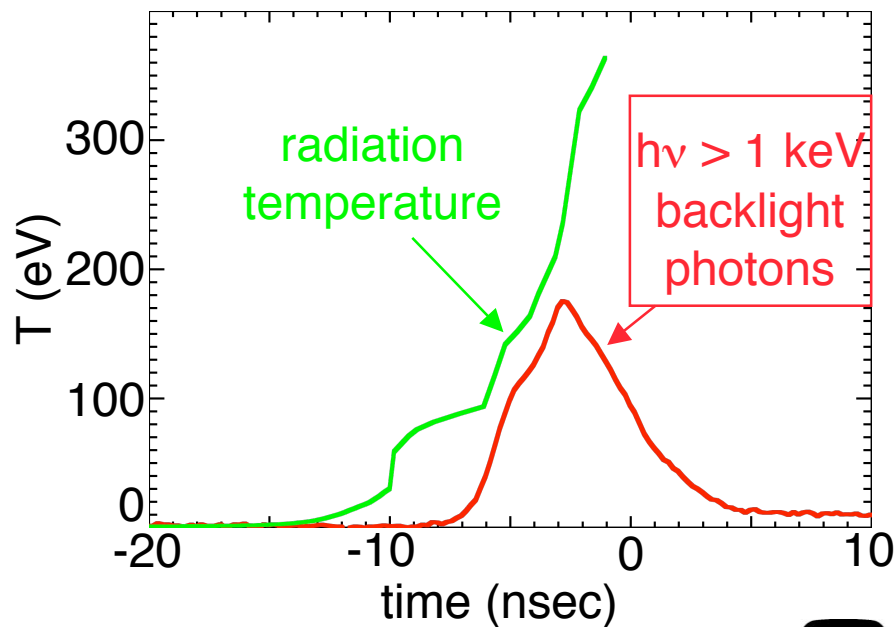
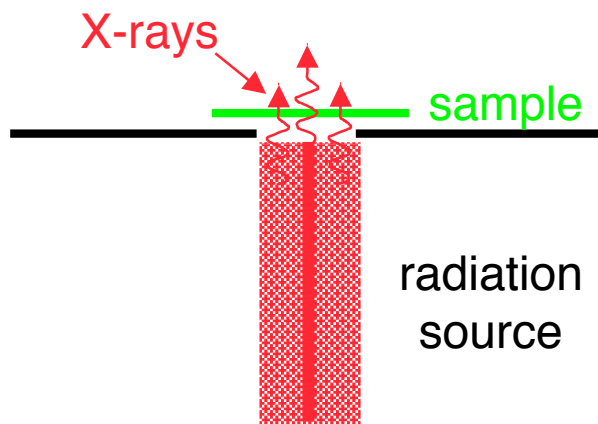
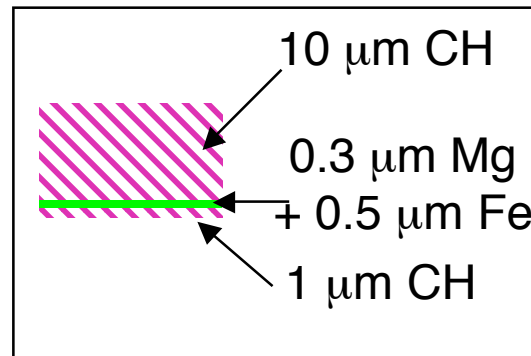
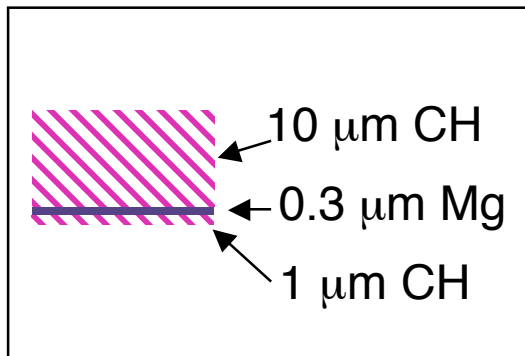
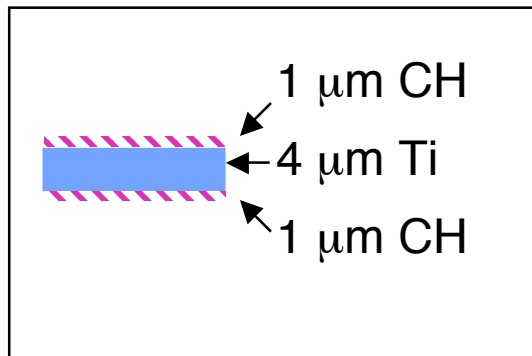


Dynamic hohlraum radiation source is created by accelerating a tungsten plasma onto a low Z foam

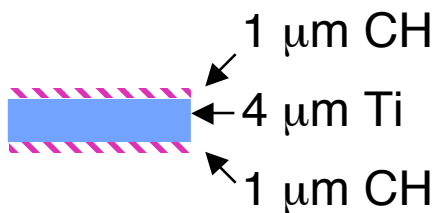
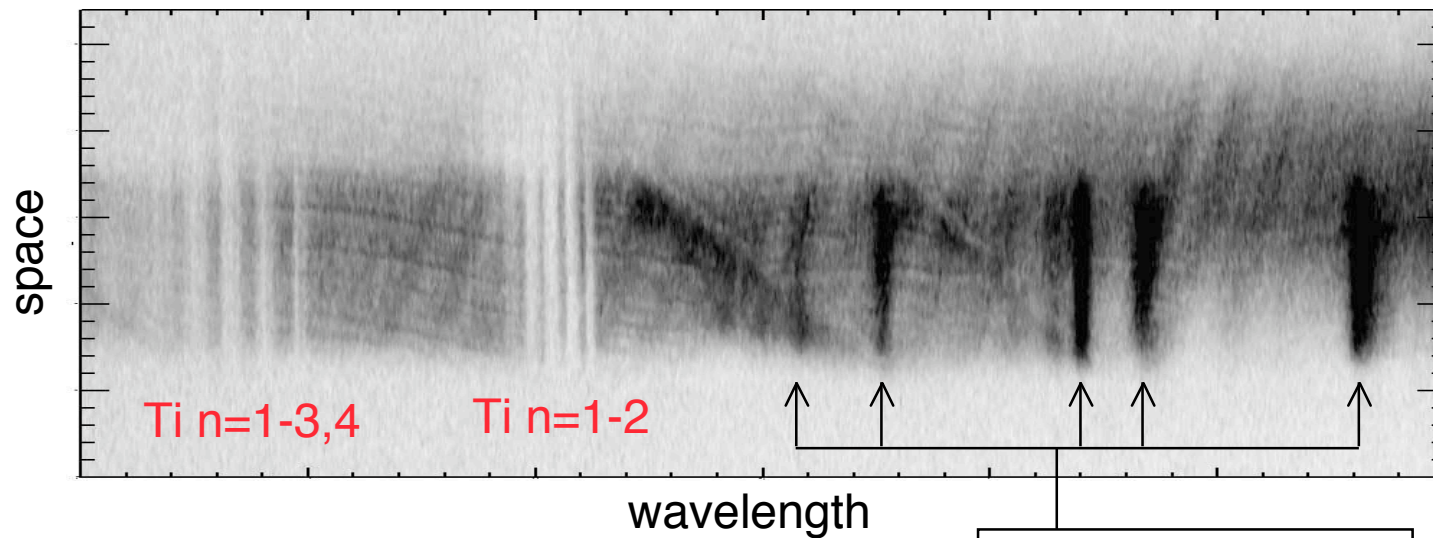




The radiation source heats and backlights the sample



Opacity measurements were strongly suggested by Ti symmetry foil absorption spectra

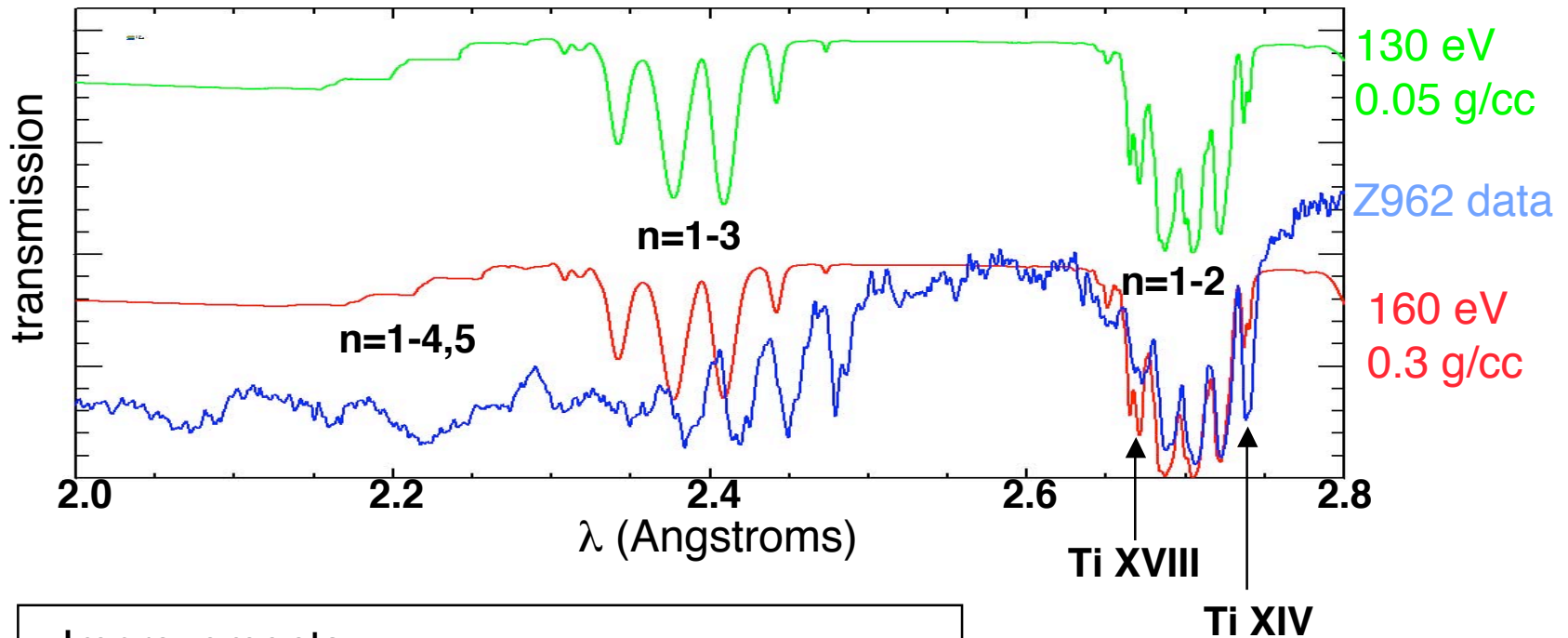


This demonstrates:

- Foils reach interesting conditions
- Self backlight source is very bright



Ti absorption spectra are a rich opportunity for atomic physics, despite lack of optimization

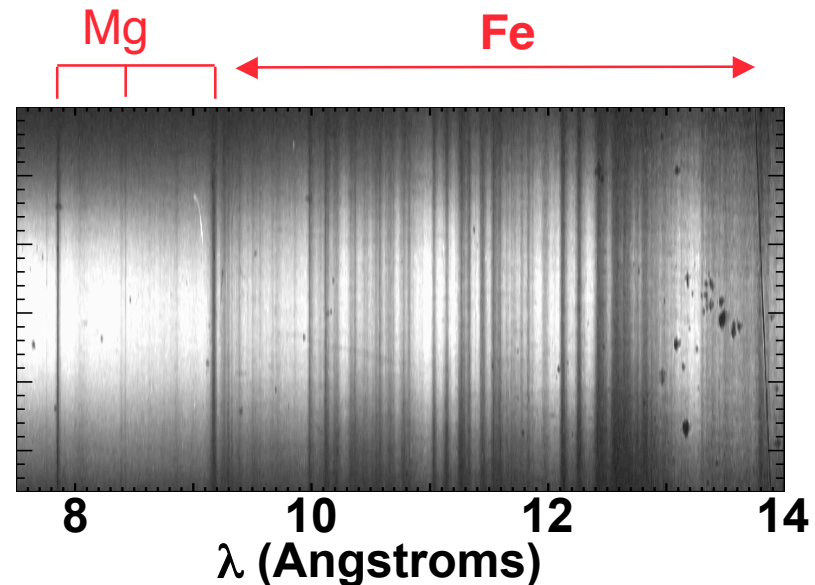
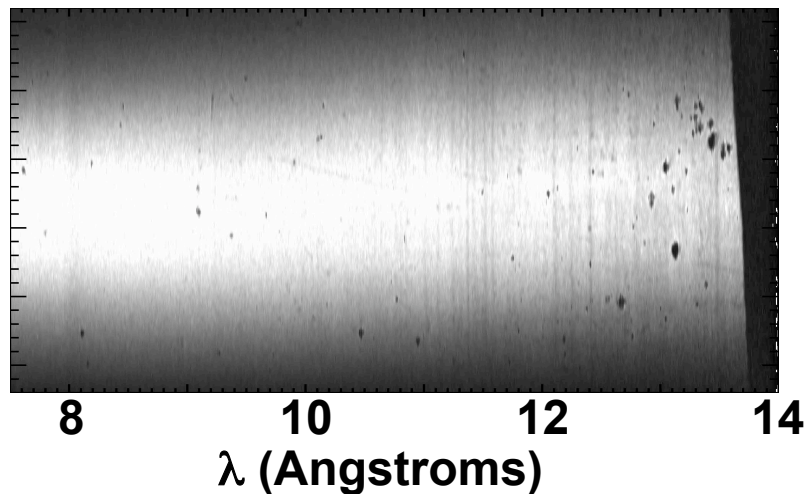
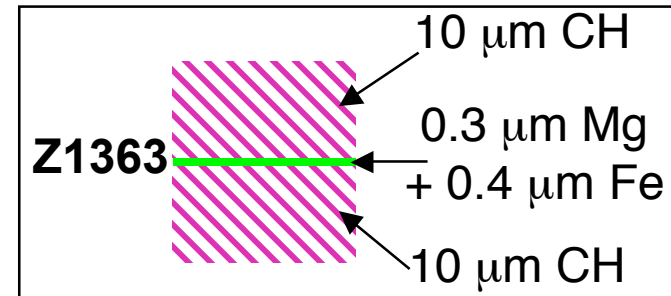
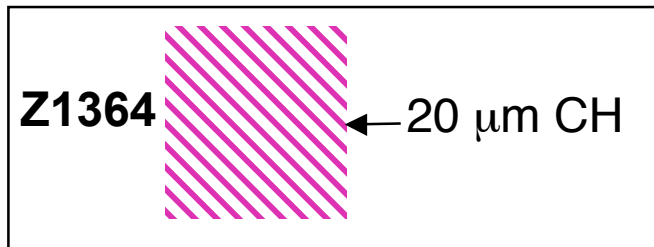


Improvements:

- Mixtures to obtain T, r diagnosis
- Reduced thickness to improve uniformity
- Better crystal quality



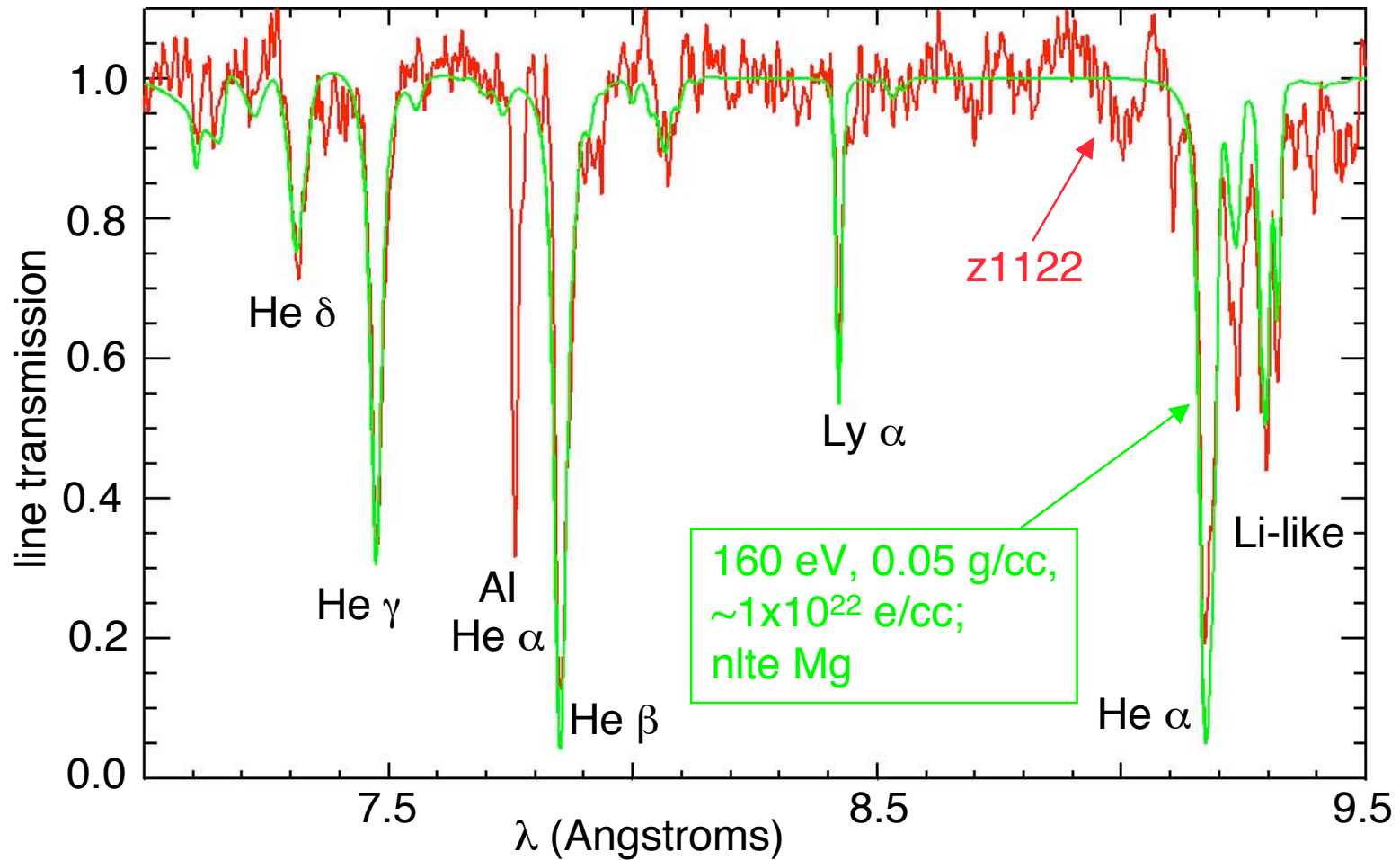
L-shell Fe absorption features have been successfully recorded



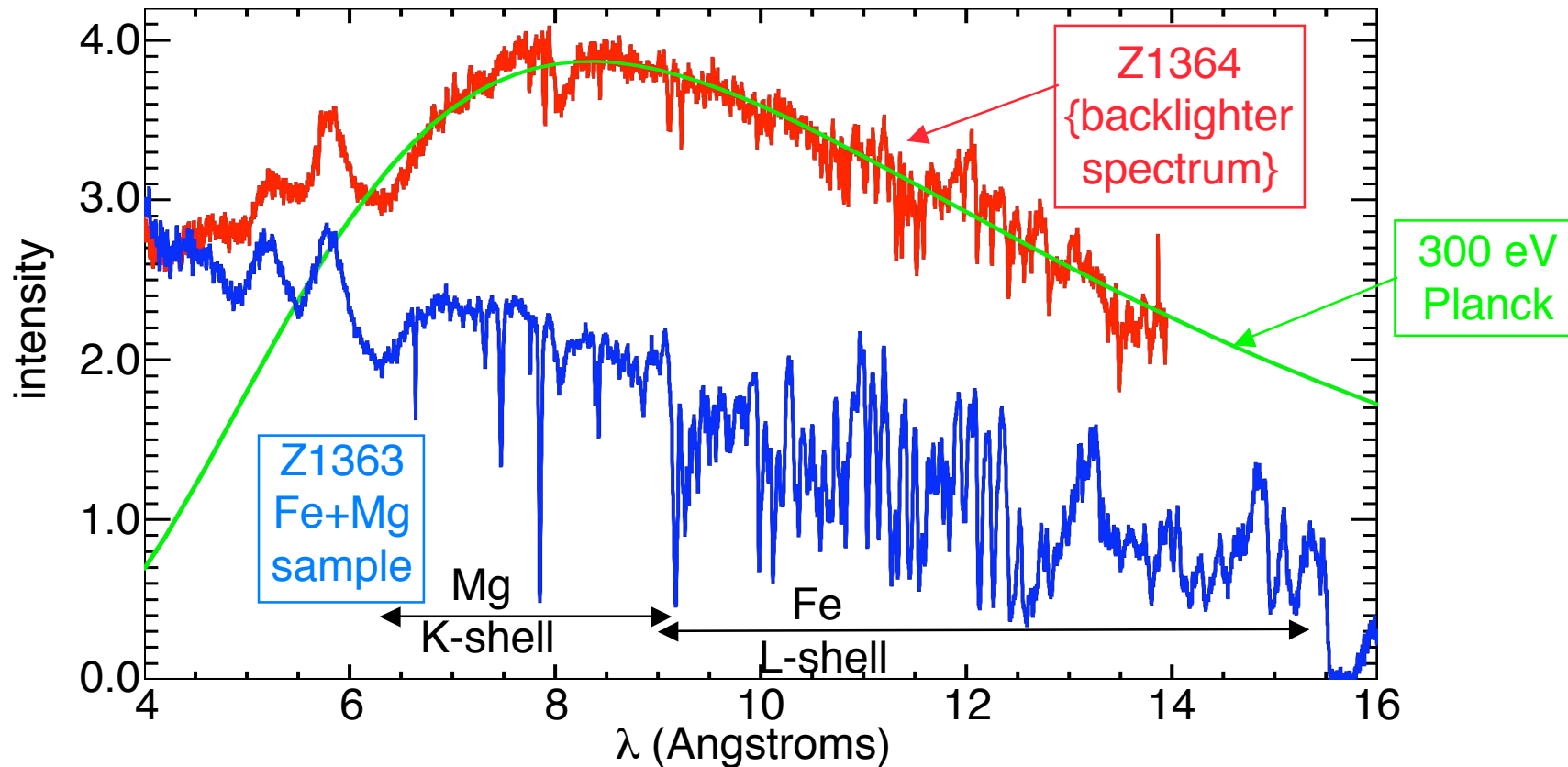
One pair of Z experiments determines the Fe + Mg transmission



The sample conditions are diagnosed from Mg absorption spectra



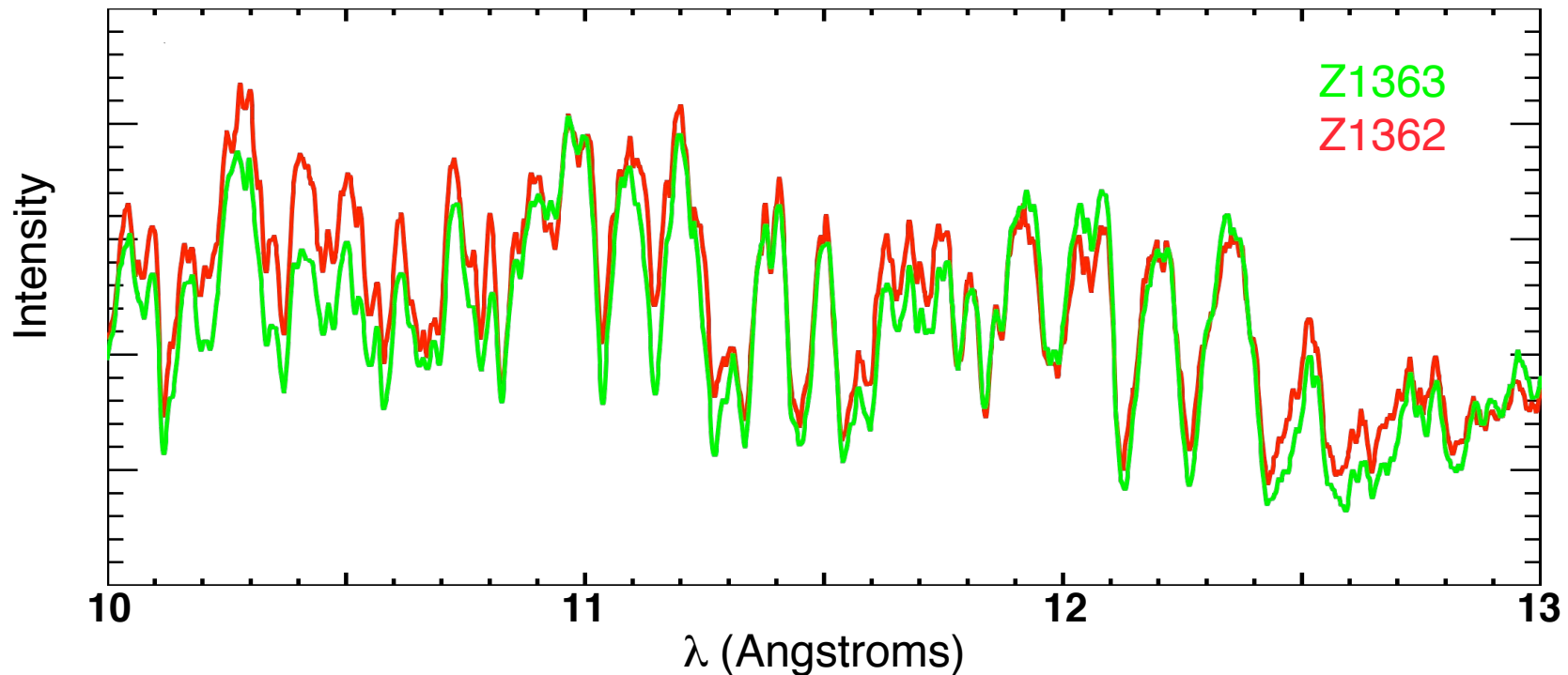
Experiments with and without Fe enable determination of the Fe transmission



- The difference between z1363 & z1364 is the Fe+Mg transmission
- Assuming shot to shot reproducibility

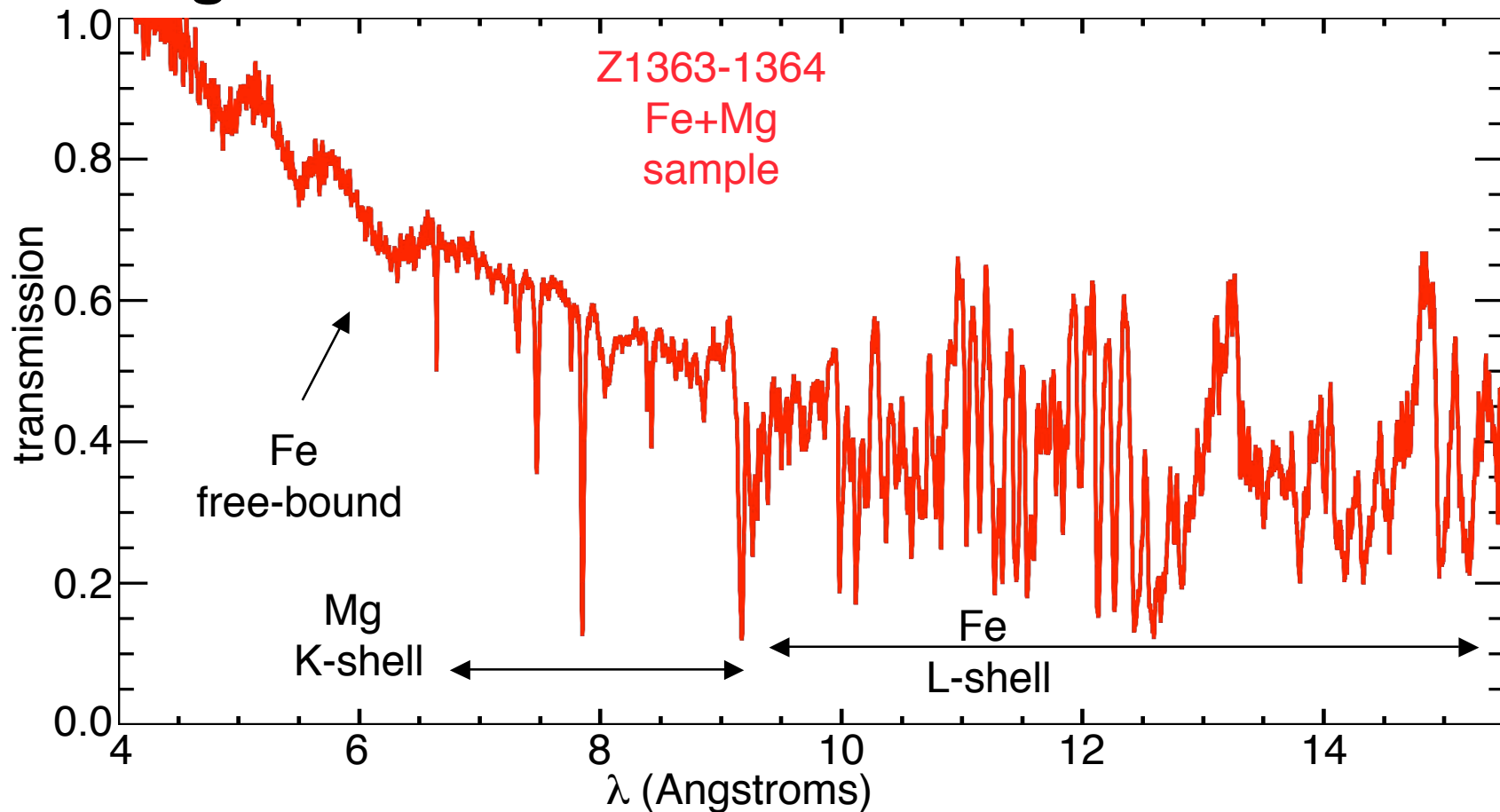


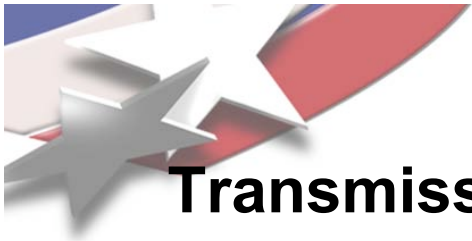
The shot to shot reproducibility is good, if conditions are carefully controlled



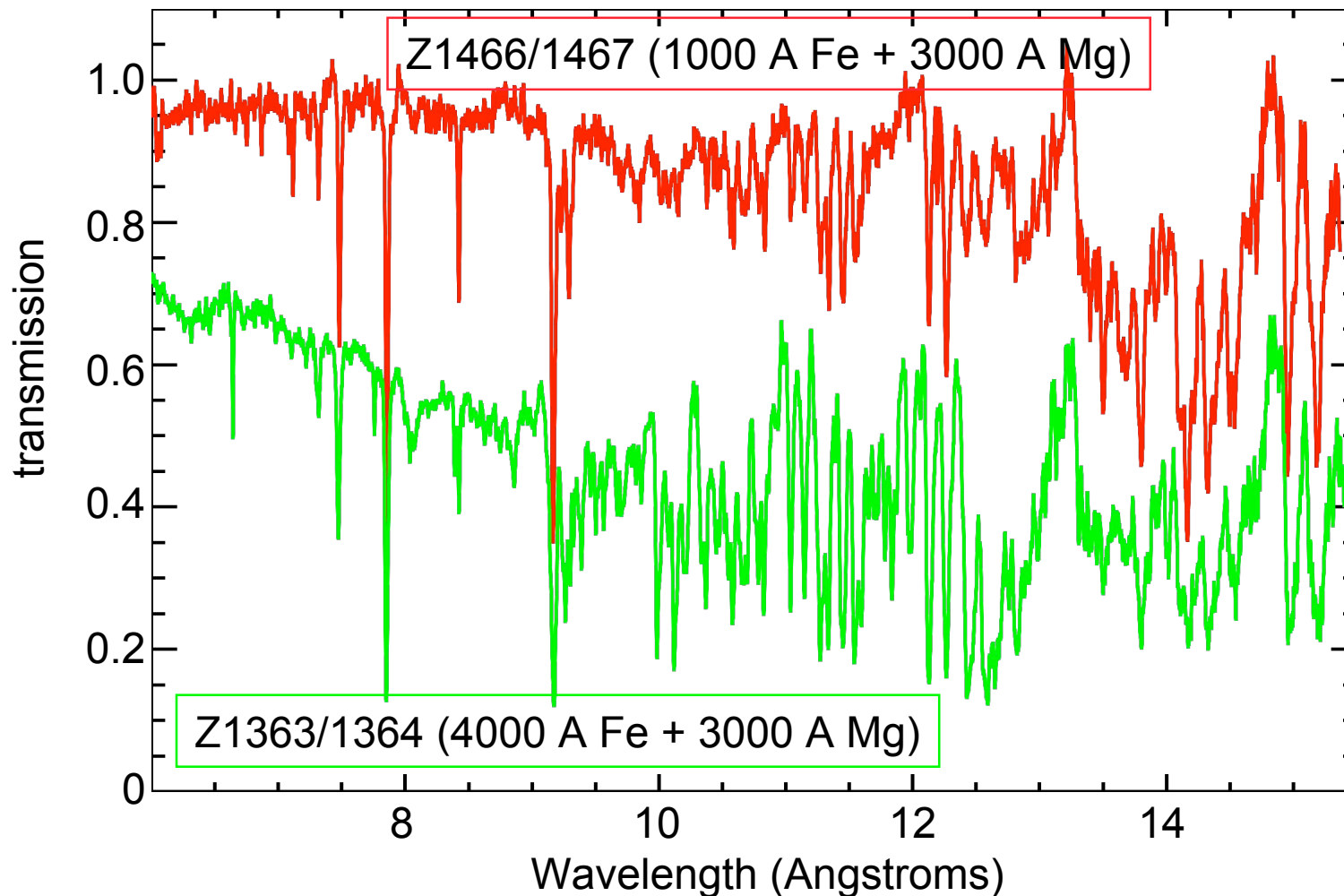
- Both experiments used 10 μm CH | 0.3 μm Mg + 0.4 μm Fe | 10 μm CH sample
- No scaling was applied for this comparison
- Reproducibility is approximately 10% or better over this wavelength range

The dynamic hohlarum backlighter measures transmission over a very broad λ range



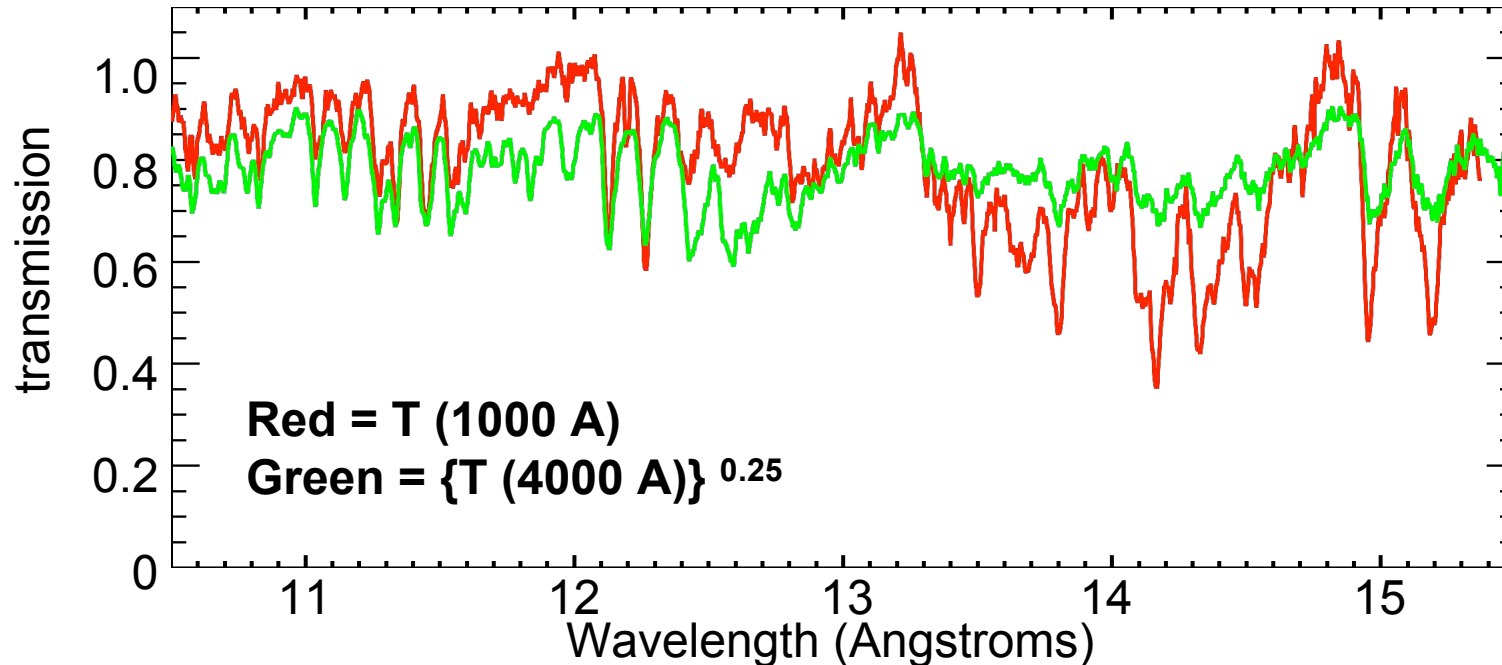


Transmission for two Fe thicknesses under similar T_e and n_e conditions has been measured





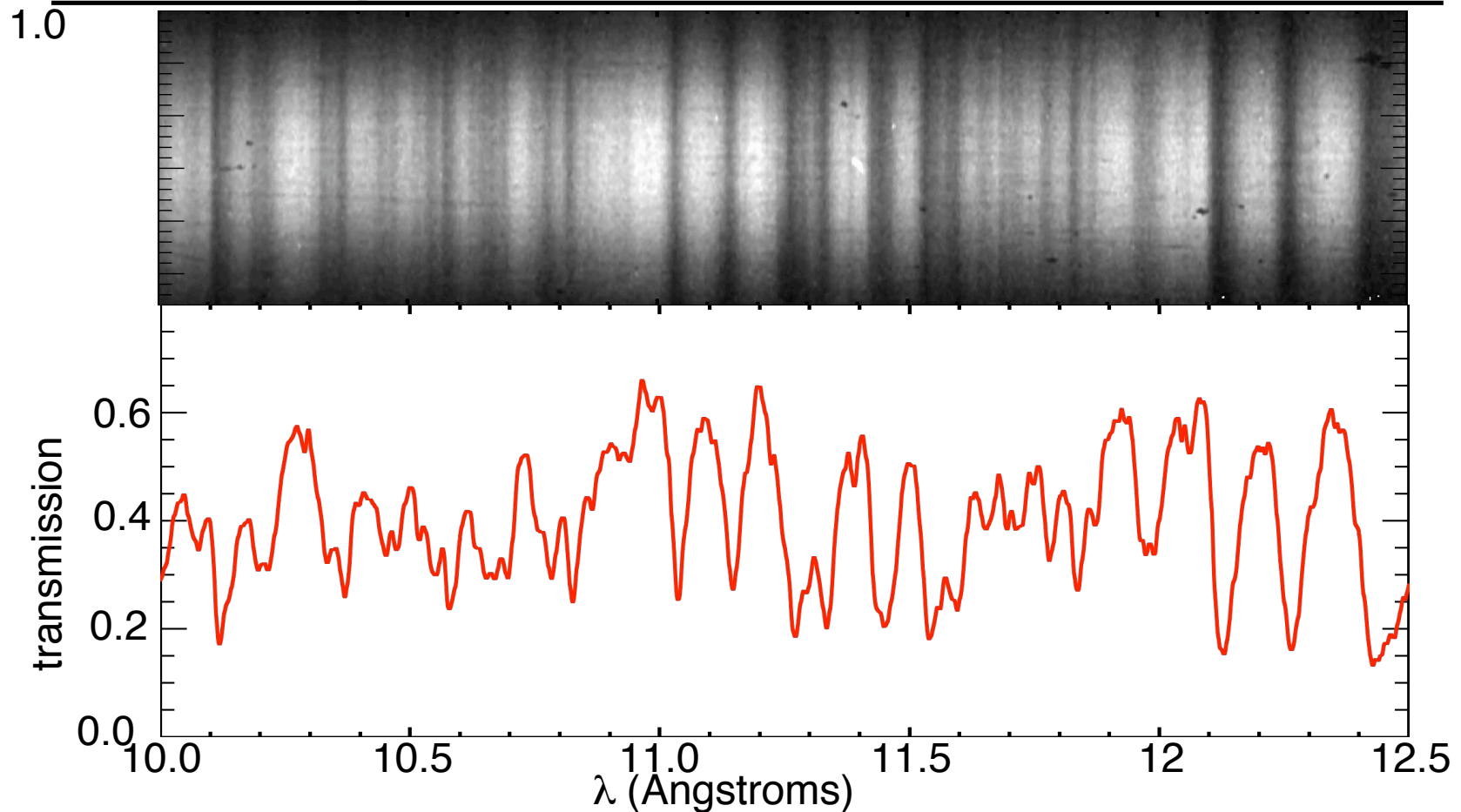
The transmission data scales with the thickness approximately as expected



- Significant portions of the spectrum scales with $\{T\}^x$, with x =thickness
- This supports method robustness - correct areal density, negligible self emission, correct film response, correct background subtraction
- Residual differences due to line saturation, possibly different T_e , n_e



The Fe L-shell spectrum exhibits a wealth of line absorption features

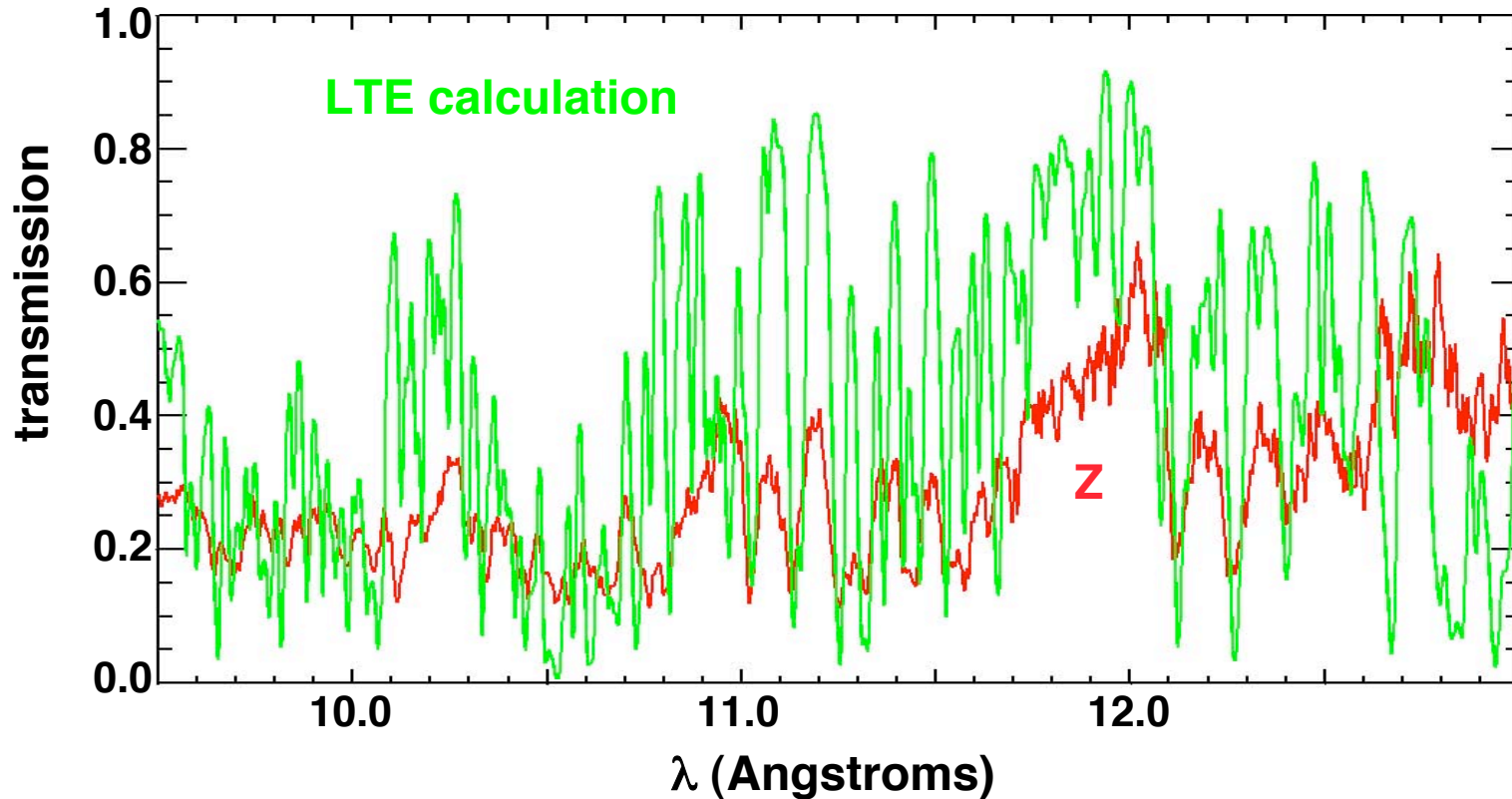


- Reproducing these features is a difficult test for any opacity model





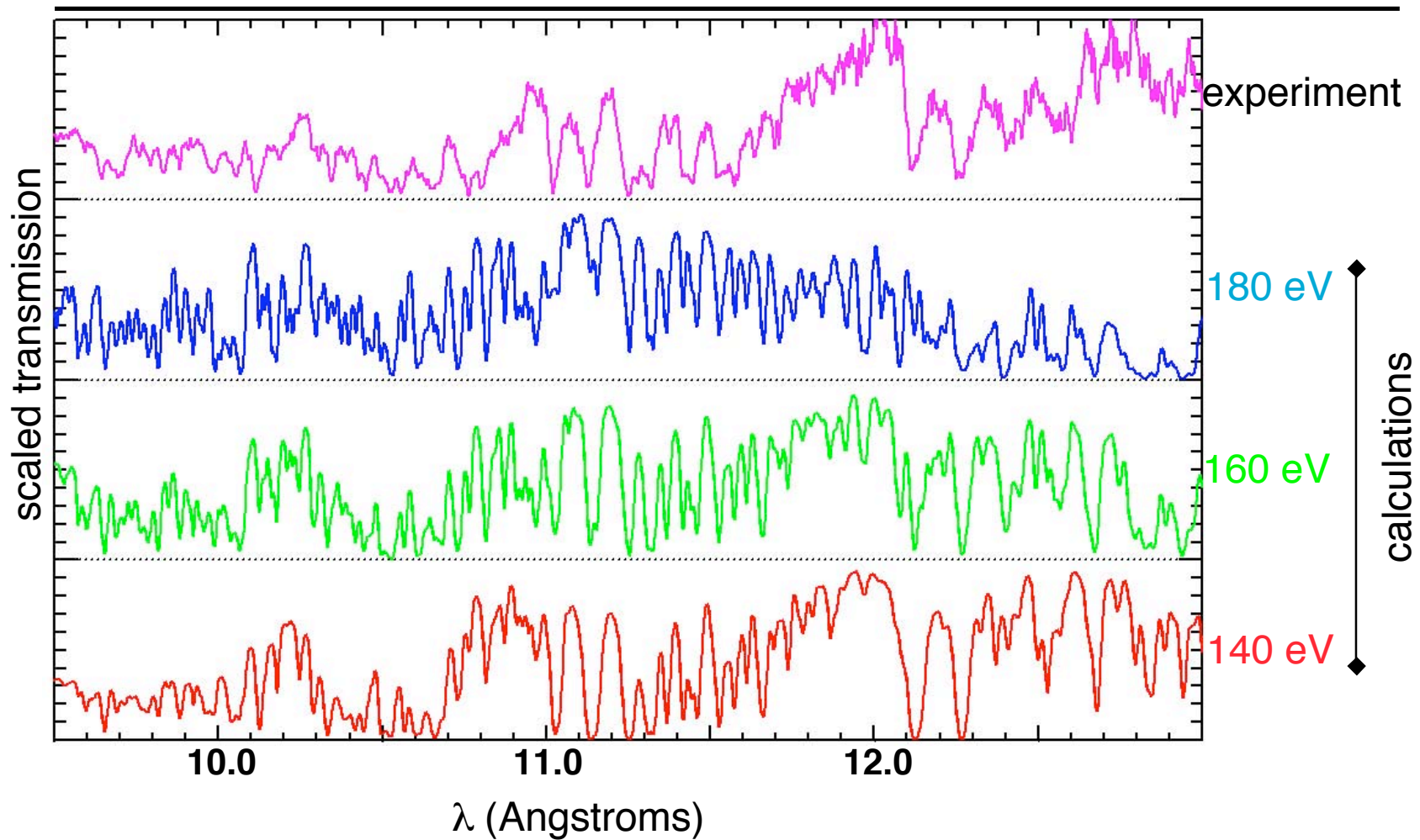
PRISMSPECT calculations exhibit respectable agreement with Fe transmission



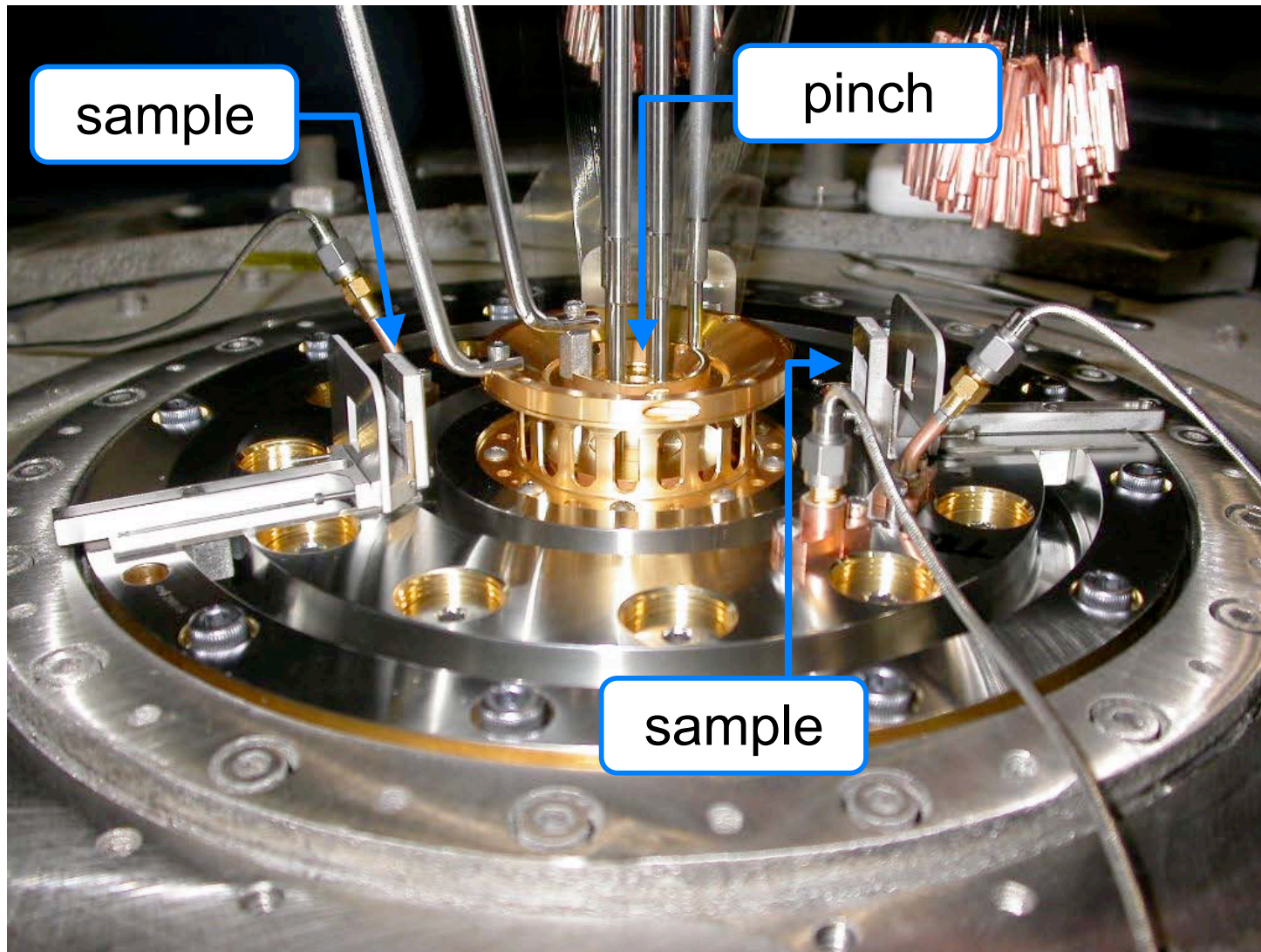
- The main features are well reproduced
- The calculated transmission has “windows” between the lines



The data enables tests of the calculated charge state distribution



Side-on opacity experiments use samples placed ~ 5 cm from the pinch



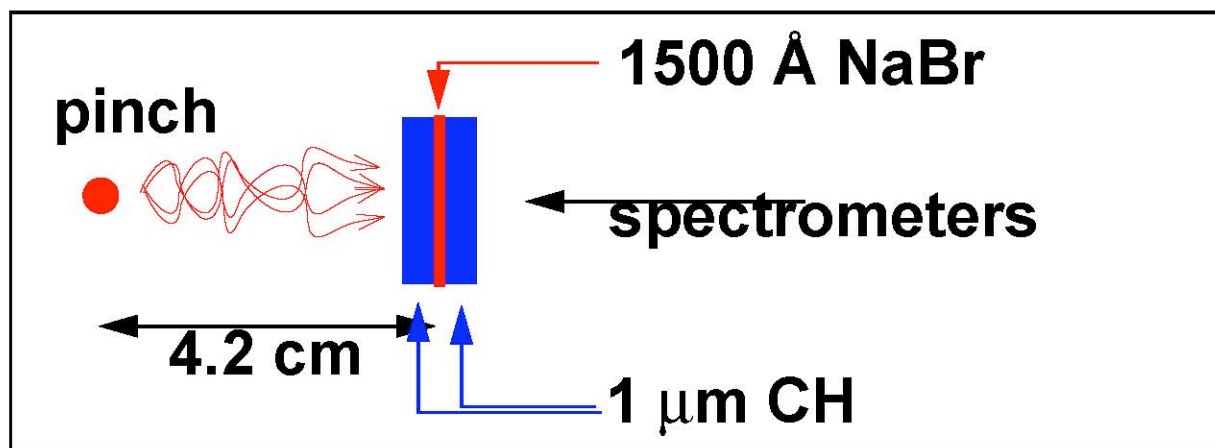
The ability to measure complex opacities is being developed using open M-shell bromine.



Goal for ride-alongs:

Use *FREE* radiation to measure opacities at

$\sim 20\text{-}70\text{ eV}$ and $\sim 10^{-3} - 10^{-2}\text{ g/cc}$



Basic idea:

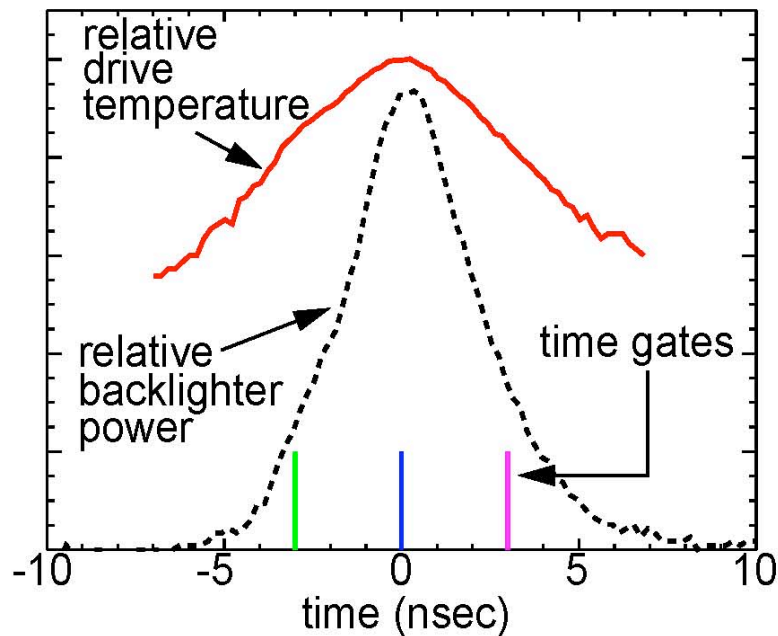
Pinch both heats and backlights sample

Na = thermometer; Br = test element

Develop method, then many elements can be measured

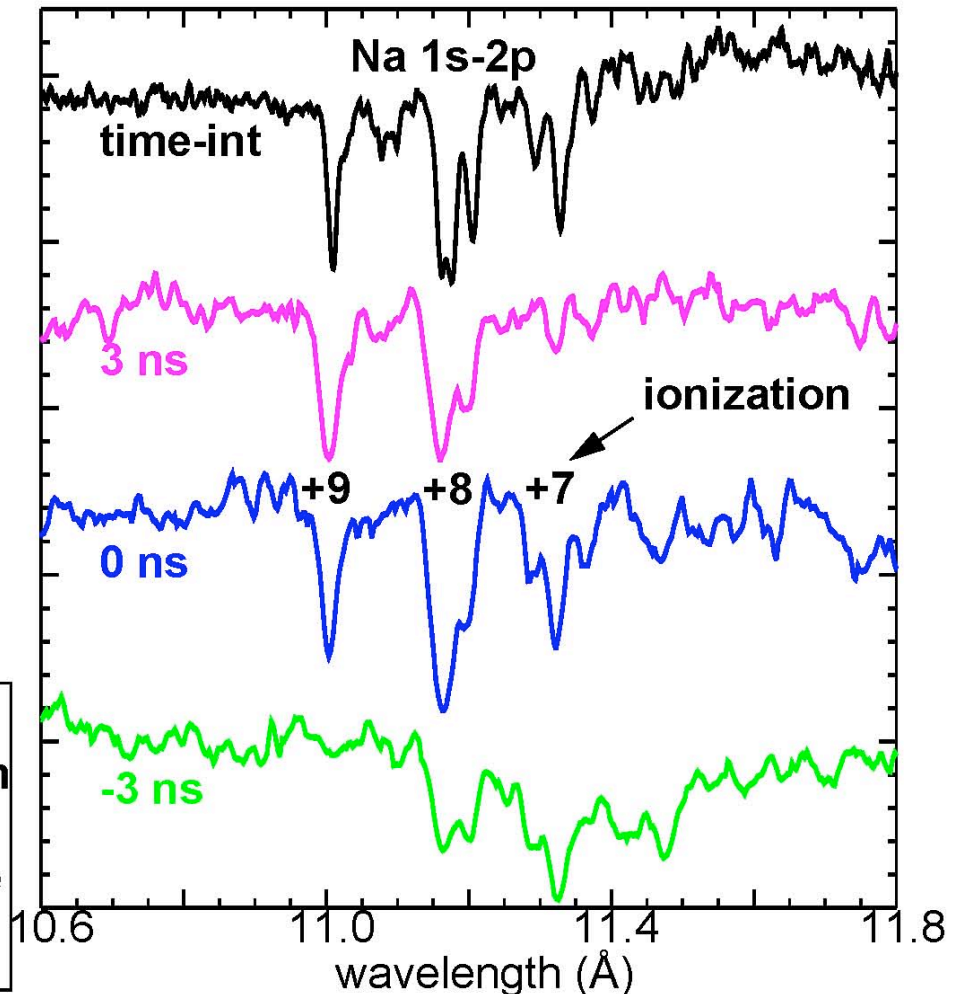


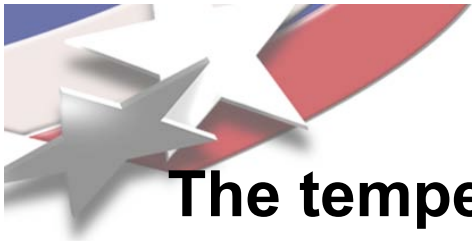
The drive temperature changes only by a modest amount over the z-pinch backlighter duration



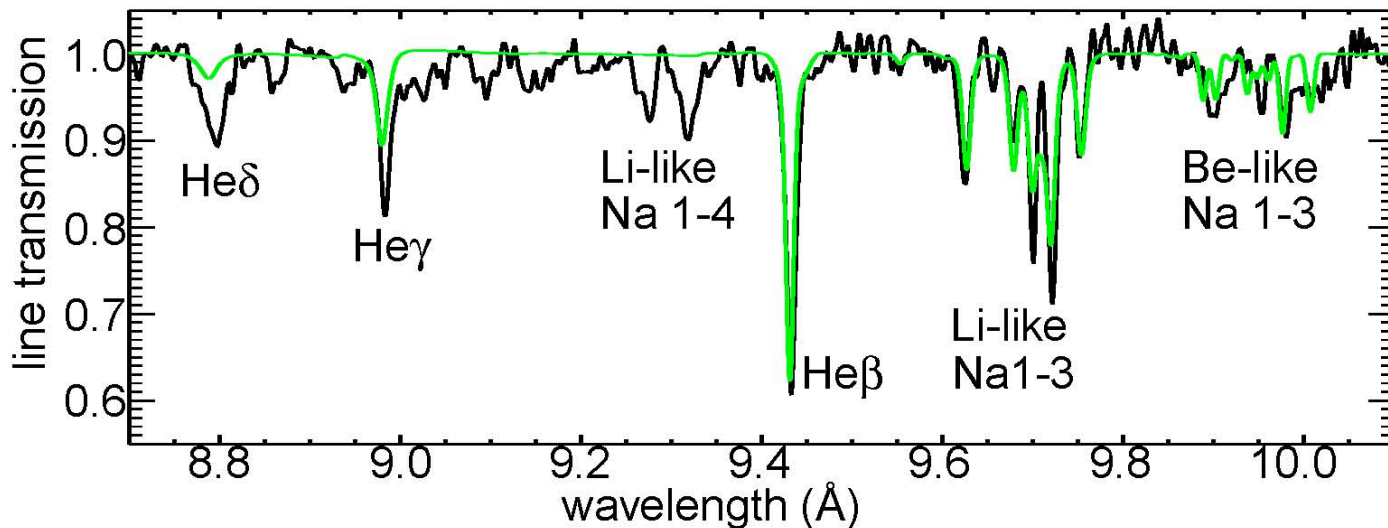
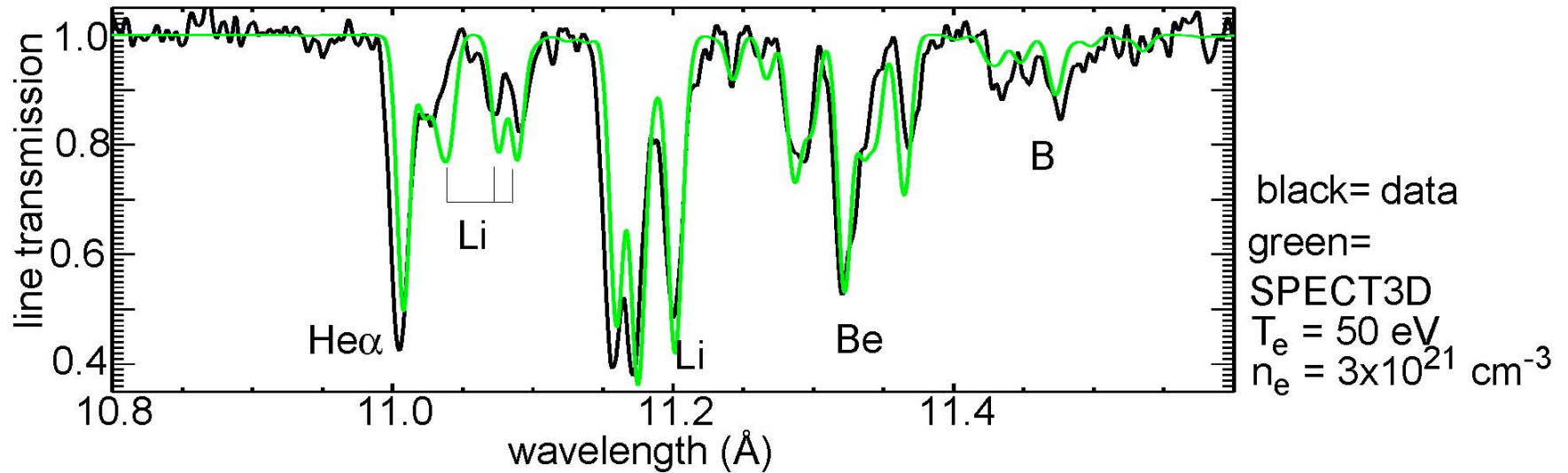
time-integrated spectrum ~
peak power time-resolved spectrum

time-integrated spectrometers have
superior range and resolution



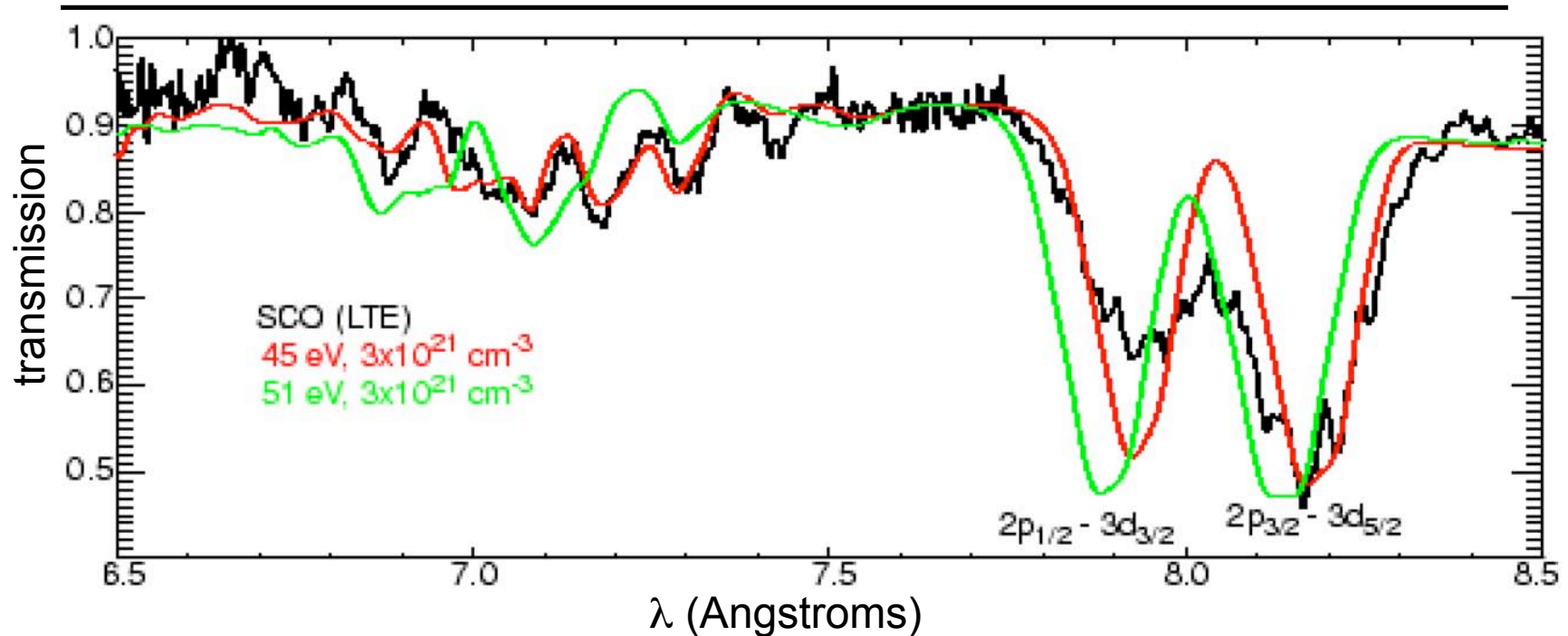


**The temperature and density are diagnosed with
roughly $\pm 10\%$ and $\pm 30\%$ uncertainties, respectively**



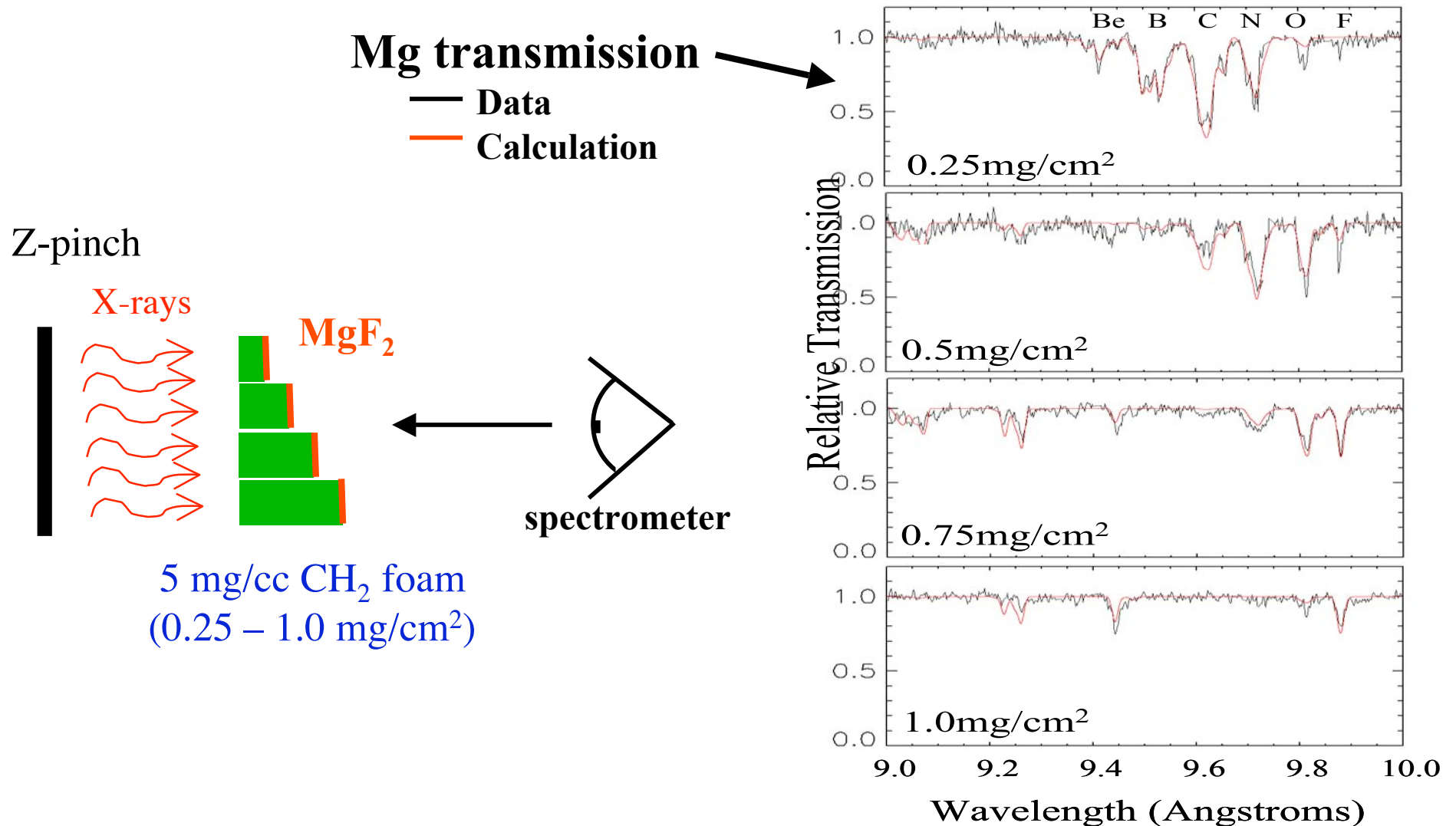



NaBr data can test opacity models



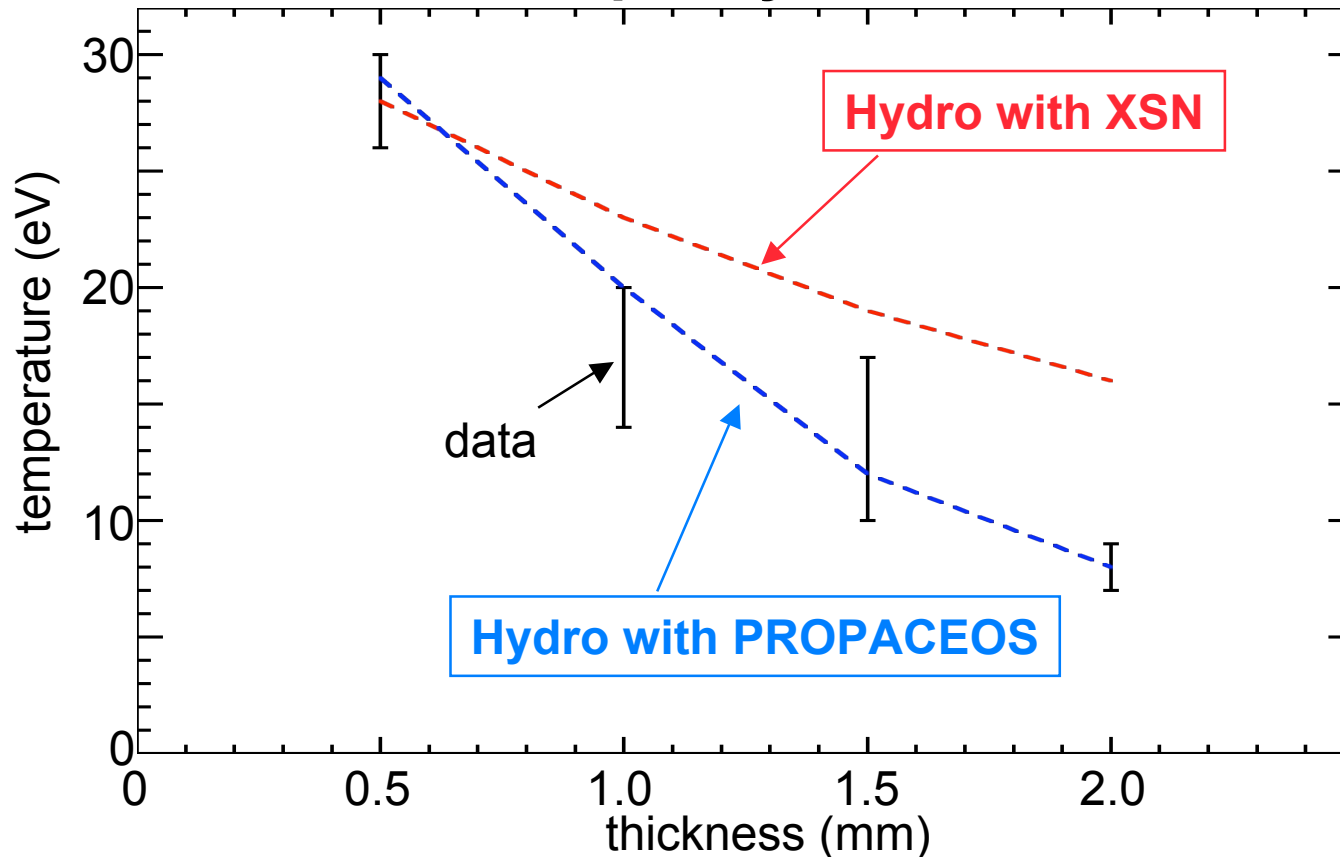
- SCO calculations by P. Arnault, T. Blenski, and G. Dejonghe (CEA France)
- J.E. Bailey et al., JQSRT 81, 31 (2003).

CH₂ foam opacity can be inferred by measuring heating of Mg foils placed behind different foam thicknesses.





Mg tracer heating behind different foam thicknesses discriminates between different CH₂ opacity models



This method is relatively indirect, but it can address a difficult to access regime



goals for future work

- **Model comparisons, feature identification**
- **Measure transmission with multiple Fe thickness on a single shot**
- **Extend to shorter and longer wavelengths**
- **Optimize tamping and sample design with benchmarked rad-hydro simulations**
- **Extend to higher densities and temperatures (ZR)**

Z opacity experiments strengthen existing database and extend measurements beyond $T \sim 150$ eV

